

## ABSTRACT

Title of Document: THE REDOX CHEMISTRY OF DIRHODIUM  
CARBOXAMIDATES: FROM  
FUNDAMENTAL STRUCTURES TO  
CATALYTIC FUNCTIONS.

Jason Michael Nichols, Ph. D., 2008

Directed By: Professor Michael P. Doyle, Department of  
Chemistry and Biochemistry

Redox chemistry is the study of molecular structure and function associated with changes in oxidation state. In this manuscript, the structures and functions of dinuclear rhodium complexes in various oxidation states are investigated. In Chapter 1, probing the structural chemistry of dirhodium(II) carboxamidates reveals that an unprecedented, stable, dirhodium(III) complex can be synthesized and characterized. *Bis*( $\sigma$ -phenyl)-*tetrakis*( $\mu$ -caprolactamato)dirhodium(III) [Rh<sub>2</sub>(cap)<sub>4</sub>Ph<sub>2</sub>] was prepared from Rh<sub>2</sub>(cap)<sub>4</sub> by a copper-catalyzed, aerobic oxidation with aryl transfer from sodium tetraphenylborate. Structural data was obtained by single crystal X-ray diffraction (XRD) of Rh<sub>2</sub>(cap)<sub>4</sub>Ph<sub>2</sub> and related structures with systematic changes in oxidation state. X-ray photoelectron spectroscopy (XPS) was used to determine binding energies for the rhodium electrons in the complexes. The structural data and XPS binding energies indicate that the Rh-Rh bonding interaction does not exist in Rh<sub>2</sub>(cap)<sub>4</sub>Ph<sub>2</sub>.

In Chapter 2, the synthesis of  $\text{Rh}_2(\text{cap})_4\text{Ph}_2$  was made general by using aryl-boronic acids as the aryl transfer agent. The synthesis provided access to an array of *bis*( $\sigma$ -aryl)- $\text{Rh}_2\text{L}_4$  complexes with varying substitution of the aryl ligands. X-ray structures, electrochemical, and computational analysis of complexes with substituents of varying electron-deficiency confirm the Rh-Rh bond cleavage. A second-order Jahn-Teller effect is proposed as the basis for the observed Rh-Rh-C bond angle distortions in the X-ray crystal structures. The delocalization of the aromatic  $\pi$ -system through the  $\text{Rh}_2$ -core was investigated and found to be absent, consistent with the calculated electronic structure.

The final chapter explores the catalytic redox chemistry of  $\text{Rh}_2(\text{cap})_4$ . The mechanism for the oxidative Mannich reaction catalyzed by  $\text{Rh}_2(\text{cap})_4$  in conjunction with *tert*-butyl hydroperoxide was investigated. This study revealed that iminium ions were formed by the oxidation of *N,N*-dialkylanilines with the  $\text{Rh}_2(\text{cap})_4/\text{TBHP}$  system.  $\text{Rh}_2(\text{cap})_4$  was found to be a catalyst for the homolytic decomposition of TBHP to yield the *tert*-butylperoxyl radical (*t*-BuOO•) in a one-electron redox couple. Iminium ions were formed in a stepwise process from *N,N*-dialkylaniline via rate-limiting, hydrogen atom transfer to *t*-BuOO• followed by rapid electron transfer to excess oxidant *in situ*. The net hydrogen atom transfer was found to be a step-wise electron transfer/proton transfer between the *N,N*-dialkylaniline and *t*-BuOO• providing evidence for a novel reactivity mode for peroxy radicals. Nucleophilic capture of the iminium ion to complete the Mannich process was found to occur without association to  $\text{Rh}_2(\text{cap})_4$  under thermodynamic control.

THE REDOX CHEMISTRY OF DIRHODIUM CARBOXAMIDATES: FROM  
FUNDAMENTAL STRUCTURES TO CATALYTIC FUNCTIONS.

By

Jason M. Nichols

Dissertation submitted to the Faculty of the Graduate School of the  
University of Maryland, College Park, in partial fulfillment  
of the requirements for the degree of  
Doctor of Philosophy  
2008

Advisory Committee:

Professor Jeff Davis, Chair  
Professor Daniel Falvey  
Professor Andrei Verdernikov  
Professor Russell Dickerson  
Professor Michael P. Doyle, Advisor

© Copyright

Jason M. Nichols

2008



# Dedication

To my wife,

Rachel Anya Petkewich

“Now this is not the end. It is not even the beginning of the end. But it is,  
perhaps, the end of the beginning.”

*-Winston Churchill, 1942*

## Acknowledgements

I must thank many people both personally and professionally for helping to get my career started. First, and foremost, I thank my mother Penny for more than her fair share of sacrifice to get me here and keep me going. Not least among those sacrifices was living with a child who asked too many questions. Little did we know at the time that asking questions was habit-forming, but I am blessed that she indulged my habit at every opportunity. And she still does.

I am grateful to my sister Shannan for keeping me humble. She enjoys a surfeit of volunteers to aid her in this task, but she has done it solo many times over the years and I am in her debt. Chief among willing volunteers is my dear friend and brother Toby Cutting. His support, friendship, and dedication continue to inspire me not to mess this up!

Many personal friends have contributed to this manuscript without knowing it. To name a few: my step-father Bill, Neal, Kerri, Raj, Gautam, Jarrod, Tanay, Marvourneen, Kazeem, Jay Pearson, Chris, Christian, and that guy at the chicken-fry shack. Many thanks to them, and all of those who were not named, for their love and support.

Professionally, I am grateful to Mike Doyle for his academic support and counsel. He has always sought excellence in our work, and his patience and guidance has taught me to do the same. I appreciate the leadership and mentoring opportunities he has provided me by incorporating undergraduate students into the research program. It has been a rewarding experience and one I intend to pay forward in the coming years. Most of all, I have come to appreciate Mike as a friend and I wish him well.

I would like to thank Dan Falvey, Jeff Davis, Andrei Vedernikov, and Russell Dickerson for serving on my committee. Special thanks to Andrei,

Dan, and Lyle Isaacs for many helpful discussions, sharing of resources, and ideas.

I would also like to thank my undergraduate mentors at Ithaca College, Professors Heinz Koch and Vincent De Turi. I still refuse to take wooden nickels, and no longer glue things into my notebook thanks to their guidance. And special thanks to my high school chemistry teacher, David Pysnik, for showing me at a very early age just how cool science can be.

I am grateful to the Organic Division of the American Chemical Society for funding through a fellowship sponsored by Bristol-Meyers-Squibb.

Chemistry is not easy work, but good collaborations turn that work into play. I am grateful to the people I have collaborated with during my graduate career for making this endeavor fun. In my collaborations with Dr. Arthur Catino, he taught me what it means to be a life-long student of chemistry. His love for the subject is infectious and his knowledge truly remarkable. I thank him for sharing them both with me. I would also like to thank Professor Lyle Isaacs, Professor Tong Ren, Professor Rinaldo Poli, Dr. Hojae Choi, Dr. Joffrey Wolf, Dr. Peter Zavalij, Dr. Bindhu Varughese, Dr. Ray Forslund, Dr. Yuanhua Wang, Mr. Yiu Liu, Mr. Sidhartha Gottipamula, Ms. Catt Edgely, Mr. James Myslinksi, Ms. Christina Wells, Mr. James Perry, Mr. Brian Nettles, and Mr. Conrad Lubek for their collaborations with me over my graduate career.

I would also like to thank Doyle group members I have worked and made merry with including Dr. Tom Weathers, Dr. Marcela Valenzuela, John Colyer, Christine Hedberg, Dr. Albert Russell, Dr. J.P. Morgan, Dr. Penglin Huang, Dr. Bing Deng, Dr. Yu Zhang, Sara Saba, Ben Von Hohenstoff, Randy Binder, Mansi Dalal, Grace Chiou, Myloan Ngyuen, and Jim Creagan. I would especially like to thank Dr. Emily McLaughlin for slogging through the unbearable first attempts at this manuscript. It has been a pleasure to work and play with all of you.

As the last person of the “core-four” to graduate from Maryland, I must thank Art Catino, Darren Bykowski, and Kousik Kundu for their friendship here. As we go our separate ways, I have pieces of you all in my head: visions of the Hindhu Elvis, Bykowski on a *JOC* cover that should never see the light of day, and the Catino-ite elves who make the Vermiculite. Gentlemen, it has been a long road, and I am glad to have walked it with you.

Rachel, I love you. And because the graduate department doesn't award degrees to spouses, this manuscript is for you. Thank you.

# Table of Contents

<b>List of Tables</b> .....	viii
<b>List of Figure</b> .....	xiii
<b>List of Abbreviations</b> .....	xiv
<b>Chapter 1. <i>Bis</i>(<math>\sigma</math>-phenyl)-<i>tetrakis</i>-(<math>\mu</math>-caprolactamato)-dirhodium(III): A Dirhodium Paddlewheel Complex With No Metal Bond</b>	
I. Synopsis.....	1
II. Introduction - Bonding in Dinuclear Metal Complexes.....	3
III. Results and Discussion .....	16
IV. Conclusion.....	32
V. Experimental .....	33
<b>Chapter 2. <i>Bis</i>(<math>\sigma</math>-aryl)-dirhodium(III) Carboxamidates – A General Class of Dinuclear Rhodium Compounds</b>	
I. Synopsis.....	82
II. Introduction - $M_2^{6+}$ complexes with M-C bonds.....	84
III. Results and Discussion .....	92
IV. Conclusion.....	129
V. Experimental .....	130
<b>Chapter 3. The Oxidative Mannich Reaction: <i>tert</i>-Butylperoxyl Radical Oxidizes Dialkylanilines by Electron/Proton Transfer</b>	
I. Synopsis.....	257
II. Introduction - Amine Oxidations and the Oxidative Mannich Reaction .....	259
III. Results and Discussion .....	286
IV. Conclusion .....	317
V. Experimental .....	318
<b>Bibliography</b> .....	342

## List of Tables

- Table 1-1.** Selected bond lengths for  $[\text{Rh}_2(\text{cap})_4 \cdot 2\text{CH}_3\text{CN}]$  (2),  $[\text{Rh}_2(\text{cap})_4(\text{OH}_2)_2]\text{OTf}$  (3),  $[\text{Rh}_2(\text{cap})_4(\text{C}_6\text{H}_5)_2]$  (1).
- Table 1-2.** Selected bond angles for  $[\text{Rh}_2(\text{cap})_4 \cdot 2\text{CH}_3\text{CN}]$  (2),  $[\text{Rh}_2(\text{cap})_4(\text{OH}_2)_2]\text{OTf}$  (3),  $[\text{Rh}_2(\text{cap})_4(\text{C}_6\text{H}_5)_2]$  (1).
- Table 1-3.** XPS Data for  $[\text{Rh}_2(\text{cap})_4 \cdot 2\text{CH}_3\text{CN}]$  (2),  $[\text{Rh}_2(\text{cap})_4(\text{OH}_2)_2]\text{OTf}$  (3),  $[\text{Rh}_2(\text{cap})_4(\text{C}_6\text{H}_5)_2]$  (1).
- Table 1-4.** Optimization for the formation of 1.
- Table 1-5.** Crystal data and structure refinement for  $[\text{Rh}_2(\text{cap})_4\text{Ph}_2] \cdot 2\text{CH}_2\text{Cl}_2$ .
- Table 1-6.** Atomic coordinates and equivalent isotropic atomic displacement parameters ( $\text{\AA}^2$ ) for  $[\text{Rh}_2(\text{cap})_4\text{Ph}_2] \cdot 2\text{CH}_2\text{Cl}_2$ .
- Table 1-7.** Anisotropic atomic displacement parameters ( $\text{\AA}^2$ ) for  $[\text{Rh}_2(\text{cap})_4\text{Ph}_2] \cdot 2\text{CH}_2\text{Cl}_2$ .
- Table 1-8.** Hydrogen atom coordinates and isotropic atomic displacement parameters ( $\text{\AA}^2$ ) for  $[\text{Rh}_2(\text{cap})_4\text{Ph}_2] \cdot 2\text{CH}_2\text{Cl}_2$ .
- Table 1-9.** Site occupancy factors that deviate from unity for disordered solvent molecule of  $\text{CH}_2\text{Cl}_2$  in  $[\text{Rh}_2(\text{cap})_4\text{Ph}_2] \cdot 2\text{CH}_2\text{Cl}_2$ .
- Table 1-10.** Bond lengths ( $\text{\AA}$ ) and angles ( $^\circ$ ) for  $[\text{Rh}_2(\text{cap})_4\text{Ph}_2] \cdot 2\text{CH}_2\text{Cl}_2$ .
- Table 1-11.** Torsion angles ( $^\circ$ ) for  $[\text{Rh}_2(\text{cap})_4\text{Ph}_2] \cdot 2\text{CH}_2\text{Cl}_2$ .
- Table 1-12.** Crystal data/structure refinement for  $[\text{Rh}_2(\text{cap})_4(\text{MeCN})_2] \cdot 2\text{CH}_3\text{CN}$ .
- Table 1-13.** Atomic coordinates and equivalent isotropic atomic displacement parameters ( $\text{\AA}^2$ ) for  $[\text{Rh}_2(\text{cap})_4(\text{MeCN})_2] \cdot 2\text{CH}_3\text{CN}$ .
- Table 1-14.** Anisotropic atomic displacement parameters ( $\text{\AA}^2$ ) for  $[\text{Rh}_2(\text{cap})_4(\text{MeCN})_2] \cdot 2\text{CH}_3\text{CN}$ .

- Table 1-15.** Hydrogen atom coordinates and isotropic atomic displacement parameters ( $\text{\AA}^2$ ) for  $[\text{Rh}_2(\text{cap})_4(\text{MeCN})_2] \cdot 2\text{CH}_3\text{CN}$ .
- Table 1-16.** Bond lengths ( $\text{\AA}$ ) and angles ( $^\circ$ ) for  $[\text{Rh}_2(\text{cap})_4(\text{MeCN})_2] \cdot 2\text{CH}_3\text{CN}$ .
- Table 1-17.** Crystal data and structure refinement for  $[\text{Rh}_2(\text{cap})_4(\text{OH}_2)_2]\text{OTf}$ .
- Table 1-18.** Atomic coordinates and equivalent isotropic atomic displacement parameters ( $\text{\AA}^2$ ) for  $[\text{Rh}_2(\text{cap})_4(\text{OH}_2)_2]\text{OTf}$ .
- Table 1-19.** Anisotropic atomic displacement parameters ( $\text{\AA}^2$ ) for  $[\text{Rh}_2(\text{cap})_4(\text{OH}_2)_2]\text{OTf}$ .
- Table 1-20.** Bond lengths ( $\text{\AA}$ ) and angles ( $^\circ$ ) for  $[\text{Rh}_2(\text{cap})_4(\text{OH}_2)_2]\text{OTf}$ .
- Table 1-21.** Torsion angles ( $^\circ$ ) for  $[\text{Rh}_2(\text{cap})_4(\text{OH}_2)_2]\text{OTf}$ .
- Table 1-22.** Site occupancy factors that deviate from unity for  $[\text{Rh}_2(\text{cap})_4(\text{OH}_2)_2]\text{OTf}$ .
- Table 1-23.** Hydrogen bond information for  $[\text{Rh}_2(\text{cap})_4(\text{OH}_2)_2]\text{OTf}$  ( $\text{\AA}$  and  $^\circ$ ).
- Table 1-24.** XPS data for **1** with selected peak graphs.
- Table 1-25.** XPS data for **2** with selected peak graphs.
- Table 1-26.** XPS data for **3** with selected peak graphs.
- Table 2-1.** Structural data for *bis*( $\sigma$ -alkynyl)- $\text{Ru}_2(\text{DMBA})_4$ .
- Table 2-2.** Electronic comparison ( $E_{1/2}$  and  $\lambda_{\text{max}}$ ) for  $\text{Rh}_2\text{L}_4\text{Ar}_2$  and  $\text{Rh}_2\text{L}_4\text{ArAr}'$ .
- Table 2-3.** Structural comparison from XRD data.
- Table 2-4.** Selected DFT-optimized geometric parameters (distances in  $\text{\AA}$ , angles in degrees) for the model compounds **55-57** compared to the crystallographic averages from Table 2-3.
- Table 2-5.** Upper-valent MOs for the completely symmetric model compound  $\text{Rh}_2(\text{HNCHO})_4\text{Ph}_2$  (**55**).



**Table 2-6.** Upper-valent MOs for the model compound  $\text{Rh}_2(\text{HNCHO})_4\text{Ph}_2$  (**56**) with a  $A_g'$  bond angle distortion.

**Table 2-7.** Upper-valent MOs for the model compound  $\text{Rh}_2(\text{HNCHO})_4\text{Ph}_2$  (**57**) with a  $B_g''$  bond angle distortion.

**Table 2-8.** Symmetry transform of irreducible representations of  $C_{2h}$  to  $G_i$ .

**Table 2-9.** Crystal data and structure refinement for **12**.

**Table 2-10.** Atomic coordinates and equivalent isotropic atomic displacement parameters ( $\text{\AA}^2$ ) for **12**.

**Table 2-11.** Anisotropic atomic displacement parameters ( $\text{\AA}^2$ ) for **12**.

**Table 2-12.** Site occupancy factors that deviate from unity for **12**.

**Table 2-13.** Bond lengths ( $\text{\AA}$ ) and angles ( $^\circ$ ) for **12**.

**Table 2-14.** Crystal data and structure refinement for **13**.

**Table 2-15.** Atomic coordinates and equivalent isotropic atomic displacement parameters ( $\text{\AA}^2$ ) for **13**.

**Table 2-16.** Anisotropic atomic displacement parameters ( $\text{\AA}^2$ ) for **13**.

**Table 2-17.** Hydrogen-atom coordinates/isotropic atomic displacement parameters ( $\text{\AA}^2$ ) for **13**.

**Table 2-18.** Bond lengths ( $\text{\AA}$ ) and angles ( $^\circ$ ) for **13**.

**Table 2-19.** Crystal data and structure refinement for **16**.

**Table 2-20.** Atomic coordinates and equivalent isotropic atomic displacement parameters ( $\text{\AA}^2$ ) for **16**.

**Table 2-21.** Site occupancy factors that deviate from unity for **16**.

**Table 2-22.** Anisotropic atomic displacement parameters ( $\text{\AA}^2$ ) for **16**.

**Table 2-23.** Hydrogen atom coordinates/isotropic atomic displacement parameters ( $\text{\AA}^2$ ) for **16**.

**Table 2-24.** Bond lengths ( $\text{\AA}$ ) and angles ( $^\circ$ ) for **16**.

- Table 2-25.** Crystal data and structure refinement for **18**.
- Table 2-26.** Atomic coordinates and equivalent isotropic atomic displacement parameters ( $\text{\AA}^2$ ) for **18**.
- Table 2-27.** Site occupancy factors that deviate from unity for **18**.
- Table 2-28.** Anisotropic atomic displacement parameters ( $\text{\AA}^2$ ) for **18**.
- Table 2-29.** Hydrogen atom coordinates/isotropic atomic displacement parameters ( $\text{\AA}^2$ ) for **18**.
- Table 2-30.** Bond lengths ( $\text{\AA}$ ) and angles ( $^\circ$ ) for **18**.
- Table 2-31.** Crystal data and structure refinement for **20**.
- Table 2-32.** Atomic coordinates and equivalent isotropic atomic displacement parameters ( $\text{\AA}^2$ ) for **20**.
- Table 2-33.** Anisotropic atomic displacement parameters ( $\text{\AA}^2$ ) for **20**.
- Table 2-34.** Hydrogen atom coords/isotropic atomic displacement parameters ( $\text{\AA}^2$ ) for **20**.
- Table 2-35.** Crystal data and structure refinement for **22**.
- Table 2-36.** Atomic coordinates and equivalent isotropic atomic displacement parameters ( $\text{\AA}^2$ ) for **22**.
- Table 2-37.** Anisotropic atomic displacement parameters ( $\text{\AA}^2$ ) for **22**.
- Table 2-38.** Hydrogen atom coordinates and isotropic atomic displacement parameters ( $\text{\AA}^2$ ) for **22**.
- Table 2-39.** Bond lengths ( $\text{\AA}$ ), valence angles, and torsion angles ( $^\circ$ ) for **22**.
- Table 2-40.** Optimized geometry for **55** in Cartesian coordinates.
- Table 2-41.** Optimized geometry for **56** in Cartesian coordinates.
- Table 2-42.** Optimized geometry for **57** in Cartesian coordinates.
- Table 2-43.** MO Calculations for **55** with energies (eV) and atomic orbital contributions (%)

**Table 2-44.** MO Calculations for **56** with energies (eV) and atomic orbital contributions (%).

**Table 2-45.** MO Calculations for **57** with energies (eV) and atomic orbital contributions (%).

**Table 3-1.** Free-energy profiles of PIE and KIE.

**Table 3-2.** Compiled raw data for adamantane product distribution.

**Table 3-3.** % Deuterium incorporation for deuterated analogues.

**Table 3-4.** Data for KIE values.

**Table 3-5.** Data for PIE values.

**Table 3-6.** Compiled raw data for LFER of amine,  $\nu_i$  and  $\log(\nu_i^{\text{rel}})$ .

**Table 3-7.** Compiled raw data for LFER of catalyst,  $\nu_i$  and  $\log(\nu_i^{\text{rel}})$ .

**Table 3-8.** Compiled raw data for kinetic order of *N,N*-dimethylaniline.

**Table 3-9.** Compiled raw data for kinetic order of dirhodium catalyst.

## List of Figures

**Figure 1-1.** Redox specific nomenclature.

**Figure 1-2.** General structure of  $M_2L_4$  paddle-wheel complexes.

**Figure 1-3.** AOs combine to give metal-metal bonding/anti-bonding interactions.

**Figure 1-4.** ORTEP drawing of  $Pd_2^{4+}(DAniF)_4$  (**5**).

**Figure 1-5.** ORTEP stereoscopic view of one of two crystallographically independent molecules of **6**•Et<sub>2</sub>O.

**Figure 1-6.** Rehybridization in  $Ti_2^{6+}$  complex (**6**).

**Figure 1-7.** General structure and ligand arrangement of dirhodium carboxamidates.

**Figure 1-8.** M-L interactions that destabilize the  $\delta^*$ -MO.

**Figure 1-9.** ORTEP drawing of one of two crystallographically independent molecules of  $[Rh_2(cap)_4(C_6H_5)_2] \cdot 2CH_2Cl_2$ .

**Figure 1-10.** ORTEP drawing of  $[Rh_2(cap)_4(CH_3CN)_2] \cdot 2CH_3CN$ ,  $C_{32}H_{52}N_8O_4Rh_2$ .

**Figure 1-11.** ORTEP drawing of  $[Rh_2(cap)_4(H_2O)_2]OTf$ ,  $C_{25}H_{44}F_3N_4O_9Rh_2S$ .

**Figure 1-12.** (a) General  $Rh_2^{n+}(cap)_4L_2$  structure with atom labels (b) A partial view of **1** with labels of the aryl ligand.

**Figure 1-13.** Rehybridization at Rh alters bonding in **1**.

**Figure 1-14.** Conversion of **9** to **1** monitored at 430 nm under various conditions.

**Figure 1-15.** A view of  $[Rh_2(cap)_4Ph_2] \cdot 2CH_2Cl_2$  showing the numbering scheme.

**Figure 1-16.** A view of  $[Rh_2(cap)_4(MeCN)_2] \cdot 2CH_3CN$  showing the numbering scheme.

**Figure 1-17.** (Top) a view of  $\text{Rh}_2(\text{cap})_4(\text{MeCN})_2$  ABAB Layer I; (Bottom) Alternative AAAA stacking of  $\text{Rh}_2(\text{cap})_4(\text{MeCN})_2$  in Layer II of the OD structure.

**Figure 1-18.** A view of  $[\text{Rh}_2(\text{cap})_4(\text{OH}_2)_2]\text{OTf}$  showing the numbering scheme.

**Figure 1-19.** XPS peak graph for the Rh 3d orbitals in **1**.

**Figure 1-20.** XPS peak graph for the Rh 3d orbitals in **2**.

**Figure 1-21.** XPS peak graph for the Rh 3d orbitals in **3**.

**Figure 2-1.** Distance dependent free energy relationship of comproportionation energies [ $(\Delta r)^2$  vs.  $\Delta E_c$ , biferrocene = 0]

**Figure 2-2.** Boronic acids that did not form  $\text{Rh}_2^{6+}$  complexes.

**Figure 2-3.** Model transition states for recalcitrant substrates.

**Figure 2-4.** CV and DPV vs. Ag/AgCl for **3** measured in  $\text{CH}_2\text{Cl}_2$  (1 mM) with tetra-*n*-butylammonium hexafluorophosphate as the supporting electrolyte.

**Figure 2-5.** LFER relationships. a)  $E_{1/2}$  vs  $\sigma_{m,p}$ ; b)  $E_s$  vs  $\sigma_p^+$ .

**Figure 2-6.** General structure with numbering scheme.

**Figure 2-7.** An ORTEP view of **1**• $2\text{CH}_2\text{Cl}_2$  looking down the  $C_2$  rotational axis with the ligands eclipsed.

**Figure 2-8.** Eclipsed ORTEP view of **12**• $2\text{CH}_2\text{Cl}_2$  illustrating the  $B_g''$  distortion mode.

**Figure 2-9.** Mutually perpendicular views of complexes **55**, **56**, and **57** with their relative energies from the DFT calculations.

**Figure 2-10.** Molecular orbital correlation diagram for the distorted geometries.

**Figure 2-11.** (a) MOs of **55** that mix in the  $A_g'$  distortion; (b) MOs in **56** that result from the MOs in **55**; (c) MOs of **55** that mix in the  $B_g''$  distortion; (d) MOs in **57** that result from the MOs in **55**.

**Figure 2-12.** Comparison of bond angle distortion in the ORTEP drawings of complexes **1**, **12**, and **13**.

**Figure 2-13.** Schematic representation showing the inverse relationship between the bond angle distortion ( $\theta$ ) and Rh-Rh bond distance ( $r$ ).

**Figure 2-14.** Electronic absorption spectra (250-400 nm) of (a) complex **16**; (b) complex **18**; (c) 1:1 mixture of complexes **16** and **18**; (d) complex **23**.

**Figure 2-15.** A view of **12** showing the numbering scheme employed.

**Figure 2-16.** A view of **13** showing the numbering scheme employed.

**Figure 2-17.** A view of **16** showing the numbering scheme employed.

**Figure 2-18.** A view of **18** showing the numbering scheme employed.

**Figure 2-19.** A view of **20** showing the numbering scheme employed.

**Figure 2-20.** A view of **22** showing the numbering scheme employed.

**Figure 3-1.** (a) LFER calculated against  $\sigma^+$  for 4-R-*N,N*-dimethylanilines; (b) LFER calculated against  $E_0$  of 4-R-*N,N*-dimethylanilines.

**Figure 3-2.** Graph showing lack of LFER for **60** and related complexes.

**Figure 3-3.** Kinetic order log/log plots for **2** and *N,N* dimethylaniline.

**Figure 3-4.** Plots of  $\nu_i$  for each substituted 4-R-*N,N*-dimethylaniline.

**Figure 3-5.** Plots of  $\nu_i$  for each dirhodium(II) complex.

**Figure 3-6.** Plots of  $\nu_i$  for each concentration of *N,N*-dimethylaniline.

**Figure 3-7.** Plots of  $\nu_i$  for each concentration of  $\text{Rh}_2(\text{cap})_4$ .

**Figure 3-8.** 1st order plot of  $\ln[\text{DMA}]$  vs. time ( $k_{\text{obs}} = -1.3 \times 10^{-3} \text{ s}^{-1}$ ;  $r^2 = 0.9999$ ).

## List of Abbreviations

AO	atomic orbital
av	average value
B3LYP	Becke-Lee Yang Parr
BDE	bond dissociation energy
Boc	<i>tert</i> -butylcarbamate
CV	cyclic voltametry
DAniF	<i>N,N'</i> -(4-anisole)-formamidinate
DCB	1,4-dicyanobenzene
DFT	density functional theory
DMA	<i>N,N</i> -dimethylaniline
DMBA	<i>N,N'</i> -dimethylbenzamidine, ArCN <sub>2</sub> (CH <sub>3</sub> ) <sub>2</sub>
DPV	differential pulse voltammetry
dr	diastereomeric ratio
ECHEM	electrochemistry
ESI	electrospray ionization
EtOAc	ethyl acetate
FAB	fast-atom bombardment
Fc	ferrocene
FWHM	full width at half maximum
GCMS	gas chromatograph/mass spectroscopy
HOMO	highest occupied molecular orbital
HRMS	high resolution mass spectroscopy
IR	infrared spectroscopy
KIE	kinetic isotope effect
LCAO	linear combinations of atomic orbitals
LFER	free energy relationship
LUMO	lowest unoccupied molecular orbital
MO	molecular orbital
<i>n</i> -BuLi	<i>n</i> -butyl lithium

NHE	normal hydrogen electrode
NHPI	<i>N</i> -hydroxyphthalimide
ORTEP	Oak Ridge Thermal Ellipsoid Program
OTf	trifluoromethanesulfonate, CF <sub>3</sub> SO <sub>3</sub>
PCET	proton-coupled electron transfer
PIE	product isotope effect
PINO	phthalimido- <i>N</i> -oxyl radical
PRE	Ingold-Fisher persistent radical effect
SCE	standard calomel electrode
SCF	self-consistent field
SD	standard deviation
TBAA	tetra- <i>n</i> -butyl ammonium acetate
TBHP	<i>tert</i> -butyl hydroperoxide
THF	tetrahydrofuran
T-HYDRO <sup>®</sup>	70% w/w aqueous TBHP
TIPS	tri-isopropylsilyl
TLC	thin layer chromatography
TMS	tetramethylsilane, Me <sub>4</sub> Si
UV/Vis	ultraviolet/visible spectroscopy
XPS	X-ray photoelectron spectroscopy
XRD	single-crystal X-ray diffraction



## Chapter 1

### *Bis*( $\sigma$ -phenyl)-*tetrakis*( $\mu$ -caprolactamato)-dirhodium(III): A Dirhodium Paddlewheel Complex With No Metal Bond

#### I. Synopsis<sup>1</sup>

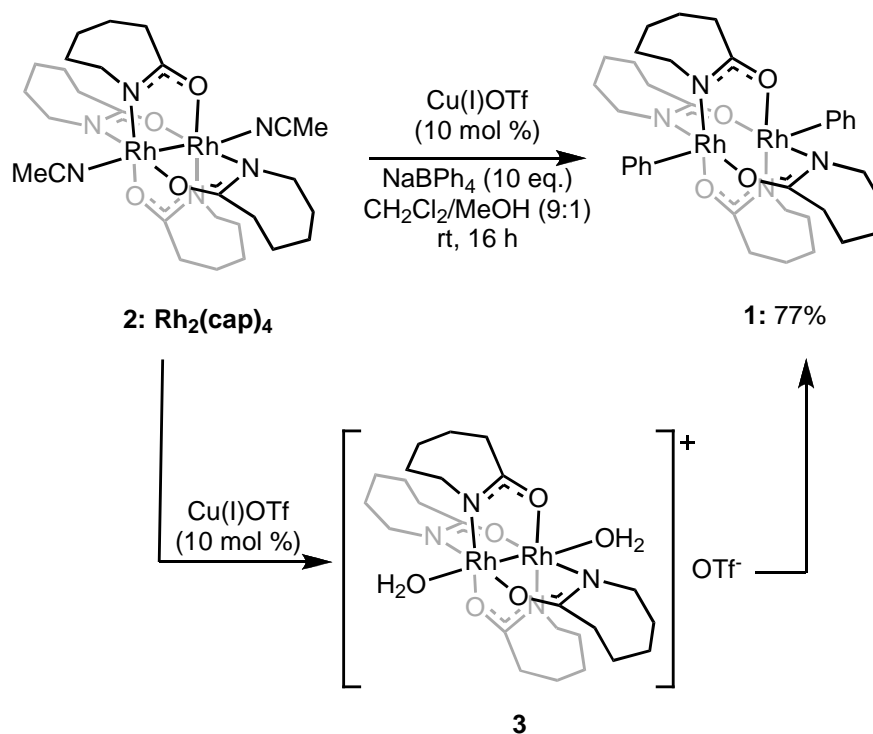
In this chapter, the first unambiguous and fully characterized dirhodium(III) paddle-wheel complex, *bis*( $\sigma$ -phenyl)-*tetrakis*( $\mu$ -caprolactamato)-dirhodium(III) (**1**:  $[\text{Rh}_2(\text{cap})_4(\text{C}_6\text{H}_5)_2]$ ) and its synthesis is described (Scheme 1). Compound **1** was prepared by the oxidation of *bis*(acetonitrile)-*tetrakis*( $\mu$ -caprolactamato)-dirhodium(II) (**2**:  $[\text{Rh}_2(\text{cap})_4(\text{CH}_3\text{CN})_2]$ ) using a catalytic amount of CuOTf (10 mol%) with molecular oxygen as the terminal oxidant and sodium tetraphenylborate ( $\text{NaBPh}_4$ ) as an aryl transfer agent. The proposed intermediate structure, *bis*-aquo-*tetrakis*( $\mu$ -caprolactamato)-dirhodium(II,III) triflate (**3**:  $[\text{Rh}_2(\text{cap})_4(\text{OH}_2)_2]\text{OTf}$ ) was prepared and a comparative electronic and structural analysis of a redox series of  $\text{Rh}_2^{n+}$  complexes ( $n = 4, 5, \text{ and } 6$ ) is reported. This analysis, including X-ray structural determination and X-ray photoelectron spectroscopy (XPS) demonstrates that **1** is a dinuclear paddlewheel complex without a formal metal-metal bond. The formation of **1** is proposed to occur through a sequential oxidation/aryl transfer mechanism in which complex **2** is oxidized by Cu(II) to yield **3** and Cu(I). Aryl transfer to **3** from  $\text{NaBPh}_4$  provides **3-Ph** that can undergo a second oxidation by Cu(II) and aryl transfer to give **1**. The process is catalyzed by copper salts as

---

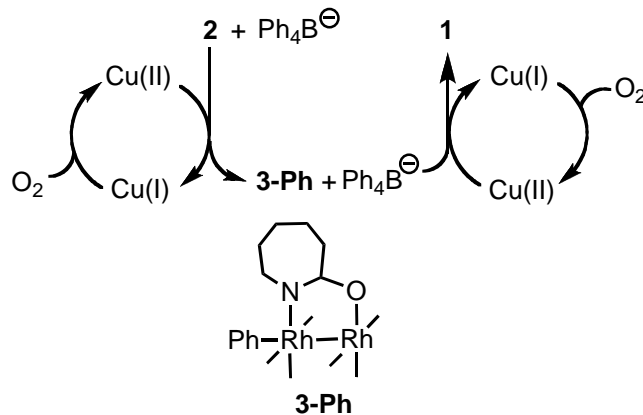
<sup>1</sup>This work was published in the Journal of the American Chemical Society. Nichols, J. M.; Wolf, J.; Zavalij, P.; Varughese, B.; Doyle, M. P. *J. Am. Chem. Soc.* **2007**, 129, 3504.

molecular oxygen regenerates Cu(II) from Cu(I). Data is presented to support the Cu(I)/Cu(II) oxidative cycle (Scheme 1-2).

**Scheme 1-1.** Synthesis of **1**, (Abbreviations: OTf = trifluoromethanesulfonate,  $\text{SO}_3\text{CF}_3$ , rt = room temperature).



**Scheme 1-2.** Proposed catalytic cycle for the formation of **1**.



## II. Introduction-Bonding in Dinuclear Metal Complexes

This chapter explores the first synthetic attempts in our labs to access stable dirhodium(III) *tetrakis*- $\mu$ -carboxamidates of the form  $M_2^{6+}$  where  $M = Rh$  and their physical characterization. Despite the preparation of a wide variety of  $M_2^{6+}$  complexes, structurally well-defined  $Rh_2^{6+}$  complexes have remained an elusive target.<sup>2</sup> As such, there exists little structural information on compounds with a  $Rh_2^{6+}$  core.

Understanding the structure and bonding in organometallic complexes is essential for understanding their applications and developing new technologies. The preparation and electronic structure of dinuclear metal complexes with a metal-metal (M-M) bond have been areas of interest since the 1967 discovery of the rhenium quadruple bond in  $K_2[Re_2Cl_8]$ .<sup>3</sup> In the last four decades, the number of isolated and characterized dinuclear metal complexes has risen to well over two thousand compounds.<sup>4</sup> These compounds have had a large impact on organometallic chemistry with applications in such areas as catalysis, materials,<sup>5</sup> molecular electronics,<sup>6</sup> and supramolecular assembly.<sup>7</sup>

---

<sup>2</sup> Chifotides, H. T.; Dunbar, K. R., *Rhodium compounds*. In *Multiple Bonds between Metal Atoms*, 3rd ed.; Cotton, Murillo and Walton, Eds. Springer Science and Business Media, Inc.: New York, **2005**, 465-589.

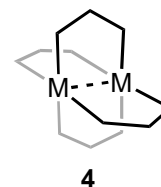
<sup>3</sup> a) Cotton, F. A.; Robinson, W. R.; Walton, R. A. *Inorg. Chem.* **1967**, *6*, 223, b) Cotton, F. A.; Harris, C. B. *Inorg. Chem.* **1967**, *6*, 924, c) Bennett, M. J.; Cotton, F. A.; Foxman, B. M.; Stokely, P. F. *J. Am. Chem. Soc.* **1967**, *89*, 2759.

<sup>4</sup> Based on a recent search of the Cambridge Crystallographic Database, as well as the compounds contained in: Cotton, F. A.; Murillo, C. A.; Walton, R. A.; Editors, *Multiple Bonds Between Metal Atoms*. 3rd ed.; Springer Science and Business Media, Inc.: New York, **2005**.

<sup>5</sup> a) Lo Schiavo, S.; Bruno, G.; Zanello, P.; Laschi, F.; Piraino, P. *Inorg. Chem.* **1997**, *36*, 1004, b) Prater, M. E.; Pence, L. E.; Clerac, R.; Finnis, G. M.; Campana, C.; Auban-Senzier, P.; Jerome, D.; Canadell, E.; Dunbar, K. R. *J. Am. Chem. Soc.* **1999**, *121*, 8005, c) Lo Schiavo, S.; Serroni, S.; Puntoriero, F.; Tresoldi, G.; Piraino, P. *Eur. J. Inorg. Chem.* **2002**, *79*, d) Chen, W.-Z.; Fanwick, P. E.; Ren, T. *Inorg. Chem.* **2007**, *46*, 3429.

<sup>6</sup> a) Ren, T. *Organometallics* **2005**, *24*, 4854, b) Ying, J.; Cordova, A.; Ren, T. Y.; Xu, G.; Ren, T. *Chem. Eur. J.* **2007**, *13*, 6874, c) Cotton, F. A.; Liu, C. Y.; Murillo, C. A.; Zhao, Q.

This overview will briefly discuss the general theories of bonding in dinuclear metal complexes with the generic chemical formula  $M_2L_4$  where M is a transition metal, and L is a  $\mu$ -bridging ligand in the so-called “lantern” or “paddlewheel” geometry (4). The ligand most often is in the form of an  $sp^2$   $X=C-Y$  donor. Examples include carboxylates ( $RCO_2$ ,  $[O=C-O]$ ), carboxamidates ( $RCONR'$ ,  $[O=C-N]$ ), amidinates ( $RC(NR')_2$ ,  $[N=C-N]$ ). The bonding will be developed from a valence-bond model to a molecular orbital (MO) model. Two illustrative examples of the bonding concepts will be provided from the literature. The discussion will then focus on the structure and bonding in dirhodium complexes with an emphasis on the dirhodium carboxamidates.



**Nomenclature.** Figure 1-1 shows a generalized naming convention for expressing the redox state of a dinuclear metal complex that is used throughout the entirety of this document to make molecular descriptions redox specific. Each of the dinuclear metal complexes with general formula  $M_2L_4$  contains two metals of oxidation state  $x$  and  $y$  and the abbreviation  $M_2^{n+}$  where  $n = x + y$  will be used to describe the oxidation state for such complexes. The identification of redox state in Figure 1-1a appears often in the literature and helps resolve ambiguities in determining the absolute oxidation state between two metals in a M-M bond. Bonding interactions between two metals with identical, or near identical nuclei, result in a valence-averaged oxidation state.<sup>8</sup> For example, the Stock notation for a mixed-valent

---

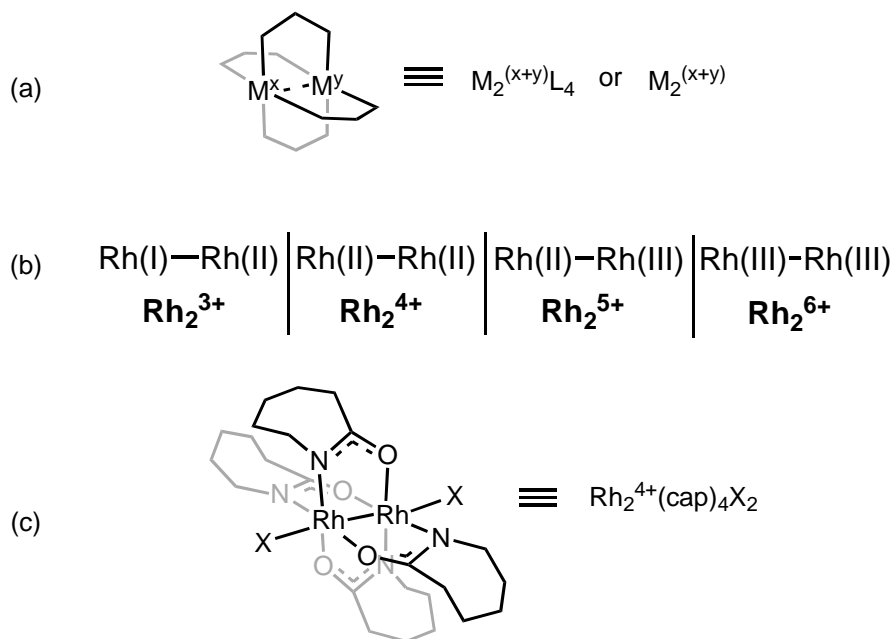
*Inorg. Chem.* **2007**, *46*, 2604, d) Cotton, F. A.; Li, Z.; Liu, C. Y.; Murillo, C. A. *Inorg. Chem.* **2007**, *46*, 7840.

<sup>7</sup> For reviews on large arrays derived from repeating axial  $M_2-L$  subunits, see: a) Cotton, F. A.; Lin, C.; Murillo, C. A. *Acc. Chem. Res.* **2001**, *34*, 759, b) Cotton, F. A.; Lin, C.; Murillo, C. A. *Proc. Natl. Acad. Sci.* **2002**, *99*, 4810, For recent expansions of this supramolecular  $M_2L_4$  chemistry, see: c) Angaridis, P.; Cotton, F. A.; Murillo, C. A.; Villagran, D.; Wang, X. *Inorg. Chem.* **2004**, *43*, 8290, d) Cotton, F. A.; Liu, C. Y.; Murillo, C. A. *Inorg. Chem.* **2004**, *43*, 2267, e) Cotton, F. A.; Murillo, C. A.; Yu, R. *Inorg. Chem.* **2005**, *44*, 8211, f) Cotton, F. A.; Li, Z.; Murillo, C. A. *Eur. J. Inorg. Chem.* **2007**, 3509.

<sup>8</sup> Ref. 4.

M(II)-M(III) system is misleading as the oxidation state of each metal is actually best described as the valence-averaged  $M^{2.5}$  (Figure 1-1b). This occurs as the odd  $d$ -electron occupies a M-M bonding/anti-bonding MO that has contributions from both metal centers. Thus, the abbreviation  $M_2^{n+}$  will be used to both reflect the valence-averaging phenomenon and simplify the discussion of oxidation states in dinuclear metal complexes.

**Figure 1-1.** Redox specific nomenclature.



The  $M_2^{n+}$  abbreviation will be used in one of two ways. When referring to a general class of complexes with a transition metal (M),  $M_2^{n+}$  will be used without a ligand identifier. For example, up to four oxidation states have been observed for the general class of dirhodium complexes,  $Rh_2^{3+}$  to  $Rh_2^{6+}$  (Figure 1-1b).<sup>9</sup> When referring a specific subclass of complexes, a ligand identifier will be appended i.e.  $M_2^{n+}L_4$ . An example would be the basic structure of *tetrakis*-( $\mu$ -caprolactamato)-dirhodium(II) with a generic axial ligand (X). The redox specific abbreviation for this complex will be  $[Rh_2^{4+}(cap)_4X_2]$  (Figure 1-1c).

<sup>9</sup> See Ref. 2.

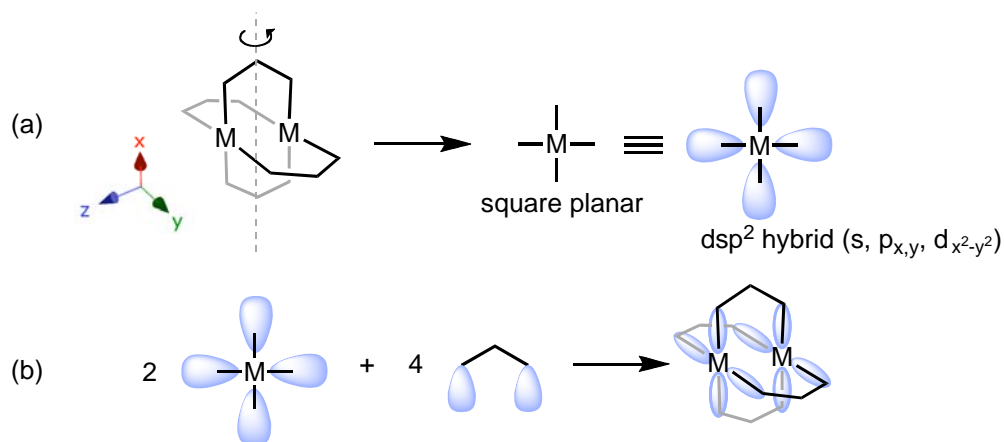
**Metal-Metal Bonding.** The extent of bonding between two metals in a dinuclear paddlewheel complex is highly dependent on the identity of the metal and the number of electrons in its outer d-shell. However, a general molecular orbital (MO) description can be formulated for the M-M bonding interactions in all such complexes using valence-bond theory and simple linear combinations of atomic orbitals (LCAO). More sophisticated treatments of the MOs in the  $M_2L_4$  complexes are available;<sup>10</sup> however, this simple description encompasses much of the M-M and M-L bonding interactions. A description of M-M bonding follows in which models for tetravalent ( $M_2^{4+}$ ) and hexavalent ( $M_2^{6+}$ ) will be described.

Rotating the generic  $M_2L_4$  structure (**4**) such that the two metals are eclipsed along the z-axis shows a simplified projection of **4** with a square planar geometry about M (Figure 1-2a). Ignoring the potential M-M bond, the square-planar geometry of M is the minimum requirement for bonding in complex **4** and can be expressed as a metal centered  $dsp^2$  hybrid atomic orbital (AO). Based on the coordinate system, the  $dsp^2$  hybrid orbital is made up of the s,  $p_{x,y}$ , and  $d_{x^2-y^2}$  AOs. The basic structure of **4** results as a combination of two empty  $dsp^2$  AOs and 4  $sp^2$  orbitals of a  $\mu$ -bridging X=C-Y donor ligand (Figure 1-2b). This combination leaves four d-orbitals and one p-orbital on each of the metal atoms that can combine in M-M or M-L bonding/anti-bonding interactions.

---

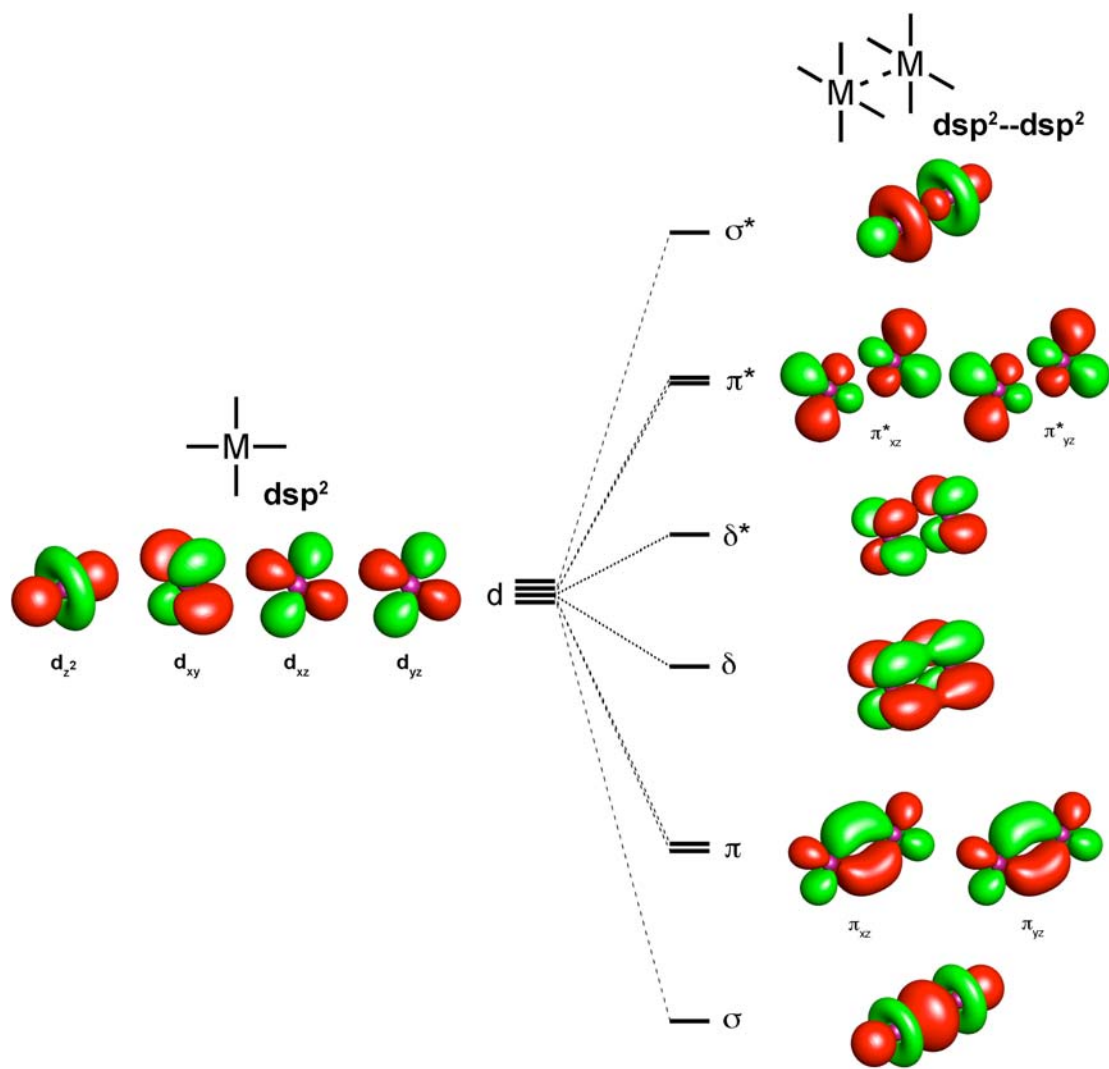
<sup>10</sup> Cotton, F. A., *Physical, spectroscopic and theoretical results on multiple bonds between metal atoms*. In *Multiple Bonds between Metal Atoms*, 3rd ed.; Springer Science and Business Media, Inc.: New York, **2005**, 707-796.

**Figure 1-2.** General structure of  $M_2L_4$  paddlewheel complexes.



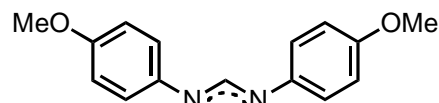
Based on the coordinate system shown in Figure 1-2a, the remaining  $d$ -orbitals are the  $d_{z^2}$ ,  $d_{xz}$ ,  $d_{yz}$ , and  $d_{xy}$  orbitals (Figure 1-3). These orbitals combine to form the M-M bonding/anti-bonding interactions in the complexes. The  $d_{z^2}$  bonding and anti-bonding combination yields the  $\sigma$  and  $\sigma^*$  MOs. The bonding and anti-bonding combinations of  $d_{xz}$  and  $d_{yz}$  yield orthogonal  $\pi$  and  $\pi^*$  MOs and  $d_{xy}$  gives the  $\delta$  and  $\delta^*$  MOs. Arranging the MOs in order of their relative bond stabilities,  $\sigma > \pi > \delta$ , gives the MO diagram in Figure 1-3. This is the general MO diagram for dinuclear metal paddlewheel complexes and determining the extent of bonding between two metals is matter of filling the diagram with the total number of  $d$ -electrons in the M-M core. In this model, the remaining  $p_z$  AO on each metal is the empty orbital primarily responsible for the axial M-L interactions.

**Figure 1-3.** AOs combine to give metal-metal bonding/anti-bonding interactions.



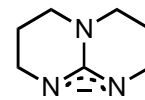


**M<sub>2</sub>L<sub>4</sub> complexes with no M-M bond.** Many complexes with a M-M bond have been prepared including those with M = Mo, Tc, W, Re, Os, Ir, Pt, Nb, Ru, and Rh.<sup>11</sup> Far less common are dinuclear paddlewheel complexes that do not have a M-M bond. These compounds are held together only by the bridging ligand interaction and often violate the 18-electron rule. Two such complexes are the dipalladium(II) complex Pd<sub>2</sub><sup>4+</sup>(DAniF)<sub>4</sub> (**5**) with a N=C-N bridging ligand,<sup>12</sup> and the dititanium(III) complex, Ti<sub>2</sub><sup>6+</sup>[μ<sup>2</sup>-O<sub>2</sub>CN(*t*-Bu)Ph]<sub>4</sub>(σ-N(*t*-Bu)Ph)<sub>2</sub> (**6**) with an O=C-O bridging ligand.<sup>13</sup> The following is a discussion of the M-M bonding within these complexes and how they fit, or do not fit, within the valence-bond model.



**DAniF** = N,N'-di-anisidine formamidinate

The Pd<sub>2</sub><sup>4+</sup> complex **5** (Figure 1-4), prepared by Berry and Wang, and co-workers, is the archetypal example of a M-M complex that does not have a M-M bond. The structure of **5** is shown in Figure 1-4. As a d<sup>8</sup>-d<sup>8</sup> complex, **5** has 16 *d*-electrons. Based on the MO diagram in Figure 1-3, this gives the complex an electronic configuration of σ<sup>2</sup>π<sup>4</sup>δ<sup>2</sup>δ\*<sup>2</sup>π\*<sup>4</sup>σ\*<sup>2</sup> and a formal bond order of zero. The lack of a Pd-Pd bond was observed in the long Pd-Pd bond length of 2.649 Å. The bond length in **5** is a 0.258 Å attenuation compared to the bond length in a related Pd<sub>2</sub><sup>6+</sup> complex (2.391 Å) with a N=C-N bridging ligand Pd<sub>2</sub>(hpp)<sub>4</sub>Cl<sub>2</sub> in which a Pd-Pd single bond is proposed.<sup>14</sup> SCF-Xα-SW calculations on analogues of **5** with aryl rings removed yielded an MO



**hpp** = 1,3,4,6,7,8-hexahydro-1H-pyrimido-[1,2-a]pyrimidinate

<sup>11</sup> See ref. 8.

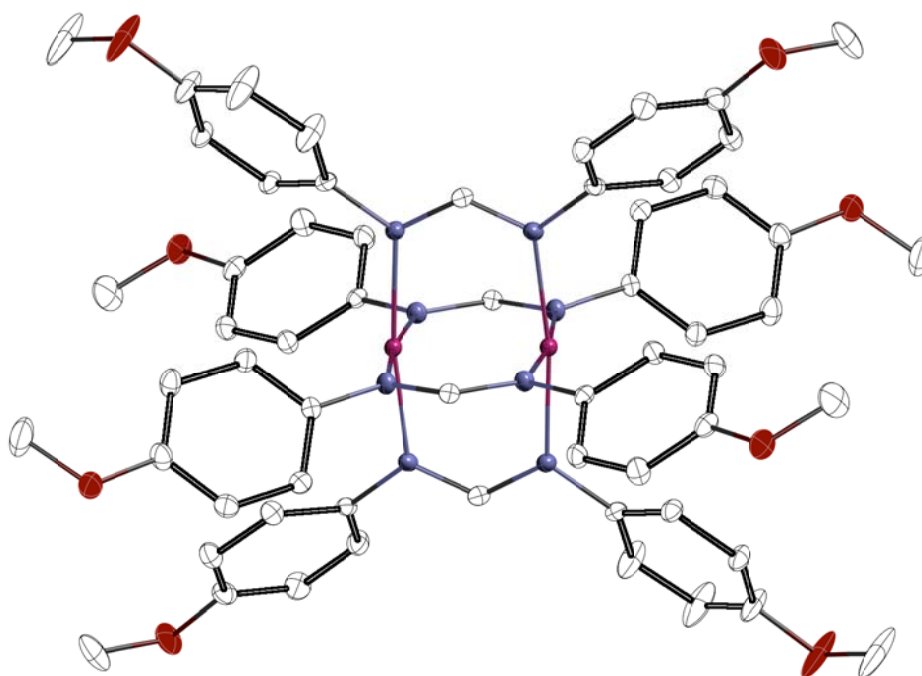
<sup>12</sup> Berry, J. F.; Cotton, F. A.; Ibragimov, S. A.; Murillo, C. A.; Wang, X. *Inorg. Chem.* **2005**, *44*, 6129.

<sup>13</sup> Mendiratta, A.; Cummins, C. C.; Cotton, F. A.; Ibragimov, S. A.; Murillo, C. A.; Villagran, D. *Inorg. Chem.* **2006**, *45*, 4328.

<sup>14</sup> a) Cotton, F. A.; Gu, J.; Murillo, C. A.; Timmons, D. J. *J. Am. Chem. Soc.* **1998**, *120*, 13280, b) Cotton, F. A.; Koshevoy, I. O.; Lahuerta, P.; Murillo, C. A.; Sanau, M.; Ubeda, M. A.; Zhao, Q. *J. Am. Chem. Soc.* **2006**, *128*, 13674.

description much like the model in Figure 1-3. The calculations confirmed the electronic configuration and the absence of a formal Pd-Pd bonding interaction.<sup>15</sup>

**Figure 1-4.** ORTEP drawing of Pd<sub>2</sub><sup>4+</sup>(DAniF)<sub>4</sub> (**5**) with thermal ellipsoids drawn at 30% probability. Hydrogen atoms have been omitted for clarity (Abbreviations: ORTEP = Oak Ridge Thermal Ellipsoid Program; Color Code: Pd = purple, O = red, N = blue, C = white).



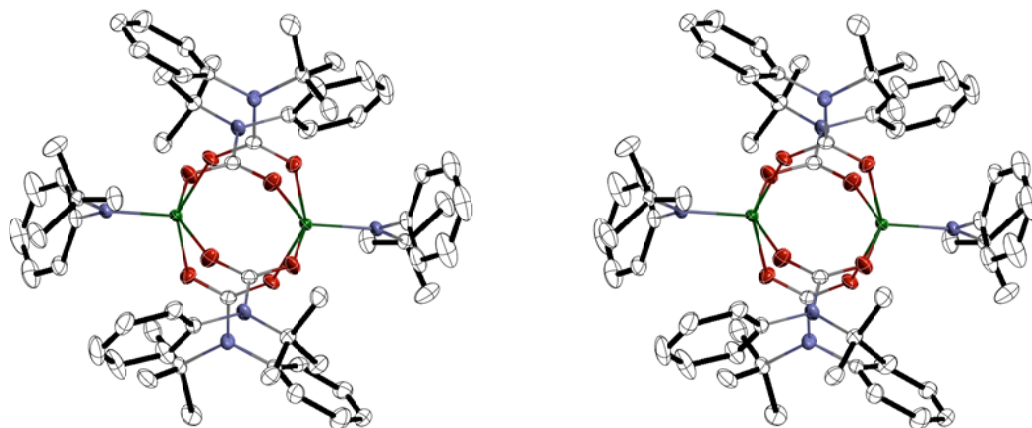
The dititanium(III) complex **6** (Figure 1-6) prepared by Cotton, Villagran, and co-workers, does not fall within the archetypical dinuclear metal complex described in Figure 1-2. The structure of **6** is shown in Figure 1-5.

---

<sup>15</sup>Cotton, F. A.; Matusz, M.; Poli, R.; Feng, X. *J. Am. Chem. Soc.* **1988**, *110*, 1144.

The  $d^1$ - $d^1$  complex has two  $d$ -electrons should produce a complex with a metal-metal bond and an electronic configuration of  $\sigma^2$  based on the model in Figure 1-3. This is not the case for **6** as the complex has an extremely long internuclear Ti-Ti distance of 3.515 Å and 3.421 Å for each of the two crystallographically independent structures. The extremely long Ti-Ti distance prevents Ti-Ti bonding interactions. The pyramidalization of the metal-ligand plane about each Ti-center ( $\text{Ti-Ti-O}_{\text{av}} = 71.3^\circ$ ) also suggests the lack of a Ti-Ti bond. In the absence of the rigid structure imposed by the paddlewheel ligand arrangement,  $\text{Ti}_2^{6+}$  complexes do form the expected M-M bonds. These complexes have  $\mu$ -alkoxo bridging ligands that do not allow the titanium centers to have a long a bond distance.<sup>16</sup> It is an interaction specific to the paddlewheel geometry that causes the cleavage of the Ti-Ti bond.

**Figure 1-5.** ORTEP stereoscopic view of one of two crystallographically independent molecules of **6**• $\text{Et}_2\text{O}$  with thermal ellipsoids drawn at 30% probability. Hydrogen atoms and solvent have been omitted for clarity (Ti = green, O = red, N = blue, C = blank).

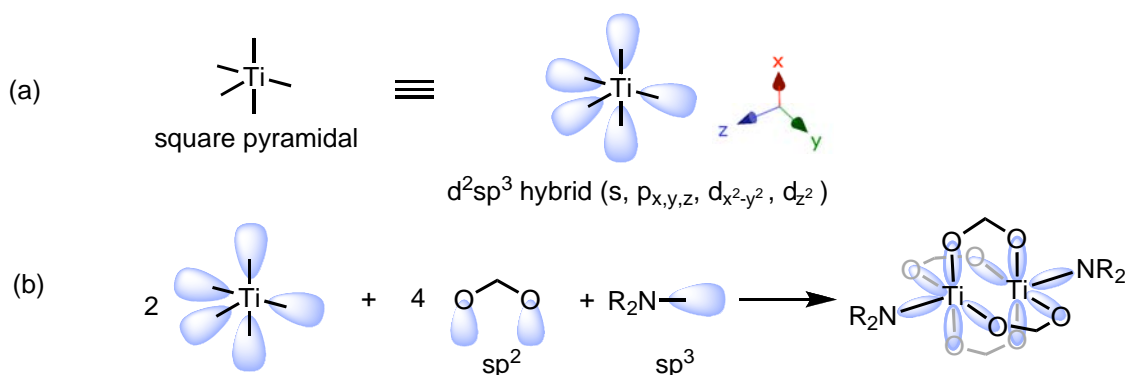


---

<sup>16</sup> Jerzykiewicz, L.; Mierzwicki, K.; Latajka, Z.; Sobota, P. *Inorg. Chem.* **2003**, *42*, 267.

The tri-valent nature of the  $Ti_2^{6+}$  core requires an alternate valence bond model than the model described in Figure 1-2. A bonding model for the titanium complex is shown in Figure 1-6. If the axial Ti-N bond is assumed to be covalent in nature, a distorted square pyramidal geometry is the minimum geometry required to satisfy all of the covalent M-L bonding in **6**. The distorted square pyramidal AO is a  $d^2sp^3$  hybrid consisting of the Ti 4s,  $4p_{x,y,z}$ ,  $3d_{x^2-y^2}$ , and  $3d_{z^2}$  AOs (Figure 1-6). The complex is then composed of the bonding interactions between the  $\mu$ -bridging ligand  $sp^2$  AOs, the axial amide  $sp^3$  AOs and the two titanium  $d^2sp^3$  AOs. The remaining three  $d$ -orbitals of the  $Ti_2$ -core make up the AOs responsible for any Ti-Ti bonding interaction.

**Figure 1-6.** Rehybridization in  $Ti_2^{6+}$  complex (**6**).



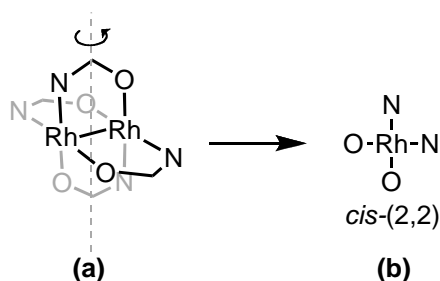
The incorporation of  $p_z$  and  $d_{z^2}$  into the  $d^2sp^3$  hybridization of titanium diminishes the  $\sigma$ -bonding and anti-bonding interactions in Figure 1-3. This reduces the available M-M bonding/anti-bonding to 6 MOs consisting of two  $\pi$  and two  $\pi^*$  MOs, as well as one  $\delta$  and one  $\delta^*$  MO. In this model, the electronic configuration of the  $Ti_2^{6+}$  complex **6** would be  $\pi^2$  with electrons in two degenerate  $\pi$ -bonding orbitals. Without the ability to make a strong M-M  $\sigma$ -bond, and without additional  $d$ -electrons to entirely fill the degenerate  $\pi$ -system, only a weak  $\pi$ -bonding interaction would exist in the  $Ti_2^{6+}$  core. Density functional (DFT) calculations performed by Cotton and co-workers show that, rather than maintain a M-M bond, M-M bonding is foregone in favor of stronger M-L interactions. The calculations show that the  $d$ -electrons

are localized in the  $d_{xy}$  AOs on each of the Ti(III) atoms and that these AOs are mixed with the  $\pi$ -system of the  $\mu$ -bridging ligand. Interestingly, the M- $\pi$  interaction leads to very strong, antiferromagnetic coupling causing the paramagnetic Ti(III) centers to be spin-paired and yielding a diamagnetic complex. The  $Ti_2^{6+}$  complex (**6**) is an example of a dinuclear metal complex that does not conform to the bonding model in Figure 1-3.

**Bonding in dirhodium carboxamidates.** The bonding in  $Rh_2^{n+}$  complexes can be discussed within the context of the description in Figure 1-3. The basic  $Rh_2^{4+}$  complex is a  $d^7$ - $d^7$  dimer with a total of 14  $d$ -electrons. Placing the electrons into the MO diagram gives an electronic configuration of  $\sigma^2\pi^4\delta^2\delta^*\pi^4$  for  $Rh_2^{4+}$  and an overall Rh-Rh single bond. Removal of an electron from the system yields  $Rh_2^{5+}$  with a formal Rh-Rh bond order of 1.5 and removal of an additional electron yields  $Rh_2^{6+}$  with a formal Rh-Rh double bond.

The dirhodium(II) carboxamidates are dinuclear paddlewheel complexes that consist of a Rh-Rh metal core surrounded by four  $\mu$ -(N=C-O) bridging ligands in the paddlewheel arrangement. The general paddlewheel structure is shown in Figure 1-7a. Rotating the structure such that the Rh-atoms are eclipsed shows the heteratom arrangement around the face of the complex (Figure 1-7a). In most carboxamidates, the two nitrogen atoms and two oxygen atoms are bound to each rhodium in a *cis*-(2,2) orientation (Figure 1-7b). Although the valence-bond approach provides an adequate phenomenological description of bonding in  $M_2L_4$  complexes, there are metal-metal and metal-ligand interactions that require a more sophisticated treatment. The interactions between the  $\mu$ -bridging amide ligand and the Rh-Rh core in dirhodium carboxamidates fall into this category.

**Figure 1-7.** General structure and ligand arrangement of dirhodium carboxamidates.



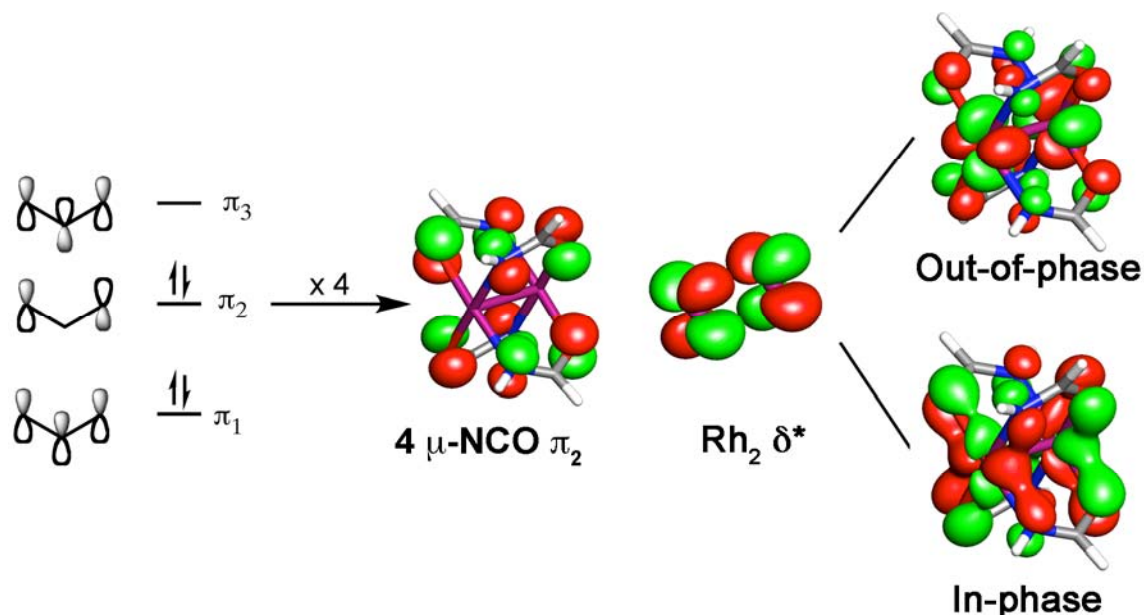
The general  $M_2^{4+}$  MO configuration is maintained for the dirhodium(II) carboxylates with  $\mu$ -(O=C-O) bridging ligands ( $\sigma^2\pi^4\delta^2\delta^*\pi^4$ ).<sup>17</sup> However, for the carboxamidates, metal-ligand interactions cause a reorganization of the  $\pi^*$  and  $\delta^*$  MOs. This was demonstrated by Bear and co-workers in a thorough set of experiments with a series of complexes with the general formula  $Rh_2(OAc)_m(acam)_n$  (acam = acetamidate).<sup>18</sup> These experiments showed that as the number of acam ligands were increased, the highest occupied molecular orbital (HOMO) changed from  $\pi^*$  to  $\delta^*$ . This inversion has been observed computationally<sup>19</sup> and can be understood as an interaction between the  $\pi$ -orbitals of the donor ligands and the  $\delta^*$  orbital of the Rh-Rh core (Figure 1-8). The combination of the four non-bonding  $\pi$ -orbitals ( $\pi^2$ ) of the  $\mu$ -bridging carboxamidate ligands yields the ligand MO shown in Figure 1-8. In-phase mixing between the this MO and  $\delta^*(Rh-Rh)$  leads to M-L bonding interactions and the out-of-phase mixing raises the energy of the  $\delta^*(Rh-Rh)$  MO above that of the  $\pi^*(Rh-Rh)$  MOs. Thus, the electronic configuration for the dirhodium(II) carboxamidates is more properly assigned as  $\sigma^2\pi^4\delta^2\pi^*\delta^*$ .

<sup>17</sup> Cotton, F. A.; Hillard, E. A.; Murillo, C. A. *J. Am. Chem. Soc.* **2002**, *124*, 5658.

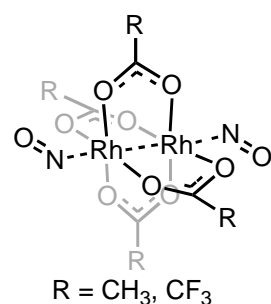
<sup>18</sup> Chavan, M. Y.; Zhu, T. P.; Lin, X. Q.; Ahsan, M. Q.; Bear, J. L.; Kadish, K. M. *Inorg. Chem.* **1984**, *23*, 4538.

<sup>19</sup> Aguirre, J. D.; Lutterman, D. A.; Angeles-Boza, A. M.; al., e. *Inorg. Chem.* **2007**, *46*, 7494.

**Figure 1-8.** M-L interactions that destabilize the  $\delta^*$ -MO.



Detailed structural analyses have been made for both  $\text{Rh}_2^{4+}$  and  $\text{Rh}_2^{5+}$  structures,<sup>20</sup> however, only the electronic absorption spectrum of a  $\text{Rh}_2^{6+}$  complex has been reported.<sup>21</sup> It has been pointed out that the bent dinitrosyl



complexes of dirhodium(II) tetracarboxylates reported by Lippard and co-workers<sup>22</sup> could be formally  $\text{Rh}_2^{6+}$  complexes with longer Rh-Rh bond lengths than the parent compounds, as with **1** (*vide supra*). The authors, however, do not make this claim, and an unambiguous electronic assignment was not made. No spectroscopic data was reported to indicate a change in the Rh-Rh bonding for the complexes. Moreover, these complexes are reversible nitric oxide (NO) rather than nitroxyl donors ( $\text{NO}^-$ ) further complicating the M-M and M-L bonding description for a potential *bis*-nitroxyl  $\text{Rh}_2^{6+}$  complex. Although the

<sup>20</sup> See ref. 2.

<sup>21</sup> Kadish, K. M.; Phan, T. D.; Giribabu, L.; Van Caemelbecke, E.; Bear, J. L. *Inorg. Chem.* **2003**, *42*, 8663.

<sup>22</sup> Hilderbrand, S. A.; Lim, M. H.; Lippard, S. J. *J. Am. Chem. Soc.* **2004**, *126*, 4972.

Rh-Rh bond attenuation is intriguing and may indicate that a change occurs within the dirhodium core upon binding of nitric oxide, it remains to be seen whether this is the case.

### III. Results and Discussion<sup>23</sup>

**Synthesis.** The investigation began with the preparation of *bis*-( $\sigma$ -phenyl)-*tetrakis*-( $\mu$ -caprolactamato)-dirhodium(III) (**1**). The development of this protocol will be discussed within the context of the mechanism of aryl transfer in the following sections. The aerobic oxidation of  $\text{Rh}_2(\text{cap})_4$  with  $\text{CuOTf}$  (10 mol %) in the presence of  $\text{NaBPh}_4$  (5 equiv.) provided **1** as a green solid in 77% yield after chromatographic purification (Scheme 1). The structure of **1** was first indicated by signals corresponding to two equivalent phenyl ligands in addition to the caprolactamato ligands observed in both the  $^1\text{H}$  and  $^{13}\text{C}$  NMR spectra. Aryl ring vibrations at  $1550\text{ cm}^{-1}$ , and the parent ion corresponding to **1** ( $\text{M}+\text{H}$ ) by high-resolution mass spectroscopy (ESI) provided further evidence for the incorporation of the aryl ring into the complex. The visible spectrum of **1** with  $\lambda_{\text{max}}$  ( $\epsilon$ ,  $\text{M}^{-1}\text{cm}^{-1}$ ) at 430 (4540) nm was consistent with previous reports of electrochemically generated  $\text{Rh}_2^{6+}$  complexes that were not isolated.<sup>24</sup> A mass magnetic susceptibility ( $\chi_{\text{g}}$ ,  $\text{m}^3\text{ kg}^{-1}$ ) of  $2.9 \times 10^{-10}$  was measured for the complex indicated that **1** was diamagnetic. X-ray diffraction (XRD) of a single crystal grown in  $\text{CH}_2\text{Cl}_2$  confirmed that **1** was indeed  $[\text{Rh}_2(\text{cap})_4(\text{C}_6\text{H}_5)_2]$  (Figure 1-9).

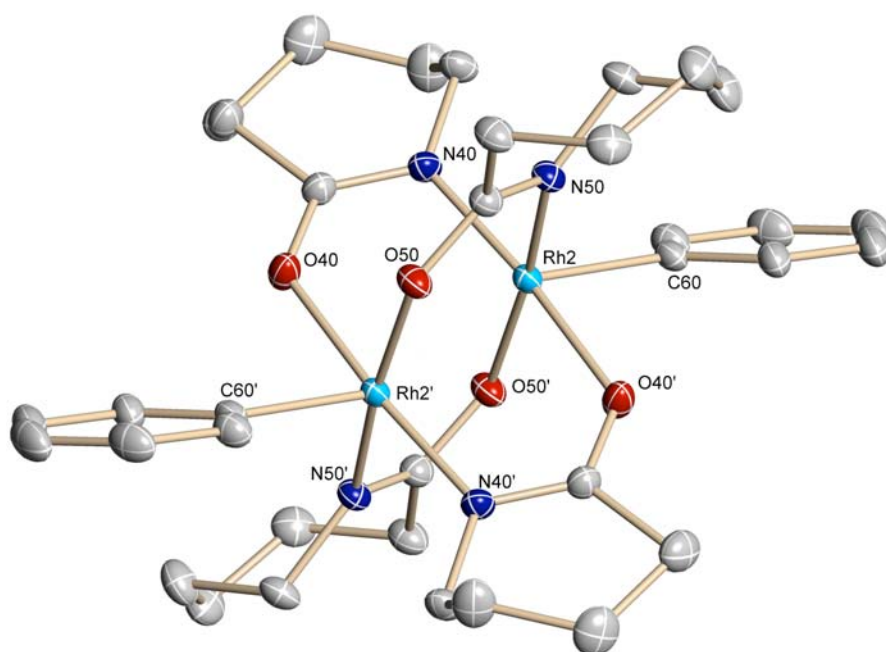
---

<sup>23</sup> This work was done in collaboration with Joffrey Wolf, Center for Coordination Chemistry, Toulouse, France.

<sup>24</sup> Kadish, K. M.; Phan, T. D.; Giribabu, L.; Van Caemelbecke, E.; Bear, J. L. *Inorg. Chem.* **2003**, *42*, 8663.



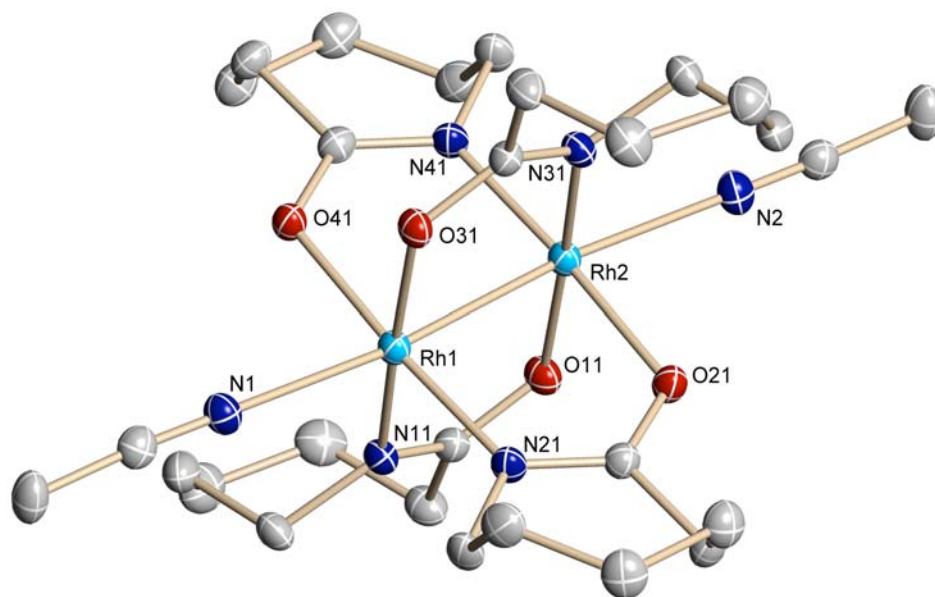
**Figure 1-9.** ORTEP drawing of one of two crystallographically independent molecules of  $[\text{Rh}_2(\text{cap})_4(\text{C}_6\text{H}_5)_2] \cdot 2\text{CH}_2\text{Cl}_2$ ,  $\text{C}_{38}\text{H}_{52}\text{N}_4\text{O}_4\text{Cl}_2\text{Rh}_2$ ,  $R_1 = 3.00\%$ . Selected bond lengths (Å) and angles (°): Rh2-Rh2' (2.519); Rh2-C60 (2.000), Rh2'-O40 (2.085); Rh2'-O50 (2.083); Rh2-N40 (2.011); Rh2-N50 (2.014); Rh2-Rh2'-C60' (155.4); Rh2'-Rh2-N40 (96.4); Rh2'-Rh2-N50 (94.0); Rh2-Rh2'-O40 (77.4); Rh2-Rh2'-O50 (79.8). CCDC #615577. Ellipsoids are shown at a 30% probability level. Solvent and hydrogen atoms are omitted for clarity.



To make structural comparisons, additional complexes were prepared as representative examples of  $\text{Rh}_2^{5+}(\text{cap})_4$  and  $\text{Rh}^{4+}(\text{cap})_4$ .  $[\text{Rh}_2(\text{cap})_4 \cdot 2\text{CH}_3\text{CN}]$  (**2**) was prepared by ligand exchange with  $\epsilon$ -caprolactam and  $\text{Rh}_2(\text{OAc})_4$  according to a published procedure.<sup>25</sup> Recrystallization of **2** from  $\text{CH}_3\text{CN}:\text{MeOH}$  (10:1) at  $-20\text{ }^\circ\text{C}$  provided deep purple crystals that were analytically pure and suitable for XRD structure determination (Figure 1-10).

<sup>25</sup> Doyle, M. P.; Westrum, L. J.; Wolthuis, W. N. E.; See, M. M.; Boone, W. P.; Bagheri, V.; Pearson, M. M. *J. Am. Chem. Soc.* **1993**, *115*, 958.

**Figure 1-10.** ORTEP drawing of  $[\text{Rh}_2(\text{cap})_4(\text{CH}_3\text{CN})_2] \cdot 2\text{CH}_3\text{CN}$ ,  $\text{C}_{32}\text{H}_{52}\text{N}_8\text{O}_4\text{Rh}_2$ ,  $R_1 = 4.29\%$ . Selected bondlengths (Å) and angles (°): Rh1-Rh2 (2.422); Rh1-N1 (2.336), Rh2-O11 (2.050); Rh1-N11 (2.038); Rh2-Rh1-N1 (174.4); Rh2-Rh1-N11 (86.7); Rh1-Rh2-O11 (89.6); Rh2-Rh1-N21 (86.9); Rh1-Rh2-O21 (89.3). CCDC #615575. Ellipsoids are shown at a 30% probability level. Non-coordinating solvent molecules and hydrogen atoms are omitted for clarity.

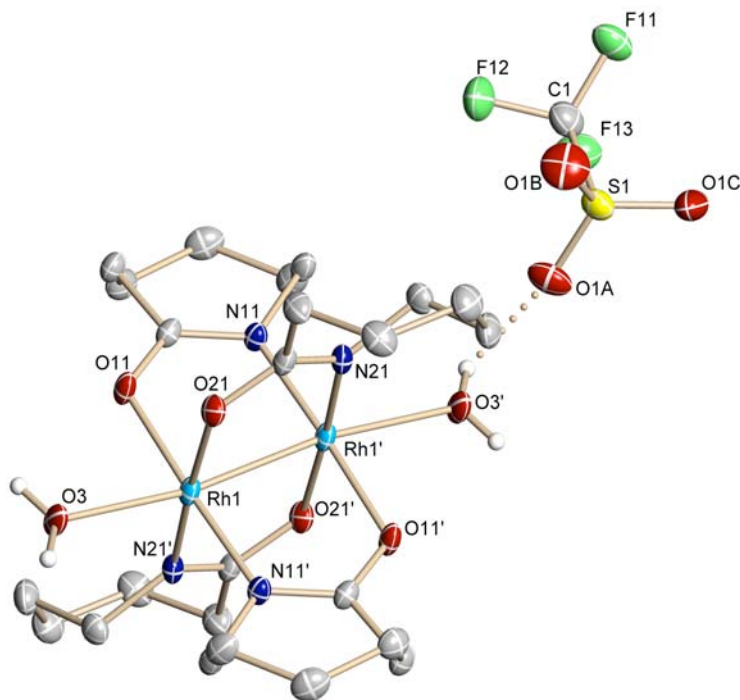


The final complex prepared for this study was  $[\text{Rh}_2(\text{cap})_4(\text{H}_2\text{O})_2]\text{OTf}$  (**3**) as an intermediate  $\text{Rh}_2^{5+}$  structure. When  $\text{Rh}_2(\text{cap})_4$  (**2**) was treated with stoichiometric amount of  $\text{Cu}(\text{OTf})_2$  in wet ethyl acetate, the solution turned from blue to deep burgundy. After 1 h, the reaction was stopped and the solvent removed (Scheme 1-3).<sup>26</sup> Recrystallization by slow diffusion of ether into dichloromethane provided pure **3** and XRD quality crystals. The visible spectrum of **3** in  $\text{CH}_2\text{Cl}_2$  was typical of  $\text{Rh}_2^{5+}$  structures with  $\lambda_{\text{max}}$  ( $\epsilon \text{ M}^{-1}\text{cm}^{-1}$ ) at

<sup>26</sup> The redox potential of the  $\text{Cu}^{\text{II}}\text{-Cu}^{\text{I}}$  couple for  $\text{Cu}(\text{ClO}_4)_2$  (1.2 eV vs SCE in  $\text{CH}_3\text{CN}$ ) suggested its ability to oxidize **2**: Sumalekshmy, S.; Gopidas, K. R. *Chem. Phys. Lett.* **2005**, *413*, 294.

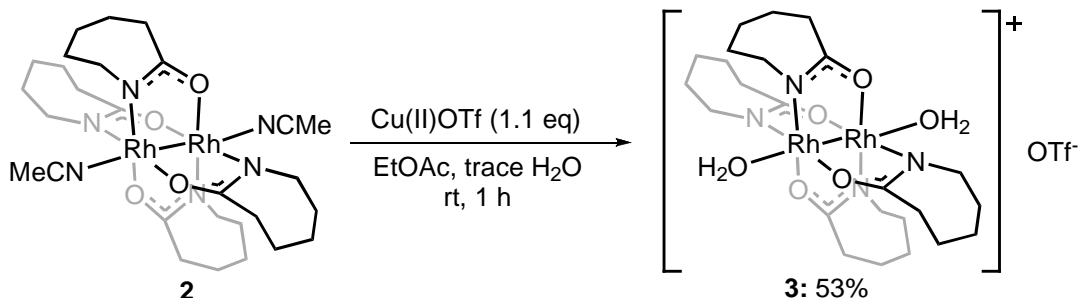
505 (4502) nm and 970 (1086) nm.<sup>27</sup> Complex **2** exhibited severe line broadening in the <sup>1</sup>H NMR consistent with its paramagnetic mixed-valent state. The resolved structure is shown in Figure 1-11. Complex **2** has the typical dirhodium core with axial aquo ligands completing its ligand sphere. Charge balance is provided by an outer sphere triflate ion hydrogen-bonded to one of the axial water ligands.

**Figure 1-11.** ORTEP drawing of **[Rh<sub>2</sub>(cap)<sub>4</sub>(H<sub>2</sub>O)<sub>2</sub>][OTf]**, C<sub>25</sub>H<sub>44</sub>F<sub>3</sub>N<sub>4</sub>O<sub>9</sub>Rh<sub>2</sub>S, R1 = 3.72%. Selected bond lengths (Å) and angles (°): Rh1-Rh1' (2.384); Rh1'-O3 (2.288), Rh1-O11 (2.023); Rh1'-N11 (1.996); Rh1-Rh1'-O3 (171.3); Rh1-Rh1'-N11 (88.4); Rh1'-Rh1-O11 (88.6); Rh1-Rh1'-N21 (88.6); Rh1'-Rh1-O21 (88.5). CCDC #615576. Ellipsoids are shown at a 30% probability level. Hydrogen atoms, except those for water, are omitted for clarity.



<sup>27</sup> Kadish, K. M.; Phan, T. D.; Giribabu, L.; Van Caemelbecke, E.; Bear, J. L. *Inorg. Chem.* **2003**, *42*, 8663.

**Scheme 1-3.** Synthesis of *bis-aquo-tetrakis*( $\mu$ -caprolactamato)-dirhodium(II,III) triflate (**2**), (Abbreviations: OTf = trifluoromethanesulfonate, EtOAc = ethyl acetate).



**Structure and Bonding.** The structural data for each of the three complexes is summarized in Table 1-1 and Table 1-2. Figure 1-12a shows a generalized structure of dirhodium caprolactamate with variable axial ligands (L) and variable Rh-Rh bond order (dashed grey/pink line). Figure 1-12b is a partial view of **1** that shows only the axial phenyl ligand with atom labels. The structures are labeled for the purposes of cross-comparison in Tables 1-1 and 1-2. The atom labels do not correspond to atom labels in the actual XRD structures for the individual complexes.

**Figure 1-12.** (a) General  $\text{Rh}_2^{n+}(\text{cap})\text{L}_2$  structure with atom labels. (b) A partial view of **1** with labels of the phenyl ligand.

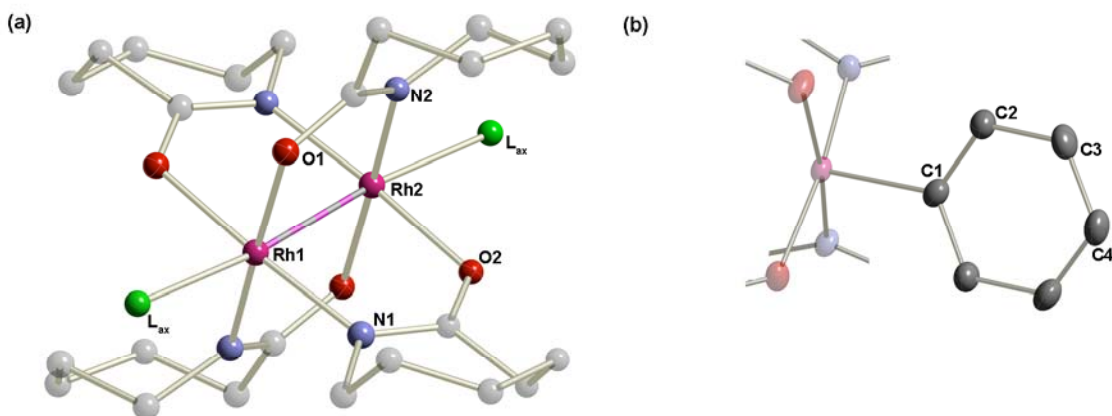


**Table 1-1.** Selected bond lengths for  $[\text{Rh}_2(\text{cap})_4 \cdot 2\text{CH}_3\text{CN}]$  (**2**),  $[\text{Rh}_2(\text{cap})_4(\text{OH}_2)_2]\text{OTf}$  (**3**),  $[\text{Rh}_2(\text{cap})_4(\text{C}_6\text{H}_5)_2]$  (**1**), [NOTE: Values in parentheses are the uncertainty in the last reported digit.].

	Complexes		
	<b>2</b>	<b>3</b>	<b>1</b>
Rh1–Rh2	2.4221(4)	2.3840(6)	2.5188(3)
Rh2–O1	2.050(2)	2.023(2)	2.0825(16)
Rh2–O2	2.053(2)	2.030(2)	2.0777(16)
Rh1–N1	2.038(3)	1.988(3)	2.012(2)
Rh1–N2	2.045(3)	1.996(3)	2.0078(19)
C1–C2	-	-	1.390 (4)
C2–C3	-	-	1.390 (4)
C3–C4	-	-	1.374 (4)
Rh–L <sub>ax</sub>	2.336(3)	2.288(2)	2.010(2)

**Table 1-2.** Selected bond angles for  $[\text{Rh}_2(\text{cap})_4 \cdot 2\text{CH}_3\text{CN}]$  (**2**),  $[\text{Rh}_2(\text{cap})_4(\text{OH}_2)_2]\text{OTf}$  (**3**),  $[\text{Rh}_2(\text{cap})_4(\text{C}_6\text{H}_5)_2]$  (**1**).

	Complexes		
	<b>2</b>	<b>3</b>	<b>1</b>
Rh1–Rh2–N1	89.62(6)	88.58(7)	79.29(4)
Rh1–Rh2–O2	89.37(6)	88.50 (7)	78.39(5)
Rh2–Rh1–N1	86.70(7)	88.42(8)	94.46(5)
Rh2–Rh1–N2	86.81(7)	88.60(8)	95.32(5)
Rh2–N1–C1	118.3(2)	119.8(2)	128.11(15)
Rh2–O2–C2	118.96(19)	119.5(2)	128.97(15)
Rh1–N1–C1	121.5(2)	120.8(2)	114.45(16)
Rh1–N2–C2	121.7(2)	121.2(2)	113.51(15)
Rh1–Rh2–L <sub>axial</sub>	174.42(7)	171.28(7)	156.19(7)
N1 –Rh–Rh–N1*	0.61	0.65	1.42
O2 –Rh–Rh–N2*	1.05	0.73	1.78

\*Torsion angles.

The structure of  $[\text{Rh}_2(\text{cap})_4 \cdot 2\text{CH}_3\text{CN}]$  (**2**) is similar to the structure of most other dirhodium(II) carboxamidates (Figure 1-9).<sup>28</sup> The Rh-Rh bond length is 2.442 Å with average Rh-O<sub>eq</sub> and Rh-N<sub>eq</sub> bond lengths of 2.052 Å and 2.042 Å respectively. The average Rh-N<sub>ax</sub> bond length is 2.336 Å and the Rh-Rh-N<sub>ax</sub> bond angle is 174.4° with little distortion of the Rh-Rh-NCMe vector from linearity. The Rh-Rh-N<sub>eq</sub> and Rh-Rh-O<sub>eq</sub> angles of the complex are 86.83° and 89.37° and maintain an overall octahedral arrangement of ligands about the Rh-Rh core.

The structure of  $[\text{Rh}_2(\text{cap})_4 \cdot \text{H}_2\text{O}]\text{OTf}$  (**3**) is similar to the structure of **2** (Figure 1-11). The average Rh-O<sub>eq</sub> and Rh-N<sub>eq</sub> bond lengths (2.027 Å and 1.992 Å respectively) are shorter than **2** consistent with the increase in oxidation state from Rh<sub>2</sub><sup>4+</sup> to Rh<sub>2</sub><sup>5+</sup>. The average Rh-O<sub>ax</sub> bond length is 2.286 Å and the Rh-Rh-O<sub>ax</sub> bond angle is 171.3° which constitutes a minor distortion of the Rh-Rh-OH<sub>2</sub> vector away from linearity. The Rh-Rh-N<sub>eq</sub> and Rh-Rh-O<sub>eq</sub> angles of the complex are 88.5° which maintain an overall octahedral arrangement of ligands about the Rh-Rh core. The main structural difference between **3** and **2** occurs in the Rh-Rh bond length with a 58 pm reduction of the Rh-Rh bond length to 2.384 Å.

In terms of its general molecular composition, the connectivity of  $[\text{Rh}_2(\text{cap})_4(\text{C}_6\text{H}_5)_2]$  (**1**) does not deviate from that in the general dirhodium(II) carboxamidate paddlewheel structure. Despite the increased oxidation state, the average Rh-O<sub>eq</sub> bond length (2.080 Å) is actually longer than the bond lengths in both the Rh<sub>2</sub><sup>4+</sup> (**2**) and Rh<sub>2</sub><sup>5+</sup> (**3**) complexes. The average Rh-N<sub>eq</sub> bond length (2.010 Å) is slightly shorter than the bond length in **2**, but longer than the bond length in **3**. The coordination sphere of **1** is completed by two axial C<sub>6</sub>H<sub>5</sub> anionic ligands with an average Rh-C<sub>ax</sub> bond length of 2.005 Å consistent with a Rh-C σ-bond. Notable structural distortions occur in **1** about

---

<sup>28</sup> See ref. 2.

the Rh-Rh-C vector. First, the Rh-Rh-N<sub>eq</sub> and Rh-Rh-O<sub>eq</sub> bond angles of the complex are 94.91° and 78.84° creating a distorted octahedral arrangement of the ligands about the Rh-Rh core. The Rh-Rh-C<sub>ax</sub> bond angle is 155.78° constituting a major distortion of the Rh-Rh-C vector from linearity. Finally, the Rh-Rh bond of **1** (2.519 Å) is lengthened compared to **2** (2.442 Å) and **3** (2.384 Å).

The increasing Rh-Rh, Rh-N, and Rh-O bond lengths in **1** are at variance with the increasing oxidation state of the dirhodium complex. Considering the general  $\sigma^2\pi^4\delta^2\pi^*4\delta^*n$  electronic structure of dirhodium paddlewheel complexes (*vide infra*), a shorter Rh-Rh bond is expected with increasing bond order upon oxidation from a Rh<sub>2</sub><sup>4+</sup> (n = 2) to a Rh<sub>2</sub><sup>6+</sup> complex (n = 0). Consistent with this electronic structure, the Rh-Rh bond length shortens modestly as oxidation occurs from **2** (n = 2) to **3** (n = 1), 2.422 Å to 2.384 Å, respectively. However, the Rh-Rh bond length in **1** (n = 0) is 77 pm *longer* than the corresponding bond length in **2** and 135 pm longer than the Rh-Rh bond length in **3**. The lengthening of the bond, and the bond angle distortions signal a change in the electronic configuration of the Rh-Rh core.<sup>29,30</sup>

X-ray photoelectron spectroscopy (XPS) allows the direct measurement of the binding energy of *d*-electrons that make up the Rh-Rh core and therefore their environment. XPS measurements on the series are summarized in Table 1-3. These measurements indicated that a fundamental change in the metal-centered orbitals did indeed occur when Rh<sub>2</sub>(cap)<sub>4</sub> was oxidized to **1**. The electron binding energy (*E<sub>b</sub>*) for the rhodium 3*d*-orbitals (Rh 3*d*<sub>5/2</sub>) increased from 308.08 eV to 309.09 eV upon oxidation from Rh<sub>2</sub><sup>5+</sup> to

---

<sup>29</sup> Kadish, K. M.; Phan, T. D.; Giribabu, L.; Van Caemelbecke, E.; Bear, J. L. *Inorg. Chem.* **2003**, *42*, 8663.

<sup>30</sup> An analogous phenomenon was observed for Ru<sub>2</sub><sup>6+</sup> complexes with a similar lengthening of the metal bond, see: Bear, J., L.; Chen, W. Z.; Han, B.; Huang, S.; Wang, L. L.; Thuriere, A.; Van Caemelbecke, E.; Kadish Karl, M.; Ren, T. *Inorg. Chem.* **2003**, *42*, 6230.

Rh<sub>2</sub><sup>6+</sup> (**2** to **3**). The ~1 eV increase in  $E_b$  is consistent with the oxidation of Rh<sub>2</sub><sup>4+</sup> to Rh<sub>2</sub><sup>5+</sup> in other dirhodium(II) complexes.<sup>31</sup> However, upon oxidation from Rh<sub>2</sub><sup>5+</sup> to Rh<sub>2</sub><sup>6+</sup> (**3** to **1**),  $E_b(\text{Rh } 3d_{5/2})$  remained virtually unchanged at 309.11 eV. The binding energy of **1** is lower than what would be expected for the removal of another electron from the standard electronic configuration to give  $\sigma^2\pi^4\delta^2\pi^*4$ . The difference in  $E_b$  suggests that **1** does not retain the  $\sigma^2\pi^4\delta^2\pi^*4\delta^{*n}$  electronic structure with  $n = 0$  and a  $dsp^2$  hybridized Rh-Rh core. Furthermore, the disappearance of the  $\delta$ - $\delta^*$  transition at 970 nm in the visible spectrum of **1** indicates that the  $\delta^*$  orbital is fully occupied.

**Table 1-3.** XPS Data for [Rh<sub>2</sub>(cap)<sub>4</sub>•2CH<sub>3</sub>CN] (**2**), [Rh<sub>2</sub>(cap)<sub>4</sub>(OH<sub>2</sub>)<sub>2</sub>]OTf (**3**), [Rh<sub>2</sub>(cap)<sub>4</sub>(C<sub>6</sub>H<sub>5</sub>)<sub>2</sub>] (**1**).

	Complexes		
	<b>2</b>	<b>3</b>	<b>1</b>
$E_b(\text{Rh } 3d_{5/2})^*$	308.080	309.094	309.105
$E_b(\text{Rh } 3d_{3/2})^*$	312.812	313.718	313.725

\*Reported in eV calibrated to C 1s at 284.6 eV.

Much like the Ti-N bonds in complex **6** (Figure 1-6), the formation of two new Rh-C bonds can be expected to change the hybridization of the Rh-centered orbitals from Rh<sub>2</sub>(cap)<sub>4</sub> ( $dsp^2$ ) to **1** ( $d^2sp^3$ ) to accommodate the new Rh-C bond (Figure 1-13). Upon rehybridization, an alternative electronic configuration of **1** would then be  $\pi^4\delta^2\pi^*4\delta^{*2}$  for a  $d^2sp^3$  dimer resulting in the formal cleavage of the Rh-Rh bond. The value of  $E_b(\text{Rh } 3d_{5/2})$  of **1** is similar to monomeric  $d^2sp^3$  hybridized Rh(III) complexes and consistent with the Rh(III) centers in **1** are  $d^2sp^3$  hybridized.<sup>32</sup> The presence of <sup>1</sup>H and <sup>13</sup>C NMR signals and the lack of a measurable magnetic susceptibility for **1** are consistent with

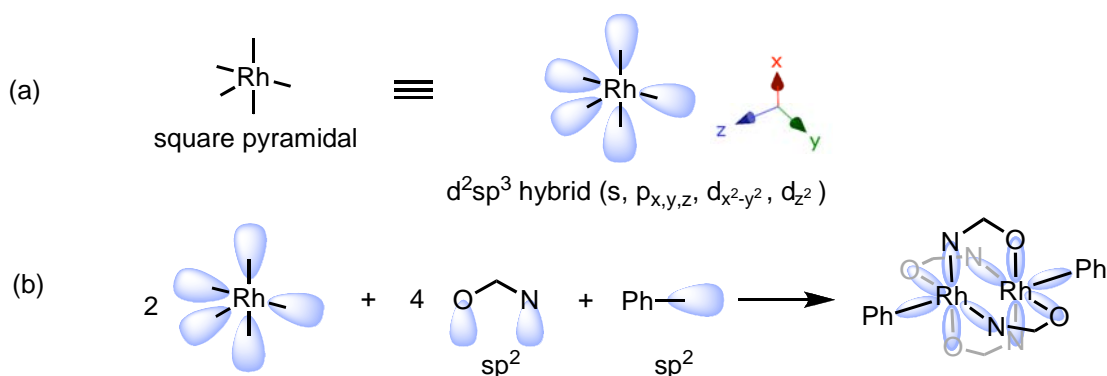
<sup>31</sup> Dennis, A. M.; Howard, R. A.; Kadish, K. M.; Bear, J. L.; Brace, J.; Winograd, N. *Inorg. Chim. Act.* **1980**, *44*, L139.

<sup>32</sup> Gassman, P. G.; Macomber, D. W.; Willging, S. M. *J. Am. Chem. Soc.* **1985**, *107*, 2380.



this closed shell assignment, as is the electronic absorption spectra. The attenuated Rh-Rh bond length in **1** is also consistent with the lack of  $\sigma$ -bonding interactions predicted by the electronic configuration. Based on this hybridization of the Rh(III) centers, a  $\pi^4\delta^2\pi^*4\delta^*2$  electron configuration for **1** is proposed. This does not mean that Rh-Rh interactions do not exist, only that there is no net bonding relationship.<sup>33</sup> Indeed, the Rh-Rh-C bond-angle distortion suggests that there exists a metal-metal or metal-ligand interaction that is not explained by simple valence-bond model. A more sophisticated treatment will be discussed in Chapter 2 that expands upon the proposed electronic structure.

**Figure 1-13.** Rehybridization at Rh alters bonding in **1**.

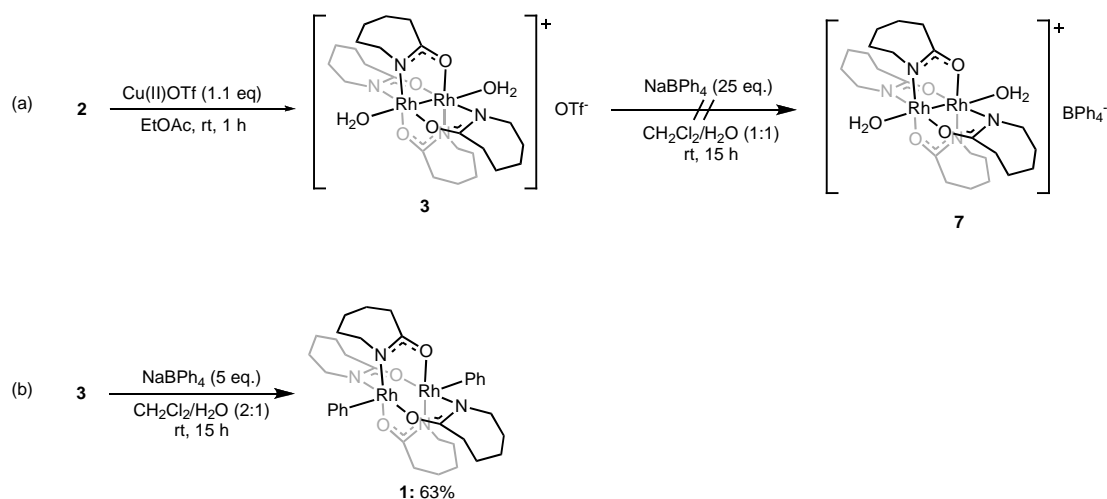


**Reaction Development and Mechanism of Aryl Transfer.** The conditions for the preparation of **1**, as reported in Scheme 1-1, were the endpoint of an interesting journey. Reaction development began with the following observation. A solution of crude  $[\text{Rh}_2(\text{cap})_4(\text{OH}_2)_2]\text{OTf}$  (**3**) in  $\text{CH}_2\text{Cl}_2$  (0.10 mmol in 10 mL) was layered with an aqueous solution of  $\text{NaBPh}_4$  (2.5 mmol in 15 mL) and vigorously stirred in an attempted anion-exchange to generate **7** (Scheme 1-4a). Upon standing open to the atmosphere for 16 h, the solution turned orange, then green. After purification, complex **1** was isolated

<sup>33</sup> The full extent of Rh-Rh bond cleavage is unclear at this time as the Rh atoms are still within the covalent radius for Rh (136 pm) by 10 pm. Pauling, L. *Acta Crystallogr., Sect. B: Struct. Sci.* **1978**, B34, 746.

and initially characterized rather than the desired anion exchange product **7**.<sup>34</sup> Based on the initial observation, the amount of sodium tetraphenylborate could be decreased from 25 to 5 equivalents (Scheme 1-4b). Under these conditions, the Rh<sub>2</sub><sup>5+</sup> complex **3** yields **1** in 63% yield over 15h. When **3** was purified by aqueous extraction, applying the conditions in Scheme 1-4b resulted in depressed yields of **1** over longer reaction times (<50% over >24 h). This suggested that impurities, most likely residual Cu(II)/Cu(I) salts, were promoting the reaction.

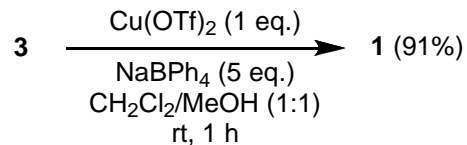
**Scheme 1-4.** Reaction development for the production of **1**.



Reaction conditions were found upon further reaction development such that all reactants were in solution. The solvent system was converted from a biphasic CH<sub>2</sub>Cl<sub>2</sub>/H<sub>2</sub>O mixture to a 1:1/CH<sub>2</sub>Cl<sub>2</sub>:MeOH solvent system in which Cu(OTf)<sub>2</sub>, NaBPh<sub>4</sub>, and Rh<sub>2</sub>(cap)<sub>4</sub> were all soluble. When Rh<sub>2</sub>(cap)<sub>4</sub> (0.014 mmol) was treated with a stoichiometric amount of Cu(OTf)<sub>2</sub> and NaBPh<sub>4</sub> (0.070 mmol), **1** was prepared in 91% isolated yield after 1 h (Scheme 1-5) in 1:1/ CH<sub>2</sub>Cl<sub>2</sub>:MeOH.

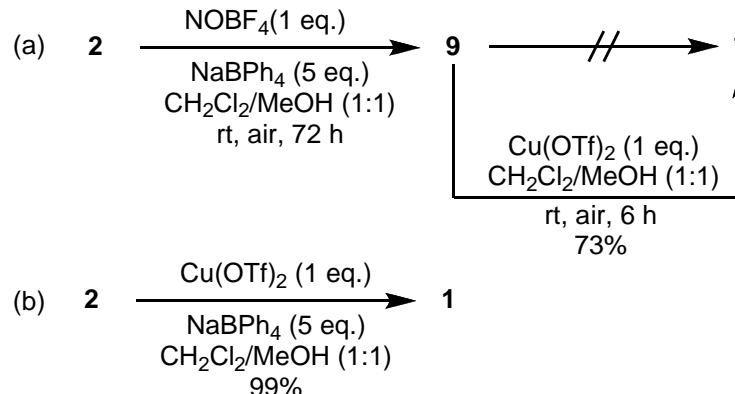
<sup>34</sup> J. Wolf made the initial observation and characterization of the formation of **1** using the biphasic CH<sub>2</sub>Cl<sub>2</sub>/H<sub>2</sub>O conditions from crude **3**.

**Scheme 1-5.** Homogenizing the reaction mixture.



With a set of homogeneous reaction conditions in hand, the role of copper salts was clearly demonstrated in the following set of experiments. Nitrosonium tetrafluoroborate (**8**: NOBF<sub>4</sub>) was used as an auxiliary one-electron oxidant to eliminate the possibility of trace copper salts. [Rh<sub>2</sub>(cap)<sub>4</sub>•2CH<sub>3</sub>CN] (**2**) (0.014 mmol) was oxidized to [Rh<sub>2</sub>(cap)<sub>4</sub>•2CH<sub>3</sub>CN]BF<sub>4</sub> (**9**) in CH<sub>2</sub>Cl<sub>2</sub> (1 mL) with a 50 μL solution of **8** in CH<sub>3</sub>CN (0.272 M). The oxidation of **2** to **9** was observed as the appearance of the characteristic π\*-δ\* transition at 970 nm and severe paramagnetic broadening of <sup>1</sup>H NMR signals. Addition of NaBPh<sub>4</sub> (0.028 mmol) in MeOH (1 mL) to this mixture did not initiate the formation of **1**, even after 72 h. At the end of the 72 h period, Cu(OTf)<sub>2</sub> (0.014 mmol) was added to the reaction and within 6 h the solution had turned the characteristic green of the Rh<sub>2</sub><sup>6+</sup> complex **1**. Compound **1** was chromatographically isolated from the reaction mixture in 73% yield (Scheme 1-6a). In an extension of using Cu(II) as an oxidant, the reaction to form **1** was initiated directly from **2** (0.014 mol) using Cu(OTf)<sub>2</sub> (0.014 mmol) and NaBPh<sub>4</sub> (0.070 mmol) in 1:1/CH<sub>2</sub>Cl<sub>2</sub>:MeOH (2 mL). Under these reaction conditions, **1** was generated directly from Rh<sub>2</sub>(cap)<sub>4</sub> in 1 h in 99% yield (Scheme 1-6b) through the intermediacy of **3**.

**Scheme 1-6.** Cu(II) is the oxidant in the formation of **1**.

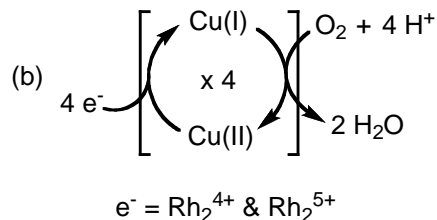
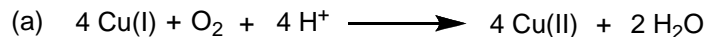


The near quantitative yield of **1** in Scheme 1-6b required almost two Cu(II)/Cu(I) turnovers for the oxidation of Rh<sub>2</sub><sup>4+</sup> to Rh<sub>2</sub><sup>6+</sup> by Cu(OTf)<sub>2</sub>. This result suggested that the reaction could be catalytic in copper via the well-documented aerobic Cu(II)/Cu(I) couple. The stoichiometric reduction of O<sub>2</sub> to water by Cu(I) is shown in Scheme 1-7a. This process is well known for its biochemical reduction of molecular oxygen<sup>35</sup> as well as operating as the co-oxidant in the Wacker oxidation.<sup>36</sup> The stoichiometric reaction can be rendered catalytic if a source of electrons are supplied to reduce Cu(II) back to Cu(I). In such a case, rather than 4 moles of Cu(I), 4 moles of electrons and 4 turnovers of the Cu(II)/Cu(I) couple are required to reduce O<sub>2</sub> to water (Scheme 1-7b). In the case of the reaction to form **1** from **2** or **3**, the Rh<sub>2</sub><sup>n+</sup> complexes would be the source of electrons and the solvent would be the source of protons.

<sup>35</sup> Solomon, E. I.; Chen, P.; Metz, M.; Lee, S.-K.; Palmer, A. E. *Angew. Chem. Int. Ed.* **2001**, *40*, 4570.

<sup>36</sup> a) Punniyamurthy, T.; Velusamy, S.; Iqbal, J. *Chem. Rev.* **2005**, *105*, 2329, b) Cornell, C. N.; Sigman, M. S. *Inorg. Chem.* **2007**, *46*, 1903.

**Scheme 1-7.** Oxidation of Cu(I) by O<sub>2</sub>.



The data in Table 1-4 show the final refinement of conditions to realize the catalytic process. Consistent with the proposed Cu(II)/Cu(I) couple, replacing Cu(OTf)<sub>2</sub> with CuOTf as its benzene solvate (CuOTf = [(CuOTf)<sub>2</sub>•C<sub>6</sub>H<sub>6</sub>]) had no deleterious effects on the production of **1** (Entries 1 and 2, Table 1-4). Reducing the amount of CuOTf made the process catalytic, and catalyst loading could be dropped to as low as 5 mol% before a substantial diminution in yield was observed (Entries 3-5, Table 1-4). The ratio of CH<sub>2</sub>Cl<sub>2</sub>:MeOH could be reduced to as low as 9:1 before reactants were no longer soluble and doing so had little effect on the production of **1** (Entries 6-8, Table 1-4). However, if polar aprotic solvents like CH<sub>3</sub>CN and tetrahydrofuran (THF) were used, no reaction occurred, consistent with the requirement of a proton source in the Cu(II)/Cu(I) cycle (Scheme 1-7b). The parameter that most affected the reaction outcome was the stoichiometry of NaBPh<sub>4</sub>. Reducing the stoichiometry of NaBPh<sub>4</sub> from 5 to 3 equivalents resulted in a 19% reduction in yield (Entry 9, Table 1-4). Further reduction of NaBPh<sub>4</sub> to 2 equivalents reduced the yield of **1** to 61% (Entry 10, Table 1-4). Entry 7 of Table 1-4 reports the conditions chosen to scale up the reaction because they minimized the amount of alcohol and CuOTf. Scale-up of the reaction conditions to 0.100 mmol of Rh<sub>2</sub>(cap)<sub>4</sub> provided **1** in 77% isolated yield.

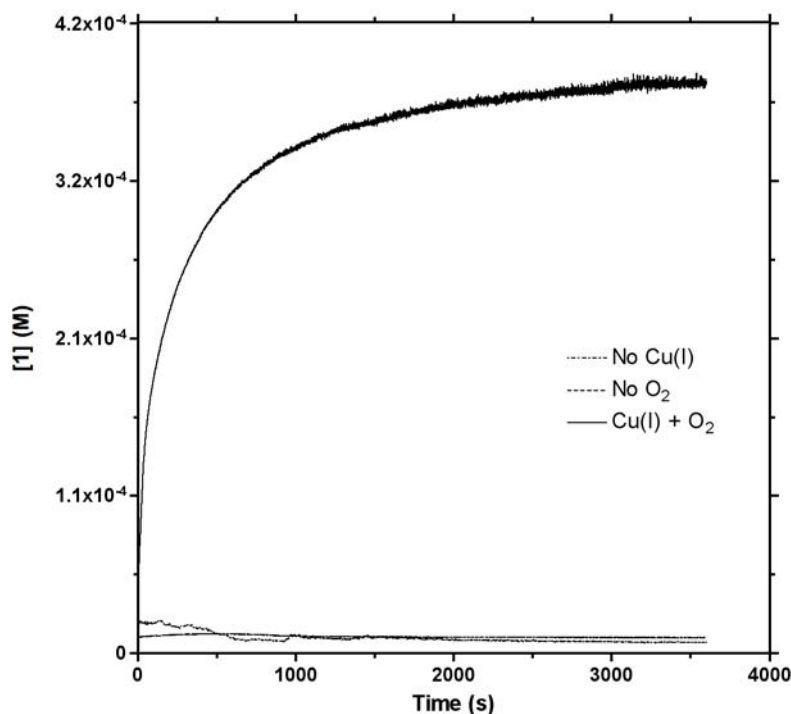
**Table 1-4.** Optimization for the formation of **1**.

entry <sup>a</sup>	Catalyst (mol %)	Solvent CH <sub>2</sub> Cl <sub>2</sub> :MeOH	NaBPh <sub>4</sub> (eq.)	Yield (%) <sup>b</sup>
<b>1</b>	Cu(OTf) <sub>2</sub> (100)	1:1	5	99
<b>2</b>	CuOTf (100)	1:1	5	99
<b>3</b>	CuOTf (33)	1:1	5	99
<b>4</b>	CuOTf (10)	1:1	5	92
<b>5</b>	CuOTf (5)	1:1	5	83
<b>6</b>	CuOTf (10)	4:1	5	92
<b>7</b>	CuOTf (10)	9:1	5	92
<b>9</b>	CuOTf (10)	9:1	3	73
<b>10</b>	CuOTf (10)	9:1	2	61

<sup>a</sup>Reaction conditions: [Rh<sub>2</sub>(cap)<sub>4</sub>(MeCN)<sub>2</sub>] (0.014 mmol), solvent (2 mL), 1 h under ambient atmosphere and temperature. <sup>b</sup>Yields are based on the mass of isolated products following preparatory chromatography.

After obtaining a set of reaction conditions that minimized the amount of NaBPh<sub>4</sub>, MeOH, and CuOTf used in the reaction, the question of mechanism was revisited. The oxidation of a [Rh<sub>2</sub>(cap)<sub>4</sub>(MeCN)<sub>2</sub>]BF<sub>4</sub> (**9**, 0.4 mmol) to [Rh<sub>2</sub>(cap)<sub>4</sub>(Ph)<sub>2</sub>] (**1**) was observed over 60 minutes *via* spectral changes at λ<sub>max</sub> of **1** (Figure 1-14). A control reaction with a mixture of **9** and NaBPh<sub>4</sub> in the absence of CuOTf under the optimal reaction conditions did not form **1**. In a demonstration of the aerobic nature of the oxidation, there was no conversion of **9** to **1** in the presence of NaBPh<sub>4</sub> and CuOTf in rigorously degassed solvents under N<sub>2</sub>. However, in the presence CuOTf (10 mol%), NaBPh<sub>4</sub>, and air, **9** rapidly formed **1** in almost complete conversion (0.37 mmol, 93%) at 60 mins.

**Figure 1-14.** Conversion of **9** to **1** monitored at 430 nm under various conditions.



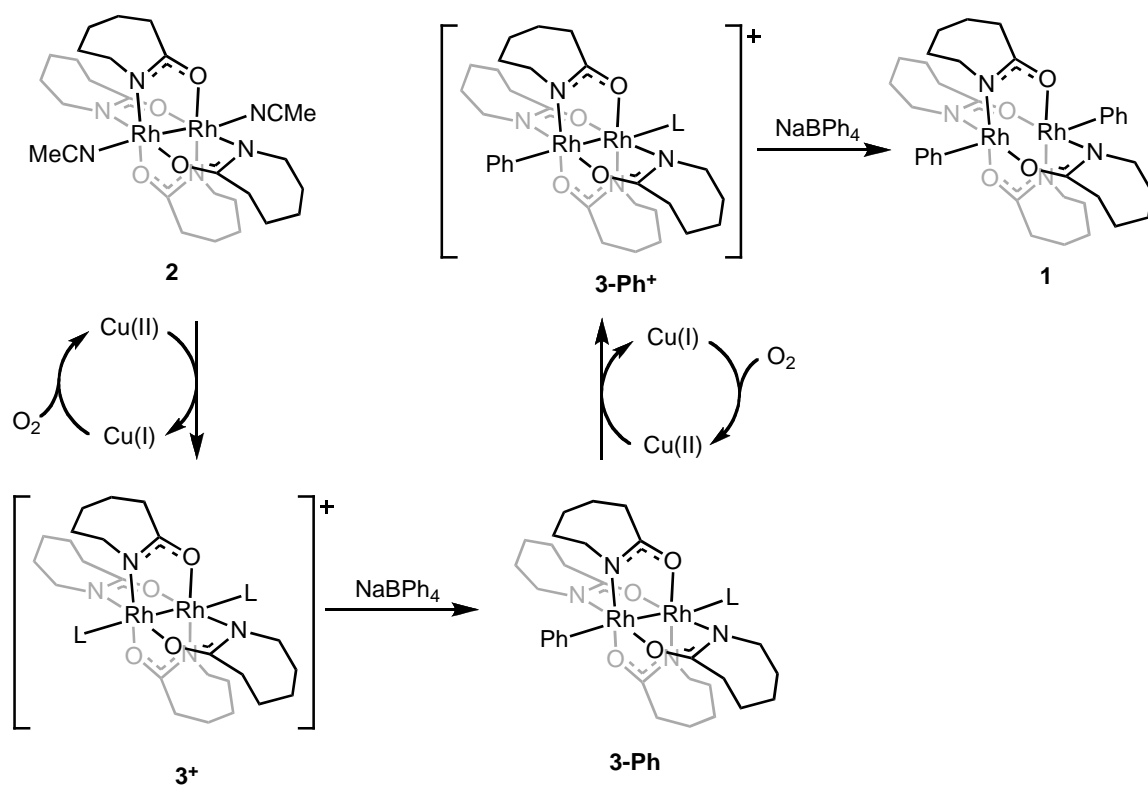
Based on these results and the data from Figure 1-14, a simple model can be proposed for the oxidation of **2** to **1** based on these data (Scheme 1-8.). A Cu(II)/Cu(I) couple with oxygen as a terminal oxidant oxidizes **2** to **3<sup>+</sup>**. An aryl transfer from NaBPh<sub>4</sub> to **3<sup>+</sup>** gives a transient **3-Ph** species lowering the Rh<sup>5+/6+</sup> oxidation potential and facilitating further oxidation by the Cu(II)/Cu(I) couple to yield **3-Ph<sup>+</sup>**. Strong,  $\sigma$ -donating ligands have been shown to decrease oxidation potentials by up to 1 eV below the parent complex.<sup>37</sup> Phenyl transfer from an additional equivalent of NaBPh<sub>4</sub> completes

---

<sup>37</sup> Axial ligands can dramatically effect oxidation potentials Bear, J. L.; Han, B.; Huang, S.; Kadish, K. M. *Inorg. Chem.* **1996**, 35, 3012.

the process and generates **1**.<sup>38</sup> The phenyl transfer process will be discussed in further detail in Chapter 2.

**Scheme 1-8.** Proposed mechanism for the formation of **1**.



<sup>38</sup>The 5<sup>+</sup>/6<sup>+</sup> redox couple for Rh<sub>2</sub>(cap)<sub>4</sub> is estimated to be ~1300 mV vs SCE in CH<sub>3</sub>CN, see: Doyle, M. P.; Ren, T., *The Influence of Ligands on Dirhodium(II) on Reactivity and Selectivity in Metal Carbene Reactions*. In *Progress in Inorganic Chemistry*, Karlin, Ed. Wiley: New York, **2001**, 49, 113-168.



## IV. Conclusion

A copper catalyzed aerobic oxidation of  $[\text{Rh}_2^{4+}(\text{cap})_4(\text{MeCN})_2]$  (**2**) with  $\text{NaBPh}_4$  as a phenyl transfer agent provides entry into the novel *bis*( $\sigma$ -phenyl)- $\text{Rh}_2^{6+}$  species (**1**). The isolation of **1** provides the first unequivocal example of a dirhodium(III) complex and its full characterization. An electronic structure of  $\pi^4\delta^2\pi^*4\delta^*2$  is proposed for **1** based on the crystallographically determined Rh-Rh bond length and XPS binding energies for the Rh  $d$ -electrons. The electronic structure suggests a cleavage of the Rh-Rh bond consistent with the electronic and structural data obtained.

## V. Experimental

**General.** All reagents were commercially obtained and used without further purification.  $^1\text{H}$  NMR (400 MHz) and  $^{13}\text{C}$  NMR (100 MHz) spectra were obtained on a Bruker DRX-400 NMR spectrometer as solutions in  $\text{CDCl}_3$  unless otherwise reported. Chemical shifts are reported in parts per million (ppm,  $\delta$ ) downfield from  $\text{Me}_4\text{Si}$  (TMS) or relative to residual solvent peaks. UV/Visible spectra were obtained on a Varian Cary 50 spectrophotometer using a xenon flash lamp. IR spectra were recorded on a JASCO FT/IR 4100 spectrometer. All preparatory silica gel columns were run with Silicycle Ultrapure silica (230-400 mesh). Elemental analyses were performed on crystals that were dried for 12 h in a vacuum oven (100 °C, 20 torr).

**XRD Crystal Structure Determination.**<sup>39</sup> The X-ray intensity data were measured at 223(2) K on a three-circle diffractometer system equipped with Bruker Smart 1000 CCD area detector using a graphite monochromator and a Mo  $K\alpha$  fine-focus sealed tube ( $\lambda = 0.71073 \text{ \AA}$ ). Data was collected using the

---

<sup>39</sup> All structures were Solved by Peter Zavalij, crystallographer at the University of Maryland, College Park.

SMART software package.<sup>40</sup> Cell determination, refinement and frames integration were done with the SAINT software package using a narrow-frame integration algorithm.<sup>40</sup> Data were corrected for absorption effects with the semi-empirical from equivalents method using XPREP for **1**<sup>41</sup> or SADABS for **2** and **3**.<sup>42</sup> Structures were solved and refined using the SHELXS-97 and SHELXL-97 software.

**XPS Binding Energy Determination.**<sup>43</sup> A Kratos Axis 165 X-ray photoelectron spectrometer was used to determine the Rh 3d binding energies in compounds **1**, **2** and **3** at a pressure of  $8 \times 10^{-10}$  Torr with non-monochromatic Mg K $\alpha$  radiation. The powder samples were dusted on to double-sided conductive carbon tape mounted on a sample stub. High-resolution measurements for various regions (Rh, N, O, F, S and C) were done in hybrid mode using both electrostatic and magnetic lenses, with a step size of 0.1 eV and a pass-energy of 40 eV. The charge neutralizer was on during the measurements to compensate surface charging and binding energies were calibrated with respect to C 1s at 284.6 eV.

**XPS Data Analysis.** Data processing was performed using Vision processing software. After subtraction of a linear background, all spectra are fitted using 60% Gaussian/40% Lorentzian peaks, taking the minimum number of peaks consistent with the best fit. The important parameters used for this fitting are peak position, full width at half maximum (FWHM), and spin orbit coupling.

---

<sup>40</sup> Bruker, SMART and SAINT. Bruker AXS Inc., Madison, Wisconsin, USA., **1999**.

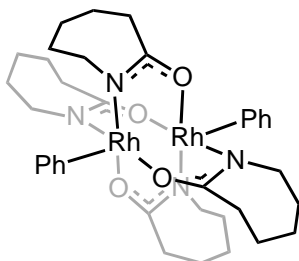
<sup>41</sup> Sheldrick, G. M., SHELXL-97 University of Göttingen, Germany, **1999**.

<sup>42</sup> Sheldrick, G. M., SADABS University of Göttingen, Germany, **1996**.

<sup>43</sup> All XPS data were collected by Bindhu Varughese, University of Maryland, College Park.

## Synthesis and Characterizations.

**Bis- $\sigma$ -(phenyl)-tetrakis-( $\mu$ -caprolactamato)-dirhodium(III) (1).** In a 250

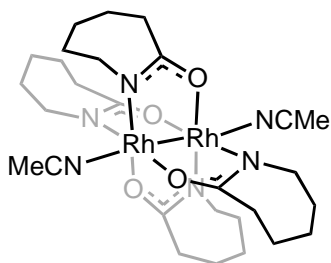


mL round bottom flask, NaBPh<sub>4</sub> (1.16 g, 3.39 mmol) and (CuOTf)<sub>2</sub>·C<sub>6</sub>H<sub>6</sub> (49 mg, 0.17 mmol) were added to a CH<sub>2</sub>Cl<sub>2</sub>/MeOH solution (100 mL, 9:1) of Rh<sub>2</sub>(cap)<sub>4</sub> (500 mg, 679 mmol). During the first minutes of reaction, the solution color turned from red-purple to green after which the reaction was left to stir at room temperature under air.

At 15 hours, the reaction was concentrated to dryness, loaded onto a silica gel column, and purified via gradient elution using pentane/CH<sub>2</sub>Cl<sub>2</sub> (5:1, 100 mL) → CH<sub>2</sub>Cl<sub>2</sub> (50 mL) → CH<sub>2</sub>Cl<sub>2</sub>/acetone (95:5, 50 mL). The desired fractions were concentrated to a dark green solid that was triturated with diethyl ether (2 x 25 mL), filtered, and dried under vacuum. Yield: 420 mg (77 %). Recrystallization from CH<sub>2</sub>Cl<sub>2</sub> provided X-ray quality crystals.

Anal. calcd. for Rh<sub>2</sub>C<sub>36</sub>H<sub>51</sub>N<sub>4</sub>O<sub>4</sub> (809.20): C(53.47), H(6.23), N(6.93) / Found: C(53.04), H(6.15), N(6.63); <sup>1</sup>H NMR (CD<sub>2</sub>Cl<sub>2</sub>):  $\delta$  7.53-7.52 (comp, 4H), 7.18-7.10 (comp, 6H), 3.04-2.91 (comp, 8H), 2.48-2.39 (comp, 8H) 1.83-1.80 (comp, 4H), 1.63-1.40 (comp, 20H) ppm; <sup>13</sup>C NMR (CD<sub>2</sub>Cl<sub>2</sub>)  $\delta$  183.5, 147.7 (d, <sup>1</sup>J<sub>C-Rh</sub> = 37.1 Hz; C<sub>ipso</sub> Ph), 137.0, 126.0, 123.8, 51.3, 38.4, 30.5, 29.6, 24.2 ppm; UV/Visible (CH<sub>2</sub>Cl<sub>2</sub>):  $\lambda_{\text{max}}$  ( $\epsilon$  M<sup>-1</sup>cm<sup>-1</sup>) = 430 nm (4490); IR(neat):  $\nu$  = 1583(N=C-O, s), 1550(aryl-C=C, s), cm<sup>-1</sup>; HRMS (ESI) calcd. for Rh<sub>2</sub>C<sub>36</sub>H<sub>51</sub>N<sub>4</sub>O<sub>4</sub> 809.2020, found 809.2018 (M+H); XRD (CCDC #615577) Crystals grown by slow evaporation of CH<sub>2</sub>Cl<sub>2</sub>.

**Bis-(acetonitrile)-tetrakis-( $\mu$ -caprolactamato)-dirhodium(II) (2).** The



preparation of  $[\text{Rh}_2(\text{cap})_4 \cdot 2\text{CH}_3\text{CN}]$  has been previously described.<sup>1</sup> Synthetic and X-ray quality material was prepared by an unpublished recrystallization for which the procedure and characterizations are given below.

Recrystallization procedure: An oven dried 250 mL, single-necked (24/40 joint) round-bottomed flask, equipped with a Teflon-coated stir-bar was charged with 3.52 g of  $\text{Rh}_2(\text{cap})_4$ , 100 mL of acetonitrile, and 10 mL of methanol. The flask was placed in an oil bath maintained at 100 °C. When the mixture reached boiling, methanol was added sparingly via Pasteur pipette until a deep purple homogeneous solution was obtained. Care was taken to avoid adding additional methanol once a homogeneous solution was obtained as excess methanol reduces the efficiency of the recrystallization. The solution was removed from the oil bath and filtered hot over a funnel containing a small cotton plug. The solution was allowed to cool to room temperature and was placed into the freezer overnight. Shiny purple crystals were isolated by removal of the supernatant liquid. The crystals were washed with acetonitrile (3 x 5 mL) and dried for 10 minutes at 0.1 mm Hg to provide  $[\text{Rh}_2(\text{cap})_4(\text{CH}_3\text{CN})_2] \cdot 2\text{CH}_3\text{CN}$  as shiny, deep purple, X-Ray quality crystals.

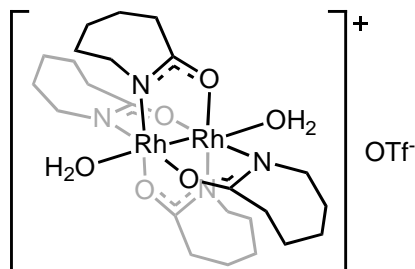
Anal. calcd. for  $\text{Rh}_2\text{C}_{28}\text{H}_{46}\text{N}_6\text{O}_4$  (736.52): C(45.66), H(6.29), N(11.41) / Found C(45.65), H(6.44), N(11.90); <sup>1</sup>H NMR  $\delta$  3.37-3.24 (comp, 8H), 2.41-2.31 (comp, 8H), 2.07 (br, 9H),<sup>44</sup> 1.67-1.39 (comp, 24H) ppm; <sup>13</sup>C NMR  $\delta$  185.3, 115.5, 53.2, 36.3, 30.3, 28.5, 23.8, 1.8 ppm; UV/Visible (MeCN/MeOH 1:1)  $\lambda_{\text{max}}$  ( $\epsilon$   $\text{M}^{-1}\text{cm}^{-1}$ ) nm = 362 (176), 516 (189); IR (neat)  $\nu$  = 1593 (N-C=O, s)  $\text{cm}^{-1}$

---

<sup>44</sup> Signals were slightly broadened due to rapid exchange of free solvent with Rh-bound solvent. The loss of excess  $\text{CH}_3\text{CN}$  accounts for discrepancy between the XRD formula and that observed by <sup>1</sup>H NMR.

<sup>1</sup>; HRMS (FAB) calcd. for Rh<sub>2</sub>C<sub>24</sub>H<sub>40</sub>N<sub>4</sub>O<sub>4</sub> 654.1160, found 654.1180 (M+H). XRD (CCDC #615575) Crystals grown in CH<sub>3</sub>CN @ -20 °C.

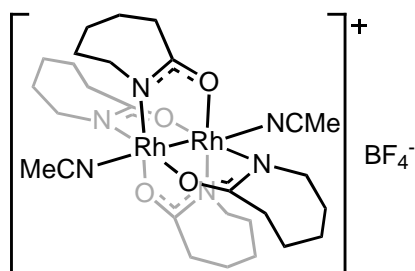
**Bis-aquo-tetrakis-(μ-caprolactamato)-dirhodium(II/III) triflate, (3).** A 125



mL Erlenmeyer flask was charged with **2** (25 mg, 0.034 mmol), 20mL of ethyl acetate was added, and the resulting mixture was sonicated for 10 minutes until a fine powder suspension was observed. Copper(II) triflate (13 mg, 0.036 mmol) was added and the ethyl acetate reaction mixture was heated to boiling until a translucent purple solution was obtained. The solution was allowed to cool to room temperature, and solvent was removed under reduced pressure to yield a purple glassy solid. Recrystallization from CH<sub>2</sub>Cl<sub>2</sub> with slow diffusion of diethyl ether yielded X-ray quality crystals. Yield: 15 mg (53%).

NMR silent; UV/Visible (CH<sub>2</sub>Cl<sub>2</sub>) λ<sub>max</sub> (ε M<sup>-1</sup>cm<sup>-1</sup>) nm = 504 (7300), 640 (1010), 966 (2330); XRD (CCDC #615576) Crystals grown by slow diffusion of ether into CH<sub>2</sub>Cl<sub>2</sub>.

**Bis-(acetonitrile)-tetrakis(μ-caprolactamato)-dirhodium(II/III)**



**tetrafluoroborate, (9).** A solution of NOBF<sub>4</sub> (54 mg, 0.46 mmol) in MeCN (10 mL) was slowly added (over 3 min) to a solution of freshly recrystallized [Rh<sub>2</sub>(cap)<sub>4</sub>(CH<sub>3</sub>CN)<sub>2</sub>] (310 mg, 0.42 mmol) in CH<sub>2</sub>Cl<sub>2</sub> (50 mL). The solution rapidly turned from blue-purple to dark red-violet. The solution was stirred 30 min at room temperature. Solvents were removed under reduced pressure. The residue was dissolved in CH<sub>2</sub>Cl<sub>2</sub> (15 mL) and filtered through Celite. The filtrate was concentrated to reduced volume (ca. 5 mL) and precipitated in diethyl ether (100 mL). The precipitate

was filtered and dried under vacuum to yield a dark red-violet solid (295 mg, 85%).

NMR silent; UV/Visible (CH<sub>2</sub>Cl<sub>2</sub>)  $\lambda_{\text{max}}$  ( $\epsilon$  M<sup>-1</sup>cm<sup>-1</sup>) nm = 507 (6350), 658 (618), 978 (1750); HRMS (EI) calcd. for Rh<sub>2</sub>C<sub>26</sub>H<sub>43</sub>N<sub>5</sub>O<sub>4</sub> (M(MeCN)<sup>+</sup>): 695.14251; found: 695.14072; MS (ESI) 87.0, (100) [BF<sub>4</sub>]<sup>-</sup>.

#### **Spectroscopic Monitoring of the Formation of 1 at 430 nm (No Cu).**

Solutions of **9** in CH<sub>2</sub>Cl<sub>2</sub> (0.800 mM) and NaBPh<sub>4</sub> in MeOH (1.60 mM) were prepared using volumetric glassware under ambient conditions. A cuvette, sealed with a septum with the inclusion of air, was charged with the solution of **9** (1.00 mL, 0.800 mmol). The reaction was initiated with the solution of NaBPh<sub>4</sub> (1.00 mL, 1.60 mmol) to give a final reaction volume of 2 mL (0.400 mM in **9**). The reaction was monitored as the change in absorbance at 430 nm.<sup>45</sup>

#### **Spectroscopic Monitoring of the Formation of 1 at 430 nm (No O<sub>2</sub>).**

Solutions of **9** in CH<sub>2</sub>Cl<sub>2</sub> (0.800 mM) and (CuOTf)<sub>2</sub>•C<sub>6</sub>H<sub>6</sub> in MeOH (0.0800 mM) were prepared using volumetric glassware. The solutions were sparged with N<sub>2</sub> for 10 min, then diluted to volume. Trace amounts of O<sub>2</sub> were removed with three freeze (-195 °C), pump (0.1 torr), and thaw (20 °C) cycles. A cuvette, sealed and purged with N<sub>2</sub>, was charged with the solution of **9** (1.00 mL, 0.800 mmol). The reaction was initiated with the solution of (CuOTf)<sub>2</sub>•C<sub>6</sub>H<sub>6</sub> (1.00 mL, 0.0800 mmol) to give a final reaction volume of 2 mL (0.400 mM in **9**). The reaction was monitored as the change in absorbance at 430 nm.

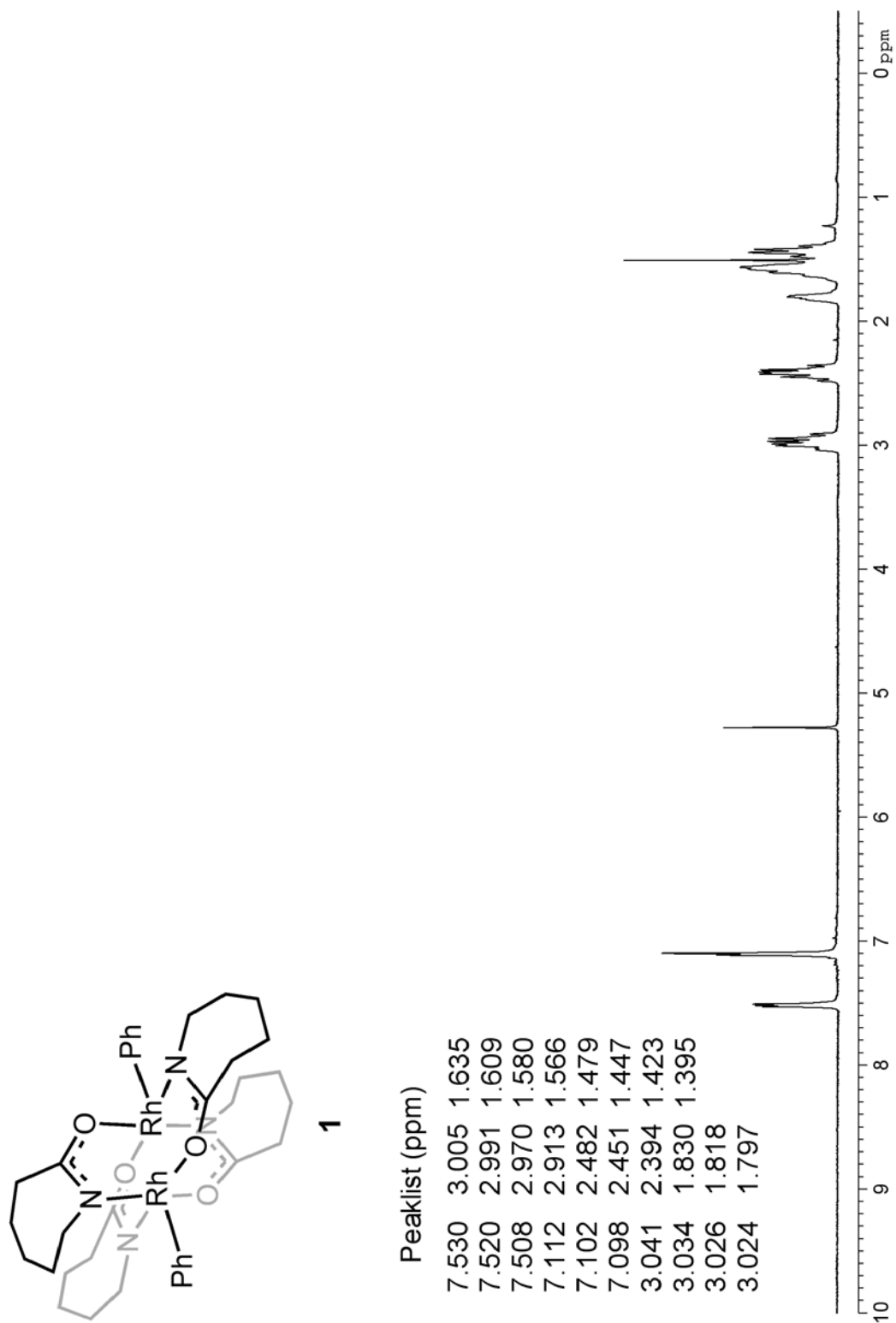
---

<sup>45</sup> The absorbances were converted to concentration values for **1** using  $\epsilon = 4490$  M<sup>-1</sup>cm<sup>-1</sup>. Although the solvent system is different than the solvent system used to determine  $\epsilon$ , the same system was used for each of the spectrophotometric analyses. Therefore, any error imposed by the solvent is systematic and does not interfere with comparisons.

**Spectroscopic Monitoring of the Formation of 1 at 430 nm (Cu + O<sub>2</sub>).** Solutions of **9** in CH<sub>2</sub>Cl<sub>2</sub> (0.800 mM), NaBPh<sub>4</sub> in MeOH (1.60 mM), and (CuOTf)<sub>2</sub>•C<sub>6</sub>H<sub>6</sub> in MeOH (8.00 mM) were prepared using volumetric glassware under ambient conditions. A cuvette was charged with the solution of **9** (1.00 mL, 0.800 mmol) and the solution of NaBPh<sub>4</sub> (1.00 mL, 1.60 mmol) and sealed with the inclusion of air. The reaction was initiated with the solution of (CuOTf)<sub>2</sub>•C<sub>6</sub>H<sub>6</sub> (0.010 mL, 0.080 mmol) to give a final reaction volume of 2.01 mL (0.398 mM in **9**). The reaction was monitored as the change in absorbance at 430 nm.

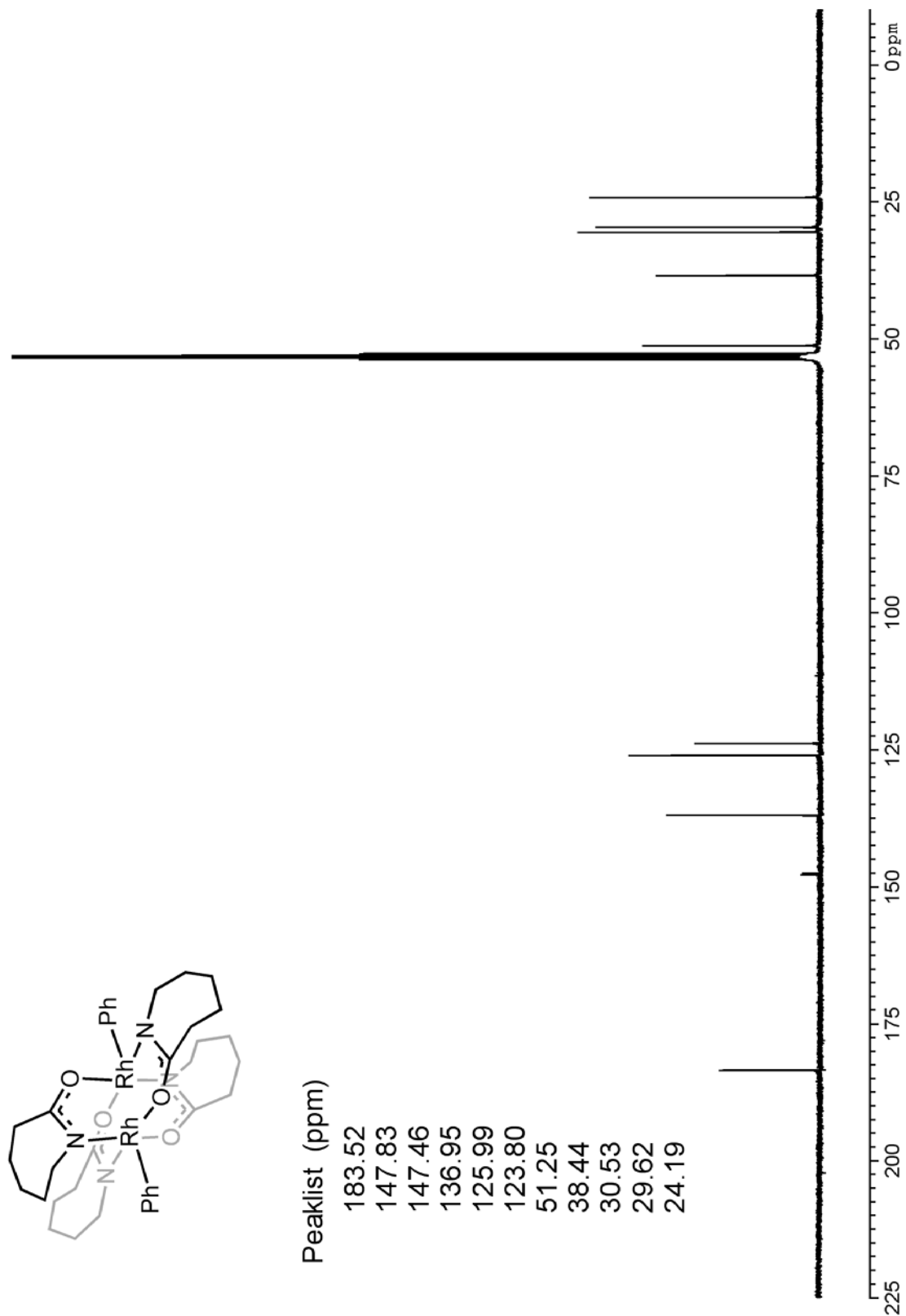
## Spectral Traces.

$^1\text{H}$  NMR Spectrum (1).

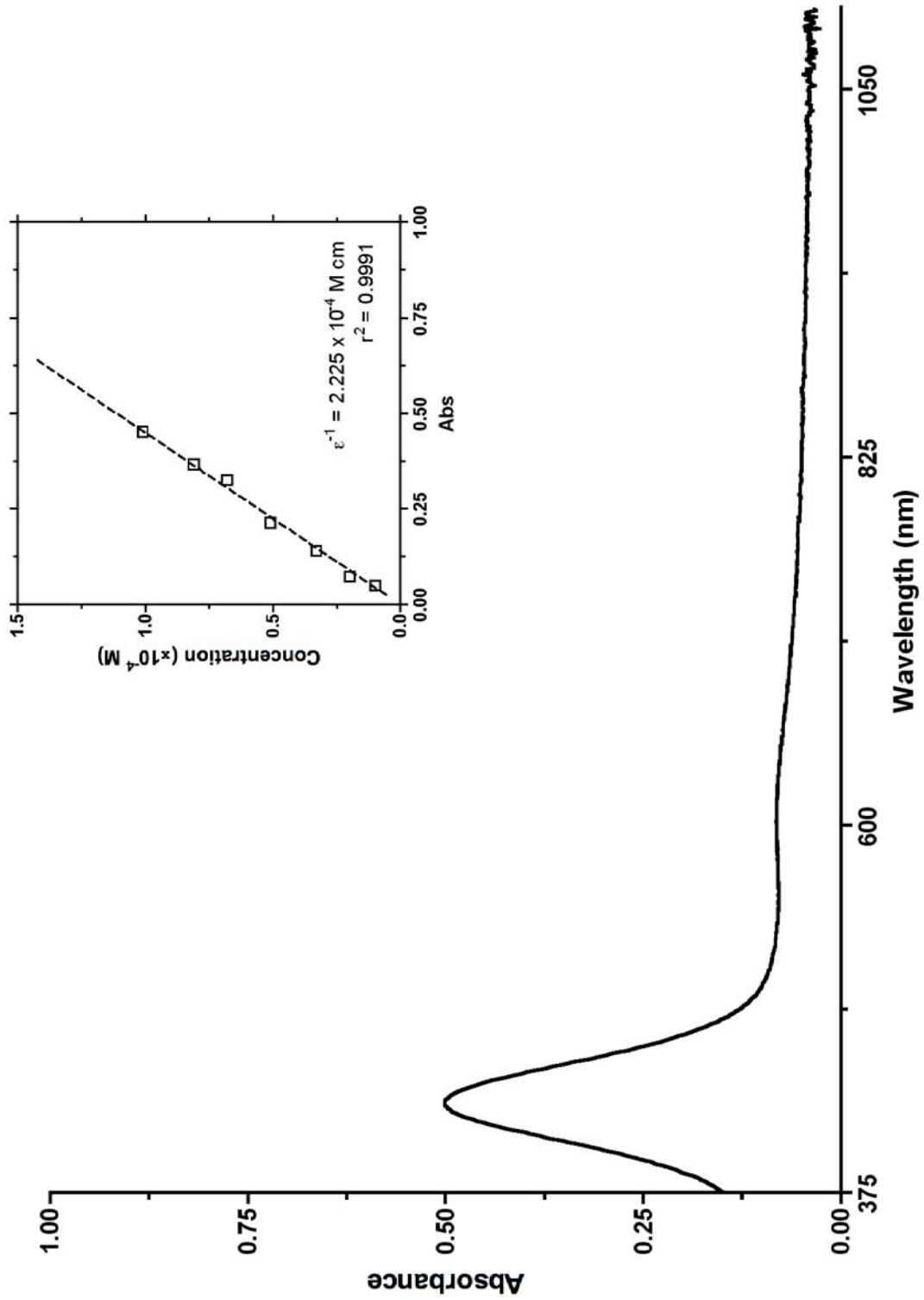




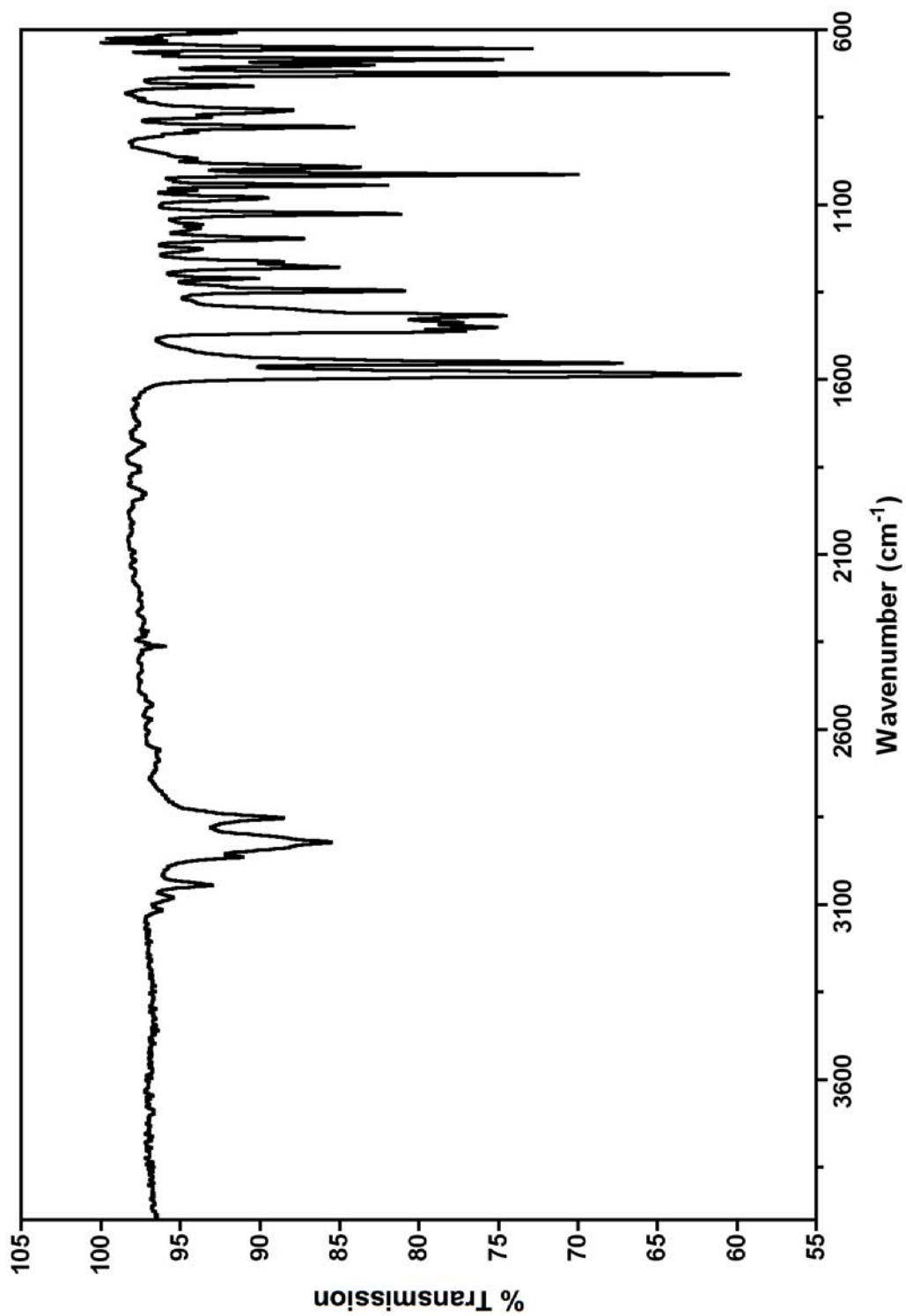
<sup>13</sup>C NMR Spectrum (1).



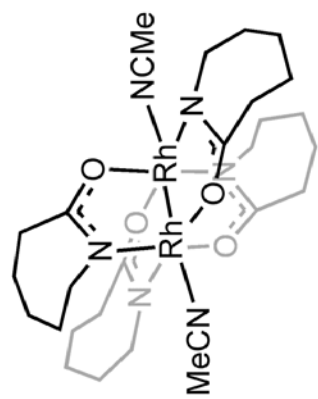
Electronic Absorption Spectrum & Molar Absorptivity (1, 375 – 1100 nm).



Vibrational Spectrum (1) (4000 – 600  $\text{cm}^{-1}$ ).



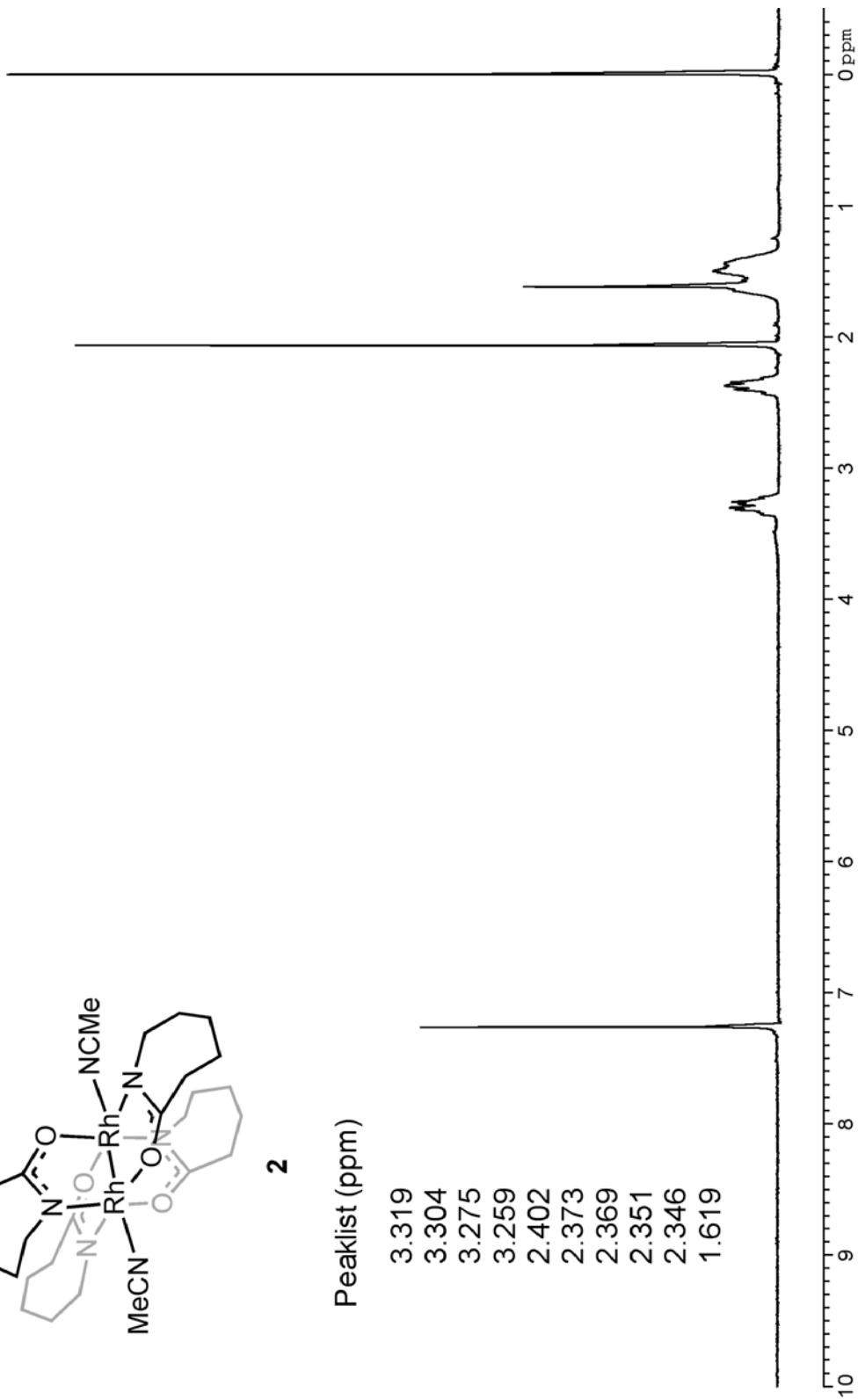
<sup>1</sup>H NMR Spectrum (2).



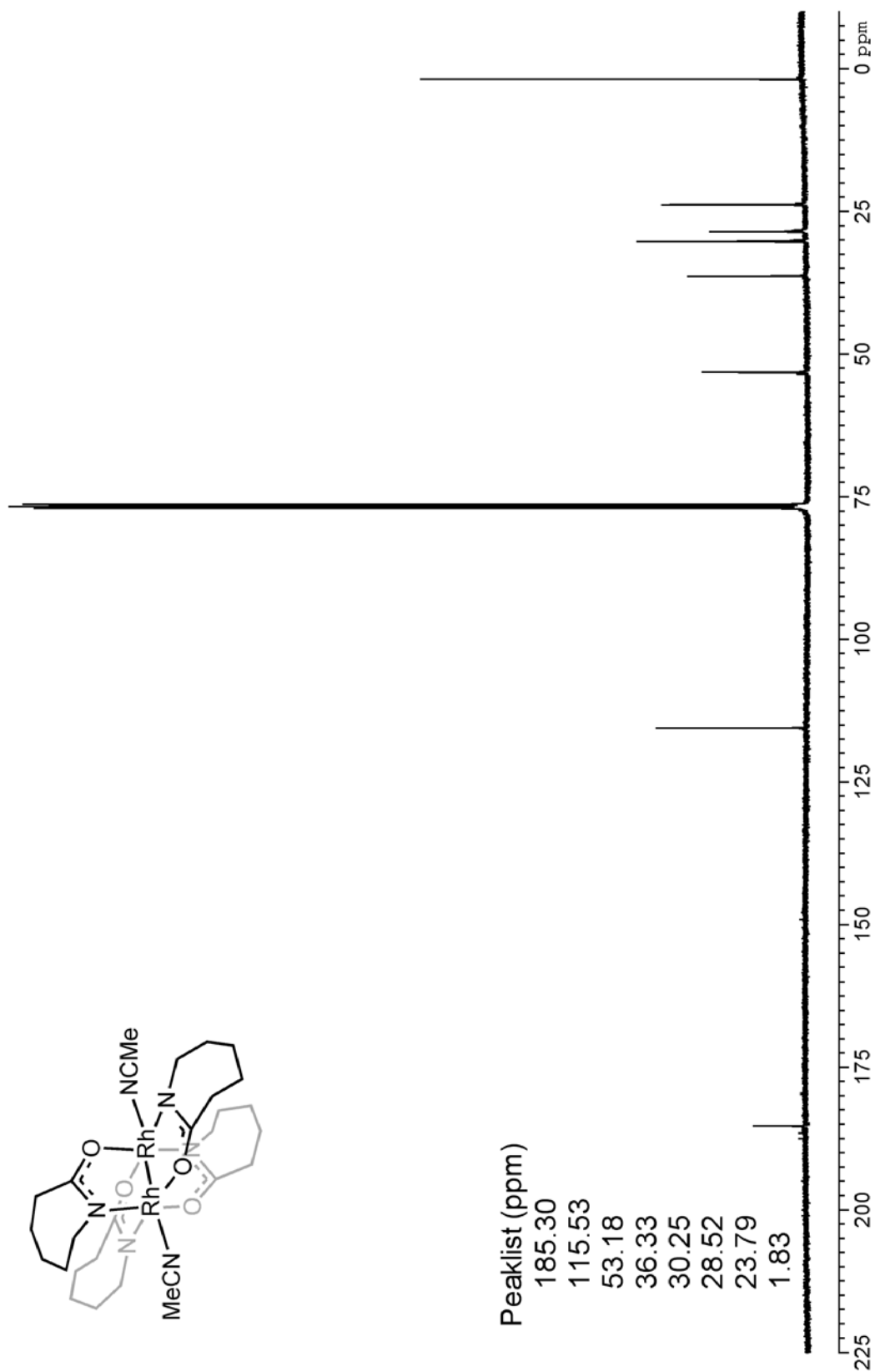
2

Peaklist (ppm)

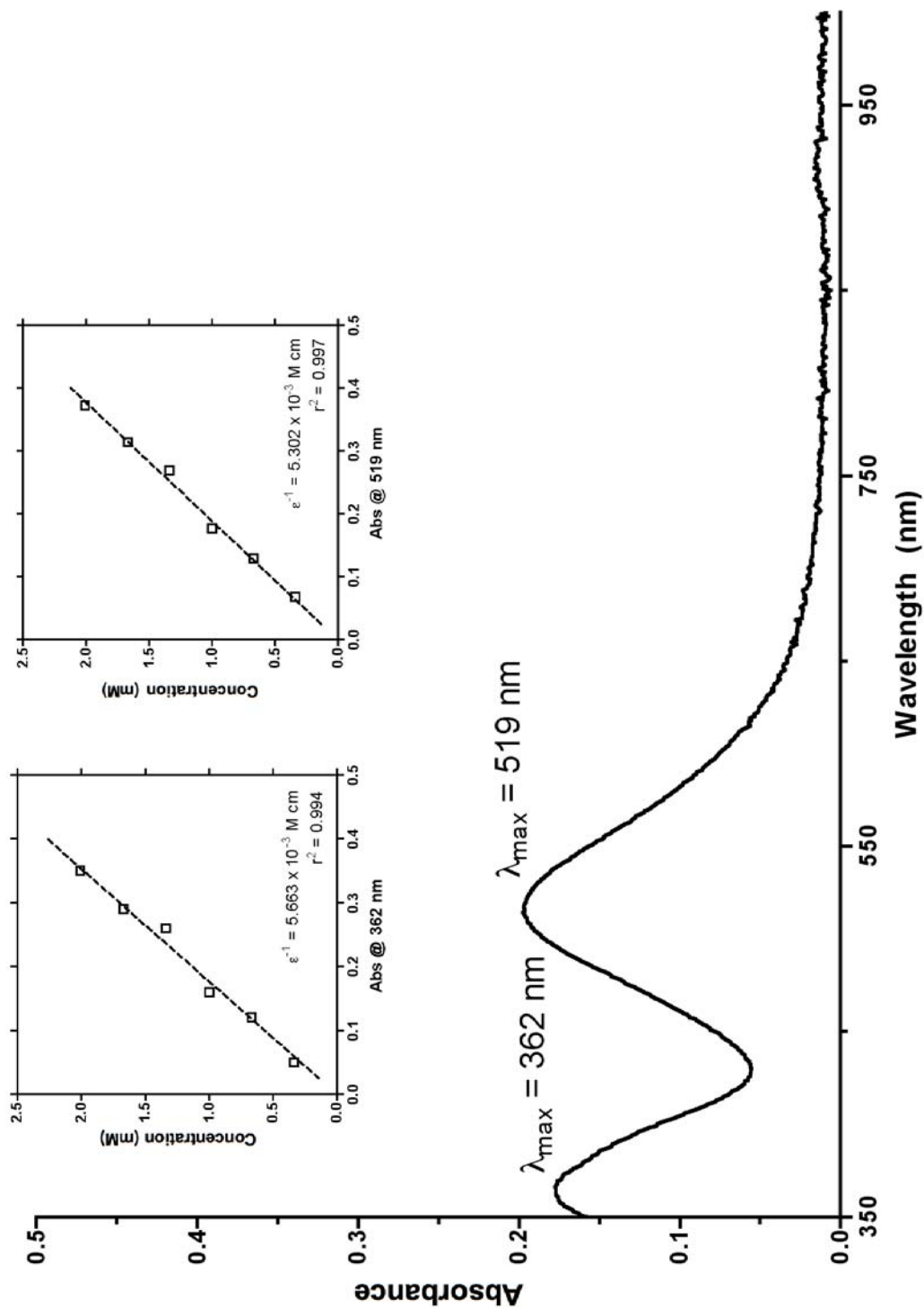
- 3.319
- 3.304
- 3.275
- 3.259
- 2.402
- 2.373
- 2.369
- 2.351
- 2.346
- 1.619



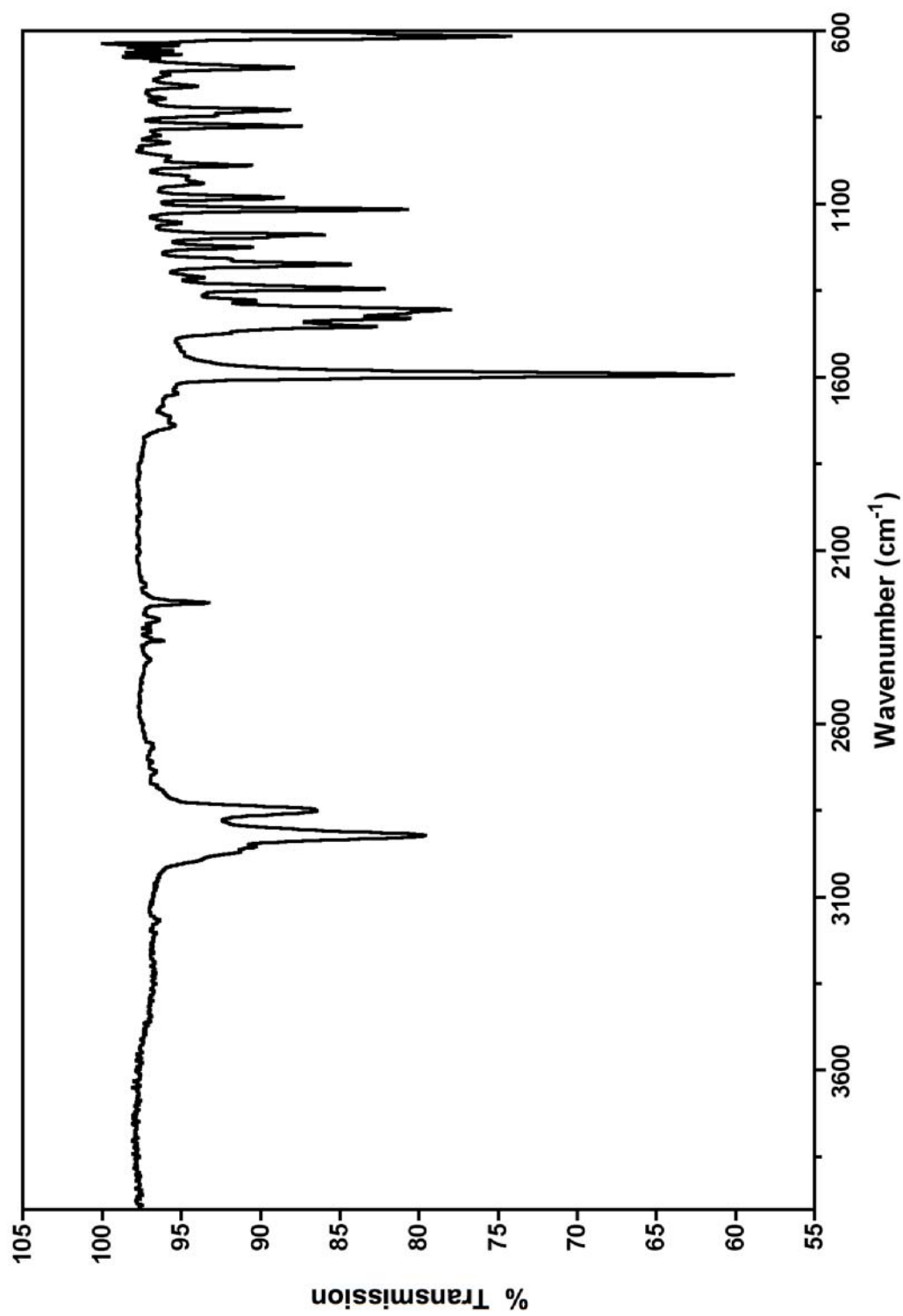
<sup>13</sup>C NMR Spectrum (2).



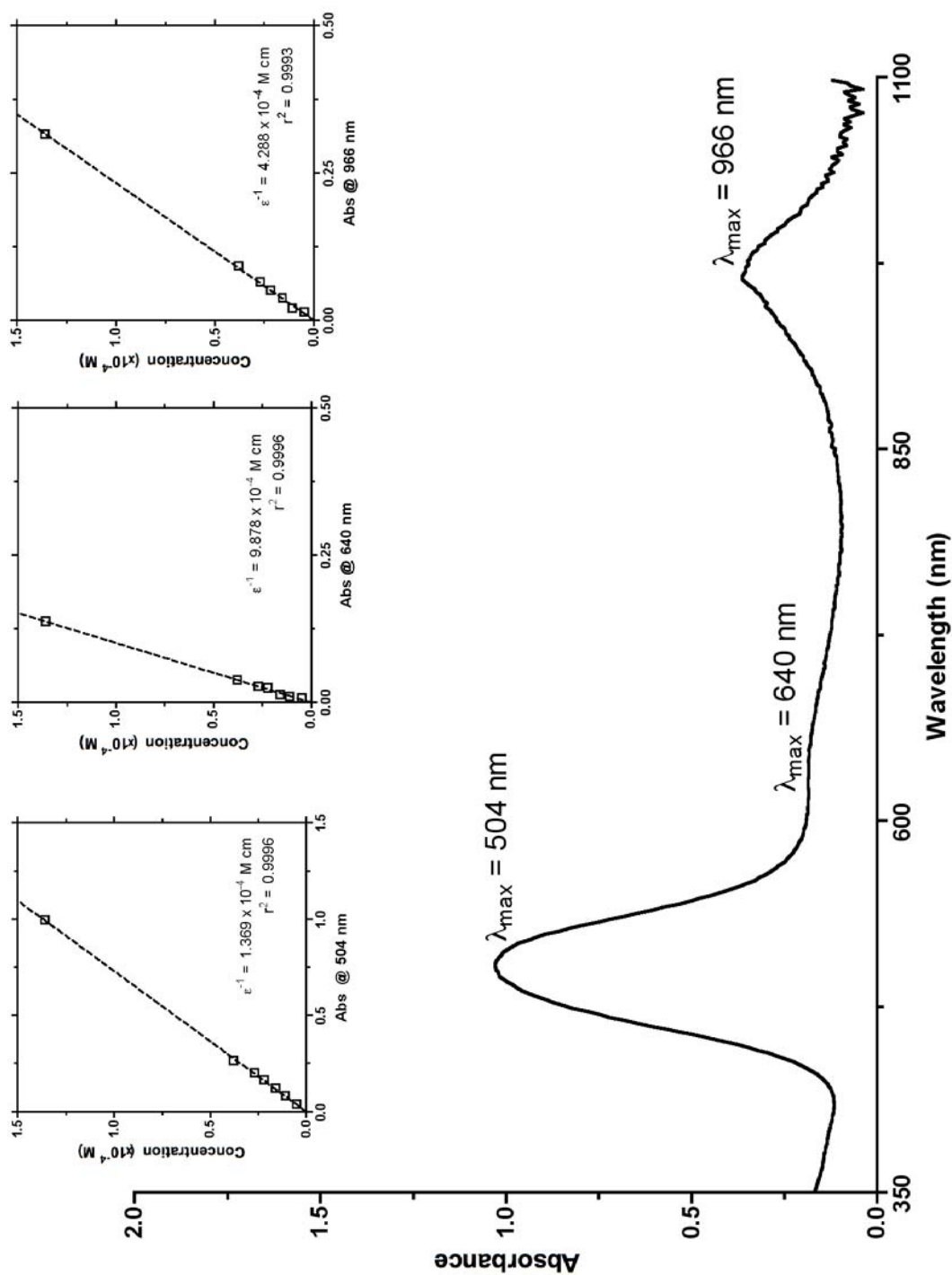
Electronic Absorption Spectrum & Molar Absorptivity (2, 350 – 1000 nm).



Vibrational Spectrum (2) (4000 – 600  $\text{cm}^{-1}$ ).

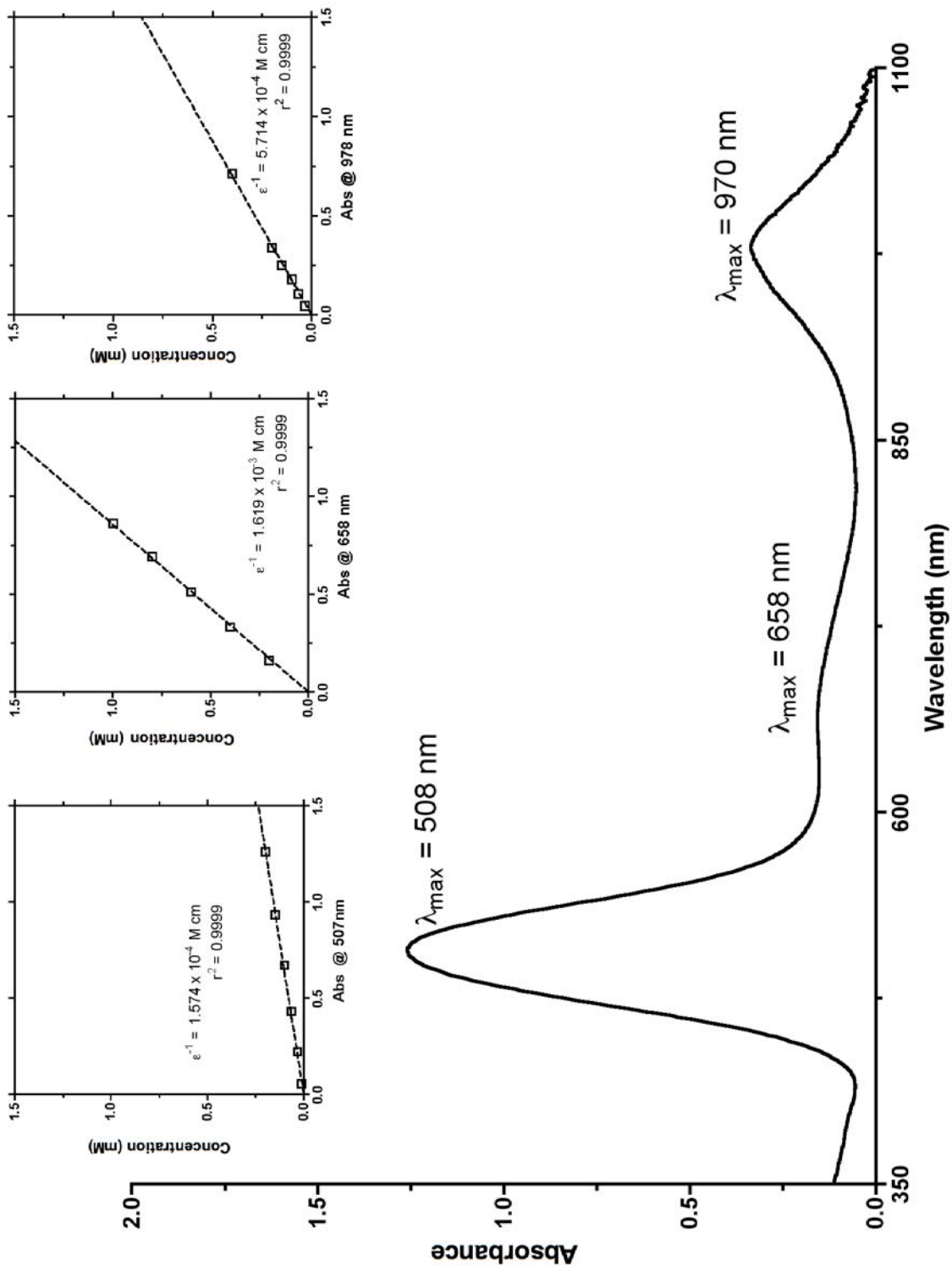


Electronic Absorption Spectrum & Molar Absorptivity (3, 350 – 1100 nm).





Electronic Absorption Spectrum & Molar Absorptivity (9, 375 – 1100 nm).



## XRD and XPS Data.

Crystallographer's<sup>46</sup> Report  $[\text{Rh}_2(\text{cap})_4\text{Ph}_2]\cdot 2\text{CH}_2\text{Cl}_2$ , CCDC #615577.

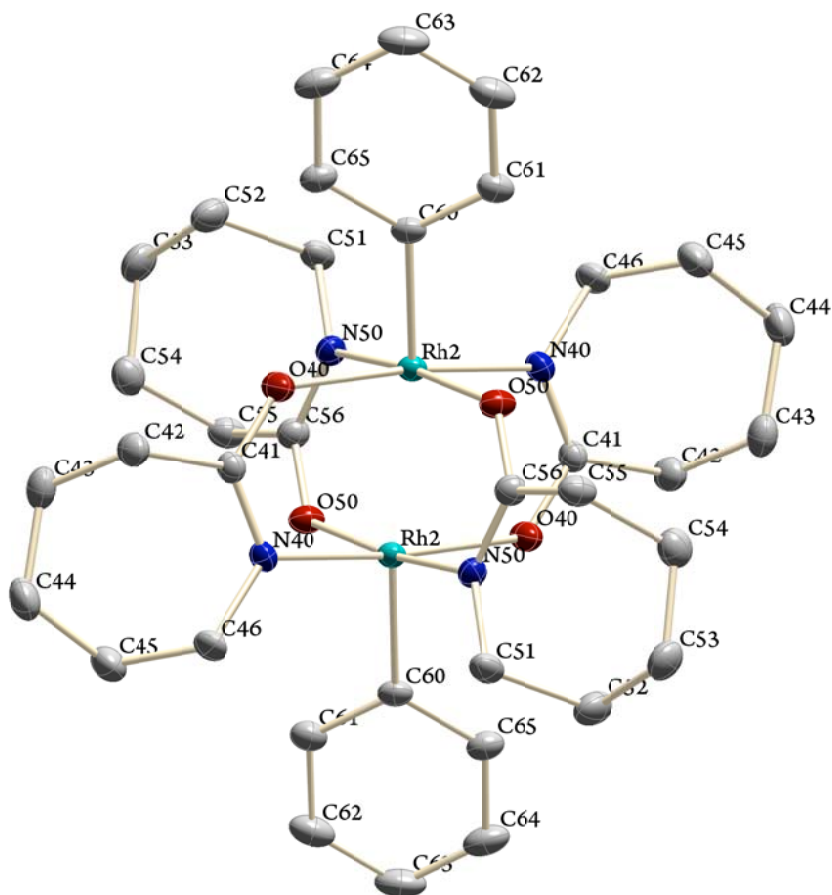


**Figure 1-15.** A view of  $[\text{Rh}_2(\text{cap})_4\text{Ph}_2]\cdot 2\text{CH}_2\text{Cl}_2$  showing the numbering scheme. Anisotropic atomic displacement ellipsoids for the non-hydrogen atoms are shown at the 30% probability level. Hydrogen atoms are omitted for clarity.

---

<sup>46</sup> See ref. 39.

A green prism of  $C_{36}H_{50}N_4O_4Rh_2 \cdot 2CH_2Cl_2$ , approximate dimensions  $0.20 \times 0.22 \times 0.345 \text{ mm}^3$ , was used for the X-ray crystallographic analysis. The X-ray intensity data were measured at 223(2) K on a three-circle diffractometer system equipped with Bruker Smart1000 CCD area detector using a graphite monochromator and a Mo  $K_\alpha$  fine-focus sealed tube ( $\lambda = 0.71073 \text{ \AA}$ ) operated at 50 kV and 20 mA. The detector was placed at a distance of 4.958 cm from the crystal.

A total of 3074 frames were collected with a scan width of  $0.3^\circ$  in  $\omega$  and an exposure time of 13 sec/frame using SMART.<sup>47</sup> The total data collection time was 17.21 hours. The frames were integrated with SAINT software<sup>48</sup> package using a narrow-frame integration algorithm. The integration of the data using a Triclinic unit cell yielded a total of 27474 reflections to a maximum  $\theta$  angle of  $27.50^\circ$ , of which 9583 were independent (completeness = 98.8%,  $R_{\text{int}} = 2.20\%$ ,  $R_{\text{sig}} = 2.27\%$ ) and 8323 were greater than  $2\sigma(I)$ . The final cell dimensions of  $a = 10.9770(3) \text{ \AA}$ ,  $b = 13.1258(4) \text{ \AA}$ ,  $c = 16.0022(5) \text{ \AA}$ ,  $\alpha = 78.8840(10)^\circ$ ,  $\beta = 74.4100(10)^\circ$ ,  $\gamma = 73.1860(10)^\circ$ , and  $V = 2109.25(11) \text{ \AA}^3$  are based upon the refinement of the XYZ-centroids of 7880 reflections with  $2.2 < \theta < 29.5^\circ$  using SAINT. Analysis of the data showed 0.14 % decay during data collection. Data were corrected for absorption effects with the Semi-empirical from equivalents method using SADABS.<sup>49</sup> The minimum and maximum transmission coefficients were 0.685 and 0.806.

The structure was solved and refined using the SHELXS-97 and SHELXL-97 software<sup>50</sup> in the space group  $P1$  with  $Z = 2$  for the formula unit  $C_{36}H_{50}N_4O_4Rh_2 \cdot 2CH_2Cl_2$ . The final anisotropic full-matrix least-squares

---

<sup>47</sup> See ref. 40.

<sup>48</sup> See ref. 40.

<sup>49</sup> See ref. 42.

<sup>50</sup> See ref. 41.

refinement on  $F^2$  with 527 variables converged at  $R_1 = 3.00\%$  for the observed data and  $wR_2 = 6.87\%$  for all data. The goodness-of-fit was 1.000. The largest peak on the final difference map was  $1.584\bar{e}/\text{\AA}^3$  and the largest hole was  $-1.001\bar{e}/\text{\AA}^3$ . On the basis of the final model, the calculated density was  $1.541\text{ g/cm}^3$  and  $F(000)$ ,  $1000\bar{e}$ .

**Table 1-5.** Crystal data and structure refinement for  $[\text{Rh}_2(\text{cap})_4\text{Ph}_2]\cdot 2\text{CH}_2\text{Cl}_2$ .

Empirical formula	$\text{C}_{36}\text{H}_{50}\text{N}_4\text{O}_4\text{Rh}_2\cdot 2\text{CH}_2\text{Cl}_2$	
Formula weight (amu)	978.47	
Temperature ( $^\circ\text{K}$ )	223(2)	
Wavelength ( $\text{\AA}$ )	0.71073	
Crystal size ( $\text{mm}^3$ )	$0.345 \times 0.22 \times 0.20$	
Crystal habit	green prism	
Crystal system	Triclinic	
Space group	$P1$	
Unit cell dimensions ( $\text{\AA}^\circ$ )	$a = 10.9770(3)$	$\alpha = 78.884(1)$
	$b = 13.1258(4)$	$\beta = 74.410(1)$
	$c = 16.0022(5)$	$\gamma = 73.186(1)$
Volume ( $\text{\AA}^3$ )	2109.25(11)	
Z	2	
Density, $\rho_{\text{calc}}$ ( $\text{g/cm}^3$ )	1.541	
Absorption coefficient, $\mu$ ( $\text{mm}^{-1}$ )	1.078	
$\theta$ Range ( $^\circ$ )	2.63 to 27.50	
Reflections collected	27474	
Independent reflections	9583	
Observed reflection, $I > 2\sigma(I)$	8323	
Max. and min. transmission <sup>a</sup>	0.806 and 0.685	
Goodness-of-fit on $F^2$	1.000	
Max $[\Delta/\sigma]$	0.002	
Final R indices: <sup>b</sup>		
$R_1, I > 2\sigma(I)$	0.0300	
$wR_2, \text{all data}$	0.0687	
$R_{\text{int}}$	0.0220	
$R_{\text{sig}}$	0.0227	
Min., max. peaks ( $\bar{e}/\text{\AA}^3$ )	1.584 and -1.001	

<sup>a</sup>Absorption correction was performed using the semi-empirical from equivalents method (SADABS). <sup>b</sup>Function minimized was  $\sum w(F_o^2 - F_c^2)^2$  where  $R_1 = \sum ||F_o| - |F_c|| / \sum |F_o|$ ,  $wR_2 = [\sum w(F_o^2 - F_c^2)^2 / \sum w(F_o^2)^2]^{1/2}$  with a weighting scheme  $w = 1/[\sigma^2(F_o^2) + (0.015P)^2 + 27.8P]$ ,  $P = [\max(F_o^2, 0) + 2F_o^2]/3$ .

**Table 1-6.** Atomic coordinates and equivalent isotropic atomic displacement parameters ( $\text{\AA}^2$ ) for  $[\text{Rh}_2(\text{cap})_4\text{Ph}_2]\cdot 2\text{CH}_2\text{Cl}_2$ .

Atom	<i>x/a</i>	<i>y/b</i>	<i>z/c</i>	$U_{\text{eq}}$
Rh1	0.537221(16)	0.584836(13)	0.970615(11)	0.02413(5)
O10	0.49649(17)	0.41192(13)	0.89538(11)	0.0328(4)
N10	0.5579(2)	0.56920(16)	0.84459(13)	0.0306(4)
C11	0.5308(2)	0.48288(19)	0.83264(16)	0.0314(5)
C12	0.5415(3)	0.4575(2)	0.74243(17)	0.0439(7)
C13	0.6792(4)	0.4369(3)	0.6862(2)	0.0586(9)
C14	0.7201(4)	0.5392(3)	0.6432(2)	0.0700(11)
C15	0.7194(4)	0.6116(3)	0.7072(2)	0.0660(10)
C16	0.5900(3)	0.6490(2)	0.76948(18)	0.0464(7)
N20	0.35704(19)	0.68076(15)	0.97360(13)	0.0292(4)
O20	0.28582(16)	0.52883(13)	1.03016(13)	0.0377(4)
C21	0.2647(2)	0.63041(19)	1.00429(17)	0.0327(5)
C22	0.1220(2)	0.6883(2)	1.0143(2)	0.0469(7)
C23	0.0740(3)	0.7692(2)	1.0803(2)	0.0533(8)
C24	0.1079(3)	0.8750(2)	1.0435(2)	0.0527(8)
C25	0.2534(3)	0.8680(2)	1.0127(2)	0.0481(7)
C26	0.3257(3)	0.79574(19)	0.94143(17)	0.0360(5)
C30	0.6442(2)	0.69023(18)	0.95839(15)	0.0285(5)
C31	0.7677(2)	0.67518(19)	0.90414(16)	0.0326(5)
C32	0.8413(2)	0.7483(2)	0.89794(18)	0.0388(6)
C33	0.7928(3)	0.8334(2)	0.94622(19)	0.0414(6)
C34	0.6701(3)	0.8469(2)	1.00153(19)	0.0411(6)
C35	0.5956(2)	0.77454(19)	1.00851(17)	0.0343(5)
Rh2	0.069546(18)	0.065600(14)	0.485535(12)	0.02830(5)
N40	0.1708(2)	0.02826(17)	0.36586(13)	0.0329(4)
O40	0.05038(18)	-0.09518(16)	0.39182(12)	0.0417(4)
C41	0.1393(2)	-0.0494(2)	0.34341(16)	0.0353(5)
C42	0.2062(3)	-0.0944(2)	0.25725(18)	0.0454(7)
C43	0.3523(3)	-0.1454(2)	0.2478(2)	0.0518(7)
C44	0.4341(3)	-0.0645(3)	0.2195(2)	0.0598(9)
C45	0.4057(3)	0.0141(3)	0.2853(2)	0.0583(8)
C46	0.2658(3)	0.0823(2)	0.30495(18)	0.0417(6)
N50	-0.0603(2)	0.18646(16)	0.43364(13)	0.0323(4)
O50	-0.19230(17)	0.07101(14)	0.46299(12)	0.0374(4)
C51	-0.0381(3)	0.2921(2)	0.39397(19)	0.0412(6)
C52	-0.1245(3)	0.3849(2)	0.4440(2)	0.0530(8)
C53	-0.2630(3)	0.4263(2)	0.4300(2)	0.0531(8)
C54	-0.3400(3)	0.3416(2)	0.4535(2)	0.0490(7)
C55	-0.2787(3)	0.2468(2)	0.40021(19)	0.0432(6)
C56	-0.1688(2)	0.1637(2)	0.43370(16)	0.0343(5)
C60	0.1784(3)	0.1453(2)	0.51616(17)	0.0350(5)
C61	0.3137(3)	0.1082(2)	0.49715(19)	0.0426(6)
C62	0.3891(3)	0.1618(3)	0.5209(2)	0.0554(8)
C63	0.3312(4)	0.2510(3)	0.5637(2)	0.0606(9)
C64	0.1976(4)	0.2871(3)	0.5835(2)	0.0558(8)
C65	0.1195(3)	0.2352(2)	0.56062(18)	0.0417(6)
C1A	0.213(2)	0.4023(9)	0.8676(10)	0.052(3)
Cl1A	0.1024(4)	0.5255(3)	0.8460(3)	0.0986(12)
Cl2A	0.2587(8)	0.3250(6)	0.7835(6)	0.0680(12)
C1B	0.204(2)	0.4324(12)	0.8709(9)	0.060(5)
Cl1B	0.1799(12)	0.5670(9)	0.8237(5)	0.097(3)
Cl2B	0.2165(11)	0.3483(9)	0.7970(8)	0.098(4)
C1C	0.167(4)	0.4684(18)	0.8763(12)	0.050(8)

Cl1C	0.2004(14)	0.5900(12)	0.8220(11)	0.048(3)
Cl2C	0.150(4)	0.392(3)	0.8058(13)	0.118(7)
C1	0.1726(5)	-0.0018(4)	0.7238(2)	0.0861(14)
Cl1	0.08958(8)	-0.10016(7)	0.77885(5)	0.05588(19)
Cl2	0.22712(11)	0.05314(9)	0.79072(7)	0.0813(3)

\*  $U_{eq}$  is defined as one third of the trace of the orthogonalized  $U_{ij}$  tensor.

**Table 1-7.** Anisotropic atomic displacement parameters ( $\text{\AA}^2$ ) for  $[\text{Rh}_2(\text{cap})_4\text{Ph}_2]\cdot 2\text{CH}_2\text{Cl}_2$ .

Atom	$U_{11}$	$U_{22}$	$U_{33}$	$U_{23}$	$U_{13}$	$U_{12}$
Rh1	0.02523(9)	0.01834(8)	0.02942(9)	-0.00229(6)	-0.00480(7)	-0.00813(6)
O10	0.0429(9)	0.0310(9)	0.0298(8)	-0.0021(7)	-0.0068(7)	-0.0202(7)
N10	0.0378(11)	0.0269(10)	0.0278(10)	-0.0027(8)	-0.0034(8)	-0.0135(8)
C11	0.0348(12)	0.0312(12)	0.0299(12)	-0.0037(10)	-0.0048(10)	-0.0135(10)
C12	0.0664(18)	0.0431(15)	0.0315(13)	-0.0059(11)	-0.0088(13)	-0.0292(14)
C13	0.080(2)	0.057(2)	0.0421(16)	-0.0217(15)	0.0105(16)	-0.0343(18)
C14	0.095(3)	0.076(2)	0.0443(18)	-0.0209(17)	0.0189(18)	-0.053(2)
C15	0.091(3)	0.070(2)	0.0475(18)	-0.0168(16)	0.0141(17)	-0.058(2)
C16	0.075(2)	0.0330(14)	0.0333(14)	0.0018(11)	-0.0069(13)	-0.0263(14)
N20	0.0290(9)	0.0192(9)	0.0388(11)	-0.0022(8)	-0.0095(8)	-0.0046(7)
O20	0.0265(8)	0.0218(8)	0.0633(12)	-0.0033(8)	-0.0094(8)	-0.0059(6)
C21	0.0282(11)	0.0243(11)	0.0455(14)	-0.0070(10)	-0.0091(10)	-0.0042(9)
C22	0.0285(12)	0.0304(13)	0.081(2)	-0.0097(14)	-0.0133(13)	-0.0044(10)
C23	0.0337(14)	0.0426(16)	0.072(2)	-0.0114(15)	-0.0018(14)	0.0011(12)
C24	0.0467(16)	0.0339(15)	0.074(2)	-0.0208(14)	-0.0144(15)	0.0045(12)
C25	0.0483(16)	0.0279(13)	0.071(2)	-0.0143(13)	-0.0165(15)	-0.0054(12)
C26	0.0395(13)	0.0224(12)	0.0449(14)	0.0011(10)	-0.0134(11)	-0.0059(10)
C30	0.0311(11)	0.0221(11)	0.0333(12)	-0.0042(9)	-0.0097(9)	-0.0054(9)
C31	0.0323(12)	0.0264(12)	0.0383(13)	-0.0043(10)	-0.0032(10)	-0.0104(9)
C32	0.0314(12)	0.0385(14)	0.0462(15)	-0.0004(12)	-0.0025(11)	-0.0176(11)
C33	0.0435(14)	0.0367(14)	0.0508(16)	-0.0023(12)	-0.0093(12)	-0.0236(12)
C34	0.0488(15)	0.0320(13)	0.0478(15)	-0.0114(12)	-0.0055(12)	-0.0191(12)
C35	0.0347(12)	0.0294(12)	0.0402(13)	-0.0064(10)	-0.0030(10)	-0.0141(10)
Rh2	0.03112(10)	0.02588(10)	0.02839(10)	-0.00213(7)	-0.00425(7)	-0.01101(7)
N40	0.0337(10)	0.0336(11)	0.0285(10)	-0.0031(8)	-0.0006(8)	-0.0105(9)
O40	0.0457(10)	0.0493(11)	0.0346(9)	-0.0132(8)	0.0010(8)	-0.0231(9)
C41	0.0358(13)	0.0392(14)	0.0295(12)	-0.0060(10)	-0.0026(10)	-0.0105(11)
C42	0.0499(16)	0.0524(17)	0.0356(14)	-0.0143(13)	-0.0008(12)	-0.0180(13)
C43	0.0551(18)	0.0470(17)	0.0439(16)	-0.0149(13)	-0.0023(14)	-0.0005(14)
C44	0.0390(16)	0.073(2)	0.060(2)	-0.0244(17)	0.0054(14)	-0.0067(15)
C45	0.0408(16)	0.071(2)	0.063(2)	-0.0209(17)	0.0064(14)	-0.0220(15)
C46	0.0459(15)	0.0375(14)	0.0367(14)	-0.0005(11)	0.0028(12)	-0.0167(12)
N50	0.0338(10)	0.0252(10)	0.0353(11)	-0.0010(8)	-0.0072(9)	-0.0058(8)
O50	0.0406(10)	0.0303(9)	0.0444(10)	0.0026(8)	-0.0167(8)	-0.0121(7)
C51	0.0399(14)	0.0323(13)	0.0473(15)	0.0062(11)	-0.0064(12)	-0.0135(11)
C52	0.0545(18)	0.0321(15)	0.074(2)	-0.0085(14)	-0.0187(16)	-0.0091(13)
C53	0.0596(19)	0.0332(15)	0.061(2)	-0.0081(14)	-0.0168(16)	0.0003(13)
C54	0.0409(15)	0.0456(17)	0.0530(17)	-0.0020(13)	-0.0111(13)	-0.0015(12)
C55	0.0433(15)	0.0366(14)	0.0504(16)	0.0048(12)	-0.0176(13)	-0.0112(12)
C56	0.0364(13)	0.0314(13)	0.0341(13)	-0.0026(10)	-0.0082(10)	-0.0076(10)
C60	0.0416(13)	0.0315(13)	0.0360(13)	0.0019(10)	-0.0103(11)	-0.0180(11)
C61	0.0418(14)	0.0424(15)	0.0461(15)	0.0015(12)	-0.0112(12)	-0.0179(12)
C62	0.0488(17)	0.062(2)	0.063(2)	0.0099(16)	-0.0208(15)	-0.0302(15)
C63	0.074(2)	0.056(2)	0.072(2)	0.0075(17)	-0.0338(19)	-0.0401(18)

C64	0.082(2)	0.0401(16)	0.0575(19)	-0.0017(14)	-0.0274(17)	-0.0272(16)
C65	0.0519(16)	0.0340(14)	0.0450(15)	-0.0029(11)	-0.0166(13)	-0.0160(12)
C1A	0.053(7)	0.049(5)	0.053(7)	-0.004(4)	-0.014(5)	-0.010(5)
C11A	0.090(3)	0.068(2)	0.114(3)	-0.0107(19)	-0.026(2)	0.0193(18)
C12A	0.076(3)	0.0628(19)	0.072(2)	-0.0224(15)	-0.016(2)	-0.0193(18)
C1B	0.044(9)	0.092(11)	0.045(7)	0.003(7)	-0.016(5)	-0.022(9)
C11B	0.116(6)	0.084(4)	0.062(3)	-0.018(3)	-0.025(4)	0.028(3)
C12B	0.117(9)	0.103(7)	0.096(6)	0.002(5)	-0.032(6)	-0.063(7)
C1C	0.049(16)	0.050(12)	0.044(12)	-0.002(9)	-0.006(10)	-0.010(12)
C11C	0.048(4)	0.052(5)	0.044(4)	0.009(3)	-0.013(3)	-0.019(4)
C12C	0.166(16)	0.143(13)	0.085(6)	-0.012(8)	-0.019(9)	-0.112(12)
C1	0.128(4)	0.110(3)	0.050(2)	0.015(2)	-0.028(2)	-0.084(3)
Cl1	0.0634(5)	0.0621(5)	0.0484(4)	0.0013(4)	-0.0153(4)	-0.0281(4)
Cl2	0.0884(7)	0.0881(7)	0.0842(7)	-0.0146(6)	-0.0193(6)	-0.0459(6)

\* The anisotropic atomic displacement factor exponent takes the form:  $-2\pi^2 [ h^2a^2U_{11} + \dots + 2hka^*b^*U_{12} ]$ .

**Table 1-8.** Hydrogen atom coordinates and isotropic atomic displacement parameters ( $\text{\AA}^2$ ) for  $[\text{Rh}_2(\text{cap})_4\text{Ph}_2]\cdot 2\text{CH}_2\text{Cl}_2$ .

Atom	<i>x/a</i>	<i>y/b</i>	<i>z/c</i>	$U_{\text{iso}}$
H12A	0.4855	0.5175	0.7126	0.053
H12B	0.5085	0.3940	0.7483	0.053
H13A	0.6854	0.3941	0.6407	0.070
H13B	0.7400	0.3948	0.7225	0.070
H14A	0.6612	0.5796	0.6051	0.084
H14B	0.8084	0.5200	0.6061	0.084
H15A	0.7843	0.5730	0.7416	0.079
H15B	0.7475	0.6748	0.6736	0.079
H16A	0.5906	0.7135	0.7915	0.056
H16B	0.5207	0.6691	0.7370	0.056
H22A	0.0699	0.6352	1.0327	0.056
H22B	0.1075	0.7258	0.9573	0.056
H23A	-0.0211	0.7821	1.1005	0.064
H23B	0.1124	0.7383	1.1310	0.064
H24A	0.0705	0.9236	1.0885	0.063
H24B	0.0665	0.9068	0.9941	0.063
H25A	0.2936	0.8415	1.0630	0.058
H25B	0.2651	0.9403	0.9907	0.058
H26A	0.2721	0.8084	0.8986	0.043
H26B	0.4072	0.8160	0.9111	0.043
H31	0.8017	0.6165	0.8718	0.039
H32	0.9248	0.7392	0.8604	0.047
H33	0.8430	0.8822	0.9416	0.050
H34	0.6368	0.9050	1.0345	0.049
H35	0.5129	0.7828	1.0470	0.041
H42A	0.1938	-0.0363	0.2092	0.054
H42B	0.1640	-0.1483	0.2518	0.054
H43A	0.3673	-0.1857	0.3039	0.062
H43B	0.3810	-0.1964	0.2047	0.062
H44A	0.4185	-0.0239	0.1635	0.072
H44B	0.5267	-0.1030	0.2100	0.072
H45A	0.4260	-0.0266	0.3402	0.070
H45B	0.4644	0.0618	0.2631	0.070
H46A	0.2645	0.1458	0.3292	0.050
H46B	0.2375	0.1072	0.2498	0.050
H51A	-0.0528	0.3062	0.3346	0.049

H51B	0.0535	0.2897	0.3892	0.049
H52A	-0.1294	0.3620	0.5066	0.064
H52B	-0.0822	0.4445	0.4271	0.064
H53A	-0.3098	0.4851	0.4653	0.064
H53B	-0.2589	0.4557	0.3684	0.064
H54A	-0.4284	0.3751	0.4445	0.059
H54B	-0.3476	0.3146	0.5157	0.059
H55A	-0.3469	0.2120	0.4008	0.052
H55B	-0.2451	0.2740	0.3394	0.052
H61	0.3542	0.0470	0.4683	0.051
H62	0.4806	0.1369	0.5075	0.066
H63	0.3828	0.2870	0.5794	0.073
H64	0.1581	0.3480	0.6129	0.067
H65	0.0280	0.2604	0.5749	0.050
H111	0.2911	0.4158	0.8774	0.062
H112	0.1728	0.3626	0.9213	0.062
H121	0.2842	0.4111	0.8929	0.072
H122	0.1309	0.4252	0.9207	0.072
H131	0.2379	0.4277	0.9050	0.060
H132	0.0860	0.4831	0.9217	0.060
H11	0.2474	-0.0338	0.6793	0.103
H12	0.1139	0.0555	0.6936	0.103

**Table 1-9.** Site occupancy factors that deviate from unity for disordered solvent molecule of CH<sub>2</sub>Cl<sub>2</sub> in [Rh<sub>2</sub>(cap)<sub>4</sub>Ph<sub>2</sub>] $\cdot$ 2CH<sub>2</sub>Cl<sub>2</sub>.

Atom	sof	Atom	sof	Atom	sof
C1A	0.415(4)	C1A	0.415(4)	Cl2A	0.415(4)
C1B	0.427(16)	C1B	0.427(16)	Cl2B	0.427(16)
C1C	0.158(16)	C1C	0.158(16)	Cl2C	0.158(16)



**Table 1-10.** Bond lengths (Å) and angles (°) for [Rh<sub>2</sub>(cap)<sub>4</sub>Ph<sub>2</sub>]**•**2CH<sub>2</sub>Cl<sub>2</sub>.

Rh1-N20	2.0078(19)	Rh1-C30	2.010(2)	Rh1-N10	2.012(2)
Rh1-O20#1	2.0777(16)	Rh1-O10#1	2.0825(16)	Rh1-Rh1#1	2.5188(3)
O10-C11	1.287(3)	O10-Rh1#1	2.0825(16)	N10-C11	1.311(3)
N10-C16	1.471(3)	C11-C12	1.510(3)	C12-C13	1.514(4)
C13-C14	1.519(4)	C14-C15	1.522(4)	C15-C16	1.510(5)
N20-C21	1.304(3)	N20-C26	1.468(3)	O20-C21	1.290(3)
O20-Rh1#1	2.0777(16)	C21-C22	1.509(3)	C22-C23	1.526(4)
C23-C24	1.511(4)	C24-C25	1.520(4)	C25-C26	1.524(4)
C30-C31	1.382(3)	C30-C35	1.387(3)	C31-C32	1.397(3)
C32-C33	1.377(4)	C33-C34	1.382(4)	C34-C35	1.394(3)
Rh2-C60	2.000(2)	Rh2-N40	2.011(2)	Rh2-N50	2.014(2)
Rh2-O50#2	2.0829(17)	Rh2-O40#2	2.0845(18)	Rh2-Rh2#2	2.5189(3)
N40-C41	1.304(3)	N40-C46	1.468(3)	O40-C41	1.291(3)
O40-Rh2#2	2.0845(18)	C41-C42	1.519(4)	C42-C43	1.526(4)
C43-C44	1.512(5)	C44-C45	1.525(4)	C45-C46	1.521(4)
N50-C56	1.309(3)	N50-C51	1.468(3)	O50-C56	1.290(3)
O50-Rh2#2	2.0829(17)	C51-C52	1.525(4)	C52-C53	1.522(4)
C53-C54	1.518(4)	C54-C55	1.531(4)	C55-C56	1.515(4)
C60-C61	1.390(4)	C60-C65	1.397(4)	C61-C62	1.390(4)
C62-C63	1.374(5)	C63-C64	1.372(5)	C64-C65	1.391(4)
C1A-C12A	1.720(7)	C1A-C11A	1.756(9)	C1B-C12B	1.722(7)
C1B-C11B	1.756(8)	C1C-C12C	1.719(9)	C1C-C11C	1.753(9)
C1-C12	1.707(3)	C1-C11	1.756(3)		
N20-Rh1-C30	102.43(8)	N20-Rh1-N10	90.29(8)	C30-Rh1-N10	101.12(9)
N20-Rh1-O20#1	173.56(7)	C30-Rh1-O20#1	84.00(8)	N10-Rh1-O20#1	88.82(8)
N20-Rh1-O10#1	88.56(8)	C30-Rh1-O10#1	85.38(8)	N10-Rh1-O10#1	173.50(7)
O20#1-Rh1-O10#1	91.61(7)	N20-Rh1-Rh1#1	95.32(5)	C30-Rh1-Rh1#1	156.19(7)
N10-Rh1-Rh1#1	94.46(5)	O20#1-Rh1-Rh1#1	78.39(5)	O10#1-Rh1-Rh1#1	79.29(4)
C11-O10-Rh1#1	128.11(15)	C11-N10-C16	120.0(2)	C11-N10-Rh1	114.45(16)
C16-N10-Rh1	125.37(16)	O10-C11-N10	123.6(2)	O10-C11-C12	114.5(2)
N10-C11-C12	121.9(2)	C11-C12-C13	114.0(2)	C12-C13-C14	113.1(3)
C13-C14-C15	114.3(3)	C16-C15-C14	115.6(3)	N10-C16-C15	114.6(3)
C21-N20-C26	120.6(2)	C21-N20-Rh1	113.51(15)	C26-N20-Rh1	125.82(16)
C21-O20-Rh1#1	128.97(15)	O20-C21-N20	123.8(2)	O20-C21-C22	114.2(2)
N20-C21-C22	122.0(2)	C21-C22-C23	113.7(2)	C24-C23-C22	113.3(3)
C23-C24-C25	114.8(2)	C24-C25-C26	114.9(2)	N20-C26-C25	114.2(2)
C31-C30-C35	120.5(2)	C31-C30-Rh1	120.13(17)	C35-C30-Rh1	119.29(17)
C30-C31-C32	119.2(2)	C33-C32-C31	120.7(2)	C32-C33-C34	119.8(2)
C33-C34-C35	120.2(2)	C30-C35-C34	119.6(2)	C60-Rh2-N40	102.31(10)
C60-Rh2-N50	101.52(9)	N40-Rh2-N50	91.15(8)	C60-Rh2-O50#2	84.99(9)
N40-Rh2-O50#2	87.70(8)	N50-Rh2-O50#2	173.49(7)	C60-Rh2-O40#2	84.21(9)
N40-Rh2-O40#2	173.48(7)	N50-Rh2-O40#2	87.57(8)	O50#2-Rh2-O40#2	92.86(8)
C60-Rh2-Rh2#2	155.37(7)	N40-Rh2-Rh2#2	96.36(6)	N50-Rh2-Rh2#2	93.97(6)
O50#2-Rh2-Rh2#2	79.81(5)	O40#2-Rh2-Rh2#2	77.37(5)	C41-N40-C46	120.8(2)
C41-N40-Rh2	112.54(16)	C46-N40-Rh2	126.59(17)	C41-O40-Rh2#2	130.07(16)
O40-C41-N40	123.6(2)	O40-C41-C42	114.2(2)	N40-C41-C42	122.2(2)
C41-C42-C43	113.9(2)	C44-C43-C42	113.3(3)	C43-C44-C45	113.7(3)
C46-C45-C44	114.9(3)	N40-C46-C45	115.2(2)	C56-N50-C51	120.1(2)
C56-N50-Rh2	114.96(16)	C51-N50-Rh2	124.92(16)	C56-O50-Rh2#2	127.54(16)
N50-C51-C52	114.7(2)	C53-C52-C51	115.5(3)	C54-C53-C52	113.9(2)
C53-C54-C55	113.8(3)	C56-C55-C54	113.8(2)	O50-C56-N50	123.7(2)
O50-C56-C55	114.6(2)	N50-C56-C55	121.7(2)	C61-C60-C65	119.4(2)
C61-C60-Rh2	119.9(2)	C65-C60-Rh2	120.6(2)	C60-C61-C62	119.9(3)
C63-C62-C61	120.7(3)	C64-C63-C62	119.5(3)	C63-C64-C65	121.1(3)
C64-C65-C60	119.3(3)	Cl2A-C1A-C11A	112.4(6)	Cl2B-C1B-C11B	111.8(6)
Cl2C-C1C-C11C	111.9(9)	Cl2-C1-C11	113.8(2)		

Symmetry transformation codes: #1 -x+1,-y+1,-z+2 #2 -x,-y,-z+1

**Table 1-11.** Torsion angles (°) for [Rh<sub>2</sub>(cap)<sub>4</sub>Ph<sub>2</sub>]**•**2CH<sub>2</sub>Cl<sub>2</sub>.

N20-Rh1-N10-C11	-96.24(18)	C30-Rh1-N10-C11	161.03(18)	O20#1-Rh1-N10-C11	77.38(18)
Rh1#1-Rh1-N10-C11	-0.88(18)	N20-Rh1-N10-C16	78.9(2)	C30-Rh1-N10-C16	-23.8(2)
O20#1-Rh1-N10-C16	107.5(2)	Rh1#1-Rh1-N10-C16	174.3(2)	Rh1#1-O10-C11-N10	4.2(4)
Rh1#1-O10-C11-C12	177.55(17)	C16-N10-C11-O10	-176.9(2)	Rh1-N10-C11-O10	-1.5(3)
C16-N10-C11-C12	4.9(4)	Rh1-N10-C11-C12	-179.7(2)	O10-C11-C12-C13	-114.1(3)
N10-C11-C12-C13	64.2(4)	C11-C12-C13-C14	-81.4(4)	C12-C13-C14-C15	60.7(5)
C13-C14-C15-C16	-58.5(5)	C11-N10-C16-C15	-69.2(3)	Rh1-N10-C16-C15	115.9(2)
C14-C15-C16-N10	79.2(4)	C30-Rh1-N20-C21	-162.68(18)	N10-Rh1-N20-C21	95.87(18)
O10#1-Rh1-N20-C21	-77.73(18)	Rh1#1-Rh1-N20-C21	1.37(18)	C30-Rh1-N20-C26	20.3(2)
N10-Rh1-N20-C26	-81.2(2)	O10#1-Rh1-N20-C26	105.21(19)	Rh1#1-Rh1-N20-C26	-175.70(19)
Rh1#1-O20-C21-N20	-1.7(4)	Rh1#1-O20-C21-C22	179.62(18)	C26-N20-C21-O20	177.0(2)
Rh1-N20-C21-O20	-0.2(3)	C26-N20-C21-C22	-4.4(4)	Rh1-N20-C21-C22	178.3(2)
O20-C21-C22-C23	114.5(3)	N20-C21-C22-C23	-64.2(4)	C21-C22-C23-C24	80.6(3)
C22-C23-C24-C25	-60.9(4)	C23-C24-C25-C26	58.9(4)	C21-N20-C26-C25	69.1(3)
Rh1-N20-C26-C25	-114.0(2)	C24-C25-C26-N20	-79.2(3)	N20-Rh1-C30-C31	-140.14(19)
N10-Rh1-C30-C31	-47.4(2)	O20#1-Rh1-C30-C31	40.25(19)	O10#1-Rh1-C30-C31	132.4(2)
Rh1#1-Rh1-C30-C31	82.6(3)	N20-Rh1-C30-C35	43.4(2)	N10-Rh1-C30-C35	136.16(19)
O20#1-Rh1-C30-C35	136.2(2)	O10#1-Rh1-C30-C35	-44.12(19)	Rh1#1-Rh1-C30-C35	-93.9(2)
C35-C30-C31-C32	-2.3(4)	Rh1-C30-C31-C32	-178.75(19)	C30-C31-C32-C33	1.1(4)
C31-C32-C33-C34	0.1(4)	C32-C33-C34-C35	0.0(4)	C31-C30-C35-C34	2.4(4)
Rh1-C30-C35-C34	178.9(2)	C33-C34-C35-C30	-1.3(4)	C60-Rh2-N40-C41	161.42(18)
N50-Rh2-N40-C41	-96.53(19)	O50#2-Rh2-N40-C41	77.06(18)	Rh2#2-Rh2-N40-C41	-2.41(18)
C60-Rh2-N40-C46	-21.8(2)	N50-Rh2-N40-C46	80.3(2)	O50#2-Rh2-N40-C46	-106.1(2)
Rh2#2-Rh2-N40-C46	174.4(2)	Rh2#2-O40-C41-N40	0.5(4)	Rh2#2-O40-C41-C42	179.94(18)
C46-N40-C41-O40	-175.3(2)	Rh2-N40-C41-O40	1.7(3)	C46-N40-C41-C42	5.3(4)
Rh2-N40-C41-C42	-177.7(2)	O40-C41-C42-C43	-117.2(3)	N40-C41-C42-C43	62.3(4)
C41-C42-C43-C44	-81.3(3)	C42-C43-C44-C45	63.2(4)	C43-C44-C45-C46	-60.1(4)
C41-N40-C46-C45	-68.4(3)	Rh2-N40-C46-C45	115.1(2)	C44-C45-C46-N40	78.8(4)
C60-Rh2-N50-C56	-158.50(19)	N40-Rh2-N50-C56	98.70(19)	O40#2-Rh2-N50-C56	-74.91(18)
Rh2#2-Rh2-N50-C56	2.24(18)	C60-Rh2-N50-C51	24.4(2)	N40-Rh2-N50-C51	-78.4(2)
O40#2-Rh2-N50-C51	107.9(2)	Rh2#2-Rh2-N50-C51	-174.90(19)	C56-N50-C51-C52	69.8(3)
Rh2-N50-C51-C52	-113.2(2)	N50-C51-C52-C53	-79.6(3)	C51-C52-C53-C54	58.0(4)
C52-C53-C54-C55	-60.4(4)	C53-C54-C55-C56	81.2(3)	Rh2#2-O50-C56-N50	-1.3(4)
Rh2#2-O50-C56-C55	179.81(17)	C51-N50-C56-O50	176.1(2)	Rh2-N50-C56-O50	-1.1(3)
C51-N50-C56-C55	-5.0(4)	Rh2-N50-C56-C55	177.67(19)	C54-C55-C56-O50	115.1(3)
C54-C55-C56-N50	-63.8(3)	N40-Rh2-C60-C61	-42.1(2)	N50-Rh2-C60-C61	-135.8(2)
O50#2-Rh2-C60-C61	44.4(2)	O40#2-Rh2-C60-C61	137.8(2)	Rh2#2-Rh2-C60-C61	96.3(3)
N40-Rh2-C60-C65	141.2(2)	N50-Rh2-C60-C65	47.4(2)	O50#2-Rh2-C60-C65	-132.3(2)
O40#2-Rh2-C60-C65	-38.9(2)	Rh2#2-Rh2-C60-C65	-80.4(3)	C65-C60-C61-C62	-1.3(4)
Rh2-C60-C61-C62	-178.0(2)	C60-C61-C62-C63	0.5(5)	C61-C62-C63-C64	0.2(5)
C62-C63-C64-C65	-0.2(5)	C63-C64-C65-C60	-0.5(5)	C61-C60-C65-C64	1.3(4)
Rh2-C60-C65-C64	178.0(2)				

Symmetry transformation codes: #1 -x+1,-y+1,-z+2 #2 -x,-y,-z+1

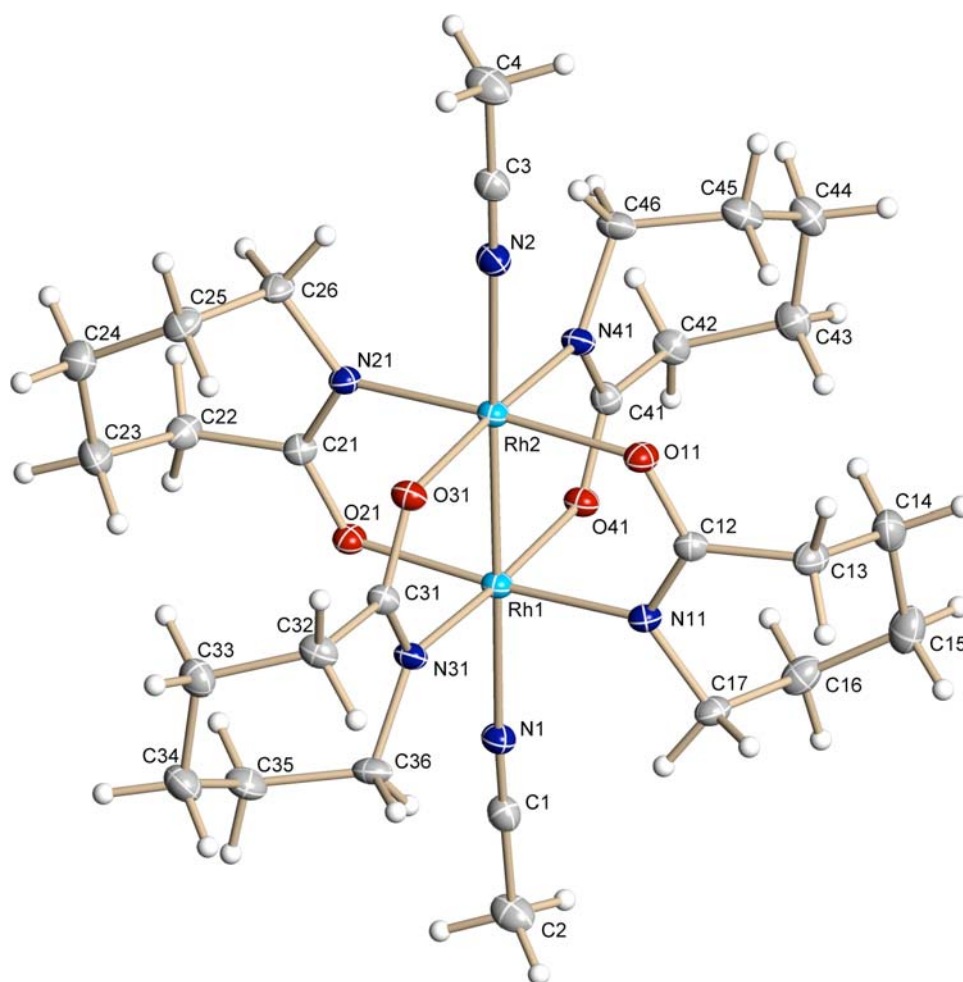


**Figure 1-16.** A view of  $[\text{Rh}_2(\text{cap})_4(\text{CH}_3\text{CN})_2] \cdot 2\text{CH}_3\text{CN}$  showing the numbering scheme. Anisotropic atomic displacement ellipsoids for the non-hydrogen atoms are shown at the 30% probability level. Hydrogen atoms are displayed with an arbitrarily small radius.

---

<sup>51</sup> See ref. 39.

A purple plate of  $C_{28}H_{46}N_6O_4Rh_2 \cdot 2(C_2H_3N)$ , approximate dimensions  $0.065 \times 0.220 \times 0.340 \text{ mm}^3$ , was used for the X-ray crystallographic analysis. The X-ray intensity data were measured at 223(2) K on a three-circle diffractometer system equipped with Bruker Smart1000 CCD area detector using a graphite monochromator and a Mo  $K_\alpha$  fine-focus sealed tube ( $\lambda = 0.71073 \text{ \AA}$ ) operated at 50 kV and 40 mA. The detector was placed at a distance of 4.958 cm from the crystal.

A total of 3124 frames were collected with a scan width of  $0.3^\circ$  in  $\omega$  and an exposure time of 15 sec/frame using SMART software package.<sup>52</sup> The total data collection time was 19.22 hours. The frames were integrated with SAINT software package<sup>53</sup> using a narrow-frame integration algorithm. The integration of the data using a monoclinic unit cell yielded a total of 36999 reflections to a maximum  $\theta$  angle of  $28.00^\circ$ , of which 8358 were independent (completeness = 97.7%,  $R_{\text{int}} = 6.82\%$ ,  $R_{\text{sig}} = 4.22\%$ ) and 6508 were greater than  $2\sigma(I)$ . The final cell dimensions of  $a = 9.3710(8) \text{ \AA}$ ,  $b = 15.8919(13) \text{ \AA}$ ,  $c = 23.994(2) \text{ \AA}$ ,  $\alpha = 90^\circ$ ,  $\beta = 97.408(2)^\circ$ ,  $\gamma = 90^\circ$ , and  $V = 3543.4(5) \text{ \AA}^3$  are based upon the refinement of the XYZ-centroids of 8854 reflections with  $2.5 < \theta < 29.8^\circ$  using SAINT. Analysis of the data showed -0.16 % decay during data collection. Data were corrected for absorption effects with the semi-empirical from equivalents method using XPREP. The minimum and maximum transmission coefficients were 0.703 and 0.938.

The structure was solved and refined using the SHELXS-97 and SHELXL-97 software<sup>54</sup> in the space group  $P 21/c$  with  $Z = 4$  for the formula unit  $C_{28}H_{46}N_6O_4Rh_2 \cdot 2(C_2H_3N)$ . The final anisotropic full-matrix least-squares refinement on  $F^2$  with 420 variables converged at  $R_1 = 4.29 \%$  for the

---

<sup>52</sup> See ref. 40.

<sup>53</sup> See ref. 40.

<sup>54</sup> See ref. 41.

observed data and  $wR_2 = 9.23\%$  for all data. The goodness-of-fit was 1.000. The largest peak on the final difference map was  $1.184\bar{e}/\text{\AA}^3$  and the largest hole was  $-0.824\bar{e}/\text{\AA}^3$ . On the basis of the final model, the calculated density was  $1.535\text{ g/cm}^3$  and  $F(000)$ ,  $1688\bar{e}$ .

**Disorder Description.** This structure was refined by duplicating main structure (Layer I, provided in this file) using  $x$ ,  $y+0.66$ ,  $z$  transformation (Layer II). The ratio of Layer I to Layer II was refined as  $0.908 : 0.092$  (~10:1). Pairs of the layers I+I and I+II are almost identical and are related to each other as a mirror image reflected perpendicularly to the crystallographic  $b$ -axis. The main structure has an ABABAB sequence of layers (Figure 1-17: Top). The secondary structure has an AAAA sequence of layers (Figure 1-17: Bottom). Thus, the crystal consists of mixed ABAB and AAAA stacking of layers in a 10:1 ratio. Because all pairs of adjacent layers are equivalent which satisfy vicinity conditions, this structure is an OD structure, according to Dornberger-Schiff.<sup>55</sup>

**Refinement.** The secondary structure from Layer II was constrained using SAME instruction to be the same as the main structure from Layer I. Thermal parameters were also restrained using DELU & ISOR instruction. The structure from Layer II should not be analyzed by itself as it represents only stacking of the layers perpendicularly to the  $b$ -axis. Thus, Layer I at  $z=0.25$  and Layer I at  $z=0.75$  form the A pair of the ABAB composite layer. Layer I at  $z=0.25$  and Layer II at  $z=0.75$  form the B pair to complete the ABAB composite layer.

---

<sup>55</sup> K. Dornberger-Schiff, H. Grezl-Niemann. *Acta Cryst.*, **14**, 167.

**Figure 1-17.** Top: a view of  $[\text{Rh}_2(\text{cap})_4(\text{CH}_3\text{CN})_2]$  ABAB Layer I; Bottom: Alternative AAAA stacking of  $[\text{Rh}_2(\text{cap})_4(\text{CH}_3\text{CN})_2]$  in Layer II of the OD structure; Anisotropic atomic displacement ellipsoids for the non-hydrogen atoms are shown at the 50% probability level. Hydrogen atoms are displayed with an arbitrarily small radius.

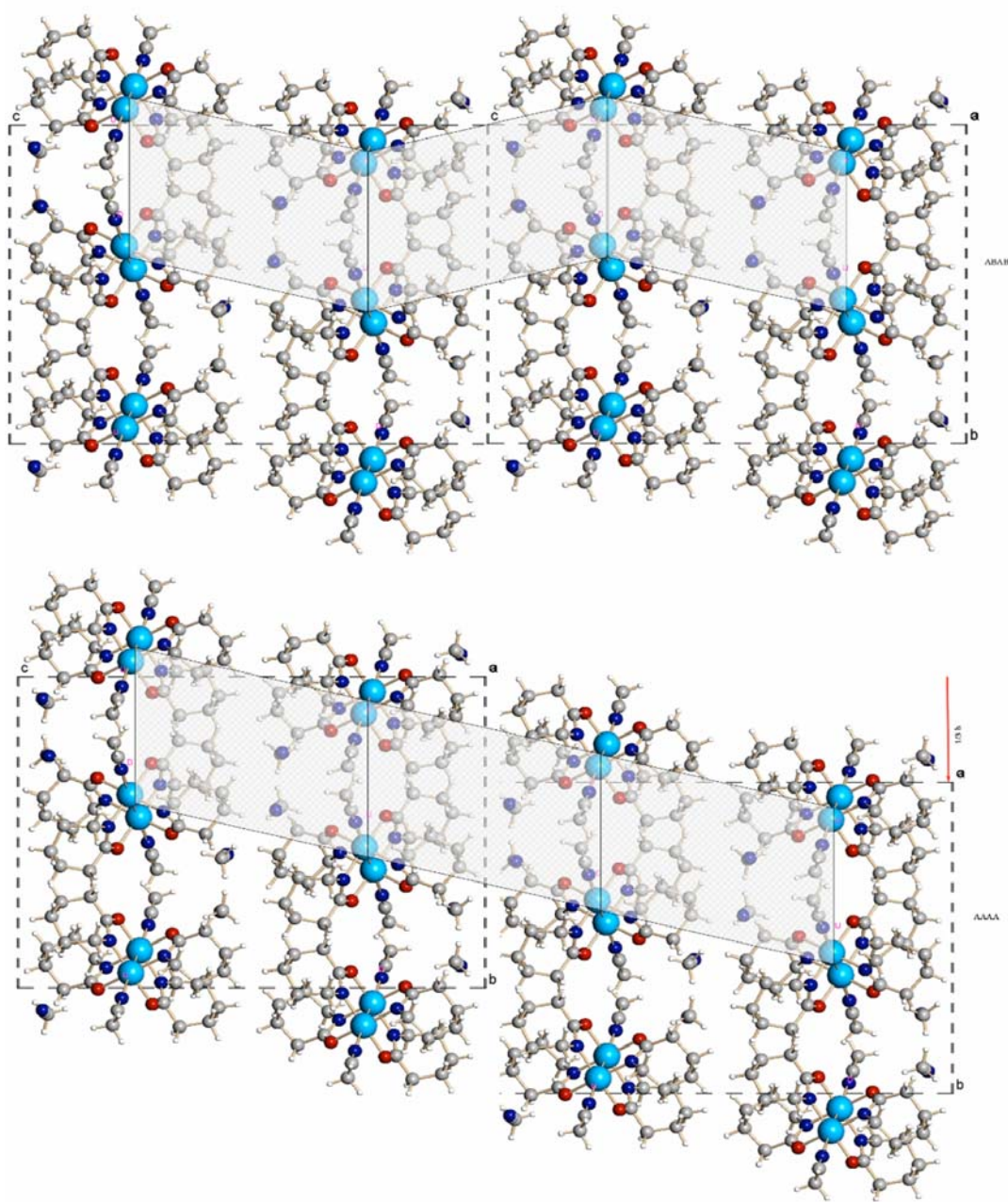


**Table 1-12.** Crystal data/structure refinement for [Rh<sub>2</sub>(cap)<sub>4</sub>(CH<sub>3</sub>CN)<sub>2</sub>]**•**2CH<sub>3</sub>CN.

Empirical formula	C <sub>32</sub> H <sub>52</sub> N <sub>8</sub> O <sub>4</sub> Rh <sub>2</sub>	
Formula weight (amu)	818.64	
Temperature (K)	223(2)	
Wavelength (Å)	0.71073	
Crystal size (mm <sup>3</sup> )	0.34×0.22×0.065	
Crystal habit	purple plate	
Crystal system	Monoclinic	
Space group	<i>P</i> 2 <sub>1</sub> / <i>c</i>	
Unit cell dimensions (Å/°)	<i>a</i> = 9.3710(8)	$\alpha$ = 90
	<i>b</i> = 15.8919(13)	$\beta$ = 97.408(2)
	<i>c</i> = 23.994(2)	$\gamma$ = 90
Volume (Å <sup>3</sup> )	3543.4(5)	
Z	4	
Density, $\rho_{\text{calc}}$ (g/cm <sup>3</sup> )	1.535	
Absorption coefficient, $\mu$ (mm <sup>-1</sup> )	0.978	
$\theta$ Range (°)	1.54 to 28.00	
Reflections collected	36999	
Independent reflections	8358	
Observed reflection, $I > 2\sigma(I)$	6508	
Max. and min. transmission <sup>a</sup>	0.938 and 0.703	
Goodness-of-fit on $F^2$	0.969	
Max [ $\Delta/\sigma$ ]	0.001	
Final R indices: <sup>b</sup>		
	$R_1, I > 2\sigma(I)$	0.0429
	$wR_2, \text{all data}$	0.0923
	$R_{\text{int}}$	0.0682
	$R_{\text{sig}}$	0.0422
Min., max. peaks ( $e/\text{\AA}^3$ )	1.184 and -0.824	

<sup>a</sup>Absorption correction was performed using the semi-empirical from equivalents method (SADABS). <sup>b</sup>Function minimized was  $\sum w(F_o^2 - F_c^2)^2$  where  $R_1 = \sum ||F_o| - |F_c|| / \sum |F_o|$ ,  $wR_2 = [\sum w(F_o^2 - F_c^2)^2 / \sum w(F_o^2)^2]^{1/2}$  with a weighting scheme  $w = 1/[\sigma^2(F_o^2) + (0.015P)^2 + 27.8P]$ ,  $P = [\max(F_o^2, 0) + 2F_o^2]/3$ .

**Table 1-13.** Atomic coordinates and equivalent isotropic atomic displacement parameters ( $\text{\AA}^2$ ) for  $[\text{Rh}_2(\text{cap})_4(\text{CH}_3\text{CN})_2] \cdot 2\text{CH}_3\text{CN}$ .

Atom	<i>x/a</i>	<i>y/b</i>	<i>z/c</i>	$U_{\text{eq}}$
Rh1	0.14847(3)	0.120491(16)	0.260737(11)	0.02709(7)
Rh2	0.36572(3)	0.048682(16)	0.242550(11)	0.02703(7)
N1	-0.0480(3)	0.20187(19)	0.27885(12)	0.0350(7)
C1	-0.1458(4)	0.2416(2)	0.28532(15)	0.0372(8)
C2	-0.2756(4)	0.2880(3)	0.29303(18)	0.0483(10)
N2	0.5621(3)	-0.03281(19)	0.22356(12)	0.0374(7)
C3	0.6579(4)	-0.0718(2)	0.21508(15)	0.0365(8)
C4	0.7849(5)	-0.1192(3)	0.20493(19)	0.0526(11)
N11	0.0509(3)	0.06571(17)	0.18895(11)	0.0298(6)
C12	0.1234(3)	0.0195(2)	0.15695(13)	0.0307(7)
C13	0.0609(4)	-0.0052(2)	0.09786(14)	0.0392(8)
C14	0.0549(4)	0.0729(3)	0.05934(16)	0.0500(10)
C15	-0.0786(5)	0.1271(3)	0.06270(17)	0.0552(12)
C16	-0.0935(4)	0.1613(2)	0.12105(16)	0.0448(9)
C17	-0.0940(4)	0.0935(2)	0.16595(15)	0.0354(8)
O11	0.2550(2)	-0.00366(15)	0.17172(10)	0.0334(5)
N21	0.4638(3)	0.10288(17)	0.31457(11)	0.0294(6)
C21	0.3932(3)	0.1513(2)	0.34573(13)	0.0304(7)
C22	0.4601(4)	0.1824(2)	0.40257(14)	0.0377(8)
C23	0.4736(5)	0.1111(3)	0.44620(19)	0.0472(10)
C24	0.6036(5)	0.0540(3)	0.4427(2)	0.0474(11)
C25	0.6083(4)	0.0117(2)	0.38583(15)	0.0402(8)
C26	0.6080(4)	0.0748(2)	0.33765(15)	0.0350(8)
O21	0.2614(2)	0.17409(14)	0.33114(9)	0.0313(5)
N31	0.1066(3)	0.01735(16)	0.30692(11)	0.0299(6)
C31	0.1932(3)	-0.04764(19)	0.31218(14)	0.0298(7)
C32	0.1637(4)	-0.1242(2)	0.34659(14)	0.0373(8)
C33	0.1803(4)	-0.1078(3)	0.41000(15)	0.0432(9)
C34	0.0530(5)	-0.0628(3)	0.4297(2)	0.0469(11)
C35	0.0185(4)	0.0219(3)	0.40149(15)	0.0434(9)
C36	-0.0182(4)	0.0171(2)	0.33779(15)	0.0370(8)
O31	0.3093(2)	-0.05197(14)	0.28873(10)	0.0317(5)
N41	0.4089(3)	0.15209(16)	0.19702(11)	0.0303(6)
C41	0.3220(3)	0.21709(19)	0.19144(13)	0.0316(7)
C42	0.3507(4)	0.2932(2)	0.15670(14)	0.0369(8)
C43	0.3333(4)	0.2755(2)	0.09330(15)	0.0424(9)
C44	0.4597(5)	0.2293(2)	0.07354(16)	0.0450(10)
C45	0.4974(4)	0.1455(2)	0.10242(15)	0.0434(9)
C46	0.5353(4)	0.1526(2)	0.16623(15)	0.0377(8)
O41	0.2053(2)	0.22088(14)	0.21434(9)	0.0309(5)
N3	-0.1697(3)	0.2444(3)	0.4335(2)	0.0780(13)
C5	-0.0486(3)	0.2462(3)	0.43539(19)	0.0520(11)
C6	0.1061(5)	0.2483(4)	0.4380(2)	0.0687(15)
N4	0.6784(5)	0.9289(3)	0.0549(2)	0.0769(13)
C7	0.5609(5)	0.9230(3)	0.0594(2)	0.0514(10)
C8	0.4087(5)	0.9167(3)	0.0648(2)	0.0593(12)

\*  $U_{\text{eq}}$  is defined as one third of the trace of the orthogonalized  $U_{ij}$  tensor.



**Table 1-14.** Anisotropic atomic displacement parameters ( $\text{\AA}^2$ ) for  $[\text{Rh}_2(\text{cap})_4(\text{CH}_3\text{CN})_2] \cdot 2\text{CH}_3\text{CN}$ .

Atom	$U_{11}$	$U_{22}$	$U_{33}$	$U_{23}$	$U_{13}$	$U_{12}$
Rh1	0.02424(13)	0.02690(13)	0.03107(14)	0.00054(10)	0.00717(10)	0.00199(10)
Rh2	0.02438(13)	0.02717(13)	0.03051(14)	0.00033(10)	0.00725(10)	0.00196(10)
N1	0.0315(16)	0.0398(16)	0.0347(16)	0.0008(13)	0.0080(13)	0.0044(13)
C1	0.043(2)	0.0368(19)	0.0327(19)	0.0029(15)	0.0067(16)	0.0013(16)
C2	0.051(2)	0.041(2)	0.056(2)	0.0084(18)	0.019(2)	0.0156(19)
N2	0.0358(17)	0.0411(17)	0.0361(16)	0.0053(13)	0.0072(13)	0.0070(14)
C3	0.038(2)	0.0358(18)	0.0371(19)	0.0031(15)	0.0092(16)	-0.0014(15)
C4	0.054(3)	0.048(2)	0.061(3)	0.011(2)	0.025(2)	0.018(2)
N11	0.0244(14)	0.0310(14)	0.0342(15)	-0.0003(11)	0.0048(11)	0.0016(11)
C12	0.0277(17)	0.0284(16)	0.0368(18)	0.0006(13)	0.0069(14)	-0.0010(13)
C13	0.0342(19)	0.042(2)	0.040(2)	-0.0102(16)	0.0027(16)	-0.0005(16)
C14	0.052(3)	0.062(3)	0.035(2)	-0.0002(18)	0.0030(18)	-0.007(2)
C15	0.062(3)	0.053(3)	0.047(2)	0.010(2)	-0.007(2)	-0.002(2)
C16	0.039(2)	0.0356(19)	0.057(2)	0.0036(17)	-0.0048(18)	0.0010(16)
C17	0.0247(17)	0.0398(19)	0.041(2)	-0.0022(15)	0.0030(15)	0.0029(14)
O11	0.0281(12)	0.0354(13)	0.0371(13)	-0.0051(10)	0.0058(10)	0.0031(10)
N21	0.0239(14)	0.0325(14)	0.0322(15)	0.0009(11)	0.0047(11)	0.0019(11)
C21	0.0307(17)	0.0257(15)	0.0349(18)	0.0002(13)	0.0046(14)	0.0001(13)
C22	0.036(2)	0.0364(19)	0.041(2)	-0.0078(15)	0.0029(16)	0.0036(15)
C23	0.047(2)	0.061(3)	0.034(2)	0.0003(19)	0.0079(18)	0.004(2)
C24	0.048(2)	0.051(3)	0.043(2)	0.007(2)	0.0016(19)	0.004(2)
C25	0.0331(19)	0.0367(19)	0.049(2)	0.0028(16)	0.0003(16)	0.0032(15)
C26	0.0265(17)	0.0406(19)	0.0380(19)	-0.0033(15)	0.0045(14)	0.0054(14)
O21	0.0282(12)	0.0315(12)	0.0346(12)	-0.0035(9)	0.0061(10)	0.0054(10)
N31	0.0259(14)	0.0327(14)	0.0328(15)	0.0043(11)	0.0097(11)	0.0012(11)
C31	0.0301(17)	0.0286(16)	0.0316(17)	0.0007(13)	0.0068(13)	-0.0004(13)
C32	0.041(2)	0.0289(17)	0.044(2)	0.0038(15)	0.0133(16)	0.0018(15)
C33	0.049(2)	0.044(2)	0.038(2)	0.0069(16)	0.0096(17)	0.0039(18)
C34	0.050(2)	0.055(3)	0.039(2)	0.0034(18)	0.0162(19)	0.004(2)
C35	0.041(2)	0.045(2)	0.048(2)	-0.0045(17)	0.0193(18)	0.0033(17)
C36	0.0252(17)	0.0393(19)	0.049(2)	0.0075(16)	0.0134(15)	0.0026(14)
O31	0.0315(12)	0.0277(11)	0.0375(13)	0.0028(10)	0.0107(10)	0.0017(10)
N41	0.0259(14)	0.0323(14)	0.0340(15)	0.0043(11)	0.0091(12)	-0.0006(11)
C41	0.0354(19)	0.0295(16)	0.0302(17)	0.0012(13)	0.0054(14)	-0.0031(14)
C42	0.042(2)	0.0283(17)	0.041(2)	0.0019(14)	0.0100(16)	-0.0037(15)
C43	0.051(2)	0.038(2)	0.039(2)	0.0053(16)	0.0082(17)	-0.0011(17)
C44	0.055(3)	0.045(2)	0.037(2)	0.0023(17)	0.0147(18)	-0.0049(19)
C45	0.043(2)	0.041(2)	0.049(2)	-0.0040(17)	0.0188(18)	-0.0038(17)
C46	0.0292(18)	0.0403(19)	0.046(2)	0.0080(16)	0.0146(16)	0.0010(15)
O41	0.0285(12)	0.0291(12)	0.0365(12)	0.0025(9)	0.0098(10)	0.0026(9)
N3	0.052(3)	0.082(3)	0.100(4)	-0.018(3)	0.006(2)	-0.002(2)
C5	0.050(3)	0.053(3)	0.052(3)	-0.010(2)	0.006(2)	-0.002(2)
C6	0.043(3)	0.080(4)	0.086(4)	-0.023(3)	0.020(3)	-0.009(3)
N4	0.050(3)	0.076(3)	0.106(4)	0.000(3)	0.015(2)	-0.002(2)
C7	0.046(3)	0.046(2)	0.063(3)	-0.001(2)	0.010(2)	-0.0001(19)
C8	0.046(3)	0.064(3)	0.070(3)	-0.004(2)	0.018(2)	-0.004(2)

\* The anisotropic atomic displacement factor exponent takes the form:  $-2\pi^2 [h^2a^{*2}U_{11} + \dots + 2hka^*b^*U_{12}]$ .

**Table 1-15.** Hydrogen atom coordinates and isotropic atomic displacement parameters ( $\text{\AA}^2$ ) for  $[\text{Rh}_2(\text{cap})_4(\text{CH}_3\text{CN})_2] \cdot 2\text{CH}_3\text{CN}$ .

Atom	$x/a$	$y/b$	$z/c$	$U_{\text{iso}}$
H21	-0.3586	0.2515	0.2850	0.072
H22	-0.2857	0.3359	0.2677	0.072
H23	-0.2691	0.3077	0.3316	0.072
H41	0.8705	-0.0866	0.2176	0.079
H42	0.7809	-0.1305	0.1650	0.079
H43	0.7879	-0.1719	0.2254	0.079
H131	-0.0362	-0.0280	0.0981	0.047
H132	0.1208	-0.0488	0.0837	0.047
H141	0.1411	0.1071	0.0699	0.060
H142	0.0557	0.0544	0.0204	0.060
H151	-0.0765	0.1747	0.0368	0.066
H152	-0.1642	0.0936	0.0497	0.066
H161	-0.0138	0.2002	0.1324	0.054
H162	-0.1833	0.1935	0.1191	0.054
H171	-0.1431	0.1153	0.1966	0.043
H172	-0.1489	0.0449	0.1497	0.043
H221	0.4007	0.2276	0.4151	0.045
H222	0.5557	0.2055	0.3995	0.045
H231	0.4812	0.1357	0.4839	0.057
H232	0.3859	0.0769	0.4408	0.057
H241	0.6914	0.0875	0.4517	0.057
H242	0.6044	0.0101	0.4714	0.057
H251	0.5249	-0.0256	0.3779	0.048
H252	0.6952	-0.0231	0.3877	0.048
H261	0.6654	0.1239	0.3512	0.042
H262	0.6542	0.0488	0.3075	0.042
H321	0.2299	-0.1693	0.3390	0.045
H322	0.0655	-0.1438	0.3344	0.045
H331	0.1941	-0.1618	0.4297	0.052
H332	0.2671	-0.0740	0.4204	0.052
H341	0.0728	-0.0541	0.4704	0.056
H342	-0.0319	-0.0991	0.4225	0.056
H351	0.1015	0.0592	0.4105	0.052
H352	-0.0629	0.0471	0.4173	0.052
H361	-0.0738	-0.0343	0.3283	0.044
H362	-0.0799	0.0651	0.3252	0.044
H421	0.4488	0.3131	0.1686	0.044
H422	0.2843	0.3384	0.1641	0.044
H431	0.2459	0.2420	0.0833	0.051
H432	0.3200	0.3292	0.0731	0.051
H441	0.5444	0.2659	0.0795	0.054
H442	0.4380	0.2194	0.0330	0.054
H451	0.5793	0.1208	0.0867	0.052
H452	0.4156	0.1071	0.0942	0.052
H461	0.5984	0.1057	0.1796	0.045
H462	0.5890	0.2049	0.1749	0.045
H61	0.1336	0.2286	0.4026	0.103
H62	0.1488	0.2122	0.4682	0.103

H63	0.1398	0.3056	0.4448	0.103
H81	0.3932	0.9319	0.1027	0.089
H82	0.3765	0.8594	0.0570	0.089
H83	0.3548	0.9545	0.0382	0.089

**Table 1-16.** Bond lengths (Å) and angles (°) for [Rh<sub>2</sub>(cap)<sub>4</sub>(CH<sub>3</sub>CN)<sub>2</sub>]**•**2CH<sub>3</sub>CN.

Rh1-N11	2.038(3)	Rh1-N31	2.045(3)	Rh1-O41	2.054(2)	Rh1-O21	2.059(2)
Rh1-N1	2.336(3)	Rh1-Rh2	2.4221(4)	Rh2-N21	2.040(3)	Rh2-N41	2.043(3)
Rh2-O11	2.050(2)	Rh2-O31	2.053(2)	Rh2-N2	2.343(3)	N1-C1	1.139(4)
C1-C2	1.455(5)	C2-H21	0.9700	C2-H22	0.9700	C2-H23	0.9700
N2-C3	1.130(4)	C3-C4	1.455(5)	C4-H41	0.9700	C4-H42	0.9700
C4-H43	0.9700	N11-C12	1.313(4)	N11-C17	1.466(4)	C12-O11	1.292(4)
C12-C13	1.515(4)	C13-C14	1.543(5)	C13-H131	0.9800	C13-H132	0.9800
C14-C15	1.530(6)	C14-H141	0.9800	C14-H142	0.9800	C15-C16	1.525(6)
C15-H151	0.9800	C15-H152	0.9800	C16-C17	1.524(5)	C16-H161	0.9800
C16-H162	0.9800	C17-H171	0.9800	C17-H172	0.9800	N21-C21	1.310(4)
N21-C26	1.463(4)	C21-O21	1.292(4)	C21-C22	1.509(4)	C22-C23	1.537(6)
C22-H221	0.9800	C22-H222	0.9800	C23-C24	1.530(6)	C23-H231	0.9800
C23-H232	0.9800	C24-C25	1.527(6)	C24-H241	0.9800	C24-H242	0.9800
C25-C26	1.530(5)	C25-H251	0.9800	C25-H252	0.9800	C26-H261	0.9800
C26-H262	0.9800	N31-C31	1.309(4)	N31-C36	1.463(4)	C31-O31	1.290(4)
C31-C32	1.516(4)	C32-C33	1.531(5)	C32-H321	0.9800	C32-H322	0.9800
C33-C34	1.518(6)	C33-H331	0.9800	C33-H332	0.9800	C34-C35	1.521(6)
C34-H341	0.9800	C34-H342	0.9800	C35-C36	1.525(5)	C35-H351	0.9800
C35-H352	0.9800	C36-H361	0.9800	C36-H362	0.9800	N41-C41	1.312(4)
N41-C46	1.474(4)	C41-O41	1.287(4)	C41-C42	1.513(4)	C42-C43	1.535(5)
C42-H421	0.9800	C42-H422	0.9800	C43-C44	1.521(5)	C43-H431	0.9800
C43-H432	0.9800	C44-C45	1.521(5)	C44-H441	0.9800	C44-H442	0.9800
C45-C46	1.531(5)	C45-H451	0.9800	C45-H452	0.9800	C46-H461	0.9800
C46-H462	0.9800	N3-C5	1.130(4)	C5-C6	1.443(5)	C6-H61	0.9700
C6-H62	0.9700	C6-H63	0.9700	N4-C7	1.124(6)	C7-C8	1.452(6)
C8-H81	0.9700	C8-H82	0.9700	C8-H83	0.9700		
N11-Rh1-N31	91.09(11)	N11-Rh1-O41	89.61(10)	N31-Rh1-O41	175.88(10)		
N11-Rh1-O21	175.77(10)	N31-Rh1-O21	90.07(10)	O41-Rh1-O21	88.95(9)		
N11-Rh1-N1	96.61(10)	N31-Rh1-N1	97.59(10)	O41-Rh1-N1	86.36(9)		
O21-Rh1-N1	87.27(9)	N11-Rh1-Rh2	86.70(7)	N31-Rh1-Rh2	86.81(7)		
O41-Rh1-Rh2	89.18(6)	O21-Rh1-Rh2	89.30(6)	N1-Rh1-Rh2	174.42(7)		
N21-Rh2-N41	90.84(11)	N21-Rh2-O11	176.40(10)	N41-Rh2-O11	89.83(10)		
N21-Rh2-O31	89.48(10)	N41-Rh2-O31	176.26(10)	O11-Rh2-O31	89.62(9)		
N21-Rh2-N2	96.82(10)	N41-Rh2-N2	97.23(10)	O11-Rh2-N2	86.60(10)		
O31-Rh2-N2	86.43(10)	N21-Rh2-Rh1	86.89(7)	N41-Rh2-Rh1	86.93(7)		
O11-Rh2-Rh1	89.62(6)	O31-Rh2-Rh1	89.37(6)	N2-Rh2-Rh1	174.36(8)		
C1-N1-Rh1	177.1(3)	N1-C1-C2	176.8(4)	C3-N2-Rh2	179.1(3)		
N2-C3-C4	177.7(4)	C12-N11-C17	118.2(3)	C12-N11-Rh1	121.5(2)		
C17-N11-Rh1	118.8(2)	O11-C12-N11	123.2(3)	O11-C12-C13	115.0(3)		
N11-C12-C13	121.7(3)	C12-C13-C14	109.4(3)	C12-C13-H131	109.8		
C14-C13-H131	109.8	C12-C13-H132	109.8	C14-C13-H132	109.8		
H131-C13-H132	108.2	C15-C14-C13	112.8(3)	C15-C14-H141	109.0		
C13-C14-H141	109.0	C15-C14-H142	109.0	C13-C14-H142	109.0		
H141-C14-H142	107.8	C16-C15-C14	114.9(3)	C16-C15-H151	108.5		
C14-C15-H151	108.5	C16-C15-H152	108.5	C14-C15-H152	108.5		
H151-C15-H152	107.5	C17-C16-C15	113.9(3)	C17-C16-H161	108.8		

C15-C16-H161	108.8	C17-C16-H162	108.8	C15-C16-H162	108.8
H161-C16-H162	107.7	N11-C17-C16	113.1(3)	N11-C17-H171	109.0
C16-C17-H171	109.0	N11-C17-H172	109.0	C16-C17-H172	109.0
H171-C17-H172	107.8	C12-O11-Rh2	118.3(2)	C21-N21-C26	118.2(3)
C21-N21-Rh2	121.7(2)	C26-N21-Rh2	119.0(2)	O21-C21-N21	123.1(3)
O21-C21-C22	115.1(3)	N21-C21-C22	121.8(3)	C21-C22-C23	111.3(3)
C21-C22-H221	109.4	C23-C22-H221	109.4	C21-C22-H222	109.4
C23-C22-H222	109.4	H221-C22-H222	108.0	C24-C23-C22	113.3(4)
C24-C23-H231	108.9	C22-C23-H231	108.9	C24-C23-H232	108.9
C22-C23-H232	108.9	H231-C23-H232	107.7	C25-C24-C23	115.1(4)
C25-C24-H241	108.5	C23-C24-H241	108.5	C25-C24-H242	108.5
C23-C24-H242	108.5	H241-C24-H242	107.5	C24-C25-C26	112.9(3)
C24-C25-H251	109.0	C26-C25-H251	109.0	C24-C25-H252	109.0
C26-C25-H252	109.0	H251-C25-H252	107.8	N21-C26-C25	113.4(3)
N21-C26-H261	108.9	C25-C26-H261	108.9	N21-C26-H262	108.9
C25-C26-H262	108.9	H261-C26-H262	107.7	C21-O21-Rh1	118.6(2)
C31-N31-C36	118.4(3)	C31-N31-Rh1	121.7(2)	C36-N31-Rh1	119.9(2)
O31-C31-N31	123.2(3)	O31-C31-C32	114.7(3)	N31-C31-C32	122.1(3)
C31-C32-C33	113.7(3)	C31-C32-H321	108.8	C33-C32-H321	108.8
C31-C32-H322	108.8	C33-C32-H322	108.8	H321-C32-H322	107.7
C34-C33-C32	113.9(3)	C34-C33-H331	108.8	C32-C33-H331	108.8
C34-C33-H332	108.8	C32-C33-H332	108.8	H331-C33-H332	107.7
C33-C34-C35	114.1(3)	C33-C34-H341	108.7	C35-C34-H341	108.7
C33-C34-H342	108.7	C35-C34-H342	108.7	H341-C34-H342	107.6
C34-C35-C36	114.2(3)	C34-C35-H351	108.7	C36-C35-H351	108.7
C34-C35-H352	108.7	C36-C35-H352	108.7	H351-C35-H352	107.6
N31-C36-C35	114.5(3)	N31-C36-H361	108.6	C35-C36-H361	108.6
N31-C36-H362	108.6	C35-C36-H362	108.6	H361-C36-H362	107.6
C31-O31-Rh2	118.96(19)	C41-N41-C46	118.2(3)	C41-N41-Rh2	121.7(2)
C46-N41-Rh2	120.0(2)	O41-C41-N41	123.0(3)	O41-C41-C42	114.8(3)
N41-C41-C42	122.3(3)	C41-C42-C43	113.3(3)	C41-C42-H421	108.9
C43-C42-H421	108.9	C41-C42-H422	108.9	C43-C42-H422	108.9
H421-C42-H422	107.7	C44-C43-C42	114.2(3)	C44-C43-H431	108.7
C42-C43-H431	108.7	C44-C43-H432	108.7	C42-C43-H432	108.7
H431-C43-H432	107.6	C43-C44-C45	115.2(3)	C43-C44-H441	108.5
C45-C44-H441	108.5	C43-C44-H442	108.5	C45-C44-H442	108.5
H441-C44-H442	107.5	C44-C45-C46	113.6(3)	C44-C45-H451	108.8
C46-C45-H451	108.8	C44-C45-H452	108.8	C46-C45-H452	108.8
H451-C45-H452	107.7	N41-C46-C45	113.8(3)	N41-C46-H461	108.8
C45-C46-H461	108.8	N41-C46-H462	108.8	C45-C46-H462	108.8
H461-C46-H462	107.7	C41-O41-Rh1	119.3(2)	N3-C5-C6	179.9(8)
N4-C7-C8	179.0(6)				
N11-Rh1-Rh2-N21	-179.75(11)	N31-Rh1-Rh2-N21	-88.46(11)	O41-Rh1-Rh2-N21	90.60(10)
O21-Rh1-Rh2-N21	1.64(10)	N11-Rh1-Rh2-N41	89.24(11)	N31-Rh1-Rh2-N41	-179.48(11)
O41-Rh1-Rh2-N41	-0.42(10)	O21-Rh1-Rh2-N41	-89.37(10)	N11-Rh1-Rh2-O11	-0.61(10)
N31-Rh1-Rh2-O11	90.67(10)	O41-Rh1-Rh2-O11	-90.26(9)	O21-Rh1-Rh2-O11	-179.22(10)
N11-Rh1-Rh2-O31	-90.23(10)	N31-Rh1-Rh2-O31	1.05(10)	O41-Rh1-Rh2-O31	-179.89(9)
O21-Rh1-Rh2-O31	91.16(9)	N31-Rh1-N11-C12	-90.6(3)	O41-Rh1-N11-C12	85.4(2)
N1-Rh1-N11-C12	171.6(2)	Rh2-Rh1-N11-C12	-3.8(2)	N31-Rh1-N11-C17	103.4(2)
O41-Rh1-N11-C17	-80.6(2)	N1-Rh1-N11-C17	5.6(2)	Rh2-Rh1-N11-C17	-169.8(2)
C17-N11-C12-O11	175.4(3)	Rh1-N11-C12-O11	9.3(4)	C17-N11-C12-C13	-0.1(5)
Rh1-N11-C12-C13	-166.2(2)	O11-C12-C13-C14	-104.4(3)	N11-C12-C13-C14	71.5(4)
C12-C13-C14-C15	-83.1(4)	C13-C14-C15-C16	59.3(5)	C14-C15-C16-C17	-56.7(5)
C12-N11-C17-C16	-71.9(4)	Rh1-N11-C17-C16	94.6(3)	C15-C16-C17-N11	82.4(4)
N11-C12-O11-Rh2	-9.8(4)	C13-C12-O11-Rh2	166.0(2)	N41-Rh2-O11-C12	-81.7(2)
O31-Rh2-O11-C12	94.6(2)	N2-Rh2-O11-C12	-179.0(2)	Rh1-Rh2-O11-C12	5.2(2)
N41-Rh2-N21-C21	88.2(3)	O31-Rh2-N21-C21	-88.0(3)	N2-Rh2-N21-C21	-174.4(2)
Rh1-Rh2-N21-C21	1.4(2)	N41-Rh2-N21-C26	-103.5(2)	O31-Rh2-N21-C26	80.2(2)
N2-Rh2-N21-C26	-6.1(2)	Rh1-Rh2-N21-C26	169.6(2)	C26-N21-C21-O21	-174.4(3)
Rh2-N21-C21-O21	-6.0(4)	C26-N21-C21-C22	3.7(5)	Rh2-N21-C21-C22	172.0(2)
O21-C21-C22-C23	105.8(3)	N21-C21-C22-C23	-72.4(4)	C21-C22-C23-C24	80.1(4)

C22-C23-C24-C25	-57.8(5)	C23-C24-C25-C26	58.4(5)	C21-N21-C26-C25	69.5(4)
Rh2-N21-C26-C25	-99.1(3)	C24-C25-C26-N21	-84.4(4)	N21-C21-O21-Rh1	7.8(4)
C22-C21-O21-Rh1	-170.3(2)	N31-Rh1-O21-C21	81.6(2)	O41-Rh1-O21-C21	-94.4(2)
N1-Rh1-O21-C21	179.2(2)	Rh2-Rh1-O21-C21	-5.2(2)	N11-Rh1-N31-C31	85.9(3)
O21-Rh1-N31-C31	-90.0(3)	N1-Rh1-N31-C31	-177.3(3)	Rh2-Rh1-N31-C31	-0.7(2)
N11-Rh1-N31-C36	-97.7(2)	O21-Rh1-N31-C36	86.4(2)	N1-Rh1-N31-C36	-0.9(3)
Rh2-Rh1-N31-C36	175.7(2)	C36-N31-C31-O31	-176.9(3)	Rh1-N31-C31-O31	-0.5(4)
C36-N31-C31-C32	3.2(5)	Rh1-N31-C31-C32	179.6(2)	O31-C31-C32-C33	110.5(3)
N31-C31-C32-C33	-69.6(4)	C31-C32-C33-C34	78.5(4)	C32-C33-C34-C35	-57.7(5)
C33-C34-C35-C36	59.9(5)	C31-N31-C36-C35	67.1(4)	Rh1-N31-C36-C35	-109.4(3)
C34-C35-C36-N31	-84.4(4)	N31-C31-O31-Rh2	1.7(4)	C32-C31-O31-Rh2	-178.3(2)
N21-Rh2-O31-C31	85.1(2)	O11-Rh2-O31-C31	-91.4(2)	N2-Rh2-O31-C31	-178.0(2)
Rh1-Rh2-O31-C31	-1.8(2)	N21-Rh2-N41-C41	-86.8(3)	O11-Rh2-N41-C41	89.7(3)
N2-Rh2-N41-C41	176.2(3)	Rh1-Rh2-N41-C41	0.1(2)	N21-Rh2-N41-C46	97.4(2)
O11-Rh2-N41-C46	-86.1(2)	N2-Rh2-N41-C46	0.4(3)	Rh1-Rh2-N41-C46	-175.8(2)
C46-N41-C41-O41	176.6(3)	Rh2-N41-C41-O41	0.7(4)	C46-N41-C41-C42	-2.6(5)
Rh2-N41-C41-C42	-178.5(2)	O41-C41-C42-C43	-109.5(3)	N41-C41-C42-C43	69.7(4)
C41-C42-C43-C44	-77.9(4)	C42-C43-C44-C45	56.6(5)	C43-C44-C45-C46	-58.9(5)
C41-N41-C46-C45	-68.5(4)	Rh2-N41-C46-C45	107.4(3)	C44-C45-C46-N41	84.3(4)
N41-C41-O41-Rh1	-1.2(4)	C42-C41-O41-Rh1	178.1(2)	N11-Rh1-O41-C41	-85.8(2)
O21-Rh1-O41-C41	90.2(2)	N1-Rh1-O41-C41	177.6(2)	Rh2-Rh1-O41-C41	0.9(2)

---

Crystallographer's<sup>56</sup> Report for Rh<sub>2</sub>(cap)<sub>4</sub>(OH<sub>2</sub>)<sub>2</sub>]OTf, CCDC #615576.

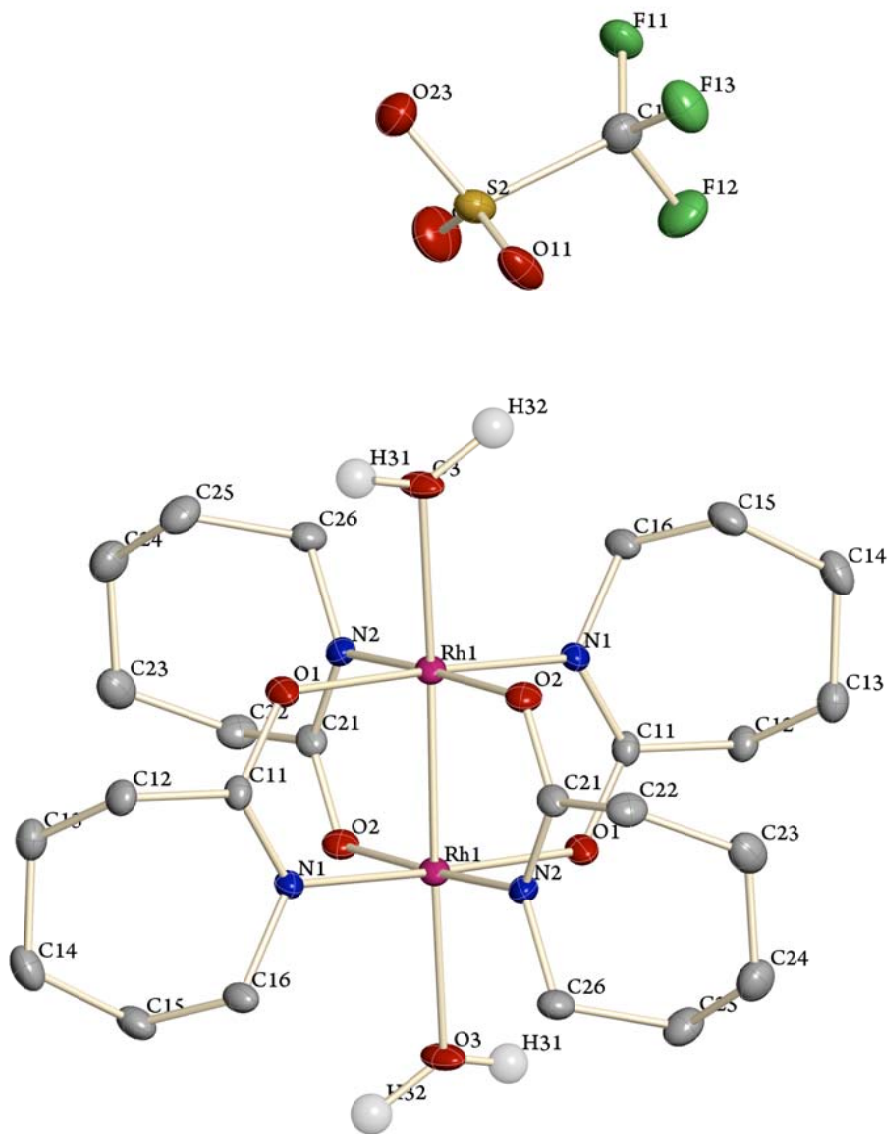


**Figure 1-18.** A view of Rh<sub>2</sub>(cap)<sub>4</sub>(OH<sub>2</sub>)<sub>2</sub>]OTf showing the numbering scheme. Thermal ellipsoids for the non-hydrogen atoms are shown at the 30% probability level. Hydrogen atoms, except for those on water, are omitted for clarity.

---

<sup>56</sup> See ref. 39.

A dark-purple plate of  $C_{25}H_{44}F_3N_4O_9Rh_2S$ , approximate dimensions  $0.035 \times 0.13 \times 0.22 \text{ mm}^3$ , was used for the X-ray crystallographic analysis. The X-ray intensity data were measured at 223(2) K on a three-circle diffractometer system equipped with Bruker Smart1000 CCD area detector using a graphite monochromator and a  $MoK\alpha$  fine-focus sealed tube ( $\lambda = 0.71073 \text{ \AA}$ ) operated at 50 kV and 40 mA. The detector was placed at a distance of 4.958 cm from the crystal.

A total of 1458 frames were collected with a scan width of  $0.3^\circ$  in  $\omega$  and an exposure time of 30 sec/frame using SMART software package.<sup>57</sup> The total data collection time was 15.05 hours. The frames were integrated with SAINT software package<sup>58</sup> using a narrow-frame integration algorithm. The integration of the data using a monoclinic unit cell yielded a total of 19459 reflections to a maximum  $\theta$  angle of  $27.49^\circ$ , of which 3464 were independent (completeness = 93.8%,  $R_{\text{int}} = 2.98\%$ ,  $R_{\text{sig}} = 3.87\%$ ) and 4172 were greater than  $2\sigma(I)$ . The final cell dimensions of  $a = 24.663(4) \text{ \AA}$ ,  $b = 7.1764(13) \text{ \AA}$ ,  $c = 21.213(4) \text{ \AA}$ ,  $\alpha = 90^\circ$ ,  $\beta = 121.245(3)^\circ$ ,  $\gamma = 90^\circ$ , and  $V = 3209.9(10) \text{ \AA}^3$  are based upon the refinement of the XYZ-centroids of 2975 reflections with  $2.2 < \theta < 27.4^\circ$  using SAINT. Analysis of the data showed 0.00 % decay during data collection. Data were corrected for absorption effects with the semi-empirical from equivalents method using SADABS.<sup>59</sup> The minimum and maximum transmission coefficients were 0.809 and 0.960.

The structure was solved and refined using the SHELXS-97 and SHELXL-97 software<sup>60</sup> in the space group  $C2/c$  with  $Z = 4$  for the formula unit  $C_{25}H_{44}F_3N_4O_9Rh_2S$ . The final anisotropic full-matrix least-squares refinement

---

<sup>57</sup> See ref. 40.

<sup>58</sup> See ref. 40.

<sup>59</sup> See ref. 42.

<sup>60</sup> See ref. 41.

on  $F^2$  with 320 variables converged at  $R_1 = 3.72\%$  for the observed data and  $wR_2 = 7.96\%$  for all data. The goodness-of-fit was 1.000. The largest peak on the final difference map was  $0.725\bar{e}/\text{\AA}^3$  and the largest hole was  $-0.490\bar{e}/\text{\AA}^3$ . On the basis of the final model, the calculated density was  $1.737\text{ g/cm}^3$  and  $F(000)$ ,  $1708\bar{e}$ .

**Table 1-17.** Crystal data and structure refinement for  $\text{Rh}_2(\text{cap})_4(\text{OH}_2)_2\text{OTf}$ .

Empirical formula	$\text{C}_{25}\text{H}_{44}\text{F}_3\text{N}_4\text{O}_9\text{Rh}_2\text{S}$	
Formula weight (amu)	839.52	
Temperature (K)	223(2)	
Wavelength ( $\text{\AA}$ )	0.71073	
Crystal size ( $\text{mm}^3$ )	$0.22 \times 0.13 \times 0.035$	
Crystal habit	dark-purple plate	
Crystal system	Monoclinic	
Space group	C 2/c	
Unit cell dimensions ( $\text{\AA}/^\circ$ )	$a = 24.663(4)$	$\alpha = 90$
	$b = 7.1764(13)$	$\beta = 121.245(3)$
	$c = 21.213(4)$	$\gamma = 90$
Volume ( $\text{\AA}^3$ )	3209.9(10)	
Z	4	
Density, $\rho_{\text{calc}}$ ( $\text{g/cm}^3$ )	1.737	
Absorption coefficient, $\mu$ ( $\text{mm}^{-1}$ )	1.165	
$\theta$ Range ( $^\circ$ )	2.25 to 27.49	
Reflections collected	19459	
Independent reflections	3464	
Observed reflection, $I > 2\sigma(I)$	4172	
Max. and min. transmission <sup>a</sup>	0.960 and 0.809	
Goodness-of-fit on $F^2$	1.060	
Max $[\Delta/\sigma]$	0.001	
Final R indices: <sup>b</sup>		
$R_1$ , $I > 2\sigma(I)$	0.0372	
$wR_2$ , all data	0.0796	
$R_{\text{int}}$	0.0298	
$R_{\text{sig}}$	0.0387	
Min., max. peaks ( $\bar{e}/\text{\AA}^3$ )	0.725 and -0.490	

<sup>a</sup>Absorption correction was performed using the semi-empirical from equivalents method (SADABS). <sup>b</sup>Function minimized was  $\sum w(F_o^2 - F_c^2)^2$  where  $R_1 = \sum ||F_o| - |F_c|| / \sum |F_o|$ ,  $wR_2 = [\sum w(F_o^2 - F_c^2)^2 / \sum w(F_o^2)^2]^{1/2}$  with a weighting scheme  $w = 1/[\sigma^2(F_o^2) + (0.015P)^2 + 27.8P]$ ,  $P = [\max(F_o^2, 0) + 2F_o^2]/3$ .



**Table 1-18.** Atomic coordinates and equivalent isotropic atomic displacement parameters ( $\text{\AA}^2$ ) for  $\text{Rh}_2(\text{cap})_4(\text{OH}_2)_2\text{OTf}$ .

Atom	<i>x/a</i>	<i>y/b</i>	<i>z/c</i>	$U_{\text{eq}}$
Rh1	0.218915(14)	0.11190(3)	0.476750(16)	0.02653(9)
O1	0.25799(12)	0.0211(3)	0.58180(14)	0.0331(6)
N1	0.31772(13)	0.2851(3)	0.62481(16)	0.0258(6)
C11	0.29800(17)	0.1252(5)	0.6357(2)	0.0279(8)
C12	0.31740(18)	0.0574(5)	0.7116(2)	0.0330(9)
C13	0.29549(19)	0.1905(5)	0.7506(2)	0.0387(10)
C14	0.3380(2)	0.3597(6)	0.7855(2)	0.0460(11)
C15	0.3440(2)	0.4877(5)	0.7325(2)	0.0412(10)
C16	0.36780(17)	0.3894(5)	0.6874(2)	0.0336(8)
N2	0.34906(13)	0.2618(4)	0.51536(16)	0.0275(7)
O2	0.29050(11)	-0.0039(3)	0.46936(14)	0.0320(6)
C21	0.34141(17)	0.0920(4)	0.4893(2)	0.0296(8)
C22	0.38982(19)	-0.0044(5)	0.4776(2)	0.0378(10)
C23	0.3995(2)	0.0909(6)	0.4196(2)	0.0448(10)
C24	0.4408(2)	0.2629(6)	0.4473(3)	0.0480(11)
C25	0.4163(2)	0.4173(5)	0.4750(2)	0.0427(10)
C26	0.40893(17)	0.3608(5)	0.5394(2)	0.0345(9)
O3	0.17332(12)	-0.1767(3)	0.44379(15)	0.0415(7)
S1	0.0174(5)	0.6051(13)	0.3013(5)	0.0420(12)
O11	0.0821(6)	0.612(3)	0.3229(11)	0.053(5)
O12	-0.0090(12)	0.768(2)	0.3136(17)	0.074(7)
O13	-0.0055(9)	0.4293(19)	0.3085(13)	0.057(5)
C1	-0.0167(7)	0.607(2)	0.2011(7)	0.051(3)
F11	-0.0778(6)	0.566(2)	0.1600(9)	0.059(4)
F12	-0.0070(10)	0.771(2)	0.1782(15)	0.074(5)
F13	0.0125(11)	0.481(3)	0.1822(15)	0.068(6)
S2	0.0191(10)	0.638(3)	0.3074(8)	0.0420(12)
O21	0.0839(10)	0.602(6)	0.3333(19)	0.045(7)
O22	0.0014(16)	0.831(3)	0.3020(15)	0.061(7)
O23	-0.013(2)	0.506(4)	0.326(2)	0.057(8)
C2	-0.0146(11)	0.576(3)	0.2104(10)	0.051(3)
F21	-0.0143(14)	0.397(3)	0.1963(13)	0.087(7)
F22	-0.0747(11)	0.643(4)	0.1686(18)	0.064(6)
F23	0.0159(11)	0.665(5)	0.1816(13)	0.088(7)
H121	0.3637	0.0455	0.7411	0.027(9)
H122	0.2991	-0.0661	0.7080	0.035(10)
H131	0.2525	0.2336	0.7147	0.038(10)
H132	0.2933	0.1213	0.7890	0.037(10)
H141	0.3215	0.4325	0.8111	0.071(15)
H142	0.3804	0.3162	0.8228	0.034(10)
H151	0.3733	0.5891	0.7606	0.041(11)
H152	0.3025	0.5433	0.6986	0.036(11)
H161	0.3854	0.4824	0.6690	0.041(11)
H162	0.4020	0.3035	0.7195	0.051(12)
H221	0.3763	-0.1334	0.4623	0.052(12)
H222	0.4304	-0.0080	0.5245	0.035(11)
H231	0.4187	0.0014	0.4020	0.042(11)
H232	0.3580	0.1256	0.3775	0.050(12)

H241	0.4453	0.3126	0.4072	0.052(12)
H242	0.4831	0.2263	0.4874	0.036(11)
H251	0.3751	0.4591	0.4342	0.043(11)
H252	0.4456	0.5232	0.4902	0.044(11)
H261	0.4445	0.2803	0.5729	0.059(13)
H262	0.4106	0.4726	0.5669	0.044(11)
H31	0.1814	-0.2275	0.4838	0.046
H32	0.1550	-0.2376	0.3905	0.048

$U_{eq}$  is defined as one third of the trace of the orthogonalized  $U_{ij}$  tensor.

**Table 1-19.** Anisotropic atomic displacement parameters ( $\text{\AA}^2$ ) for  $\text{Rh}_2(\text{cap})_4(\text{OH}_2)_2\text{OTf}$ .

Atom	$U_{11}$	$U_{22}$	$U_{33}$	$U_{23}$	$U_{13}$	$U_{12}$
Rh1	0.03728(16)	0.01598(13)	0.02618(16)	0.00028(13)	0.01636(12)	-0.00331(13)
O1	0.0479(16)	0.0194(12)	0.0291(15)	0.0006(11)	0.0179(13)	-0.0073(11)
N1	0.0336(16)	0.0200(14)	0.0240(16)	-0.0026(12)	0.0151(14)	-0.0030(12)
C11	0.037(2)	0.0236(17)	0.0267(19)	0.0035(16)	0.0192(17)	0.0039(16)
C12	0.041(2)	0.0285(19)	0.030(2)	0.0062(16)	0.0193(19)	0.0011(16)
C13	0.043(2)	0.045(2)	0.033(2)	0.0058(19)	0.023(2)	0.0041(19)
C14	0.055(3)	0.051(3)	0.029(2)	-0.004(2)	0.020(2)	0.008(2)
C15	0.051(3)	0.031(2)	0.032(2)	-0.0060(18)	0.014(2)	-0.0015(19)
C16	0.039(2)	0.0243(17)	0.027(2)	0.0015(17)	0.0104(17)	-0.0053(17)
N2	0.0353(16)	0.0219(14)	0.0286(17)	-0.0006(13)	0.0189(14)	-0.0059(13)
O2	0.0397(15)	0.0178(12)	0.0390(16)	-0.0036(11)	0.0207(13)	-0.0034(10)
C21	0.040(2)	0.0198(17)	0.027(2)	0.0023(15)	0.0165(17)	-0.0006(16)
C22	0.040(2)	0.0252(19)	0.049(3)	-0.0028(18)	0.023(2)	0.0023(17)
C23	0.044(2)	0.049(2)	0.047(3)	-0.013(2)	0.027(2)	-0.004(2)
C24	0.047(3)	0.054(3)	0.053(3)	0.001(2)	0.033(2)	-0.004(2)
C25	0.043(2)	0.036(2)	0.057(3)	0.006(2)	0.031(2)	-0.0039(19)
C26	0.036(2)	0.028(2)	0.037(2)	-0.0071(17)	0.0172(19)	-0.0072(17)
O3	0.0493(16)	0.0185(11)	0.0390(16)	0.0013(12)	0.0103(13)	-0.0104(11)
S1	0.0356(17)	0.041(3)	0.0429(18)	-0.008(2)	0.0155(16)	-0.006(2)
O11	0.036(5)	0.067(10)	0.044(8)	-0.025(7)	0.013(5)	-0.005(6)
O12	0.081(11)	0.075(9)	0.081(10)	-0.016(8)	0.054(8)	0.015(7)
O13	0.040(7)	0.061(7)	0.059(9)	0.020(7)	0.019(6)	0.004(6)
C1	0.043(6)	0.063(6)	0.050(5)	-0.003(5)	0.026(4)	-0.008(5)
F11	0.047(5)	0.078(8)	0.042(6)	-0.015(6)	0.016(4)	-0.019(5)
F12	0.074(8)	0.072(7)	0.079(9)	0.020(7)	0.042(7)	-0.013(6)
F13	0.067(8)	0.077(9)	0.052(8)	-0.008(7)	0.026(7)	0.010(7)
S2	0.0356(17)	0.041(3)	0.0429(18)	-0.008(2)	0.0155(16)	-0.006(2)
O21	0.043(7)	0.055(12)	0.036(11)	-0.014(10)	0.018(7)	0.006(7)
O22	0.058(11)	0.042(7)	0.070(11)	-0.006(7)	0.023(8)	0.008(7)
O23	0.058(12)	0.065(12)	0.051(11)	0.007(8)	0.030(9)	-0.007(8)
C2	0.043(6)	0.063(6)	0.050(5)	-0.003(5)	0.026(4)	-0.008(5)
F21	0.108(12)	0.069(7)	0.066(9)	-0.022(7)	0.033(8)	-0.008(7)
F22	0.054(7)	0.067(10)	0.049(9)	0.020(8)	0.010(6)	-0.007(7)
F23	0.093(10)	0.117(13)	0.080(10)	0.019(9)	0.062(9)	-0.009(8)

The anisotropic atomic displacement factor exponent takes the form:  $-2\pi^2 [h^2a^{*2}U_{11} + \dots + 2hka^*b^*U_{12}]$ .

**Table 1-20.** Bond lengths (Å) and angles (°) for Rh<sub>2</sub>(cap)<sub>4</sub>(OH<sub>2</sub>)<sub>2</sub>]OTf.

Rh1-N2#1	1.988(3)	Rh1-N1#1	1.996(3)	Rh1-O1	2.023(2)	Rh1-O2	2.030(2)
Rh1-O3	2.286(2)	Rh1-Rh1#1	2.3840(6)	O1-C11	1.291(4)	N1-C11	1.312(4)
N1-C16	1.465(4)	N1-Rh1#1	1.996(3)	C11-C12	1.505(5)	C12-C13	1.533(5)
C12-H121	0.9800	C12-H122	0.9800	C13-C14	1.522(5)	C13-H131	0.9800
C13-H132	0.9800	C14-C15	1.519(6)	C14-H141	0.9800	C14-H142	0.9800
C15-C16	1.530(5)	C15-H151	0.9800	C15-H152	0.9800	C16-H161	0.9800
C16-H162	0.9800	N2-C21	1.311(4)	N2-C26	1.471(4)	N2-Rh1#1	1.988(3)
O2-C21	1.296(4)	C21-C22	1.508(5)	C22-C23	1.530(5)	C22-H221	0.9800
C22-H222	0.9800	C23-C24	1.512(5)	C23-H231	0.9800	C23-H232	0.9800
C24-C25	1.519(5)	C24-H241	0.9800	C24-H242	0.9800	C25-C26	1.524(5)
C25-H251	0.9800	C25-H252	0.9800	C26-H261	0.9800	C26-H262	0.9800
O3-H31	0.8480	O3-H32	1.0691	S1-O11	1.415(7)	S1-O13	1.422(8)
S1-O12	1.425(8)	S1-C1	1.836(8)	C1-F11	1.323(10)	C1-F13	1.340(10)
C1-F12	1.347(10)	S2-O21	1.419(11)	S2-O23	1.424(12)	S2-O22	1.438(11)
S2-C2	1.831(8)	C2-F21	1.320(13)	C2-F23	1.350(14)	C2-F22	1.360(14)
N2#1-Rh1-N1#1	89.58(11)	N2#1-Rh1-O1	89.70(11)	N1#1-Rh1-O1	176.94(10)		
N2#1-Rh1-O2	177.01(10)	N1#1-Rh1-O2	89.61(11)	O1-Rh1-O2	90.96(10)		
N2#1-Rh1-O3	97.83(10)	N1#1-Rh1-O3	97.47(10)	O1-Rh1-O3	85.58(9)		
O2-Rh1-O3	85.12(9)	N2#1-Rh1-Rh1#1	88.60(8)	N1#1-Rh1-Rh1#1	88.42(8)		
O1-Rh1-Rh1#1	88.58(7)	O2-Rh1-Rh1#1	88.50(7)	O3-Rh1-Rh1#1	171.28(7)		
C11-O1-Rh1	119.8(2)	C11-N1-C16	120.2(3)	C11-N1-Rh1#1	120.8(2)		
C16-N1-Rh1#1	119.0(2)	O1-C11-N1	122.2(3)	O1-C11-C12	115.7(3)		
N1-C11-C12	122.0(3)	C11-C12-C13	111.8(3)	C11-C12-H121	109.3		
C13-C12-H121	109.3	C11-C12-H122	109.3	C13-C12-H122	109.3		
H121-C12-H122	107.9	C14-C13-C12	114.4(3)	C14-C13-H131	108.6		
C12-C13-H131	108.6	C14-C13-H132	108.6	C12-C13-H132	108.6		
H131-C13-H132	107.6	C15-C14-C13	115.4(3)	C15-C14-H141	108.4		
C13-C14-H141	108.4	C15-C14-H142	108.4	C13-C14-H142	108.4		
H141-C14-H142	107.5	C14-C15-C16	113.7(3)	C14-C15-H151	108.8		
C16-C15-H151	108.8	C14-C15-H152	108.8	C16-C15-H152	108.8		
H151-C15-H152	107.7	N1-C16-C15	112.7(3)	N1-C16-H161	109.1		
C15-C16-H161	109.1	N1-C16-H162	109.1	C15-C16-H162	109.1		
H161-C16-H162	107.8	C21-N2-C26	119.6(3)	C21-N2-Rh1#1	121.1(2)		
C26-N2-Rh1#1	119.3(2)	C21-O2-Rh1	119.5(2)	O2-C21-N2	122.3(3)		
O2-C21-C22	114.8(3)	N2-C21-C22	122.9(3)	C21-C22-C23	113.2(3)		
C21-C22-H221	108.9	C23-C22-H221	108.9	C21-C22-H222	108.9		
C23-C22-H222	108.9	H221-C22-H222	107.8	C24-C23-C22	114.1(4)		
C24-C23-H231	108.7	C22-C23-H231	108.7	C24-C23-H232	108.7		
C22-C23-H232	108.7	H231-C23-H232	107.6	C23-C24-C25	115.0(3)		
C23-C24-H241	108.5	C25-C24-H241	108.5	C23-C24-H242	108.5		
C25-C24-H242	108.5	H241-C24-H242	107.5	C24-C25-C26	114.2(3)		
C24-C25-H251	108.7	C26-C25-H251	108.7	C24-C25-H252	108.7		
C26-C25-H252	108.7	H251-C25-H252	107.6	N2-C26-C25	112.5(3)		
N2-C26-H261	109.1	C25-C26-H261	109.1	N2-C26-H262	109.1		
C25-C26-H262	109.1	H261-C26-H262	107.8	Rh1-O3-H31	105.1		
Rh1-O3-H32	124.4	H31-O3-H32	129.4	O11-S1-O13	116.2(8)		
O11-S1-O12	117.2(7)	O13-S1-O12	117.6(8)	O11-S1-C1	97.9(8)		
O13-S1-C1	99.2(12)	O12-S1-C1	103.1(12)	F11-C1-F13	105.1(12)		
F11-C1-F12	108.1(12)	F13-C1-F12	104.9(12)	F11-C1-S1	116.3(11)		
F13-C1-S1	110.4(14)	F12-C1-S1	111.3(15)	O21-S2-O23	117.0(15)		
O21-S2-O22	116.1(13)	O23-S2-O22	118.2(14)	O21-S2-C2	98.9(12)		
O23-S2-C2	99.0(14)	O22-S2-C2	101.7(13)	F21-C2-F23	106.6(16)		
F21-C2-F22	109.3(17)	F23-C2-F22	102.3(15)	F21-C2-S2	116.0(15)		
F23-C2-S2	111.1(15)	F22-C2-S2	110.6(18)				

Symmetry transformation codes: #1 -x+1/2,-y+1/2,-z+1

**Table 1-21.** Torsion angles (°) for Rh<sub>2</sub>(cap)<sub>4</sub>(OH<sub>2</sub>)<sub>2</sub>]OTf.

N2#1-Rh1-O1-C11	-87.0(3)	O2-Rh1-O1-C11	90.0(3)	O3-Rh1-O1-C11	175.1(3)
Rh1#1-Rh1-O1-C11	1.6(2)	Rh1-O1-C11-N1	-4.4(4)	Rh1-O1-C11-C12	171.8(2)
C16-N1-C11-O1	-173.9(3)	Rh1#1-N1-C11-O1	5.2(5)	C16-N1-C11-C12	10.1(5)
Rh1#1-N1-C11-C12	-170.8(2)	O1-C11-C12-C13	-115.1(3)	N1-C11-C12-C13	61.1(5)
C11-C12-C13-C14	-80.9(4)	C12-C13-C14-C15	61.1(5)	C13-C14-C15-C16	-56.7(5)
C11-N1-C16-C15	-75.7(4)	Rh1#1-N1-C16-C15	105.2(3)	C14-C15-C16-N1	79.6(4)
N1#1-Rh1-O2-C21	88.5(3)	O1-Rh1-O2-C21	-88.4(3)	O3-Rh1-O2-C21	-173.9(3)
Rh1#1-Rh1-O2-C21	0.1(2)	Rh1-O2-C21-N2	1.1(5)	Rh1-O2-C21-C22	-176.9(2)
C26-N2-C21-O2	177.8(3)	Rh1#1-N2-C21-O2	-2.0(5)	C26-N2-C21-C22	-4.3(5)
Rh1#1-N2-C21-C22	175.8(3)	O2-C21-C22-C23	114.0(4)	N2-C21-C22-C23	-64.0(5)
C21-C22-C23-C24	78.5(4)	C22-C23-C24-C25	-59.8(5)	C23-C24-C25-C26	60.1(5)
C21-N2-C26-C25	70.9(4)	Rh1#1-N2-C26-C25	-109.2(3)	C24-C25-C26-N2	-82.2(4)
O11-S1-C1-F11	167.7(14)	O13-S1-C1-F11	49.4(15)	O12-S1-C1-F11	-71.9(15)
O11-S1-C1-F13	48.2(15)	O13-S1-C1-F13	-70.1(14)	O12-S1-C1-F13	168.6(15)
O11-S1-C1-F12	-67.9(13)	O13-S1-C1-F12	173.8(12)	O12-S1-C1-F12	52.5(13)
O21-S2-C2-F21	71(2)	O23-S2-C2-F21	-49(3)	O22-S2-C2-F21	-170(2)
O21-S2-C2-F23	-51(2)	O23-S2-C2-F23	-171(2)	O22-S2-C2-F23	68(2)
O21-S2-C2-F22	-164(2)	O23-S2-C2-F22	76(2)	O22-S2-C2-F22	-45(2)

Symmetry transformation codes: #1 -x+1/2,-y+1/2,-z+1

**Table 1-22.** Site occupancy factors that deviate from unity for Rh<sub>2</sub>(cap)<sub>4</sub>(OH<sub>2</sub>)<sub>2</sub>]OTf.

Atom	sof	Atom	sof	Atom	sof	Atom	sof
S1	0.323(12)	O11	0.323(12)	O12	0.323(12)	O13	0.323(12)
C1	0.323(12)	F11	0.323(12)	F12	0.323(12)	F13	0.323(12)
S2	0.177(12)	O21	0.177(12)	O22	0.177(12)	O23	0.177(12)
C2	0.177(12)	F21	0.177(12)	F22	0.177(12)	F23	0.177(12)

**Table 1-23.** Hydrogen bond information for Rh<sub>2</sub>(cap)<sub>4</sub>(OH<sub>2</sub>)<sub>2</sub>]OTf (Å and °).

D—H...A*	d(D—H) ∠(DHA)	d(H...A)	d(D...A)	
O3—H31...O2#2	0.85	2.11	2.782(3)	135.4
O3—H32...O11#3	1.07	1.94	2.819(16)	136.8
O3—H32...F22#4	1.07	1.91	2.69(2)	127.0
O3—H32...O21#3	1.07	1.91	2.74(3)	131.4
O3—H32...F11#4	1.07	2.15	2.902(15)	125.0

\* D-donor atom, H-hydrogen, A-acceptor.

Symmetry transformation codes: #1 -x+1/2,-y+1/2,-z+1 #2 -x+1/2,-y-1/2,-z+1 #3 x,y-1,z  
#4 -x,y-1,-z+1/2

**Table 1-24.** XPS data for **1** with selected peak graphs.

Peak	Position (eV)	FWHM (eV)	Atomic Conc %
Rh 3d <sub>5/2</sub>	309.105	1.571	1.10
Rh 3d <sub>3/2</sub>	313.725	1.892	0.72
N 1s a	398.290	1.405	3.94
N 1s b	399.783	1.436	0.49
O 1s a	531.210	1.911	6.77
O 1s b	532.934	2.050	4.07
C 1s a	284.610	1.613	69.96
C 1s b	286.404	1.498	11.09
C 1s c	288.289	1.697	1.85

**Figure 1-19.** XPS peak graph for the Rh 3d orbitals in **1**.

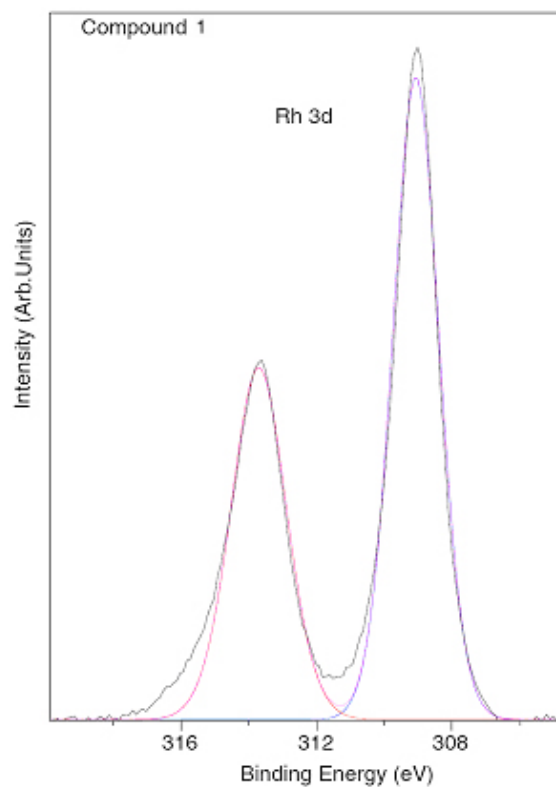


**Table 1-25.** XPS data for **2** with selected peak graphs.

Peak	Position (eV)	FWHM (eV)	Atomic Conc %
Rh 3d <sub>5/2</sub>	308.080	1.532	2.05
Rh 3d <sub>3/2</sub>	312.812	1.838	1.36
N 1s a	397.874	1.577	6.51
N 1s b	399.284	1.626	1.58
O 1s a	530.982	1.878	10.54
O 1s b	532.832	2.144	4.88
C 1s a	284.600	1.611	55.91
C 1s b	286.259	1.334	10.10
C 1s c	288.029	2.311	7.07

**Figure 1-20.** XPS peak graph for the Rh 3d orbitals in **2**.

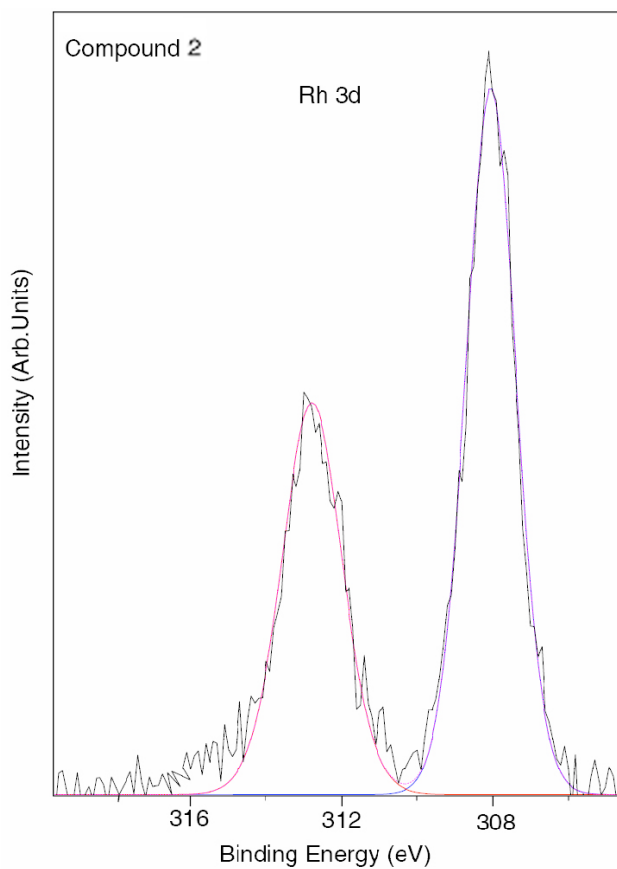
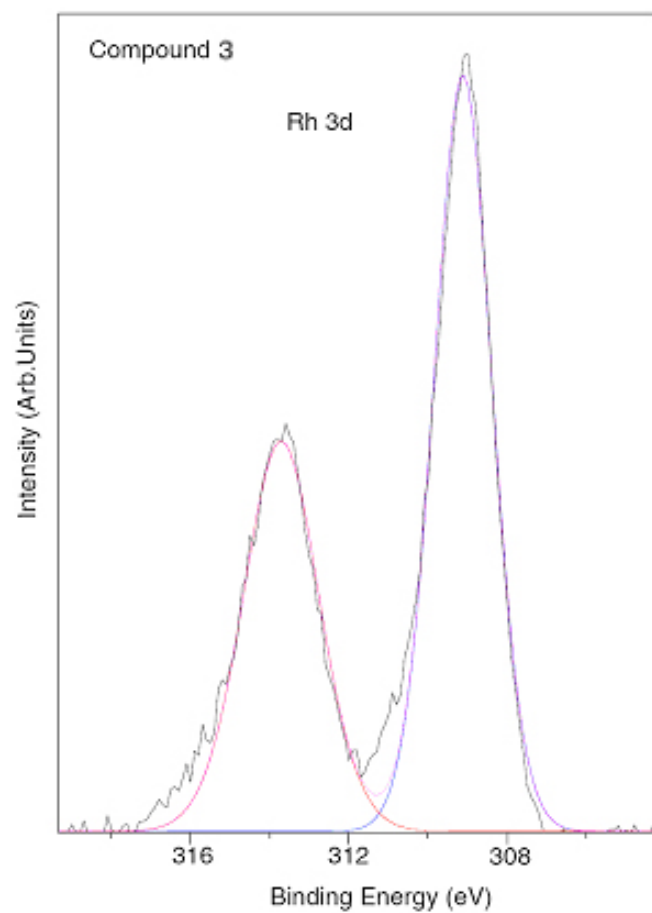


**Table 1-26.** XPS data for **3** with selected peak graphs.

Peak	Position (eV)	FWHM (eV)	Atomic Conc %
Rh 3d <sub>5/2</sub>	309.094	1.578	1.68
Rh 3d <sub>3/2</sub>	313.718	2.202	1.32
N 1s a	398.282	1.600	5.79
N 1s b	400.105	1.950	0.89
O 1s a	531.120	1.692	14.15
O 1s b	532.534	1.525	3.81
O 1s c	534.018	1.580	1.27
C 1s a	284.600	1.708	47.21
C 1s b	286.471	1.981	13.15
C 1s c	291.874	1.233	1.68
C 1s d	288.851	1.879	2.23
F 1s a	687.470	1.719	3.98
F 1s b	688.801	1.648	1.14
S 2p 3/2	167.505	1.859	0.99
S 2p 1/2	168.685	1.859	0.69



**Figure 1-21.** XPS peak graph for the Rh 3d orbitals in **3**.



## Chapter 2

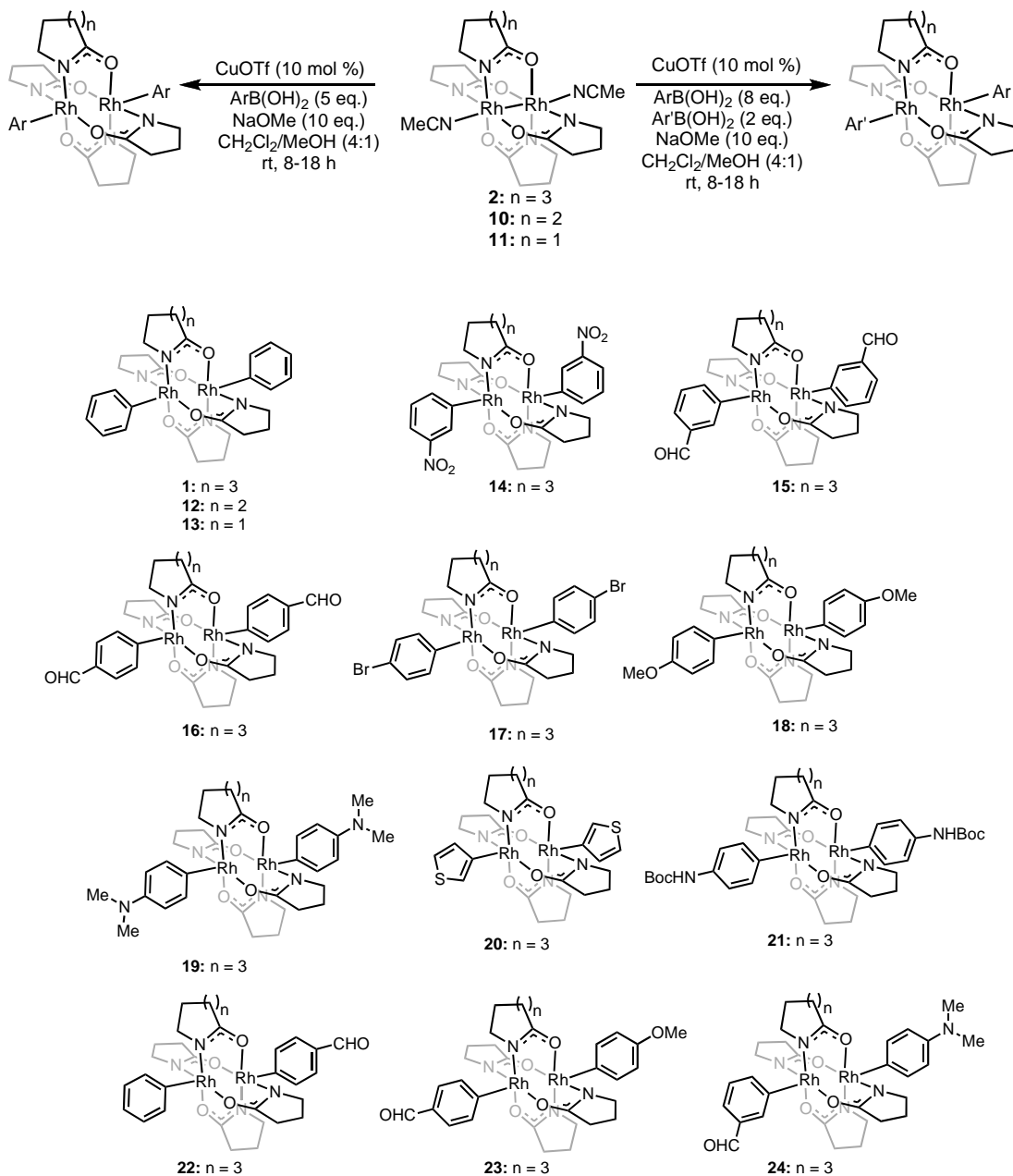
# *Bis*( $\sigma$ -Aryl)-Dirhodium(III) Carboxamidates – A General Class of Dinuclear Rhodium Compounds

### I. Synopsis

General access to the *bis*( $\sigma$ -aryl)-Rh<sub>2</sub><sup>6+</sup>L<sub>4</sub> core structure is necessary in order to explore the capabilities of such complexes as materials or chemical agents. This chapter focuses on the expansion of *bis*( $\sigma$ -aryl)-Rh<sub>2</sub><sup>6+</sup>L<sub>4</sub> complexes into a general class of compounds. The synthesis of these complexes was accomplished with arylboronic acids under basic conditions in conjunction with the aerobic, copper catalyzed oxidation developed in Chapter 1. Starting from either *tetrakis*( $\mu$ -caprolactamato)dirhodium(II) [**2**: Rh<sub>2</sub>(cap)<sub>4</sub>], *tetrakis*( $\mu$ -valerolactamato)dirhodium(II) [**10**: Rh<sub>2</sub>(val)<sub>4</sub>], or *tetrakis*( $\mu$ -pyrrolidinato)dirhodium(II) [**11**: Rh<sub>2</sub>(pyr)<sub>4</sub>], both homosubstituted *bis*( $\sigma$ -aryl)-Rh<sub>2</sub><sup>6+</sup>L<sub>4</sub> complexes (**1**, **12-21**), and heterosubstituted, [( $\sigma$ -aryl), ( $\sigma$ -aryl')]-Rh<sub>2</sub><sup>6+</sup>L<sub>4</sub> complexes (**22-24**) can be prepared from commercially available arylboronic acids (Scheme 2-1). Reaction variables, steric dependencies, and a proposed mechanism for aryl-transfer are discussed.

A comparative analysis of both the molecular and electronic structure of a range of *bis*( $\sigma$ -aryl)-Rh<sub>2</sub><sup>6+</sup>L<sub>4</sub> complexes is presented. The molecular structure is largely unperturbed by substitutional variations on the aryl-ligand. These variations had a minor impact on the electronic structure as observed in both the voltammetry and electronic absorption spectra. Structural distortions were explored computationally and a second-order Jahn-Teller distortion is proposed to rationalize the Rh-Rh-C bond angle distortions. Finally, analysis of the UV spectra of the aryl ligands in a series of related complexes demonstrate the absence of delocalization of the aryl  $\pi$ -system through the dirhodium core.

**Scheme 2-1.** General preparation of  $\text{Rh}_2^{6+}\text{L}_4\text{Ar}_2$  and  $\text{Rh}_2^{6+}\text{L}_4\text{ArAr}'$  complexes (Abbreviations: OTf = trifluoromethanesulfonate,  $\text{CF}_3\text{SO}_3^-$ ;  $(\ )_n$  indicates the number of methylenes in the backbone.<sup>61</sup>)



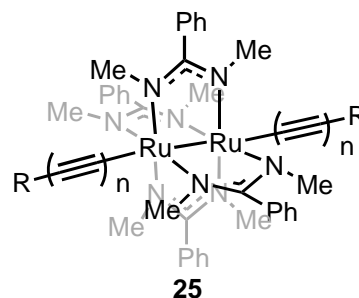
<sup>61</sup> $(\ )_n$  is shown for only one of the ligands for clarity, however, it refers to each of the bridging ligands shown in the complex.

## II. Introduction – $M_2^{6+}$ complexes with M-C bonds.

Although there are many  $M_2^{6+}$  complexes, it is relatively rare for these compounds to have a metal-carbon (M-C) bond linking the  $M_2^{6+}$  core to the axial ligand. The same general statement could be made for dinuclear metal paddlewheel complexes irrespective of their oxidation state.<sup>62</sup> In addition to its structural significance, the M-C bond confers functionality to some of these compounds.<sup>63</sup> To demonstrate this concept, the following discussion will provide a brief look at the largest class of dinuclear metal paddlewheel complexes with a M-C bond, and the functionality that results.

The largest groups of dinuclear metal complexes with a M-C bond are diruthenium<sup>64</sup> and diosmium<sup>65</sup> structures that feature an organometallic bond between the metal and an sp-hybridized carbon.

Within this family, *bis*( $\sigma$ -alkynyl)-*tetrakis*[ $\mu$ -(*N,N'*-dimethylbenzamidinato)] diruthenium(III) complexes (*N,N'*-dimethylbenzamidine =  $ArCN_2(CH_3)_2$ , DMBA) of the general structure  $Ru_2(DMBA)_4[(C_2)_nR]_2$  (**25**) provide examples of a



<sup>62</sup> Cotton, F. A.; Murillo, C. A.; Walton, R. A.; Editors, *Multiple Bonds Between Metal Atoms*. 3rd ed.; Springer Science and Business Media, Inc.: New York, **2005**.

<sup>63</sup> Examples of  $M_2^{6+}$  paddlewheel complexes with materials, or catalytic function: a) Ying, J. W.; Sobransingh, D. R.; Xu, G. L.; Kaifer, A. E.; Ren, T. *Chem. Commun.* **2005**, 357, b) Gois, P. M.; Trindade, A. F.; Veiros, L. F.; Andre, V.; Duarte, M. T.; Afonso, C. A.; Caddick, S.; Cloke, F. G. *Angew. Chem., Int. Ed.* **2007**, *46*, 5750, c) Ying, J. W.; Cordova, A.; Ren, T. Y.; Xu, G. L.; Ren, T. *Chem. Eur. J.* **2007**, *13*, 6874.

<sup>64</sup> For examples of diruthenium(III) complexes, see: a) Bear, J. L.; Han, B.; Huang, S. *J. Am. Chem. Soc.* **1993**, *115*, 1175, For early examples, see: b) Zou, G.; Alvarez, J. C.; Ren, T. *J. Organomet. Chem.* **2000**, *152*, 152, c) Hurst, S. K.; Ren, T. *J. Organomet. Chem.* **2002**, *660*, 1, d) Xu, G. L.; Campana, C.; Ren, T. *Inorg. Chem.* **2002**, *41*, 3521, e) Xu, G. L.; Ren, T. *J. Organomet. Chem.* **2002**, *655*, 239, f) Chen, W.-Z.; Ren, T. *Inorg. Chem.* **2003**, *42*, 8847.

<sup>65</sup> For a diosmium(III) example, see: Shi, Y. H.; Chen, W. Z.; John, K. D.; Da Re, R. E.; Cohn, J. L. *Inorg. Chem.* **2005**, *44*, 5719.

conjugated organometallic complex that have a range of interesting molecular properties and functions. These functions are primarily derived from the linkage between the Ru<sub>2</sub>-core and a carbon-centered  $\pi$ -system.

**Ru<sub>2</sub>-C<sub>sp</sub> as a Molecular Wire.** The description of *bis*( $\sigma$ -alkynyl)-Ru<sub>2</sub><sup>6+</sup>L<sub>4</sub> complexes as part of a conjugated organometallic framework is reported in a series of elegant publications from the labs of Ren et al.<sup>66</sup> The following discussion will focus on the most recent developments from the Ren lab that demonstrate how charge can be transferred through the diruthenium-core of an organometallic poly-yne.<sup>67</sup>

The development of the *bis*( $\sigma$ -alkynyl)-Ru<sub>2</sub><sup>6+</sup>L<sub>4</sub> complexes was made possible through a relatively simple method of preparation (Scheme 2-2). The first generation synthesis of these compounds proceeded *via* anionic metathesis between Ru<sub>2</sub>(DMBA)<sub>4</sub>Cl<sub>2</sub> (**26**) and the preformed lithium salt of a terminal acetylene (i.e. hard deprotonation). The procedure was later simplified by replacing the hard deprotonation conditions with softer conditions using an alkylamine base with Ru<sub>2</sub>(DMBA)<sub>4</sub>(BF<sub>4</sub>)<sub>2</sub> (**27**) as the Ru<sub>2</sub><sup>6+</sup> source. The softer base conditions allowed a greater range of functionality within the complex, (e.g. Ru<sub>2</sub>(DMBA)<sub>4</sub>[(4-NO<sub>2</sub>-C<sub>6</sub>H<sub>4</sub>)-C<sub>2</sub>]<sub>2</sub>)<sup>68</sup> and made it easier to prepare [( $\sigma$ -alkynyl), ( $\sigma'$ -alkynyl)]-Ru<sub>2</sub><sup>6+</sup>L<sub>4</sub> complexes with mixtures of terminal acetylenes (R  $\neq$  R' and/or m  $\neq$  n, Scheme 2-2).

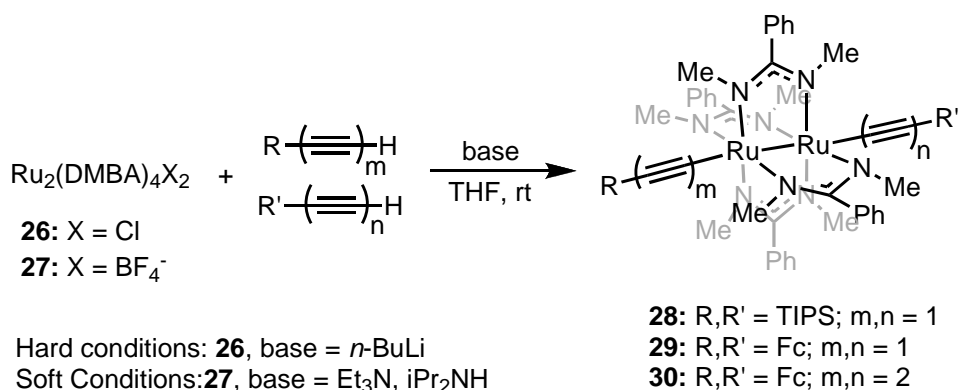
---

<sup>66</sup> a) Xu, G. L.; Jablonski, C. G.; Ren, T. *J. Organomet. Chem.* **2003**, 683, 388, b) Xu, G.; DeRosa, M. C.; Crutchley, R. J.; Ren, T. *J. Am. Chem. Soc.* **2004**, 126, 3728, c) Xu, G. L.; Cordova, A.; Ren, T. *J. Clust. Sci.* **2004**, 15, 413, For a comprehensive review of conjugated diruthenium complexes with a M-C bond, see: d) Ren, T. *Organometallics* **2005**, 24, 4854.

<sup>67</sup> The data described in the in this section comes from the following: a) Shi, Y. H.; Yee, G. T.; Wang, G. B.; Ren, T. *J. Am. Chem. Soc.* **2004**, 126, 10552, b) Szuchmacher Blum, A.; Ren, T.; Parish, D. A.; Trammell, S. A.; Moore, M. H.; Kushmerick, J. G.; Xu, G. L.; Deschamps, J. R.; Pollack, S. K.; Shashidhar, R. *J. Am. Chem. Soc.* **2005**, 127, 10010, c) Xu, G. L.; Crutchley, R. J.; DeRosa, M. C.; Pan, Q. J.; Zhang, H. X.; Wang, X.; Ren, T. *J. Am. Chem. Soc.* **2005**, 127, 13354.

<sup>68</sup> See ref 63a and references therein.

**Scheme 2-2.** Synthesis of *bis*( $\sigma$ -alkynyl)-Ru<sub>2</sub>(DMBA)<sub>4</sub>. (Abbreviations: TIPS = tri-isopropylsilyl, Fc = ferrocene, *n*-BuLi = *n*-butyl-lithium)



The Ru<sub>2</sub><sup>6+</sup> complexes **28**,<sup>69</sup> **29**,<sup>70</sup> and **30**<sup>9</sup> (Scheme 2-2) were prepared using the hard deprotonation conditions from Ru<sub>2</sub>(DMBA)<sub>4</sub>Cl<sub>2</sub> with TIPS-ethyne, ferrocenylacetylene, and ferrocenylbutadi-yne respectively. A brief summary of structural information for these complexes is shown in (Table 2-1). The Ru-Ru bond lengths average 2.445 Å for complexes **28**, **29**, and **30**. The bond is elongated more than 100 pm compared to mono-( $\sigma$ -alkynyl)-Ru<sub>2</sub><sup>6+</sup>L<sub>4</sub> species characteristic of a cleavage of the Ru-Ru  $\sigma$ -bond. This suggests a  $\pi^4\delta^2\pi^4$  electronic configuration for the core d-orbitals of Ru<sub>2</sub><sup>6+</sup> where the  $\sigma$ -bonding interaction is destroyed by the formation of Ru-C bonds.<sup>71</sup> Based on this configuration a weak Ru-Ru  $\delta$ -bond exists maintaining a Ru-Ru bonding interaction. The complexes all have short M-C bonds (<2.000 Å) indicative of a back-bonding interaction between the M and C  $\pi$ -systems. For compounds **28** and **30**, the C-Ru-Ru bond angle is nearly linear at 174.8° and 178.1°, respectively. Complex **29** has a C-Ru-Ru bond angle of 163.4°, which is a significant departure from linearity. This distortion has

<sup>69</sup> This complex was reported in ref. 64f.

<sup>70</sup> These complexes were reported in ref. 67c.

<sup>71</sup> Bear, J. L.; Han, B.; Huang, S.; Kadish, K. M. *Inorg. Chem.* **1996**, *35*, 3012.

been attributed to a second-order Jahn-Teller distortion.<sup>72</sup> Overall, it is apparent that the *bis*( $\sigma$ -alkynyl)-Ru<sub>2</sub>(DMBA)<sub>4</sub> family of Ru<sub>2</sub><sup>6+</sup> complexes have structural features that are desirable for a linearly conjugated organometallic complex.

**Table 2-1.** Structural data for *bis*( $\sigma$ -alkynyl)-Ru<sub>2</sub>(DMBA)<sub>4</sub>.

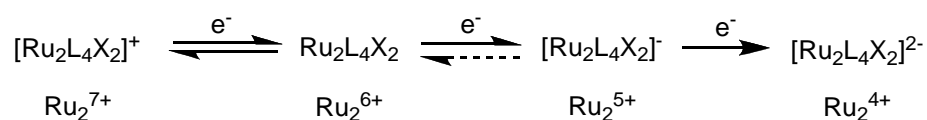
Compound			
	<b>28</b>	<b>29</b>	<b>30</b>
Selected Bond Lengths (Å)			
Ru-Ru	2.450	2.439	2.447
Ru-C <sub>av</sub>	1.955	1.979	1.986
Ru-N <sub>av</sub>	2.046	2.042	2.047
C <sub>ω</sub> -C <sub>ω'</sub>	-	11.58	16.58
Selected Bond Angles (°)			
C-Ru-Ru	174.8	163.4	178.1

The redox chemistry of *bis*( $\sigma$ -alkynyl)-Ru<sub>2</sub><sup>6+</sup>L<sub>4</sub> complexes is shown in Scheme 2-3. In general, a reversible Ru<sub>2</sub><sup>7+/6+</sup>, quasi-reversible Ru<sub>2</sub><sup>6+/5+</sup>, and irreversible Ru<sub>2</sub><sup>5+/4+</sup> couples can be observed for *bis*( $\sigma$ -alkynyl)-Ru<sub>2</sub><sup>6+</sup>L<sub>4</sub> complexes within the potential limit of the solvent. Complex **28** demonstrates each of these with a reversible Ru<sub>2</sub><sup>7+/6+</sup> anodic wave at 0.558 V, reversible Ru<sub>2</sub><sup>6+/5+</sup> cathodic wave at -1.141 V, and an irreversible Ru<sub>2</sub><sup>5+/4+</sup> cathodic wave at -2.324 V in THF versus a Ag/AgCl reference electrode. The Ru<sub>2</sub><sup>7+/6+</sup> redox couple is a reversible process that adds/removes an electron from the highest occupied molecular orbital (HOMO) of the Ru<sub>2</sub><sup>6+</sup> ground state. The Ru<sub>2</sub><sup>6+/5+</sup> redox couple is a reversible process that add/removes an electron from the lowest unoccupied molecular orbital (LUMO) of the Ru<sub>2</sub><sup>6+</sup> ground state. Thus, the HOMO-LUMO gap ( $E_g$ ) for the lowest singlet excitation energy can be estimated directly from the electrochemistry of these compounds by

<sup>72</sup> Lin, C.; Ren, T.; Valente, E. J.; Zubkowsky, J. D. *J. Chem. Soc., Dalton Trans.* **1998**, 571.

comparing the  $\text{Ru}_2^{7+/6+}$  and  $\text{Ru}_2^{6+/5+}$  redox couples in the relationship:  $E_g = E(\text{Ru}_2^{7+/6+}) - E(\text{Ru}_2^{6+/5+})$ . The estimated  $E_g$  for **28** is remarkably low at 1.7 eV; indeed, almost all of *bis*( $\sigma$ -alkynyl)- $\text{Ru}_2^{6+}\text{L}_4$  complexes have an  $E_g$  between 1.2 and 1.8 eV. This range is lower than the  $E_g$  for many organic molecules used in organic conductors like thiophene (5.3 eV), styrene (5.2 eV), or phenylacetylene (5.2 eV).<sup>73</sup> In addition to its molecular structure, the small  $E_g$  of **28** is a desirable property for organometallic conjugation.

**Scheme 2-3.** Redox related chemical steps in electrochemistry of  $\text{Ru}_2\text{L}_4\text{X}_2$



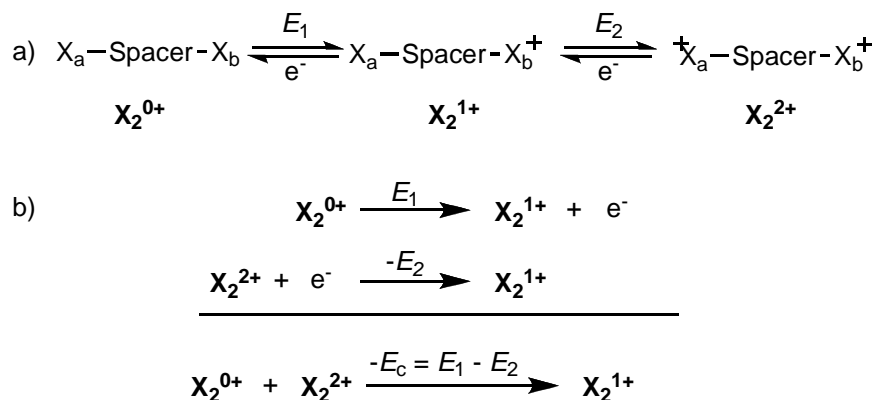
With favorable structural and electrochemical parameters for a conjugated system in **28** and related complexes, Ren and co-workers went on to demonstrate charge mobility across the Ru-Ru core using ferrocene-containing complexes like **29** and **30** (Scheme 2-2). In a beautiful set of comproportionation experiments, ferrocene (Fc) was used as an electrochemical reporter of conjugation and charge mobility. The classical definition of comproportionation is the tendency of a solution containing a metal (M) in a mixture of oxidation states to react to give a single oxidation state, i.e.  $\text{M}^{n+} + \text{M}^{n+2} \rightarrow \text{M}^{n+1}$ .<sup>74</sup> A schematic for a general comproportionation experiment that measures charge mobility within a molecule can be found in Scheme 2-4.

<sup>73</sup> Pretsch, E.; Clerc, T.; Seibl, J.; Simon, W., *Tables of Spectral Data for Structure Determination of Organic Compounds*. Springer-Verlag: Berlin, **1983**.

<sup>74</sup> Bard, A. J.; Faulkner, L. R., *Electrochemical Methods: Fundamentals and Applications*. Wiley: New York, **1980**.



**Scheme 2-4.** Comproportionation experiment.



A conducting spacer is placed between two identical, redox active, reporter molecules,  $X_a$  and  $X_b$  (Scheme 2-4a). Ferrocene has a stable, solvent independent redox couple and is a common redox reporter in such experiments.<sup>75</sup> This gives the molecule three possible oxidation states,  $X_2^{0+}$ ,  $X_2^{1+}$ , and  $X_2^{2+}$ . Conjugation through the spacer stabilizes the mixed-valent  $X_2^{1+}$  state and destabilizes the  $X_2^{2+}$  state, widening the energy difference between  $X_2^{1+}$  and  $X_2^{2+}$  ( $E_2$ ). The extent of differentiation is a measure of the electronic communication between  $X_a$  and  $X_b$  and is called the comproportionation energy ( $E_c$ ). Scheme 2-4b shows a thermochemical cycle that derives  $E_c$  and shows the relationship between this experiment and the classic comproportionation experiment.

The comproportionation energy is typically measured electrochemically and reported as a positive value ( $E_c = E_2 - E_1$ ). Upon electrochemical oxidation of the sample molecule,  $X_2^{0+} \rightarrow X_2^{2+}$ , there are two possible experimental observations. In the absence of conjugation between  $X_a$  and  $X_b$ , a single, two-electron anodic wave will be observed. Because there is no stabilization of the  $X_2^{1+}$  state over the  $X_2^{2+}$  state,  $X_a$  and  $X_b$  behave as two separate and equivalent redox sites. If there is complete, efficient conjugation

<sup>75</sup> Launay, J. P. *Chem. Soc. Rev.* **2001**, 30, 386.

between  $X_a$  and  $X_b$ , then a stabilized, mixed-valent state exists for  $X_2^{1+}$  in which the oxidation state of  $X_a$  and  $X_b$  are averaged ( $X_2^{1+} = X_a^{0.5+} + X_b^{0.5+}$ ). In this case, a broadening, or splitting, of the anodic wave for  $X$  is observed as the  $X_2^{1+}$  state is differentiated from the  $X_2^{2+}$  state by  $E_c$ . The comproportionation energy ( $E_c$ ) is measured as the difference in half-wave potentials for the  $X_2^{0+/1+}$  and  $X_2^{1+/2+}$  redox couples. The comproportionation energy is essentially the stabilization energy of the mixed valent,  $X_2^{1+}$  state afforded to the complex by conjugation of the electroactive reporter groups through the spacer.

In the case of the  $Ru_2^{6+}$  complexes **29** and **30** of Ren and co-workers, the comproportionation energies were large with an  $E_c$  of 0.31 V (7.1 kcal/mol) and 0.27 V (6.2 kcal/mol) respectively. The comproportionation energies are remarkable in that they are close to the  $E_c$  value of biferrocene (0.35 V), an electroactive complex with no spacer and a bond distance of 1.45 Å.<sup>76</sup> Moreover, because conduction is distance dependent,  $E_c$  is inversely related to the distance between the reporter groups.<sup>77</sup> For example, organic conductors like ethynyl and butadiynyl spacers place the ferrocenyl groups 4.0 Å and 6.8 Å apart.<sup>78</sup> As a result of the distance dependence, the ethynyl spacer yields an  $E_c$  of 0.23 V, but  $E_c$  for the butadiynyl spacer is reduced to 0.1 V. Thus, the comproportionation values for **29** and **30** become truly remarkable, as the crystallographic distance between reporter groups are 11.58 Å and 16.58 Å, respectively.

Perhaps the easiest way to demonstrate the impact of the diruthenium spacer is to compare the charge transport efficiency using  $E_c$  and the separation distance ( $r$ ) of biferrocene as a reference. The following free-energy relationship relates the change in  $E_c$  to a coulombic distance

---

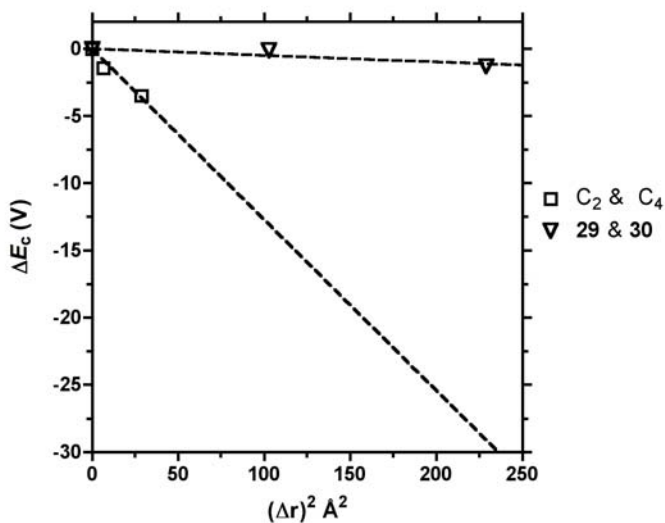
<sup>76</sup> Powers, M. J.; Meyer, T. J. *J. Am. Chem. Soc.* **1978**, *100*, 4393.

<sup>77</sup> See ref. 75.

<sup>78</sup> Levanda, C.; Bechgaard, K.; Cowan, D. O. *J. Org. Chem.* **1976**, *41*, 2700.

dependence  $[(\Delta r)^2 \text{ vs. } \Delta E_c]$ . A graph comparing the organic alkynyl spacers and the  $(\sigma\text{-alkynyl})\text{-Ru}_2^{6+}$  spacers is shown in Figure 2-1. The distance dependence for the organic alkynyl spacers (slope =  $-0.10 \text{ V/\AA}^2$ ,  $r^2 = 0.996$ ) is much stronger than the  $\text{Ru}_2^{6+}$  spacers (slope =  $-0.005 \text{ V/\AA}^2$ ,  $r^2 = 0.91$ ). Despite the poor linear correlation for the  $\text{Ru}_2^{6+}$  spacers, the graph in Figure 2-1 clearly shows the increased efficiency derived by inserting a  $\text{Ru}_2^{6+}$  complex into an organic conductor. The authors performed a much more rigorous spectroscopic analysis of this phenomenon and demonstrated the increased efficiency through application of Marcus-Hush theory. The reader is referred to the primary literature for a more complete description of the electronic coupling.<sup>79</sup>

**Figure 2-1.** Distance dependent free energy relationship of comproportionation energies [Graph:  $(\Delta r)^2 \text{ vs. } \Delta E_c$ , biferrocene = 0]



The work by Ren and co-workers demonstrates how a diruthenium(III) core with a M-C bond can play a beneficial role in promoting conjugation within an organometallic framework. It sets the stage for asking similar

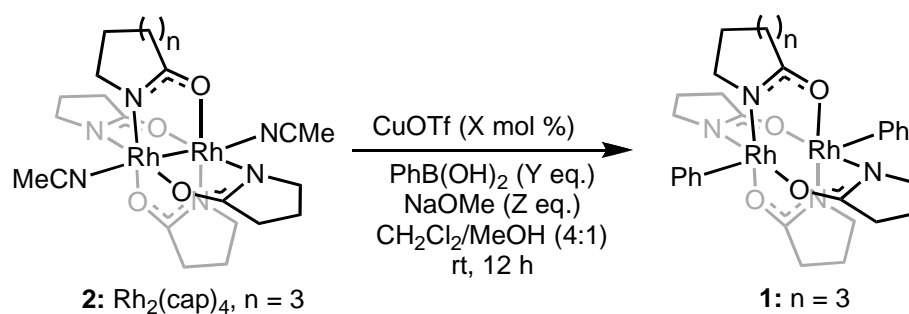
<sup>79</sup> See ref. 67.

questions of the dirhodium(III) core by analogy. The following section describes the expansion of the synthesis of *bis*( $\sigma$ -aryl)-Rh<sub>2</sub><sup>6+</sup>L<sub>4</sub> complexes and an analysis of their molecular and electronic structure in an effort to place the capabilities of Rh<sub>2</sub><sup>6+</sup> within the context of Ru<sub>2</sub><sup>6+</sup>.

### III. Results and Discussion.

**Synthesis.** The general synthesis of *bis*( $\sigma$ -aryl)-Rh<sub>2</sub><sup>6+</sup>L<sub>4</sub> compounds was developed to enable the further exploration of the physical characteristics and potential function of these complexes. The synthesis reported in Chapter 1 used sodium tetraphenylborate as an aryl-donor under aerobic oxidation conditions catalyzed by a copper(I) salt to generate Rh<sub>2</sub>(cap)<sub>4</sub>Ph<sub>2</sub> (**1**) in excellent yield (Scheme 2-5) from Rh<sub>2</sub>(cap)<sub>4</sub> (**2**). To make the synthesis in Scheme 2-5 a general process, variation of the aryl-ring in the tetraarylborate salt was envisioned. Although there are reported procedures for the preparation of tetra-arylborate salts, they are not general over a wide range of aryl substitution patterns and are potentially dangerous to perform.<sup>80</sup> Thus, an alternative to the aryl donor in Scheme 2-5 was pursued.

**Scheme 2-5.** First generation procedure for the preparation of **1**.<sup>81</sup>

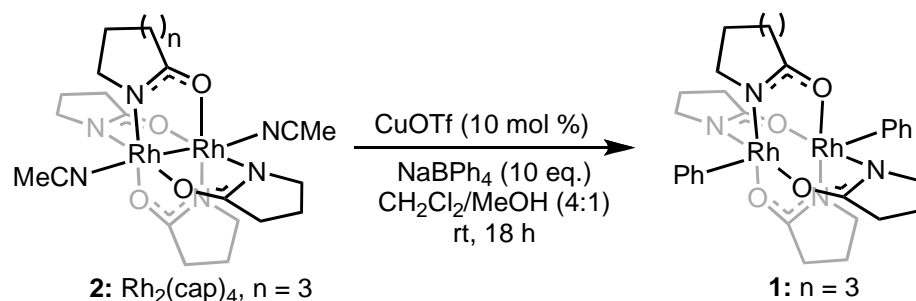


<sup>80</sup> Yakelis, N. A.; Bergman, R. G. *Organometallics* **2005**, *24*, 3579.

<sup>81</sup> Nichols, J. M.; Wolf, J.; Zavalij, P.; Varughese, B.; Doyle, M. P. *J. Am. Chem. Soc.* **2007**, *129*, 3504.

Arylboronic acids are widely available, easily prepared,<sup>82</sup> and well-documented transmetalating agents in the preparation of transition-metal aryl species.<sup>83</sup> Thus, phenylboronic acid was targeted as an aryl-donor in the preparation of **1** under the copper-catalyzed oxidation conditions in Scheme 2-5 using sodium methoxide (NaOMe) to generate an arylborate salt *in situ* (Scheme 2-6).

**Scheme 2-6.** Reaction Development.



Entry <sup>a</sup>	Cu <sup>b</sup> (X mol %)	PhB(OH) <sub>2</sub> (Y eq.)	NaOMe (Z eq.)	% yield <sup>c</sup>
1	10	2	2	0
2	10	2	10	48
3	10	5	10	98
4	10	10	10	98
5	10	10	0	66
6	10	10	5	78
7	0	10	10	0

<sup>a</sup>Reaction conditions: Rh<sub>2</sub>(cap)<sub>4</sub>(CH<sub>3</sub>CN)<sub>2</sub> (0.027 mmol), solvent (5 mL), ambient temperature and atmosphere. <sup>b</sup>[CuOTf]<sub>2</sub>-C<sub>6</sub>H<sub>6</sub> was used. <sup>c</sup>Isolated by silica gel chromatography.

<sup>82</sup> a) Li, W.; Nelson, D. P.; Jensen, M. S.; Hoerner, R. S.; Cai, D. *J. Org. Chem.* **2002**, *67*, 5394. b) Brown, H. C.; Bhat, N. G.; Somayaji, V. *Organometallics* **1983**, *2*, 1311.

<sup>83</sup> Miyaura, N.; Suzuki, A. *Chem. Rev.* **1995**, *95*, 2457.

In Scheme 2-6, all stoichiometries and yields are relative to  $\text{Rh}_2(\text{cap})_4$  as the limiting reagent. Initial attempts with stoichiometric amounts of phenylboronic acid and sodium methoxide (Entry 1, Scheme 2-6) were unsuccessful. Sodium methoxide was poorly soluble in the solvent system ( $\text{CH}_2\text{Cl}_2:\text{MeOH}$ ) as there was partially undissolved salt in the reaction mixture. Thus, to increase and maintain the amount of the dissolved salt, the amount of NaOMe was increased to 10 equivalents based on  $\text{Rh}_2(\text{cap})_4$ . The formation of **1** was immediately observed as a color change from red to green in the reaction and **1** was isolated in 48% yield (Entry 2, Scheme 2-6). Increasing the amount of phenylboronic acid to 5 equivalents (Entry 3, Scheme 2-6) and 10 equivalents (Entry 4, Scheme 2-6) provided **1** in nearly quantitative yield. NaOMe was not necessary for the reaction to proceed, but was requisite for the reaction to proceed to completion (Entries 5 & 6, Scheme 2-6). CuOTf was also necessary under these conditions, similar to the original methodology (Entry 7, Scheme 2-6).

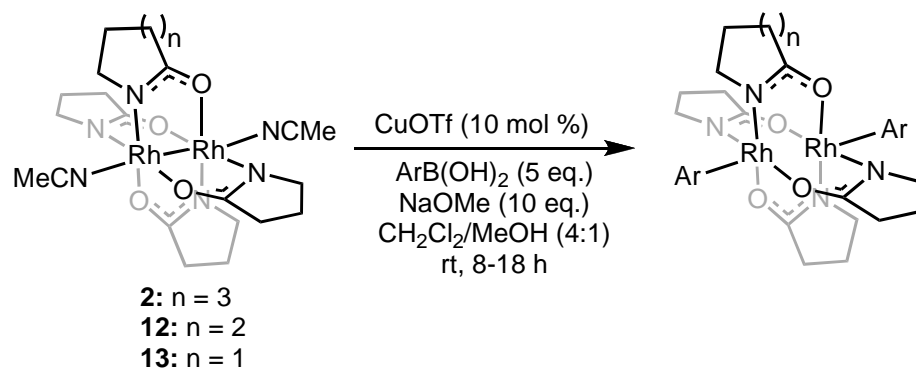
With reaction conditions in hand, the scope of the transformation was explored. The results are enumerated in Scheme 2-7. Varying the number of methylenes ( $n$ ) in the  $\mu$ -bridging ligand varies the oxidation potential of the complex by approximately 150 mV, decreasing from  $n = 1$  to  $n = 3$ .<sup>84</sup> The reaction proceeded smoothly with  $n = 1$  to yield  $\text{Rh}_2(\text{pyr})_4\text{Ph}_2$  (**13**, Entry 1, Scheme 2-7) and  $n = 3$  to form **1** (Entry 3, Scheme 2-7). However, reaction yield suffered for  $n = 2$  to form  $\text{Rh}_2(\text{val})_4\text{Ph}_2$  (**12**, Entry 2, Scheme 2-7). The reaction was tolerant of varying boronic acid substitution.  $\text{Rh}_2(\text{cap})_4\text{Ar}_2$  complexes with electron-withdrawing aryl rings were prepared in moderate to good yield (Entries 4-7, Scheme 2-7). Complexes with electron-donating aryl rings were prepared in poor to moderate yield (Entries 8, 9 and 11, Scheme

---

<sup>84</sup> Doyle, M. P.; Ren, T., *The Influence of Ligands on Dirhodium(II) on Reactivity and Selectivity in Metal Carbene Reactions*. In *Progress in Inorganic Chemistry*, Karlin, Ed. Wiley: New York, **2001**, 49, 113-168.

2-7) as was the heteroaromatic thiophene complex (**20**, Entry 10, Scheme 2-7).

**Scheme 2-7.** Second-generation procedure for the preparation of  $\text{Rh}_2\text{L}_4\text{Ar}_2$  complexes.



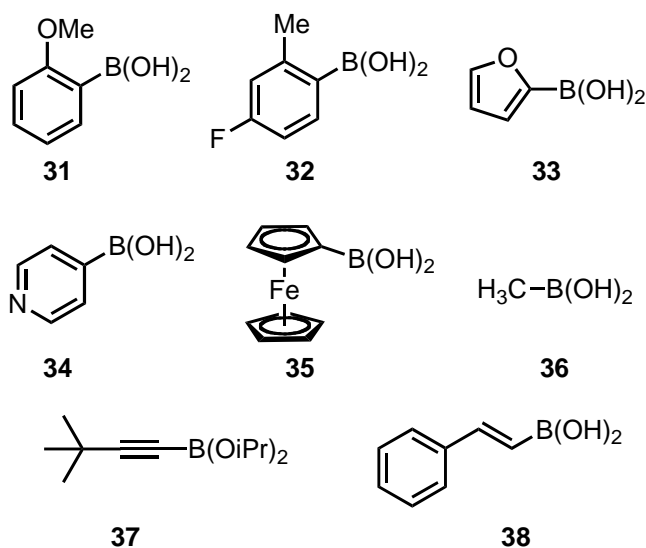
Entry <sup>a</sup>	n	Ar	% yield <sup>b</sup>
<b>1</b>	1-pyr	<b>1</b> : $\text{C}_6\text{H}_5^-$	98
<b>2</b>	2-val	<b>12</b> : $\text{C}_6\text{H}_5^-$	48(2) <sup>d</sup>
<b>3</b>	3-cap	<b>13</b> : $\text{C}_6\text{H}_5^-$	98(1) <sup>d</sup>
<b>4</b>	3	<b>14</b> : 3- $\text{NO}_2\text{-C}_6\text{H}_4^-$	59(5) <sup>c, d</sup>
<b>5</b>	3	<b>15</b> : 3- $\text{CHO-C}_6\text{H}_4^-$	54 <sup>c</sup>
<b>6</b>	3	<b>16</b> : 4- $\text{CHO-C}_6\text{H}_4^-$	99 <sup>c</sup>
<b>7</b>	3	<b>17</b> : 4- $\text{Br-C}_6\text{H}_4^-$	91
<b>8</b>	3	<b>18</b> : 4- $\text{MeO-C}_6\text{H}_4^-$	88(1) <sup>d</sup>
<b>9</b>	3	<b>19</b> : 4- $(\text{NMe}_2)\text{-C}_6\text{H}_4^-$	34
<b>10</b>	3	<b>20</b> : 3- $(\text{C}_4\text{H}_3\text{S})^-$	76(6) <sup>d</sup>
<b>11</b>	3	<b>21</b> : 4- $(\text{NHBoc})\text{-C}_6\text{H}_4^-$	71 <sup>c</sup>

<sup>a</sup>Reaction conditions:  $\text{Rh}_2(\text{cap})_4(\text{CH}_3\text{CN})_2$  (0.027 mmol), solvent (5 mL), ambient temperature and atmosphere. <sup>b</sup>Isolated yield based on  $\text{Rh}_2\text{L}_4$  from a single run unless otherwise noted. <sup>c</sup> $\text{RB(OH)}_2$  (10 eq.). <sup>d</sup>Average of duplicate reactions. Variation in the last reported digit is shown in parentheses.

The reaction was not tolerant of all arylboronic acids, however (Figure 2-2). Any ortho-substitution in the form of 2-substituted arylboronic acids (**31** and **32**) or 2-furanylboronic acid (**33**) provided no isolable amount of the

corresponding  $\text{Rh}_2^{6+}\text{L}_4\text{Ar}_2$  complexes. 4-Pyridylboronic acid (**34**) and ferrocenylboronic acid (**35**) also did not produce the expected complexes. In addition to these substrates, the reaction was not tolerant of non-aromatic substituents. Reactions with methylboronic acid (**36**), *trans*-cinnamyl boronic acid (**37**), or *bis*-isopropoxy-*tert*-butylethynylboronic ester (**38**) were all unsuccessful and provided no isolable dirhodium(III) complex.<sup>85</sup>

**Figure 2-2.** Boronic acids that did not form isolable  $\text{Rh}_2^{6+}$  complexes.



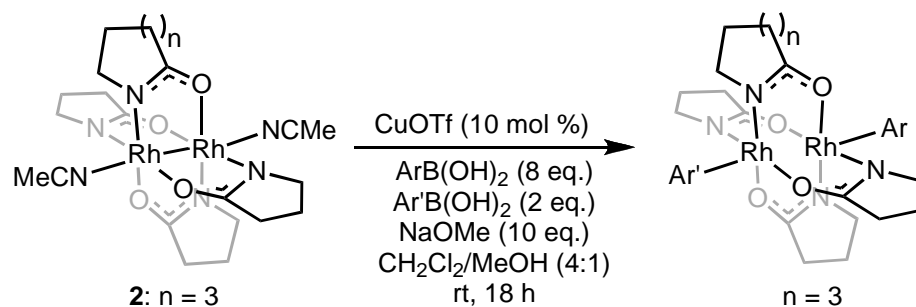
The synthetic methodology was further expanded to include the preparation of  $[(\sigma\text{-aryl})(\sigma\text{-aryl}')]\text{-Rh}_2\text{L}_4$  complexes with two different aryl rings as axial ligands (Scheme 2-8). Considering the formation of the *bis*( $\sigma\text{-aryl}$ )- $\text{Rh}_2^{6+}$  complexes as a stepwise oxidation/aryl transfer, it was assumed that electron rich aryl rings would transfer faster than electron-deficient aryl rings under the reaction conditions. Varying the relative stoichiometry of the boronic acids within the reaction conditions confirmed this assumption and a 4:1 mixture of 4-formylphenyl- and phenylboronic acid was optimal for the preparation of *trans*- $[\sigma\text{-(4-CHO-C}_6\text{H}_4), (\sigma\text{-C}_6\text{H}_5)]\text{-Rh}_2(\text{cap})_4$

<sup>85</sup> The  $\text{Rh}_2^{6+}$  complexes from **37** and **38** could be observed *in situ* with absorption maxima at ~430 nm.



(**22**, Entry 1, Scheme 2-8). Thus, the more electron-rich aryl ring was used as the minor portion of a 4:1 mixture of boronic acids with  $\text{Rh}_2(\text{cap})_4$  to yield the corresponding heterosubstitution pattern.

**Scheme 2-8.** Preparation of  $\text{Rh}_2\text{L}_4\text{ArAr}'$  complexes (Abbreviations: OTf – see Scheme 2-1).



Entry <sup>a</sup>	Ar	Ar'	% yield Ar/Ar' <sup>b, c</sup>	% yield Ar <sub>2</sub> <sup>b, c</sup>	% yield Ar' <sub>2</sub> <sup>b, c</sup>
1			55 ( <b>22</b> )	23 ( <b>16</b> )	13 ( <b>1</b> )
2			48 ( <b>23</b> )	16 ( <b>16</b> )	4 ( <b>18</b> )
3			23 ( <b>24</b> )	7 ( <b>15</b> )	NA <sup>d</sup>

<sup>a</sup>Reaction conditions:  $\text{Rh}_2(\text{cap})_4(\text{CH}_3\text{CN})_2$  (0.027 mmol), solvent (5 mL), ambient temperature and atmosphere. <sup>b</sup>Isolated yield for each purified complex recovered from a single experiment based on  $\text{Rh}_2\text{L}_4$  as the limiting reagent. <sup>c</sup>Compound references are in parentheses. <sup>d</sup>Not isolated from the reaction mixture.

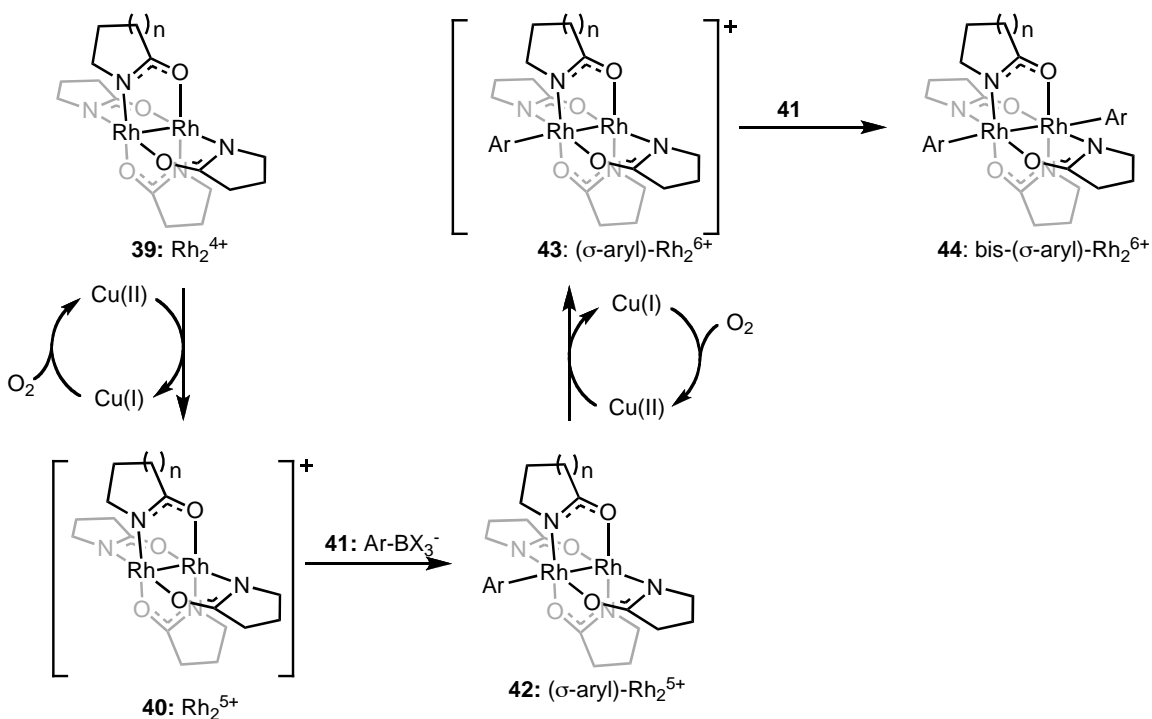
Using this strategy, mixtures of electron-rich arylboronic acids with 4-formylphenyl boronic acid (Entries 1 and 2, Scheme 2-8) or 3-formylphenyl boronic acid (Entry 3, Scheme 2-8) yielded the corresponding heterosubstituted product in low to moderate yield. In each case, the product was separated from a mixture of *bis*( $\sigma$ -aryl)-, *bis*( $\sigma$ -aryl')-, and [( $\sigma$ -aryl), ( $\sigma$ -aryl')]- $\text{Rh}_2(\text{cap})_4$  complexes. The ratio of each product was determined based

on pure materials isolated from column chromatography. Compound **22** was isolated in 55% yield from a 4:2:1 mixture of Ar/Ar', Ar<sub>2</sub>, and Ar'<sub>2</sub>. Compound **23** was isolated in 48% yield from a 3:4:1 mixture of similar composition. Compound **24** was isolated in 23% yield from a 3:1 mixture of Ar/Ar' and Ar<sub>2</sub> and the Ar<sub>2</sub>' complex (**19**) was not observed. The overall low yield of **24** can be attributed to poor conversion as well as the oxidative dealkylation of *N,N*-dimethylaniline containing compounds. The poor conversion was observed as a substantial amount of Rh<sub>2</sub><sup>5+</sup>(cap)<sub>4</sub> in the visible spectrum of the crude mixture and *N*-methylaniline products were observed in <sup>1</sup>H-NMR spectrum of the crude reaction mixture. These products were not isolated.

The methodology described here provides general access to *bis*( $\sigma$ -aryl)- and [( $\sigma$ -aryl), ( $\sigma$ -aryl')]-Rh<sub>2</sub><sup>6+</sup> carboxamidates with considerable possibilities for substitutional variation. In light of the importance of group transfer reactions between boronic acids and transition metals, the mechanism of aryl transfer became a point of interest. The following discussion describes a brief inquiry into the mechanism of aryl transfer under the reaction conditions.

**Aryl Transfer Mechanism.** The following discussion will develop a basic model for the aryl transfer reaction. It is not intended to be a rigorous definition of mechanism for the reaction. The basic mechanism described in Chapter 1 for the formation of **1** is restated and generalized in Scheme 2-9. The formation of Rh<sub>2</sub><sup>6+</sup> from Rh<sub>2</sub><sup>4+</sup> is a net two-electron oxidation. The oxidation occurs through the Cu(I)/Cu(II) couple with molecular oxygen as the terminal oxidant. The reaction begins with the oxidation of a Rh<sub>2</sub><sup>4+</sup> complex (**39**) to a Rh<sub>2</sub><sup>5+</sup> complex (**40**). Aryl transfer from an aryl donor (**41**: ArBX<sub>3</sub><sup>-</sup>) then generates a ( $\sigma$ -aryl)-Rh<sub>2</sub><sup>5+</sup> complex (**42**). The formation of **42** lowers the Rh<sub>2</sub><sup>5+</sup>  $\rightarrow$  Rh<sub>2</sub><sup>6+</sup> oxidation potential and facilitates further oxidation. Oxidation of **42** by the Cu(I)/Cu(II) couple yields a ( $\sigma$ -aryl)-Rh<sub>2</sub><sup>6+</sup> complex (**43**) and subsequent aryl transfer from **41** to **43** yields a stable *bis*( $\sigma$ -aryl)-Rh<sub>2</sub><sup>6+</sup> complex (**44**).

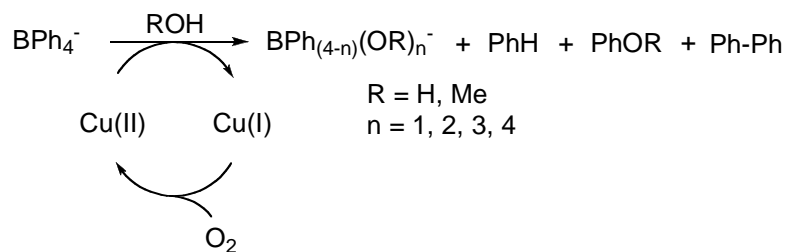
**Scheme 2-9.** Proposed mechanism for  $\text{Rh}_2^{6+}$  formation.



The evidence for the oxidation portion of the mechanism was provided in Chapter 1 and can be summarized as a rate dependence on both the copper salt and molecular oxygen under the reaction conditions. The preparation of  $[(\sigma\text{-aryl}), (\sigma\text{-aryl}')]\text{-Rh}_2\text{L}_4$  complexes speaks to the stepwise nature of the aryl transfer process. The identity of X in  $\text{Ar-BX}_3^-$  (**41**) is complicated when  $\text{NaBPh}_4$  is used as the aryl-transfer reagent. Copper-catalyzed solvolysis of  $\text{NaBPh}_4$  generates an ensemble of potential aryl-transfer reagents (Scheme 2-10).<sup>86</sup> Fortunately, this complication does not exist for arylboronic acids making the aryl transfer event more accessible to interrogation under the second-generation reaction conditions.

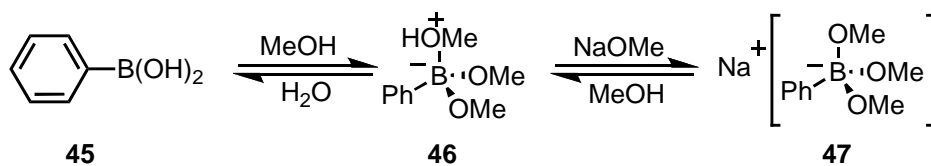
<sup>86</sup> Crawford, C. L.; Barnes, M. J.; Peterson, R. A.; Wilmarth, W. R. *J. Organomet. Chem.* **1999**, *581*, 194.

**Scheme 2-10.** Copper-catalyzed solvolysis of NaBPh<sub>4</sub>.



Initial mechanistic considerations begin with the state of the arylboronic acid in the presence of base in an alcohol solvent. Based on the reactivity of boronic acids with alcohols,<sup>87</sup> the arylboronic acid is expected to undergo the basic solvolysis shown in Scheme 2-11. Phenylboronic acid (**45**), when dissolved in a 4:1 mixture of CH<sub>2</sub>Cl<sub>2</sub>:MeOH, enters into a solvolytic equilibrium with its solvated methylborinic ester (**46**). Deprotonation of **46** in the presence of NaOMe yields the anionic methylborate ester (**47**) as the proposed aryl transfer agent.

**Scheme 2-11.** Reaction of phenylboronic acid in alcohol solvent with base.



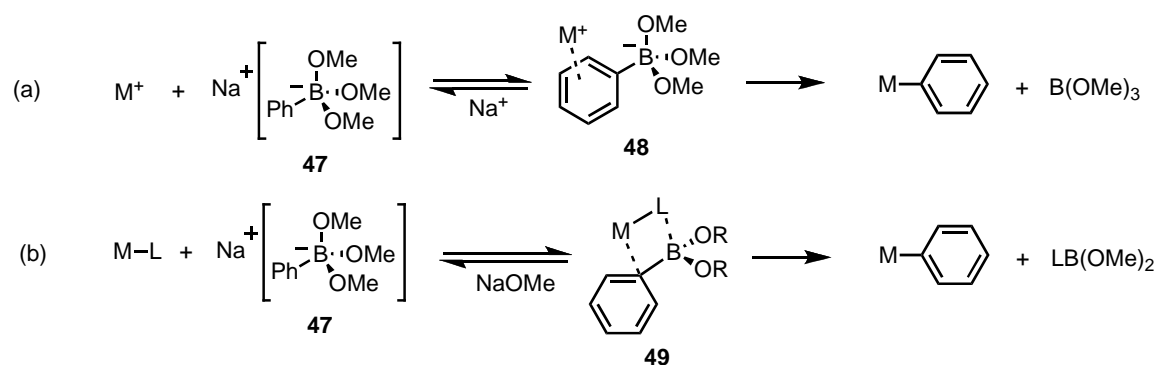
There are two reaction mechanisms for aryl transfer that dominate the literature. These mechanisms are shown in Scheme 2-12 using **47** as the putative aryl transfer agent. The first involves a cation- $\pi$  association between a cationic metal salt and an arylborate (Scheme 2-12a).<sup>88</sup> This mechanism begins with an initial association between the aryl ring of the borate anion and the transition metal cation to form a cation- $\pi$  complex (**48**). Group transfer of the aryl ring from the boron to the metal generates a new metal-aryl bond and

<sup>87</sup> Roy, C. D.; Brown, H. C. *J. Organomet. Chem.* **2007**, 692, 784.

<sup>88</sup> Strauss, S. H. *Chem. Rev.* **1993**, 93, 927.

a neutral, trivalent boron species. Facile cation- $\pi$  transfers are known for cationic Rh(I) and Au(I) complexes with tetra-arylborates and have been well characterized.<sup>89</sup> The second mechanism is a transmetalation between a transition metal and an arylboronic acid, or ester (Scheme 2-12b). This mechanism begins with the formation of a boron-metalloccycle (**49**) with both the aryl ring and a coordinating ligand bridging the transition metal and boron atoms. Ligand migration within the boron-metalloccycle results in the simultaneous transfer of an aryl-ring to the metal and the coordinating ligand to boron to yield a new metal-aryl bond and a neutral, trivalent boron species. This type of transfer has been observed for Rh(I) and Pt(IV) complexes.<sup>90</sup>

**Scheme 2-12.** Aryl transfer mechanisms.



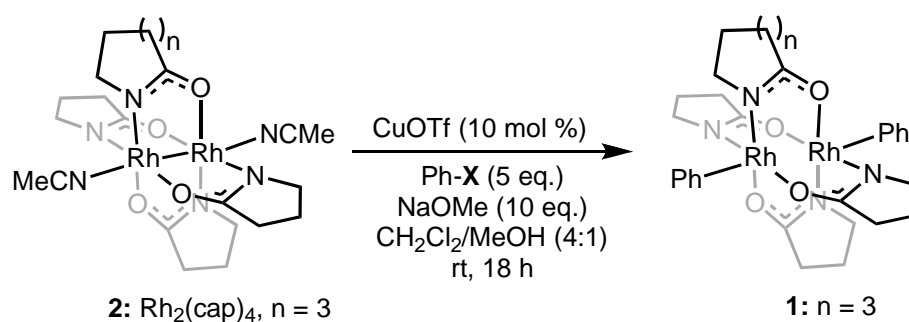
To test the solvolysis model in Scheme 2-11, the formation of  $\text{Rh}_2(\text{cap})_4\text{Ph}_2$  (**1**) from  $\text{Rh}_2(\text{cap})_4$  with various boronic ester precursors was monitored (Scheme 2-13). Under the standard reaction conditions with phenylboronic acid, **1** was prepared in 98% isolated yield. When boronic esters prepared from chelating alcohols with increasing steric bulk were used, little to no formation of **1** was observed (Entries 2 and 3, Scheme 2-13). As the chelating alcohols are less likely to undergo the solvolysis with MeOH

<sup>89</sup> a) Forward, J. M.; Fackler, J. P., Jr.; Staples, R. J. *Organometallics* **1995**, *14*, 4194, b) Aresta, M.; Quaranta, E.; Tommasi, I.; Derien, S.; Dunach, E. *Organometallics* **1995**, *14*, 3349.

<sup>90</sup> a) Khaskin, E.; Zavalij, P. Y.; Vedernikov, A. N. *Angew. Chem., Int. Ed.* **2007**, *46*, 6309, b) Zhao, P.; Incarvito, C. D.; Hartwig, J. F. *J. Am. Chem. Soc.* **2007**, *129*, 1876.

under the reaction conditions, it follows that the steric bulk of the oxygen substituent of the arylboronate directly impacts the formation of **1**. Sodium phenyltrifluoroborate was submitted to the reaction conditions and did not provide **1** (Entry 4, Scheme 2-13). The lack of reaction with potassium phenyltrifluoroborate is unlikely due to steric effects, but suggests that the simple cation- $\pi$  mechanism described in Scheme 2-12a is not a sufficient model for this reaction.

**Scheme 2-13.** Effect of boron substituents on the formation of **1**.



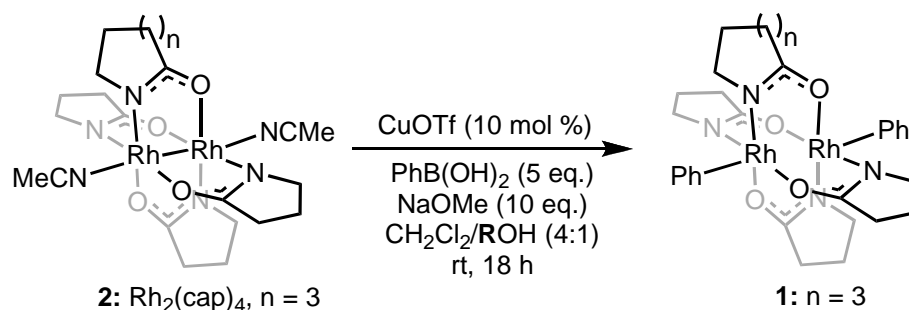
entry	X	% yield <sup>a</sup>
1	-B(OH) <sub>2</sub>	98
2		18
3		0
4	Na <sup>+</sup>	0

<sup>a</sup>Isolated yields from chromatography. Reaction conditions: Rh<sub>2</sub>(cap)<sub>4</sub>(CH<sub>3</sub>CN)<sub>2</sub> (0.027 mmol), solvent (5 mL), ambient temperature and atmosphere.

The possibility of a boronic ester (**46**, Scheme 2-11) as the aryl transfer agent was explored. Phenylboronic acid was stirred in methanol with NaOMe

for 90 minutes to undergo solvolysis. Removal of solvent under reduced pressure provided a clear oil that was immediately submitted to the reaction conditions in Scheme 2-14 as a substitute for phenylboronic acid, NaOMe, and methanol. The reaction proceeded to **1** in 55% isolated yield after chromatography. A similar reaction using 2-propanol did not proceed to **1** within the 12 h reaction time.

**Scheme 2-14.** Effect of alcohol co-solvent on the formation of **1**.



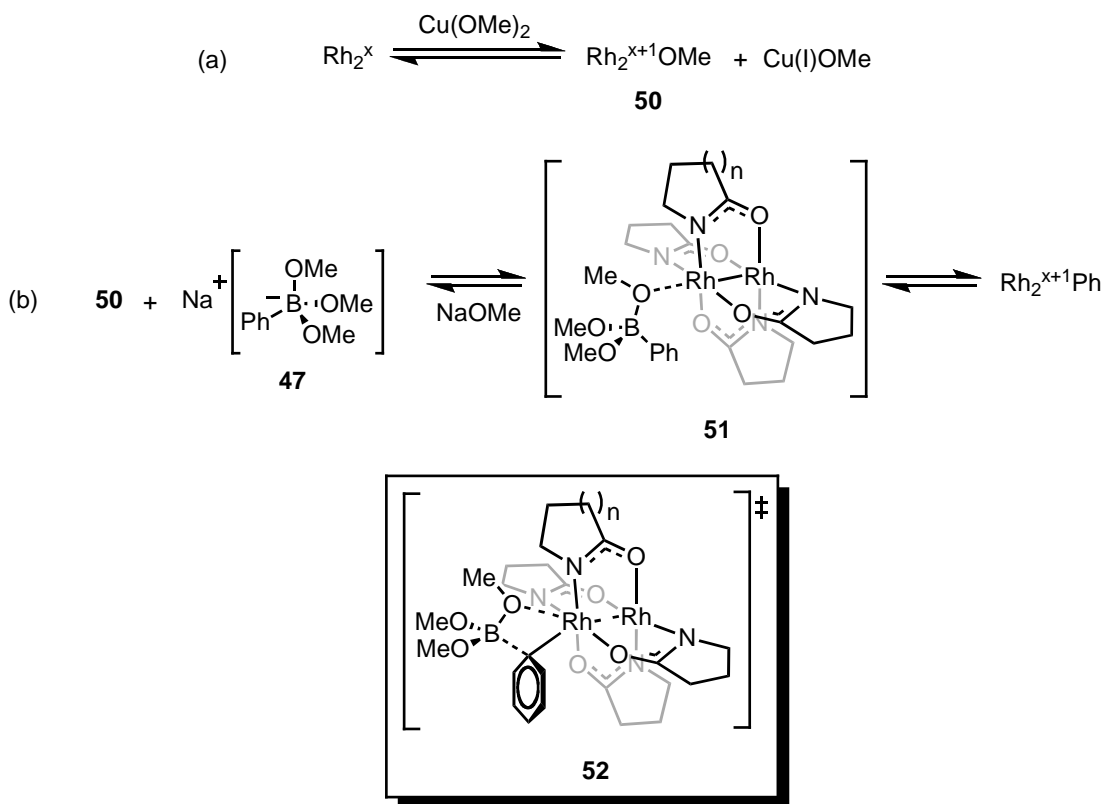
entry	R	% yield <sup>a</sup>
<b>1</b>	Me	98
<b>2</b>	Et	29
<b>3</b>	<i>n</i> -Bu	16
<b>4</b>	<i>i</i> -Bu	4
<b>5</b>	<i>i</i> -Pr	0
<b>6</b>	<i>t</i> -Bu	0

<sup>a</sup>Isolated yields from chromatography. Reaction conditions:  $\text{Rh}_2(\text{cap})_4(\text{CH}_3\text{CN})_2$  (0.027 mmol), solvent (5 mL), ambient temperature and atmosphere.

Further probing of the solvolysis model shown in Scheme 2-11 with alcohol co-solvents of varying steric bulk revealed dramatic size dependencies consistent with the formation of an arylboronate like **47**. Scheme 2-14 is a summary of co-solvents arranged by increasing bulk. In the reaction of **2** with phenylboronic acid to form **1**, changing the alcohol from MeOH to EtOH caused a sharp decrease in yield (Entries 1 and 2). Longer chain (Entry 3),  $\alpha$ -branched (Entries 5 and 6), and  $\beta$ -branched (Entry 4) alcohols all inhibited the formation of **1**. As an electron-transfer, the oxidation

of  $\text{Rh}_2(\text{cap})_4$  by  $\text{Cu}(\text{II})$  would depend on the dielectric constant of the solvent and the observed reaction dependencies could be the result of a decreasing dielectric constant with the increasing hydrocarbon character of the alcohol. This is not the case, however, as *n*-butyl, *i*-butyl, and *t*-butyl alcohol all have similar dielectric constants,<sup>91</sup> yet the formation of **1** is diminished with increasing bulk near the boron center.

**Scheme 2-15.** Proposed transmetalation-type mechanism for aryl-transfer.



Based on the strong steric influence imposed by the substituents on the borate ester and the elimination of a cation- $\pi$  mechanism, a transmetalation mechanism is proposed in Scheme 2-15. Copper(II) methoxide [ $\text{Cu}(\text{OMe})_2$ ] is the most likely copper(II) species present under reaction conditions with a large excess of  $\text{NaOMe}$ . Likewise, the oxidation of

<sup>91</sup> Danhauser, W.; Cole, R. H. *J. Chem. Phys.* **1955**, 23, 1762.



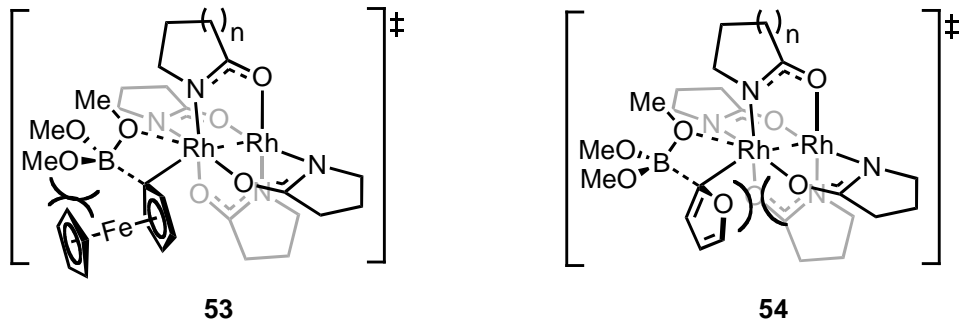
the dirhodium complex by  $\text{Cu}(\text{OMe})_2$  in the presence of a large excess of  $\text{NaOMe}$  generates a dirhodium-methoxide salt (**50**, Scheme 2-15a).<sup>92</sup> Anion exchange between the aryl transfer reagent (**47**) yields a contact ion pair (**51**) with the dirhodium complex ligating one of the methoxide substituents of **47**. Analogous to the mechanism in Scheme 2-12b, a ligand exchange between dirhodium and boron in **51** through a transmetalation-like transition state (**52**) yields a new dirhodium-aryl bond and a neutral, trivalent boron species (Scheme 2-15b). The proposed intimate contact between the aryl transfer reagent and the dirhodium species in the transition state is consistent with the observed steric effects and the proposed geometry is consistent with the lack of reactivity with sodium phenyltrifluoroborate.

The aryl transfer model in Scheme 2-15 helps to explain some of the recalcitrant substrates in Figure 2-2. For example, the inability to transfer the ferrocenyl group from ferrocenyl boronic acid (**35**, Figure 2-2) is reasonable based on the proposed transmetalation. The required geometry (**53**) would force the iron center of ferrocene into the ligand sphere of boron causing a severe steric interaction. The inability to transfer the 2-furanyl group can also be understood by electronic repulsions in the proposed transition state (**54**). When the heteroatom is moved to the 3-position, as was the case with 3-thienylboronic acid, the transfer proceeds smoothly to **20** (Scheme 2-1). This model provides a rational tool for constructing other  $(\sigma\text{-aryl})\text{-Rh}_2^{6+}\text{L}_4$  complexes, however, more work is necessary to validate the model chemically.

---

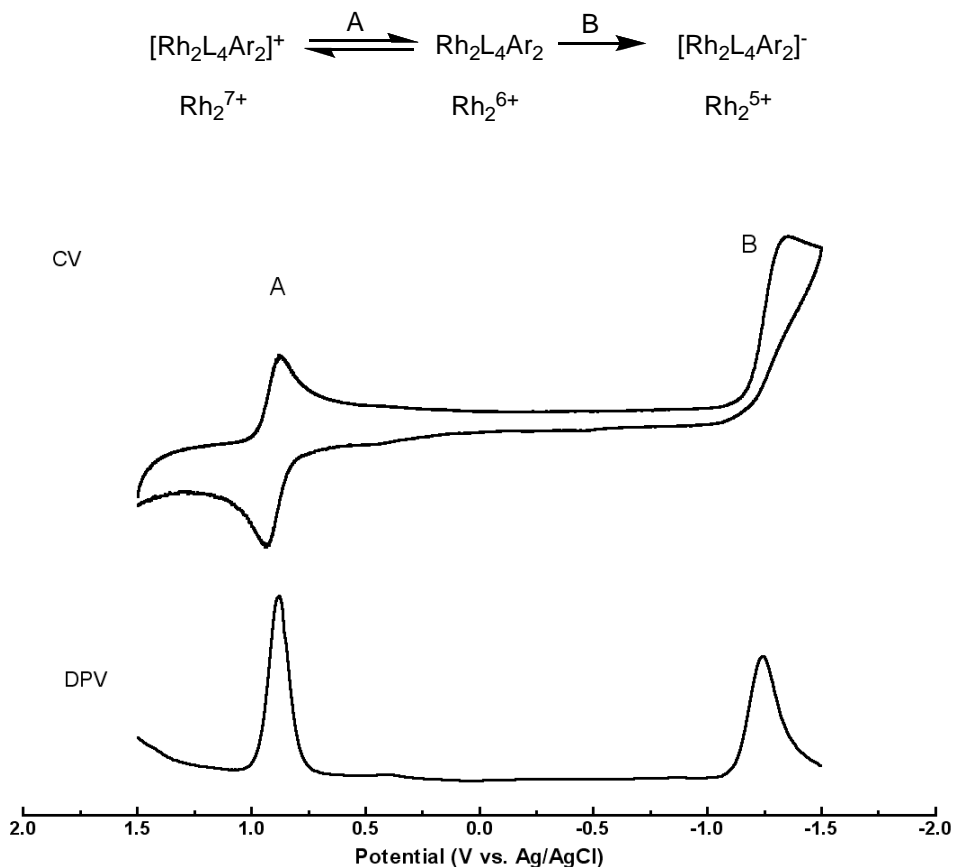
<sup>92</sup> An inner sphere electron transfer with concurrent ligand transfer could also generate X, Astruc, D., *Electron-Transfer and Radical Processes in Transition Metal Chemistry*. Wiley: New York, **1995**.

**Figure 2-3.** Model transition states for recalcitrant substrates.



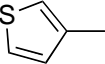
**Voltammetric and Spectroscopic Properties.** The electrochemistry of complexes **1**, **12-14**, **16**, **18**, **20**, **21**, and **23** was measured in CH<sub>2</sub>Cl<sub>2</sub> by cyclic and differential pulse voltammetry (CV and DPV, respectively). The half-wave potentials ( $E_{1/2}$ ) are reported in Table 2-2. The electrochemistry for the remaining compounds in Table 2-2 was not measured due to poor solubility or limited availability. Figure 2-4 shows the CV and DPV traces for Rh<sub>2</sub>(pyr)<sub>4</sub>Ph<sub>2</sub> (**13**) as a representative example. For all of the complexes measured, a reversible Rh<sub>2</sub><sup>7+/6+</sup> redox couple (A) was observed. For complexes **13**, **14**, **16**, **18**, and **23** an additional irreversible redox couple near the reduction limit of the solvent was observed and is assigned to the Rh<sub>2</sub><sup>6+/5+</sup> redox couple (B). Electronic absorption maxima ( $\lambda_{\text{max}}$ ) are also reported in Table 2-2 along with their conversion to singlet transition energies based on the formula  $E_s = 10^7/8065.5\lambda$ .

**Figure 2-4.** CV and DPV vs Ag/AgCl for Rh<sub>2</sub>(pyr)<sub>4</sub>(C<sub>6</sub>H<sub>5</sub>)<sub>2</sub> (**11**) measured in CH<sub>2</sub>Cl<sub>2</sub> (1 mM) with tetra-*n*-butylammonium hexafluorophosphate as the supporting electrolyte.



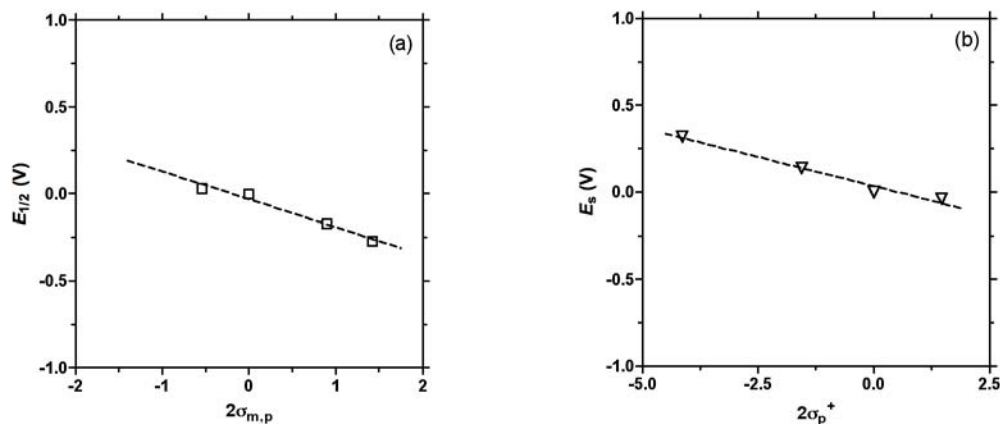
Comparison of  $E_{1/2}$  and  $\lambda_{\text{max}}$  for complexes with varying aryl substitution follows a logical progression. As the electron-withdrawing nature of the ligand increases, the oxidation potential increases slightly. The Rh<sub>2</sub><sup>7+/6+</sup> redox couple for the electron rich complex with Ar = 4-methoxyphenyl- (**18**) is 0.75 V. The redox couple shifts anodically to 0.78 V for Ar = phenyl (**1**) and to 1.05 V for Ar = 3-nitrophenyl- (**14**). The singlet-excitation energy ( $E_s$ ) calculated from the electronic absorption spectrum also increases as the electron-withdrawing nature of the aryl ring increases. The singlet-excitation energy is 2.56 eV (485 nm) for Ar = 4-(*N,N*-dimethylphenyl)- (**19**) and  $E_s$  increases to 2.93 eV (423 nm) for complex Ar = 3-nitrophenyl- (**14**).

**Table 2-2.** Electronic comparison ( $E_{1/2}$  and  $\lambda_{\max}$ ) for  $\text{Rh}_2\text{L}_4\text{Ar}_2$  and  $\text{Rh}_2\text{L}_4\text{ArAr}'$ .[NOTE: Table is organized by increasing value of  $\lambda_{\max}$ ].

Entry	Ar	$E_{1/2}$ (V) <sup>a,b</sup>	$\lambda_{\max}$ (nm) <sup>c</sup>	$E_s$ (eV)
1	1: C <sub>6</sub> H <sub>5</sub> -	0.78	430	2.88
2	12: C <sub>6</sub> H <sub>5</sub> -	0.81	429	2.89
3	13: C <sub>6</sub> H <sub>5</sub> -	0.91(-1.36)	442	2.81
4	14: 3-NO <sub>2</sub> -C <sub>6</sub> H <sub>4</sub> -	1.05(-1.23)	423	2.93
5	16: 4-CHO-C <sub>6</sub> H <sub>4</sub> -	0.95(-1.34)	425	2.92
6	15: 3-CHO-C <sub>6</sub> H <sub>4</sub> -	-	425	2.92
7	22: (4-CHO-C <sub>6</sub> H <sub>4</sub> )-(C <sub>6</sub> H <sub>5</sub> )-	-	425	2.92
8	23: (4-CHO-C <sub>6</sub> H <sub>4</sub> )-(4-MeO-C <sub>6</sub> H <sub>4</sub> )-	0.85(-1.46)	430	2.88
9	17: 4-Br-C <sub>6</sub> H <sub>4</sub> -	-	432	2.87
10	24: (3-CHO-C <sub>6</sub> H <sub>4</sub> )-(4-Me <sub>2</sub> N-C <sub>6</sub> H <sub>4</sub> )-	-	438	2.83
11	21: 4-NHBoc-C <sub>6</sub> H <sub>4</sub> -	0.80	450	2.76
12	18: 4-MeO-C <sub>6</sub> H <sub>4</sub> -	0.75	452	2.74
13	20: 	0.85	458	2.71
14	19: 4-Me <sub>2</sub> N-C <sub>6</sub> H <sub>4</sub> -	-	485	2.56

<sup>a</sup>Reversible, anodic wave (A) reported as  $E_{1/2}$ , measured with platinum wire/glassy carbon working electrodes against a Ag/AgCl reference electrode in CH<sub>2</sub>Cl<sub>2</sub> with *n*-Bu<sub>4</sub>NPF<sub>6</sub> as the supporting electrolyte. <sup>b</sup>Irreversible, cathodic reduction (B) reported as cathodic peak potential ( $E_{pc}$ ) in parentheses. <sup>c</sup>Measured in CH<sub>2</sub>Cl<sub>2</sub>.

**Figure 2-5.** LFER relationships. a)  $E_{1/2}$  vs  $\sigma_{m,p}$ ; b)  $E_s$  vs  $\sigma_p^+$ .



The trends in half-wave potential and electronic absorption are experimentally consistent with the proposed electronic structure for these complexes of  $\pi^4\delta^2\pi^*4\delta^*2$ . A linear free energy relationship (LFER) can be calculated between  $\Delta E_{1/2}$  and  $2\sigma$  for the complexes **1**, **14**, **16**, and **18** where  $\Delta E_{1/2} = E_{1/2}(\mathbf{1}) - E_{1/2}(\mathbf{X})$ . A similar free energy relationship can be established for  $\Delta E_s$  and  $2\sigma$  for complexes **1**, **16**, **18**, and **19** where  $\Delta E_s = E_s(\mathbf{1}) - E_s(\mathbf{X})$ . The LFER for the  $\text{Rh}_2^{7+/6+}$  redox couple is -159 mV with a moderate correlation versus  $\sigma_m$  and  $\sigma_p$  ( $r^2 = 0.971$ ) and no correlation with  $\sigma_p^+$  (Figure 2-5a). This indicates that there is a weak interaction between the aryl ring and the HOMO of the complex.<sup>93</sup> In the proposed electronic structure,  $\delta^*$  constitutes the HOMO and is not of the appropriate symmetry to mix with the  $\pi$ -system of the aryl rings. Thus, the LFER is most likely the result of inductive interactions consistent with the lack of correlation with  $\sigma_p^+$ .

The LFER for  $E_s$  is -67 mV with a moderate correlation versus  $\sigma_p^+$  ( $r^2 = 0.977$ ) and very poor correlation ( $r^2 = 0.887$ ) with  $\sigma_{m,p}$  (Figure 2-5b). The

<sup>93</sup> a) Hansch, C.; Leo, A.; Taft, R. W. *Chem. Rev.* **1991**, *91*, 165, b) Ren, T. *Coord. Chem. Rev.* **1998**, *175*, 43, c) Lin, C.; Ren, T.; Valente, E. J.; Zubkowski, J. D. *J. Organomet. Chem.* **1999**, *570*, 114.

correlation with  $\sigma_p^+$  suggests that the change in  $E_s$  is due to  $\pi$ - $\pi$  interactions between the Rh-Rh core and the aryl ring. As  $E_s$  and the LFER were calculated from  $\lambda_{\max}$ , it follows that  $\pi^*$ - $\delta^*$  transitions make a substantial contribution to the absorptions between 420 and 500 nm. Similar assignments have been made for diruthenium(III) systems.<sup>94</sup> Consistent with this assignment, the negative LFER value for  $E_s$  indicates a destabilizing interaction between the orbitals responsible for the  $\pi^*$ - $\delta^*$  transitions in  $\lambda_{\max}$  with increasing electron-density in the  $\pi$ -system of the aryl rings.

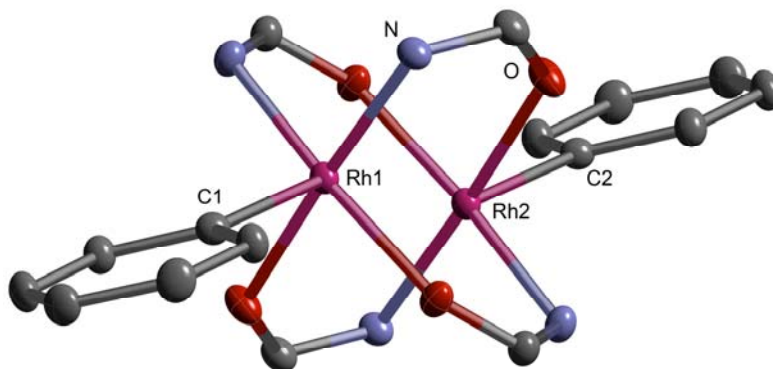
The HOMO-LUMO gaps ( $E_g$ ) for the complexes indicate that singlet transitions from the HOMO to the LUMO are not responsible for the absorptions between 420 and 500 nm. The average  $E_g$  for **13**, **14**, **16**, and **23** is 2.29(2) V and are estimated from the oxidation and reduction potentials determined by voltammetry. The  $E_g$  value is 0.54 V lower than the average  $E_s$  of 2.89(5). The relative difference in gap energies,  $E_g < E_s$ , indicates that the  $\pi^*$ (Rh-Rh) orbitals responsible for the  $\pi^*$ - $\delta^*$  singlet transitions are lower in energy than the HOMO. This is consistent with the proposed electronic configuration  $\pi^4 \delta^2 \pi^* \delta^* 2$ .

**Molecular Structure.** With the accessibility to a range of structures provided by the second-generation methodology, a more thorough examination of molecular and electronic structure was possible. Figure 2-6 shows the general structure of the core ligand sphere of the dirhodium(III) complexes studied. The following is a discussion of the comparative analysis of the molecular and electronic structure of the dirhodium(III) core.

---

<sup>94</sup> See ref. 64a

**Figure 2-6.** General structure with numbering scheme. [NOTE: The carbocyclic carboxamidate backbone and aryl ring substituents are not shown. The numbering scheme is generalized for the sake of comparison and does not correspond to the individual crystal structure data.]



X-ray crystal structures were obtained for seven of the complexes prepared in this study by single crystal X-ray diffraction spectroscopy (XRD). Structural parameters relevant to the dirhodium core and the Rh-aryl bond are compiled for each of these structures in Table 2-3. The overall homogeneity of the ( $\sigma$ -aryl)-Rh<sub>2</sub><sup>6+</sup> structures irrespective of substitution is readily apparent from the data. The Rh-Rh bond lengths for each of the Rh<sub>2</sub><sup>6+</sup> complexes averaged 2.521(23)<sup>95</sup> Å. The Rh-N, and Rh-O bond lengths were also tightly grouped with average values amounting to 2.015(70) Å and 2.086(5) Å, respectively. The Rh-C bond lengths were remarkably unperturbed by electronic substitution of the aryl-ring and average 1.993(8) Å. Bond angles were similarly uniform with average values of 157.1(33)°, 85.5(13)°, and 101.0(9)° for the C-Rh-Rh, C-Rh-O, and C-Rh-N bond angles respectively. The eclipsed configuration of the Rh<sub>2</sub>(NCO)<sub>4</sub> core is maintained with average torsion angles of 180.0(0)° for the C1-Rh1-Rh2-C2 angle and 1.9(4)° for the N-Rh1-Rh2-O angles.

---

<sup>95</sup> Values in parentheses are standard deviations calculated from the average values.

**Table 2-3.** Structural Comparison from XRD Data.

Parameter	Compound							Mean(SD) <sup>c</sup>
	<b>1</b> <sup>a</sup>	<b>12</b>	<b>13</b>	<b>16</b>	<b>23</b> <sup>b</sup>	<b>18</b>	<b>20</b>	
Bond Length (Å)								
Rh1-Rh2	2.519	2.516	2.570	2.515	2.519	2.511	2.494	2.521(23)
Rh-C <sub>av</sub>	1.999	1.996	1.982	1.984	1.995	2.003	1.995	1.993(8)
Rh-N <sub>av</sub>	2.013	2.027	2.003	2.016	2.018	2.013	2.012	2.015(7)
Rh-O <sub>av</sub>	2.083	2.083	2.096	2.086	2.089	2.086	2.080	2.086(5)
Bond angles (°)								
C-Rh-Rh <sub>av</sub>	155.4	157.3	164.2	154.6	155.3	157.3	155.8	157.1(33)
C-Rh-O <sub>av</sub>	84.6	87.1	87.1	85.7	85.4	85.0	83.6	85.5(13)
C-Rh-N <sub>av</sub>	101.9	99.9	99.9	100.8	101.0	101.1	102.1	101.0(9)
C1-Rh1-Rh2-C2 <sup>d</sup>	180.0	180.0	179.9	180.0	180.0	180.0	180.0	180.0(0)
N-Rh1-Rh2-O <sub>av</sub> <sup>d</sup>	1.9	2.7	1.7	2.2	1.9	1.5	1.5	1.9(4)

av = Average value. <sup>a</sup>Data reported in Ref. 81. <sup>b</sup>**23** is the Ar/Ar' complex related to **16** (Ar<sub>2</sub>) and **18** (Ar'<sub>2</sub>). <sup>c</sup>Values in parentheses are the variability in the last reported digit ( $\pm 1$  standard deviation from the mean). <sup>d</sup>Torsion angles.

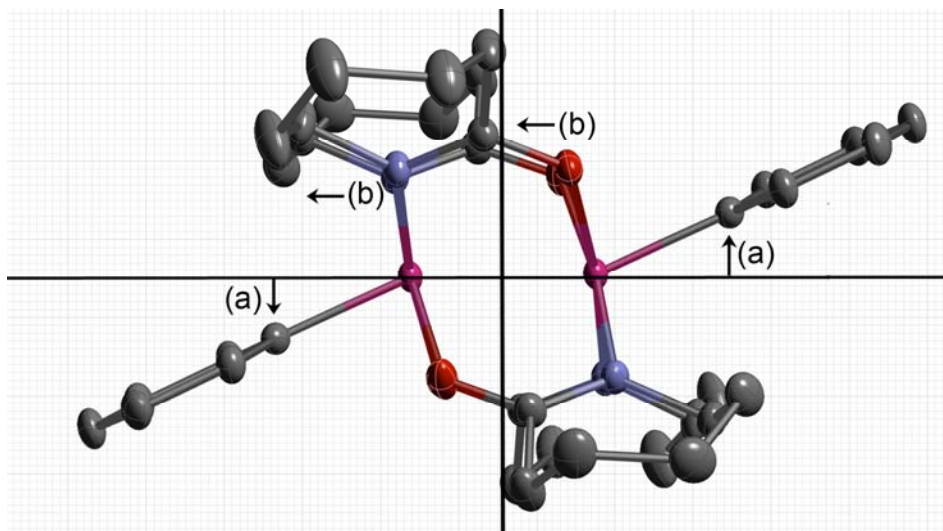
A general set of distortions away from the ideal octahedral geometry were observed for each complex in Table 2-3. The first distortion is an attenuated Rh-Rh bond distance in the *bis*( $\sigma$ -aryl)-Rh<sub>2</sub><sup>6+</sup>L<sub>4</sub> complexes in comparison with the parent Rh<sub>2</sub><sup>4+</sup> structures. Based on the interpretation provided in Chapter 1, the elongated Rh-Rh bond lengths are the result of changes in the electronic structure from Rh<sub>2</sub><sup>4+</sup> to *bis*( $\sigma$ -aryl)-Rh<sub>2</sub><sup>6+</sup>L<sub>4</sub>. In short, the new  $\sigma$ (Rh-C) bonds between the aryl-ligand and the dirhodium core effectively eliminates the  $\sigma$ (Rh-Rh) bond. Thus, the electronic configuration of the dirhodium MOs in the *bis*( $\sigma$ -aryl)-Rh<sub>2</sub><sup>6+</sup>L<sub>4</sub> complexes is  $\pi^4\delta^2\pi^*4\delta^*2$  resulting in a net Rh-Rh bond order of zero and longer Rh-Rh bond distances.

An ORTEP view of [Rh<sub>2</sub>(cap)<sub>4</sub>Ph<sub>2</sub>] $\cdot$ 2CH<sub>2</sub>Cl<sub>2</sub> (**[1]** $\cdot$ **2CH<sub>2</sub>Cl<sub>2</sub>**) in Figure 2-10 shows the second structural deformation. Two bond angle distortions are revealed when looking at the structure along the C<sub>2</sub>-axis of symmetry. The first is a distortion of the Rh-Rh-C angle away from the ideal value of 180° by an average of 23.9(33)° (Figure 2-7a). Accompanying the distortion along the



Rh-Rh vector, the oxygen atoms are shifted towards the center of the Rh-Rh bond to yield a more acute average angle by  $4.5(13)^\circ$ , while the nitrogen atoms are shifted in the same direction expanding the average Rh-Rh-N angle by  $11.0^\circ(9)$  (Figure 2-7b). This distortion occurs within the xy-plane and is symmetric about the  $C_2$ -rotational axis, the horizontal mirror plane ( $\sigma_h$ ), and the center of inversion maintaining an idealized  $C_{2h}$  symmetry. Thus, the Mulliken label associated with the symmetry of bond angle mode ( $A_g'$ ) will be used to indicate this type of structural deformation. Although only complex **1** is shown in Figure 2-7, the  $A_g'$  distortion is general for all of the complexes in Table 2-3.

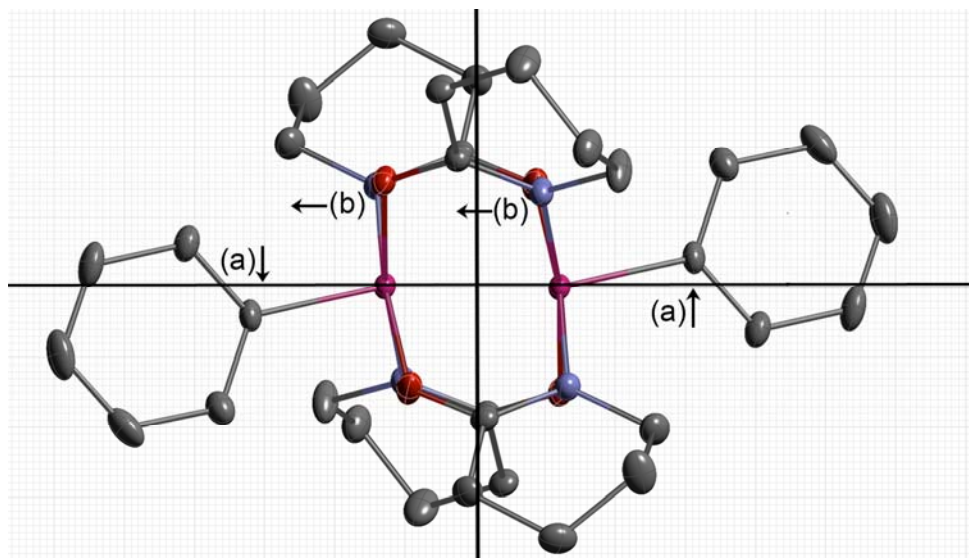
**Figure 2-7.** An ORTEP view of **[1]•2CH<sub>2</sub>Cl<sub>2</sub>** looking down the  $C_2$  rotational axis with the ligands eclipsed. Thermal ellipsoids are drawn at 30% probability. Hydrogens and solvent have been eliminated for clarity. Cross-hairs are provided as a reference for ideal bond angles.



Another related bond angle deformation can be found when looking at the xz-plane perpendicular to the  $C_2$ -axis of the complex. The angular distortion is analogous to the  $A_g'$  distortion mode, however, it occurs perpendicular to the horizontal mirror plane ( $\sigma_h$ ). An ORTEP drawing of  $[\text{Rh}_2(\text{val})_4\text{Ph}_2]\cdot 2\text{CH}_2\text{Cl}_2$  (**[12]•2CH<sub>2</sub>Cl<sub>2</sub>**) is shown in Figure 2-8 illustrating the

second bond angle distortion. Again, the Rh-Rh-C angle is non-linear by an average of  $9.8(36)^\circ$ . The two Rh-Rh-N $_\alpha$  and Rh-Rh-N $_\beta$  bond angles are inequivalent with N $_\alpha$  shifted toward the center of the Rh-Rh bond an average of  $11.3^\circ$  and N $_\beta$  is shifted away an average of  $4.6^\circ$ . A similar trend is observed for the Rh-Rh-O $_\alpha$  and Rh-Rh-O $_\beta$  bond angles where O $_\alpha$  is shifted toward the center of the Rh-Rh bond an average of  $9.7^\circ$  and O $_\beta$  is shifted away an average of  $3.8^\circ$ . Thus, it reduces the ideal C $_{2h}$  symmetry of the complexes to the C $_i$  point group. This distortion is common to each of the structures prepared in Table 2-3 *except* complexes **1** and **13**. The distortion is not symmetric about the C $_2$ -rotational axis or the  $\sigma_h$  mirror plane, but maintains a center of inversion. This distortion will be referred to by the Mulliken symbol associated with the bond angle distortion mode (B $_g''$ ).

**Figure 2-8.** Eclipsed ORTEP view of **12**•2CH $_2$ Cl $_2$  illustrating the B $_g''$  distortion mode looking perpendicular to the C $_2$ -rotational axis. Hydrogens and solvent have been eliminated for clarity. Cross-hairs are provided as a reference.



**Electronic Effects on Molecular Structure.** To get a more complete picture of the interactions responsible for the observed molecular distortions, calculations were performed on model compounds of a *bis*( $\sigma$ -phenyl)-dirhodium(III) complex using density functional theory (DFT) and Fenske-Hall molecular orbital (MO) calculations.<sup>96</sup> The model compound was derived from the basic *bis*( $\sigma$ -phenyl)-dirhodium(III) structure by replacing the cyclic  $\mu$ -bridging carboxamidate ligand with formamidinate ( $\text{CN}_2\text{H}_2$ ). The geometry of each of the complexes was optimized with the B3LYP functional using the LANL2DZ basis set. Fenske-Hall MO calculations were performed on these optimized structures. There are two main advantages of the Fenske-Hall calculation.<sup>97</sup> The method is very inexpensive computationally, yet remarkably accurate. In many cases, the Fenske-Hall calculations accurately give the MO configurations predicted by more sophisticated DFT calculations.<sup>98</sup> Moreover, the Fenske-Hall calculations use linear combinations of atomic orbitals (LCAO) to build the MOs for a given structure. This facilitates a chemical interpretation of the MO output that can be difficult to obtain from DFT calculations.

The model complexes are shown in Figure 2-9. Complex **55** is an approximation of the idealized Rh-Rh-C bond angle ( $180^\circ$ ) and has  $C_{2h}$  symmetry. Complex **56** models the symmetric  $A_g'$  bond angle distortion maintaining the  $C_{2h}$  symmetry and complex **57** models the anti-symmetric  $B_g''$  bond-angle distortion that reduces the  $C_{2h}$  symmetry to the  $C_i$  point group.

---

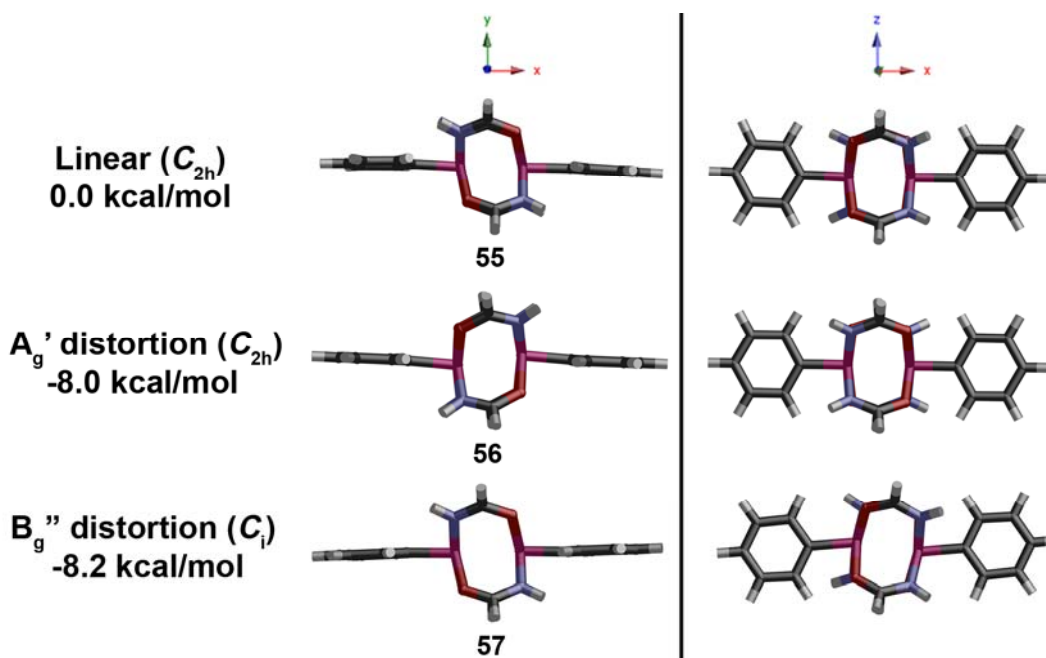
<sup>96</sup> Rinaldo Poli, Professor, Center for Coordination Chemistry, Toulouse, Fr. Performed the DFT calculations that provided the optimized geometries. The Fenske-Hall MO calculations were performed by the author.

<sup>97</sup> Bursten, B. E. *Pure Appl. Chem.* **1991**, 63, 839.

<sup>98</sup> For application of Fenske-Hall MO calculations to dinuclear metal complexes, see: a) Sargent, A. L.; Rollog, M. E.; Eagle, C. T. *Theor. Chem. Acc.* **1997**, 97, 283, b) Lichtenberger, D. L.; Lynn, M. A.; Chisholm, M. H. *J. Am. Chem. Soc.* **1999**, 121, 12167, For more recent applications of Fenske-Hall calculations, see: c) Adams, R. D.; Captain, B.; Zhu, L. *J. Am. Chem. Soc.* **2006**, 128, 13672, d) Adams, R. D.; Captain, B.; Trufan, E.; Zhu, L. *J. Am. Chem. Soc.* **2007**, 129, 7545.

Symmetry was not imposed computationally during the optimization of complexes **55** and **57**. Thus the geometries are formally  $C_1$ , however their *pseudo*-symmetries will be used in the description that follows. Each of the complexes was found independently as local minima on the potential energy surface during geometry optimization. Energetically, the  $A_g'$  (**56**) and  $B_g''$  (**57**) bond angle distortions are nearly equivalent in their stabilization of the idealized linear complex (**55**) with stabilization energies of 8.0 and 8.2 kcal/mol, respectively.

**Figure 2-9.** Mutually perpendicular views of complexes **55**, **56**, and **57**, with their relative energies from the DFT calculations. (Axes are shown for reference.)



The calculated molecular structures compare well with the XRD data for the related complexes (Table 2-4). The average Rh-C and Rh-N bond lengths, and the C-Rh-Rh-C torsion angle are all within one standard deviation of the average crystallographic value. However, the average Rh-O and Rh-Rh bond lengths, and the C-Rh-N/O bond angles are well outside of the average crystallographic values. The overestimation of the Rh-Rh bond

length by the DFT calculation<sup>99</sup> is the likely cause for the relaxation of the angular distortions compared to the crystallographic data. The coupling of the bond angle distortion with the Rh-Rh bond distance will be discussed in the context of the MO calculations that follow.

**Table 2-4.** Selected DFT-optimized geometric parameters (distances in Å, angles in degrees) for the model compounds **55-57** compared to the crystallographic averages from Table 2-3.

Parameter	Compound				
	<b>55</b>	<b>56</b>	<b>57</b>	Mean	XRD Mean(SD) <sup>a</sup>
Bond length (Å)					
Rh-Rh	2.640	2.639	2.644	2.641	2.521(23)
Rh-C	1.999	1.999	1.999	1.999	1.993(8)
Rh-N	2.022	2.022	2.025 2.053	2.022	2.015(7)
Rh-O	2.138	2.138	2.095 2.133	2.138	2.086(5)
Bond angles (°)					
C-Rh-Rh	180.0	166.5 <sup>b</sup>	166.9 <sup>c</sup>	166.7 <sup>b</sup>	157.1(33)
C-Rh-O <sub>av</sub>	98.9	89.4	99.4 89.2	92.7 <sup>b</sup>	85.5(13)
C-Rh-N <sub>av</sub>	89.2 86.5	98.8	99.0 89.1	95.6 <sup>b</sup>	101.0(9)
Torsion angles (°)					
C1-Rh1-Rh2-C2	179.9 177.2	180.0	180.0	180.0	180.0(0)
N-Rh1-Rh2-O	0.9	1.0	0.3, 1.1	1.0	1.9(4)

<sup>a</sup>Values in parentheses are the uncertainty in the last reported digit based on the average value (SD = standard deviation) <sup>b</sup>Angle measured in the xy-plane. <sup>c</sup>Angle measured in the xz-plane.

<sup>99</sup> Jensen, K. P.; Roos, B. O.; Ryde, U. *J. Chem. Phys.* **2007**, *126*, 14103.

The calculation data for the frontier MOs in **55** are compiled in Table 2-5. The MO labels have been modified with symmetry assignments based on its *pseudo-C<sub>2h</sub>* molecular symmetry. Five MOs with greater than 40% contribution from Rh-centered orbitals are listed and are labeled as they appear in the calculation output. The orbitals are 67a<sub>g</sub> [ $\pi$ (Rh-Rh)], 68b<sub>g</sub> [ $\pi$ (Rh-Rh)], 69b<sub>u</sub> [ $\delta$ (Rh-Rh)], 70b<sub>g</sub> [ $\pi^*$ (Rh-Rh)], 71a<sub>g</sub> [ $\pi^*$ (Rh-Rh)], 72b<sub>u</sub> [ $\delta^*$ (Rh-Rh)], and 73a<sub>g</sub> [ $\sigma^*$ (Rh-C)]. These orbitals are consistent with the expected ground state electronic configuration of *bis*( $\sigma$ -aryl)-dirhodium(III) complexes ( $\pi^4\delta^2\pi^4\delta^{*2}$ ). The  $\pi^*$ (Rh-Rh) orbitals are nearly degenerate with  $\Delta E$  of 0.04 eV (0.9 kcal/mol) and the HOMO-LUMO gap of this model complex is 1.64 eV.

**Table 2-5.** Upper-valent MOs for the completely symmetric model compound Rh<sub>2</sub>(HNCHO)<sub>4</sub>Ph<sub>2</sub> (**55**).

MO	E (eV)	Assignment	Contributions (%)
73a <sub>g</sub>	-6.94	LUMO [ $\sigma^*$ (Rh-C)]	Rh dsp <sub><math>\sigma</math></sub> (64), C sp <sup>2</sup> <sub><math>\sigma</math></sub> (30)
72b <sub>u</sub>	-8.58	HOMO [ $\delta^*$ (Rh-Rh)]	Rh d <sub><math>z^2</math></sub> (49), Rh d <sub><math>x^2-y^2</math></sub> (18), O p <sub><math>x,z</math></sub> (18), N p <sub><math>x,z</math></sub> (14)
71b <sub>g</sub>	-9.51	$\pi_{xz}^*$ (Rh-Rh)	Rh d <sub><math>xz</math></sub> (78)
70a <sub>g</sub>	-9.55	$\pi_{xy}^*$ (Rh-Rh)	Rh d <sub><math>xy</math></sub> (78)
69a <sub>g</sub>	-11.03	$\delta$ (Rh-Rh)	Rh d <sub><math>z^2</math></sub> (51), Rh d <sub><math>x^2-y^2</math></sub> (21), Rh d <sub><math>xy</math></sub> (10)
68b <sub>u</sub>	-11.05	$\pi_{xy}$ (Rh-Rh)	Rh d <sub><math>xy</math></sub> (48), Rh dsp <sub><math>\sigma</math></sub> (13), O p <sub><math>x,y,z</math></sub> (18)
67a <sub>g</sub>	-11.19	$\pi_{xz}$ (Rh-Rh)	Rh d <sub><math>yz</math></sub> (65), O p <sub><math>x,y,z</math></sub> (24)

The calculation data for the frontier MOs of the A<sub>g</sub>' symmetric distortion (**56**) are shown in Table 2-6. The MO labels have been modified with symmetry labels assigned based on the C<sub>2h</sub> symmetry of the complex. Compared to **55**, the occupied MOs are stabilized by an average of 0.13 eV with the exception of 70'a<sub>g</sub> which is stabilized by 0.76 eV. The breaking of the  $\pi^*$ (Rh-Rh) degeneracy occurs as a result of symmetry allowed orbital mixing

between MOs 70'a<sub>g</sub> [ $\pi_{xy}^*(\text{Rh-Rh})$ ] and 73'a<sub>g</sub> [ $\sigma^*(\text{Rh-Rh})$ ]. This is observed as a contribution of Rh d<sub>xy</sub> character to 73'a<sub>g</sub> with concomitant Rh dsp<sub>σ</sub> and C sp<sup>2</sup><sub>σ</sub> contributions to 70'a<sub>g</sub>. The HOMO is stabilized by 0.12 eV and the  $\pi_{xy}^*/\sigma^*$  mixing leads to a significantly larger HOMO-LUMO gap of 2.25 eV consistent with the increased overall stability of the complex over the undistorted **55**. The ground state electronic configuration is not maintained from **55** as an inversion of the  $\delta(\text{Rh-Rh})$  and  $\pi_{xy}(\text{Rh-Rh})$  occurs to yield a  $\pi^2\delta^2\pi^2\pi^{*4}\delta^{*2}$  electronic configuration with the  $\pi_{xy}(\text{Rh-Rh})$  raised 0.08 eV over  $\delta(\text{Rh-Rh})$ .

**Table 2-6.** Upper-valent MOs for the model compound Rh<sub>2</sub>(HNCHO)<sub>4</sub>Ph<sub>2</sub> with a A<sub>g</sub>' bond angle distortion (**56**).

MO	E (eV)	Assignment	LCAO Contributions (%)
73'a <sub>g</sub>	-6.45	LUMO [ $\sigma^*(\text{Rh-C})$ ]	Rh dsp <sub>σ</sub> (60), Rh d <sub>xy</sub> (9), C sp <sup>2</sup> <sub>σ</sub> (21)
72'b <sub>u</sub>	-8.70	HOMO [ $\delta^*(\text{Rh-Rh})$ ]	Rh d <sub>z<sup>2</sup></sub> (47), Rh d <sub>x<sup>2</sup>-y<sup>2</sup></sub> (18), O p <sub>xyz</sub> (19), N p <sub>xyz</sub> (14)
71'b <sub>g</sub>	-9.66	$\pi_{xz}^*(\text{Rh-Rh})$	Rh d <sub>xz</sub> (87)
70'a <sub>g</sub>	-10.31	$\pi_{xy}^*(\text{Rh-Rh})$	Rh d <sub>xy</sub> (64), Rh dsp <sub>σ</sub> (9), C sp <sup>2</sup> <sub>σ</sub> (5), C <sub>ipso/ortho/para</sub> p <sub>xyz</sub> (12)
69'a <sub>g</sub>	-11.10	$\pi_{xy}(\text{Rh-Rh})$	Rh d <sub>xy</sub> (58), C sp <sup>2</sup> <sub>σ</sub> (5) C <sub>ipso/ortho/para</sub> p <sub>xyz</sub> (25)
68'b <sub>u</sub>	-11.18	$\delta(\text{Rh-Rh})$	Rh d <sub>z<sup>2</sup></sub> (55), Rh d <sub>x<sup>2</sup>-y<sup>2</sup></sub> (24),
67'a <sub>g</sub>	-11.36	$\pi_{xz}(\text{Rh-Rh})$	Rh d <sub>xz</sub> (66), O p <sub>xyz</sub> (24)

The calculation data for the frontier MOs of the B<sub>g</sub>' anti-symmetric distortion (**57**) are shown in Table 2-7 with symmetry labels assigned based on its *pseudo*-C<sub>i</sub> symmetry. Compared to **55**, the occupied MOs are stabilized by an average of 0.13 eV with the exception of 70'a<sub>g</sub> which is stabilized by 0.76 eV. A new set of orbital interactions can occur as a result of the reduction of molecular symmetry from the C<sub>2h</sub> to C<sub>i</sub> point group from complexes **55** to **57**. The reduction of symmetry converts all orbitals with centers of inversion (g) to the symmetric A<sub>g</sub> representation (Table 2-8). Thus,

the symmetry forbidden mixing of the MOs 71b<sub>g</sub> [ $\pi_{xz}^*(\text{Rh-Rh})$ ] and 73a<sub>g</sub> [ $\sigma^*(\text{Rh-Rh})$ ] in **55** (Table 2-5) is allowed in **57** as b<sub>g</sub> transforms to a<sub>g</sub> with the reduction of symmetry ( $C_{2h} \rightarrow C_i$ , Table 2-8).

Similar to the A<sub>g</sub>' bond angle distortion, the  $\pi^*(\text{Rh-Rh})$  degeneracy is broken as a result of the new symmetry allowed orbital mixing between MOs 70''a<sub>g</sub> [ $\pi_{xz}^*(\text{Rh-Rh})$ ] and 73''a<sub>g</sub> [ $\sigma^*(\text{Rh-Rh})$ ] MOs. This is observed as a cross contribution of Rh d<sub>xy</sub> character to 73''a<sub>g</sub> and Rh dsp<sub>σ</sub> and C sp<sup>2</sup><sub>σ</sub> character to 70''a<sub>g</sub>. The HOMO is stabilized by 0.19 eV and the  $\pi_{xy}^*/\sigma^*$  mixing leads to a larger HOMO-LUMO gap of 2.26 eV relative to **55**. The ground state electronic configuration is not maintained from either **56** or **57** as another inversion of the  $\delta(\text{Rh-Rh})$  and  $\pi(\text{Rh-Rh})$  occurs to yield a  $\delta^2\pi^4\pi^*4\delta^*2$  electronic configuration with 69''a<sub>g</sub> [ $\pi_{xz}(\text{Rh-Rh})$ ] raised 0.13 eV over 68''a<sub>u</sub> [ $\delta(\text{Rh-Rh})$ ]. MOs 69''a<sub>g</sub> [ $\pi_{xz}(\text{Rh-Rh})$ ] and 68''a<sub>u</sub> [ $\delta(\text{Rh-Rh})$ ] are nearly degenerate with  $\Delta E_V = 0.01$  eV (0.2 kcal/mol)

**Table 2-7.** Upper-valent MOs for the model compound Rh<sub>2</sub>(HNCHO)<sub>4</sub>Ph<sub>2</sub> with a B<sub>g</sub>'' bond angle distortion (**57**).

MO	E (eV)	Assignment	LCAO Contributions (%)
73''a <sub>g</sub>	-6.51	LUMO [ $\sigma^*(\text{Rh-C})$ ]	Rh dsp <sub>σ</sub> (59), Rh d <sub>xz</sub> (13), C sp <sup>2</sup> <sub>σ</sub> (21)
72''a <sub>u</sub>	-8.77	HOMO [ $\delta^*(\text{Rh-Rh})$ ]	Rh d <sub>z<sup>2</sup></sub> (50), Rh d <sub>x<sup>2</sup>-y<sup>2</sup></sub> (15), O p <sub>xyz</sub> (19), N p <sub>xyz</sub> (15)
71''a <sub>g</sub>	-9.78	$\pi_{xy}^*(\text{Rh-Rh})$	Rh d <sub>xy</sub> (74), O p <sub>xyz</sub> (19) C <sub>ipso/ortho/para</sub> p <sub>xyz</sub> (14)
70''a <sub>g</sub>	-10.32	$\pi_{xz}^*(\text{Rh-Rh})$	Rh d <sub>xz</sub> (71), Rh dsp <sub>σ</sub> (11)
69''a <sub>g</sub>	-11.20	$\pi_{xz}(\text{Rh-Rh})$	Rh d <sub>xz</sub> (45), Rh d <sub>xy</sub> (16), Rh dsp <sub>σ</sub> (8), O p <sub>xyz</sub> (14), C sp <sup>2</sup> <sub>σ</sub> (4) C <sub>ipso/ortho/para</sub> p <sub>xyz</sub> (7)
68''a <sub>g</sub>	-11.34	$\pi_{xy}(\text{Rh-Rh})$	Rh d <sub>xy</sub> (45), Rh d <sub>xz</sub> (23), O p <sub>xyz</sub> (12), C <sub>ipso/ortho/para</sub> p <sub>xyz</sub> (7)
67''a <sub>u</sub>	-11.33	$\delta(\text{Rh-Rh})$	Rh d <sub>z<sup>2</sup></sub> (63), Rh d <sub>x<sup>2</sup>-y<sup>2</sup></sub> (20),



**Table 2-8.** Symmetry transform of irreducible representations of  $C_{2h}$  to  $C_i$ .

$C_{2h}$		$C_i$
$A_g$	→	$A_g$
$B_g$	→	$A_g$
$A_u$	→	$A_u$
$B_u$	→	$A_u$

The data provided in Table 2-5 to Table 2-7 is summarized in the MO correlation diagram provided in Figure 2-10. Based on this data, the  $A_g'$  and  $B_g''$  bond angle deformations in the model complexes can be understood as a symmetric and anti-symmetric second-order Jahn-Teller distortion. A second order Jahn-Teller distortion occurs as excited state MOs mix with ground state MOs to break orbital degeneracies and stabilize the HOMO of the molecule.<sup>100</sup> A similar phenomenon is found in *bis*( $\sigma$ -alkynyl)- $Ru_2^{6+}L_4$  complexes.<sup>101</sup>

In the case of the model  $Rh_2^{6+}$  complexes this distortion is manifested as the LUMO of the complex [ $\sigma^*(Rh-Rh)$ ] mixes with lower lying  $\pi^*$  orbitals of commensurate symmetry. The  $A_g'$  distortion occurs along the xy-plane of the molecule. Thus mixing occurs with the  $\pi_{xy}^*(Rh-Rh)$  orbital that lies on the horizontal mirror plane and results in a stabilized  $\pi_{xy}^*(Rh-Rh)$  and destabilized  $\sigma^*(Rh-Rh)$  MO (Linear( $C_{2h}$ ) →  $A_g'(C_{2h})$ , Figure 2-10). The  $B_g''$  distortion occurs along the xz-plane of the molecule. Therefore, the  $\pi_{xz}^*(Rh-Rh)$  MO mixes with  $\sigma^*(Rh-Rh)$  as allowed by the reduction of molecular symmetry. The mixing results in similar stabilization of  $\pi_{xz}^*(Rh-Rh)$  and a destabilized  $\sigma^*(Rh-Rh)$  MO (Linear( $C_{2h}$ ) →  $B_g''(C_{2h})$ , Figure 2-10). Therefore, the  $A_g'$  and  $B_g''$  bond angle deformations are a result of second-order Jahn-Teller

---

<sup>100</sup> a) Pearson, R. G. *Proc. Natl. Acad. Sci.* **1975**, 72, 2104, b) Bersuker, I. B. *Chem. Rev.* **2001**, 101, 1067.

<sup>101</sup> Lin, C.; Ren, T.; Valente, E. J.; Zubkowski, J. D. *J. Chem. Soc., Dalton Trans.* **1998**, 571.

distortion. A graphical representation of the MOs involved in the distortions are provided in Figure 2-11.

**Figure 2-10.** Molecular orbital correlation diagram for the distorted geometries (NOTE: MO labels correspond to the labels in Table 2-5 and Table 2-6).

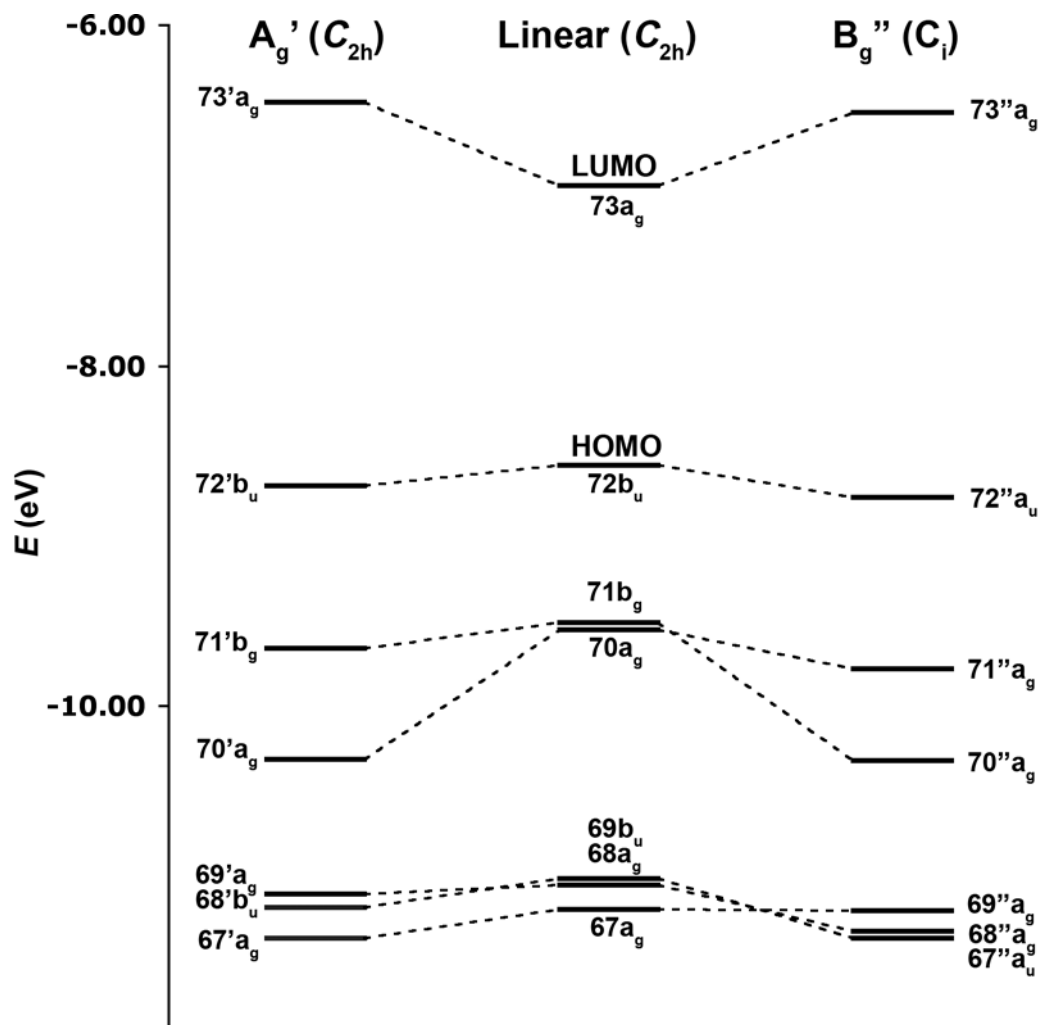
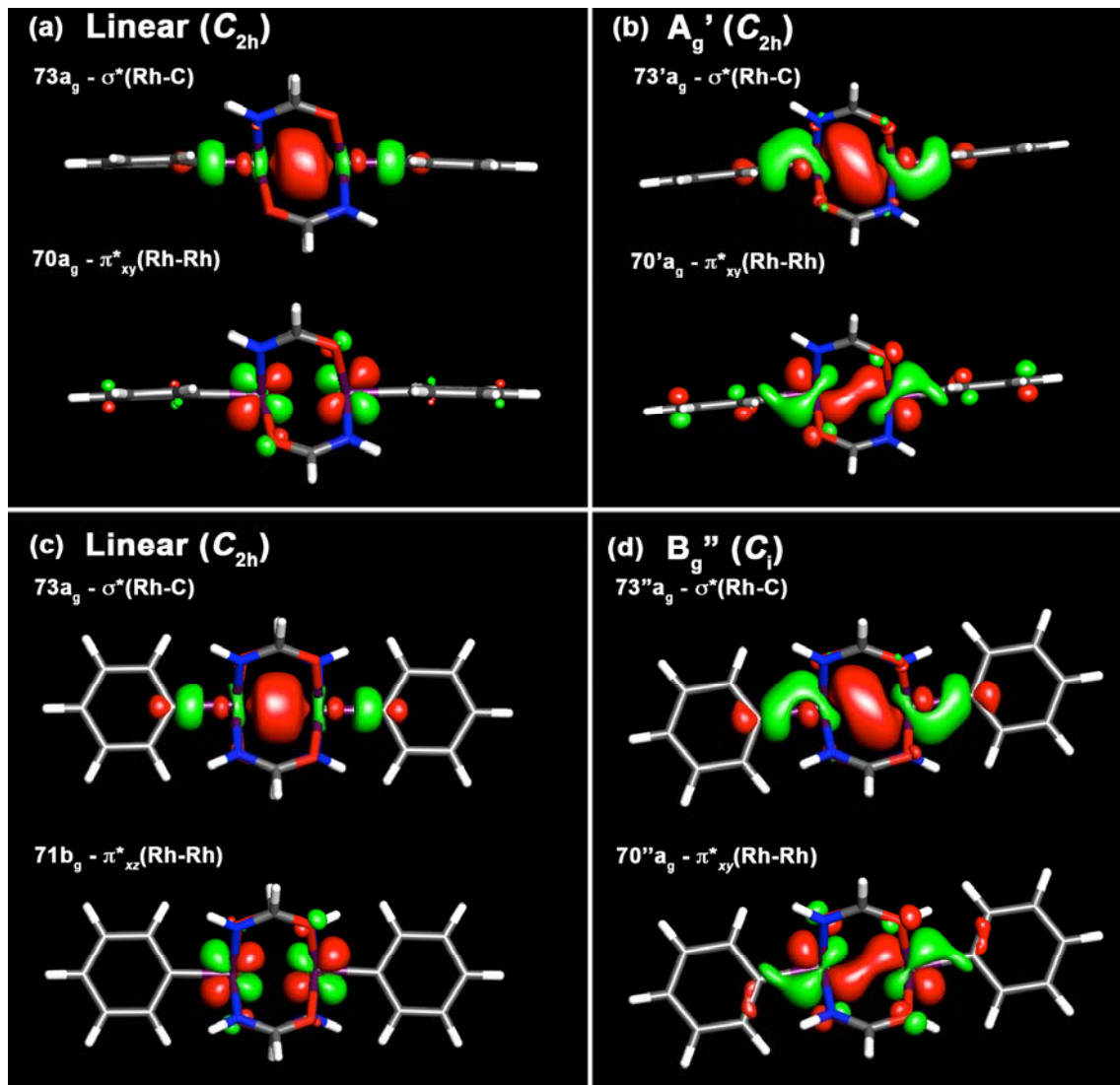


**Figure 2-11.** (a) MOs of **55** that mix in the  $A_g'$  distortion; (b) MOs in **56** that result from the MOs in **55**; (c) MOs of **55** that mix in the  $B_g''$  distortion; (d) MOs in **57** that result from the MOs in **55**.



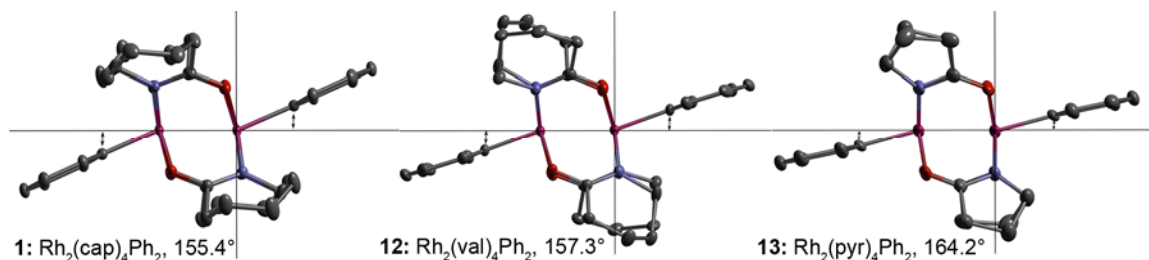
The distortion dependent reorganization of the electronic configuration is a curious feature of the calculations. The overall configuration changes from the expected  $\pi^4\delta^2\pi^*4\delta^*2$  for the linear model (**55**) to  $\pi^2\delta^2\pi^2\pi^*4\delta^*2$  and  $\delta^2\pi^4\pi^*4\delta^*2$  for the  $A_g'$  (**56**) and  $B_g''$  (**57**) distortions respectively. This restructuring does not affect the experimentally probed  $\pi^*$  and  $\delta^*$  orbitals. It occurs in the lower lying the  $\delta(\text{Rh-Rh})$ ,  $\pi_{xy}(\text{Rh-Rh})$ , and  $\pi_{xz}(\text{Rh-Rh})$  metal bonding MOs. The total energy difference between each of these MOs

averages 0.18 eV (4.2 kcal/mol). Thus, the orbitals in question are very close in energy and minor electronic perturbations may account for the change. A rational trend can be observed in the relative stability of the  $\pi(\text{Rh-Rh})$  MOs. In general, the  $\pi(\text{Rh-Rh})$  MO that corresponds to the  $\pi^*(\text{Rh-Rh})$  MO involved in the second-order Jahn-Teller distortion is destabilized (Figure 2-10), probably as a result of poorer overlap of the  $\pi$ -symmetry d-orbitals in the distorted structure. This distortion could account for the observed reorganization of the electronic configuration.

Trends in the structural data for the  $\text{bis}(\sigma\text{-aryl})\text{-Rh}_2^{6+}\text{L}_4$  complexes provide experimental support for the second-order Jahn-Teller distortion. Comparison of Rh-Rh bond length and the Rh-Rh-C bond angle for complexes **1**, **12**, and **13** where the number of methylenes ( $n$ ) is varied ( $n = 3, 2, 1$  respectively) shows a decrease of the bond angle distortion as  $n$  decreases (Figure 2-12). Considering the cleavage of the Rh-Rh bond in the dirhodium(III) complexes, the Rh-Rh distance would be imposed mainly by the  $\mu$ -bridging ligands rather than a metal-metal bonding interaction. The homogeneity of the Rh-Rh bond length within complexes with the same  $\mu$ -bridging carboxamidate ligand is consistent with this interpretation (**1**, **14-24**, Table 2-3).

For complexes **1** and **12**, the Rh-Rh bond lengths are 2.519 Å and 2.516 Å, respectively. The Rh-Rh-C bond angle distortions for **1** and **12** are also similar with values of 155.4° and 157.3°, respectively. Within the series, the outlier is **13** where  $n = 1$ . For **13**, the Rh-Rh bond length is 2.570 Å and the Rh-Rh-C bond angle is 164.2°. Also, recall the overestimation of the Rh-Rh bond length by the DFT optimization of the model complexes **56** and **57**. The average Rh-Rh bond length was 2.641 Å, which is 74 pm longer than Rh-Rh distance in **13**. The average Rh-Rh-C angle for complexes **56** and **57** was 2.6° more obtuse than **13** and 13.3° wider than complex **1** (Table 2-4).

**Figure 2-12.** Comparison of bond angle distortion in the ORTEP drawings of complexes **1**, **12**, and **13**. [NOTE: The bond-angle reported in the graphic refers to the Rh-Rh-C bond angle for the complex.]

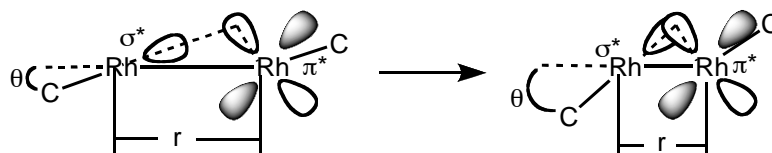


When looking at the trend in bond angle alone, a steric argument could explain the  $A_g'$  distortion mode as the methylene group over the axial binding site is forced closer to the aryl ring as the ring size increases. However, if both bond angle distortion modes and the bond length attenuations are taken into account, the distortion imposed by the MO mixing required by the second order Jahn-Teller distortion is a more complete rationalization of the observed trends. It explains the presence of significant distortions in the crystal structure of **13** and the calculated structures **56** and **57** where there is little to no steric crowding provided by the  $\mu$ -bridging carboxamidate ligand. Moreover, the Jahn-Teller description rationalizes the  $B_g''$  distortion mode, which cannot be explained with a steric argument.

When looking at both the bond length and bond angle trends, a coupling of the two distortions becomes apparent. Based on the Jahn-Teller description, this coupling can be rationalized from an MO standpoint. In essence, the smaller ring size of the ligand in **13**, or the DFT calculations of **56** and **57**, allows the Rh-Rh distance ( $r$ ) to be longer than in complexes **1** and **12**. Consequently, the metal-centered orbitals are moved further apart and the bond-angle distortion ( $\theta$ ) relaxes to facilitate  $\sigma^*(\text{Rh-C})-\pi^*(\text{Rh-Rh})$  mixing. Conversely, the Rh-Rh bond length in complexes **1** and **12** is constrained to a shorter distance by the  $\mu$ -bridging carboxamidate ligands and

the bond-angle distortion becomes more severe to maximize  $\sigma^*(\text{Rh-C})-\pi^*(\text{Rh-Rh})$  overlap. Consequently, the severity of the second-order Jahn-Teller distortion is proposed to be a function of Rh-Rh bond length (Figure 2-13).

**Figure 2-13.** Schematic representation showing the inverse relationship between the bond angle distortion ( $\theta$ ) and Rh-Rh bond distance ( $r$ ).



**Experimental Evidence Against Extended  $\pi$ -delocalization.**<sup>102</sup> With a clear picture of the electronic structure, the ability of *bis*( $\sigma$ -aryl)-dirhodium(III) complexes to function as molecular wires was assessed. The first requirement of a molecular wire is to provide a pathway for electronic communication at a distance. In terms of a molecular orbital picture, this pathway would be in the form of an extended, delocalized  $\pi$ -system as one of the frontier MOs and a small HOMO-LUMO gap.<sup>103</sup> Model calculations revealed that there is not a strong interaction between the  $\pi$ -system of aryl rings and the  $\pi$ -symmetry MOs in the model complexes. The energy gap based on the optically determined  $E_s$  was an average of 2.83 eV over all aryl-substitutions patterns measured. This value is outside of the range reported for *bis*( $\sigma$ -alkynyl)- $\text{Ru}_2^{6+}\text{L}_4$  complexes (1.2-1.8 eV), but well below the value for organic molecules typically used in conducting polymers. The linear free energy relationship between the aryl-ring substituents and the corresponding  $E_{1/2}$  was relatively weak consistent with the weak interactions between the  $\pi$ -system of the arylring and the dirhodium(III) core.

<sup>102</sup> This work was done in collaboration with Conrad Lubek, undergraduate, University of Maryland.

<sup>103</sup> Kertesz, M.; Choi, C. H.; Yang, S. J. *Chem. Rev.* **2005**, *105*, 3448.

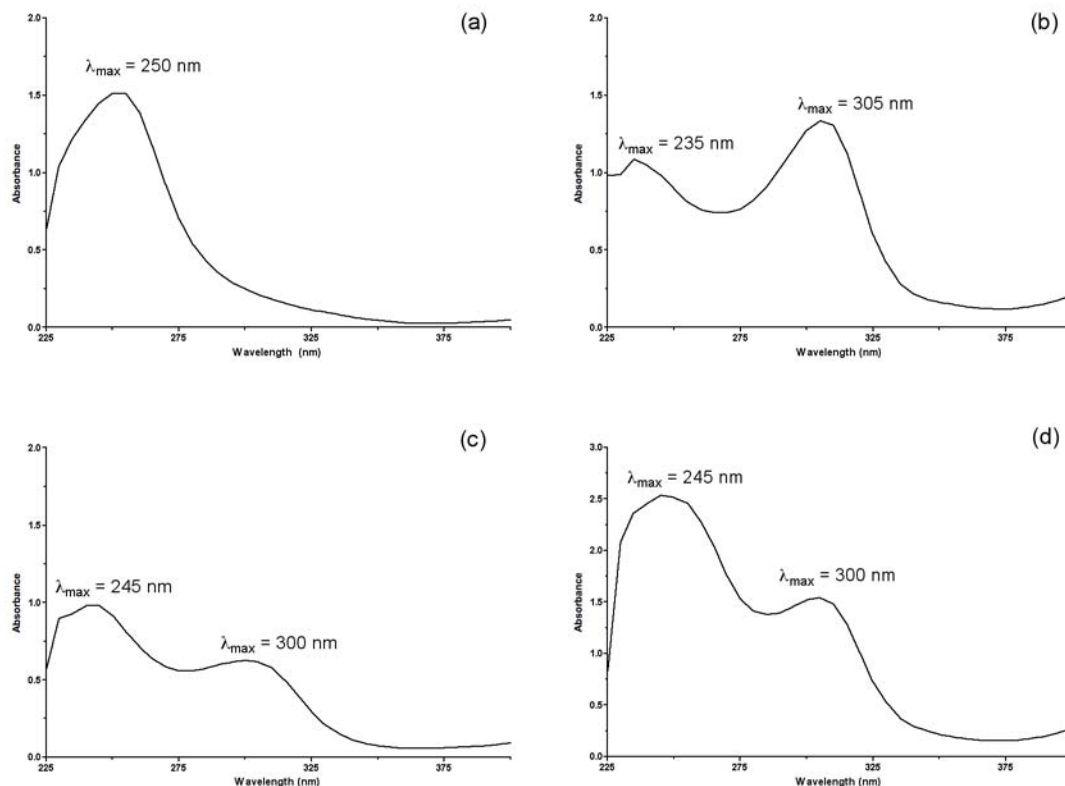
In addition to these indicators, the extent of delocalization in a  $\pi$ -system can be experimentally determined. In a conjugated system, there is a diagnostic bathochromic shift of electronic absorptions that correspond to the  $\pi$ - $\pi^*$  transitions of the aryl  $\pi$ -system relative to a known, unconjugated system with similar substitution.<sup>104</sup> The ability to prepare  $[(\sigma\text{-aryl}), (\sigma\text{-aryl}')] \text{-dirhodium(III)}$  complexes provides an opportunity to assess the amount of delocalization of the aromatic system through the dirhodium(III) core by providing an intermediate structure between two *bis*( $\sigma$ -aryl)-dirhodium(III) complexes.

The UV absorption spectra of *bis*[ $\sigma$ -(4-formylphenyl)]-Rh<sub>2</sub>(cap)<sub>4</sub> (**16**), *bis*[ $\sigma$ -(4-methoxyphenyl)]-Rh<sub>2</sub>(cap)<sub>4</sub> (**18**), and [ $\sigma$ -(4-formylphenyl),  $\sigma$ -(4-methoxyphenyl)]-Rh<sub>2</sub>(cap)<sub>4</sub> (**23**), are shown in Figure 2-14. The absorption maxima of **16** and **18** are at 250 nm and 305 nm respectively. A 1:1 stoichiometric mixture of **16** and **18** is an approximation of a complex with zero delocalization. The mixture has absorption maxima at 245 nm and 300 nm (Figure 2-14c). If complete delocalization were to occur in the intermediate structure (**23**) then the spectrum would be a single maximum above 245 nm. In the case of weak, or partial delocalization, the spectrum of **23** could be expected to be similar to the model spectrum in Figure 2-14c with the absorption maxima shifted towards higher wavelengths. The UV absorption spectrum of **23** (Figure 2-14d) is nearly identical to the model spectrum in Figure 2-14c with absorption maxima at 245 nm and 300 nm. This indicates that no delocalization of the aryl- $\pi$  system occurs through the dirhodium(III) core.

---

<sup>104</sup> a) Hicks, R. G.; Nodwell, M. B. *J. Am. Chem. Soc.* **2000**, *122*, 6746, b) Daminelli, G.; Widany, J.; Di Carlo, A.; Lugli, P. *J. Chem. Phys.* **2001**, *115*, 4919, c) Radhakrishnan, S.; Parthasarathi, R.; Subramanian, V.; Somanathan, N. *J. Phys. Chem. B* **2006**, *110*, 14078.

**Figure 2-14.** Electronic absorption spectra (250-400 nm) of 0.1 to 0.2 mM solutions of (a) complex **16**, (b) complex **18**, (c) 1:1 mixture of complexes **16** and **18**, (d) complex **23**.



The lack of significant delocalization in **23** is not a general indication that delocalization is not possible for *bis*( $\sigma$ -aryl)-Rh<sub>2</sub><sup>6+</sup>L<sub>4</sub> complexes. Rather, this experiment only demonstrates that there is poor energetic matching, or orbital overlap between the  $\pi$ -system of the dirhodium(III) core and the aromatic  $\pi$ -system in complex **23**. However, this experiment in the context of the physical and theoretical characterization of the electronic structure suggests that, unlike the related *bis*( $\sigma$ -alkynyl)-Ru<sub>2</sub><sup>6+</sup>L<sub>4</sub> complexes, *bis*( $\sigma$ -aryl)-Rh<sub>2</sub><sup>6+</sup>L<sub>4</sub> complexes with  $\mu$ -caprolactamato bridging ligands are not suitable as molecular wires. This is partly due to the Rh-Rh-C bond angle distortion disfavoring orbital overlap as well as energetic mismatches between the ligand  $\pi$ -system and the Rh-Rh core.



## IV. Conclusion

A general preparation for complexes with formula  $\text{Rh}_2\text{L}_4\text{Ar}_2$  and  $\text{Rh}_2\text{L}_4\text{ArAr}'$  was developed using arylboronic acids with a  $\text{Cu(I)}/\text{O}_2$  oxidation system. The reaction is proposed to occur through a stepwise oxidation/aryl exchange with  $\text{Cu(II)}$  as the oxidant and an arylborate ester as the transfer reagent through a transmetalation type transition state.

Comparative analysis of the  $\text{Rh}_2\text{L}_4\text{Ar}_2$  and  $\text{Rh}_2\text{L}_4\text{ArAr}'$  molecular structures revealed very little influence of aryl ring substituents on the molecular structure. Two main structural distortions, first observed in Chapter 1, as an attenuation of the Rh-Rh bond length and a distortion of the Rh-Rh-C bond angle away from the ideal value of  $180^\circ$  were consistent across all complexes for which data was obtained. The bond angle distortion was found to be a composite of two separate distortions, one symmetric and one anti-symmetric to the molecular plane of symmetry in the idealized complex. The Rh-Rh-C bond angle deformation was rationalized as the result of a second-order Jahn-Teller distortion that allows orbital mixing between the LUMO and the  $\pi^*(\text{Rh-Rh})$  orbitals to stabilize the complex.

The electronic structure of  $\text{Rh}_2\text{L}_4\text{Ar}_2$  and  $\text{Rh}_2\text{L}_4\text{ArAr}'$  complexes were experimentally probed through voltammetry and electronic absorption analysis. Variations in the aryl-ring substituents and the  $\mu$ -bridging carboxamidate ligands led to predictable free energy trends in  $E_{1/2}$  and  $\lambda_{\text{max}}$  that confirm the proposed electronic structure of  $\pi^2\delta^2\pi^2\pi^*\delta^*2$ . A lack of  $\pi$ -delocalization was found for the differentially substituted complex, [ $\sigma$ -(4-formylphenyl),  $\sigma$ -(4-methoxyphenyl)]- $\text{Rh}_2(\text{cap})_4$  (**23**) indicating that the  $\pi$ -systems of each aryl ring are independent of one another.

## V. Experimental

**General.** All reactions were performed under an ambient atmosphere unless otherwise noted. Moisture sensitive reactions were performed using oven-dried glassware under a dried nitrogen atmosphere. All reagents were commercially obtained unless otherwise noted. The preparation of  $\text{Rh}_2(\text{cap})_4 \cdot [\text{CH}_3\text{CN}]_2$ ,<sup>105</sup>  $\text{Rh}_2(\text{val})_4 \cdot [\text{CH}_3\text{CN}]_2$ , and  $\text{Rh}_2(\text{pyr})_4 \cdot [\text{CH}_3\text{CN}]_2$  have been previously described.<sup>106</sup>

$^1\text{H}$  (400 MHz) and  $^{13}\text{C}$  NMR (100 MHz) spectra were obtained on a Bruker DRX-400 NMR spectrometer as solutions in  $\text{CDCl}_3$  or  $\text{CD}_2\text{Cl}_2$  at 20 °C unless otherwise noted. Chemical shifts are reported in parts per million (ppm,  $\delta$ ) downfield from  $\text{Me}_4\text{Si}$  (TMS) or relative to the residual solvent signal in  $\text{CD}_2\text{Cl}_2$ . Preparative chromatographic purification was performed using SiliCycle (60 Å, 40 – 63 mesh) silica gel according to the method of Still.<sup>107</sup> Thin layer chromatography (TLC) was performed on Merck 0.25 mm silica gel 60 F<sub>254</sub> plates with visualization by fluorescence quenching or chemical stain. UV/Visible spectra were obtained on a Varian Cary 50 spectrophotometer using a xenon flash lamp. IR spectra were recorded on a JASCO FT/IR 4100 spectrometer. Both cyclic and differential pulse voltammetry were measured in anhydrous  $\text{CH}_2\text{Cl}_2$  on a CH Instruments 660C potentiostat equipped with glassy carbon and Pt working electrodes and a Ag/AgCl reference electrode. The electrochemical analyses were performed on 1 mM solutions of the analytes in anhydrous and degassed  $\text{CH}_2\text{Cl}_2$  with tetrabutylammonium hexafluorophosphate (0.25 M) as the supporting electrolyte. Anhydrous

---

<sup>105</sup> Doyle, M. P.; Westrum, L. J.; Wolthuis, W. N. E.; See, M. M.; Boone, W. P.; Bagheri, V.; Pearson, M. M. *J. Am. Chem. Soc.* **1993**, *115*, 958.

<sup>106</sup> Bear, J. L.; Lifsey, R. S.; Chau, L. K.; Ahsan, M. Q.; Korp, J. D.; Chavan, M.; Kadish, K. M. *J. Chem. Soc., Dalton Trans.* **1989**, 93.

<sup>107</sup> Pangborn, A. B.; Giardello, M. A.; Grubbs, R. H.; Rosen, R. K.; Timmers, F. J. *Organometallics* **1996**, *15*, 1518.

CH<sub>2</sub>Cl<sub>2</sub> and THF were purified prior to use by nitrogen forced-flow over activated alumina as described by Grubbs.<sup>108</sup>

**XRD Crystal Structure Determination.**<sup>109</sup> The X-ray intensity data were measured at 223(2) K on a three-circle diffractometer system equipped with Bruker Smart 1000 CCD area detector using a graphite monochromator and a Mo K $\alpha$  fine-focus sealed tube ( $\lambda$ = 0.71073 Å). Data was collected using the SMART software package.<sup>110</sup> Cell determination, refinement and frames integration were done with the SAINT software package using a narrow-frame integration algorithm.<sup>110</sup> Data were corrected for absorption effects with the semi-empirical from equivalents method using XPREP for **1**<sup>111</sup> or SADABS for **2** and **3**.<sup>112</sup> Structures were solved and refined using the SHELXS-97 and SHELXL-97 software.

**Note.** The prepared compounds were poorly soluble in all solvents. As such, two compounds (**17** and **19**) could not be effectively characterized by <sup>13</sup>C NMR. Compound **17** was so poorly soluble (<0.1 mg/mL) in CH<sub>2</sub>Cl<sub>2</sub>, CHCl<sub>3</sub>, CH<sub>3</sub>OH, acetone, THF, CH<sub>3</sub>CN, dimethylsulfoxide, dimethylformamide, and acetic acid that <sup>1</sup>H NMR could not be effectively obtained.

---

<sup>108</sup> Still, W. C.; Kahn, M.; Mitra, A. *J. Org. Chem.* **1978**, *43*, 2923.

<sup>109</sup> All crystal structures were collected and solved by Peter Zavalij, Crystallographer, University of Maryland.

<sup>110</sup> Bruker, SMART and SAINT. Bruker AXS Inc., Madison, Wisconsin, USA., **1999**.

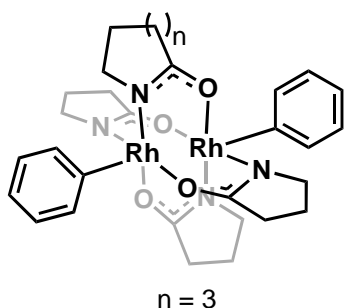
<sup>111</sup> Sheldrick, G. M., SHELXL-97 University of Göttingen, Germany, **1999**.

<sup>112</sup> Sheldrick, G. M., SADABS University of Göttingen, Germany, **1996**.

## Synthesis and Characterizations.

**General Preparation of *Bis*( $\sigma$ -aryl)-Rh<sub>2</sub><sup>6+</sup> Complexes.** Rh<sub>2</sub>L<sub>4</sub> (0.027 mmol) and [Cu(OTf)]<sub>2</sub>•C<sub>6</sub>H<sub>6</sub> (3  $\mu$ mol) were diluted in CH<sub>2</sub>Cl<sub>2</sub>/MeOH (1.5 mL, 4:1) and sonicated for 5 minutes. This solution was added dropwise to a vigorously stirring mixture of boronic acid (0.15 – 0.30 mmol) and NaOMe (0.30 mmol) in CH<sub>2</sub>Cl<sub>2</sub>/MeOH (1.5 mL, 4:1). An additional 2 mL of CH<sub>2</sub>Cl<sub>2</sub>/MeOH (4:1) was used to transfer the Rh<sub>2</sub>L<sub>4</sub> solution and bring the final reaction volume to 5 mL ([Rh<sub>2</sub>L<sub>4</sub>] = 5.4 mM). The reaction was left to stir at room temperature until completion (8-18 hrs). The solvent was removed *in vacuo* to yield a crude residue. The residue was purified either by chromatography on silica gel or trituration with MeOH.

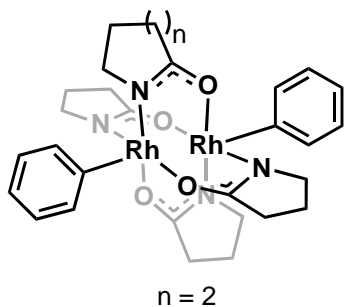
***Bis*( $\sigma$ -phenyl)-*tetrakis*( $\mu$ -caprolactamato)dirhodium(III) (1).** The general



procedure for the the synthesis of Rh<sub>2</sub>L<sub>4</sub>Ar<sub>2</sub> was followed using *tetrakis*( $\mu$ -caprolactamato)dirhodium(II) (0.027 mmol) and phenylboronic acid (0.15 mmol). Purified by silica gel chromatography (5:1 CH<sub>2</sub>Cl<sub>2</sub>/pentane  $\rightarrow$  CH<sub>2</sub>Cl<sub>2</sub>  $\rightarrow$  50:1 CH<sub>2</sub>Cl<sub>2</sub>/acetone); green solid; TLC R<sub>f</sub> =

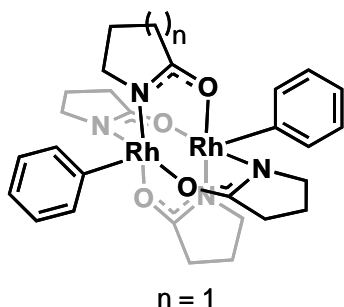
0.25 (CH<sub>2</sub>Cl<sub>2</sub>); <sup>1</sup>H NMR  $\delta$  7.55-7.49 (comp, 4H), 7.18-7.11 (comp, 6H), 3.10-3.00 (comp, 8H), 2.53-2.48 (comp, 4H), 2.44-2.40 (comp, 4H), 2.85-1.78 (comp, 4H), 1.70-1.45 (comp, 20H) ppm; ECHEM E<sub>1/2</sub> ( $\Delta E_p$ , I<sub>pa</sub>/I<sub>pc</sub>) 0.78 V (0.069 V, 1.02).

**Bis( $\sigma$ -phenyl)-tetrakis( $\mu$ -valerolactamato)dirhodium(III) (12).<sup>113</sup>** The



general procedure for the the synthesis of  $Rh_2L_4Ar_2$  complexes was followed using *tetrakis*( $\mu$ -valerolactamato)dirhodium(II) (0.027 mmol) and phenylboronic (0.15 mmol) acid. Purified by silica gel chromatography (5:1  $CH_2Cl_2$ /pentane  $\rightarrow$   $CH_2Cl_2$   $\rightarrow$  50:1  $CH_2Cl_2$ /acetone); green solid; TLC  $R_f = 0.20$  ( $CH_2Cl_2$ );  $^1H$  NMR  $\delta$  7.52-7.50 (comp, 4H), 7.14-7.12 (comp, 6H), 3.50-3.44 (comp, 4H), 2.80-2.74 (comp, 4H), 2.42-2.28 (comp, 8H), 1.68-1.59 (br, 12H), 1.46-1.40 (comp, 4H) ppm;  $^{13}C$  NMR  $\delta$  176.8, 136.6, 126.2, 123.9, 49.5, 32.4, 23.7, 20.8 ppm; UV/Visible ( $CH_2Cl_2$ )  $\lambda_{max}$  ( $\epsilon$   $M^{-1}cm^{-1}$ ) nm = 429 (5040); IR(neat)  $\tilde{\nu} = 1592$  (N-C=O, s), 1552 (aryl-C=C, s)  $cm^{-1}$ ; HRMS (ESI) calcd. for  $Rh_2C_{32}H_{43}N_4O_4$  753.1394, found 753.1416 (M+H); EChem  $E_{1/2}$  ( $\Delta E_p$ ,  $I_{pa}/I_{pc}$ ) 0.81 V (0.069 V, 1.07); XRD: crystals grown by slow evaporation from  $CH_2Cl_2$ .

**Bis( $\sigma$ -phenyl)-tetrakis( $\mu$ -pyrrolidinato)dirhodium(III) (13).<sup>113</sup>** The general



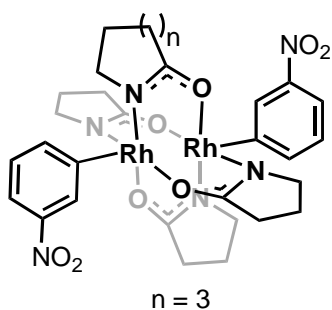
procedure for the the synthesis of  $Rh_2L_4Ar_2$  complexes was followed using *tetrakis*( $\mu$ -pyrrolidinato)dirhodium(II) acetonitrile solvate (0.027 mmol) and phenylboronic acid (0.15 mmol). Purified by silica gel chromatography (5:1  $CH_2Cl_2$ /pentane  $\rightarrow$   $CH_2Cl_2$   $\rightarrow$  50:1  $CH_2Cl_2$ /acetone); yellow solid; TLC  $R_f = 0.15$  ( $CH_2Cl_2$ );  $^1H$  NMR  $\delta$  7.34-7.32 (comp, 4H), 7.11-7.09 (comp, 6H), 3.67-3.61 (comp, 4H), 3.04-2.98 (comp, 4H), 2.57-2.37 (comp, 8H), 1.90-1.74 (comp, 8H), ppm;  $^{13}C$  NMR  $\delta$  182.2, 135.8, 126.7, 124.4, 52.7, 33.4, 21.0 ppm; UV/Visible ( $CH_2Cl_2$ )  $\lambda_{max}$  ( $\epsilon$   $M^{-1}cm^{-1}$ ) nm = 442 (4500); IR(neat)  $\tilde{\nu} = 1585$  (N-C=O, s), 1549 (aryl-C=C, s)  $cm^{-1}$ ; HRMS (ESI) calcd. for

---

<sup>113</sup>The  $^1H$  and  $^{13}C$  NMR spectra and XRD quality crystals for compounds **12** and **13** were provided by J. Wolf.

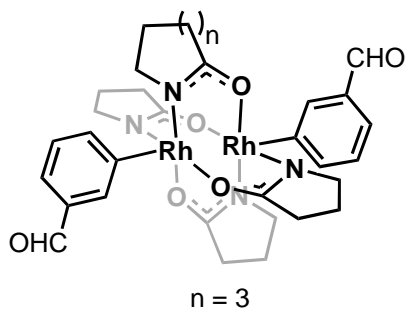
$\text{Rh}_2\text{C}_{28}\text{H}_{35}\text{N}_4\text{O}_4$  697.0768, found 697.0758 (M+H); ECHEM  $E_{1/2}$  ( $\Delta E_p$ ,  $I_{pa}/I_{pc}$ ) 0.91 V (0.054 V, 1.05); XRD crystals grown by slow evaporation from  $\text{CH}_2\text{Cl}_2$ .

**Bis[ $\sigma$ -(3-nitrophenyl)]-tetrakis( $\mu$ -caprolactamato)dirhodium(III) (14).** The



general procedure for the synthesis of  $\text{Rh}_2\text{L}_4\text{Ar}_2$  complexes was followed using tetrakis( $\mu$ -caprolactamato)dirhodium(II) (0.027 mmol) and 3-nitrophenylboronic acid (0.30 mmol). Purified by passing through a silica plug with  $\text{CH}_2\text{Cl}_2$ ; green solid; TLC  $R_f = 0.53$  (98:2  $\text{CH}_2\text{Cl}_2$ /acetone);  $^1\text{H}$  NMR  $\delta$  8.38 (s, 2H), 8.04 (d, 2H,  $J = 8$  Hz), 7.92 (d, 2H,  $J = 8$  Hz), 7.28 (t, 2H,  $J = 8$  Hz) 3.03-2.91 (comp, 8H), 2.53-2.41 (comp, 8H), 1.90-1.85 (comp, 4H), 1.73-1.56 (comp, 12H), 1.54-1.43 (comp, 8H) ppm;  $^{13}\text{C}$  NMR  $\delta$  184.6, 145.6, 143.4, 131.2, 126.1, 119.9, 51.9, 39.0, 30.7, 29.6, 24.4 ppm; UV/Visible ( $\text{CH}_2\text{Cl}_2$ ),  $\lambda_{\text{max}}$  ( $\epsilon \text{ M}^{-1}\text{cm}^{-1}$ ) nm = 423 (6440); IR(neat)  $\tilde{\nu} = 1582$  (N-C=O, s), 1512 (aryl-C=C, s), 1339 (O-N=O, s)  $\text{cm}^{-1}$ ; HRMS (FAB) calcd. for  $\text{C}_{36}\text{H}_{48}\text{N}_6\text{O}_8\text{Rh}_2$  898.1644, found 898.1653 (M+); ECHEM  $E_{1/2}$  ( $\Delta E_p$ ,  $I_{pa}/I_{pc}$ ) 1.05 V (0.089 V, 1.13).

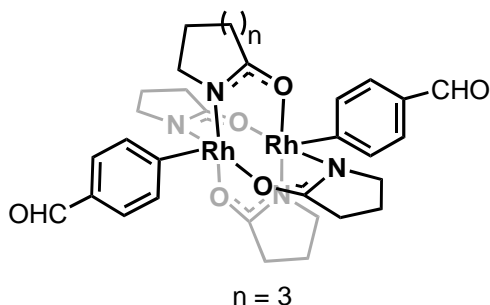
**Bis[ $\sigma$ -(3-formylphenyl)]-tetrakis( $\mu$ -caprolactamato)dirhodium (III) (15).**



The general procedure for the synthesis of  $\text{Rh}_2\text{L}_4\text{Ar}_2$  complexes was followed using tetrakis( $\mu$ -caprolactamato)dirhodium(II) (0.027 mmol) and 3-formylphenylboronic acid (0.30 mmol). Purified by silica gel chromatography (5:1  $\text{CH}_2\text{Cl}_2$ /pentane  $\rightarrow$   $\text{CH}_2\text{Cl}_2$   $\rightarrow$  50:1  $\text{CH}_2\text{Cl}_2$ /acetone); green solid; TLC  $R_f = 0.76$  (98:2  $\text{CH}_2\text{Cl}_2$ /acetone);  $^1\text{H}$  NMR  $\delta$  10.00 (s, 2H), 8.08 (s, 2H), 7.87 (d, 2H,  $J = 7.6$  Hz), 7.67 (d, 2H,  $J = 7.6$  Hz), 7.31 (t, 2H,  $J = 7.6$  Hz), 3.02-2.93 (comp, 8H), 2.52-2.39 (comp, 8H), 1.85-1.81 (comp, 4H), 1.63-1.46 (comp, 20H) ppm;  $^{13}\text{C}$  NMR ( $\text{CD}_2\text{Cl}_2$ )  $\delta$  191.2, 182.9, 146.6 (d,  $^1J_{\text{Rh-C}} = 37.9$  Hz), 142.3, 137.6, 134.4, 125.5, 124.4, 50.5, 37.6, 29.5, 28.6, 23.2 ppm; UV/Visible ( $\text{CH}_2\text{Cl}_2$ )  $\lambda_{\text{max}}$  ( $\epsilon \text{ M}^{-1}\text{cm}^{-1}$ ) nm = 425

(6320); IR (neat)  $\tilde{\nu}$  = 1729 (C=O, s), 1694 (C=O, s), 1589 (N-C=O, s), 1545 (aryl-C=C, s)  $\text{cm}^{-1}$ ; HRMS (ESI) calcd. for  $\text{C}_{38}\text{H}_{48}\text{N}_4\text{O}_6\text{Rh}_2$  865.1919 (M), found 865.1838 (M+H).

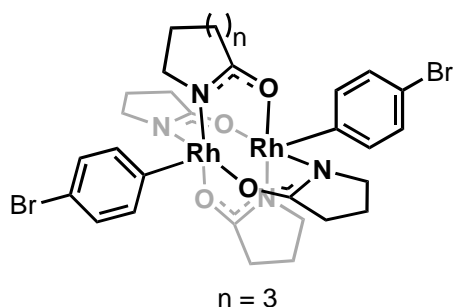
***Bis*[\mathit{\sigma}-(4-formylphenyl)]-*tetrakis*(\mathit{\mu}-caprolactamato)dirhodium(III) (16).**



The general procedure for the the synthesis of  $\text{Rh}_2\text{L}_4\text{Ar}_2$  complexes was followed using *tetrakis*(\mathit{\mu}-caprolactamato)dirhodium(II) (0.027 mmol) and 4-formylphenylboronic acid (0.30 mmol). Purified by trituration with

MeOH (3 x 5 mL); green solid; TLC  $R_f$  = 0.14 (98:2  $\text{CH}_2\text{Cl}_2$ /acetone);  $^1\text{H}$  NMR  $\delta$  10.03 (s, 1H), 7.79 (d, 2H,  $J$  = 8.4 Hz), 7.61 (d, 2H,  $J$  = 8.4 Hz), 2.99-2.92 (comp, 8H), 2.51-2.39 (comp, 8H), 1.87-1.83 (comp, 4H), 1.63-1.39 (comp, 20H) ppm;  $^{13}\text{C}$  NMR ( $\text{CD}_2\text{Cl}_2$ ) 192.1 184.1 161.5 (d,  $^1J_{\text{Rh-C}}$  = 37.1 Hz) ppm; UV/Visible ( $\text{CH}_2\text{Cl}_2$ ):  $\lambda_{\text{max}}$  ( $\epsilon$   $\text{M}^{-1}\text{cm}^{-1}$ ) nm = 422 (7790); IR(neat)  $\tilde{\nu}$  = 1690 (C=O, s), 1586 (N-C=O, s), 1549 (aryl-C=C, s)  $\text{cm}^{-1}$ ; HRMS (FAB) calcd. for  $\text{C}_{38}\text{H}_{50}\text{N}_4\text{O}_6\text{Rh}_2$  864.1841, found 864.1831 (M+); ECHEM  $E_{1/2}$  ( $\Delta E_p$ ,  $I_{pa}/I_{pc}$ ) 0.95 V (0.077 V, 1.04); XRD crystals grown by slow evaporation from 4:1  $\text{CHCl}_3/\text{MeOH}$ .

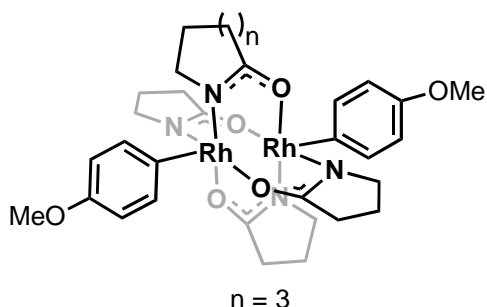
***Bis*[\mathit{\sigma}-(4-bromophenyl)]-*tetrakis*(\mathit{\mu}-caprolactamato)dirhodium(III) (17).**



The general procedure for the synthesis of  $\text{Rh}_2\text{L}_4\text{Ar}_2$  complexes was followed using *tetrakis*(\mathit{\mu}-caprolactamato)dirhodium(II) (0.027 mmol) and 4-bromophenylboronic acid (0.15 mmol). Purified by passing through a silica plug with  $\text{CH}_2\text{Cl}_2$ ; green solid; TLC  $R_f$  = 0.32 (98:2  $\text{CH}_2\text{Cl}_2$ /acetone);

UV/Visible (CH<sub>2</sub>Cl<sub>2</sub>),  $\lambda_{\max}$  ( $\epsilon$  M<sup>-1</sup>cm<sup>-1</sup>) nm = 432 (7780); IR(neat)  $\tilde{\nu}$  = 1604 (N-C=O, s), 1549 (aryl-C=C, s) cm<sup>-1</sup>; HRMS (ESI) calcd. for C<sub>36</sub>H<sub>48</sub>N<sub>4</sub>O<sub>4</sub>Rh<sub>2</sub>Br<sub>2</sub> 989.0034, found 988.9886 (M+Na).

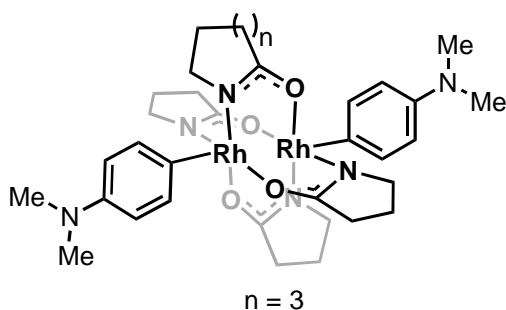
**Bis[ $\sigma$ -(4-methoxyphenyl)]-tetrakis( $\mu$ -caprolactamato)dirhodium(III) (18).**



The general procedure for the the synthesis of Rh<sub>2</sub>L<sub>4</sub>Ar<sub>2</sub> complexes was followed using *tetrakis*-( $\mu$ -caprolactamato)dirhodium(II) (0.027 mmol) and 4-methoxyphenylboronic acid (0.15 mmol). Purified by trituration with MeOH (3 x 5 mL); yellow solid; TLC R<sub>f</sub> =

0.28 (98:2 CH<sub>2</sub>Cl<sub>2</sub>/acetone); <sup>1</sup>H NMR  $\delta$  7.41 (d, 2H, *J* = 8 Hz), 6.83 (d, 2H, *J* = 8 Hz), 3.86 (s, 6H), 3.08-2.95 (comp, 8H), 2.50-2.37 (comp, 8H), 1.84-1.80 (comp, 4H), 1.62-1.55 (comp, 12H), 1.55-1.42 (comp, 8H) ppm; <sup>13</sup>C NMR (CD<sub>2</sub>Cl<sub>2</sub>)  $\delta$  183.4, 157.7, 136.6, 112.0, 55.2, 51.3, 38.5, 30.6, 29.7, 24.3 ppm; UV/Visible (CH<sub>2</sub>Cl<sub>2</sub>):  $\lambda_{\max}$  ( $\epsilon$  M<sup>-1</sup>cm<sup>-1</sup>) nm = 452 (6210); IR(neat)  $\tilde{\nu}$  = 1588 (N-C=O, s), 1474 (aryl-C=C, s) cm<sup>-1</sup>; HRMS (FAB) calcd. for C<sub>38</sub>H<sub>54</sub>N<sub>4</sub>O<sub>6</sub>Rh<sub>2</sub> 864.2153, found 864.2135 (M+); ECHEM *E*<sub>1/2</sub> ( $\Delta E_p$ , *I*<sub>pa</sub>/*I*<sub>pc</sub>) 0.75 V (0.068 V, 1.06); XRD crystals grown by slow evaporation from 4:1 CHCl<sub>3</sub>/MeOH.

**Bis[ $\sigma$ -[4-(*N,N*-dimethylamino)phenyl]]-tetrakis( $\mu$ -caprolactamato)**



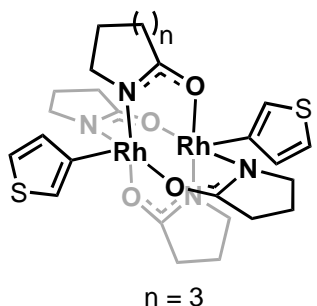
**dirhodium(III) (19).** The general procedure for the synthesis of Rh<sub>2</sub>L<sub>4</sub>Ar<sub>2</sub> complexes was followed using *tetrakis*-( $\mu$ -caprolactamato)dirhodium(II) (0.027 mmol) and 4-(*N,N*-dimethylamino)-phenylboronic acid (0.30 mmol).

Purified by silica gel chromatography (5:1 CH<sub>2</sub>Cl<sub>2</sub>/pentane → CH<sub>2</sub>Cl<sub>2</sub> → 50:1 CH<sub>2</sub>Cl<sub>2</sub>/acetone); green solid; TLC R<sub>f</sub> = 0.76 (98:2 CH<sub>2</sub>Cl<sub>2</sub>/acetone); <sup>1</sup>H NMR  $\delta$  7.35 (d, 4H, *J* = 8.8Hz), 6.72 (d, 4H, *J* = 8.8), 3.12-2.96 (comp, 8H), 2.98 (s, 12 H), 2.46-2.36 (m, 8H), 1.83-1.80 (comp, 4H), 1.61-1.37 (comp, 20H) ppm;



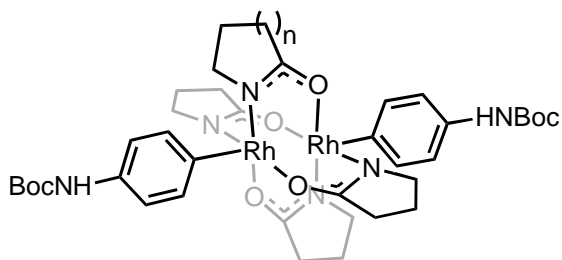
UV/Visible (CH<sub>2</sub>Cl<sub>2</sub>)  $\lambda_{\max}$  ( $\epsilon$  M<sup>-1</sup>cm<sup>-1</sup>) nm = 485 (3050); IR (neat)  $\tilde{\nu}$  = 1589 (N-C=O, s) cm<sup>-1</sup>; HRMS (ESI) calcd. for C<sub>40</sub>H<sub>60</sub>N<sub>6</sub>O<sub>4</sub>Rh<sub>2</sub> 895.2864, found 895.2848 (M+H).

**Bis[ $\sigma$ -(3-thienyl)]-tetrakis( $\mu$ -caprolactamato)dirhodium(III) (20).** The



general procedure for the synthesis of Rh<sub>2</sub>L<sub>4</sub>Ar<sub>2</sub> complexes was followed using *tetrakis*-( $\mu$ -caprolactamato)dirhodium(II) (0.027 mmol) and 3-thienylboronic acid (0.15 mmol). Purified by trituration with MeOH (3 x 5 mL); yellow solid; TLC R<sub>f</sub> = 0.32 (98:2 CH<sub>2</sub>Cl<sub>2</sub>/acetone); <sup>1</sup>H NMR  $\delta$  7.41 (d, 2H, *J* = 3 Hz), 7.34 (d, 2H, *J* = 3 Hz), 7.11 (2, 2H), 3.08-2.97 (comp, 8H), 2.53-2.37 (comp, 8H), 1.89-1.85 (comp, 4H), 1.63-1.55 (comp, 12H), 1.54-1.39 (comp, 8H) ppm; <sup>13</sup>C NMR  $\delta$  184.2, 133.4, 120.5, 119.9, 52.1, 39.3, 31.2, 30.2, 24.9 ppm; UV/Visible (CH<sub>2</sub>Cl<sub>2</sub>):  $\lambda_{\max}$  ( $\epsilon$  M<sup>-1</sup>cm<sup>-1</sup>) nm = 457 (5880); IR(neat):  $\tilde{\nu}$  = 1585 (N-C=O, s) cm<sup>-1</sup>; HRMS (FAB) calcd. for C<sub>32</sub>H<sub>46</sub>N<sub>4</sub>O<sub>4</sub>Rh<sub>2</sub>S<sub>2</sub> 820.1071, found 820.1054 (M+); ECHEM *E*<sub>1/2</sub> ( $\Delta E_p$ , *I*<sub>pa</sub>/*I*<sub>pc</sub>) 0.85 V (0.063 V, 1.00); XRD crystals grown by slow evaporation from 4:1 CHCl<sub>3</sub>/MeOH.

**Bis[ $\sigma$ -[4-(*tert*-butylcarbamato)-phenyl]]-tetrakis( $\mu$ -caprolactamato)dirhodium(III) (21).** The general procedure for the synthesis of Rh<sub>2</sub>L<sub>4</sub>Ar<sub>2</sub> complexes was followed using *tetrakis*-( $\mu$ -caprolactamato)dirhodium(II) (0.027 mmol) and 4-*N*-Boc-phenylboronic acid (0.30 mmol). Purified by trituration with MeOH (3 x 5 mL); green solid; TLC R<sub>f</sub> = 0.11 (98:2 CH<sub>2</sub>Cl<sub>2</sub>/acetone); <sup>1</sup>H NMR  $\delta$  7.42 (d, 4H, *J* = 8.4 Hz), 7.17 (d, 4H, *J* = 8.4 Hz), 6.44 (s, 2H), 3.06-2.92 (comp, 8H), 2.47-2.35 (comp, 8H), 1.81-1.79 (comp, 4H), 1.65-1.37 (comp, 38H) ppm; <sup>13</sup>C NMR  $\delta$  183.4, 152.7, 138.2 (d, *J* = 37.9 Hz), 136.2, 134.7, 117.1, 79.6, 51.1, 38.4, 30.3, 29.3, 28.0, 24.0 ppm; UV/Visible



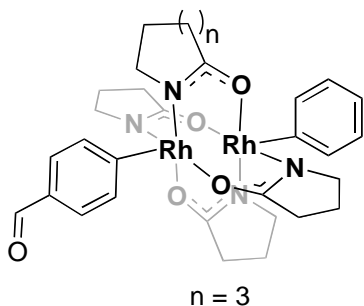
**dirhodium(III) (21).** The general procedure for the synthesis of Rh<sub>2</sub>L<sub>4</sub>Ar<sub>2</sub> complexes was followed using *tetrakis*-( $\mu$ -caprolactamato)dirhodium(II) (0.027

mmol) and 4-*N*-Boc-phenylboronic acid (0.30 mmol). Purified by trituration with MeOH (3 x 5 mL); green solid; TLC R<sub>f</sub> = 0.11 (98:2 CH<sub>2</sub>Cl<sub>2</sub>/acetone); <sup>1</sup>H NMR  $\delta$  7.42 (d, 4H, *J* = 8.4 Hz), 7.17 (d, 4H, *J* = 8.4 Hz), 6.44 (s, 2H), 3.06-2.92 (comp, 8H), 2.47-2.35 (comp, 8H), 1.81-1.79 (comp, 4H), 1.65-1.37 (comp, 38H) ppm; <sup>13</sup>C NMR  $\delta$  183.4, 152.7, 138.2 (d, *J* = 37.9 Hz), 136.2, 134.7, 117.1, 79.6, 51.1, 38.4, 30.3, 29.3, 28.0, 24.0 ppm; UV/Visible

(CH<sub>2</sub>Cl<sub>2</sub>):  $\lambda_{\max}$  ( $\epsilon$  M<sup>-1</sup>cm<sup>-1</sup>) nm = 450 (7960); IR(neat)  $\tilde{\nu}$  = 3451 (N-H, s), 1726(carbamate, s), 1586 (N-C=O, s), 1496 (aryl-C=C, s) cm<sup>-1</sup>; HRMS (FAB) calcd. for C<sub>46</sub>H<sub>68</sub>N<sub>6</sub>O<sub>8</sub>Rh<sub>2</sub> 1038.3209, found 1038.3233 (M<sup>+</sup>); ECHEM  $E_{1/2}$  ( $\Delta E_p$ ,  $I_{pa}/I_{pc}$ ) 0.80 V (0.067 V, 1.17).

**General Preparation of  $[(\sigma\text{-aryl}), (\sigma\text{-aryl}')]\text{-Rh}_2^{6+}$  Complexes.** Rh<sub>2</sub>L<sub>4</sub> (0.027 mmol) and [Cu(OTf)]<sub>2</sub>•C<sub>6</sub>H<sub>6</sub> (3 mmol) were diluted in CH<sub>2</sub>Cl<sub>2</sub>/MeOH (1.5 mL, 4:1) and sonicated for 5 minutes. This solution was added dropwise to a vigorously stirring mixture of electron deficient boronic acid (0.06 mmol), electron-rich boronic acid (0.24 mmol), and NaOMe (0.30 mmol) in CH<sub>2</sub>Cl<sub>2</sub>/MeOH (1.5 mL, 4:1). An additional 2 mL of CH<sub>2</sub>Cl<sub>2</sub>/MeOH (4:1) was used to transfer the Rh<sub>2</sub>L<sub>4</sub> solution and bring the final reaction volume to 5 mL ([Rh<sub>2</sub>L<sub>4</sub>] = 5.4 mM). The reaction was left to stir at room temperature until completion. The solvent was removed *in vacuo* to yield a crude residue. The residue was purified by chromatography on silica gel to yield  $[(\sigma\text{-aryl}), (\sigma\text{-aryl}')]\text{Rh}_2\text{L}_4$ , *bis*( $\sigma\text{-aryl}$ )Rh<sub>2</sub>L<sub>4</sub>, and *bis*( $\sigma\text{-aryl}'$ )Rh<sub>2</sub>L<sub>4</sub> complexes.

**$[(\sigma\text{-4-formylphenyl}), \sigma\text{-phenyl}]\text{-tetrakis}(\mu\text{-caprolactamato})\text{dirhodium(III)}$**



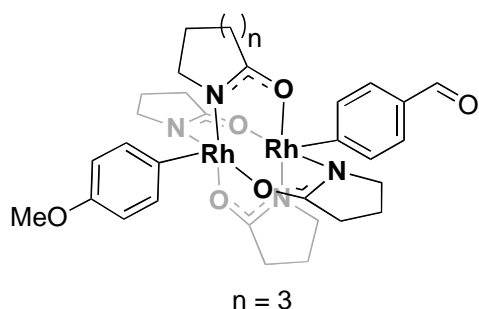
**(22).** The general procedure for the the synthesis of hetero-substituted Rh<sub>2</sub><sup>6+</sup> complexes was followed using *tetrakis*-( $\mu$ -caprolactamato)dirhodium(II) (0.027 mmol), 4-formylphenylboronic acid (0.06 mmol) and phenylboronic acid (0.24 mmol). Purified by chromatography on silica (5:1 CH<sub>2</sub>Cl<sub>2</sub>/pentane →

CH<sub>2</sub>Cl<sub>2</sub> → 50:1 CH<sub>2</sub>Cl<sub>2</sub>/acetone); green solid;<sup>114</sup> TLC R<sub>f</sub> = 0.20 (98:2 CH<sub>2</sub>Cl<sub>2</sub>/acetone); <sup>1</sup>H NMR  $\delta$  10.03 (s, 1H), 7.84 (d, 2H,  $J$  = 8 Hz), 7.61 (d, 2H,  $J$  = 8 Hz), 7.53-7.50 (comp, 2H), 7.15-7.13 (comp, 3H), 3.06-2.96 (comp, 8H), 2.51-2.39 (comp, 8H), 1.84-1.79 (comp, 4H), 1.63-1.39 (comp, 20H) ppm; <sup>13</sup>C

<sup>114</sup>*Bis*( $\sigma$ -phenyl)Rh<sub>2</sub>(cap)<sub>4</sub> and *bis*{ $\sigma$ -(4-formyl)phenyl}Rh<sub>2</sub>(cap)<sub>4</sub> were also isolated from the chromatography, however **22** was cleanly separable from the mixture.

NMR  $\delta$  192.7, 184.4, 184.0, 137.8, 136.8, 133.5, 126.7, 126.6, 124.5, 51.7, 51.5, 39.0, 38.9, 30.7, 29.9, 29.7, 24.4 ppm; UV/Visible (CH<sub>2</sub>Cl<sub>2</sub>):  $\lambda_{\text{max}}$  ( $\epsilon$  M<sup>-1</sup>cm<sup>-1</sup>) nm = 425 (8880); IR(neat)  $\tilde{\nu}$  = 1692 (C=O, s), 1586 (N-C=O, s), 1568 (aryl-C=C, s), 1555 (aryl'-C=C, s) cm<sup>-1</sup>; HRMS (ESI) calcd. for C<sub>37</sub>H<sub>50</sub>N<sub>4</sub>O<sub>5</sub>Rh<sub>2</sub> 837.1970, found 837.1921 (M+H); XRD crystals grown by slow evaporation from 4:1 CHCl<sub>3</sub>/MeOH.

***trans*-[ $\sigma$ -(4-methoxyphenyl)- $\sigma$ -(4-formylphenyl)]-tetrakis-( $\mu$ -**



**caprolactamato) dirhodium(III)**

**caprolactamate (23).** The general

procedure for the the synthesis of hetero-

substituted Rh<sub>2</sub><sup>6+</sup> complexes was followed

using *tetrakis*-( $\mu$ -

caprolactamato)dirhodium(II) (0.027

mmol), 4-formyl-phenylboronic acid (0.06 mmol) and 4-methoxy-

phenylboronic acid (0.24 mmol). Purified by chromatography on silica (5:1

CH<sub>2</sub>Cl<sub>2</sub>/pentane  $\rightarrow$  CH<sub>2</sub>Cl<sub>2</sub>  $\rightarrow$  25:1 CH<sub>2</sub>Cl<sub>2</sub>/acetone);<sup>115</sup> green solid; TLC R<sub>f</sub> =

0.31 (CH<sub>2</sub>Cl<sub>2</sub>:acetone); <sup>1</sup>H NMR  $\delta$  10.03 (s, 1H), 7.83 (d, 1H, *J* = 8 Hz), 7.60

(d, 1H, *J* = 8Hz), 7.39-7.37 (comp, 2H), 6.84-6.81 (comp, 3H), 3.86 (s, 3H),

3.04-2.96 (comp, 8H), 2.47-2.42 (comp, 2H), 1.84-1.82 (comp, 4H), 1.63-1.39

(comp, 20H) ppm; <sup>13</sup>C NMR (CD<sub>2</sub>Cl<sub>2</sub>)  $\delta$  192.1, 183.9, 183.5, 157.8, 127.7,

136.3, 133.3, 126.1, 112.1, 55.2, 51.5, 51.2, 38.5, 30.5, 29.7, 29.6, 29.5, 24.2

ppm; UV/Visible (CH<sub>2</sub>Cl<sub>2</sub>):  $\lambda_{\text{max}}$  ( $\epsilon$  M<sup>-1</sup>cm<sup>-1</sup>) nm = 438 (8390); IR(neat)  $\tilde{\nu}$  = 1685

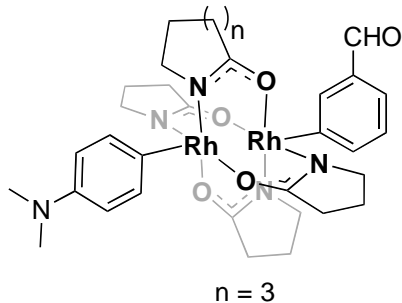
(C=O, s), 1590 (N-C=O, s), 1564 (aryl-C=C, s), 1550 (aryl'-C=C, s) cm<sup>-1</sup>;

HRMS (ESI) calcd. for C<sub>38</sub>H<sub>51</sub>N<sub>4</sub>O<sub>6</sub>Rh<sub>2</sub> 866.1997, found 866.1877 (M+H);

ECHM *E*<sub>1/2</sub> ( $\Delta E_p$ , *I*<sub>pa</sub>/*I*<sub>pc</sub>) 0.85 V (0.057 V, 1.15).

<sup>115</sup>*Bis*{ $\sigma$ -(4-formyl)phenyl}Rh<sub>2</sub>(cap)<sub>4</sub> and *bis*{ $\sigma$ -(4-methoxy)phenyl}Rh<sub>2</sub>(cap)<sub>4</sub> were also isolated from the chromatography. Complex **23** was not 100% separable from the product mixture as there were a small number of fractions that contained both **18** and **23**.

***trans*-[ $\sigma$ -(4-(*N,N*-dimethylaminophenyl))- $\sigma$ -(4-formylphenyl)]-tetrakis-( $\mu$ -caprolactamato) dirhodium(III) (24).**



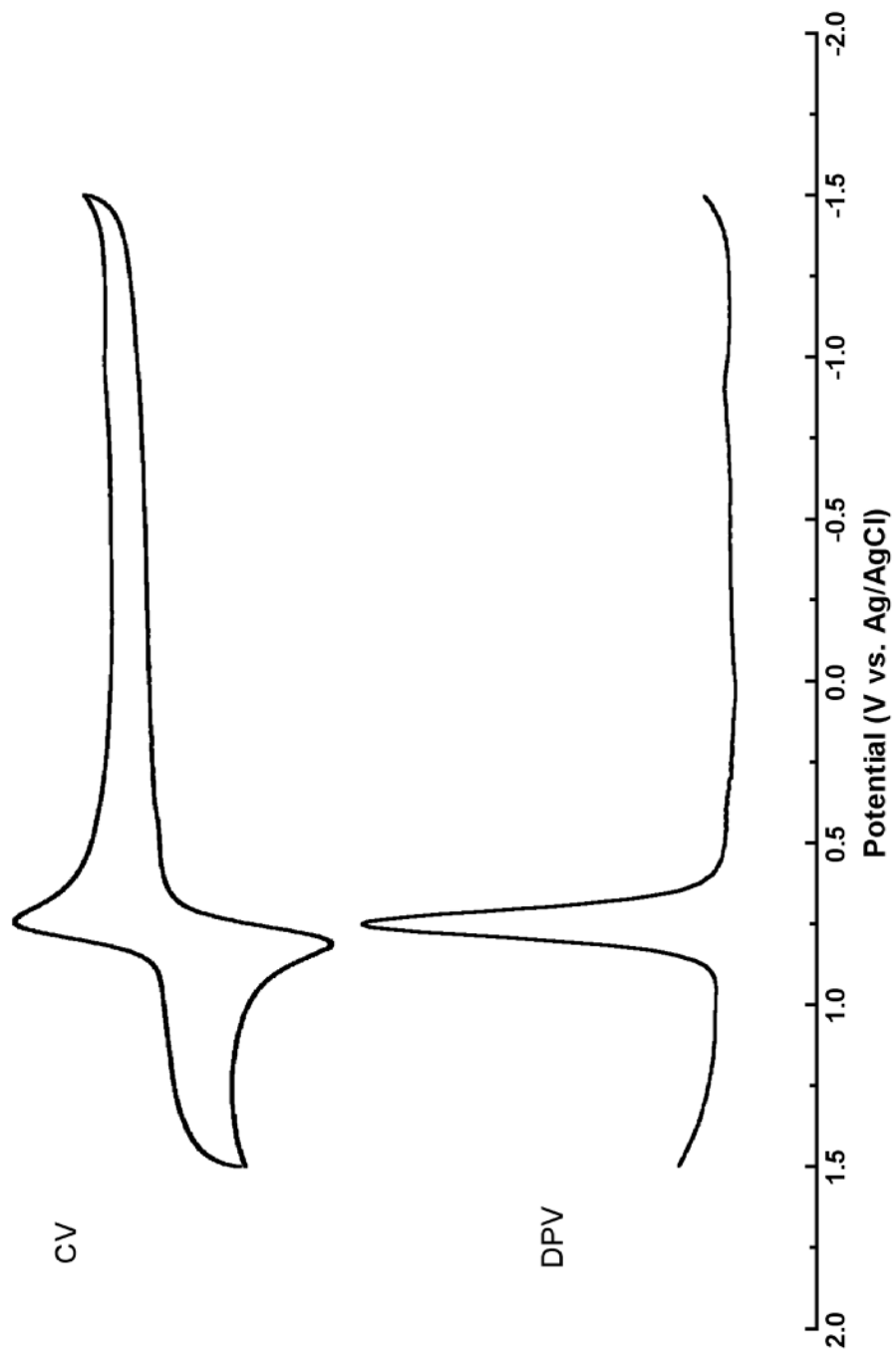
The general procedure for the synthesis of hetero-substituted  $\text{Rh}_2^{6+}$  complexes was followed using tetrakis-( $\mu$ -caprolactamato)dirhodium(II) (0.027 mmol), 3-formylphenylboronic acid (0.06 mmol) and

4-(*N,N*-dimethylamino)-phenylboronic acid (0.24 mmol). Purified by chromatography on silica ((5:1  $\text{CH}_2\text{Cl}_2$ /pentane  $\rightarrow$   $\text{CH}_2\text{Cl}_2$   $\rightarrow$  25:1  $\text{CH}_2\text{Cl}_2$ /acetone));<sup>116</sup> green solid; TLC  $R_f = 0.22$  ( $\text{CH}_2\text{Cl}_2$ );  $^1\text{H}$  NMR  $\delta$  9.99 (s, 1H), 8.10 (s, 1H), 7.87 (d, 1H,  $J = 8$  Hz), 7.62 (d, 1H,  $J = 8$  Hz), 7.32-7.23 (comp, 3H), 6.69 (d, 1H,  $J = 8$  Hz), 3.10-2.95 (comp, 14H), 2.48-2.36 (comp, 8H), 1.81-1.19 (comp, 24H) ppm;  $^{13}\text{C}$  NMR ( $\text{CD}_2\text{Cl}_2$ ) 192.7, 184.0, 183.6, 149.3, 143.9, 139.3, 136.3, 135.4, 126.5, 125.2, 112.5, 51.7, 51.6, 41.2, 38.8, 38.7, 30.8, 30.0, 29.8, 24.5 ppm; UV/Visible ( $\text{CH}_2\text{Cl}_2$ )  $\lambda_{\text{max}}$  ( $\epsilon \text{ M}^{-1}\text{cm}^{-1}$ ) nm = 430 (4090); IR (neat) 1730 (C=O, s), 1598 (N-C=O, s)  $\text{cm}^{-1}$ ; HRMS (ESI) calcd. for  $\text{C}_{39}\text{H}_{56}\text{N}_5\text{O}_5\text{Rh}_2$  880.2391, found 880.2081 (M+H).

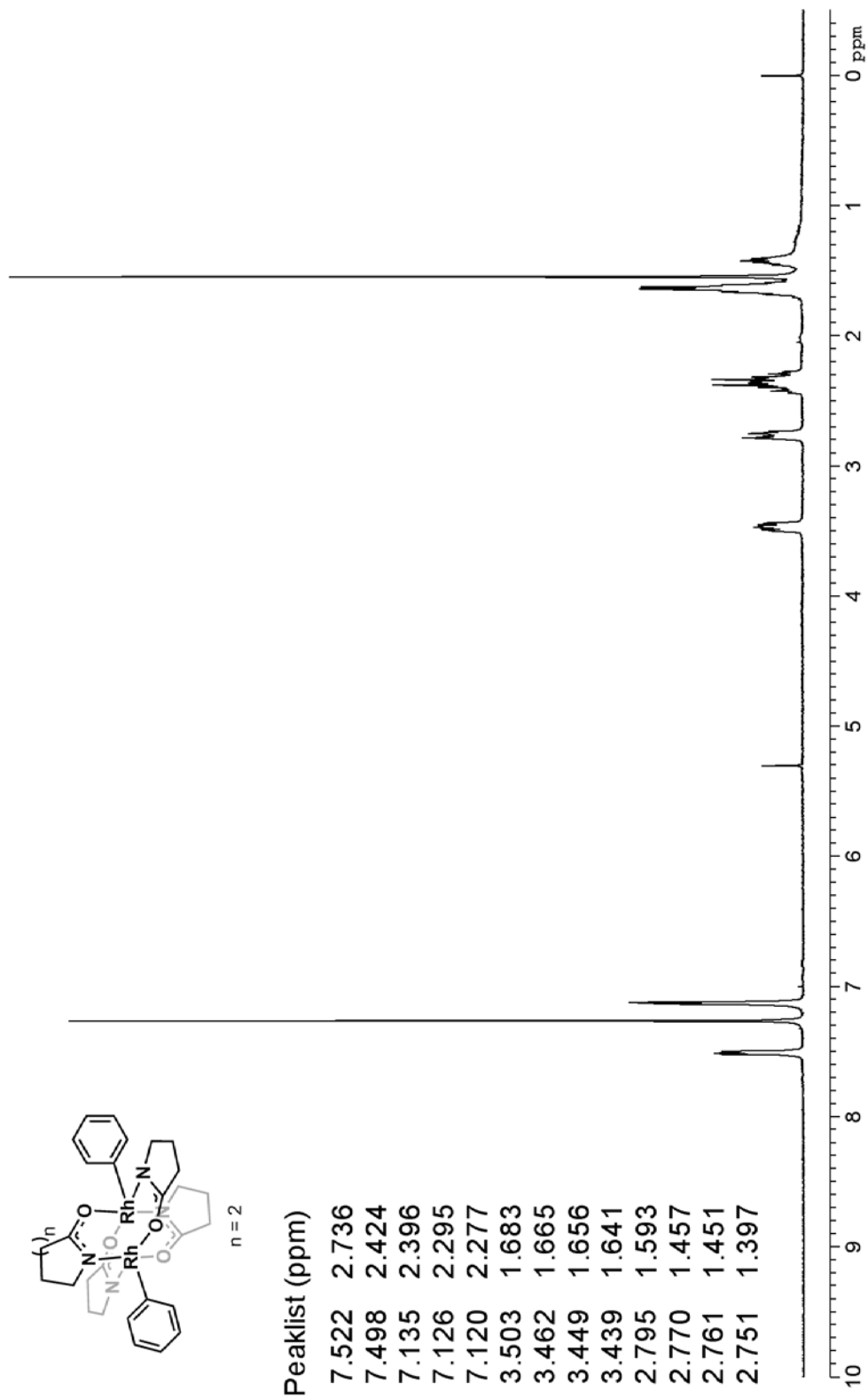
<sup>116</sup> *Bis*{ $\sigma$ -(4-dimethylamino)phenyl} $\text{Rh}_2(\text{cap})_4$  was also isolated from the chromatography and it was cleanly separable from the product mixture.

## Spectral Traces and Voltammetry.

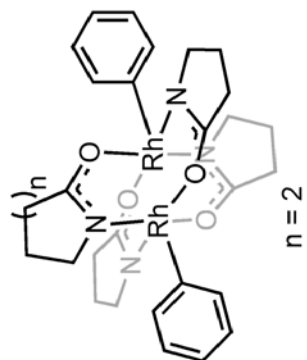
Voltammetry (1).



<sup>1</sup>H NMR Spectrum – (12)

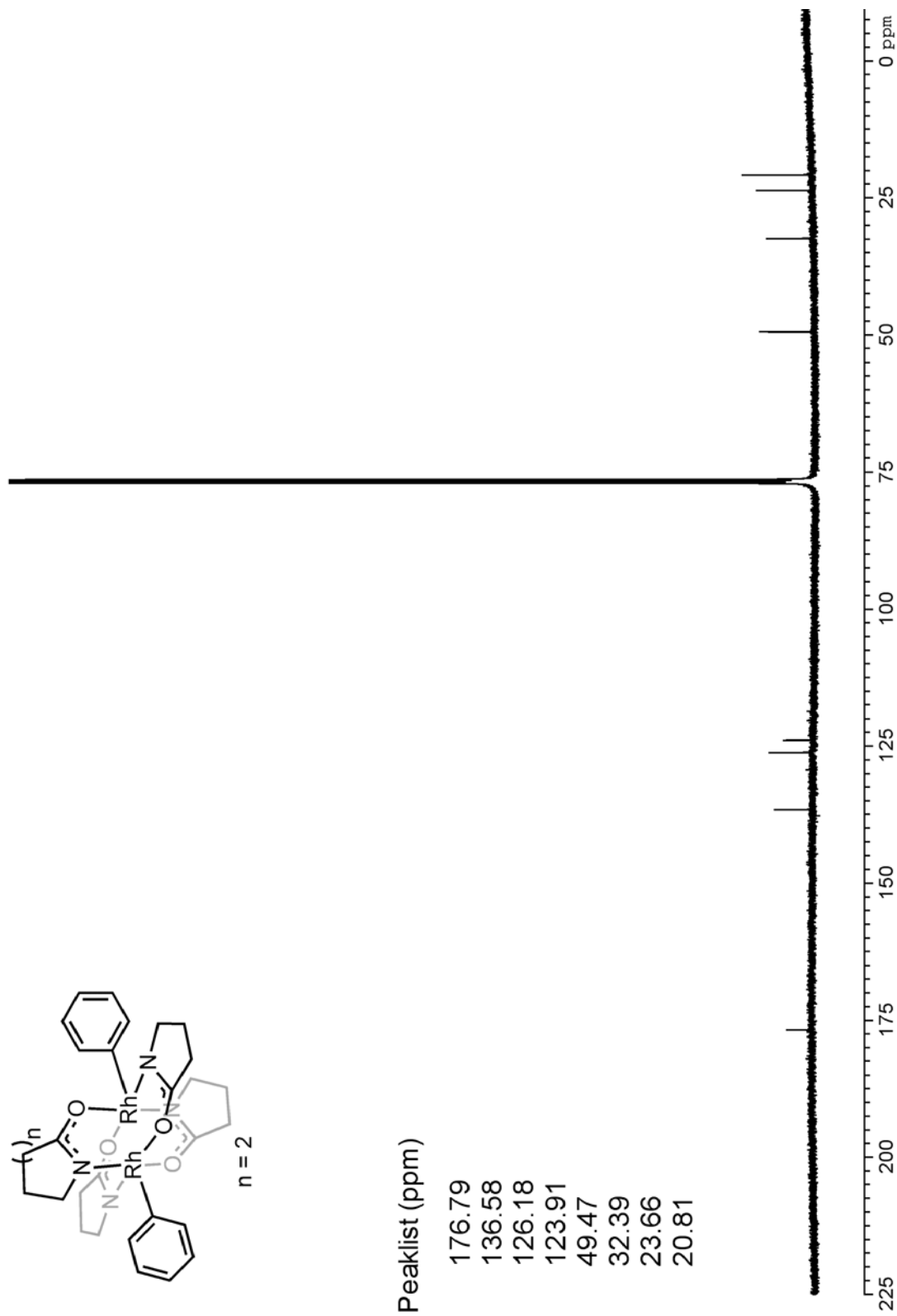


<sup>13</sup>C NMR Spectrum (12)

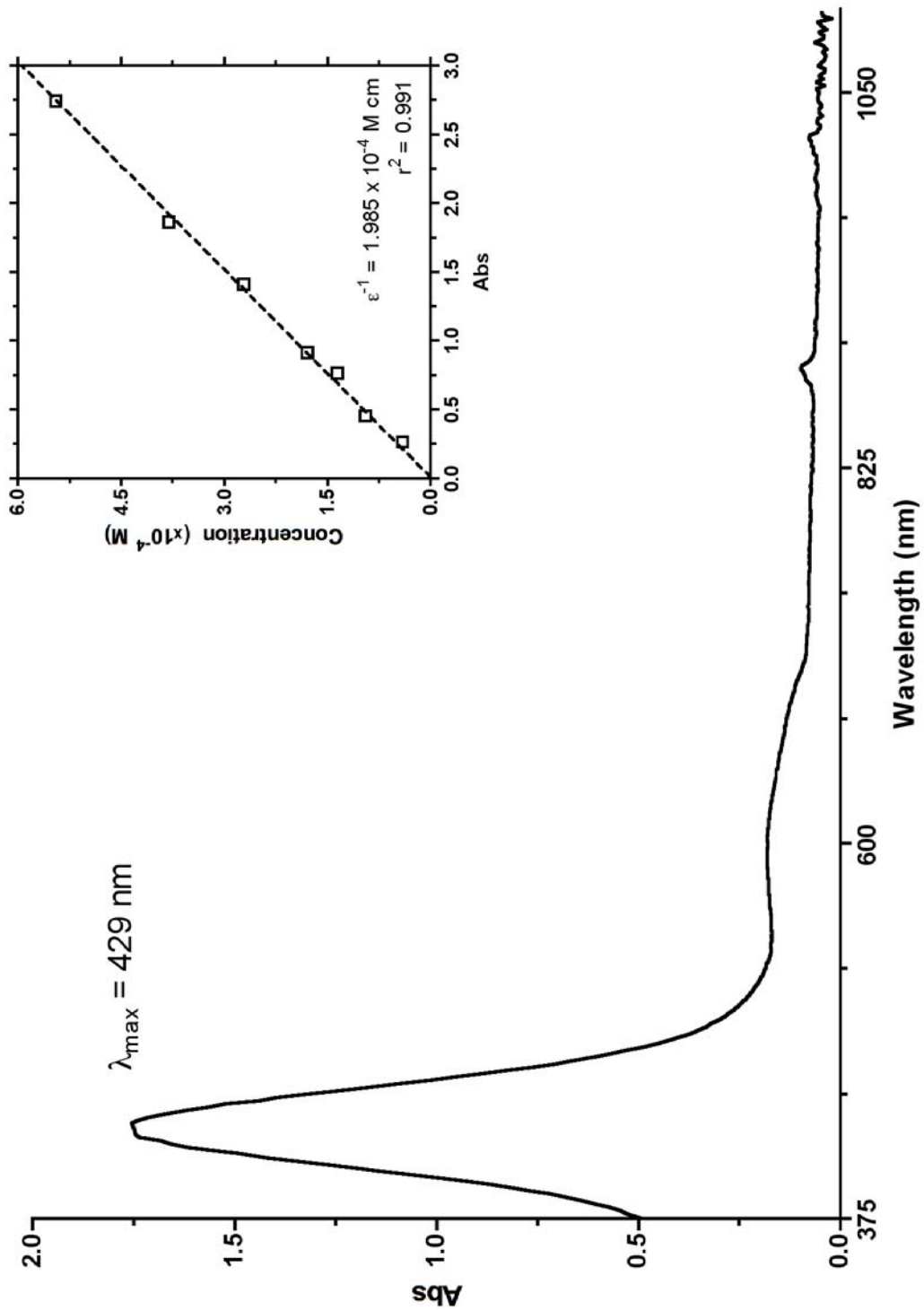


Peaklist (ppm)

- 176.79
- 136.58
- 126.18
- 123.91
- 49.47
- 32.39
- 23.66
- 20.81

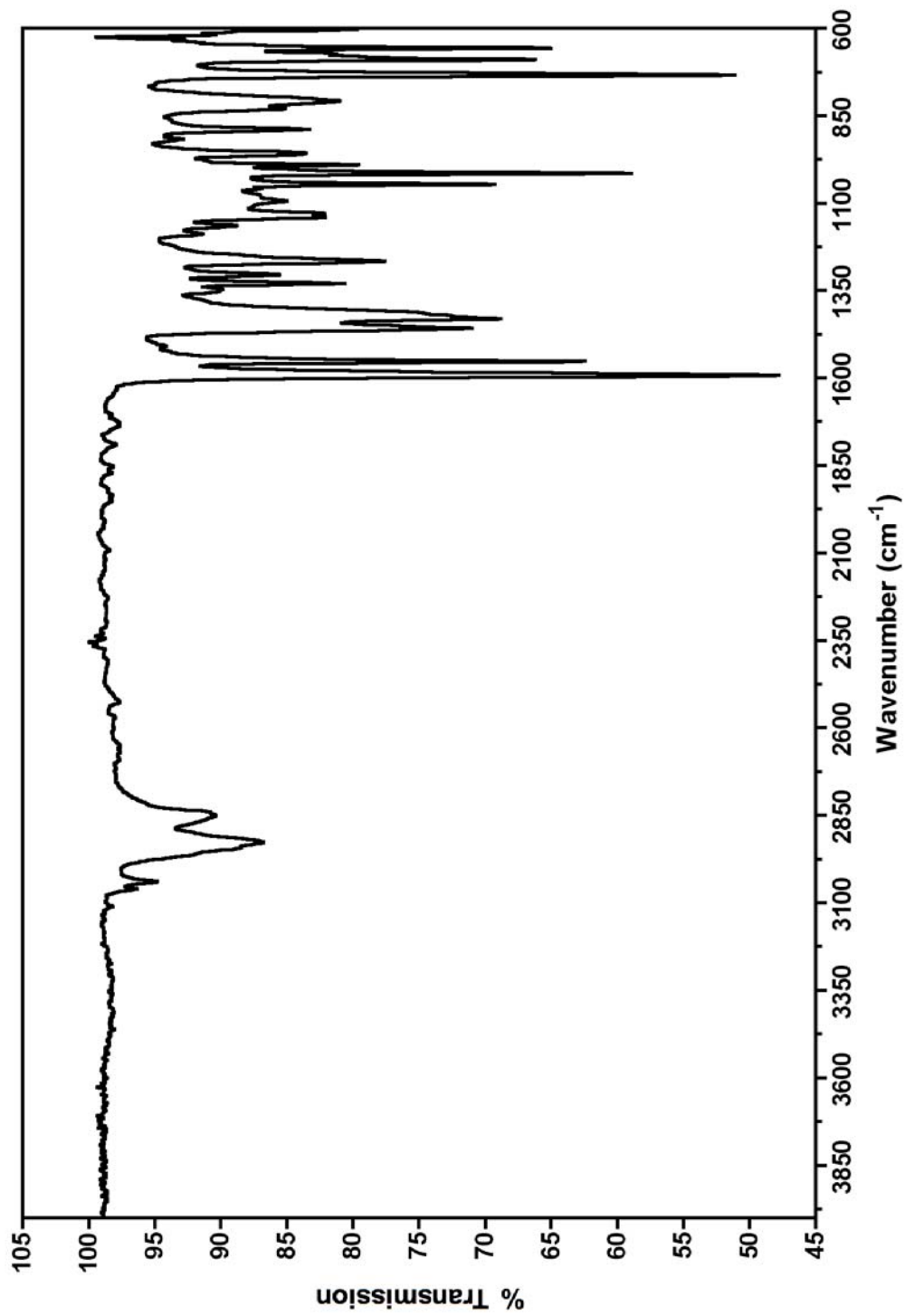


Electronic Absorption Spectrum & Molar Absorptivity (12, 375 – 1100 nm).

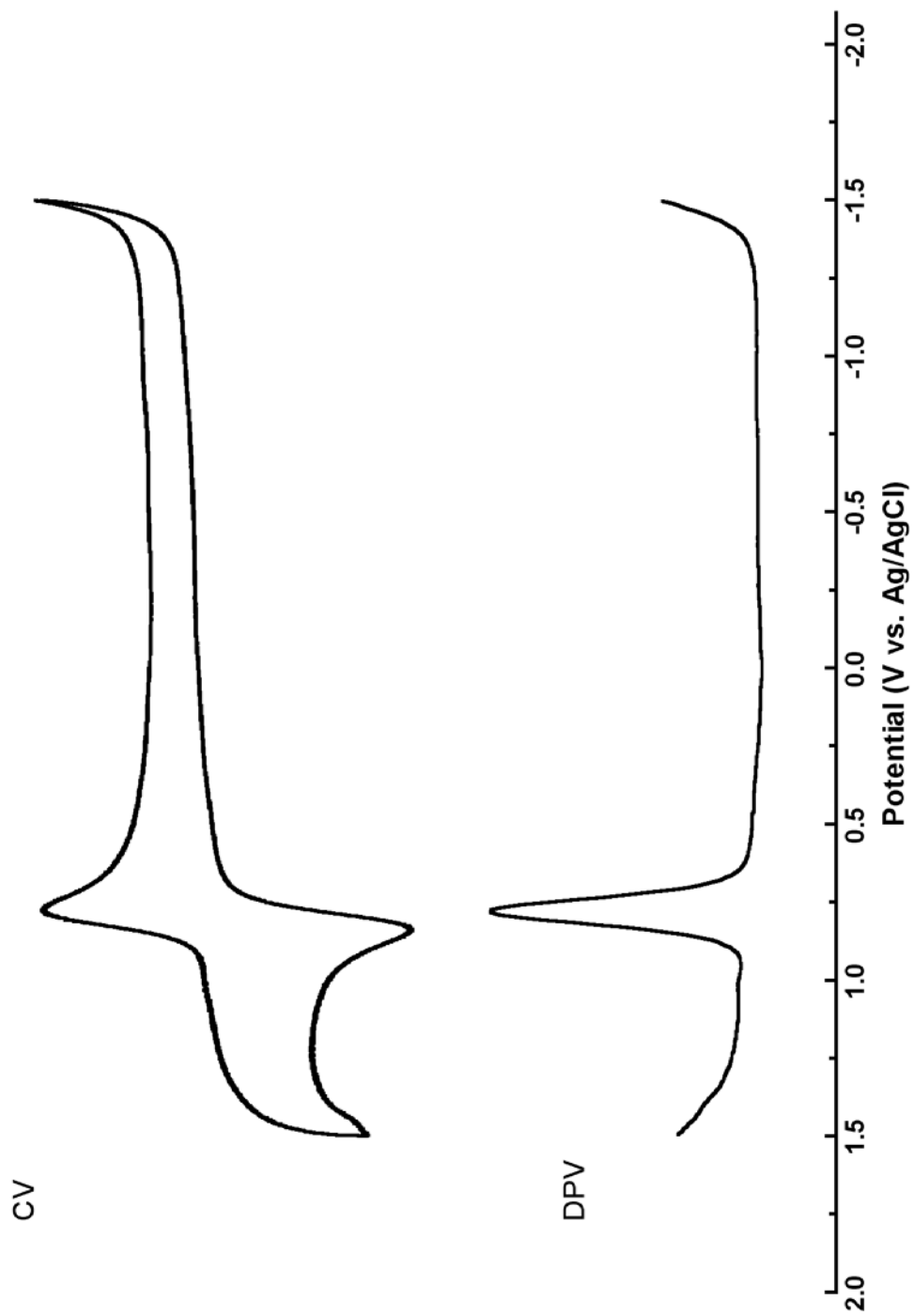




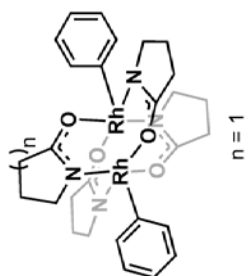
Vibrational Spectrum (12, 4000 – 600  $\text{cm}^{-1}$ ).



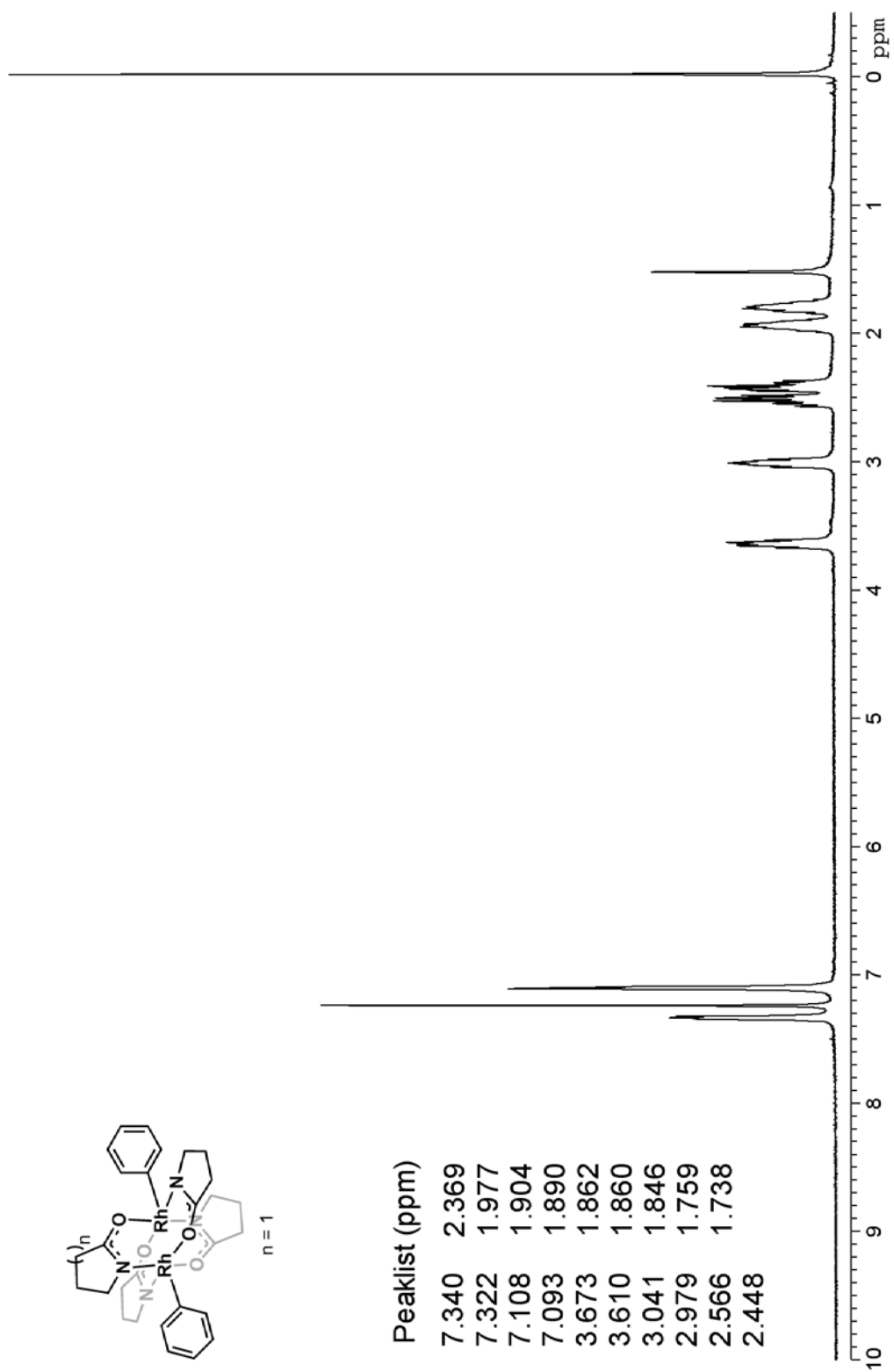
Voltammetry (12).



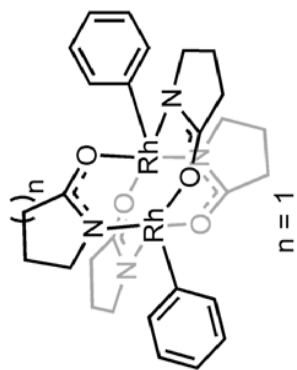
<sup>1</sup>H NMR Spectrum (13).



Peaklist (ppm)
7.340
7.322
7.108
7.093
3.673
3.610
3.041
2.979
2.566
2.448

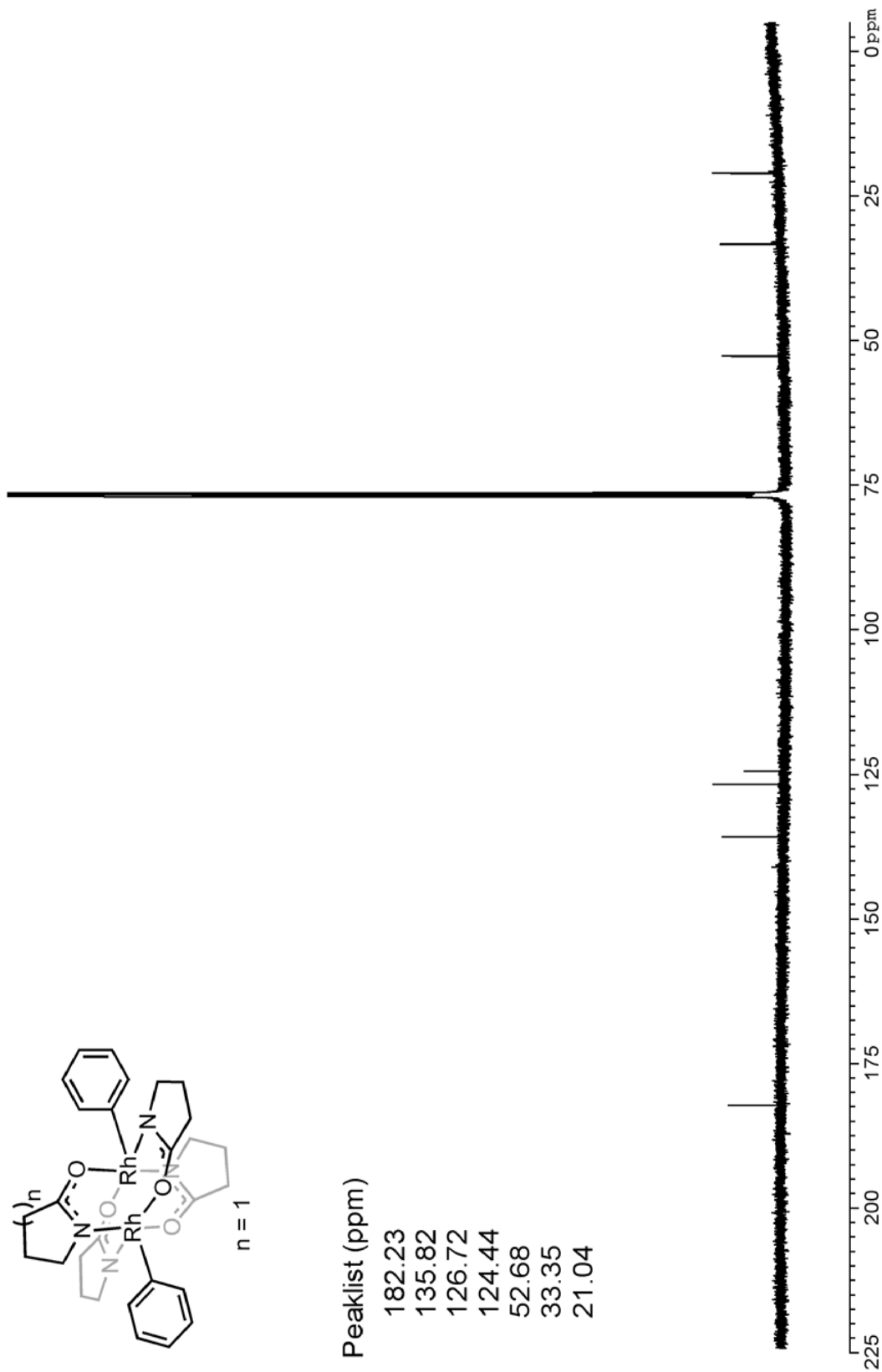


<sup>13</sup>C NMR Spectrum-(13)

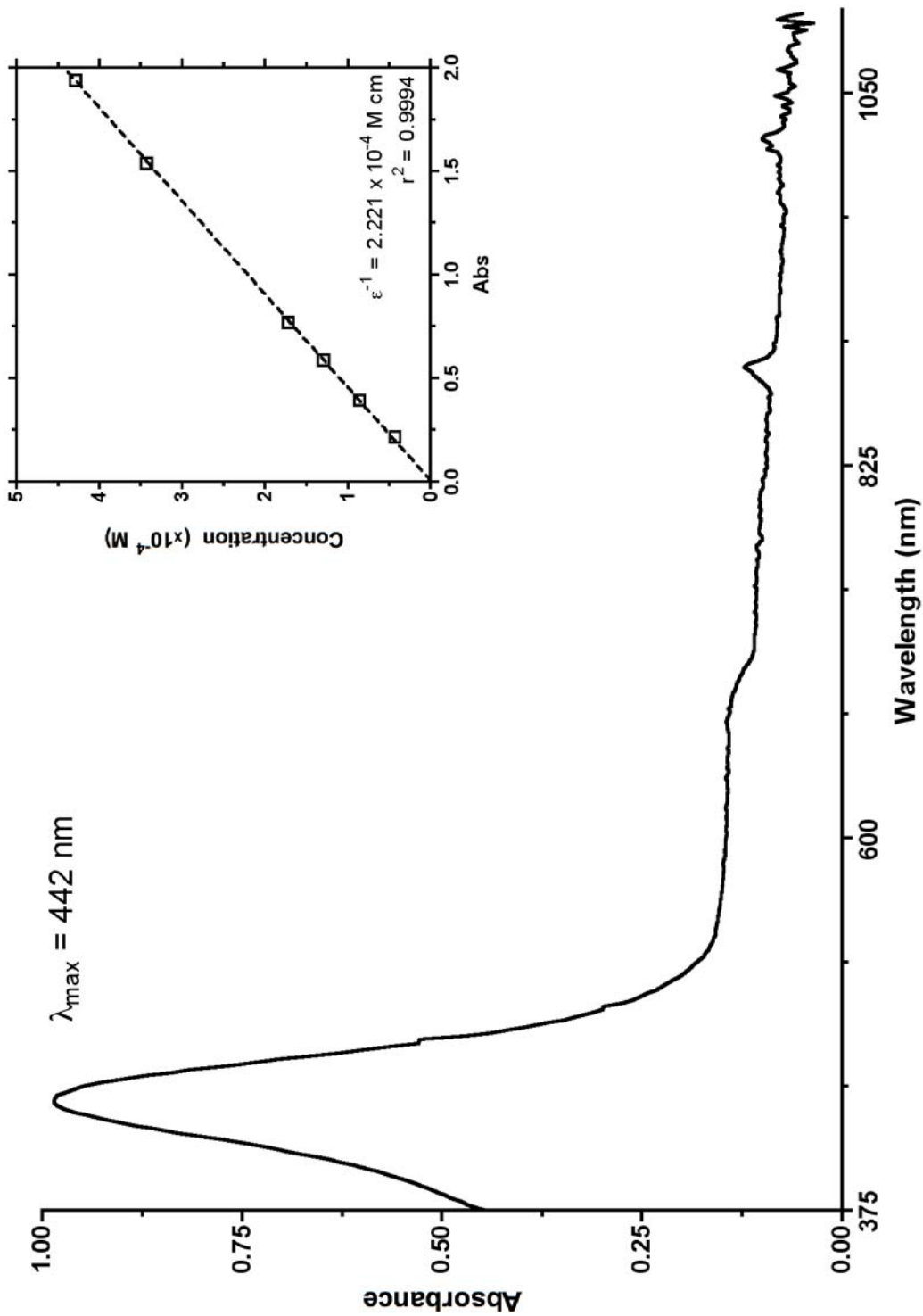


Peaklist (ppm)

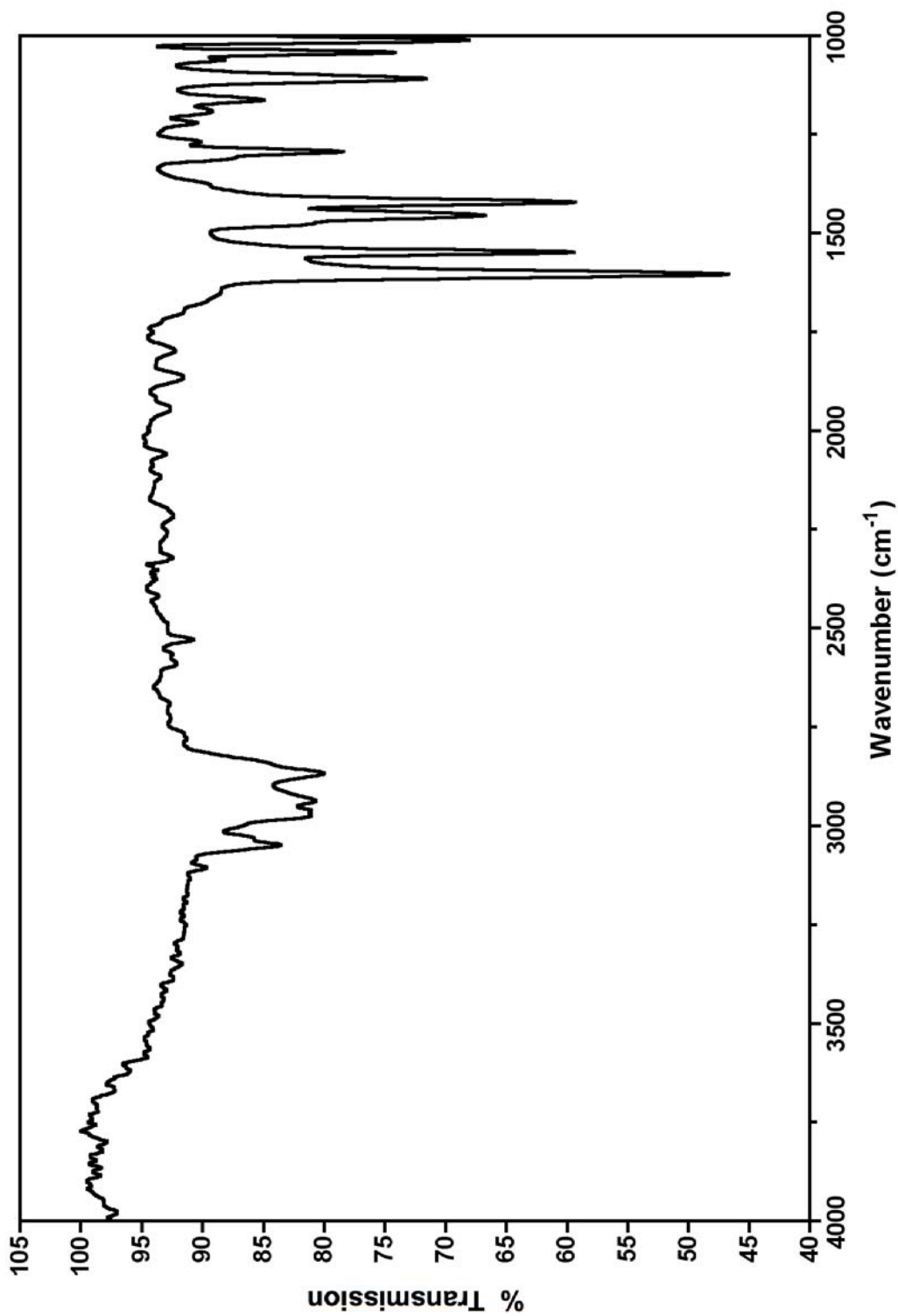
- 182.23
- 135.82
- 126.72
- 124.44
- 52.68
- 33.35
- 21.04



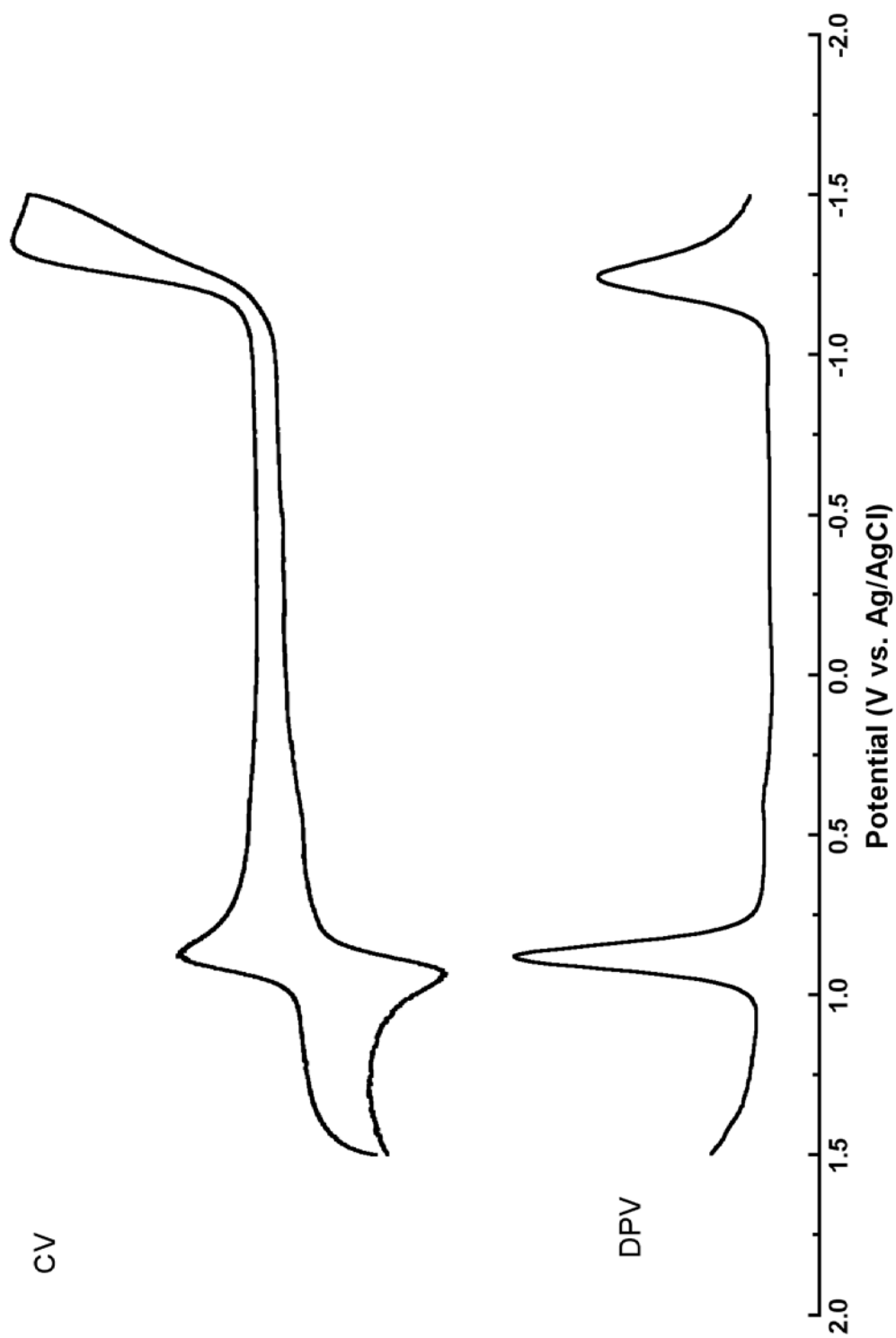
Electronic Absorption Spectrum & Molar Absorptivity (13, 375 – 1100 nm)



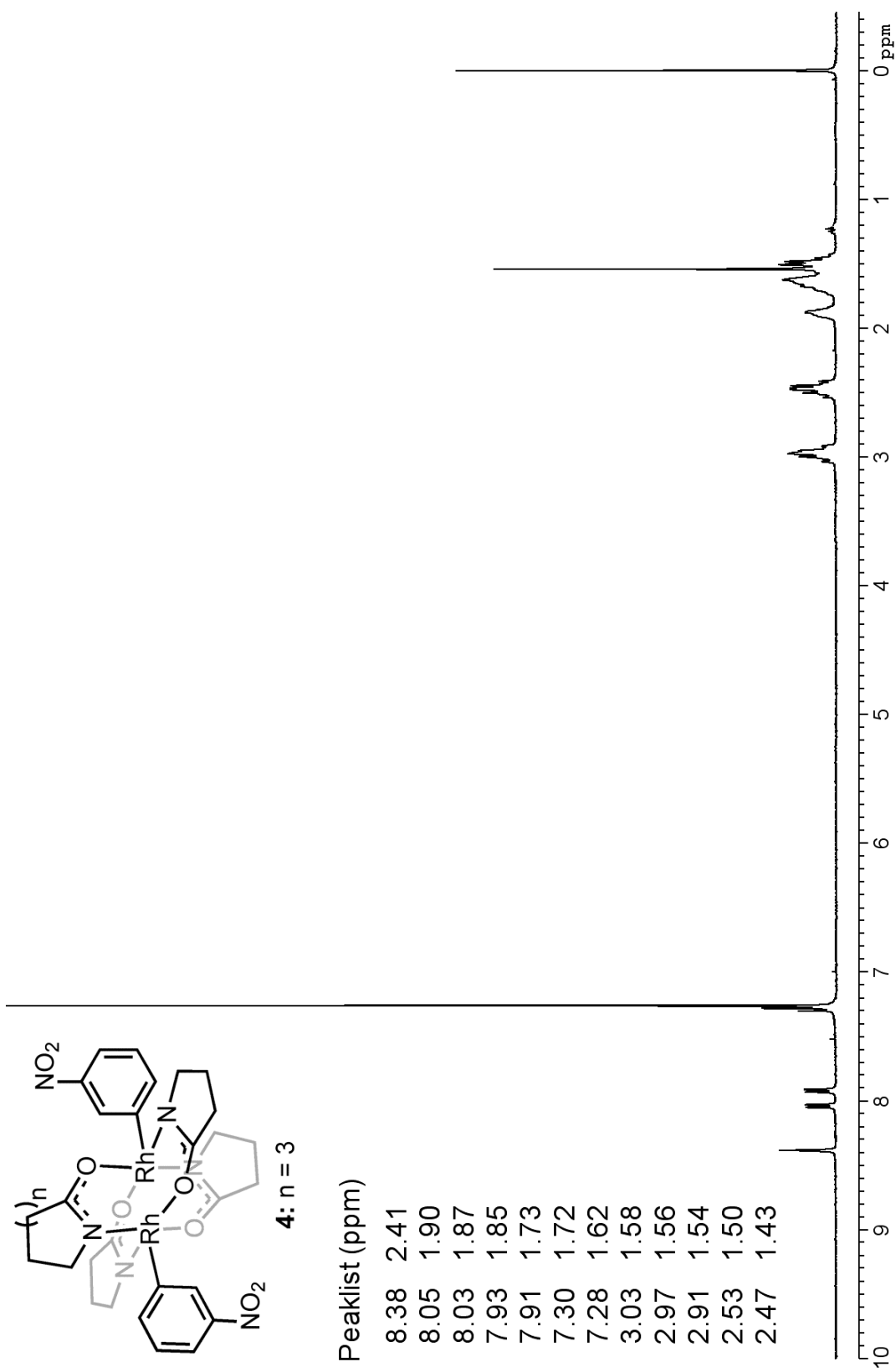
Vibrational Spectrum (13, 4000 – 600  $\text{cm}^{-1}$ )



Voltammetry (13)

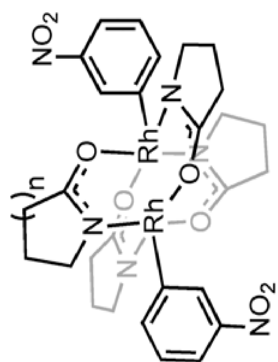


$^1\text{H}$  NMR Spectrum (**14**).



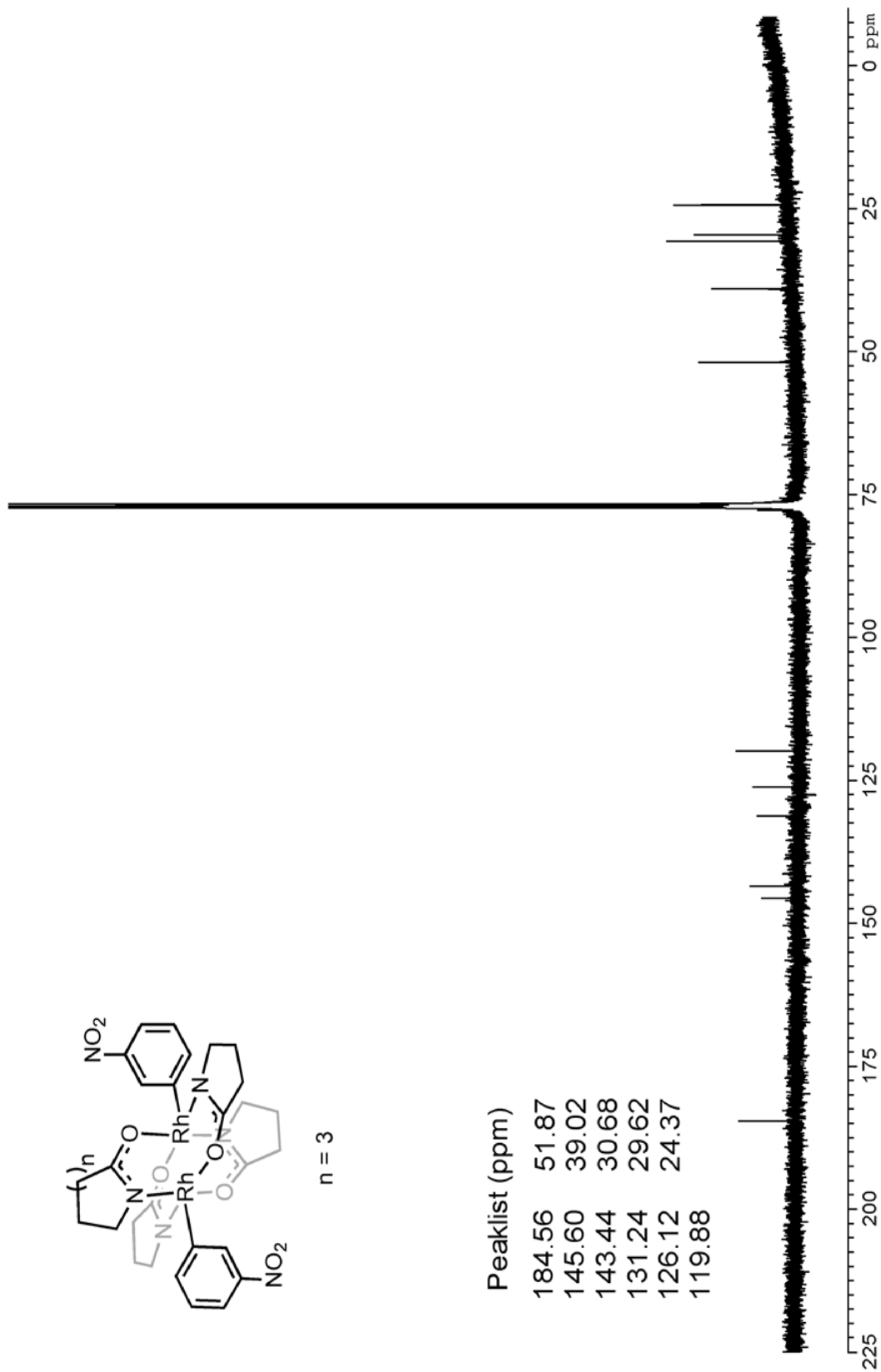


<sup>13</sup>C NMR Spectrum (14).

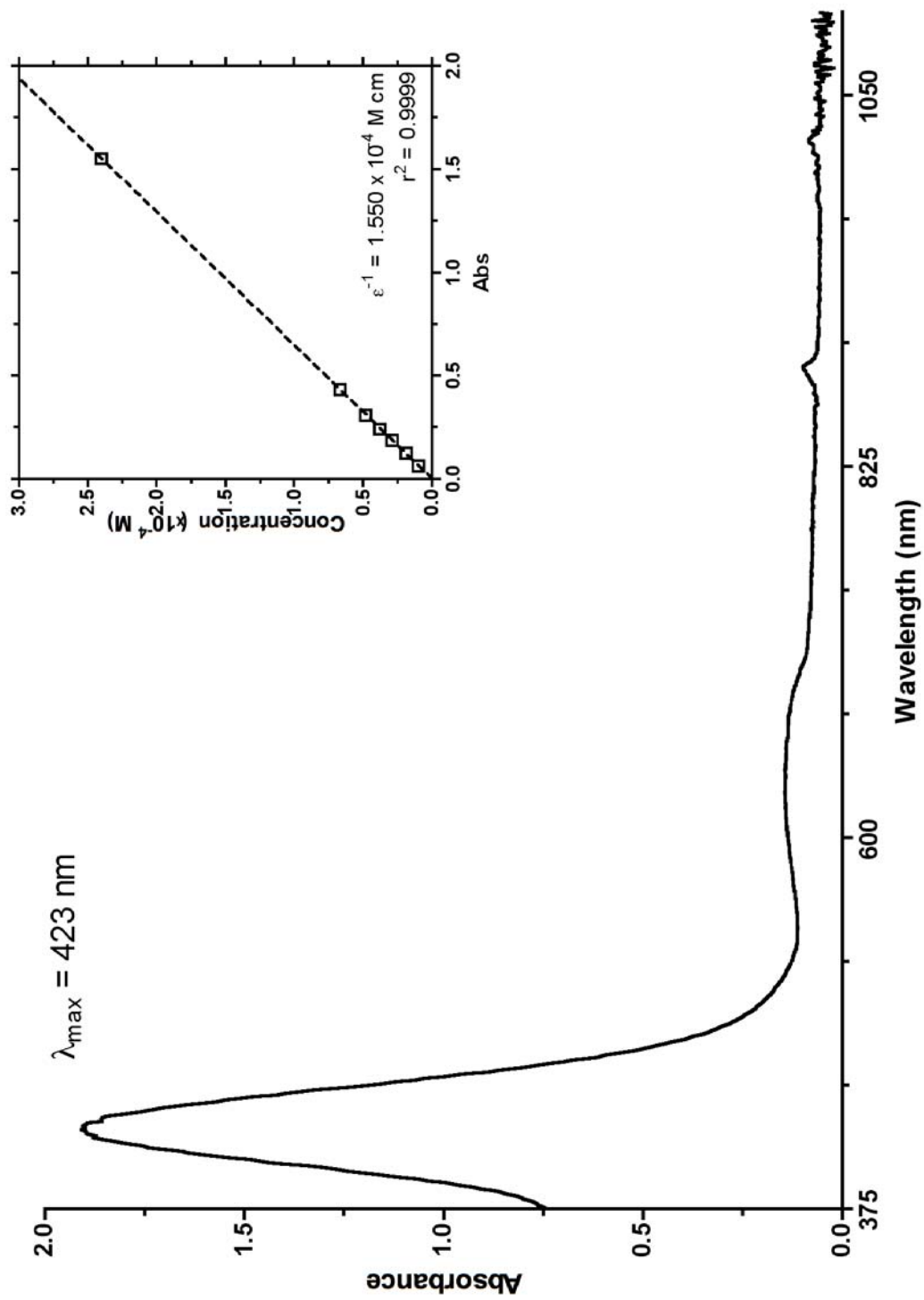


$n = 3$

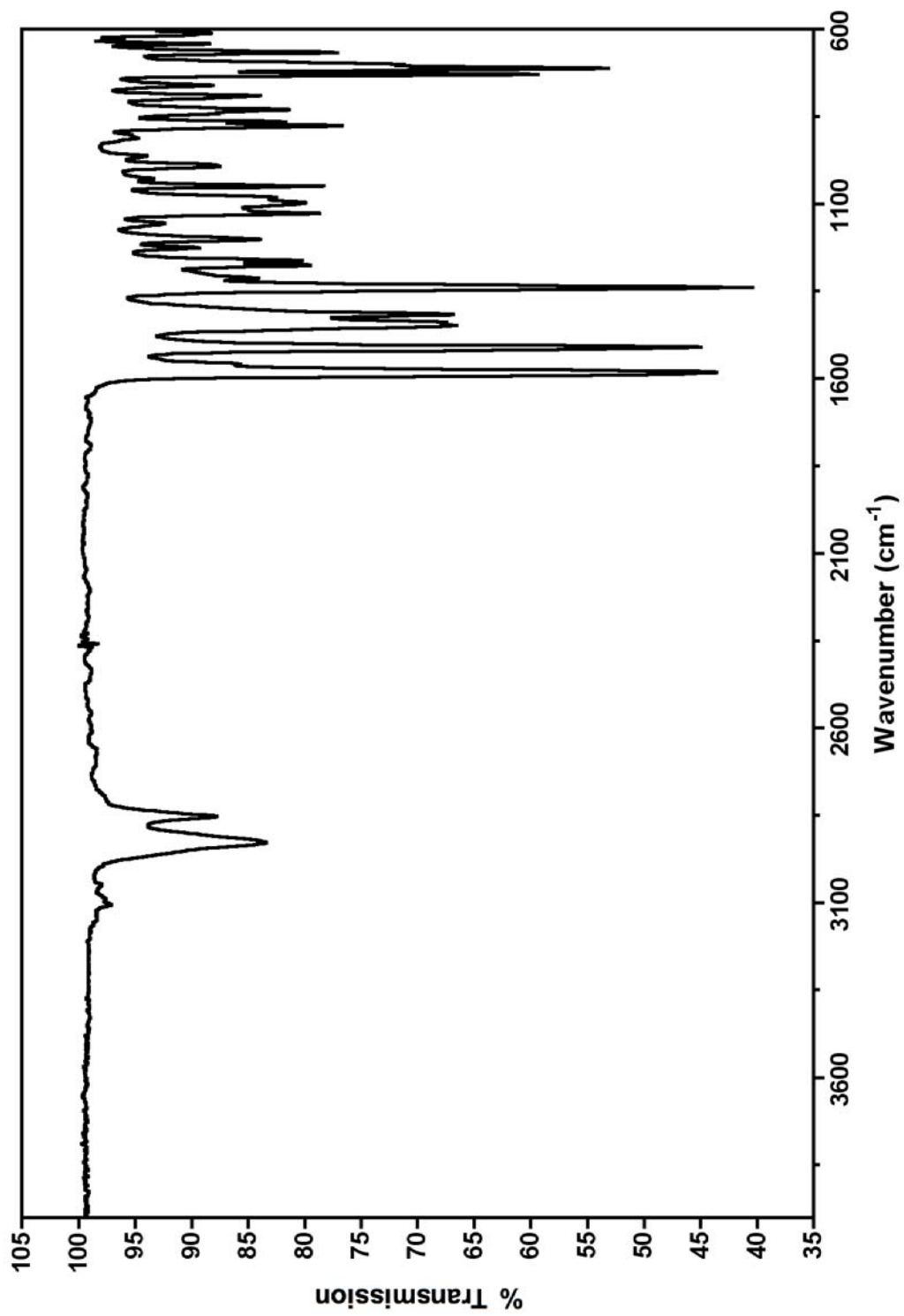
Peaklist (ppm)	
184.56	51.87
145.60	39.02
143.44	30.68
131.24	29.62
126.12	24.37
119.88	



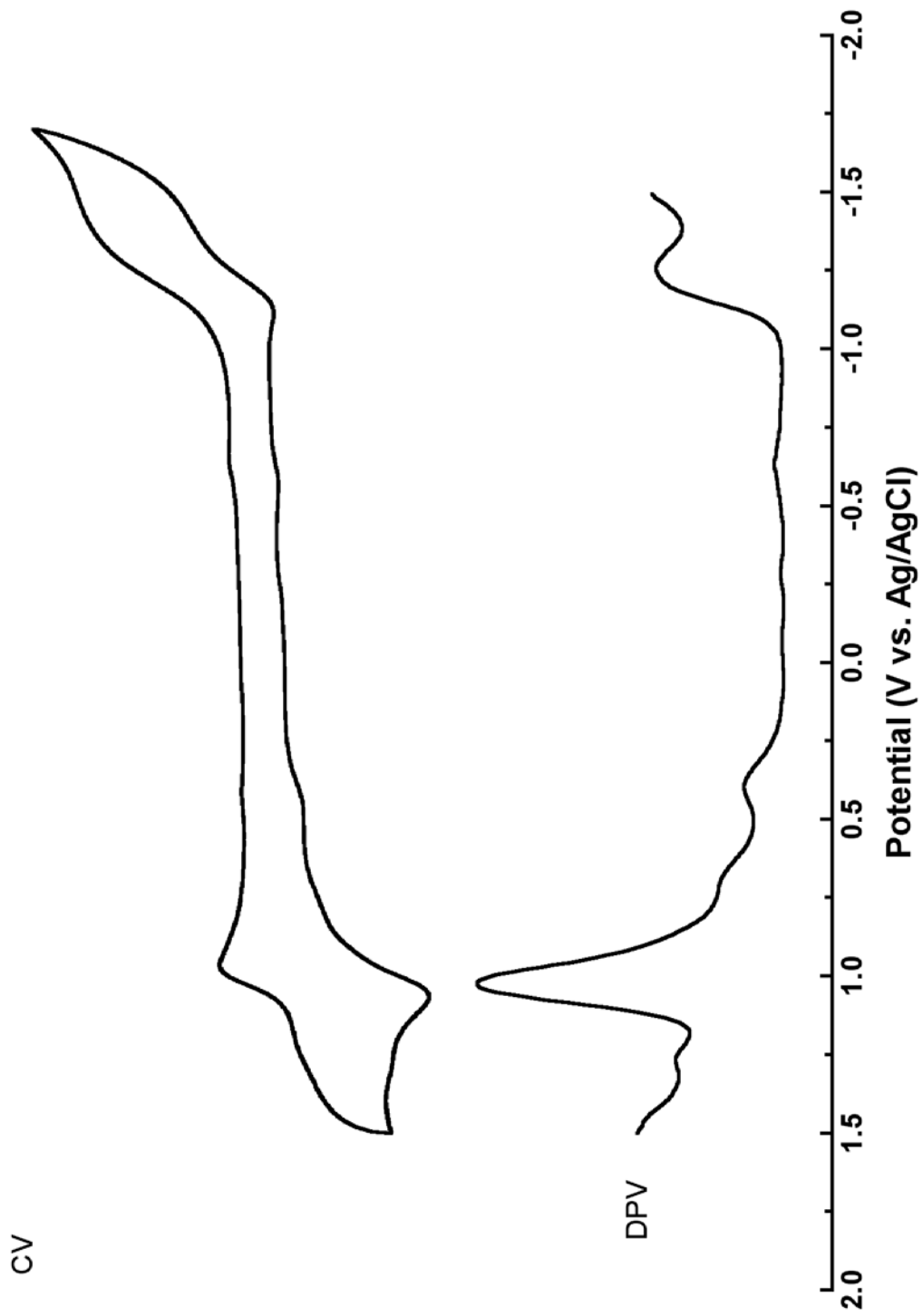
Electronic Absorption Spectrum & Molar Absorptivity (14, 375 – 1100 nm).



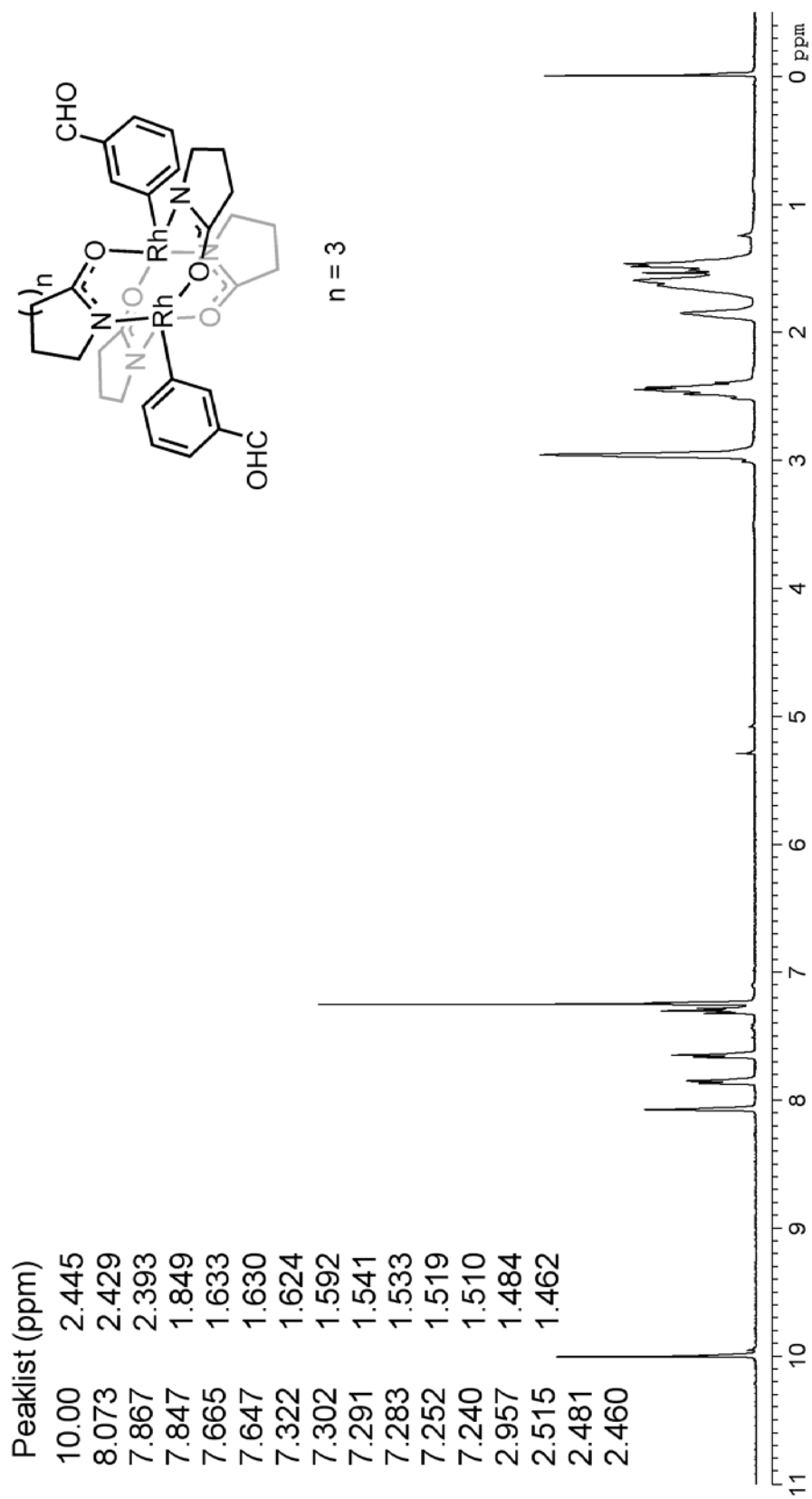
Vibrational Spectrum (**14**, 4000 – 600  $\text{cm}^{-1}$ ).



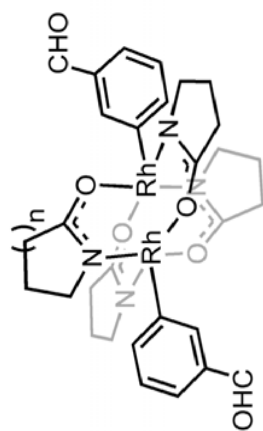
Voltammetry-(14).



<sup>1</sup>H NMR Spectrum (15).



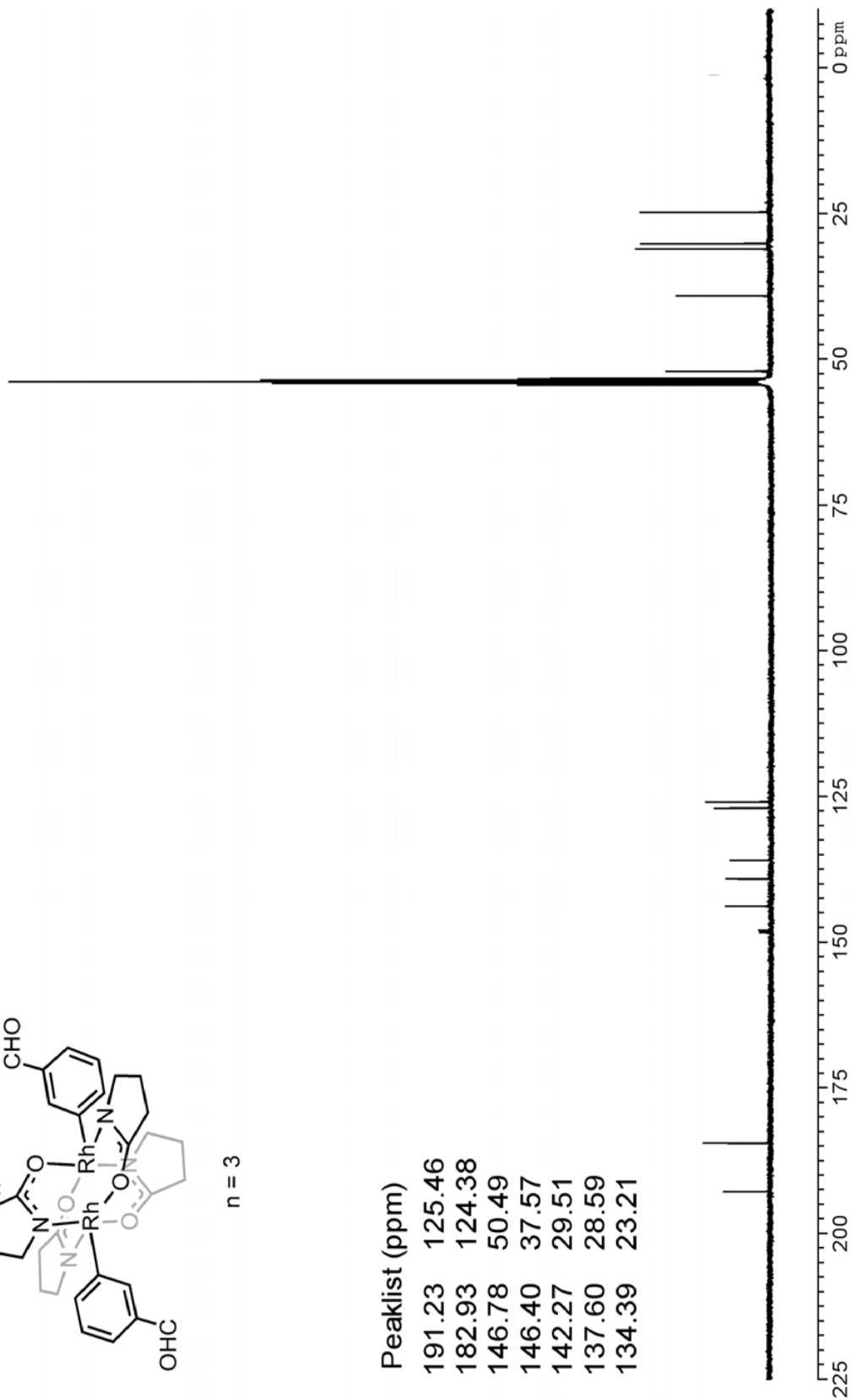
<sup>13</sup>C NMR Spectrum (15).



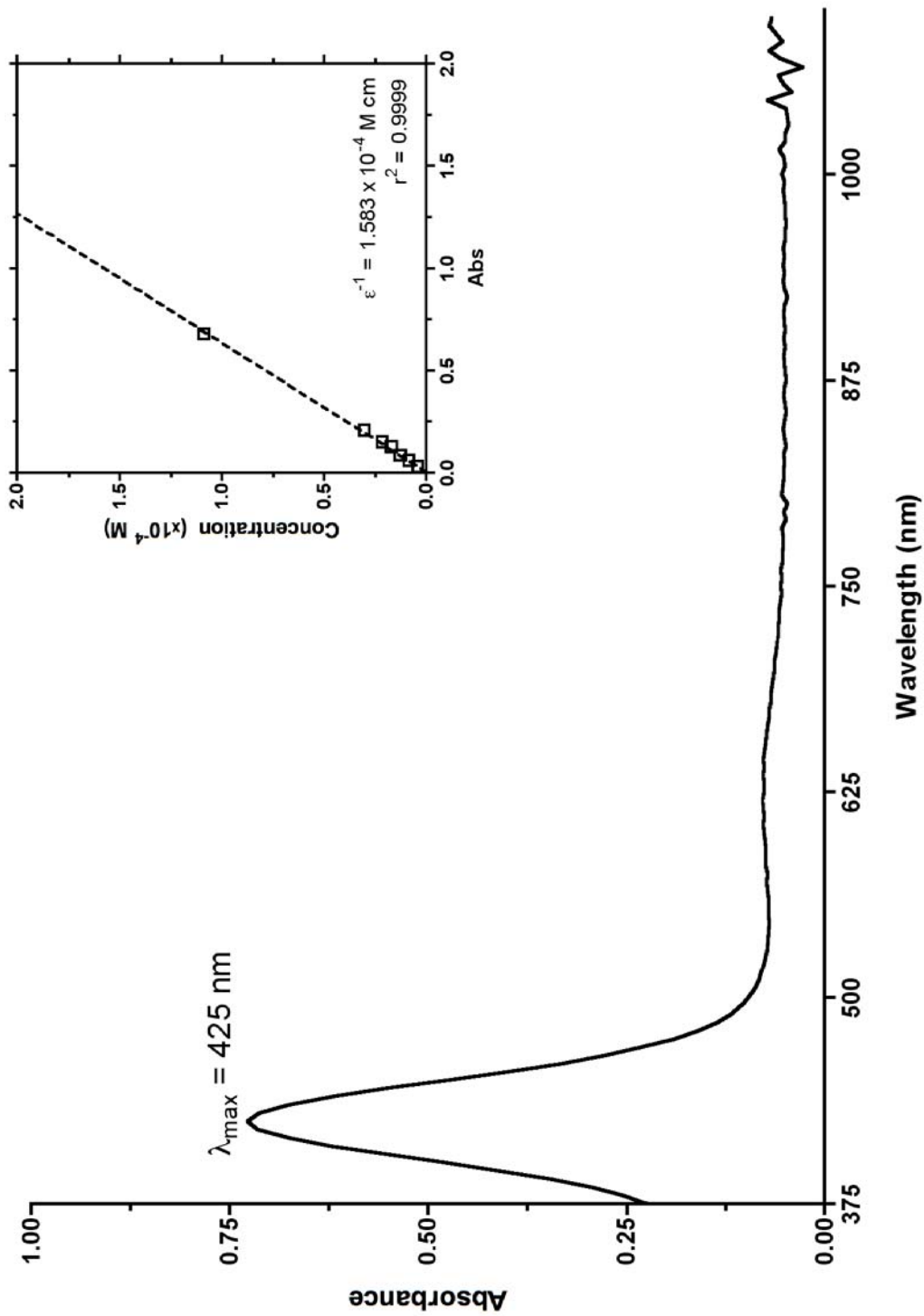
$n = 3$

Peaklist (ppm)
191.23
182.93
146.78
146.40
142.27
137.60
134.39
125.46
124.38
50.49
37.57
29.51
28.59
23.21

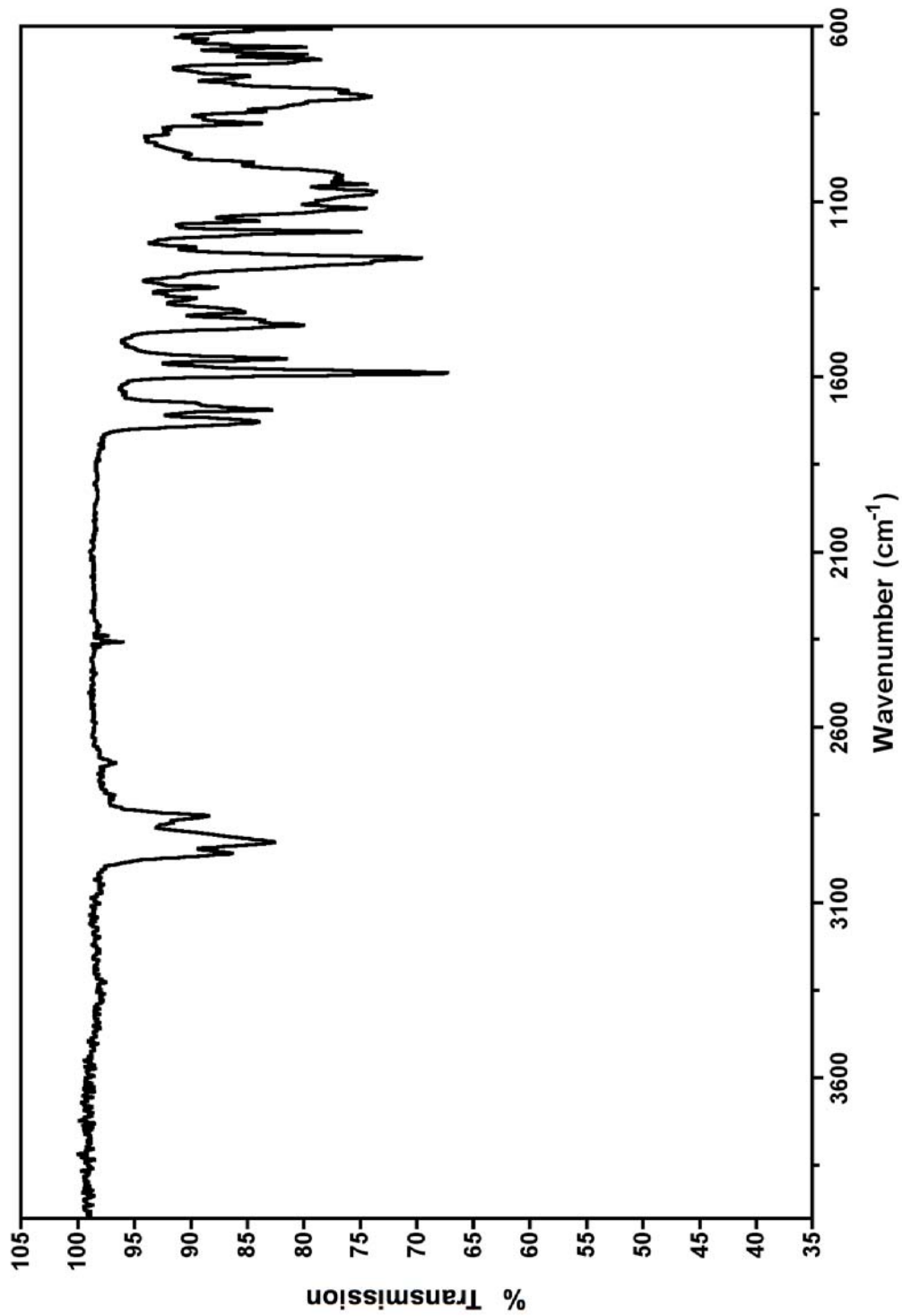
158



Electronic Absorption Spectrum & Molar Absorptivity (15, 375 – 1100 nm).

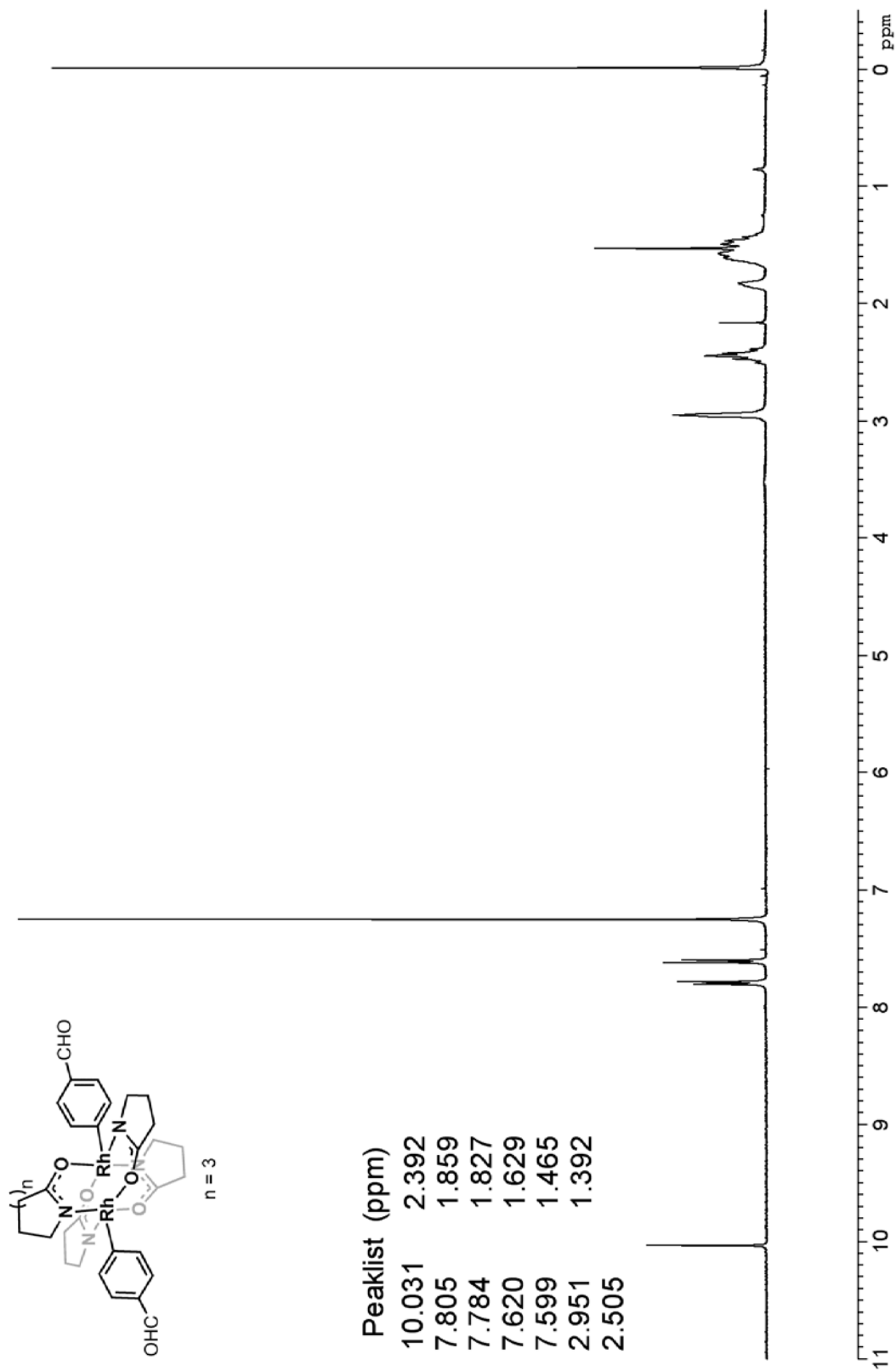


Vibrational Spectrum (15, 4000 – 600  $\text{cm}^{-1}$ ).

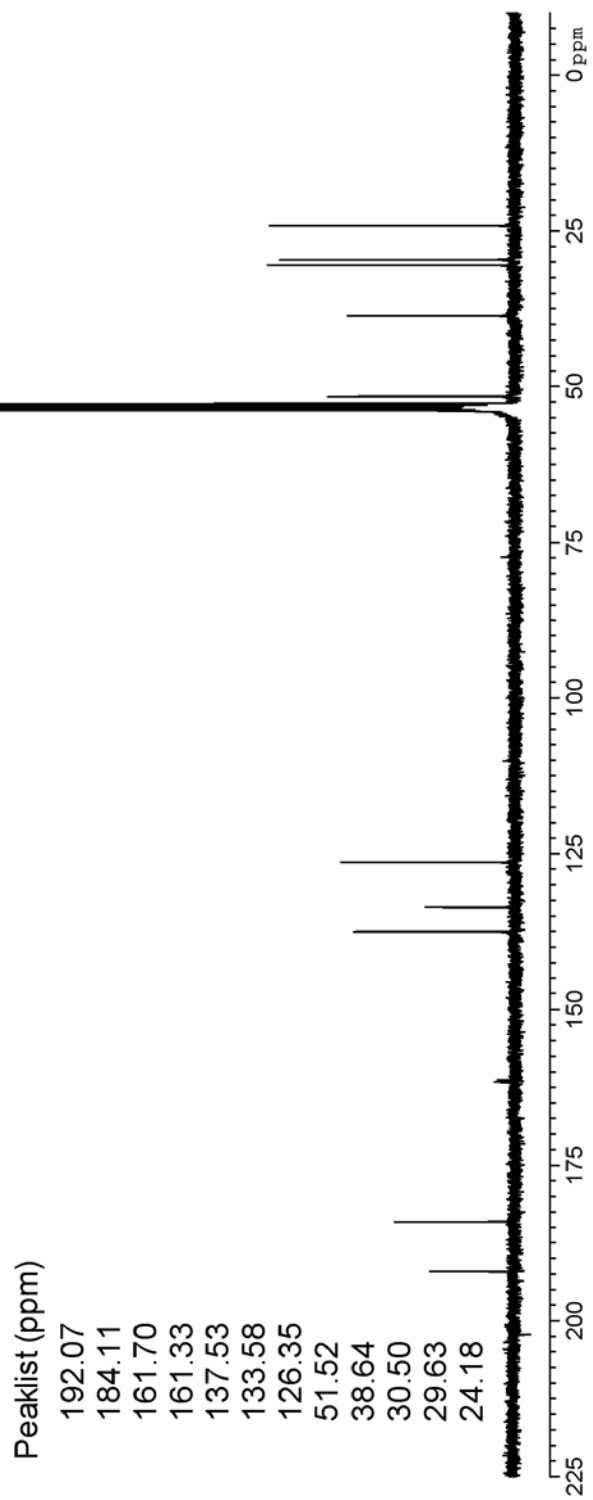
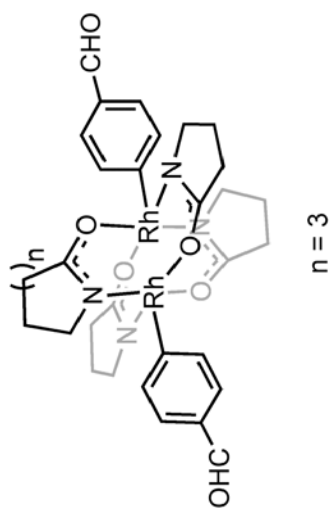




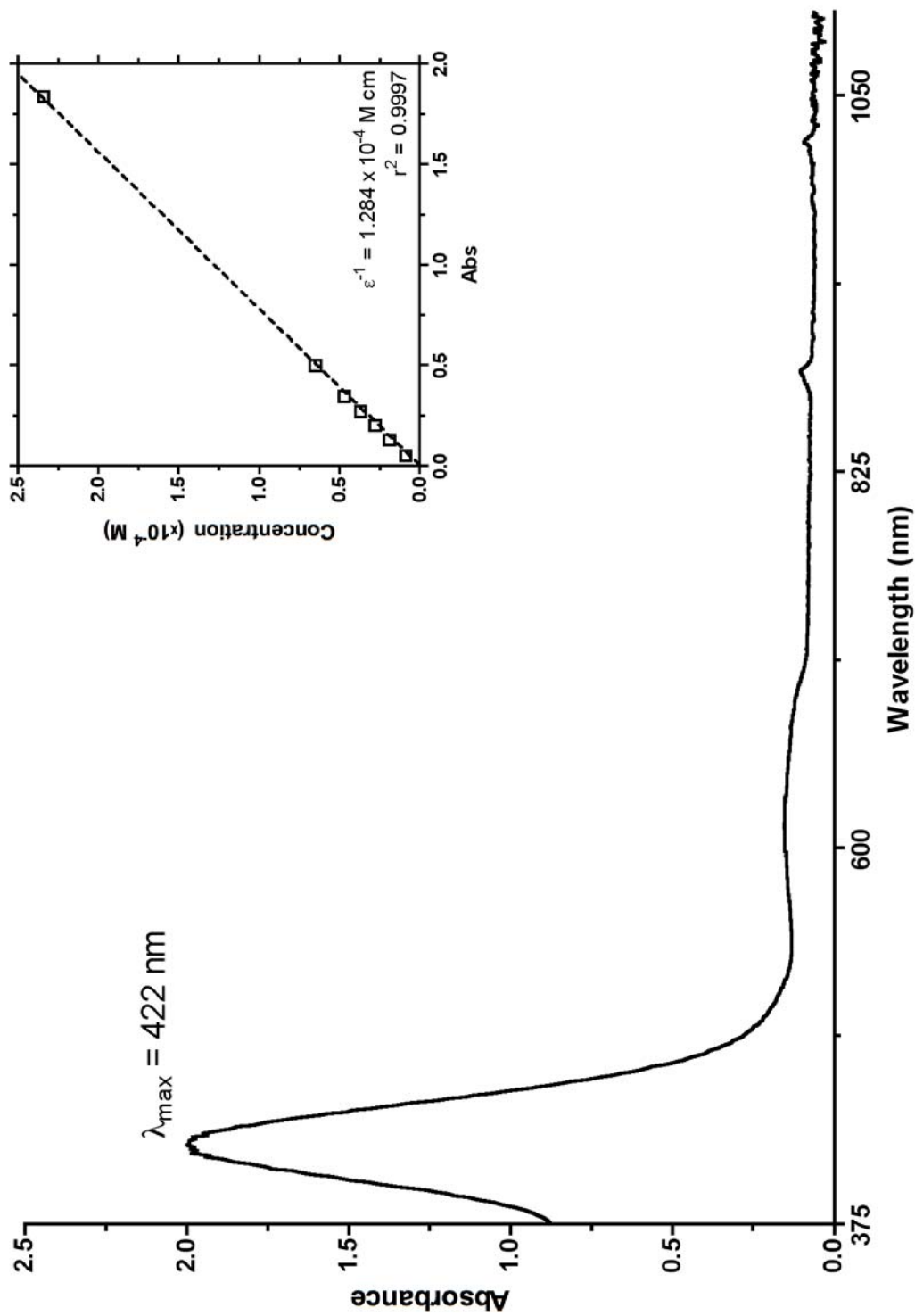
<sup>1</sup>H NMR Spectrum (**16**).



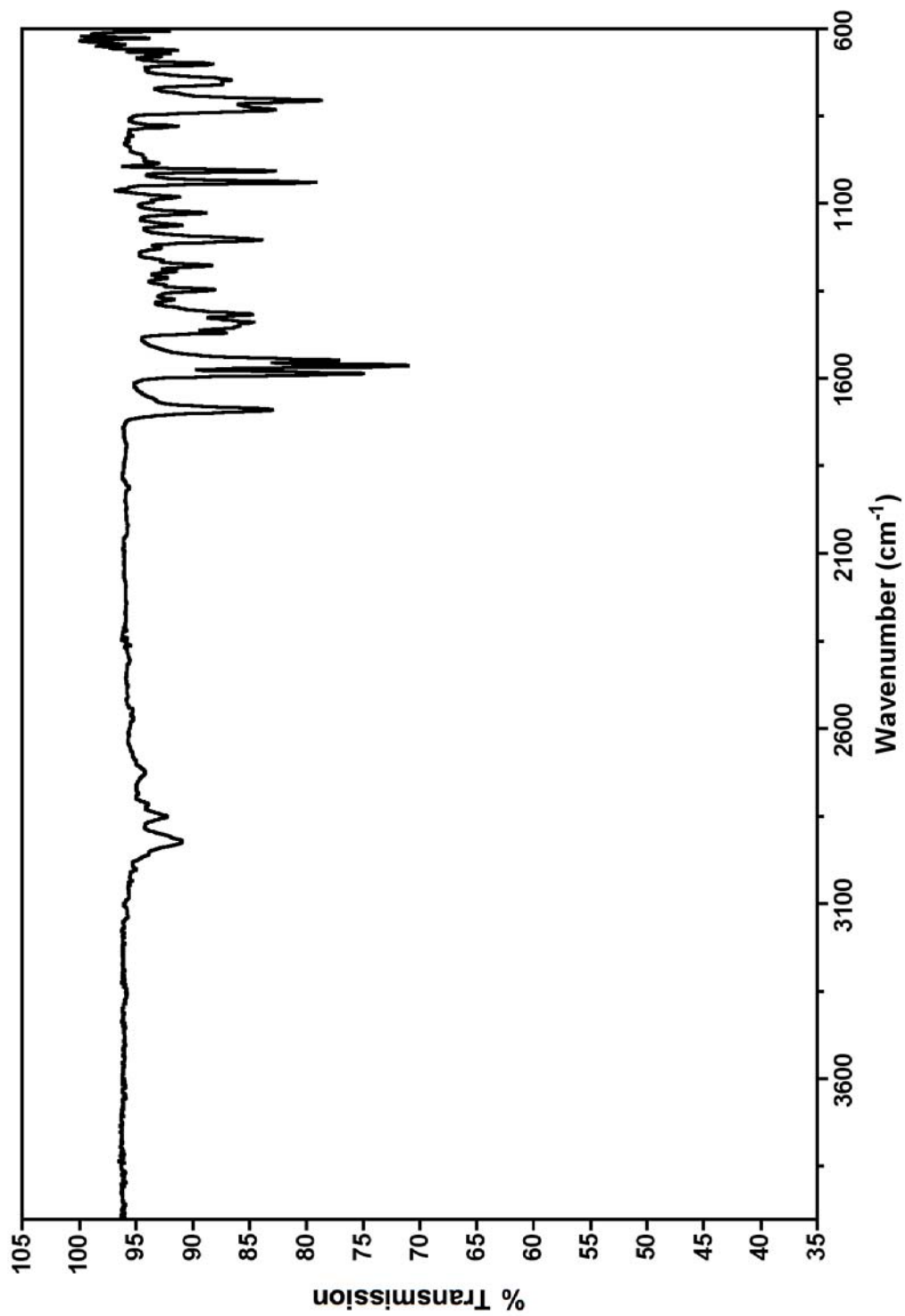
<sup>13</sup>C NMR Spectrum (**16**).



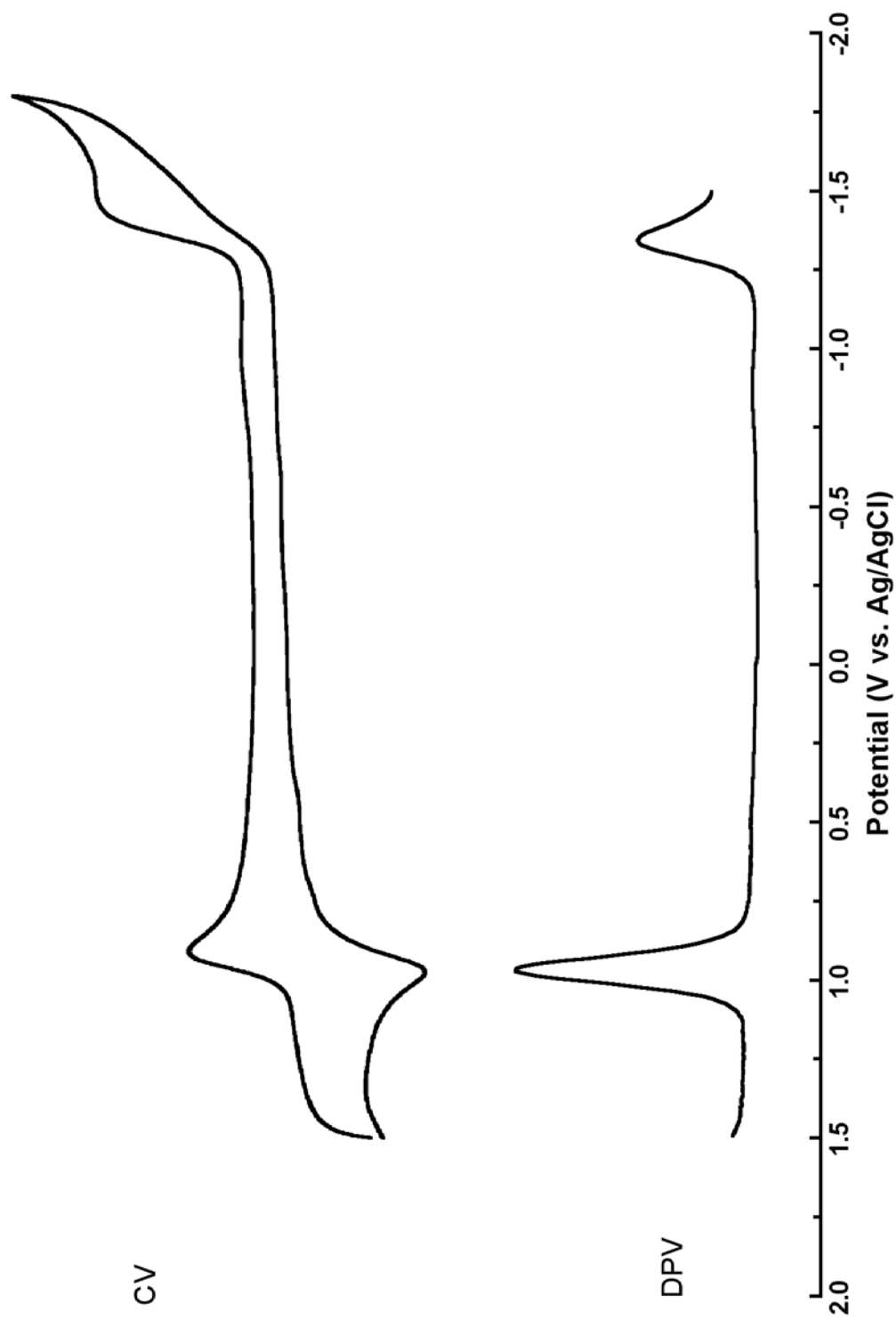
Electronic Absorption Spectrum & Molar Absorptivity (16, 375 – 1100 nm)



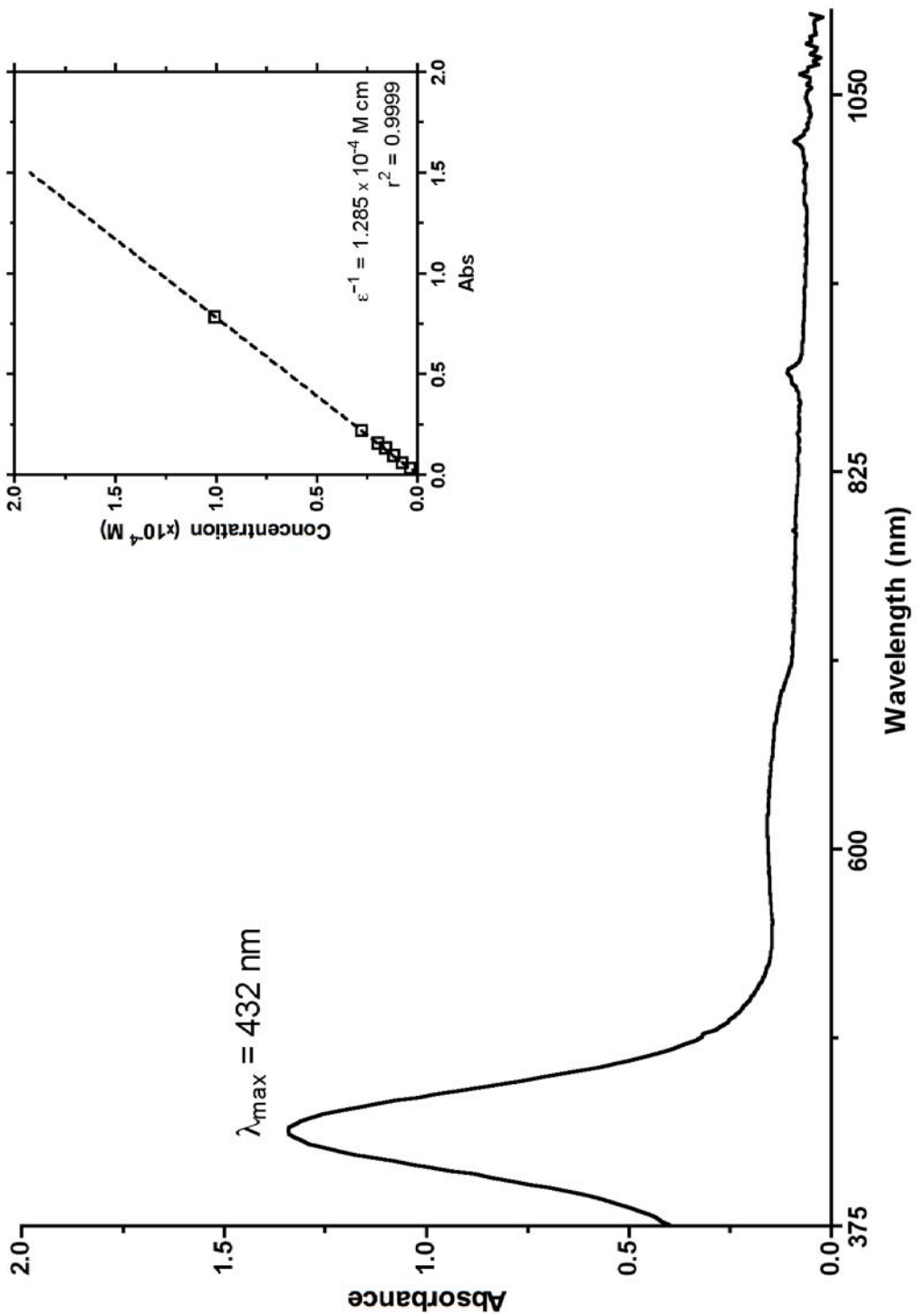
Vibrational Spectrum (**16**, 4000 – 600  $\text{cm}^{-1}$ ).



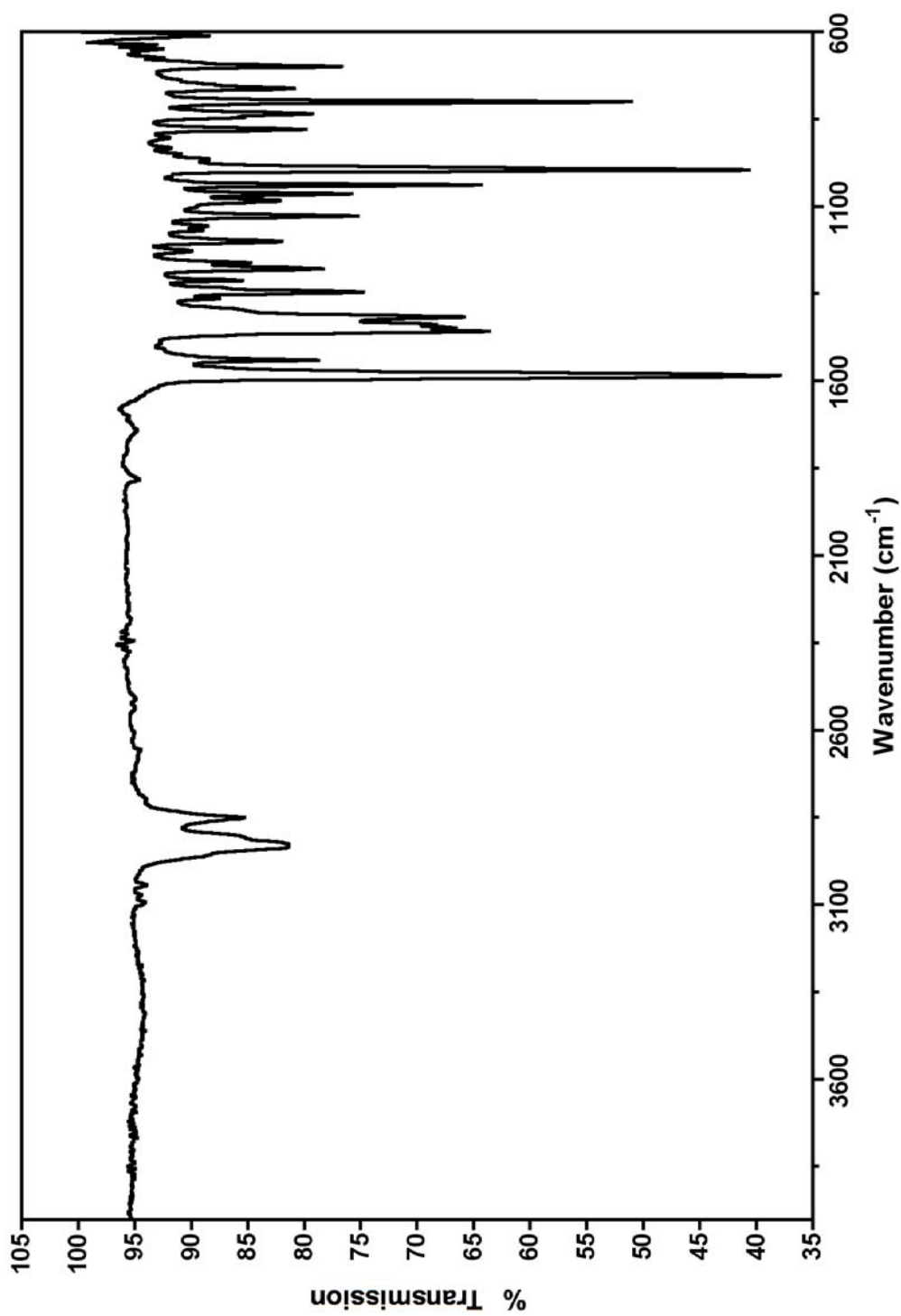
Voltammetry (16).



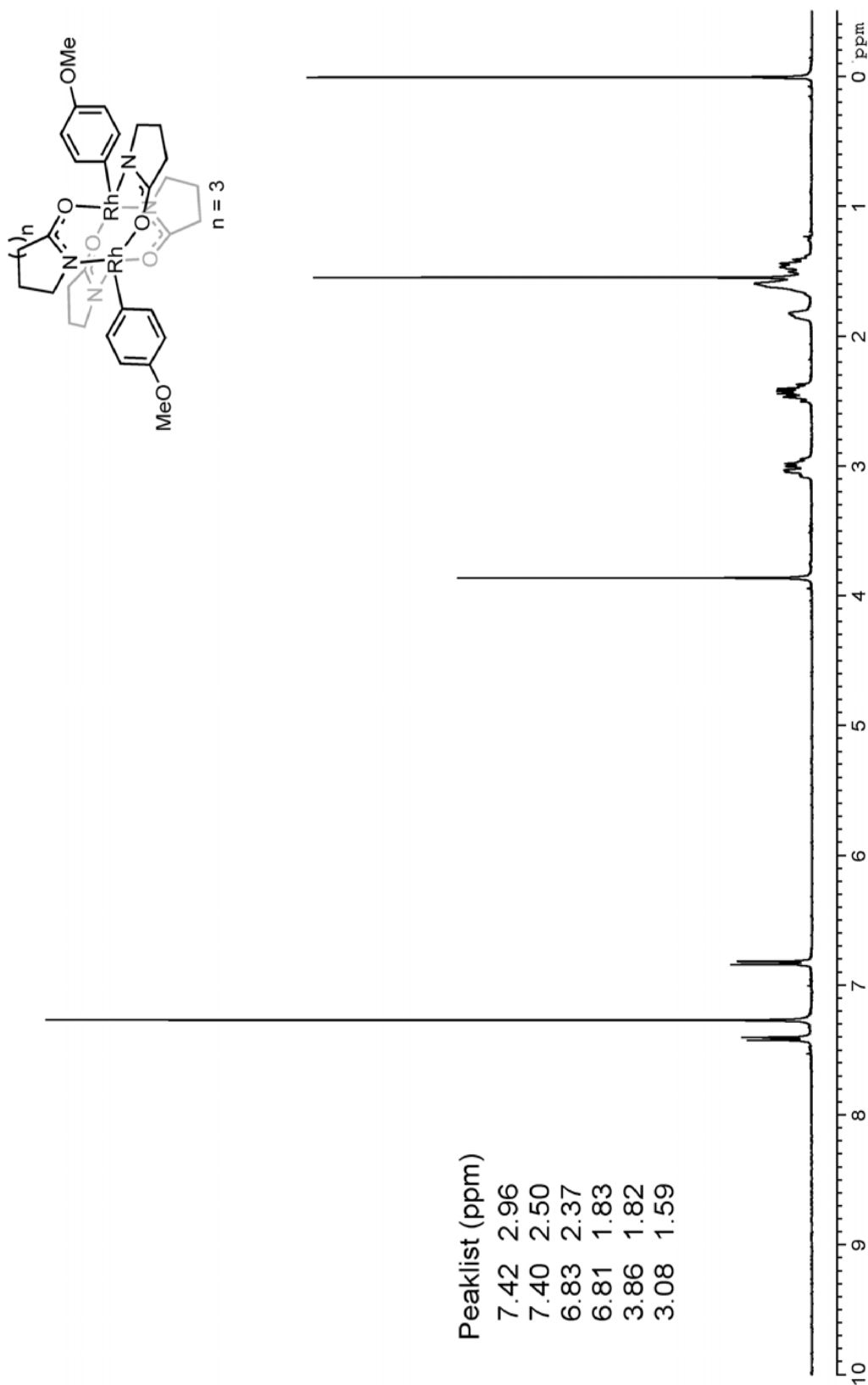
Electronic Absorption Spectrum & Molar Absorptivity (17, 375 – 1100 nm).



Vibrational Spectrum (17). 4000 – 600  $\text{cm}^{-1}$ ).

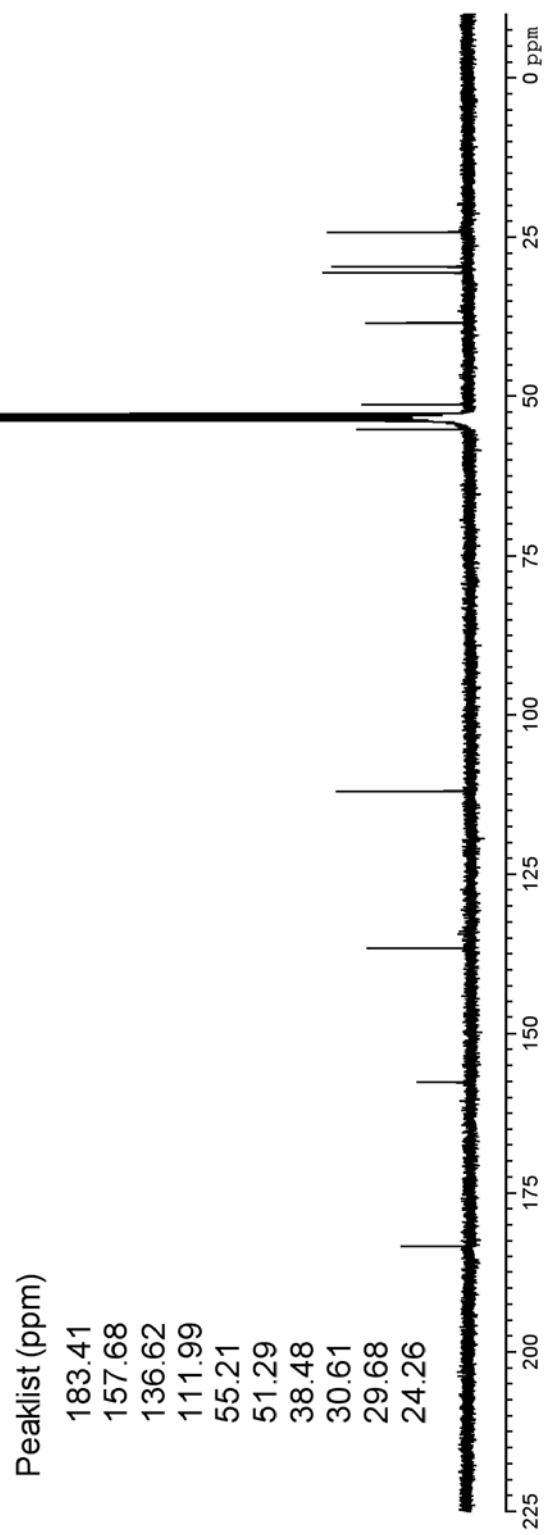
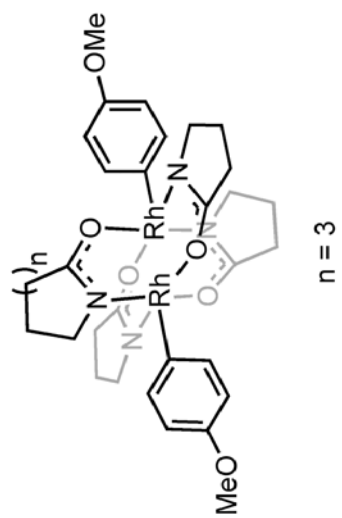


<sup>1</sup>H NMR Spectrum (**18**).

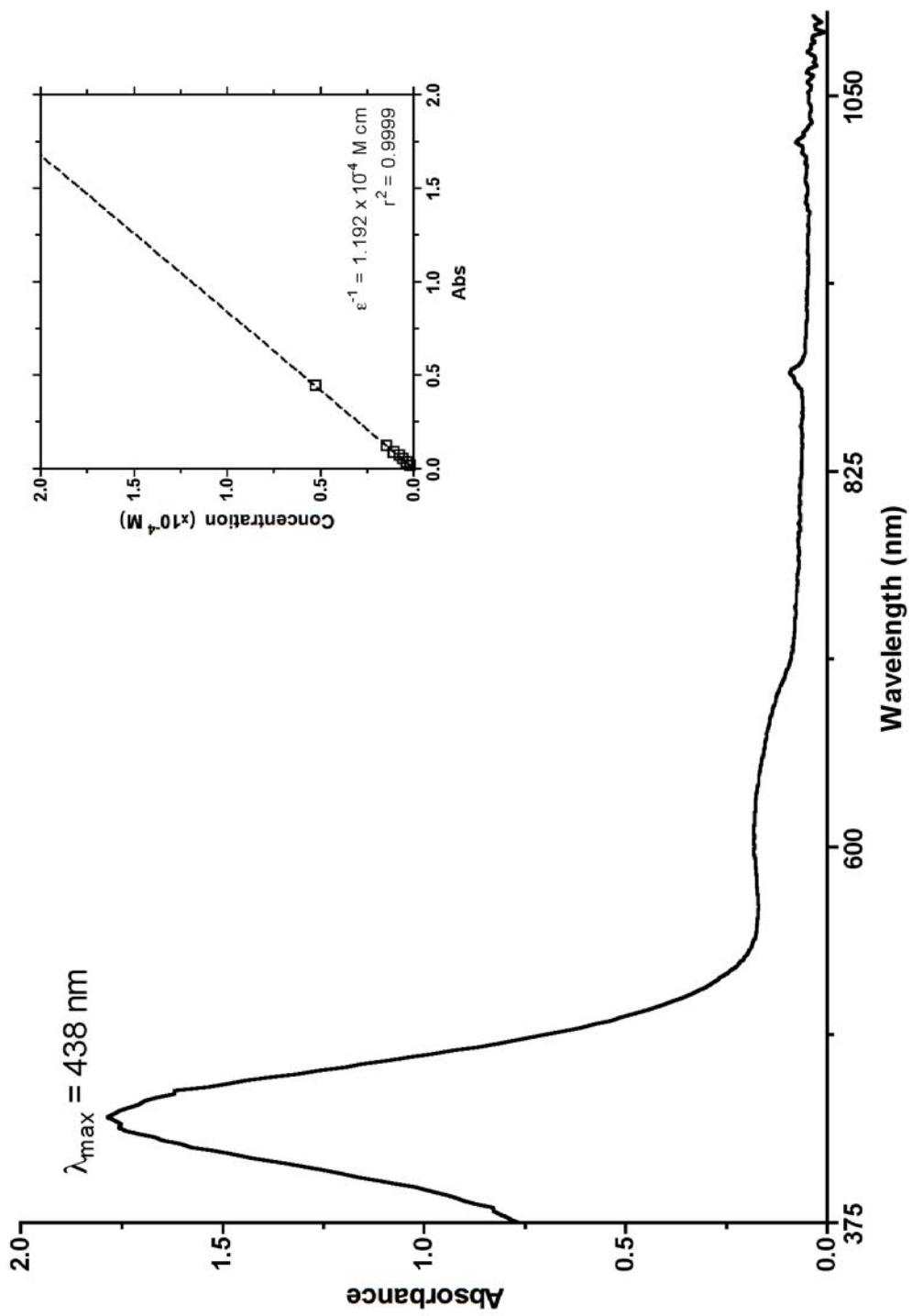




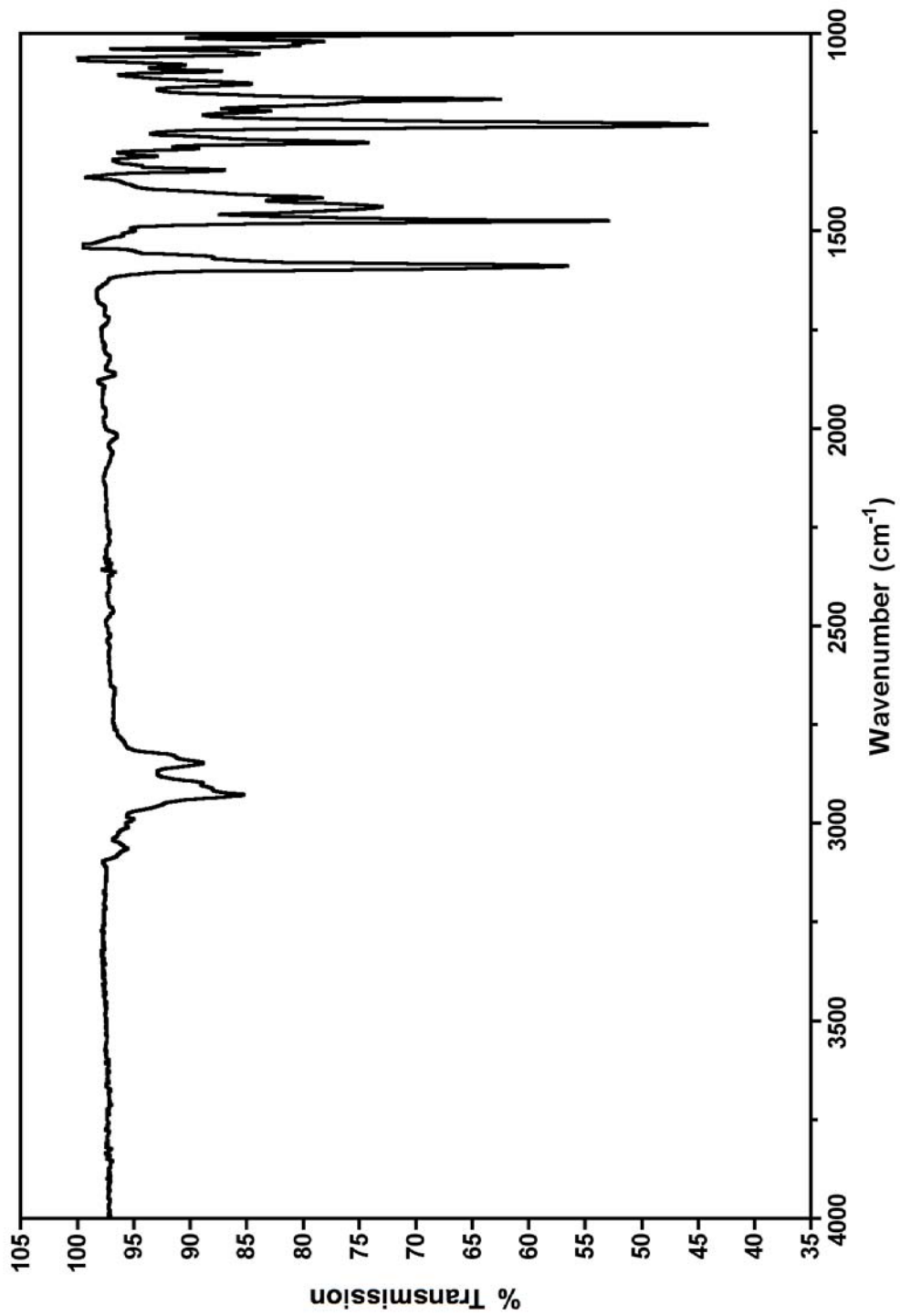
<sup>13</sup>C NMR Spectrum (**18**).



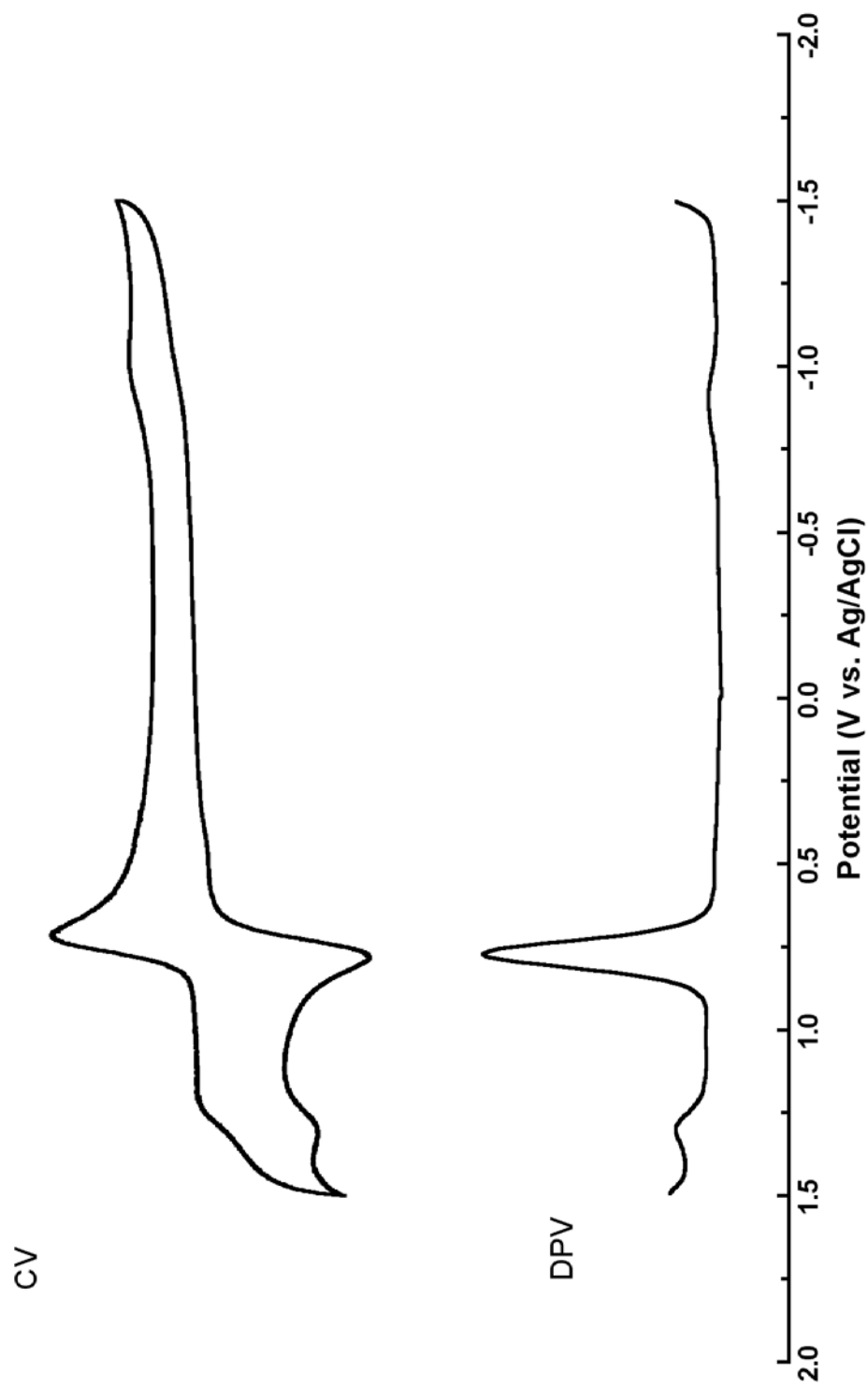
Electronic Absorption Spectrum & Molar Absorptivity (**18**, 375 – 1100 nm).



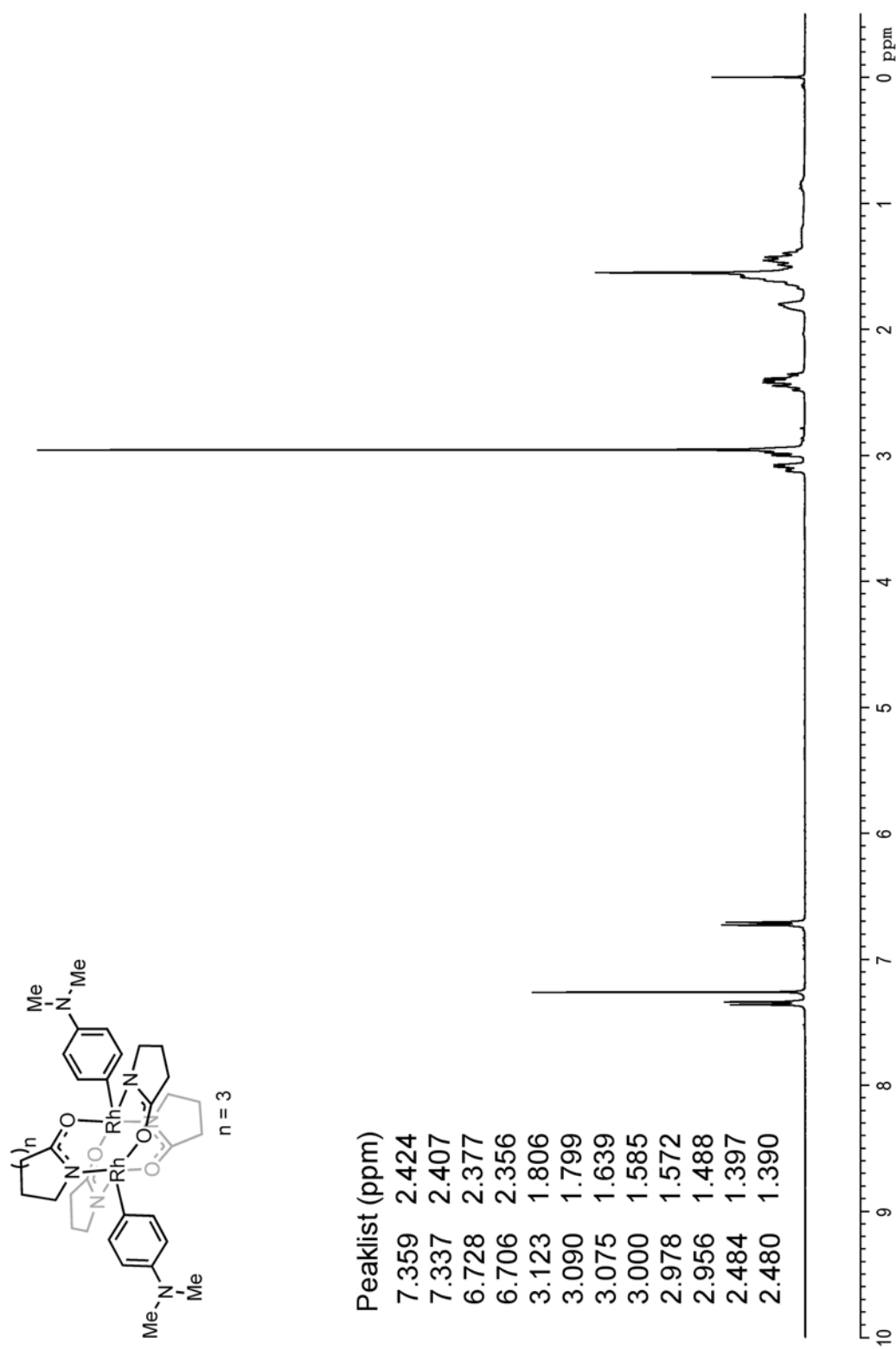
Vibrational Spectrum (**18**, 4000 – 1000  $\text{cm}^{-1}$ ).



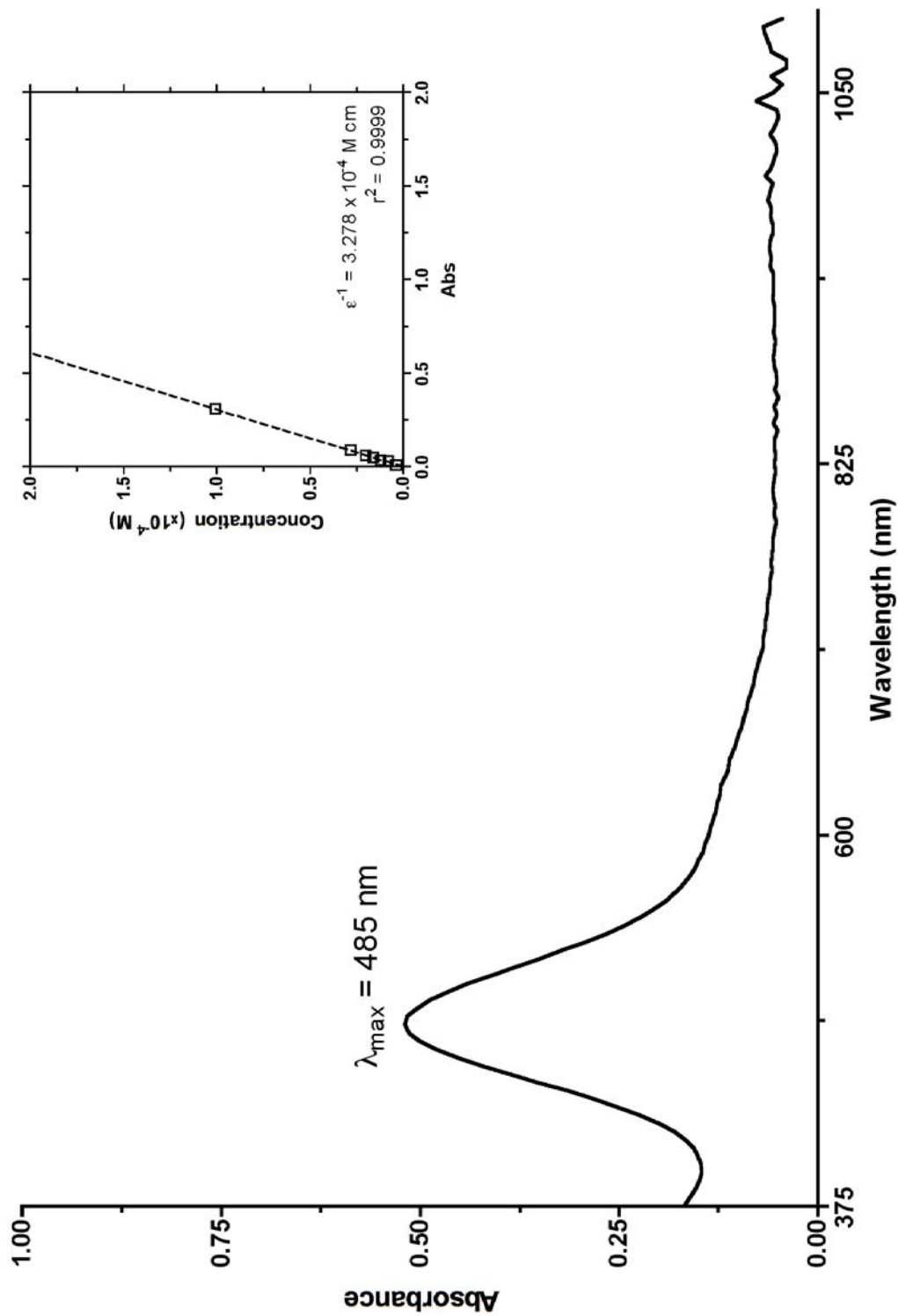
Voltammetry (18).



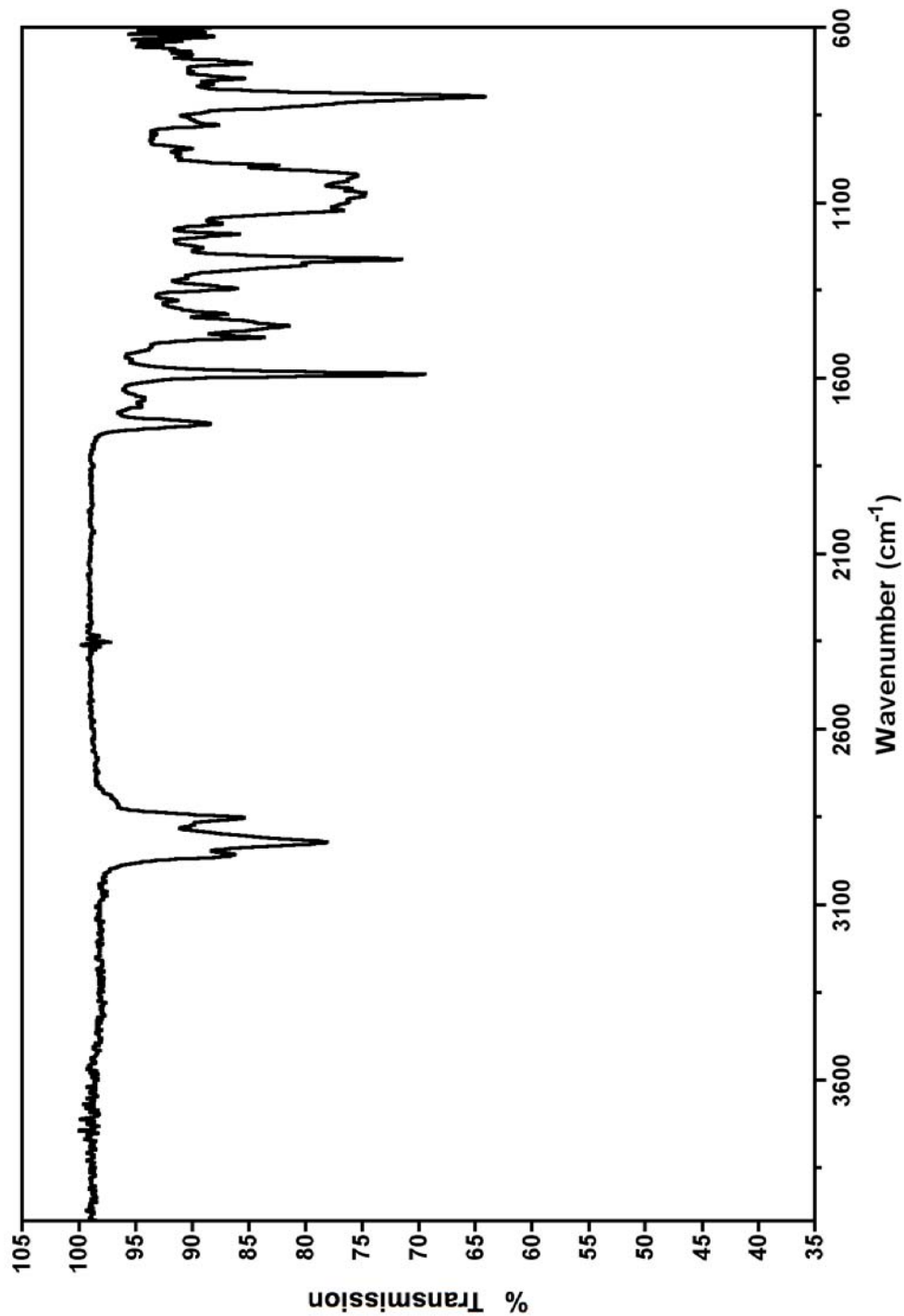
<sup>1</sup>H NMR Spectrum (**19**).



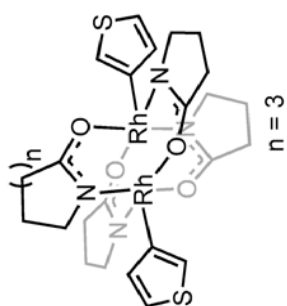
Electronic Absorption Spectrum & Molar Absorptivity (19, 375 – 1100 nm),



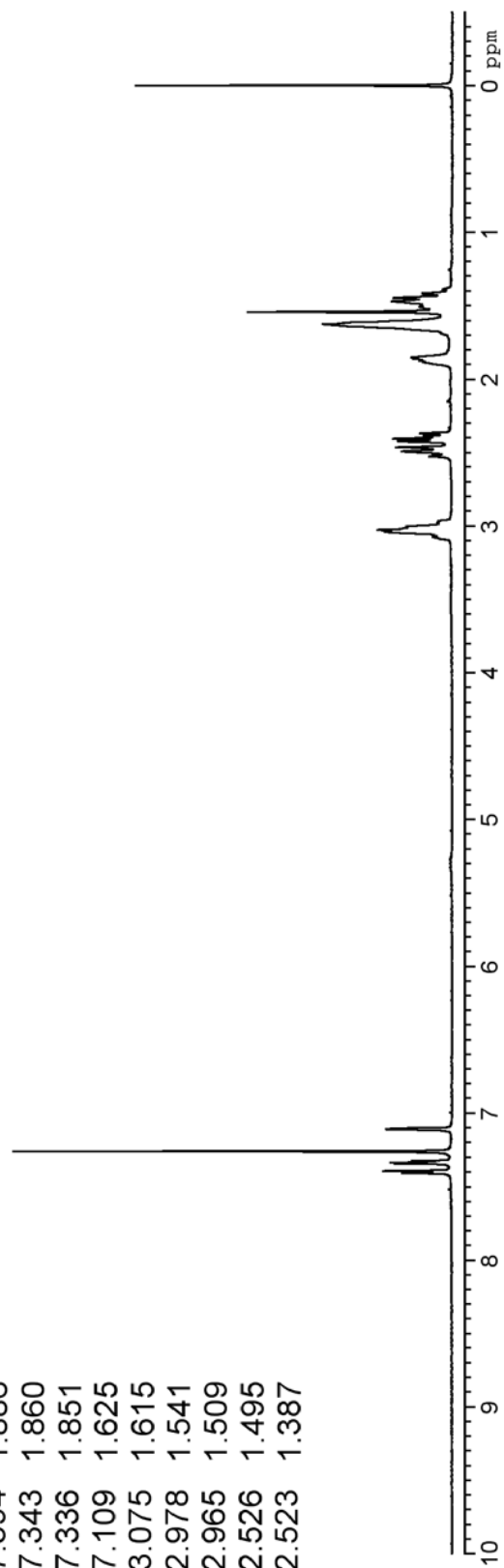
Vibrational Spectrum (19, 4000 – 600  $\text{cm}^{-1}$ )



<sup>1</sup>H NMR Spectrum (**20**).

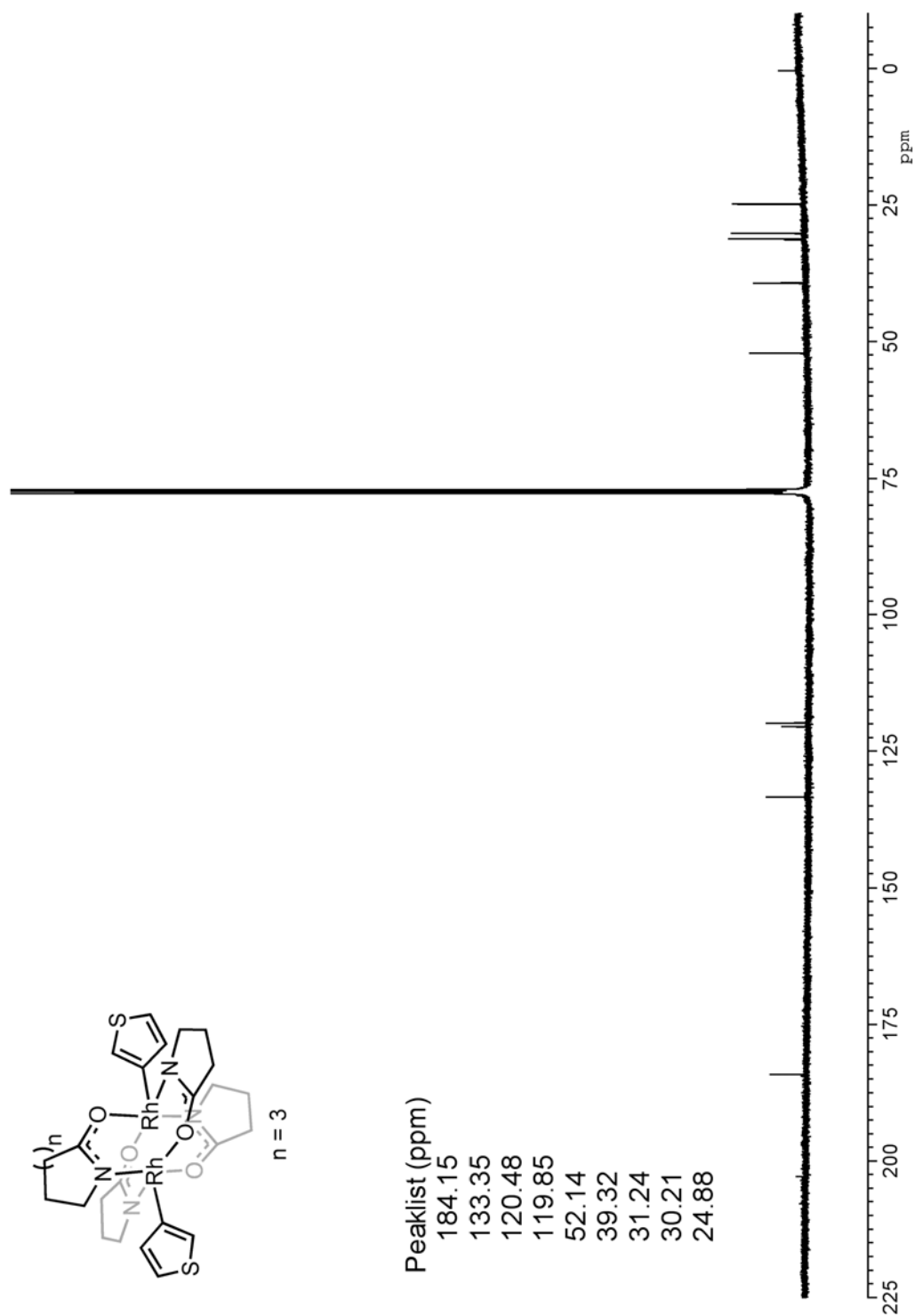


Peaklist (ppm)
7.401
2.369
7.394
1.886
7.343
1.860
7.336
1.851
7.109
1.625
3.075
1.615
2.978
1.541
2.965
1.509
2.526
1.495
2.523
1.387

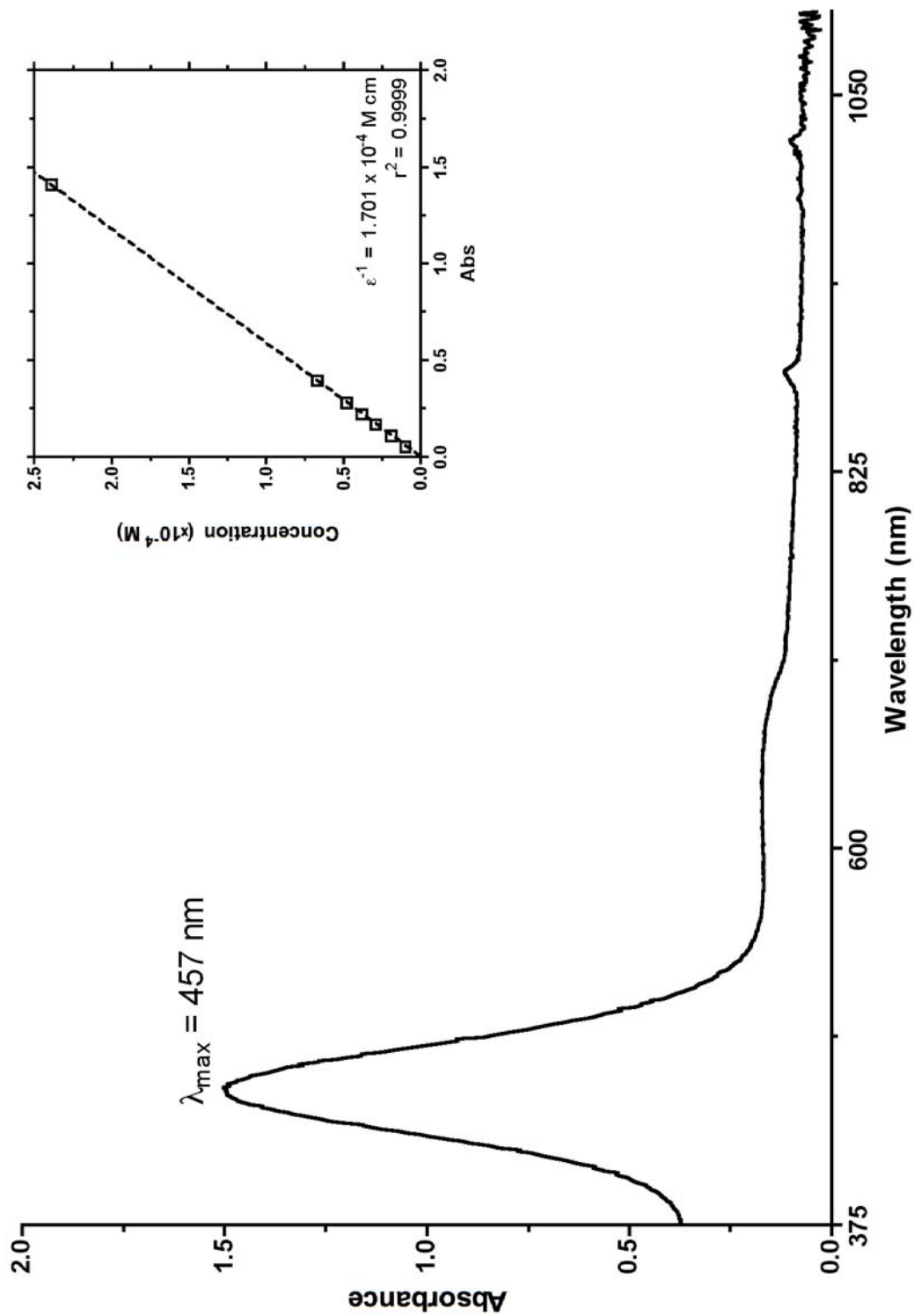




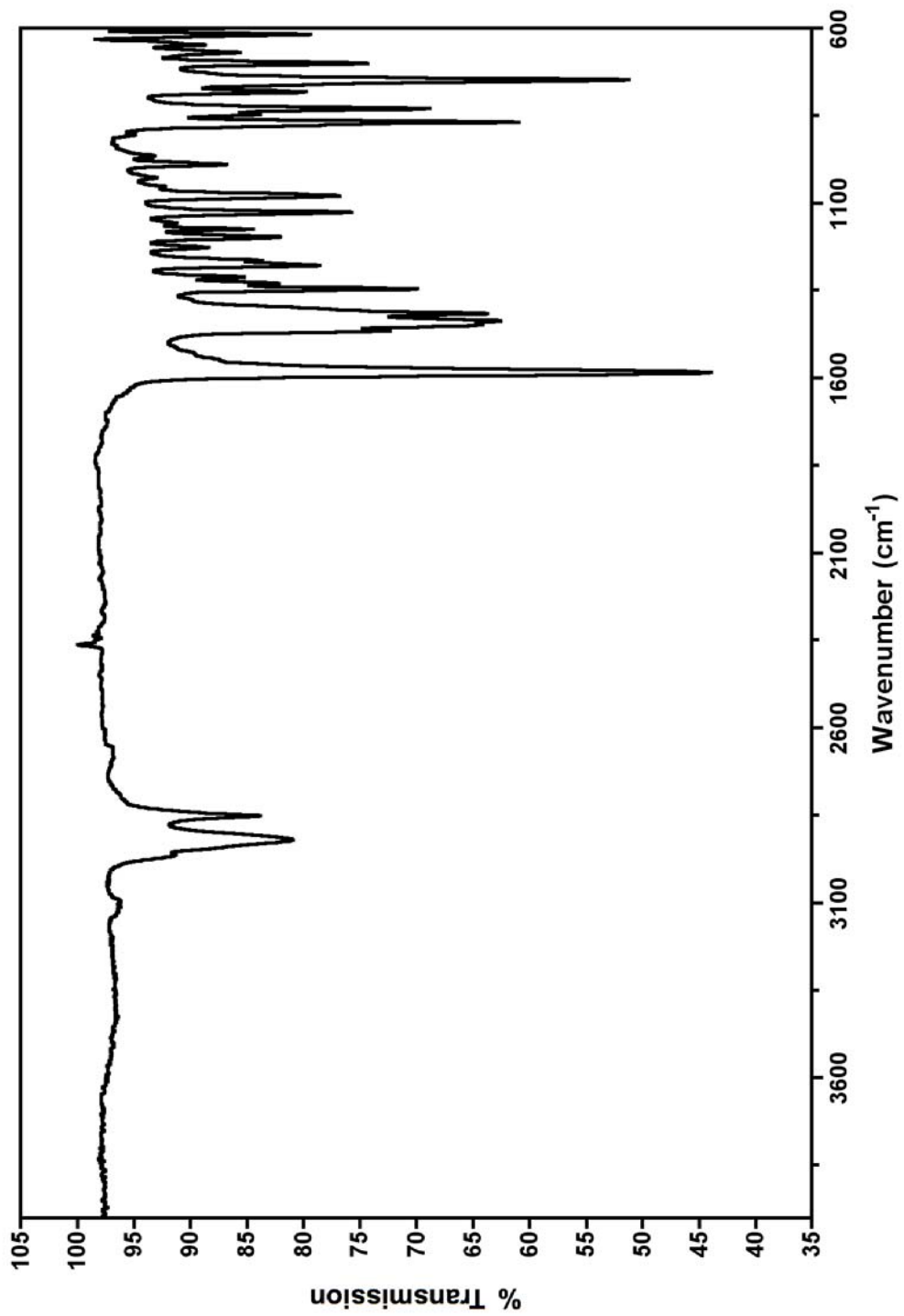
<sup>13</sup>C NMR Spectrum (**20**).



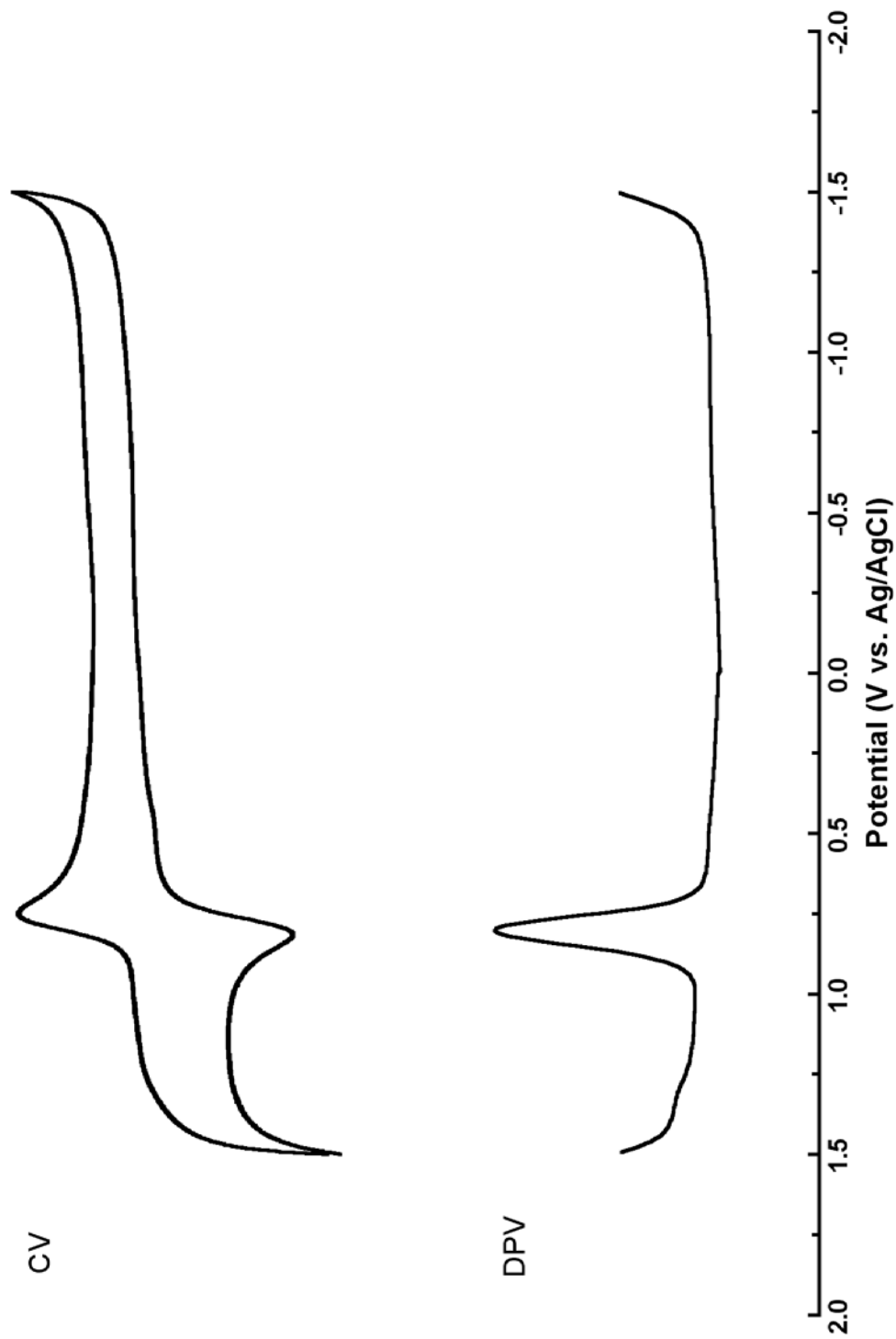
Electronic Absorption Spectrum & Molar Absorptivity (20, 375 – 1100 nm)



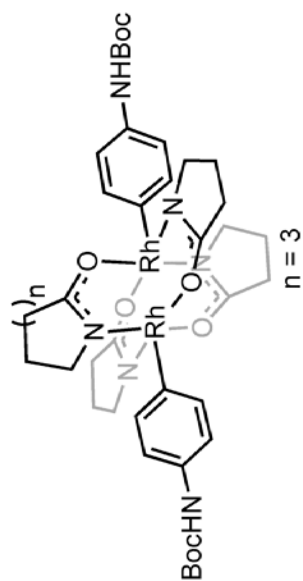
Vibrational Spectrum (**20**, 4000 – 600  $\text{cm}^{-1}$ ).



Voltammetry (20).

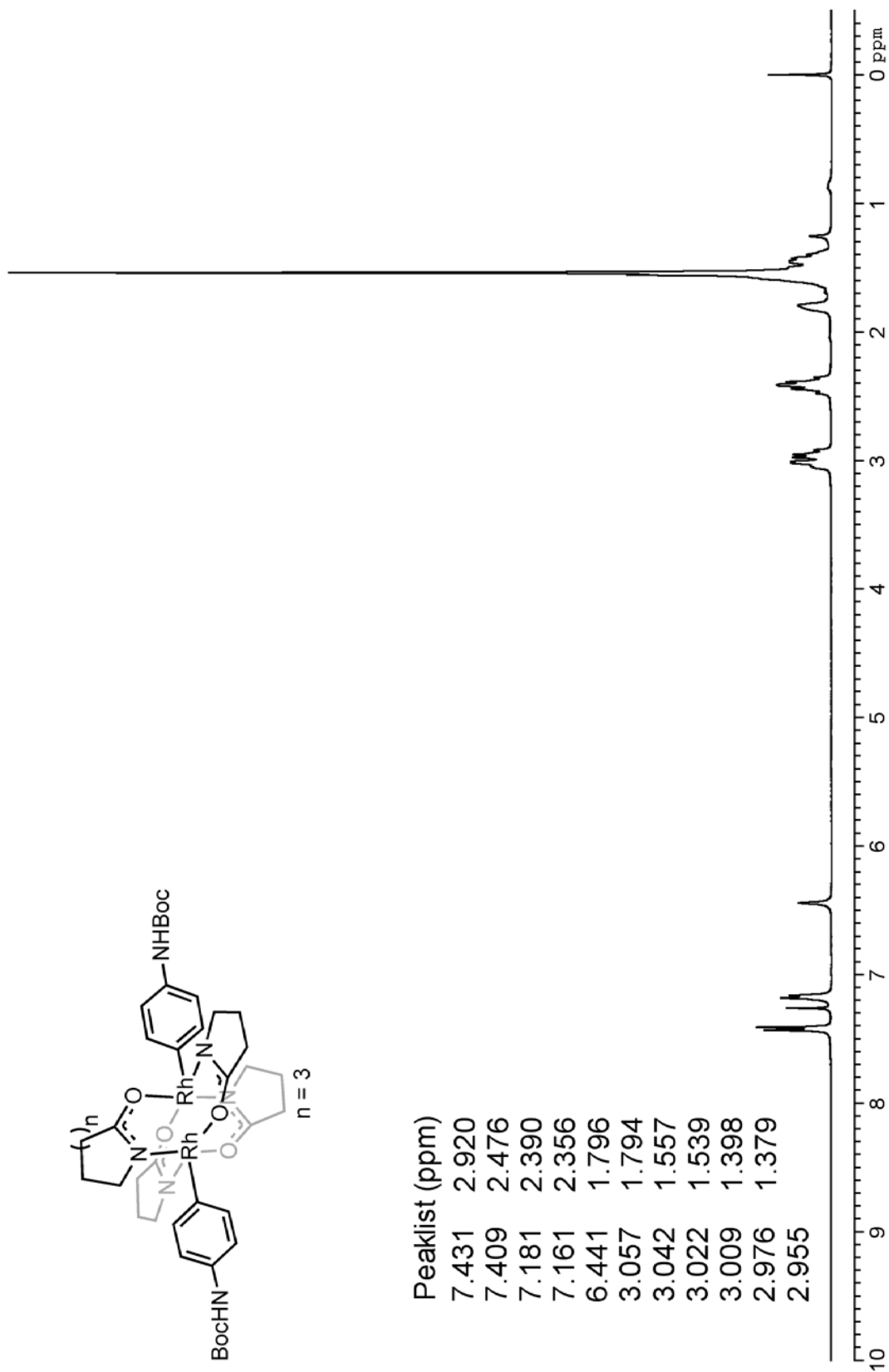


<sup>1</sup>H NMR Spectrum (**21**).

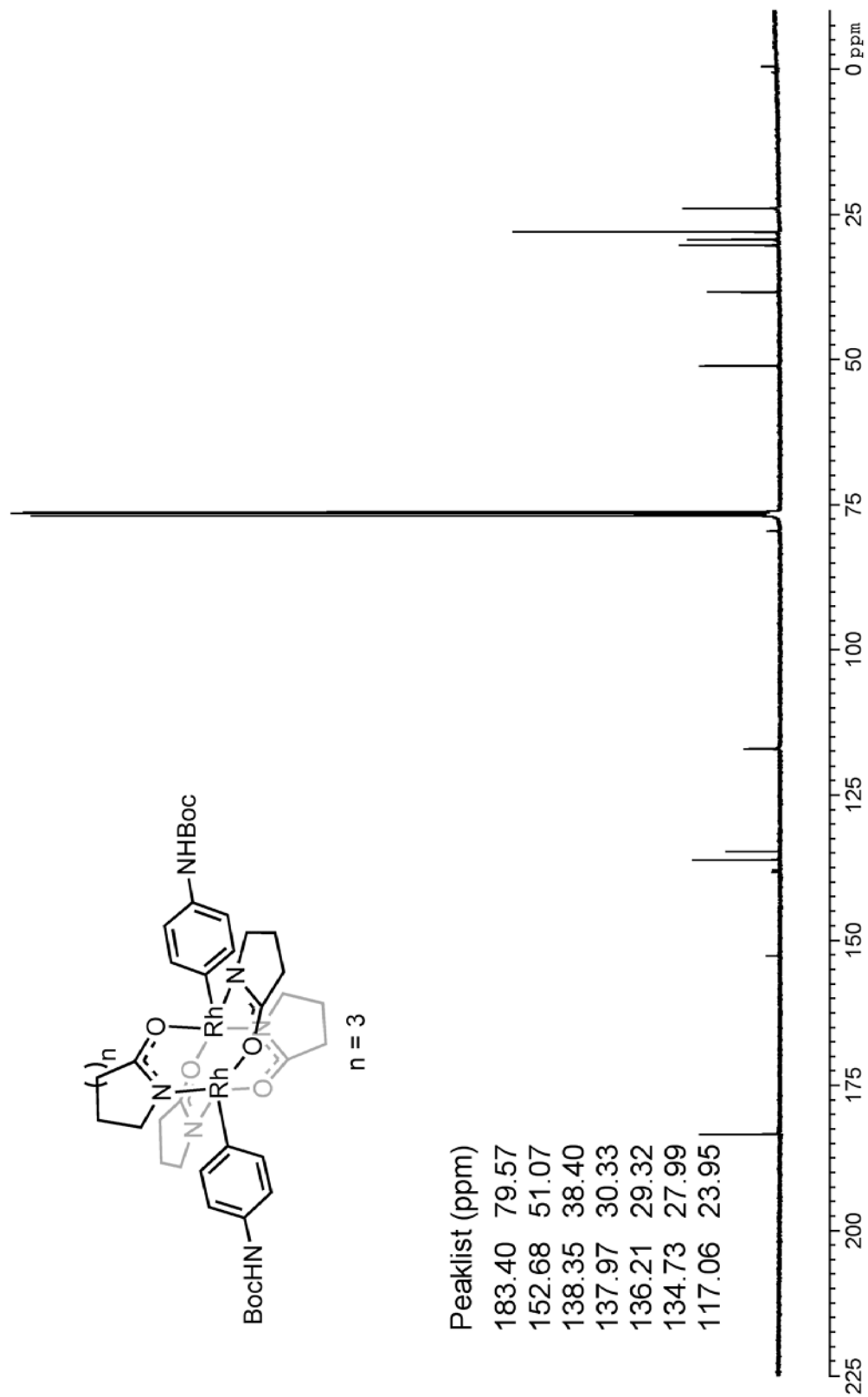


Peaklist (ppm)

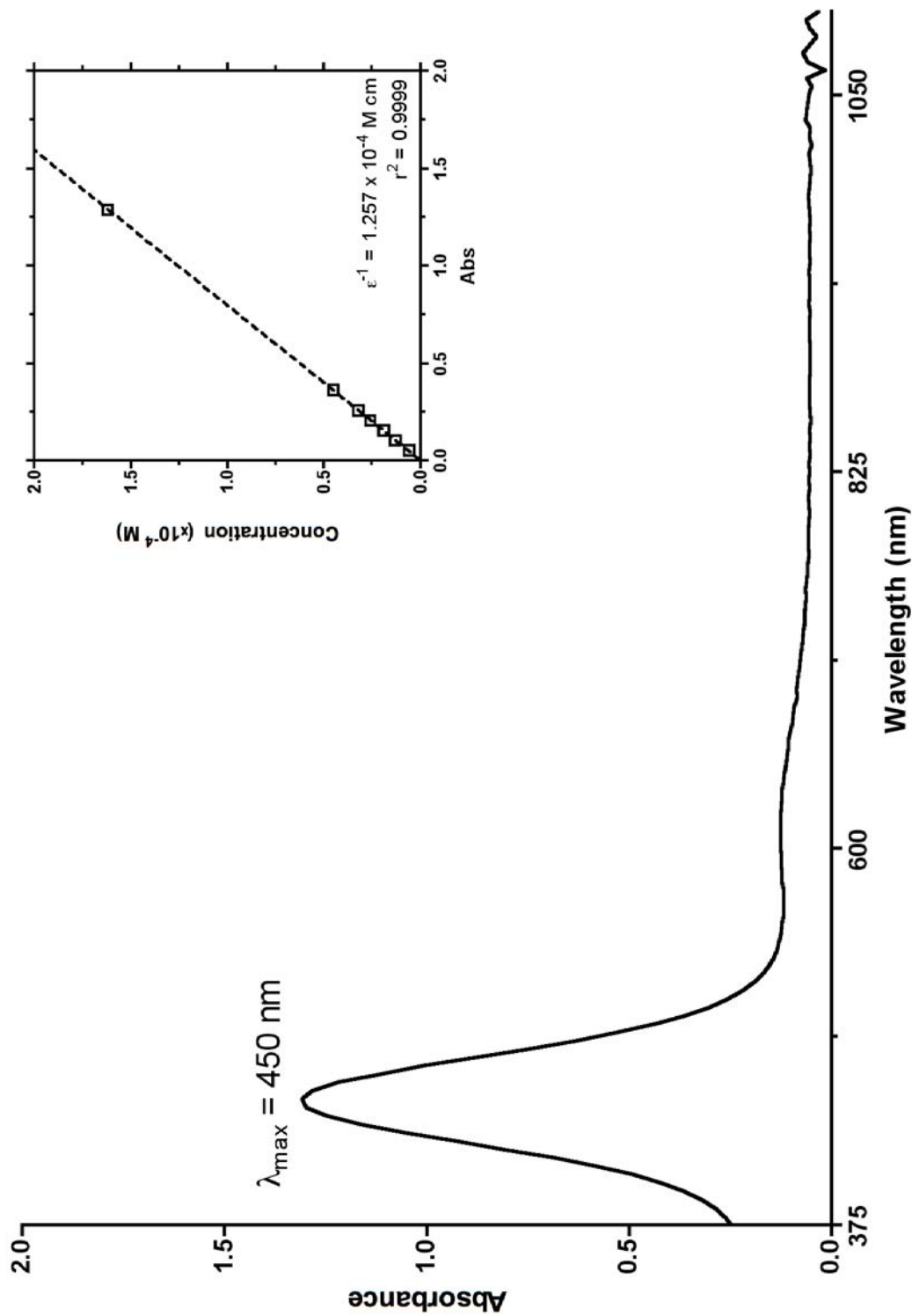
7.431	2.920
7.409	2.476
7.181	2.390
7.161	2.356
6.441	1.796
3.057	1.794
3.042	1.557
3.022	1.539
3.009	1.398
2.976	1.379
2.955	



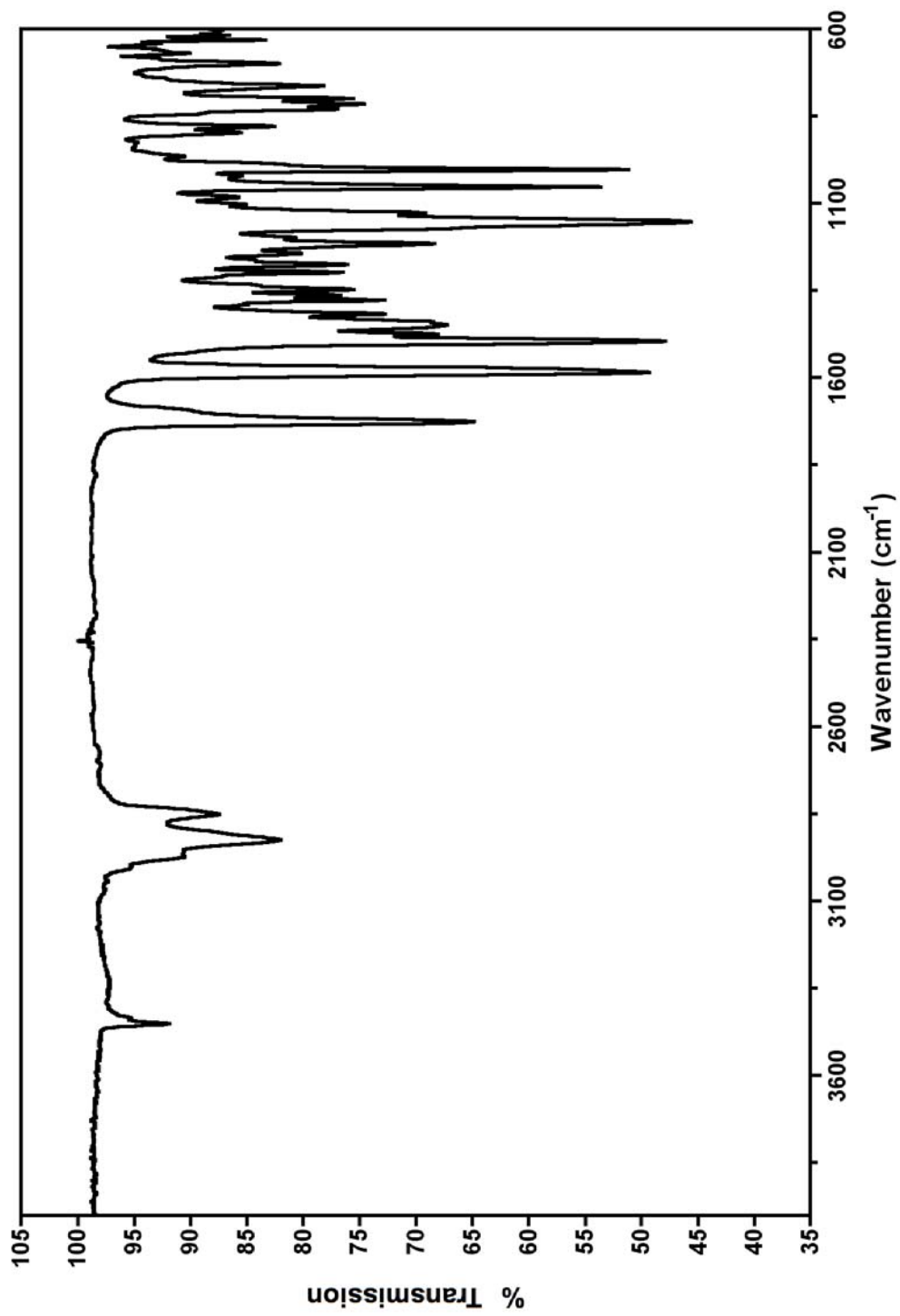
<sup>13</sup>C NMR Spectrum (21).



Electronic Absorption Spectrum & Molar Absorptivity (21, 375 – 1100 nm).

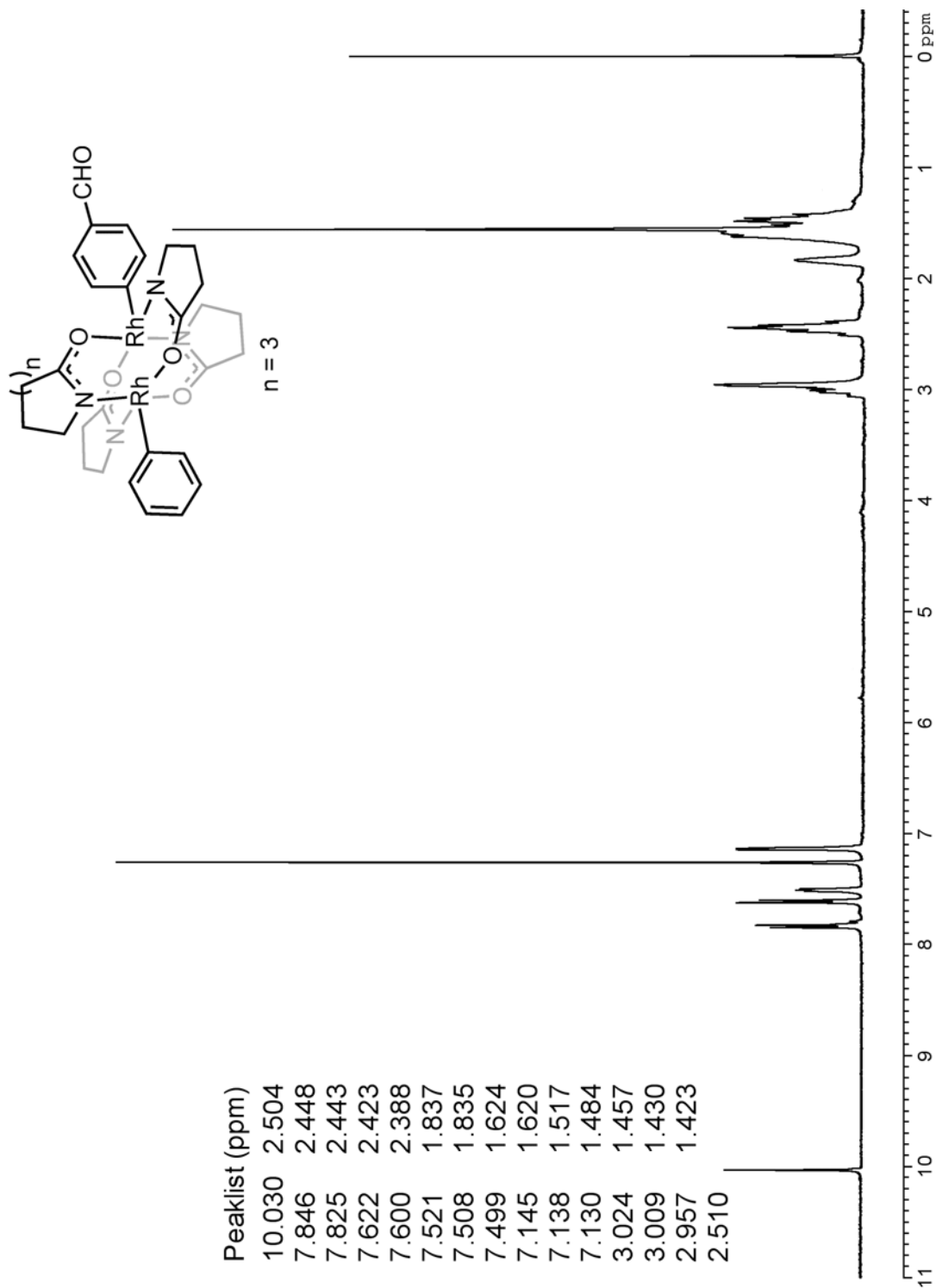


Vibrational Spectrum (21, 4000 – 600  $\text{cm}^{-1}$ ).

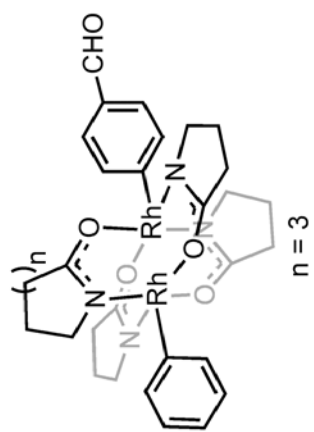




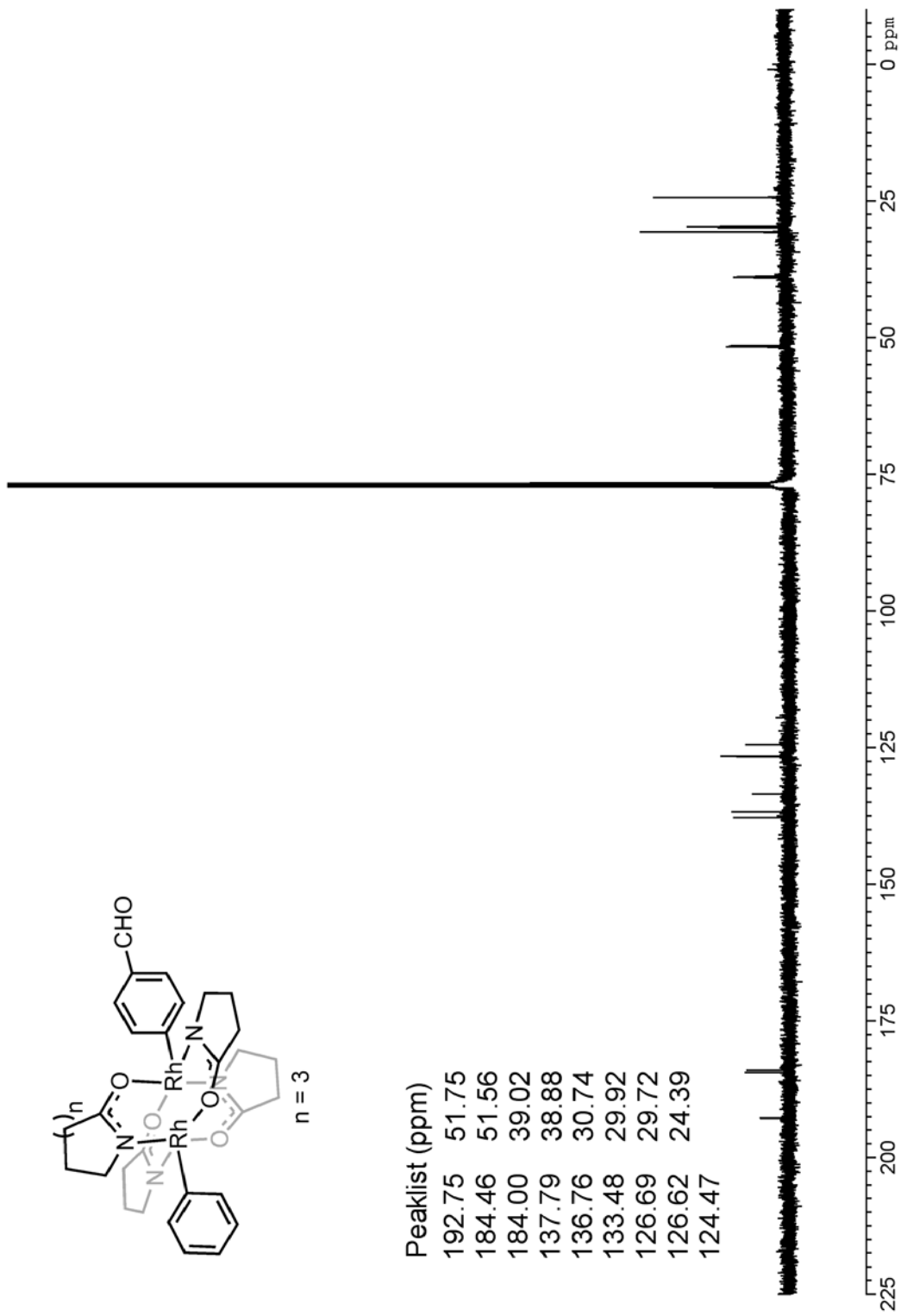
<sup>1</sup>H NMR Spectrum (**22**).



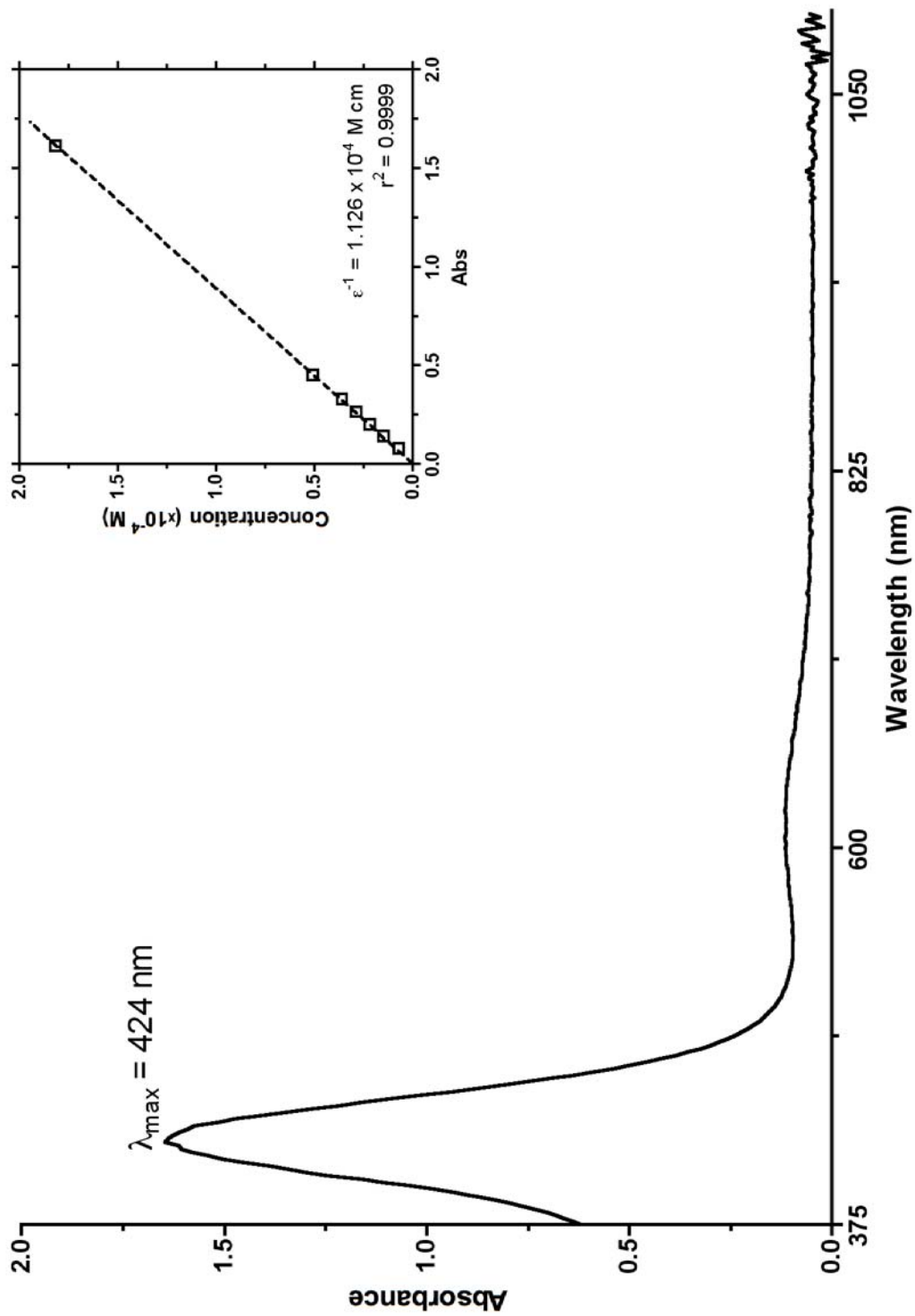
<sup>13</sup>C NMR Spectrum (**22**).



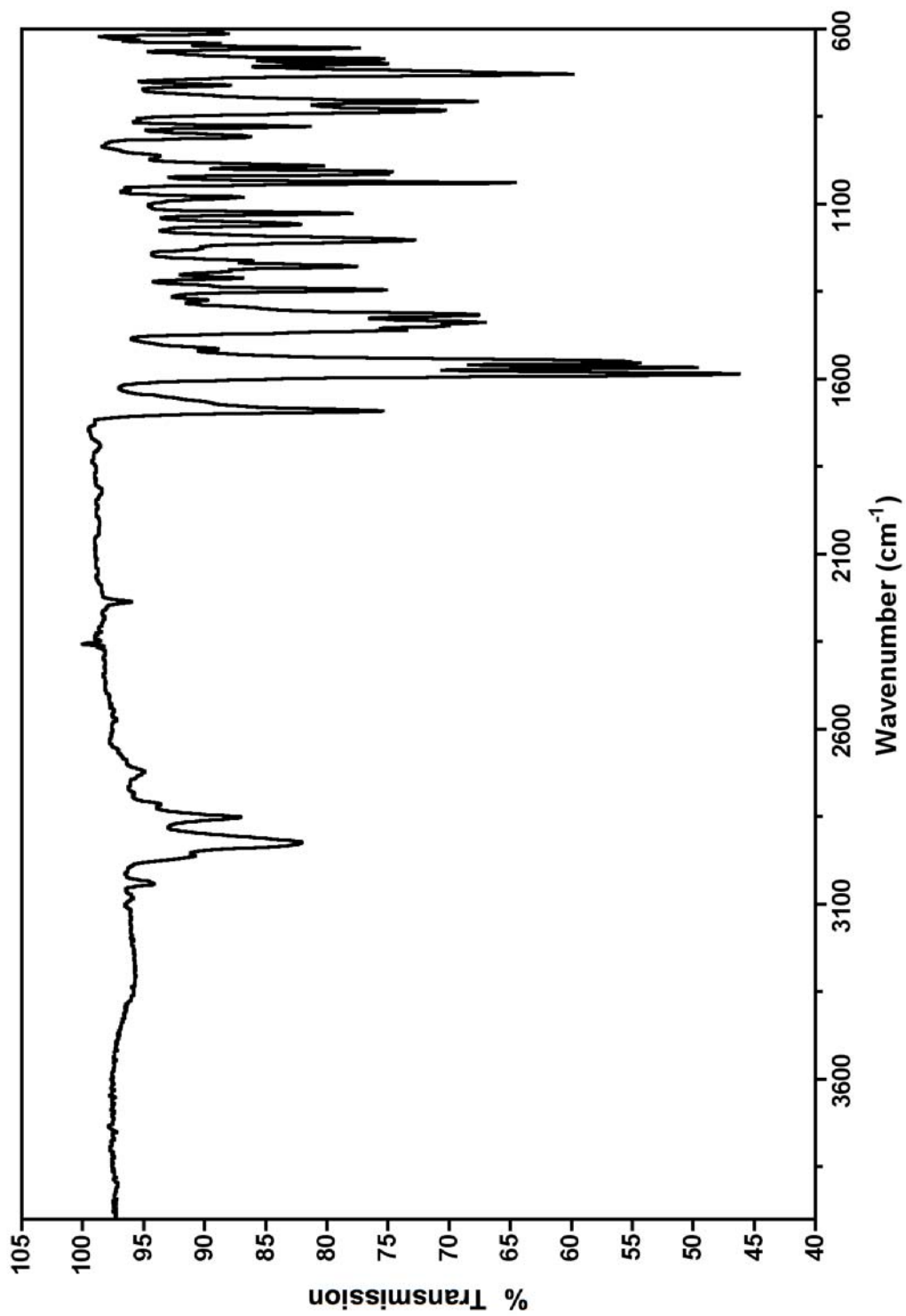
Peaklist (ppm)
192.75
184.46
184.00
137.79
136.76
133.48
126.69
126.62
124.47
51.75
51.56
39.02
38.88
30.74
29.92
29.72
24.39



Electronic Absorption Spectrum & Molar Absorptivity (22, 375 – 1100 nm)

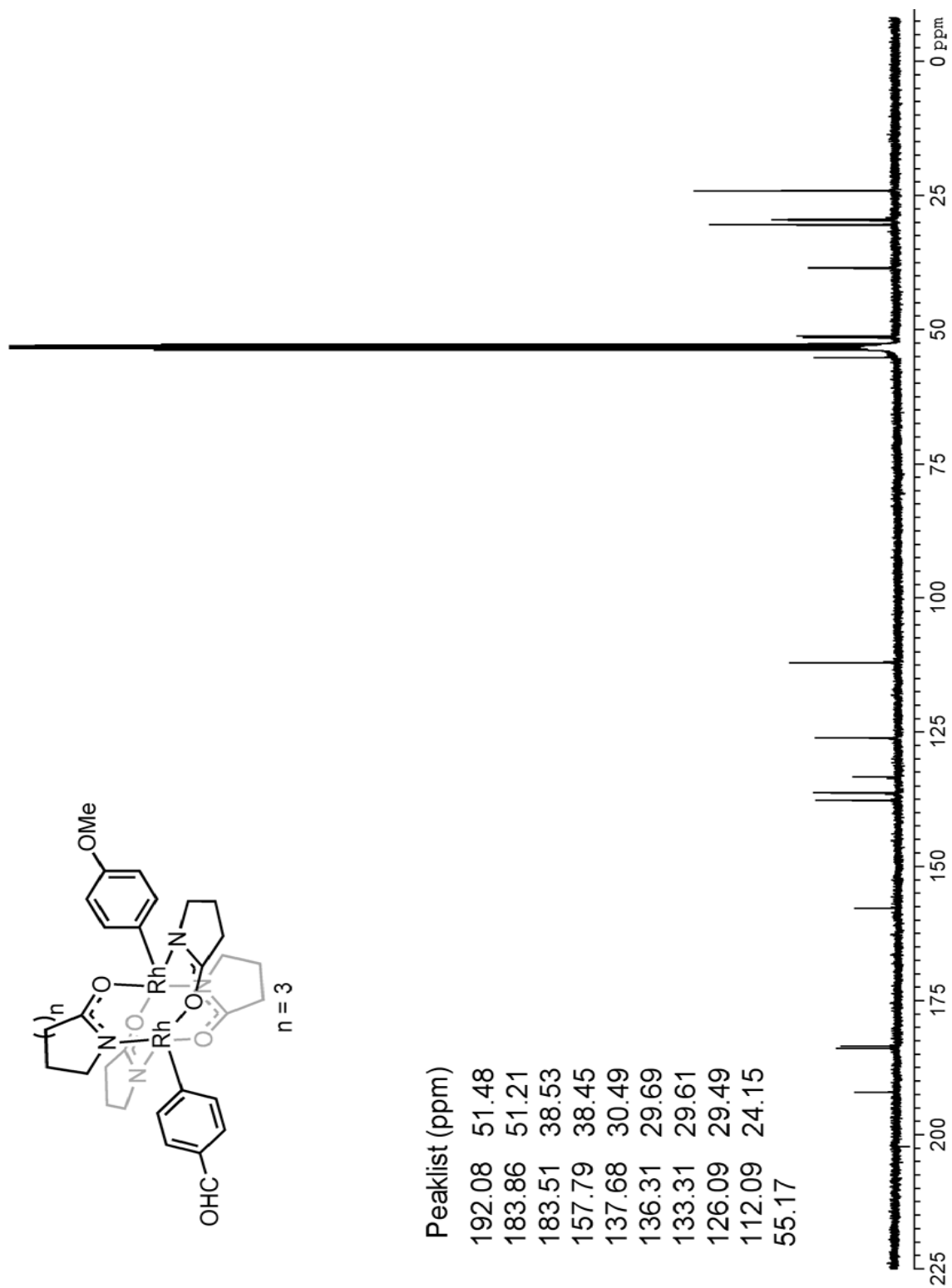


Vibrational Spectrum (22, 4000 – 600  $\text{cm}^{-1}$ )

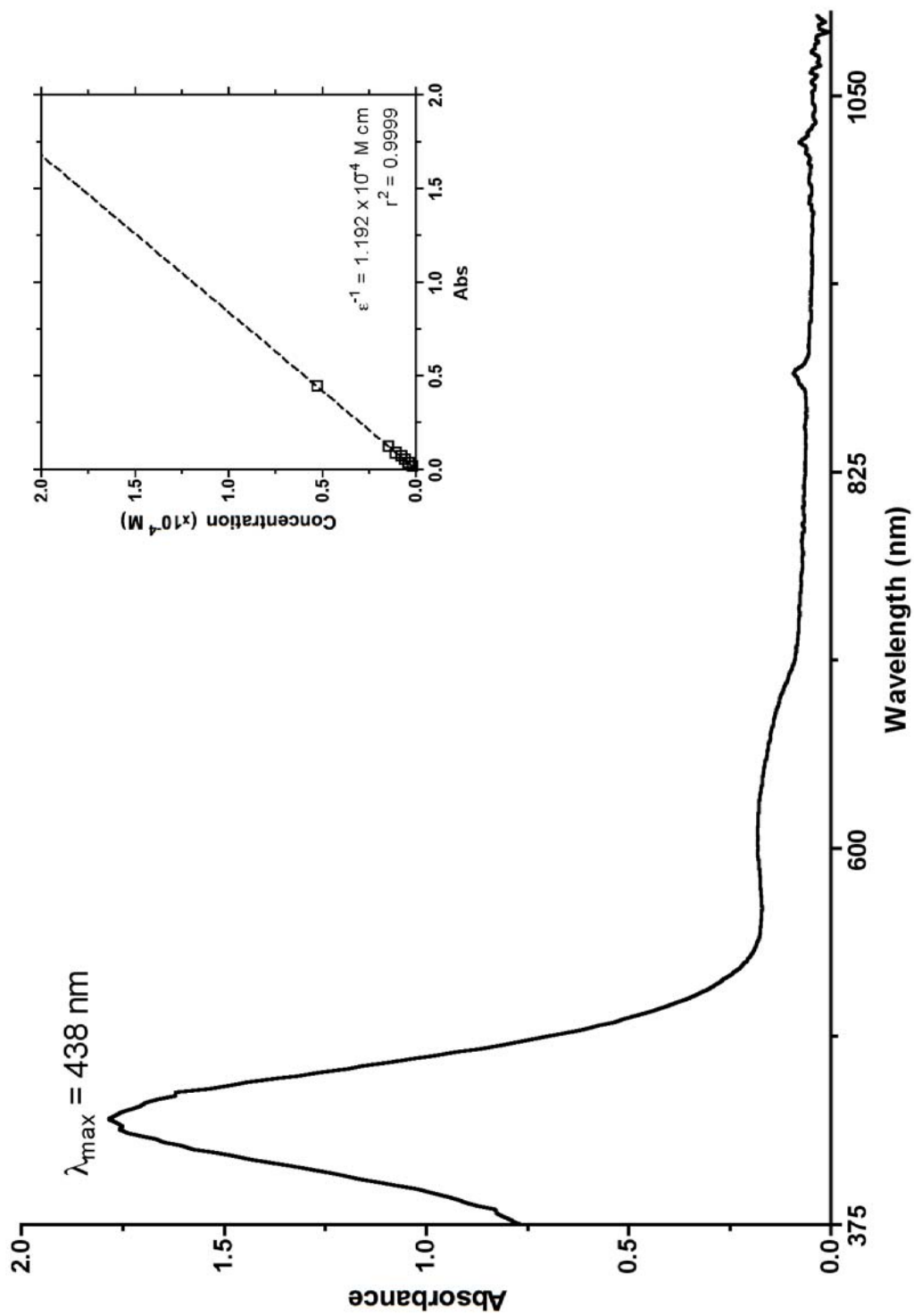




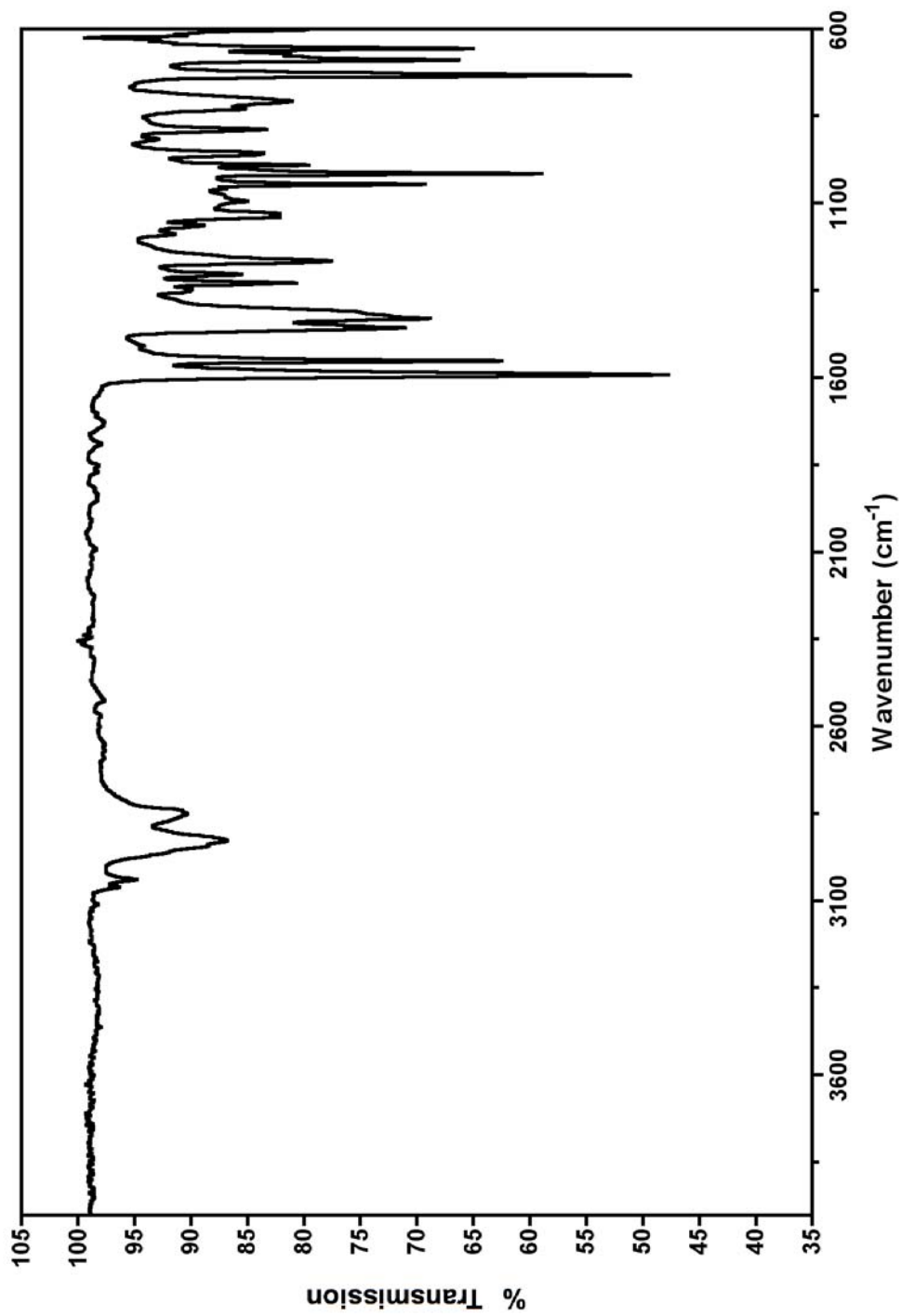
<sup>13</sup>C NMR Spectrum (23).



Electronic Absorption Spectrum & Molar Absorptivity (23, 375 – 1100 nm)

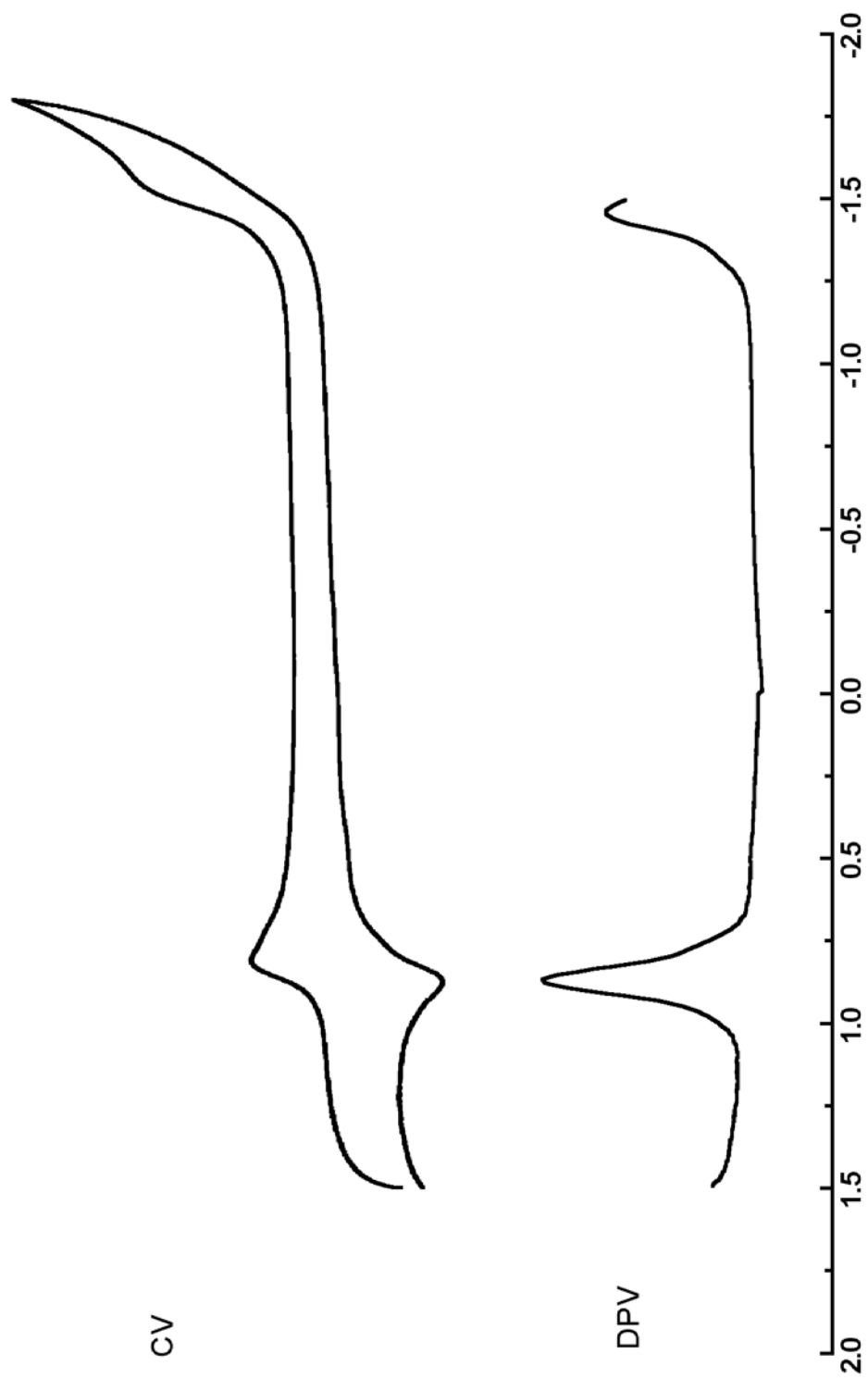


Vibrational Spectrum (23, 4000 – 600  $\text{cm}^{-1}$ )

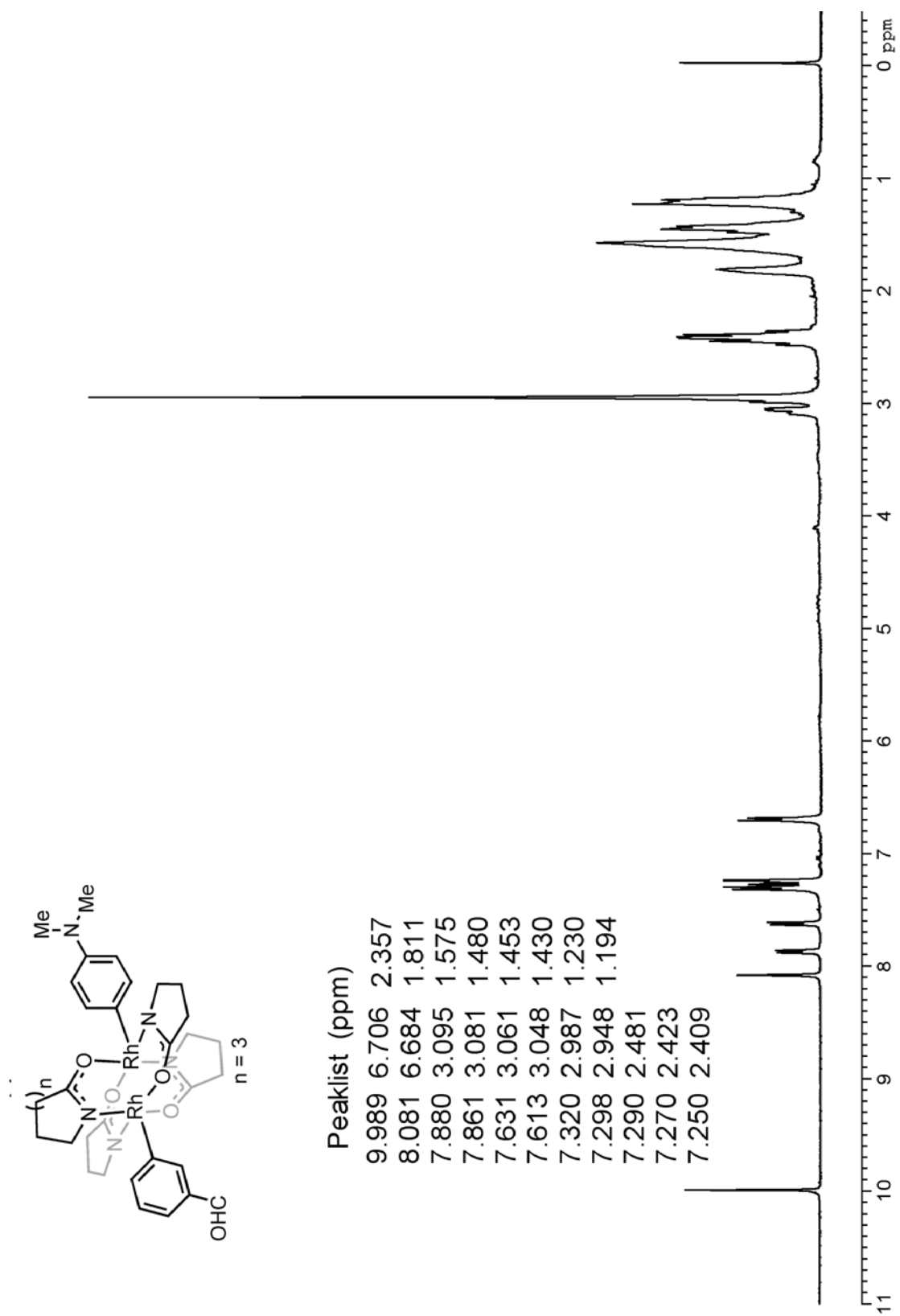




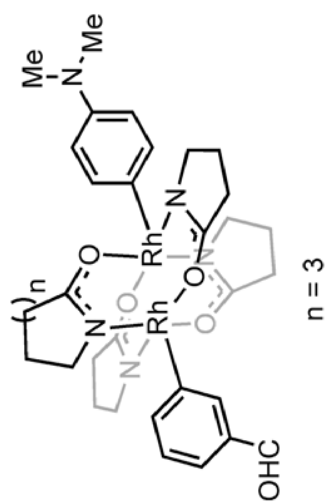
Voltammetry (23)



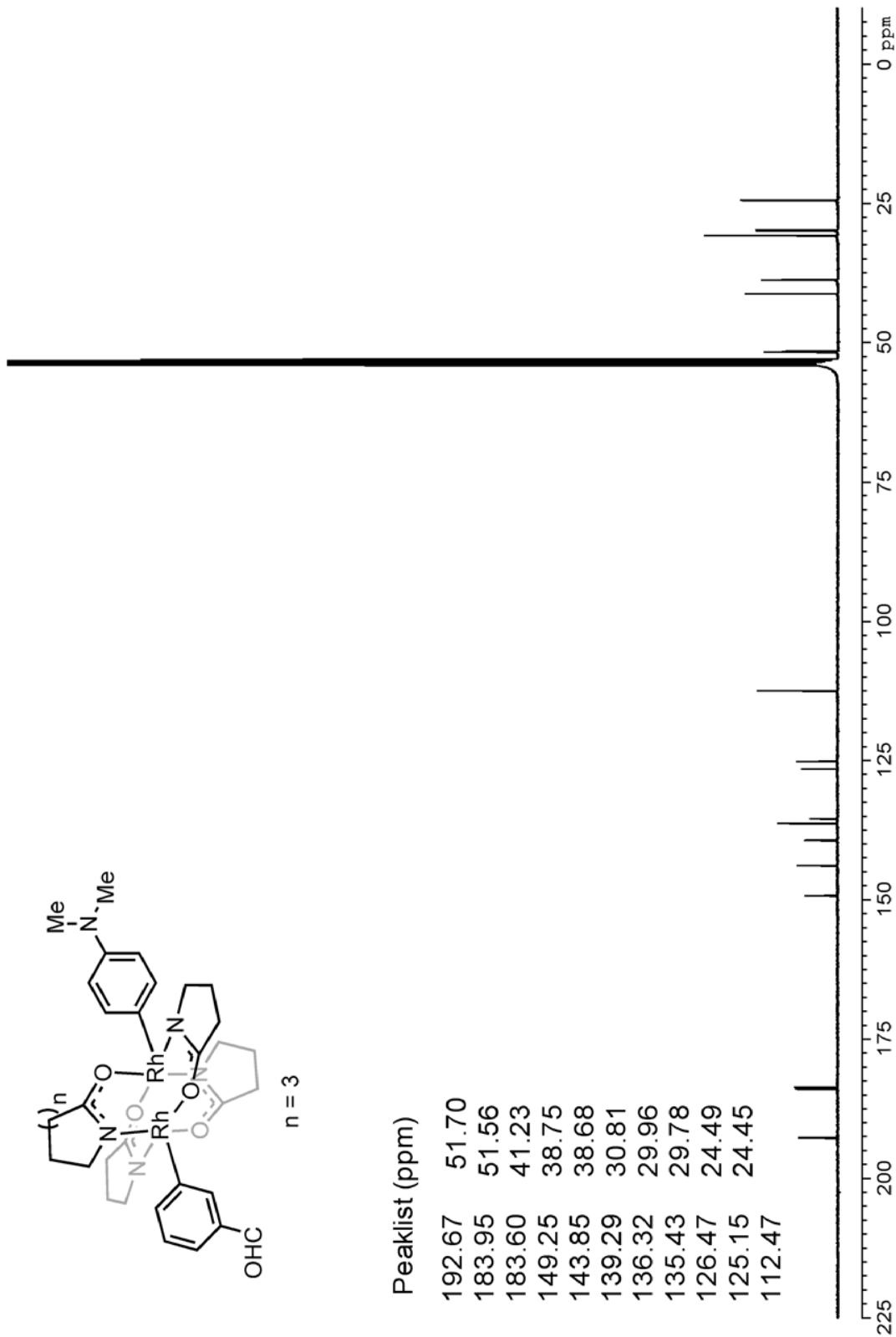
<sup>1</sup>H NMR Spectrum (**24**).



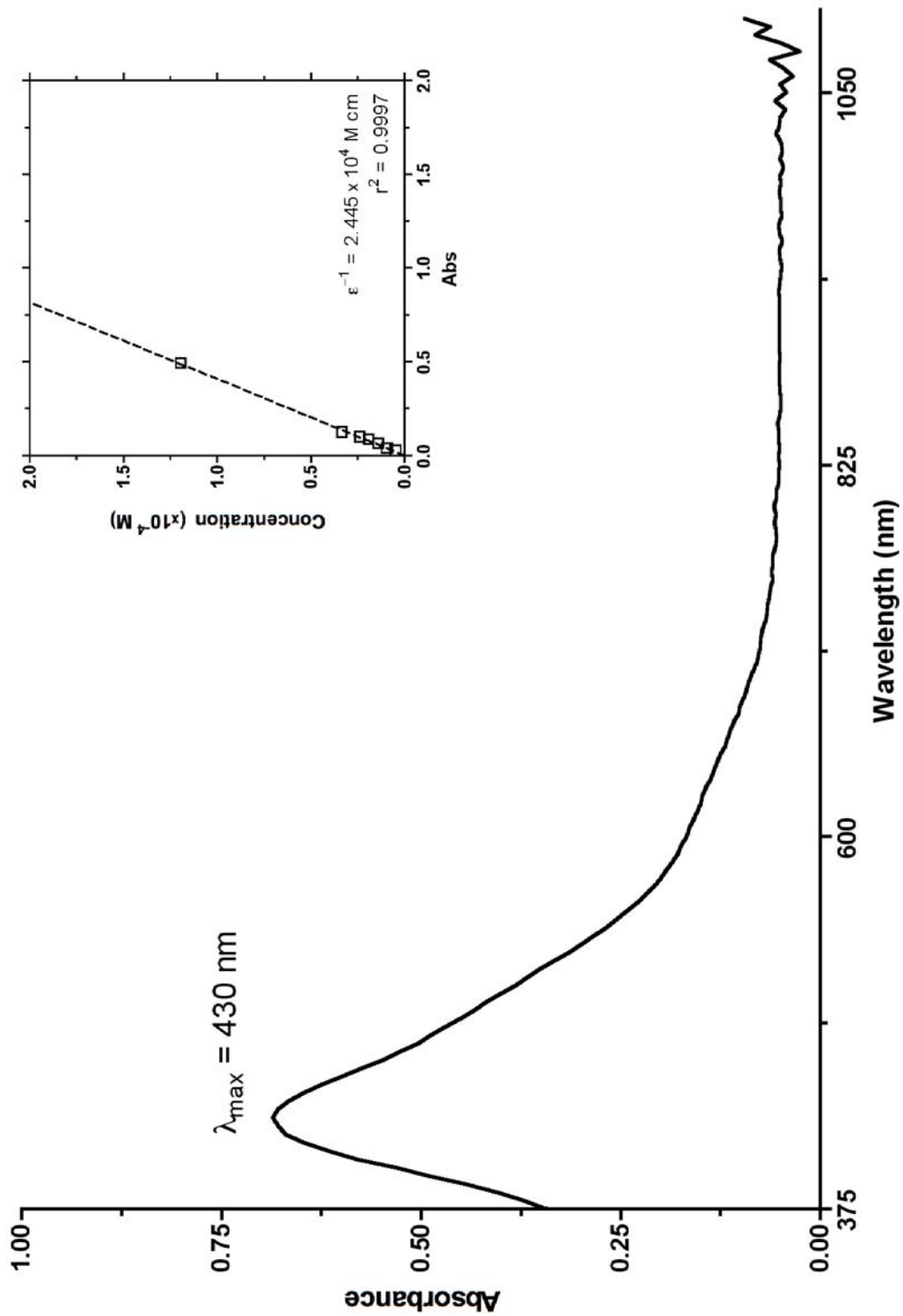
<sup>13</sup>C NMR Spectrum (**24**).



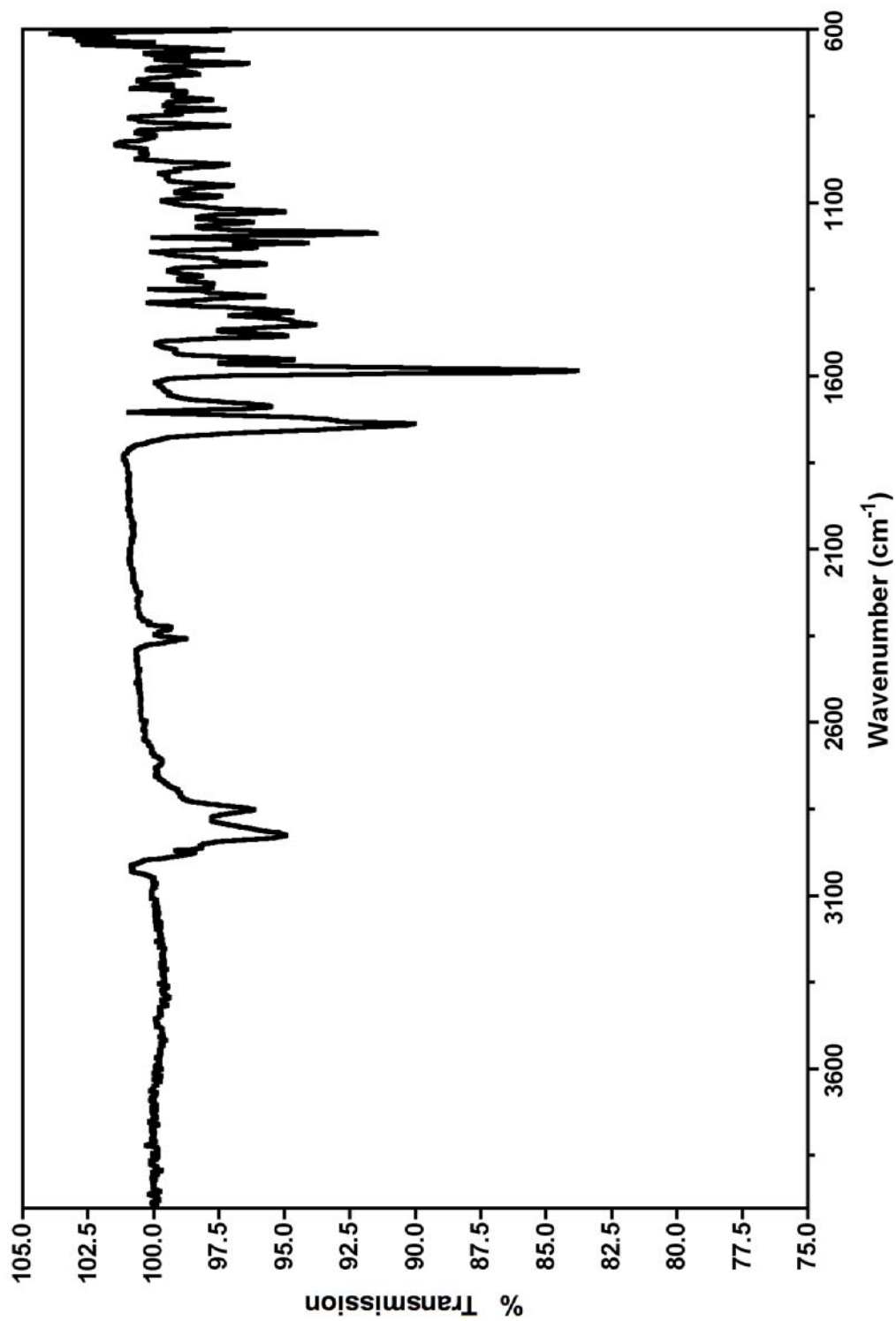
Peaklist (ppm)	51.70
192.67	51.70
183.95	51.56
183.60	41.23
149.25	38.75
143.85	38.68
139.29	30.81
136.32	29.96
135.43	29.78
126.47	24.49
125.15	24.45
112.47	



Electronic Absorption Spectrum & Molar Absorptivity (24, 375 – 1100 nm)



Vibrational Spectrum-(**24**, 4000 – 600  $\text{cm}^{-1}$ )



## XRD Data.

XRD Crystallographer's<sup>117</sup> Report (12).

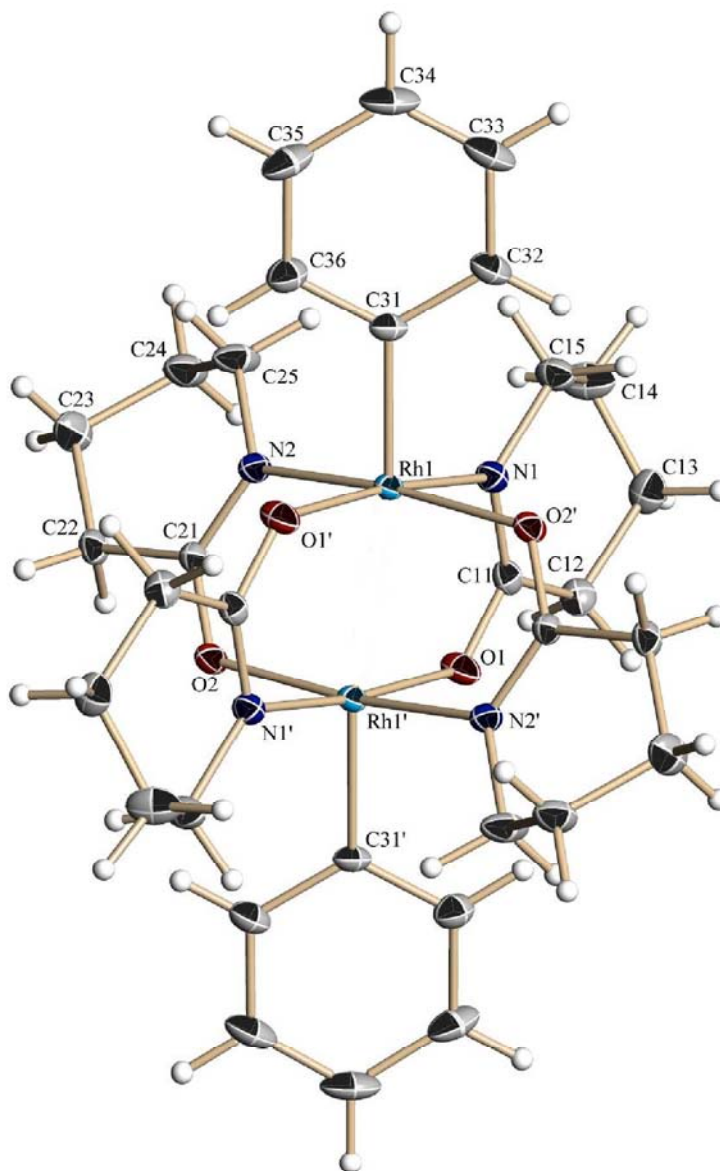


**Figure 2-15.** A view of **12** showing the numbering scheme employed. Anisotropic atomic displacement ellipsoids for the non-hydrogen atoms are shown at the 30% probability level. Hydrogen atoms are displayed with an arbitrarily small radius.

---

<sup>117</sup> See ref. 109.

A dark-yellow prism of  $C_{32}H_{42}N_4O_4Rh_2$ , approximate dimensions 0.05 x 0.15 x 0.22 mm<sup>3</sup>, was used for the X-ray crystallographic analysis. The X-ray intensity data were measured at 220(2) K on a three-circle diffractometer system equipped with Bruker Smart1000 CCD area detector using a graphite monochromator and a Mo  $K\alpha$  fine-focus sealed tube ( $\lambda = 0.71073 \text{ \AA}$ ) operated at 50 kV and 30 mA. The detector was placed at a distance of 4.939 cm from the crystal.

A total of 3024 frames were collected with a scan width of  $0.3^\circ$  in  $\omega$  and an exposure time of 33 sec/frame using SMART.<sup>118</sup> The total data collection time was 33.73 hours. The frames were integrated with SAINT<sup>119</sup> software package using a narrow-frame integration algorithm. The integration of the data using a Monoclinic unit cell yielded a total of 13641 reflections to a maximum  $\theta$  angle of  $27.51^\circ$ , of which 3399 were independent (completeness = 99.9%,  $R_{\text{int}} = 2.73\%$ ,  $R_{\text{sig}} = 2.29\%$ ) and 2924 were greater than  $2\sigma(I)$ . The final cell dimensions of  $a = 8.3492(6) \text{ \AA}$ ,  $b = 12.2916(8) \text{ \AA}$ ,  $c = 14.5016(10) \text{ \AA}$ ,  $\alpha = 90^\circ$ ,  $\beta = 90.1910(10)^\circ$ ,  $\gamma = 90^\circ$ , and  $V = 1488.22(18) \text{ \AA}^3$  are based upon the refinement of the XYZ-centroids of 7232 reflections with  $2.2 < \theta < 28.3^\circ$  using SAINT. Analysis of the data showed 0.00 % decay during data collection. Data were corrected for absorption effects with the semi-empirical from equivalents method using SADABS.<sup>120</sup> The minimum and maximum transmission coefficients were 0.807 and 0.944.

The structure was solved and refined using the SHELXS-97 and SHELXL-97 software<sup>121</sup> in the space group  $P2_1/n$  with  $Z = 2$  for the formula unit  $C_{32}H_{42}N_4O_4Rh_2$ . The final anisotropic full-matrix least-squares refinement

---

<sup>118</sup> See ref. 110.

<sup>119</sup> See ref. 110.

<sup>120</sup> See ref. 112.

<sup>121</sup> See ref. 111.

on  $F^2$  with 215 variables converged at  $R_1 = 3.27\%$  for the observed data and  $wR_2 = 8.70\%$  for all data. The goodness-of-fit was 1.000. The largest peak on the final difference map was  $1.162\bar{e}/\text{\AA}^3$  and the largest hole was  $-0.591\bar{e}/\text{\AA}^3$ . On the basis of the final model, the calculated density was  $1.679\text{ g/cm}^3$  and  $F(000)$ ,  $768\bar{e}$ .

**Table 2-9.** Crystal data and structure refinement for **12**.

Empirical formula	$C_{32}H_{42}N_4O_4Rh_2$	
Formula weight (amu)	752.52	
Temperature (K)	220(2)	
Wavelength ( $\text{\AA}$ )	0.71073 (Mo $K\alpha$ )	
Crystal size ( $\text{mm}^3$ )	0.22 × 0.15 × 0.05	
Crystal habit	dark-yellow prism	
Crystal system	Monoclinic	
Space group	$P2_1/n$	
Unit cell dimensions ( $\text{\AA} / ^\circ$ )	$a = 8.3492(6)$	$\alpha = 90$
	$b = 12.2916(8)$	$\beta = 90.1910(10)$
	$c = 14.5016(10)$	$\gamma = 90^\circ$
Volume ( $\text{\AA}^3$ )	1488.22(18)	
Z	2	
Density, $\rho_{\text{calc}}$ ( $\text{g/cm}^3$ )	1.679	
Absorption coefficient, $\mu$ ( $\text{mm}^{-1}$ )	1.153	
$\theta$ Range ( $^\circ$ )	2.17 to 27.51 $^\circ$	
Reflections collected	13641	
Independent reflections	3399	
Observed reflection, $I > 2\sigma(I)$	2924	
Max. and min. transmission <sup>a</sup>	0.944 and 0.807	
Goodness-of-fit on $F^2$	0.996	
Max $[\Delta/\sigma]$	0.001	
Final R indices: <sup>b</sup>		
$R_1$ , $I > 2\sigma(I)$	0.0327	
$wR_2$ , all data	0.0870	
$R_{\text{int}}$	0.0273	
$R_{\text{sig}}$	0.0229	
Min., max. peaks ( $\bar{e}/\text{\AA}^3$ )	1.162 and $-0.591^-$	

<sup>a</sup>Absorption correction was performed using the semi-empirical from equivalents method (SADABS). <sup>b</sup>Function minimized was  $\sum w(F_o^2 - F_c^2)^2$  where  $R_1 = \sum ||F_o| - |F_c|| / \sum |F_o|$ ,  $wR_2 = [\sum w(F_o^2 - F_c^2)^2 / \sum w(F_o^2)^2]^{1/2}$  with a weighting scheme  $w = 1/[\sigma^2(F_o^2) + (0.015P)^2 + 27.8P]$ ,  $P = [\max(F_o^2, 0) + 2F_o^2]/3$ .



**Table 2-10.** Atomic coordinates and equivalent isotropic atomic displacement parameters ( $\text{\AA}^2$ ) for **12**.

Atom	$x/a$	$y/b$	$z/c$	$U_{\text{eq}}$
Rh1	0.51711(3)	0.404978(19)	0.469330(17)	0.02524(9)
O1	0.2700(3)	0.5128(2)	0.56475(19)	0.0399(6)
N1	0.3079(3)	0.3419(2)	0.5089(2)	0.0312(6)
C11	0.2211(4)	0.4144(3)	0.5514(2)	0.0316(7)
C12	0.0595(4)	0.3926(3)	0.5874(3)	0.0377(8)
C13	0.0106(8)	0.2717(5)	0.5840(5)	0.0457(16)
C14	0.0760(8)	0.2123(6)	0.5022(6)	0.053(2)
C15	0.2575(8)	0.2258(8)	0.5024(5)	0.0416(18)
C12A	0.0595(4)	0.3926(3)	0.5874(3)	0.0377(8)
C13A	-0.0182(15)	0.2906(9)	0.5461(12)	0.0457(16)
C14A	0.101(2)	0.1998(11)	0.5388(14)	0.053(2)
C15A	0.231(2)	0.242(2)	0.4743(15)	0.0416(18)
O2	0.3953(3)	0.63038(19)	0.40106(16)	0.0333(5)
N2	0.4088(4)	0.4538(2)	0.35106(19)	0.0320(6)
C21	0.3676(4)	0.5556(3)	0.3407(2)	0.0281(7)
C22	0.2847(5)	0.5954(3)	0.2540(2)	0.0341(8)
C23	0.2409(9)	0.5111(4)	0.1832(4)	0.0560(18)
C24	0.2047(8)	0.4046(4)	0.2312(4)	0.0490(15)
C25	0.3558(18)	0.3727(11)	0.2832(6)	0.055(3)
C22A	0.2847(5)	0.5954(3)	0.2540(2)	0.0341(8)
C23A	0.179(4)	0.513(2)	0.208(3)	0.0560(18)
C24A	0.276(6)	0.4099(19)	0.195(3)	0.0490(15)
C25A	0.324(18)	0.373(10)	0.291(5)	0.055(3)
C31	0.6315(4)	0.2772(3)	0.4159(2)	0.0323(7)
C32	0.6304(5)	0.1786(3)	0.4628(3)	0.0401(9)
C33	0.7034(6)	0.0872(3)	0.4224(4)	0.0536(12)
C34	0.7779(6)	0.0944(4)	0.3391(4)	0.0595(14)
C35	0.7864(5)	0.1951(4)	0.2942(3)	0.0543(12)
C36	0.7136(5)	0.2860(4)	0.3327(3)	0.0428(9)
H12A	-0.0182	0.4350	0.5516	0.045
H12B	0.0544	0.4177	0.6515	0.045
H13A	0.0483	0.2358	0.6404	0.055
H13B	-0.1066	0.2668	0.5829	0.055
H14A	0.0304	0.2421	0.4453	0.064
H14B	0.0480	0.1349	0.5058	0.064
H15A	0.3027	0.1856	0.5547	0.050
H15B	0.3010	0.1943	0.4457	0.050
H12C	-0.0091	0.4554	0.5744	0.045
H12D	0.0659	0.3842	0.6545	0.045
H13C	-0.1076	0.2675	0.5851	0.055
H13D	-0.0608	0.3075	0.4847	0.055
H14C	0.0507	0.1344	0.5132	0.064
H14D	0.1460	0.1822	0.5995	0.064
H15C	0.3133	0.1858	0.4666	0.050
H15D	0.1842	0.2568	0.4136	0.050
H22A	0.1864	0.6332	0.2723	0.041
H22B	0.3544	0.6491	0.2245	0.041

H23A	0.3298	0.5012	0.1400	0.067
H23B	0.1468	0.5352	0.1481	0.067
H24A	0.1764	0.3485	0.1859	0.059
H24B	0.1150	0.4135	0.2740	0.059
H25A	0.3367	0.3036	0.3151	0.066
H25B	0.4421	0.3609	0.2387	0.066
H22C	0.2197	0.6591	0.2697	0.041
H22D	0.3665	0.6189	0.2100	0.041
H23C	0.1425	0.5400	0.1476	0.067
H23D	0.0845	0.4980	0.2457	0.067
H24C	0.3716	0.4246	0.1582	0.059
H24D	0.2122	0.3539	0.1642	0.059
H25C	0.2263	0.3494	0.3237	0.066
H25D	0.3925	0.3084	0.2853	0.066
H32	0.5814	0.1731	0.5208	0.044(12)
H33	0.7008	0.0200	0.4534	0.065(15)
H34	0.8231	0.0322	0.3120	0.061(14)
H35	0.8414	0.2012	0.2380	0.065(15)
H36	0.7199	0.3536	0.3026	0.054(13)

---

$U_{eq}$  is defined as one third of the trace of the orthogonalized  $U_{ij}$  tensor.

**Table 2-11.** Anisotropic atomic displacement parameters ( $\text{\AA}^2$ ) for **12**.

Atom	$U_{11}$	$U_{22}$	$U_{33}$	$U_{23}$	$U_{13}$	$U_{12}$
Rh1	0.03002(15)	0.01960(13)	0.02611(14)	-0.00108(9)	-0.00113(9)	0.00245(10)
O1	0.0359(14)	0.0265(12)	0.0572(16)	-0.0023(12)	0.0112(12)	0.0011(10)
N1	0.0330(15)	0.0267(14)	0.0338(15)	-0.0015(12)	0.0006(12)	-0.0031(12)
C11	0.0341(17)	0.0299(17)	0.0309(17)	0.0058(13)	-0.0031(13)	0.0014(14)
C12	0.0307(17)	0.040(2)	0.042(2)	0.0030(16)	0.0030(15)	0.0047(15)
C13	0.039(3)	0.056(3)	0.043(4)	0.002(3)	0.000(3)	-0.016(3)
C14	0.032(3)	0.052(3)	0.075(6)	-0.022(4)	-0.007(3)	-0.009(2)
C15	0.044(3)	0.032(4)	0.048(5)	-0.006(3)	0.001(3)	-0.007(3)
C12A	0.0307(17)	0.040(2)	0.042(2)	0.0030(16)	0.0030(15)	0.0047(15)
C13A	0.039(3)	0.056(3)	0.043(4)	0.002(3)	0.000(3)	-0.016(3)
C14A	0.032(3)	0.052(3)	0.075(6)	-0.022(4)	-0.007(3)	-0.009(2)
C15A	0.044(3)	0.032(4)	0.048(5)	-0.006(3)	0.001(3)	-0.007(3)
O2	0.0457(14)	0.0242(11)	0.0301(12)	0.0005(10)	-0.0081(10)	0.0032(10)
N2	0.0430(17)	0.0268(14)	0.0260(14)	-0.0027(11)	-0.0053(12)	0.0054(12)
C21	0.0313(17)	0.0275(16)	0.0255(16)	0.0016(13)	-0.0021(13)	0.0004(13)
C22	0.040(2)	0.0324(18)	0.0293(17)	0.0074(14)	-0.0063(14)	0.0016(15)
C23	0.086(5)	0.046(3)	0.036(3)	0.003(2)	-0.024(3)	0.000(3)
C24	0.066(4)	0.035(2)	0.046(3)	-0.009(2)	-0.017(3)	0.003(2)
C25	0.088(8)	0.036(2)	0.041(3)	-0.015(2)	-0.031(3)	0.018(4)
C22A	0.040(2)	0.0324(18)	0.0293(17)	0.0074(14)	-0.0063(14)	0.0016(15)
C23A	0.086(5)	0.046(3)	0.036(3)	0.003(2)	-0.024(3)	0.000(3)
C24A	0.066(4)	0.035(2)	0.046(3)	-0.009(2)	-0.017(3)	0.003(2)
C25A	0.088(8)	0.036(2)	0.041(3)	-0.015(2)	-0.031(3)	0.018(4)
C31	0.0371(18)	0.0269(16)	0.0330(17)	-0.0084(14)	-0.0068(14)	0.0075(14)
C32	0.046(2)	0.0266(17)	0.048(2)	-0.0033(16)	-0.0124(17)	0.0045(16)
C33	0.059(3)	0.0255(19)	0.077(3)	-0.008(2)	-0.023(2)	0.0084(18)
C34	0.056(3)	0.045(3)	0.077(3)	-0.033(2)	-0.015(2)	0.021(2)
C35	0.049(2)	0.070(3)	0.043(2)	-0.023(2)	-0.0024(19)	0.023(2)
C36	0.046(2)	0.045(2)	0.037(2)	-0.0061(17)	-0.0031(16)	0.0120(18)

The anisotropic atomic displacement factor exponent takes the form:  $-2\pi^2 [h^2a^2U_{11} + \dots + 2hka^*b^*U_{12}]$ .

**Table 2-12.** Site occupancy factors that deviate from unity for **12**.

Atom	sof	Atom	sof	Atom	sof
C12 – C15	0.705(10)	C12a – C15a	0.295(10)		
C22 – C25	0.886(11)	C22a – C25a	0.114(11)		

**Table 2-13.** Bond lengths (Å) and angles (°) for **12**.

Rh1-C31	1.996(3)	Rh1-N1	1.997(3)	Rh1-N2	2.027(3)
Rh1-O2#1	2.061(2)	Rh1-O1#1	2.105(3)	Rh1-Rh1#1	2.5162(5)
O1-C11	1.291(4)	O1-Rh1#1	2.105(3)	N1-C11	1.304(5)
N1-C15	1.490(10)	C11-C12	1.473(5)	C12-C13	1.541(7)
C13-C14	1.498(8)	C14-C15	1.524(7)	O2-C21	1.290(4)
O2-Rh1#1	2.061(2)	N2-C21	1.306(4)	N2-C25	1.468(15)
C21-C22	1.514(4)	C22-C23	1.503(6)	C23-C24	1.514(7)
C24-C25	1.520(10)	C31-C32	1.389(5)	C31-C36	1.394(5)
C32-C33	1.407(6)	C33-C34	1.364(8)	C34-C35	1.400(8)
C35-C36	1.390(6)				
C31-Rh1-N1	103.07(14)	C31-Rh1-N2	96.74(13)	N1-Rh1-N2	88.28(12)
C31-Rh1-O2#1	91.10(12)	N1-Rh1-O2#1	87.95(11)	N2-Rh1-O2#1	171.90(11)
C31-Rh1-O1#1	83.19(13)	N1-Rh1-O1#1	173.67(11)	N2-Rh1-O1#1	91.94(12)
O2#1-Rh1-O1#1	91.03(11)	C31-Rh1-Rh1#1	157.34(11)	N1-Rh1-Rh1#1	99.10(8)
N2-Rh1-Rh1#1	88.47(8)	O2#1-Rh1-Rh1#1	85.05(7)	O1#1-Rh1-Rh1#1	74.58(7)
C11-O1-Rh1#1	133.0(2)	C11-N1-C15	121.8(4)	C11-N1-Rh1	111.0(2)
C15-N1-Rh1	126.9(3)	O1-C11-N1	122.3(3)	O1-C11-C12	114.0(3)
N1-C11-C12	123.7(3)	C11-C12-C13	114.0(4)	C14-C13-C12	113.5(5)
C13-C14-C15	108.1(6)	N1-C15-C14	112.7(6)	C21-O2-Rh1#1	122.1(2)
C21-N2-C25	119.7(4)	C21-N2-Rh1	119.8(2)	C25-N2-Rh1	119.9(3)
O2-C21-N2	123.9(3)	O2-C21-C22	114.4(3)	N2-C21-C22	121.6(3)
C23-C22-C21	117.0(3)	C22-C23-C24	109.3(4)	C23-C24-C25	106.5(7)
N2-C25-C24	113.9(7)	C32-C31-C36	119.7(3)	C32-C31-Rh1	119.5(3)
C36-C31-Rh1	120.8(3)	C31-C32-C33	119.3(4)	C34-C33-C32	121.1(4)
C33-C34-C35	119.6(4)	C36-C35-C34	120.1(4)	C35-C36-C31	120.1(4)
C31-Rh1-N1-C11	175.9(2)	N2-Rh1-N1-C11	-87.6(2)	O2#1-Rh1-N1-C11	85.2(2)
Rh1#1-Rh1-N1-C11	0.6(2)	C31-Rh1-N1-C15	2.3(5)	N2-Rh1-N1-C15	98.8(4)
O2#1-Rh1-N1-C15	-88.3(4)	Rh1#1-Rh1-N1-C15	-173.0(4)	Rh1#1-O1-C11-N1	-0.2(5)
Rh1#1-O1-C11-C12	-179.6(2)	C15-N1-C11-O1	173.6(4)	Rh1-N1-C11-O1	-0.3(4)
C15-N1-C11-C12	-7.1(6)	Rh1-N1-C11-C12	179.0(3)	O1-C11-C12-C13	-171.7(4)
N1-C11-C12-C13	8.9(6)	C11-C12-C13-C14	-34.5(8)	C12-C13-C14-C15	55.6(11)
C11-N1-C15-C14	29.8(9)	C15A-N1-C15-C14	-59(2)	Rh1-N1-C15-C14	-157.4(5)
C13-C14-C15-N1	-52.6(10)	C11-N1-C15A-C14A	-37.0(17)	C15-N1-C15A-C14A	66(2)
Rh1-N1-C15A-C14A	162.4(8)	C13A-C14A-C15A-N1	59.0(19)	C31-Rh1-N2-C21	-154.4(3)
N1-Rh1-N2-C21	102.6(3)	O1#1-Rh1-N2-C21	-71.0(3)	Rh1#1-Rh1-N2-C21	3.5(3)
C31-Rh1-N2-C25	34.5(7)	N1-Rh1-N2-C25	-68.5(7)	O1#1-Rh1-N2-C25	117.9(7)
Rh1#1-Rh1-N2-C25	-167.6(7)	Rh1#1-O2-C21-N2	-8.3(5)	Rh1#1-O2-C21-C22	172.8(2)
C25-N2-C21-O2	173.1(7)	C25A-N2-C21-O2	161(6)	Rh1-N2-C21-O2	1.9(5)
C25-N2-C21-C22	-8.1(8)	C25A-N2-C21-C22	-21(6)	Rh1-N2-C21-C22	-179.3(2)
O2-C21-C22-C23	-176.7(4)	N2-C21-C22-C23	4.4(6)	C21-C22-C23-C24	31.2(8)
C22-C23-C24-C25	-59.8(10)	C21-N2-C25-C24	-24.5(13)	Rh1-N2-C25-C24	146.6(6)
C23-C24-C25-N2	58.7(11)	C21-N2-C25A-C24A	34(10)	C25-N2-C25A-C24A	-75(17)
C23A-C24A-C25A-N2	-55(9)	N1-Rh1-C31-C32	-45.2(3)	N2-Rh1-C31-C32	-135.0(3)
O2#1-Rh1-C31-C32	43.0(3)	O1#1-Rh1-C31-C32	133.9(3)	Rh1#1-Rh1-C31-C32	122.7(3)
N1-Rh1-C31-C36	135.5(3)	N2-Rh1-C31-C36	45.7(3)	O2#1-Rh1-C31-C36	-136.4(3)
O1#1-Rh1-C31-C36	-45.5(3)	Rh1#1-Rh1-C31-C36	-56.6(4)	C36-C31-C32-C33	-4.2(6)
Rh1-C31-C32-C33	176.4(3)	C31-C32-C33-C34	1.4(6)	C32-C33-C34-C35	2.1(7)
C33-C34-C35-C36	-2.6(7)	C34-C35-C36-C31	-0.2(6)	C32-C31-C36-C35	3.7(6)
Rh1-C31-C36-C35	-177.0(3)				

Symmetry transformation codes: #1 -x+1,-y+1,-z+1

XRD Crystallographer's<sup>122</sup> Report (13).

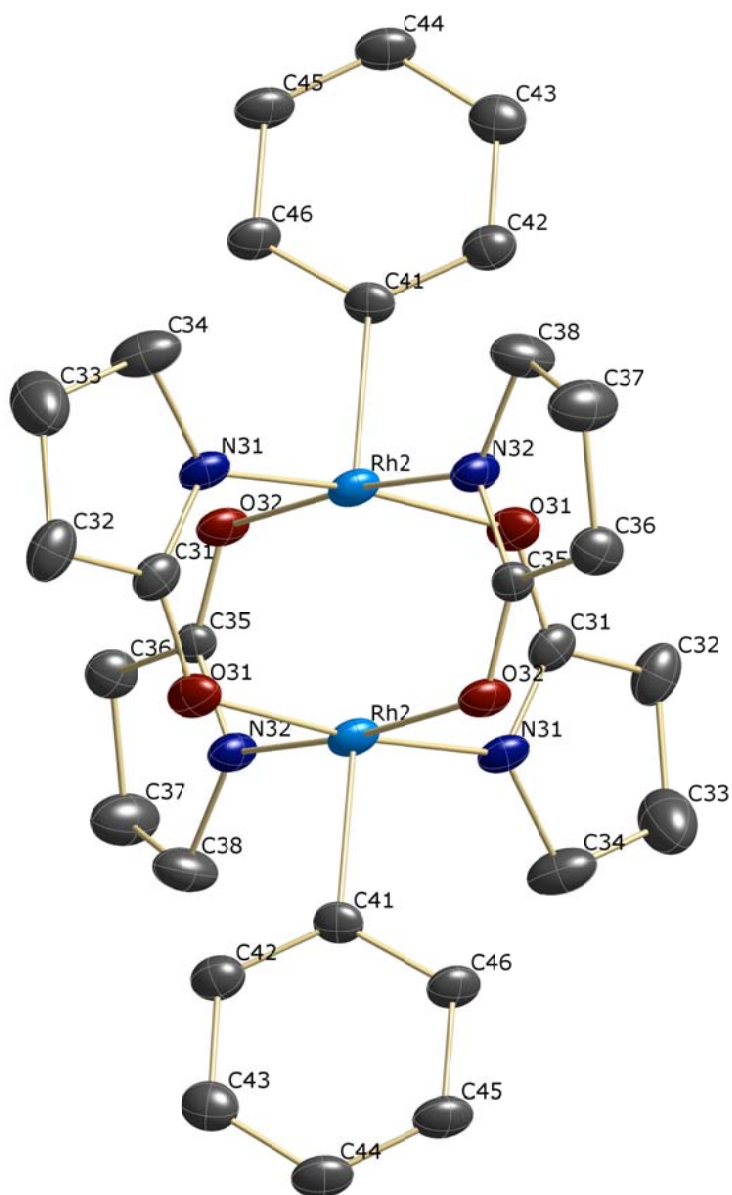


**Figure 2-16.** A view of **13** showing the numbering scheme employed. Anisotropic atomic displacement ellipsoids for the non-hydrogen atoms are shown at the 30% probability level.

---

<sup>122</sup> See ref. 109.

A yellow prism of  $C_{28}H_{34}N_4O_4Rh_2$ , approximate dimensions  $0.025 \times 0.08 \times 0.385 \text{ mm}^3$ , was used for the X-ray crystallographic analysis. The X-ray intensity data were measured at 223(2) K on a three-circle diffractometer system equipped with Bruker Smart1000 CCD area detector using a graphite monochromator and a Mo  $K\alpha$  fine-focus sealed tube ( $\lambda = 0.71073 \text{ \AA}$ ) operated at 50 kV and 30 mA. The detector was placed at a distance of 4.940 cm from the crystal.

A total of 1448 frames were collected with a scan width of  $0.3^\circ$  in  $\omega$  and an exposure time of 53 sec/frame using SMART.<sup>123</sup> The total data collection time was 24.19 hours. The frames were integrated with SAINT software<sup>124</sup> package using a narrow-frame integration algorithm. The integration of the data using a Triclinic unit cell yielded a total of 6374 reflections to a maximum  $\theta$  angle of  $25.00^\circ$ , of which 4126 were independent (completeness = 87.0%,  $R_{\text{int}} = 7.27\%$ ,  $R_{\text{sig}} = 7.07\%$ ) and 3186 were greater than  $2\sigma(I)$ . The final cell dimensions of  $a = 8.2971(13) \text{ \AA}$ ,  $b = 11.5643(18) \text{ \AA}$ ,  $c = 14.670(2) \text{ \AA}$ ,  $\alpha = 78.139(3)^\circ$ ,  $\beta = 81.744(2)^\circ$ ,  $\gamma = 79.456(3)^\circ$ , and  $V = 1346.1(4) \text{ \AA}^3$  are based upon the refinement of the XYZ-centroids of 3360 reflections with  $2.5 < \theta < 25.0^\circ$  using SAINT. Analysis of the data showed 0.00 % decay during data collection. Data were corrected for absorption effects with the semi-empirical from equivalents method using XPREP as implemented in the SAINT software package. The minimum and maximum transmission coefficients were 0.680 and 0.969.

The structure was solved and refined using the SHELXL-97 software<sup>125</sup> in the space group  $P1$  with  $Z = 2$  for the formula unit  $C_{28}H_{34}N_4O_4Rh_2$ . The final anisotropic full-matrix least-squares refinement on  $F^2$  with 343 variables

---

<sup>123</sup> See ref. 110.

<sup>124</sup> See ref. 110.

<sup>125</sup> See ref. 111.

converged at  $R_1 = 5.69\%$  for the observed data and  $wR_2 = 12.97\%$  for all data. The goodness-of-fit was 1.000. The largest peak on the final difference map was  $1.056 \text{ e}/\text{\AA}^3$  and the largest hole was  $-0.596 \text{ e}/\text{\AA}^3$ . On the basis of the final model, the calculated density was  $1.718 \text{ g}/\text{cm}^3$  and  $F(000)$ , 704 e.

**Table 2-14.** Crystal data and structure refinement for **13**.

Empirical formula	$\text{C}_{28}\text{H}_{34}\text{N}_4\text{O}_4\text{Rh}_2$	
Formula weight (amu)	696.41	
Temperature (K)	223(2)	
Wavelength (Å)	0.71073 (Mo $K\alpha$ )	
Crystal size (mm <sup>3</sup> )	0.385 × 0.08 × 0.025	
Crystal habit	yellow prism	
Crystal system	Triclinic	
Space group	P1	
Unit cell dimensions (Å / °)	$a = 8.2971(13)$	$\alpha = 78.139(3)$
	$b = 11.5643(18)$	$\beta = 81.744(2)$
	$c = 14.670(2)$	$\gamma = 79.456(3)$
Volume (Å <sup>3</sup> )	1346.1(4)	
Z	2	
Density, $\rho_{\text{calc}}$ (g/cm <sup>3</sup> )	1.718	
Absorption coefficient, $\mu$ (mm <sup>-1</sup> )	1.268	
$\theta$ Range (°)	2.51 to 25.00	
Reflections collected	6374	
Independent reflections	4126	
Observed reflection, $I > 2\sigma(I)$	3186	
Max. and min. transmission <sup>a</sup>	0.969 and 0.680	
Goodness-of-fit on $F^2$	0.999	
Max [ $\Delta/\sigma$ ]	0.001	
Final R indices: <sup>b</sup>		
	$R_1, I > 2\sigma(I)$	0.0569
	$wR_2, \text{all data}$	0.1297
	$R_{\text{int}}$	0.0727
	$R_{\text{sig}}$	0.0707
Min., max. peaks ( $\text{e}/\text{\AA}^3$ )	1.056 and -0.596	

<sup>a</sup>Absorption correction was performed using the semi-empirical from equivalents method (SADABS). <sup>b</sup>Function minimized was  $\sum w(F_o^2 - F_c^2)^2$  where  $R_1 = \sum ||F_o| - |F_c|| / \sum |F_o|$ ,  $wR_2 = [\sum w(F_o^2 - F_c^2)^2 / \sum w(F_o^2)^2]^{1/2}$  with a weighting scheme  $w = 1/[\sigma^2(F_o^2) + (0.015P)^2 + 27.8P]$ ,  $P = [\max(F_o^2, 0) + 2F_o^2]/3$ .

**Table 2-15.** Atomic coordinates and equivalent isotropic atomic displacement parameters ( $\text{\AA}^2$ ) for **13**.

Atom	<i>x/a</i>	<i>y/b</i>	<i>z/c</i>	$U_{\text{eq}}$
Rh1	0.09091(7)	0.07613(5)	0.50651(4)	0.03856(18)
O11	0.2766(6)	-0.0128(4)	0.4235(3)	0.0419(12)
N11	0.1018(7)	-0.1437(6)	0.4087(4)	0.0399(15)
C11	0.2388(9)	-0.0947(7)	0.3881(5)	0.0375(17)
C12	0.3531(10)	-0.1479(7)	0.3113(5)	0.048(2)
C13	0.2731(10)	-0.2536(8)	0.3022(6)	0.050(2)
C14	0.0932(10)	-0.2196(7)	0.3415(6)	0.048(2)
N12	-0.1793(7)	0.0193(5)	0.3776(4)	0.0389(15)
O12	-0.0215(6)	0.1624(5)	0.3844(4)	0.0473(14)
C15	-0.1273(9)	0.1223(7)	0.3450(5)	0.0426(18)
C16	-0.1902(11)	0.1831(8)	0.2556(6)	0.055(2)
C17	-0.2475(11)	0.0835(8)	0.2218(6)	0.058(2)
C18	-0.2908(10)	-0.0021(8)	0.3145(5)	0.0477(19)
C21	0.2094(9)	0.2156(6)	0.4802(5)	0.0395(18)
C22	0.3811(9)	0.1937(7)	0.4846(5)	0.0416(18)
C23	0.4670(10)	0.2907(8)	0.4676(5)	0.049(2)
C24	0.3866(11)	0.4058(8)	0.4455(5)	0.053(2)
C25	0.2160(11)	0.4265(8)	0.4404(6)	0.052(2)
C26	0.1282(10)	0.3307(7)	0.4564(5)	0.047(2)
Rh2	0.07885(7)	0.56995(6)	1.02788(4)	0.04201(19)
N31	-0.2032(7)	0.5696(6)	0.8933(4)	0.0420(15)
O31	-0.0711(7)	0.7019(5)	0.9434(4)	0.0507(14)
C31	-0.1736(9)	0.6760(8)	0.8937(5)	0.0454(19)
C32	-0.2628(11)	0.7738(9)	0.8228(6)	0.064(3)
C33	-0.3643(16)	0.7029(11)	0.7853(8)	0.093(4)
C34	-0.3118(13)	0.5751(10)	0.8202(6)	0.071(3)
N32	0.0949(8)	0.4189(6)	0.8621(4)	0.0438(16)
O32	0.2479(6)	0.5400(5)	0.9113(3)	0.0459(13)
C35	0.2196(9)	0.4787(6)	0.8544(5)	0.0368(17)
C36	0.3319(10)	0.4667(8)	0.7640(5)	0.052(2)
C37	0.2375(13)	0.4084(11)	0.7120(7)	0.079(3)
C38	0.0997(12)	0.3623(9)	0.7816(6)	0.067(3)
C41	0.1980(10)	0.7063(7)	1.0355(5)	0.0407(18)
C42	0.1087(11)	0.8139(8)	1.0488(5)	0.052(2)
C43	0.1910(12)	0.9031(8)	1.0594(6)	0.058(2)
C44	0.3619(11)	0.8846(9)	1.0551(6)	0.058(2)
C45	0.4501(11)	0.7750(8)	1.0405(6)	0.055(2)
C46	0.3688(10)	0.6829(8)	1.0299(5)	0.047(2)

$U_{\text{eq}}$  is defined as one third of the trace of the orthogonalized  $U_{ij}$  tensor.



**Table 2-16.** Anisotropic atomic displacement parameters ( $\text{\AA}^2$ ) for **13**.

Atom	$U_{11}$	$U_{22}$	$U_{33}$	$U_{23}$	$U_{13}$	$U_{12}$
Rh1	0.0295(3)	0.0410(4)	0.0488(3)	-0.0066(3)	-0.0008(3)	-0.0193(3)
O11	0.036(3)	0.038(3)	0.057(3)	-0.013(2)	0.005(2)	-0.021(2)
N11	0.032(3)	0.041(3)	0.049(3)	-0.011(3)	0.004(3)	-0.015(3)
C11	0.032(4)	0.034(4)	0.048(4)	-0.007(3)	-0.005(3)	-0.008(3)
C12	0.040(4)	0.053(5)	0.052(4)	-0.012(4)	0.003(3)	-0.013(4)
C13	0.044(4)	0.049(5)	0.057(4)	-0.010(4)	0.004(4)	-0.014(4)
C14	0.052(4)	0.041(4)	0.057(4)	-0.017(3)	0.002(4)	-0.023(4)
N12	0.033(3)	0.040(3)	0.047(3)	-0.002(3)	-0.004(3)	-0.019(3)
O12	0.043(3)	0.049(3)	0.053(3)	0.004(2)	-0.007(2)	-0.028(3)
C15	0.040(4)	0.040(4)	0.049(4)	-0.001(3)	-0.002(3)	-0.019(3)
C16	0.047(4)	0.058(5)	0.061(4)	0.006(4)	-0.011(4)	-0.024(4)
C17	0.045(4)	0.072(5)	0.053(4)	-0.003(4)	-0.007(4)	-0.010(4)
C18	0.042(4)	0.049(4)	0.058(4)	-0.011(4)	-0.016(3)	-0.016(4)
C21	0.037(4)	0.029(4)	0.055(4)	-0.007(3)	0.008(3)	-0.022(3)
C22	0.029(4)	0.045(4)	0.054(4)	-0.004(3)	-0.004(3)	-0.021(3)
C23	0.044(4)	0.055(5)	0.052(4)	-0.005(4)	-0.004(3)	-0.025(4)
C24	0.056(5)	0.058(5)	0.052(4)	-0.007(4)	-0.002(4)	-0.037(4)
C25	0.060(5)	0.042(4)	0.056(4)	-0.006(3)	-0.001(4)	-0.019(4)
C26	0.043(4)	0.041(4)	0.057(4)	-0.002(3)	-0.003(3)	-0.022(3)
Rh2	0.0340(4)	0.0543(4)	0.0428(3)	-0.0077(3)	-0.0005(3)	-0.0244(3)
N31	0.035(3)	0.055(4)	0.041(3)	-0.005(3)	-0.002(3)	-0.026(3)
O31	0.057(3)	0.040(3)	0.058(3)	0.004(2)	-0.014(3)	-0.022(3)
C31	0.033(4)	0.057(5)	0.045(4)	-0.004(3)	0.003(3)	-0.016(4)
C32	0.043(5)	0.080(6)	0.062(5)	0.003(4)	0.002(4)	-0.013(4)
C33	0.092(7)	0.102(7)	0.088(6)	-0.033(6)	-0.029(5)	0.009(6)
C34	0.065(5)	0.093(6)	0.063(5)	0.001(5)	-0.024(4)	-0.036(5)
N32	0.033(3)	0.058(4)	0.046(3)	-0.017(3)	0.003(3)	-0.020(3)
O32	0.036(3)	0.059(3)	0.050(3)	-0.015(2)	0.004(2)	-0.027(2)
C35	0.033(4)	0.034(4)	0.044(4)	-0.005(3)	0.000(3)	-0.013(3)
C36	0.046(4)	0.057(5)	0.052(4)	-0.008(4)	0.008(4)	-0.021(4)
C37	0.068(6)	0.109(7)	0.071(5)	-0.035(5)	0.011(5)	-0.036(5)
C38	0.074(6)	0.079(6)	0.061(5)	-0.032(4)	0.007(4)	-0.036(5)
C41	0.048(4)	0.035(4)	0.039(4)	0.002(3)	-0.001(3)	-0.020(3)
C42	0.053(5)	0.052(5)	0.055(4)	-0.005(4)	-0.008(4)	-0.020(4)
C43	0.069(5)	0.055(5)	0.051(4)	-0.006(4)	-0.007(4)	-0.019(4)
C44	0.060(5)	0.062(5)	0.059(4)	-0.008(4)	-0.003(4)	-0.037(4)
C45	0.050(4)	0.067(5)	0.057(4)	-0.013(4)	0.003(4)	-0.036(4)
C46	0.040(4)	0.055(5)	0.050(4)	-0.008(3)	0.005(3)	-0.027(4)

The anisotropic atomic displacement factor exponent takes the form:  $-2\pi^2 [h^2a^2U_{11} + \dots + 2hka^*b^*U_{12}]$ .

**Table 2-17.** Hydrogen-atom coordinates/isotropic atomic displacement parameters ( $\text{\AA}^2$ ) for **13**.

Atom	$x/a$	$y/b$	$z/c$	$U_{\text{iso}}$
H121	0.4650	-0.1749	0.3294	0.058
H122	0.3576	-0.0898	0.2524	0.058
H131	0.3247	-0.3284	0.3389	0.060
H132	0.2813	-0.2624	0.2366	0.060
H141	0.0266	-0.1756	0.2916	0.057
H142	0.0454	-0.2910	0.3726	0.057
H161	-0.1030	0.2161	0.2110	0.066
H162	-0.2819	0.2476	0.2651	0.066
H171	-0.1596	0.0437	0.1814	0.069
H172	-0.3444	0.1139	0.1876	0.069
H181	-0.4067	0.0178	0.3389	0.057
H182	-0.2689	-0.0856	0.3059	0.057
H22	0.4371	0.1150	0.4988	0.050
H23	0.5813	0.2768	0.4714	0.059
H24	0.4456	0.4703	0.4339	0.063
H25	0.1604	0.5054	0.4261	0.062
H26	0.0144	0.3448	0.4509	0.056
H321	-0.3324	0.8363	0.8532	0.077
H322	-0.1849	0.8102	0.7734	0.077
H331	-0.4815	0.7256	0.8059	0.111
H332	-0.3490	0.7194	0.7166	0.111
H341	-0.2517	0.5358	0.7694	0.085
H342	-0.4075	0.5357	0.8468	0.085
H361	0.3519	0.5453	0.7285	0.062
H362	0.4379	0.4168	0.7771	0.062
H371	0.3094	0.3422	0.6872	0.095
H372	0.1921	0.4663	0.6597	0.095
H381	-0.0056	0.3846	0.7547	0.081
H382	0.1228	0.2750	0.7996	0.081
H42	-0.0068	0.8271	1.0507	0.063
H43	0.1305	0.9773	1.0697	0.069
H44	0.4171	0.9458	1.0620	0.069
H45	0.5658	0.7620	1.0377	0.066
H46	0.4278	0.6084	1.0195	0.056

**Table 2-18.** Bond lengths (Å) and angles (°) for **13**.

Rh1-C21	1.982(6)	Rh1-N12i	1.984(6)	Rh1-N11i	2.021(6)
Rh1-O11	2.075(5)	Rh1-O12	2.116(5)	Rh1-Rh1i	2.5702(11)
O11-C11	1.274(9)	N11-C11	1.332(9)	N11-C14	1.465(9)
N11-Rh1i	2.021(6)	C11-C12	1.521(10)	C12-C13	1.530(11)
C13-C14	1.532(11)	N12-C15	1.315(9)	N12-C18	1.482(9)
N12-Rh1i	1.984(6)	O12-C15	1.313(9)	C15-C16	1.473(11)
C16-C17	1.517(12)	C17-C18	1.547(11)	C21-C26	1.378(11)
C21-C22	1.409(10)	C22-C23	1.397(10)	C23-C24	1.372(12)
C24-C25	1.402(12)	C25-C26	1.398(11)		
Rh2-N31ii	1.993(7)	Rh2-N32ii	2.012(6)	Rh2-C41	2.037(7)
Rh2-O31	2.093(6)	Rh2-O32	2.095(5)	Rh2-Rh2ii	2.5738(12)
N31-C31	1.299(10)	N31-C34	1.482(11)	N31-Rh2ii	1.993(7)
O31-C31	1.306(10)	C31-C32	1.529(12)	C32-C33	1.503(15)
C33-C34	1.467(15)	N32-C35	1.325(9)	N32-C38	1.456(10)
N32-Rh2ii	2.012(6)	O32-C35	1.271(9)	C35-C36	1.522(10)
C36-C37	1.492(13)	C37-C38	1.515(12)	C41-C42	1.362(11)
C41-C46	1.387(11)	C42-C43	1.382(12)	C43-C44	1.389(12)
C44-C45	1.384(13)	C45-C46	1.405(11)		
C21-Rh1-N12i	102.4(3)	C21-Rh1-N11i	97.3(3)	N12i-Rh1-N11i	86.6(3)
C21-Rh1-O11	89.8(2)	N12i-Rh1-O11	91.3(2)	N11i-Rh1-O11	172.9(2)
C21-Rh1-O12	84.3(3)	N12i-Rh1-O12	173.2(2)	N11i-Rh1-O12	92.3(2)
O11-Rh1-O12	89.1(2)	C21-Rh1-Rh1i	163.2(2)	N12i-Rh1-Rh1i	94.27(17)
N11i-Rh1-Rh1i	85.69(17)	O11-Rh1-Rh1i	87.76(13)	O12-Rh1-Rh1i	78.98(14)
C11-O11-Rh1	117.0(4)	C11-N11-C14	110.7(6)	C11-N11-Rh1i	121.0(5)
C14-N11-Rh1i	125.5(5)	O11-C11-N11	127.8(6)	O11-C11-C12	121.4(6)
N11-C11-C12	110.9(6)	C11-C12-C13	103.0(6)	C12-C13-C14	103.2(6)
N11-C14-C13	104.2(6)	C15-N12-C18	110.1(6)	C15-N12-Rh1i	116.4(5)
C18-N12-Rh1i	133.5(5)	C15-O12-Rh1	126.8(5)	O12-C15-N12	123.6(7)
O12-C15-C16	123.7(7)	N12-C15-C16	112.6(7)	C15-C16-C17	103.0(7)
C16-C17-C18	102.5(7)	N12-C18-C17	102.9(6)	C26-C21-C22	120.4(6)
C26-C21-Rh1	121.5(6)	C22-C21-Rh1	118.1(5)	C23-C22-C21	119.1(8)
C24-C23-C22	120.8(8)	C23-C24-C25	119.6(8)	C26-C25-C24	120.4(8)
C21-C26-C25	119.6(8)	N31ii-Rh2-N32ii	88.3(3)	N31ii-Rh2-C41	102.4(3)
N32ii-Rh2-C41	99.9(3)	N31ii-Rh2-O31	172.9(2)	N32ii-Rh2-O31	90.0(2)
C41-Rh2-O31	84.7(3)	N31ii-Rh2-O32	89.8(2)	N32ii-Rh2-O32	172.9(2)
C41-Rh2-O32	87.2(2)	O31-Rh2-O32	91.0(2)	N31ii-Rh2-Rh2ii	90.61(18)
N32ii-Rh2-Rh2ii	89.32(18)	C41-Rh2-Rh2ii	164.2(2)	O31-Rh2-Rh2ii	82.43(15)
O32-Rh2-Rh2ii	83.87(14)	C31-N31-C34	110.0(7)	C31-N31-Rh2ii	118.5(5)
C34-N31-Rh2ii	130.9(6)	C31-O31-Rh2	122.4(5)	N31-C31-O31	126.0(8)
N31-C31-C32	113.4(8)	O31-C31-C32	120.5(8)	C33-C32-C31	101.0(8)
C34-C33-C32	108.8(9)	C33-C34-N31	105.7(9)	C35-N32-C38	112.0(6)
C35-N32-Rh2ii	118.0(5)	C38-N32-Rh2ii	129.7(5)	C35-O32-Rh2	121.1(4)
O32-C35-N32	127.5(6)	O32-C35-C36	121.8(6)	N32-C35-C36	110.7(6)
C37-C36-C35	103.5(7)	C36-C37-C38	106.6(7)	N32-C38-C37	105.2(7)
C42-C41-C46	122.9(7)	C42-C41-Rh2	119.6(6)	C46-C41-Rh2	117.5(6)
C41-C42-C43	118.8(8)	C45-C44-C43	119.3(8)	C44-C45-C46	120.8(8)
C41-C46-C45	117.4(8)				
C21-Rh1-O11-C11	-156.0(6)	N12i-Rh1-O11-C11	101.6(5)	O12-Rh1-O11-C11	-71.7(5)
Rh1i-Rh1-O11-C11	7.3(5)	Rh1-O11-C11-N11	-11.3(10)	Rh1-O11-C11-C12	167.5(5)
C14-N11-C11-O11	170.2(7)	Rh1i-N11-C11-O11	8.2(11)	C14-N11-C11-C12	-8.6(9)
Rh1i-N11-C11-C12	-170.6(5)	O11-C11-C12-C13	171.2(7)	N11-C11-C12-C13	-9.8(9)
C11-C12-C13-C14	22.9(8)	C11-N11-C14-C13	23.5(9)	Rh1i-N11-C14-C13	-175.5(5)
C12-C13-C14-N11	-28.1(8)	C21-Rh1-O12-C15	177.2(6)	N11i-Rh1-O12-C15	-85.7(6)
O11-Rh1-O12-C15	87.4(6)	Rh1i-Rh1-O12-C15	-0.5(6)	Rh1-O12-C15-N12	0.0(11)

Rh1-O12-C15-C16	-174.8(6)	C18-N12-C15-O12	-177.1(7)	Rh1i-N12-C15-O12	0.7(10)
C18-N12-C15-C16	-1.7(9)	Rh1i-N12-C15-C16	176.1(5)	O12-C15-C16-C17	158.3(8)
N12-C15-C16-C17	-17.1(9)	C15-C16-C17-C18	27.3(8)	C15-N12-C18-C17	19.4(9)
Rh1i-N12-C18-C17	-157.9(6)	C16-C17-C18-N12	-28.4(8)	N12i-Rh1-C21-C26	-134.4(6)
N11i-Rh1-C21-C26	-46.3(7)	O11-Rh1-C21-C26	134.4(6)	O12-Rh1-C21-C26	45.2(6)
Rh1i-Rh1-C21-C26	52.9(11)	N12i-Rh1-C21-C22	46.9(6)	N11i-Rh1-C21-C22	135.0(6)
O11-Rh1-C21-C22	-44.3(6)	O12-Rh1-C21-C22	-133.5(6)	Rh1i-Rh1-C21-C22	-125.8(7)
C26-C21-C22-C23	2.2(11)	Rh1-C21-C22-C23	-179.1(6)	C21-C22-C23-C24	-1.0(12)
C22-C23-C24-C25	0.3(12)	C23-C24-C25-C26	-0.9(12)	C22-C21-C26-C25	-2.7(12)
Rh1-C21-C26-C25	178.6(6)	C24-C25-C26-C21	2.0(12)	N32ii-Rh2-O31-C31	-92.4(6)
C41-Rh2-O31-C31	167.6(6)	O32-Rh2-O31-C31	80.6(6)	Rh2ii-Rh2-O31-C31	-3.1(5)
C34-N31-C31-O31	-173.5(7)	Rh2ii-N31-C31-O31	-1.8(10)	C34-N31-C31-C32	2.1(9)
Rh2ii-N31-C31-C32	173.8(5)	Rh2-O31-C31-N31	3.9(10)	Rh2-O31-C31-C32	-171.5(5)
N31-C31-C32-C33	4.6(10)	O31-C31-C32-C33	-179.5(8)	C31-C32-C33-C34	-9.4(11)
C32-C33-C34-N31	11.0(12)	C31-N31-C34-C33	-8.2(10)	Rh2ii-N31-C34-C33	-178.5(7)
N31ii-Rh2-O32-C35	94.9(6)	C41-Rh2-O32-C35	-162.7(6)	O31-Rh2-O32-C35	-78.0(6)
Rh2ii-Rh2-O32-C35	4.3(6)	Rh2-O32-C35-N32	-5.8(11)	Rh2-O32-C35-C36	173.6(5)
C38-N32-C35-O32	178.0(8)	Rh2ii-N32-C35-O32	3.3(11)	C38-N32-C35-C36	-1.4(10)
Rh2ii-N32-C35-C36	-176.2(5)	O32-C35-C36-C37	-169.8(8)	N32-C35-C36-C37	9.6(10)
C35-C36-C37-C38	-13.5(11)	C35-N32-C38-C37	-7.3(11)	Rh2ii-N32-C38-C37	166.6(7)
C36-C37-C38-N32	13.1(11)	N31ii-Rh2-C41-C42	-136.4(6)	N32ii-Rh2-C41-C42	-45.9(6)
O31-Rh2-C41-C42	43.2(6)	O32-Rh2-C41-C42	134.4(6)	Rh2ii-Rh2-C41-C42	78.9(10)
N31ii-Rh2-C41-C46	41.5(6)	N32ii-Rh2-C41-C46	132.0(6)	O31-Rh2-C41-C46	-139.0(6)
O32-Rh2-C41-C46	-47.7(6)	Rh2ii-Rh2-C41-C46	-103.2(9)	C46-C41-C42-C43	-1.5(12)
Rh2-C41-C42-C43	176.2(6)	C41-C42-C43-C44	1.1(12)	C42-C43-C44-C45	-0.4(13)
C43-C44-C45-C46	0.1(13)	C42-C41-C46-C45	1.3(11)	Rh2-C41-C46-C45	-176.5(6)
C44-C45-C46-C41	-0.5(12)				

---

Symmetry transformation codes: (i) -x,-y,-z+1; (ii) -x,-y+1,-z+2

XRD Crystallographer's<sup>126</sup> Report (**16**•2CHCl<sub>3</sub>).

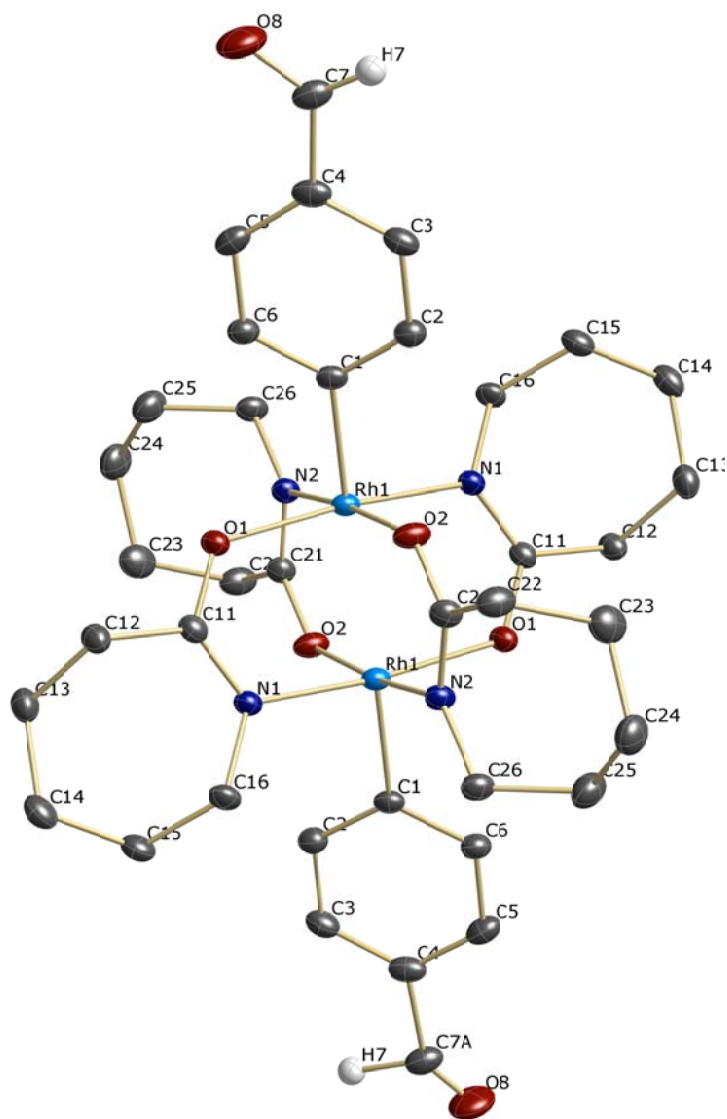


**Figure 2-17.** A view of **16** showing the numbering scheme employed. Anisotropic atomic displacement ellipsoids for the non-hydrogen atoms are shown at the 30% probability level. Solvent and aliphatic hydrogen atoms are omitted for clarity.

---

<sup>126</sup> See ref. 109.

A green prism of  $C_{38}H_{50}N_4O_6Rh_2 \cdot 2CHCl_3$ , approximate dimensions  $0.07 \times 0.13 \times 0.16 \text{ mm}^3$ , was used for the X-ray crystallographic analysis. The X-ray intensity data were measured at 220(2) K on a three-circle diffractometer system equipped with Bruker Smart1000 CCD area detector using a graphite monochromator and a Mo  $K\alpha$  fine-focus sealed tube ( $\lambda = 0.71073 \text{ \AA}$ ) operated at 50 kV and 30 mA. The detector was placed at a distance of 4.950 cm from the crystal.

A total of 1889 frames were collected with a scan width of  $0.5^\circ$  in  $\omega$  and an exposure time of 38 sec/frame using SMART.<sup>127</sup> The total data collection time was 24.1 hours. The frames were integrated with SAINT software<sup>128</sup> package using a narrow-frame integration algorithm. The integration of the data using a Triclinic unit cell yielded a total of 12762 reflections to a maximum  $\theta$  angle of  $27.50^\circ$ , of which 4988 were independent (completeness = 98.4%,  $R_{\text{int}} = 2.74\%$ ,  $R_{\text{sig}} = 3.20\%$ ) and 4412 were greater than  $2\sigma(I)$ . The final cell dimensions of  $a = 10.5426(14) \text{ \AA}$ ,  $b = 10.8903(15) \text{ \AA}$ ,  $c = 11.9923(16) \text{ \AA}$ ,  $\alpha = 100.031(2)^\circ$ ,  $\beta = 108.350(2)^\circ$ ,  $\gamma = 115.113(2)^\circ$ , and  $V = 1104.8(3) \text{ \AA}^3$  are based upon the refinement of the XYZ-centroids of 6760 reflections with  $2.2 < \theta < 28.8^\circ$  using SAINT. Analysis of the data showed 0 % decay during data collection. Data were corrected for absorption effects with the Semi-empirical from equivalents method using SADABS.<sup>129</sup> The minimum and maximum transmission coefficients were 0.835 and 0.922.

The structure was solved and refined using the SHELXS-97 and SHELXL-97 software<sup>130</sup> in the space group  $P1$  with  $Z = 1$  for the formula unit  $C_{38}H_{50}N_4O_6Rh_2 \cdot 2CHCl_3$ . The final anisotropic full-matrix least-squares

---

<sup>127</sup> See ref. 110.

<sup>128</sup> See ref. 110.

<sup>129</sup> See ref. 112.

<sup>130</sup> See ref. 111.

refinement on  $F^2$  with 301 variables converged at  $R_1 = 2.55\%$  for the observed data and  $wR_2 = 5.98\%$  for all data. The goodness-of-fit was 1.000. The largest peak on the final difference map was  $1.030\text{e}/\text{\AA}^3$  and the largest hole was  $-0.366\text{e}/\text{\AA}^3$ . On the basis of the final model, the calculated density was  $1.658\text{ g/cm}^3$  and  $F(000)$ , 560 e.

**Table 2-19.** Crystal data and structure refinement for **16**.

Empirical formula	$\text{C}_{38}\text{H}_{50}\text{N}_4\text{O}_6\text{Rh}_2 \cdot 2\text{CHCl}_3$
Formula weight (amu)	1103.38
Temperature (K)	220(2)
Wavelength ( $\text{\AA}$ )	0.71073 (Mo $K\alpha$ )
Crystal size	$0.16 \times 0.13 \times 0.07\text{ mm}^3$
Crystal habit	green prism
Crystal system	Triclinic
Space group	P1
Unit cell dimensions ( $\text{\AA} / ^\circ$ )	$a = 10.5426(14)$ $\alpha = 100.031(2)$ $b = 10.8903(15)$ $\beta = 108.350(2)$ $c = 11.9923(16)$ $\gamma = 115.113(2)$
Volume ( $\text{\AA}^3$ )	1104.8(3)
Z	1
Density, $\rho_{\text{calc}}$ ( $\text{g/cm}^3$ )	1.658
Absorption coefficient, $\mu$ ( $\text{mm}^{-1}$ )	1.160
$\theta$ Range ( $^\circ$ )	2.81 to 27.50
Reflections collected	12762
Independent reflections	4988
Observed reflection, $I > 2\sigma(I)$	4412
Max. and min. transmission <sup>a</sup>	0.922 and 0.835
Goodness-of-fit on $F^2$	0.999
Max $[\Delta/\sigma]$	0.001
Final R indices: <sup>b</sup>	
$R_1, I > 2\sigma(I)$	0.0255
$wR_2, \text{all data}$	0.0598
$R_{\text{int}}$	0.0274
$R_{\text{sig}}$	0.0320
Min., max. peaks ( $\text{e}/\text{\AA}^3$ )	1.030 and -0.366

<sup>a</sup>Absorption correction was performed using the semi-empirical from equivalents method (SADABS). <sup>b</sup>Function minimized was  $\sum w(F_o^2 - F_c^2)^2$  where  $R_1 = \sum ||F_o| - |F_c|| / \sum |F_o|$ ,  $wR_2 = [\sum w(F_o^2 - F_c^2)^2 / \sum w(F_o^2)^2]^{1/2}$  with a weighting scheme  $w = 1/[\sigma^2(F_o^2) + (0.015P)^2 + 27.8P]$ ,  $P = [\max(F_o^2, 0) + 2F_o^2]/3$ .

**Table 2-20.** Atomic coordinates and equivalent isotropic atomic displacement parameters ( $\text{\AA}^2$ ) for **16**.

Atom	<i>x/a</i>	<i>y/b</i>	<i>z/c</i>	$U_{\text{eq}}$
Rh1	0.411781(19)	0.529702(18)	0.533838(14)	0.02135(5)
C1	0.3304(2)	0.5717(2)	0.65483(18)	0.0241(4)
C2	0.2592(3)	0.4654(2)	0.7009(2)	0.0281(5)
C3	0.2011(3)	0.4942(3)	0.7841(2)	0.0313(5)
C4	0.2168(3)	0.6297(3)	0.8255(2)	0.0323(5)
C5	0.2933(3)	0.7372(3)	0.7837(2)	0.0330(5)
C6	0.3498(3)	0.7086(2)	0.6981(2)	0.0286(5)
C7	0.152(4)	0.644(3)	0.916(3)	0.034(3)
O8	0.1522(6)	0.7530(5)	0.9571(5)	0.0598(16)
C7A	0.152(4)	0.672(4)	0.910(3)	0.034(3)
O8A	0.0747(5)	0.5874(6)	0.9467(4)	0.0472(14)
N1	0.2289(2)	0.32706(19)	0.42244(16)	0.0233(4)
O1	0.39140(17)	0.26605(16)	0.36935(14)	0.0268(3)
C11	0.2551(2)	0.2362(2)	0.35966(19)	0.0243(4)
C12	0.1253(3)	0.0856(2)	0.2689(2)	0.0290(5)
C13	0.0299(3)	-0.0108(2)	0.3247(2)	0.0338(5)
C14	-0.0955(3)	0.0180(3)	0.3360(2)	0.0351(5)
C15	-0.0305(3)	0.1714(3)	0.4239(2)	0.0320(5)
C16	0.0674(2)	0.2932(2)	0.3879(2)	0.0275(4)
N2	0.3358(2)	0.60315(19)	0.40070(16)	0.0239(4)
O2	0.49275(19)	0.54894(18)	0.33477(14)	0.0303(3)
C21	0.3982(3)	0.5971(2)	0.32298(19)	0.0258(4)
C22	0.3672(3)	0.6492(3)	0.2141(2)	0.0348(5)
C23	0.4293(3)	0.8128(3)	0.2551(3)	0.0420(6)
C24	0.3239(3)	0.8553(3)	0.2924(3)	0.0421(6)
C25	0.3007(3)	0.8171(3)	0.4038(2)	0.0397(6)
C26	0.2271(3)	0.6559(2)	0.3834(2)	0.0281(5)
C10	0.3050(3)	0.2456(3)	0.0629(2)	0.0386(6)
Cl1	0.26401(9)	0.06585(7)	0.03085(6)	0.04794(16)
Cl2	0.13524(9)	0.25403(8)	0.03350(7)	0.05087(17)
Cl3	0.39307(10)	0.32250(9)	-0.02863(9)	0.0628(2)

$U_{\text{eq}}$  is defined as one third of the trace of the orthogonalized  $U_{ij}$  tensor.

**Table 2-21.** Site occupancy factors that deviate from unity for **16**.

Atom	sof	Atom	sof
C7 – O8	0.526(6)	C7A – O8A	0.474(6)



**Table 2-22.** Anisotropic atomic displacement parameters ( $\text{\AA}^2$ ) for **16**.

Atom	$U_{11}$	$U_{22}$	$U_{33}$	$U_{23}$	$U_{13}$	$U_{12}$
Rh1	0.02124(9)	0.02658(9)	0.02260(8)	0.01090(6)	0.01214(6)	0.01480(7)
C1	0.0204(10)	0.0329(11)	0.0223(9)	0.0095(8)	0.0096(8)	0.0164(9)
C2	0.0291(12)	0.0315(12)	0.0287(11)	0.0117(9)	0.0147(9)	0.0176(10)
C3	0.0257(12)	0.0418(13)	0.0293(11)	0.0156(10)	0.0154(9)	0.0161(11)
C4	0.0266(12)	0.0494(14)	0.0246(10)	0.0116(10)	0.0116(9)	0.0227(11)
C5	0.0341(13)	0.0386(13)	0.0313(11)	0.0080(10)	0.0140(10)	0.0246(11)
C6	0.0282(12)	0.0327(12)	0.0322(11)	0.0137(9)	0.0170(9)	0.0182(10)
C7	0.0392(16)	0.050(9)	0.027(3)	0.015(4)	0.0157(18)	0.032(5)
O8	0.085(4)	0.069(3)	0.059(3)	0.024(2)	0.052(3)	0.052(3)
C7A	0.0392(16)	0.050(9)	0.027(3)	0.015(4)	0.0157(18)	0.032(5)
O8A	0.046(3)	0.073(3)	0.039(2)	0.023(2)	0.029(2)	0.034(3)
N1	0.0205(9)	0.0251(9)	0.0259(8)	0.0106(7)	0.0115(7)	0.0116(8)
O1	0.0228(8)	0.0280(8)	0.0293(8)	0.0072(6)	0.0131(6)	0.0127(7)
C11	0.0237(11)	0.0275(11)	0.0251(10)	0.0132(8)	0.0128(8)	0.0130(9)
C12	0.0262(12)	0.0282(11)	0.0278(11)	0.0059(9)	0.0133(9)	0.0107(10)
C13	0.0354(13)	0.0257(11)	0.0339(12)	0.0097(9)	0.0155(10)	0.0106(10)
C14	0.0294(13)	0.0343(13)	0.0341(12)	0.0137(10)	0.0163(10)	0.0079(10)
C15	0.0265(12)	0.0377(13)	0.0350(12)	0.0150(10)	0.0189(10)	0.0145(10)
C16	0.0191(11)	0.0325(12)	0.0340(11)	0.0141(9)	0.0122(9)	0.0143(9)
N2	0.0232(9)	0.0290(9)	0.0261(9)	0.0133(7)	0.0124(7)	0.0162(8)
O2	0.0370(9)	0.0468(10)	0.0290(8)	0.0217(7)	0.0204(7)	0.0320(8)
C21	0.0251(11)	0.0311(11)	0.0261(10)	0.0134(9)	0.0116(9)	0.0168(10)
C22	0.0436(15)	0.0509(15)	0.0327(12)	0.0260(11)	0.0230(11)	0.0341(13)
C23	0.0436(16)	0.0494(16)	0.0463(15)	0.0322(13)	0.0246(13)	0.0254(13)
C24	0.0547(17)	0.0375(14)	0.0500(15)	0.0256(12)	0.0262(14)	0.0305(13)
C25	0.0531(17)	0.0386(14)	0.0450(14)	0.0203(12)	0.0272(13)	0.0318(13)
C26	0.0274(12)	0.0363(12)	0.0315(11)	0.0167(9)	0.0151(9)	0.0218(10)
C10	0.0353(14)	0.0365(13)	0.0344(13)	0.0096(10)	0.0119(11)	0.0141(11)
Cl1	0.0575(4)	0.0408(4)	0.0436(3)	0.0148(3)	0.0225(3)	0.0234(3)
Cl2	0.0454(4)	0.0595(4)	0.0543(4)	0.0239(3)	0.0242(3)	0.0291(4)
Cl3	0.0516(5)	0.0604(5)	0.0809(6)	0.0378(4)	0.0401(4)	0.0196(4)

The anisotropic atomic displacement factor exponent takes the form:  $-2\pi^2 [h^2 a^{*2} U_{11} + \dots + 2hka^* b^* U_{12}]$ .

**Table 2-23.** Hydrogen atom coordinates/isotropic atomic displacement parameters ( $\text{\AA}^2$ ) for **16**.

Atom	$x/a$	$y/b$	$z/c$	$U_{\text{iso}}$
H2	0.2510	0.3746	0.6754	0.022(6)
H3	0.1504	0.4217	0.8130	0.036(7)
H5	0.3071	0.8299	0.8135	0.037(7)
H6	0.4008	0.7815	0.6696	0.021(6)
H7	0.1101	0.5663	0.9432	0.026(16)
H7A	0.1721	0.7679	0.9344	0.026(16)
H12A	0.1704	0.0366	0.2331	0.037(7)
H12B	0.0546	0.0950	0.1996	0.042(7)
H13A	-0.0195	-0.1127	0.2718	0.032(6)
H13B	0.1005	0.0039	0.4084	0.039(7)
H14A	-0.1556	-0.0522	0.3669	0.045(8)
H14B	-0.1668	0.0025	0.2522	0.039(7)
H15A	0.0334	0.1833	0.5091	0.036(7)
H15B	-0.1177	0.1816	0.4262	0.040(7)
H16A	0.0151	0.2669	0.2966	0.034(7)
H16B	0.0703	0.3815	0.4278	0.027(6)
H22A	0.2547	0.5971	0.1613	0.033(7)
H22B	0.4155	0.6253	0.1627	0.048(8)
H23A	0.5323	0.8636	0.3268	0.036(7)
H23B	0.4418	0.8452	0.1860	0.046(8)
H24A	0.2220	0.8067	0.2198	0.039(7)
H24B	0.3684	0.9603	0.3133	0.047(8)
H25A	0.4021	0.8698	0.4775	0.044(8)
H25B	0.2349	0.8511	0.4229	0.057(9)
H26A	0.1806	0.6369	0.4421	0.029(6)
H26B	0.1430	0.6006	0.2978	0.029(6)
H10	0.3784	0.3024	0.1528	0.049(8)

**Table 2-24.** Bond lengths (Å) and angles (°) for **16**.

Rh1-C1	1.984(2)	Rh1-N2	2.0035(17)	Rh1-N1	2.0277(18)
Rh1-O1 <sup>i</sup>	2.0657(15)	Rh1-O2 <sup>i</sup>	2.1054(14)	Rh1-Rh1 <sup>i</sup>	2.5152(4)
C1-C6	1.392(3)	C1-C2	1.399(3)	C2-C3	1.382(3)
C3-C4	1.392(3)	C4-C5	1.390(3)	C4-C7	1.475(9)
C5-C6	1.392(3)	C7-O8	1.201(19)	N1-C11	1.314(3)
N1-C16	1.475(3)	O1-C11	1.292(3)	O1-Rh1 <sup>i</sup>	2.0657(15)
C11-C12	1.511(3)	C12-C13	1.528(3)	C13-C14	1.521(3)
C14-C15	1.527(3)	C15-C16	1.527(3)	N2-C21	1.306(3)
N2-C26	1.461(3)	O2-C21	1.292(3)	O2-Rh1 <sup>i</sup>	2.1054(14)
C21-C22	1.511(3)	C22-C23	1.532(4)	C23-C24	1.525(4)
C24-C25	1.527(3)	C25-C26	1.523(3)	C10-Cl3	1.752(3)
C10-Cl1	1.756(3)	C10-Cl2	1.757(3)		
C1-Rh1-N2	103.92(8)	C1-Rh1-N1	97.71(8)	N2-Rh1-N1	88.83(7)
C1-Rh1-O1 <sup>i</sup>	89.44(8)	N2-Rh1-O1 <sup>i</sup>	88.51(7)	N1-Rh1-O1 <sup>i</sup>	172.79(6)
C1-Rh1-O2 <sup>i</sup>	82.02(7)	N2-Rh1-O2 <sup>i</sup>	173.91(6)	N1-Rh1-O2 <sup>i</sup>	91.71(7)
O1#1-Rh1-O2 <sup>i</sup>	90.23(6)	C1-Rh1-Rh1 <sup>i</sup>	154.58(6)	N2-Rh1-Rh1 <sup>i</sup>	100.28(5)
N1-Rh1-Rh1 <sup>i</sup>	90.38(5)	O1#1-Rh1-Rh1 <sup>i</sup>	83.50(4)	O2#1-Rh1-Rh1 <sup>i</sup>	73.65(4)
C6-C1-C2	119.88(19)	C6-C1-Rh1	120.25(16)	C2-C1-Rh1	119.81(16)
C3-C2-C1	119.8(2)	C2-C3-C4	120.6(2)	C5-C4-C3	119.5(2)
C5-C4-C7	126.6(9)	C3-C4-C7	113.9(9)	C4-C5-C6	120.4(2)
C5-C6-C1	119.7(2)	O8-C7-C4	121.5(14)	C11-N1-C16	119.44(18)
C11-N1-Rh1	117.87(14)	C16-N1-Rh1	121.01(14)	C11-O1-Rh1 <sup>i</sup>	123.82(13)
O1-C11-N1	123.9(2)	O1-C11-C12	114.22(18)	N1-C11-C12	121.90(19)
C11-C12-C13	115.57(18)	C14-C13-C12	114.0(2)	C13-C14-C15	113.3(2)
C14-C15-C16	114.91(19)	N1-C16-C15	115.69(18)	C21-N2-C26	121.33(17)
C21-N2-Rh1	109.41(14)	C26-N2-Rh1	129.26(13)	C21-O2-Rh1 <sup>i</sup>	133.91(13)
O2-C21-N2	122.73(19)	O2-C21-C22	115.13(18)	N2-C21-C22	122.12(19)
C21-C22-C23	113.4(2)	C24-C23-C22	113.5(2)	C23-C24-C25	114.2(2)
C26-C25-C24	114.7(2)	N2-C26-C25	114.17(19)	Cl3-C10-Cl1	109.91(14)
Cl3-C10-Cl2	109.84(14)	Cl1-C10-Cl2	111.26(14)		
N2-Rh1-C1-C6	-48.44(19)	N1-Rh1-C1-C6	-139.15(17)	O1 <sup>i</sup> -Rh1-C1-C6	39.88(18)
O2 <sup>i</sup> -Rh1-C1-C6	130.20(18)	Rh1 <sup>i</sup> -Rh1-C1-C6	113.36(18)	N2-Rh1-C1-C2	134.31(17)
N1-Rh1-C1-C2	43.60(18)	O1 <sup>i</sup> -Rh1-C1-C2	-137.37(17)	O2 <sup>i</sup> -Rh1-C1-C2	-47.06(17)
Rh1 <sup>i</sup> -Rh1-C1-C2	-63.9(3)	C6-C1-C2-C3	3.4(3)	Rh1-C1-C2-C3	-179.30(16)
C1-C2-C3-C4	-1.9(3)	C2-C3-C4-C5	-0.8(3)	C2-C3-C4-C7	-178.5(15)
C2-C3-C4-C7A	176.5(19)	C3-C4-C5-C6	2.0(3)	C7-C4-C5-C6	179.4(16)
C7A-C4-C5-C6	-175.6(17)	C4-C5-C6-C1	-0.5(3)	C2-C1-C6-C5	-2.2(3)
Rh1-C1-C6-C5	-179.48(17)	C5-C4-C7-O8	5(4)	C3-C4-C7-O8	-177(2)
C7A-C4-C7-O8	-16(11)	C1-Rh1-N1-C11	-154.01(15)	N2-Rh1-N1-C11	102.10(15)
O2 <sup>i</sup> -Rh1-N1-C11	-71.83(15)	Rh1 <sup>i</sup> -Rh1-N1-C11	1.82(15)	C1-Rh1-N1-C16	40.83(16)

N2-Rh1-N1-C16	-63.06(15)	O2 <sup>i</sup> -Rh1-N1-C16	123.01(15)	Rh1 <sup>i</sup> -Rh1-N1-C16	-163.34(14)
Rh1 <sup>i</sup> -O1-C11-N1	-8.6(3)	Rh1 <sup>i</sup> -O1-C11-C12	171.42(13)	C16-N1-C11-O1	168.82(18)
Rh1-N1-C11-O1	3.4(3)	C16-N1-C11-C12	-11.2(3)	Rh1-N1-C11-C12	-176.65(15)
O1-C11-C12-C13	122.1(2)	N1-C11-C12-C13	-57.8(3)	C11-C12-C13-C14	81.2(3)
C12-C13-C14-C15	-62.4(3)	C13-C14-C15-C16	58.2(3)	C11-N1-C16-C15	72.6(3)
Rh1-N1-C16-C15	-122.43(17)	C14-C15-C16-N1	-79.1(3)	C1-Rh1-N2-C21	172.46(15)
N1-Rh1-N2-C21	-89.89(15)	O1 <sup>i</sup> -Rh1-N2-C21	83.41(15)	Rh1 <sup>i</sup> -Rh1-N2-C21	0.29(15)
C1-Rh1-N2-C26	-8.2(2)	N1-Rh1-N2-C26	89.42(19)	O1 <sup>i</sup> -Rh1-N2-C26	-97.28(18)
Rh1 <sup>i</sup> -Rh1-N2-C26	179.60(17)	Rh1 <sup>i</sup> -O2-C21-N2	-1.4(3)	Rh1 <sup>i</sup> -O2-C21-C22	177.33(16)
C26-N2-C21-O2	-178.9(2)	Rh1-N2-C21-O2	0.4(3)	C26-N2-C21-C22	2.5(3)
Rh1-N2-C21-C22	-178.17(18)	O2-C21-C22-C23	-114.0(2)	N2-C21-C22-C23	64.7(3)
C21-C22-C23-C24	-79.9(3)	C22-C23-C24-C25	61.2(3)	C23-C24-C25-C26	-60.3(3)
C21-N2-C26-C25	-67.8(3)	Rh1-N2-C26-C25	113.0(2)	C24-C25-C26-N2	80.0(3)

---

Symmetry transformation codes: (i) -x+1,-y+1,-z+1

XRD Crystallographer's<sup>131</sup> Report (**18**•4CHCl<sub>3</sub>).

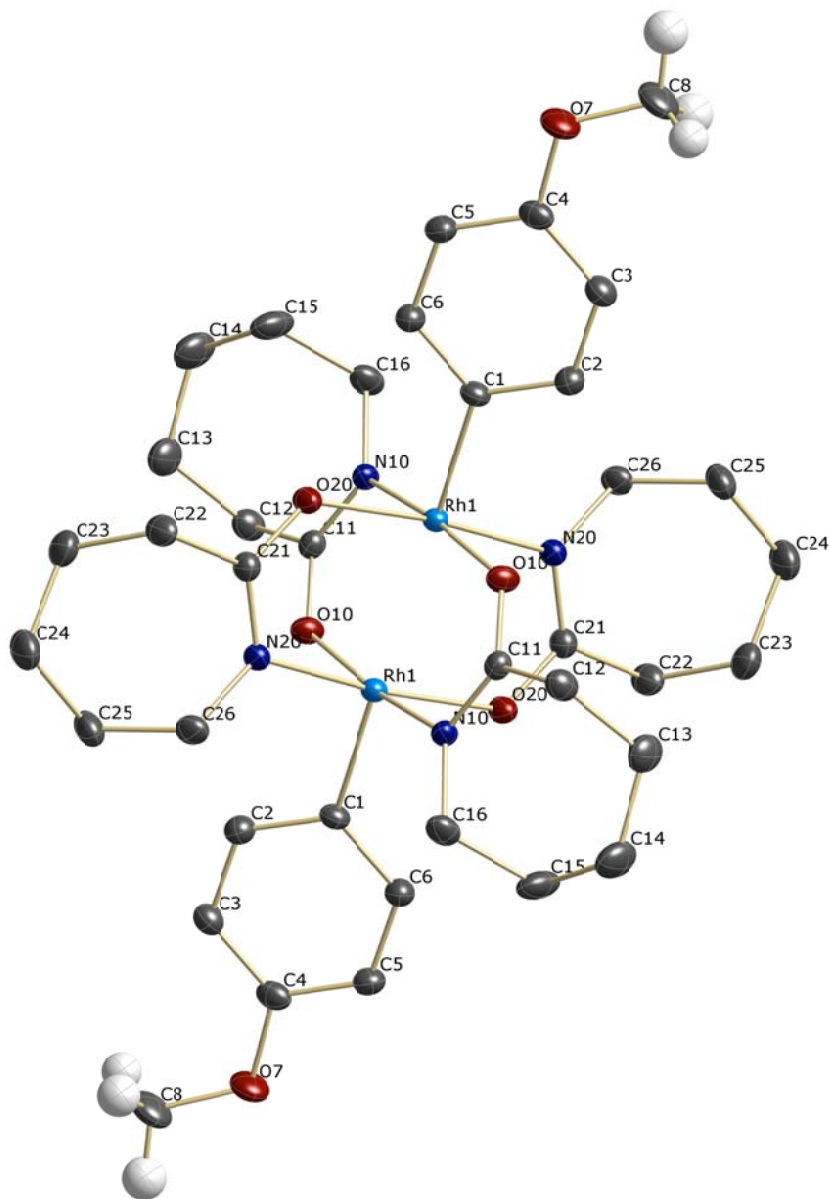


**Figure 2-18.** A view of **18** showing the numbering scheme employed. Anisotropic atomic displacement ellipsoids for the non-hydrogen atoms are shown at the 30% probability level. Solvent and hydrogen atoms are omitted for clarity.

---

<sup>131</sup> See ref. 109.

A green prism of  $C_{38}H_{54}N_4O_6Rh_2 \cdot 4CHCl_3$ , approximate dimensions  $0.14 \times 0.155 \times 0.165 \text{ mm}^3$ , was used for the X-ray crystallographic analysis. The X-ray intensity data were measured at 220(2) K on a three-circle diffractometer system equipped with Bruker Smart1000 CCD area detector using a graphite monochromator and a Mo  $K\alpha$  fine-focus sealed tube ( $\lambda = 0.71073 \text{ \AA}$ ) operated at 50 kV and 30 mA. The detector was placed at a distance of 4.950 cm from the crystal.

A total of 1824 frames were collected with a scan width of  $0.5^\circ$  in  $\omega$  and an exposure time of 38 sec/frame using SMART.<sup>132</sup> The total data collection time was 22.9 hours. The frames were integrated with SAINT software<sup>133</sup> package using a narrow-frame integration algorithm. The integration of the data using a Monoclinic unit cell yielded a total of 34996 reflections to a maximum  $\theta$  angle of  $27.50^\circ$ , of which 6342 were independent (completeness = 100.0%,  $R_{\text{int}} = 4.27\%$ ,  $R_{\text{sig}} = 2.77\%$ ) and 5370 were greater than  $2\sigma(I)$ . The final cell dimensions of  $a = 11.8973(11) \text{ \AA}$ ,  $b = 21.281(2) \text{ \AA}$ ,  $c = 10.9890(10) \text{ \AA}$ ,  $\alpha = 90^\circ$ ,  $\beta = 97.667(2)^\circ$ ,  $\gamma = 90^\circ$ , and  $V = 2757.4(4) \text{ \AA}^3$  are based upon the refinement of the XYZ-centroids of 6828 reflections with  $2.1 < \theta < 28.7^\circ$  using SAINT. Analysis of the data showed 0 % decay during data collection. Data were corrected for absorption effects with the semi-empirical from equivalents method using SADABS.<sup>134</sup> The minimum and maximum transmission coefficients were 0.773 and 0.842.

The structure was solved and refined using the SHELXS-97 and SHELXL-97 software<sup>135</sup> in the space group  $P2_1/c$  with  $Z = 2$  for the formula unit  $C_{38}H_{54}N_4O_6Rh_2 \cdot 4CHCl_3$ . The final anisotropic full-matrix least-squares

---

<sup>132</sup> See ref. 110.

<sup>133</sup> See ref. 110.

<sup>134</sup> See ref. 112.

<sup>135</sup> See ref. 111.

refinement on  $F^2$  with 355 variables converged at  $R_1 = 2.81\%$  for the observed data and  $wR_2 = 6.31\%$  for all data. The goodness-of-fit was 1.001. The largest peak on the final difference map was  $0.742\bar{e}/\text{\AA}^3$  and the largest hole was  $-0.487\bar{e}/\text{\AA}^3$ . On the basis of the final model, the calculated density was  $1.621\text{ g/cm}^3$  and  $F(000)$ ,  $1360\bar{e}$ .

**Table 2-25.** Crystal data and structure refinement for **18**.

Empirical formula	$C_{38}H_{54}N_4O_6Rh_2 \cdot 4CHCl_3$	
Formula weight (amu)	1346.14	
Temperature (K)	220(2)	
Wavelength ( $\text{\AA}$ )	0.71073 (Mo $K\alpha$ )	
Crystal size ( $\text{mm}^3$ )	$0.165 \times 0.155 \times 0.14$	
Crystal habit	green prism	
Crystal system	Monoclinic	
Space group	$P2_1/c$	
Unit cell dimensions ( $\text{\AA} / ^\circ$ )	$a = 11.8973(11)$	$\alpha = 90$
	$b = 21.281(2)$	$\beta = 97.667(2)$
	$c = 10.9890(10)$	$\gamma = 90$
Volume ( $\text{\AA}^3$ )	2757.4(4)	
Z	2	
Density, $\rho_{\text{calc}}$ ( $\text{g/cm}^3$ )	1.621	
Absorption coefficient, $\mu$ ( $\text{mm}^{-1}$ )	1.226	
$\theta$ Range ( $^\circ$ )	1.97 to 27.50	
Reflections collected	34996	
Independent reflections	6342	
Observed reflection, $I > 2\sigma(I)$	5370	
Max. and min. transmission <sup>a</sup>	0.842 and 0.773	
Goodness-of-fit on $F^2$	1.016	
Max $[\Delta/\sigma]$	0.002	
Final R indices: <sup>b</sup>		
$R_1$ , $I > 2\sigma(I)$	0.0281	
$wR_2$ , all data	0.0631	
$R_{\text{int}}$	0.0427	
$R_{\text{sig}}$	0.0277	
Min., max. peaks ( $\bar{e}/\text{\AA}^3$ )	0.742 and -0.487	

<sup>a</sup>Absorption correction was performed using the semi-empirical from equivalents method (SADABS). <sup>b</sup>Function minimized was  $\sum w(F_o^2 - F_c^2)^2$  where  $R_1 = \sum ||F_o| - |F_c|| / \sum |F_o|$ ,  $wR_2 = [\sum w(F_o^2 - F_c^2)^2 / \sum w(F_o^2)^2]^{1/2}$  with a weighting scheme  $w = 1/[\sigma^2(F_o^2) + (0.015P)^2 + 27.8P]$ ,  $P = [\max(F_o^2, 0) + 2F_o^2]/3$ .

**Table 2-26.** Atomic coordinates and equivalent isotropic atomic displacement parameters ( $\text{\AA}^2$ ) for **18**.

Atom	$x/a$	$y/b$	$z/c$	$U_{\text{eq}}$
Rh1	0.480557(13)	0.548274(7)	0.434915(14)	0.02139(5)
C1	0.38808(17)	0.61112(10)	0.32902(19)	0.0252(4)
C2	0.33955(19)	0.66153(10)	0.3831(2)	0.0301(5)
C3	0.2818(2)	0.70838(11)	0.3114(2)	0.0329(5)
C4	0.27020(19)	0.70365(10)	0.1845(2)	0.0319(5)
C5	0.3133(2)	0.65183(11)	0.1302(2)	0.0346(5)
C6	0.3716(2)	0.60553(11)	0.2020(2)	0.0310(5)
O7	0.21518(16)	0.74747(8)	0.10508(16)	0.0431(4)
C8	0.1909(3)	0.80654(12)	0.1546(3)	0.0555(8)
O10	0.34216(12)	0.54698(7)	0.53456(14)	0.0284(3)
N10	0.38086(15)	0.45816(8)	0.65030(16)	0.0248(4)
C11	0.31889(18)	0.50760(10)	0.61705(19)	0.0259(4)
C12	0.21456(19)	0.52323(11)	0.6762(2)	0.0330(5)
C13	0.2421(2)	0.54257(13)	0.8111(2)	0.0450(6)
C14	0.2646(3)	0.48711(15)	0.8986(3)	0.0548(8)
C15	0.3632(3)	0.44522(15)	0.8735(2)	0.0517(8)
C16	0.3498(2)	0.41571(11)	0.7453(2)	0.0369(5)
O20	0.40548(13)	0.48158(7)	0.31210(14)	0.0304(3)
N20	0.43551(15)	0.39504(8)	0.43640(15)	0.0242(4)
C21	0.39491(18)	0.42232(10)	0.33306(19)	0.0270(4)
C22	0.3319(2)	0.38590(11)	0.2270(2)	0.0366(5)
C23	0.4016(3)	0.33373(12)	0.1771(2)	0.0454(6)
C24	0.4077(3)	0.27329(12)	0.2516(3)	0.0494(7)
C25	0.4615(3)	0.28071(12)	0.3839(2)	0.0456(7)
C26	0.4055(2)	0.32923(10)	0.4584(2)	0.0327(5)
C31	0.1299(2)	0.52458(14)	0.3032(3)	0.0472(7)
Cl31	0.10037(7)	0.45572(4)	0.38152(8)	0.05713(19)
Cl32	0.05816(7)	0.58923(4)	0.35659(8)	0.0597(2)
Cl33	0.09162(8)	0.51558(5)	0.14512(8)	0.0762(3)
C41	0.0430(3)	0.20888(11)	0.4897(3)	0.0772(10)
Cl41	0.0750(6)	0.2712(3)	0.5917(8)	0.170(3)
Cl42	0.0390(3)	0.1409(3)	0.5863(4)	0.1110(16)
Cl43	0.1294(6)	0.2003(5)	0.3891(5)	0.182(3)
C41A	0.0430(3)	0.20888(11)	0.4897(3)	0.0772(10)
Cl44	0.1470(3)	0.1771(3)	0.4085(4)	0.1099(16)
Cl45	0.0953(4)	0.28662(18)	0.5302(5)	0.1071(15)
Cl46	0.0235(4)	0.1683(4)	0.6101(6)	0.178(3)

$U_{\text{eq}}$  is defined as one third of the trace of the orthogonalized  $U_{ij}$  tensor.

**Table 2-27.** Site occupancy factors that deviate from unity for **18**.

Atom	sof	Atom	sof
C41 – Cl43	0.503(9)	C41A – Cl46	0.497(9)



**Table 2-28.** Anisotropic atomic displacement parameters ( $\text{\AA}^2$ ) for **18**.

Atom	$U_{11}$	$U_{22}$	$U_{33}$	$U_{23}$	$U_{13}$	$U_{12}$
Rh1	0.02605(8)	0.01917(8)	0.01901(8)	0.00178(6)	0.00316(6)	0.00097(6)
C1	0.0282(10)	0.0213(10)	0.0255(10)	0.0050(8)	0.0010(8)	0.0010(8)
C2	0.0345(11)	0.0300(11)	0.0254(11)	0.0009(9)	0.0027(9)	0.0030(9)
C3	0.0366(12)	0.0261(11)	0.0358(12)	0.0013(9)	0.0036(10)	0.0052(9)
C4	0.0331(11)	0.0251(11)	0.0353(12)	0.0082(9)	-0.0030(9)	-0.0001(9)
C5	0.0455(13)	0.0319(12)	0.0251(11)	0.0041(9)	-0.0001(10)	0.0009(10)
C6	0.0395(12)	0.0272(11)	0.0258(11)	0.0012(9)	0.0021(9)	0.0038(9)
O7	0.0518(11)	0.0305(9)	0.0430(10)	0.0113(8)	-0.0076(8)	0.0082(8)
C8	0.070(2)	0.0300(14)	0.0622(19)	0.0095(13)	-0.0069(16)	0.0163(13)
O10	0.0279(7)	0.0297(8)	0.0290(8)	0.0085(6)	0.0086(6)	0.0040(6)
N10	0.0304(9)	0.0232(9)	0.0221(8)	0.0022(7)	0.0084(7)	0.0019(7)
C11	0.0272(10)	0.0271(11)	0.0236(10)	-0.0014(8)	0.0047(8)	-0.0018(8)
C12	0.0311(11)	0.0336(12)	0.0365(12)	0.0038(10)	0.0129(10)	0.0042(10)
C13	0.0519(15)	0.0474(16)	0.0399(14)	-0.0036(12)	0.0210(12)	0.0114(13)
C14	0.068(2)	0.067(2)	0.0352(15)	0.0057(13)	0.0254(14)	0.0173(16)
C15	0.0655(19)	0.0631(19)	0.0299(13)	0.0170(13)	0.0188(13)	0.0209(16)
C16	0.0435(13)	0.0309(12)	0.0398(13)	0.0102(10)	0.0179(11)	0.0041(10)
O20	0.0410(9)	0.0239(8)	0.0242(8)	0.0013(6)	-0.0041(7)	-0.0027(7)
N20	0.0291(9)	0.0203(8)	0.0231(9)	0.0001(7)	0.0033(7)	-0.0007(7)
C21	0.0307(11)	0.0238(11)	0.0260(11)	-0.0030(8)	0.0023(9)	0.0002(8)
C22	0.0471(14)	0.0290(12)	0.0301(12)	-0.0025(10)	-0.0083(10)	-0.0030(10)
C23	0.0678(18)	0.0374(14)	0.0301(13)	-0.0105(11)	0.0036(12)	-0.0022(13)
C24	0.0701(19)	0.0296(13)	0.0457(16)	-0.0126(11)	-0.0029(14)	0.0039(13)
C25	0.0646(18)	0.0245(12)	0.0444(15)	-0.0040(11)	-0.0045(13)	0.0047(12)
C26	0.0412(13)	0.0258(11)	0.0307(12)	0.0032(9)	0.0038(10)	-0.0083(9)
C31	0.0340(13)	0.0628(18)	0.0457(16)	-0.0002(13)	0.0086(12)	-0.0038(12)
Cl31	0.0552(4)	0.0572(4)	0.0605(5)	0.0030(4)	0.0133(3)	-0.0032(3)
Cl32	0.0551(4)	0.0545(4)	0.0694(5)	-0.0087(4)	0.0083(4)	-0.0026(3)
Cl33	0.0766(6)	0.1116(8)	0.0415(4)	-0.0042(4)	0.0113(4)	0.0029(5)
C41	0.0534(19)	0.078(2)	0.095(3)	0.009(2)	-0.0088(18)	0.0061(18)
Cl41	0.152(4)	0.128(4)	0.218(7)	-0.101(4)	-0.016(4)	0.031(3)
Cl42	0.0789(19)	0.117(3)	0.128(3)	0.052(2)	-0.0180(19)	0.0015(18)
Cl43	0.227(6)	0.204(6)	0.135(4)	-0.012(4)	0.092(4)	-0.052(5)
C41A	0.0534(19)	0.078(2)	0.095(3)	0.009(2)	-0.0088(18)	0.0061(18)
Cl44	0.088(2)	0.131(3)	0.107(2)	-0.051(2)	0.0000(18)	0.032(2)
Cl45	0.0910(19)	0.0773(17)	0.157(4)	-0.029(2)	0.031(2)	-0.0005(14)
Cl46	0.120(3)	0.196(5)	0.235(5)	0.132(5)	0.085(3)	0.050(3)

The anisotropic atomic displacement factor exponent takes the form:  $-2\pi^2 [h^2a^{*2}U_{11} + \dots + 2hka^*b^*U_{12}]$ .

**Table 2-29.** Hydrogen atom coordinates/isotropic atomic displacement parameters ( $\text{\AA}^2$ ) for **18**.

Atom	$x/a$	$y/b$	$z/c$	$U_{\text{iso}}$
H2	0.3457	0.6641	0.4692	0.034(7)
H3	0.2510	0.7429	0.3487	0.038(7)
H5	0.3030	0.6480	0.0442	0.039(7)
H6	0.4000	0.5703	0.1644	0.039(7)
H8A	0.1352	0.8013	0.2107	0.048(8)
H8B	0.1610	0.8346	0.0886	0.059(9)
H8C	0.2599	0.8242	0.1984	0.056(9)
H12A	0.1645	0.4865	0.6707	0.034(7)
H12B	0.1735	0.5576	0.6304	0.039(7)
H13A	0.3091	0.5698	0.8201	0.047(8)
H13B	0.1786	0.5671	0.8344	0.066(10)
H14A	0.1957	0.4614	0.8934	0.043(8)
H14B	0.2802	0.5032	0.9827	0.077(11)
H15A	0.3721	0.4115	0.9347	0.067(10)
H15B	0.4329	0.4702	0.8845	0.061(10)
H16A	0.3972	0.3780	0.7476	0.039(7)
H16B	0.2707	0.4026	0.7232	0.046(8)
H22A	0.3068	0.4153	0.1602	0.044(7)
H22B	0.2641	0.3672	0.2538	0.046(8)
H23A	0.3685	0.3243	0.0926	0.051(8)
H23B	0.4788	0.3492	0.1747	0.055(9)
H24A	0.3307	0.2568	0.2508	0.059(9)
H24B	0.4511	0.2421	0.2116	0.056(9)
H25A	0.5412	0.2924	0.3845	0.049(8)
H25B	0.4599	0.2399	0.4249	0.061(9)
H26A	0.3231	0.3247	0.4398	0.039(7)
H26B	0.4265	0.3199	0.5458	0.042(7)
H31	0.2125	0.5327	0.3193	0.047(8)
H41	-0.0341	0.2157	0.4454	0.116
H41A	-0.0296	0.2122	0.4343	0.116

**Table 2-30.** Bond lengths (Å) and angles (°) for **18**.

Rh1-C1	2.003(2)	Rh1-N10#1	2.0065(17)	Rh1-N20#1	2.0188(17)
Rh1-O20	2.0766(15)	Rh1-O10	2.0957(14)	Rh1-Rh1#1	2.5109(3)
C1-C6	1.389(3)	C1-C2	1.389(3)	C2-C3	1.394(3)
C3-C4	1.386(3)	C4-O7	1.381(3)	C4-C5	1.384(3)
C5-C6	1.388(3)	O7-C8	1.415(3)	O10-C11	1.291(2)
N10-C11	1.308(3)	N10-C16	1.465(3)	N10-Rh1#1	2.0065(17)
C11-C12	1.513(3)	C12-C13	1.531(3)	C13-C14	1.524(4)
C14-C15	1.528(4)	C15-C16	1.531(4)	O20-C21	1.291(3)
N20-C21	1.309(3)	N20-C26	1.473(3)	N20-Rh1#1	2.0188(17)
C21-C22	1.512(3)	C22-C23	1.530(4)	C23-C24	1.521(4)
C24-C25	1.517(4)	C25-C26	1.525(3)	C31-Cl33	1.747(3)
C31-Cl31	1.758(3)	C31-Cl32	1.760(3)	C41-Cl43	1.617(5)
C41-Cl41	1.746(4)	C41-Cl42	1.798(4)		
C1-Rh1-N10#1	101.32(8)	C1-Rh1-N20#1	100.95(8)	N10#1-Rh1-N20#1	90.41(7)
C1-Rh1-O20	85.61(7)	N10#1-Rh1-O20	87.65(7)	N20#1-Rh1-O20	173.41(6)
C1-Rh1-O10	84.46(7)	N10#1-Rh1-O10	174.13(6)	N20#1-Rh1-O10	89.52(7)
O20-Rh1-O10	91.76(6)	C1-Rh1-Rh1#1	157.30(6)	N10#1-Rh1-Rh1#1	96.30(5)
N20#1-Rh1-Rh1#1	193.08(5)	O20-Rh1-Rh1#1	80.88(4)	O10-Rh1-Rh1#1	77.85(4)
C6-C1-C2	119.03(19)	C6-C1-Rh1	121.33(16)	C2-C1-Rh1	119.64(15)
C1-C2-C3	120.8(2)	C4-C3-C2	119.5(2)	O7-C4-C5	115.9(2)
O7-C4-C3	124.2(2)	C5-C4-C3	119.9(2)	C4-C5-C6	120.4(2)
C5-C6-C1	120.2(2)	C4-O7-C8	117.4(2)	C11-O10-Rh1	129.21(13)
C11-N10-C16	120.56(18)	C11-N10-Rh1#1	113.08(14)	C16-N10-Rh1#1	126.29(14)
O10-C11-N10	123.52(19)	O10-C11-C12	115.08(18)	N10-C11-C12	121.38(19)
C11-C12-C13	113.1(2)	C14-C13-C12	113.6(2)	C13-C14-C15	114.3(2)
C14-C15-C16	114.7(2)	N10-C16-C15	113.4(2)	C21-O20-Rh1	126.54(13)
C21-N20-C26	119.65(18)	C21-N20-Rh1#1	115.68(14)	C26-N20-Rh1#1	124.13(14)
O20-C21-N20	123.67(19)	O20-C21-C22	114.40(19)	N20-C21-C22	121.92(19)
C21-C22-C23	114.3(2)	C24-C23-C22	114.2(2)	C25-C24-C23	114.3(2)
C24-C25-C26	115.2(2)	N20-C26-C25	115.0(2)	Cl33-C31-Cl31	110.65(16)
Cl33-C31-Cl32	110.08(16)	Cl31-C31-Cl32	110.56(15)	Cl43-C41-Cl41	114.8(3)
Cl43-C41-Cl42	112.5(3)	Cl41-C41-Cl42	104.6(2)		
N10#1-Rh1-C1-C6	47.83(19)	N20#1-Rh1-C1-C6	140.48(18)		
O20-Rh1-C1-C6	-38.89(18)	O10-Rh1-C1-C6	-131.09(19)		
Rh1#1-Rh1-C1-C6	-92.4(2)	N10#1-Rh1-C1-C2	-131.96(17)		
N20#1-Rh1-C1-C2	-39.31(19)	O20-Rh1-C1-C2	141.33(18)		
O10-Rh1-C1-C2	49.12(18)	Rh1#1-Rh1-C1-C2	87.9(2)		
C6-C1-C2-C3	-4.5(3)	Rh1-C1-C2-C3	175.27(17)		
C1-C2-C3-C4	1.8(3)	C2-C3-C4-O7	-179.7(2)		
C2-C3-C4-C5	1.6(4)	O7-C4-C5-C6	179.0(2)		
C3-C4-C5-C6	-2.2(4)	C4-C5-C6-C1	-0.6(4)		
C2-C1-C6-C5	3.9(3)	Rh1-C1-C6-C5	-175.86(18)		
C5-C4-O7-C8	-167.2(2)	C3-C4-O7-C8	14.1(4)		
C1-Rh1-O10-C11	166.45(19)	N20#1-Rh1-O10-C11	-92.50(18)		
O20-Rh1-O10-C11	81.03(18)	Rh1#1-Rh1-O10-C11	0.75(17)		
Rh1-O10-C11-N10	-2.3(3)	Rh1-O10-C11-C12	176.44(14)		
C16-N10-C11-O10	179.5(2)	Rh1#1-N10-C11-O10	2.4(3)		
C16-N10-C11-C12	0.9(3)	Rh1#1-N10-C11-C12	-176.22(16)		
O10-C11-C12-C13	-111.1(2)	N10-C11-C12-C13	67.6(3)		
C11-C12-C13-C14	-80.4(3)	C12-C13-C14-C15	59.3(4)		

C13-C14-C15-C16	-59.3(4)	C11-N10-C16-C15	-68.5(3)
Rh1#1-N10-C16-C15	108.2(2)	C14-C15-C16-N10	81.5(3)
C1-Rh1-O20-C21	-157.92(19)	N10#1-Rh1-O20-C21	100.53(18)
O10-Rh1-O20-C21	-73.62(18)	Rh1#1-Rh1-O20-C21	3.77(17)
Rh1-O20-C21-N20	-2.9(3)	Rh1-O20-C21-C22	177.62(15)
C26-N20-C21-O20	171.4(2)	Rh1#1-N20-C21-O20	-0.6(3)
C26-N20-C21-C22	-9.2(3)	Rh1#1-N20-C21-C22	178.84(17)
O20-C21-C22-C23	119.2(2)	N20-C21-C22-C23	-60.3(3)
C21-C22-C23-C24	80.8(3)	C22-C23-C24-C25	-60.6(3)
C23-C24-C25-C26	56.7(4)	C21-N20-C26-C25	72.4(3)
Rh1#1-N20-C26-C25	-116.34(19)	C24-C25-C26-N20	-78.9(3)

---

Symmetry transformation codes: #1 -x+1,-y+1,-z+1

XRD Crystallographer's<sup>136</sup> Report (**20**•2CHCl<sub>3</sub>).

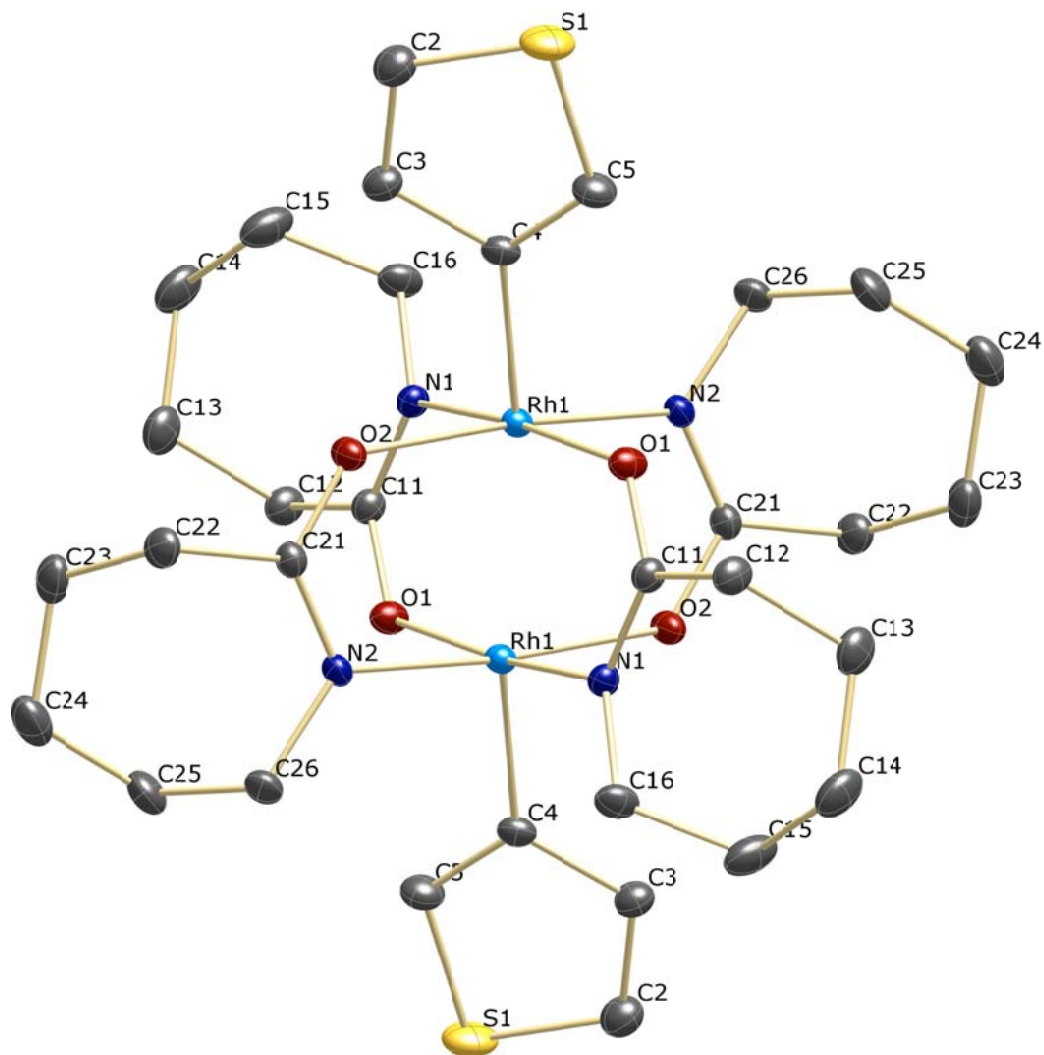


**Figure 2-19.** A view of **20** showing the numbering scheme employed. Anisotropic atomic displacement ellipsoids for the non-hydrogen atoms are shown at the 30% probability level. Solvent and hydrogen atoms are omitted for clarity.

---

<sup>136</sup> See ref. 109.

A green prism of  $(C_{32}H_{46}N_4O_4Rh_2S_2) \cdot 2(CHCl_3)$ , approximate dimensions  $0.09 \times 0.14 \times 0.22 \text{ mm}^3$ , was used for the X-ray crystallographic analysis. The X-ray intensity data were measured at 220(2) K on a three-circle diffractometer system equipped with Bruker Smart1000 CCD area detector using a graphite monochromator and a Mo  $K\alpha$  fine-focus sealed tube ( $\lambda = 0.71073 \text{ \AA}$ ) operated at 50 kV and 30 mA. The detector was placed at a distance of 4.960 cm from the crystal.

A total of 1824 frames were collected with a scan width of  $0.5^\circ$  in  $\omega$  and an exposure time of 38 sec/frame using SMART.<sup>137</sup> The total data collection time was 22.9 hours. The frames were integrated with SAINT software<sup>138</sup> package using a narrow-frame integration algorithm. The integration of the data using a Triclinic unit cell yielded a total of 12928 reflections to a maximum  $\theta$  angle of  $27.50^\circ$ , of which 4840 were independent (completeness = 98.8%,  $R_{\text{int}} = 2.50\%$ ,  $R_{\text{sig}} = 2.60\%$ ) and 4431 were greater than  $2\sigma(I)$ . The final cell dimensions of  $a = 10.3382(9) \text{ \AA}$ ,  $b = 11.3040(10) \text{ \AA}$ ,  $c = 11.4509(10) \text{ \AA}$ ,  $\alpha = 64.8490(10)^\circ$ ,  $\beta = 63.3810(10)^\circ$ ,  $\gamma = 70.9100(10)^\circ$ , and  $V = 1067.38(16) \text{ \AA}^3$  are based upon the refinement of the XYZ-centroids of 8822 reflections with  $2.1 < \theta < 29.2^\circ$  using SAINT. Analysis of the data showed 0 % decay during data collection. Data were corrected for absorption effects with the semi-empirical from equivalents method using SADABS.<sup>139</sup> The minimum and maximum transmission coefficients were 0.803 and 0.891.

The structure was solved and refined using the SHELXS-97 and SHELXL-97 software<sup>140</sup> in the space group  $P1$  with  $Z = 1$  for the formula unit  $(C_{32}H_{46}N_4O_4Rh_2S_2) \cdot 2(CHCl_3)$ . The final anisotropic full-matrix least-squares

---

<sup>137</sup> See ref. 110.

<sup>138</sup> See ref. 110.

<sup>139</sup> See ref. 112.

<sup>140</sup> See ref. 111.

refinement on  $F^2$  with 281 variables converged at  $R_1 = 2.75\%$  for the observed data and  $wR_2 = 6.46\%$  for all data. The goodness-of-fit was 0.999. The largest peak on the final difference map was  $1.065 \text{ e}/\text{\AA}^3$  and the largest hole was  $-0.750 \text{ e}/\text{\AA}^3$ . On the basis of the final model, the calculated density was  $1.648 \text{ g/cm}^3$  and  $F(000)$ , 536  $e^-$ .

**Table 2-31.** Crystal data and structure refinement for **20**.

Empirical formula	$(\text{C}_{32}\text{H}_{46}\text{N}_4\text{O}_4\text{Rh}_2\text{S}_2) \cdot 2(\text{CHCl}_3)$	
Formula weight (amu)	1059.40	
Temperature (K)	220(2)	
Wavelength ( $\text{\AA}$ )	0.71073 (Mo $K\alpha$ )	
Crystal size	$0.22 \times 0.14 \times 0.09 \text{ mm}^3$	
Crystal habit	green prism	
Crystal system	Triclinic	
Space group	P1	
Unit cell dimensions ( $\text{\AA} / ^\circ$ )	$a = 10.3382(9)$	$\alpha = 64.8490(10)$
	$b = 11.3040(10)$	$\beta = 63.3810(10)$
	$c = 11.4509(10)$	$\gamma = 70.9100(10)$
Volume ( $\text{\AA}^3$ )	1067.38(16)	
Z	1	
Density, $\rho_{\text{calc}}$ ( $\text{g/cm}^3$ )	1.648	
Absorption coefficient, $\mu$ ( $\text{mm}^{-1}$ )	1.287	
$\theta$ Range	2.40 to 27.50°	
Reflections collected	12928	
Independent reflections	4840	
Observed reflection, $I > 2\sigma(I)$	4431	
Max. and min. transmission <sup>a</sup>	0.891 and 0.803	
Goodness-of-fit on $F^2$	0.997	
Max $[\Delta/\sigma]$	0.001	
Final R indices: <sup>b</sup>		
$R_1, I > 2\sigma(I)$	0.0275	
$wR_2, \text{ all data}$	0.0646	
$R_{\text{int}}$	0.0250	
$R_{\text{sig}}$	0.0260	
Min., max. peaks ( $\text{e}/\text{\AA}^3$ )	1.065 and -0.750	

<sup>a</sup>Absorption correction was performed using the semi-empirical from equivalents method (SADABS). <sup>b</sup>Function minimized was  $\sum w(F_o^2 - F_c^2)^2$  where  $R_1 = \sum ||F_o| - |F_c|| / \sum |F_o|$ ,  $wR_2 = [\sum w(F_o^2 - F_c^2)^2 / \sum w(F_o^2)^2]^{1/2}$  with a weighting scheme  $w = 1/[\sigma^2(F_o^2) + (0.015P)^2 + 27.8P]$ ,  $P = [\max(F_o^2, 0) + 2F_o^2]/3$ .

**Table 2-32.** Atomic coordinates and equivalent isotropic atomic displacement parameters ( $\text{\AA}^2$ ) for **20**.

Atom	<i>x/a</i>	<i>y/b</i>	<i>z/c</i>	$U_{\text{eq}}$
Rh1	0.420272(18)	0.444067(16)	0.491428(16)	0.02237(6)
S1 <sup>i</sup>	0.3023(4)	0.2520(2)	0.2878(3)	0.0514(6)
C2 <sup>i</sup>	0.3574(17)	0.1331(13)	0.4194(13)	0.043(2)
C3 <sup>i</sup>	0.401(3)	0.1895(10)	0.4769(17)	0.034(3)
C4 <sup>i</sup>	0.3754(2)	0.3314(2)	0.4239(2)	0.0282(4)
C5 <sup>i</sup>	0.335(3)	0.3768(8)	0.313(2)	0.039(2)
S1A <sup>ii</sup>	0.3441(9)	0.1361(6)	0.3889(6)	0.0487(11)
C2A <sup>ii</sup>	0.309(3)	0.2919(10)	0.2774(19)	0.057(4)
C3A <sup>ii</sup>	0.314(5)	0.3866(13)	0.317(4)	0.039(2)
C4A <sup>ii</sup>	0.3754(2)	0.3314(2)	0.4239(2)	0.0282(4)
C5A <sup>ii</sup>	0.377(5)	0.1982(16)	0.484(3)	0.034(3)
N1	0.6630(2)	0.64503(18)	0.30186(18)	0.0248(4)
O1	0.50991(18)	0.55080(16)	0.28382(16)	0.0300(3)
C11	0.6085(2)	0.6246(2)	0.2298(2)	0.0259(4)
C12	0.6540(3)	0.6895(2)	0.0746(2)	0.0337(5)
C13	0.6241(3)	0.8410(3)	0.0270(3)	0.0436(6)
C14	0.7411(4)	0.8998(3)	0.0190(3)	0.0514(8)
C15	0.7559(4)	0.8621(3)	0.1573(3)	0.0521(8)
C16	0.7884(3)	0.7145(3)	0.2316(3)	0.0371(6)
N2	0.7519(2)	0.40746(18)	0.50054(19)	0.0258(4)
O2	0.61057(17)	0.30134(16)	0.48296(17)	0.0301(3)
C21	0.7286(2)	0.3043(2)	0.4937(2)	0.0271(4)
C22	0.8394(3)	0.1767(2)	0.5010(3)	0.0371(5)
C23	0.8487(3)	0.1039(3)	0.6450(3)	0.0453(7)
C24	0.9383(3)	0.1624(3)	0.6760(3)	0.0518(7)
C25	0.8828(3)	0.3071(3)	0.6665(3)	0.0458(7)
C26	0.8826(3)	0.4013(3)	0.5231(3)	0.0342(5)
C30	1.2570(4)	0.6947(3)	-0.1633(3)	0.0487(7)
Cl1	0.21813(14)	0.86711(9)	0.78393(13)	0.0863(3)
Cl2	0.3013(2)	0.62887(14)	0.98517(12)	0.1110(5)
Cl3	0.10873(10)	0.63064(9)	0.86383(10)	0.0673(2)

$U_{\text{eq}}$  is defined as one third of the trace of the orthogonalized  $U_{ij}$  tensor. Occupation factors: for: (i) S1 – C5 = 0.621(4) and (ii) S1A – C5A = 0.379(4)



**Table 2-33.** Anisotropic atomic displacement parameters ( $\text{\AA}^2$ ) for **20**.

Atom	$U_{11}$	$U_{22}$	$U_{33}$	$U_{23}$	$U_{13}$	$U_{12}$
Rh1	0.02394(9)	0.02325(9)	0.02286(9)	-0.00753(6)	-0.01030(7)	-0.00494(6)
S1	0.0618(11)	0.0664(13)	0.0504(11)	-0.0294(11)	-0.0230(9)	-0.0226(11)
C2	0.048(4)	0.038(3)	0.047(6)	-0.017(3)	-0.016(4)	-0.009(2)
C3	0.035(8)	0.0340(17)	0.038(2)	-0.0176(16)	-0.012(4)	-0.005(3)
C4	0.0264(11)	0.0340(12)	0.0285(11)	-0.0124(9)	-0.0076(9)	-0.0107(9)
C5	0.047(8)	0.0412(17)	0.0398(19)	-0.017(2)	-0.022(4)	-0.009(2)
S1A	0.064(2)	0.0484(16)	0.051(3)	-0.0249(16)	-0.0174(16)	-0.0231(14)
C2A	0.083(8)	0.070(8)	0.037(5)	-0.007(6)	-0.025(5)	-0.047(8)
C3A	0.047(8)	0.0412(17)	0.0398(19)	-0.017(2)	-0.022(4)	-0.009(2)
C4A	0.0264(11)	0.0340(12)	0.0285(11)	-0.0124(9)	-0.0076(9)	-0.0107(9)
C5A	0.035(8)	0.0340(17)	0.038(2)	-0.0176(16)	-0.012(4)	-0.005(3)
N1	0.0258(9)	0.0240(9)	0.0222(8)	-0.0044(7)	-0.0080(7)	-0.0067(7)
O1	0.0362(9)	0.0350(9)	0.0224(7)	-0.0066(6)	-0.0107(7)	-0.0141(7)
C11	0.0295(11)	0.0239(10)	0.0219(10)	-0.0061(8)	-0.0086(9)	-0.0047(9)
C12	0.0443(14)	0.0337(12)	0.0227(10)	-0.0063(9)	-0.0107(10)	-0.0120(11)
C13	0.0560(17)	0.0337(14)	0.0310(12)	-0.0011(10)	-0.0181(12)	-0.0050(12)
C14	0.077(2)	0.0334(14)	0.0365(14)	-0.0014(11)	-0.0152(15)	-0.0212(14)
C15	0.077(2)	0.0445(16)	0.0391(15)	-0.0072(13)	-0.0145(15)	-0.0337(16)
C16	0.0351(13)	0.0464(15)	0.0306(12)	-0.0064(11)	-0.0085(10)	-0.0211(11)
N2	0.0233(9)	0.0268(9)	0.0287(9)	-0.0074(7)	-0.0131(8)	-0.0027(7)
O2	0.0292(8)	0.0281(8)	0.0396(9)	-0.0164(7)	-0.0162(7)	-0.0002(7)
C21	0.0250(11)	0.0272(11)	0.0278(10)	-0.0093(9)	-0.0107(9)	-0.0006(9)
C22	0.0305(12)	0.0310(13)	0.0471(14)	-0.0156(11)	-0.0143(11)	0.0024(10)
C23	0.0393(15)	0.0301(13)	0.0528(16)	-0.0038(12)	-0.0194(13)	0.0014(11)
C24	0.0418(16)	0.0511(18)	0.0532(17)	-0.0029(14)	-0.0285(14)	0.0002(13)
C25	0.0434(15)	0.0528(17)	0.0481(16)	-0.0081(13)	-0.0306(13)	-0.0076(13)
C26	0.0238(11)	0.0360(13)	0.0442(14)	-0.0093(11)	-0.0162(10)	-0.0064(10)
C30	0.0593(19)	0.0439(16)	0.0365(14)	-0.0168(12)	-0.0100(13)	-0.0070(14)
Cl1	0.1124(9)	0.0417(5)	0.1010(8)	-0.0263(5)	-0.0318(7)	-0.0144(5)
Cl2	0.1835(15)	0.1071(9)	0.0625(6)	-0.0201(6)	-0.0656(8)	-0.0289(9)
Cl3	0.0557(5)	0.0525(5)	0.0743(6)	-0.0223(4)	-0.0030(4)	-0.0136(4)

The anisotropic atomic displacement factor exponent takes the form:  $-2\pi^2 [h^2a^2U_{11} + \dots + 2hka^*b^*U_{12}]$ .

**Table 2-34.** Hydrogen atom coordinates/isotropic atomic displacement parameters ( $\text{\AA}^2$ ) for **20**.

Atom	$x/a$	$y/b$	$z/c$	$U_{\text{iso}}$
H2	0.3572	0.0419	0.4479	0.052
H3	0.4441	0.1402	0.5444	0.041
H5	0.3263	0.4661	0.2563	0.046
H2A	0.2895	0.3092	0.1986	0.068
H3A	0.2817	0.4776	0.2797	0.046
H5A	0.3946	0.1471	0.5673	0.041
H12A	0.6014	0.6598	0.0417	0.050(9)
H12B	0.7592	0.6595	0.0318	0.039(8)
H13A	0.6167	0.8750	-0.0645	0.052(9)
H13B	0.5293	0.8704	0.0912	0.053(9)
H14A	0.7183	0.9966	-0.0187	0.061(10)
H14B	0.8356	0.8706	-0.0456	0.052(9)
H15A	0.8346	0.9033	0.1421	0.067(11)
H15B	0.6645	0.8999	0.2183	0.049(9)
H16A	0.8650	0.6731	0.1641	0.036(7)
H16B	0.8281	0.7019	0.3002	0.059(10)
H22A	0.9364	0.1972	0.4336	0.046(8)
H22B	0.8121	0.1182	0.4756	0.034(7)
H23A	0.7491	0.1058	0.7145	0.050(9)
H23B	0.8925	0.0109	0.6535	0.062(10)
H24A	0.9390	0.1101	0.7694	0.058(10)
H24B	1.0399	0.1536	0.6111	0.062(10)
H25A	0.9443	0.3346	0.6921	0.058(9)
H25B	0.7826	0.3154	0.7340	0.055(9)
H26A	0.8881	0.4904	0.5126	0.032(7)
H26B	0.9700	0.3719	0.4524	0.039(7)
H30	1.3432	0.6684	-0.2385	0.044(8)

**Table 5.** Bond lengths (Å) and angles (°) for **20**.

Rh1-C4	1.995(2)	Rh1-N2#1	2.0059(18)	Rh1-N1#1	2.0181(18)
Rh1-O1	2.0700(15)	Rh1-O2	2.0901(16)	Rh1-Rh1#1	2.4939(3)
S1-C5	1.712(9)	S1-C2	1.718(11)	C2-C3	1.364(13)
C3-C4	1.433(11)	C4-C5	1.354(11)	N1-C11	1.309(3)
N1-C16	1.463(3)	N1-Rh1#1	2.0182(18)	O1-C11	1.292(3)
C11-C12	1.512(3)	C12-C13	1.529(4)	C13-C14	1.513(4)
C14-C15	1.522(4)	C15-C16	1.518(4)	N2-C21	1.305(3)
N2-C26	1.461(3)	N2-Rh1#1	2.0059(18)	O2-C21	1.292(3)
C21-C22	1.518(3)	C22-C23	1.530(4)	C23-C24	1.522(4)
C24-C25	1.519(4)	C25-C26	1.532(4)	C30-Cl1#2	1.740(3)
C30-Cl2#2	1.747(3)	C30-Cl3#2	1.755(3)	C30-H30	0.9900
Cl1-C30#3	1.740(3)	Cl2-C30#3	1.747(3)	Cl3-C30#3	1.755(3)
C4-Rh1-N2#1	102.99(8)	C4-Rh1-N1#1	101.19(8)	N2#1-Rh1-N1#1	91.43(7)
C4-Rh1-O1	84.92(8)	N2#1-Rh1-O1	86.57(7)	N1#1-Rh1-O1	173.87(7)
C4-Rh1-O2	82.24(8)	N2#1-Rh1-O2	174.46(7)	N1#1-Rh1-O2	89.31(7)
O1-Rh1-O2	92.13(7)	C4-Rh1-Rh1#1	155.84(7)	N2#1-Rh1-Rh1#1	96.01(5)
N1#1-Rh1-Rh1#1	93.02(5)	O1-Rh1-Rh1#1	81.43(4)	O2-Rh1-Rh1#1	78.46(4)
C5-S1-C2	92.3(5)	C3-C2-S1	110.5(10)	C2-C3-C4	113.1(10)
C5-C4-C3	111.5(6)	C5-C4-Rh1	124.9(4)	C3-C4-Rh1	123.1(4)
C4-C5-S1	111.9(7)	C11-N1-C16	120.20(19)	C11-N1-Rh1#1	115.64(15)
C16-N1-Rh1#1	123.72(15)	C11-O1-Rh1	126.02(13)	O1-C11-N1	123.75(19)
O1-C11-C12	114.08(19)	N1-C11-C12	122.2(2)	C11-C12-C13	113.9(2)
C14-C13-C12	113.5(2)	C13-C14-C15	114.1(2)	C16-C15-C14	115.6(2)
N1-C16-C15	115.4(2)	C21-N2-C26	120.79(19)	C21-N2-Rh1#1	113.38(14)
C26-N2-Rh1#1	125.09(15)	C21-O2-Rh1	128.53(14)	O2-C21-N2	123.4(2)
O2-C21-C22	115.1(2)	N2-C21-C22	121.5(2)	C21-C22-C23	112.6(2)
C24-C23-C22	113.8(2)	C25-C24-C23	114.6(2)	C24-C25-C26	114.2(2)
N2-C26-C25	112.6(2)	Cl1#2-C30-Cl2#2	111.28(17)	Cl1#2-C30-Cl3#2	110.35(18)
Cl2#2-C30-Cl3#2	110.93(17)				
C5-S1-C2-C3	-1.1(18)	S1-C2-C3-C4	6(2)	C2-C3-C4-C5	-10(2)
C2-C3-C4-Rh1	177.7(12)	N2#1-Rh1-C4-C5	49.2(16)	N1#1-Rh1-C4-C5	143.4(16)
O1-Rh1-C4-C5	-36.0(16)	O2-Rh1-C4-C5	-128.9(16)	Rh1#1-Rh1-C4-C5	-91.7(16)
N2#1-Rh1-C4-C3	-139.5(12)	N1#1-Rh1-C4-C3	-45.4(12)	O1-Rh1-C4-C3	135.2(12)
O2-Rh1-C4-C3	42.4(12)	Rh1#1-Rh1-C4-C3	79.5(12)	C3-C4-C5-S1	9(2)
Rh1-C4-C5-S1	-178.9(7)	C2-S1-C5-C4	-4.7(19)	C4-Rh1-O1-C11	-156.68(19)
N2#1-Rh1-O1-C11	99.94(18)	O2-Rh1-O1-C11	-74.67(18)	Rh1#1-Rh1-O1-C11	3.33(17)
Rh1-O1-C11-N1	-2.1(3)	Rh1-O1-C11-C12	179.43(15)	C16-N1-C11-O1	171.4(2)
Rh1#1-N1-C11-O1	-1.3(3)	C16-N1-C11-C12	-10.2(3)	Rh1#1-N1-C11-C12	177.08(17)
O1-C11-C12-C13	119.2(2)	N1-C11-C12-C13	-59.4(3)	C11-C12-C13-C14	81.9(3)
C12-C13-C14-C15	-62.6(3)	C13-C14-C15-C16	57.3(4)	C11-N1-C16-C15	71.6(3)
Rh1#1-N1-C16-C15	-116.3(2)	C14-C15-C16-N1	-77.2(3)	C4-Rh1-O2-C21	168.7(2)
N1#1-Rh1-O2-C21	-89.89(19)	O1-Rh1-O2-C21	84.15(19)	Rh1#1-Rh1-O2-C21	3.34(18)
Rh1-O2-C21-N2	-6.1(3)	Rh1-O2-C21-C22	172.63(15)	C26-N2-C21-O2	175.3(2)
Rh1#1-N2-C21-O2	4.8(3)	C26-N2-C21-C22	-3.3(3)	Rh1#1-N2-C21-C22	-173.90(17)
O2-C21-C22-C23	-108.7(2)	N2-C21-C22-C23	70.1(3)	C21-C22-C23-C24	-78.6(3)
C22-C23-C24-C25	58.5(4)	C23-C24-C25-C26	-61.0(3)	C21-N2-C26-C25	-66.4(3)
Rh1#1-N2-C26-C25	103.0(2)	C24-C25-C26-N2	83.3(3)		

Symmetry transformation codes: #1 -x+1,-y+1,-z+1 #2 x+1,y,z-1 #3 x-1,y,z+1

XRD Crystallographer's<sup>141</sup> Report (**22**•2CHCl<sub>3</sub>).

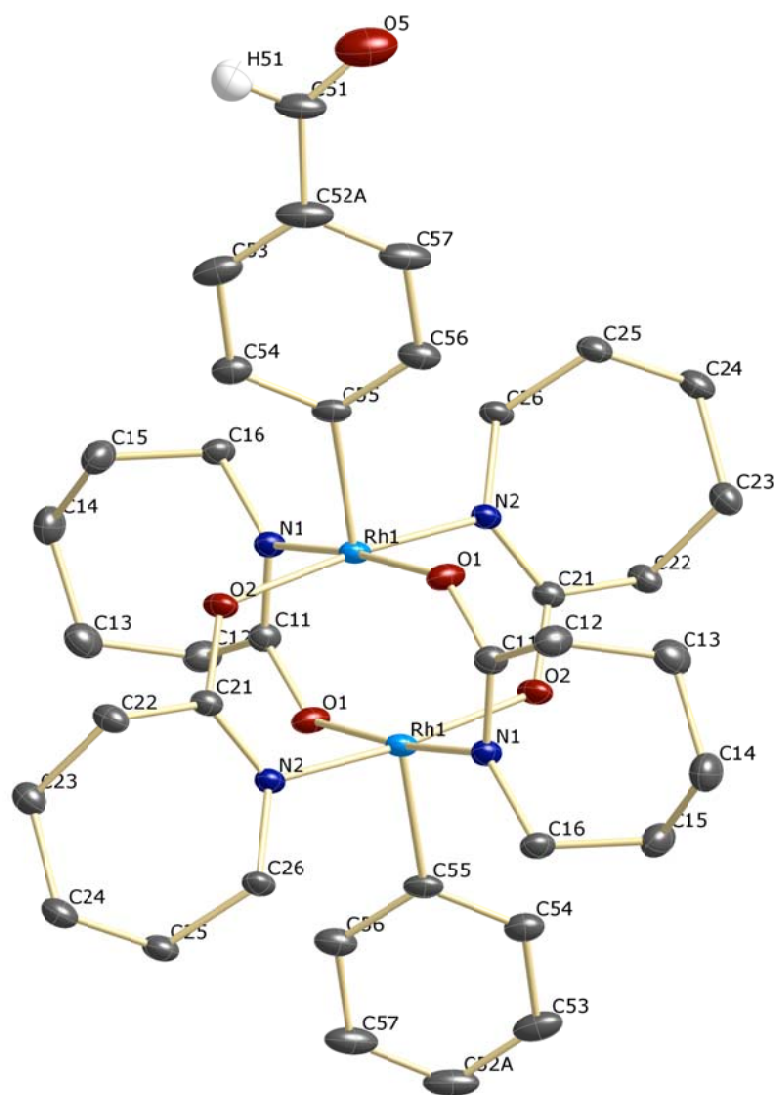


**Figure 2-20.** A view of **22** showing the numbering scheme employed. Anisotropic atomic displacement ellipsoids for the non-hydrogen atoms are shown at the 30% probability level. Solvent and hydrogen atoms are omitted for clarity.

---

<sup>141</sup> See ref. 109.

A green prism of  $C_{37}H_{50}N_4O_5Rh_2 \cdot 2CHCl_3$ , approximate dimensions  $0.07 \times 0.17 \times 0.19 \text{ mm}^3$ , was used for the X-ray crystallographic analysis. The X-ray intensity data were measured at 220(2) K on a three-circle diffractometer system equipped with Bruker Smart1000 CCD area detector using a graphite monochromator and a MoK $\alpha$  fine-focus sealed tube ( $\lambda = 0.71073 \text{ \AA}$ ) operated at 50 kV and 30 mA. The detector was placed at a distance of 4.950 cm from the crystal.

A total of 2916 frames were collected with a scan width of  $0.3^\circ$  in  $\omega$  and an exposure time of 30 sec/frame using SMART.<sup>142</sup> The total data collection time was 30.1 hours. The frames were integrated with SAINT software<sup>143</sup> package using a narrow-frame integration algorithm. The integration of the data using a Triclinic unit cell yielded a total of 19686 reflections to a maximum  $\theta$  angle of  $27.50^\circ$ , of which 5036 were independent (completeness = 99.7%,  $R_{\text{int}} = 2.87\%$ ,  $R_{\text{sig}} = 2.11\%$ ) and 4647 were greater than  $2\sigma(I)$ . The final cell dimensions of  $a = 10.5747(10) \text{ \AA}$ ,  $b = 10.8426(10) \text{ \AA}$ ,  $c = 11.9089(11) \text{ \AA}$ ,  $\alpha = 101.1210(10)^\circ$ ,  $\beta = 108.2940(10)^\circ$ ,  $\gamma = 113.9120(10)^\circ$ , and  $V = 1101.61(18) \text{ \AA}^3$  are based upon the refinement of the XYZ-centroids of 6480 reflections with  $2.2 < \theta < 28.9^\circ$  using SAINT. Analysis of the data showed 0 % decay during data collection. Data were corrected for absorption effects with the semi-empirical from equivalents method using SADABS.<sup>144</sup> The minimum and maximum transmission coefficients were 0.744 and 0.922.

The structure was solved and refined using the SHELXS-97 and SHELXL-97 software<sup>145</sup> in the space group  $P-1$  with  $Z = 1$  for the formula unit  $C_{37}H_{50}N_4O_5Rh_2 \cdot 2CHCl_3$ . The final anisotropic full-matrix least-squares

---

<sup>142</sup> See ref. 110.

<sup>143</sup> See ref. 110.

<sup>144</sup> See ref. 112.

<sup>145</sup> See ref. 111.

refinement on  $F^2$  with 288 variables converged at  $R_1 = 3.10\%$  for the observed data and  $wR_2 = 7.46\%$  for all data. The goodness-of-fit was 1.000. The largest peak on the final difference map was  $1.313\bar{e}/\text{\AA}^3$  and the largest hole was  $-0.893\bar{e}/\text{\AA}^3$ . On the basis of the final model, the calculated density was  $1.621\text{ g/cm}^3$  and  $F(000)$ ,  $546\bar{e}$ .

**Table 2-35.** Crystal data and structure refinement for **22**.

Empirical formula	$C_{37}H_{50}N_4O_5Rh_2 \cdot 2CHCl_3$
Formula weight	1075.37
Temperature	220(2) K
Wavelength	0.71073 $\text{\AA}$
Crystal size	$0.19 \times 0.17 \times 0.07\text{ mm}^3$
Crystal habit	green prism
Crystal system	Triclinic
Space group	P-1
Unit cell dimensions	$a = 10.5747(10)\text{ \AA}$ $\alpha = 101.1210(10)^\circ$ $b = 10.8426(10)\text{ \AA}$ $\beta = 108.2940(10)^\circ$ $c = 11.9089(11)\text{ \AA}$ $\gamma = 113.9120(10)^\circ$
Volume	$1101.61(18)\text{ \AA}^3$
Z	1
Density, $\rho_{\text{calc}}$	$1.621\text{ g/cm}^3$
Absorption coefficient, $\mu$	$1.159\text{ mm}^{-1}$
$\theta$ range for data collection	$2.34$ to $27.50^\circ$
Reflections collected	19686
Independent reflections	5036
Observed reflection, $I > 2\sigma(I)$	4647
Max. and min. transmission <sup>a</sup>	0.922 and 0.744
Goodness-of-fit on $F^2$	1.000
$\Delta/\sigma_{\text{max}}$	0.001
Final R indices: <sup>b</sup>	
$R_1, I > 2\sigma(I)$	0.0310
$wR_2, \text{ all data}$	0.0746
$R_{\text{int}}$	0.0287
$R_{\text{sig}}$	0.0211
Min., max. peaks ( $\bar{e}/\text{\AA}^3$ )	1.313 and -0.893

<sup>a</sup>Absorption correction was performed using the semi-empirical from equivalents method (SADABS). <sup>b</sup>Function minimized was  $\sum w(F_o^2 - F_c^2)^2$  where  $R_1 = \sum ||F_o| - |F_c|| / \sum |F_o|$ ,  $wR_2 = [\sum w(F_o^2 - F_c^2)^2 / \sum w(F_o^2)^2]^{1/2}$  with a weighting scheme  $w = 1/[\sigma^2(F_o^2) + (0.015P)^2 + 27.8P]$ ,  $P = [\max(F_o^2, 0) + 2F_o^2]/3$ .

**Table 2-36.** Atomic coordinates and equivalent isotropic atomic displacement parameters ( $\text{\AA}^2$ ) for **22**.

Atom	$x/a$	$y/b$	$z/c$	$U_{\text{eq}}$
Rh1	0.41361(2)	0.53281(2)	0.535394(19)	0.02687(7)
N1	0.3371(2)	0.6025(2)	0.3985(2)	0.0287(4)
O1	0.4917(2)	0.5433(2)	0.33002(18)	0.0363(4)
C11	0.3977(3)	0.5932(3)	0.3188(3)	0.0310(5)
C12	0.3650(4)	0.6429(4)	0.2084(3)	0.0401(7)
C13	0.4254(4)	0.8065(4)	0.2488(3)	0.0471(7)
C14	0.3229(4)	0.8529(4)	0.2882(3)	0.0478(8)
C15	0.3017(4)	0.8177(4)	0.4017(3)	0.0451(7)
C16	0.2291(3)	0.6573(3)	0.3814(3)	0.0333(6)
N2	0.2315(2)	0.3305(2)	0.4259(2)	0.0280(4)
O2	0.3901(2)	0.2639(2)	0.36890(18)	0.0332(4)
C21	0.2558(3)	0.2370(3)	0.3613(2)	0.0291(5)
C22	0.1266(3)	0.0862(3)	0.2697(3)	0.0344(6)
C23	0.0344(3)	-0.0074(3)	0.3275(3)	0.0381(6)
C24	-0.0870(3)	0.0264(3)	0.3426(3)	0.0390(6)
C25	-0.0217(3)	0.1799(3)	0.4320(3)	0.0377(6)
C26	0.0723(3)	0.2997(3)	0.3940(3)	0.0328(6)
O5**	0.0781(8)	0.5981(9)	0.9483(6)	0.084(2)
C51**	0.1557(7)	0.6771(9)	0.9155(6)	0.0483(16)
C52A**	0.2299(4)	0.6567(5)	0.8333(3)	0.0571(10)
C52**	0.2299(4)	0.6567(5)	0.8333(3)	0.0571(10)
C53	0.3046(4)	0.7598(4)	0.7887(3)	0.0516(9)
C54	0.3586(3)	0.7246(4)	0.7009(3)	0.0397(6)
C55	0.3372(3)	0.5865(3)	0.6596(2)	0.0328(6)
C56	0.2667(3)	0.4840(4)	0.7084(3)	0.0413(7)
C57	0.2116(4)	0.5202(5)	0.7940(3)	0.0540(9)
C80	0.3022(4)	0.2435(4)	0.0597(3)	0.0490(8)
Cl81	0.13209(10)	0.25071(11)	0.03245(9)	0.0601(2)
Cl82	0.26478(11)	0.06386(11)	0.02668(9)	0.0584(2)
Cl83	0.38378(13)	0.31851(13)	-0.03498(12)	0.0762(3)

$U_{\text{eq}}$  is defined as one third of the trace of the orthogonalized  $U_{ij}$  tensor. \*\*50% occupancy.

**Table 2-37.** Anisotropic atomic displacement parameters ( $\text{\AA}^2$ ) for **22**.

Atom	$U_{11}$	$U_{22}$	$U_{33}$	$U_{23}$	$U_{13}$	$U_{12}$
Rh1	0.02218(10)	0.03664(12)	0.02976(11)	0.01475(8)	0.01513(8)	0.01765(8)
N1	0.0248(10)	0.0356(11)	0.0331(11)	0.0163(9)	0.0152(9)	0.0181(9)
O1	0.0399(11)	0.0549(12)	0.0363(10)	0.0245(9)	0.0237(9)	0.0342(10)
C11	0.0280(12)	0.0386(14)	0.0318(13)	0.0157(11)	0.0137(10)	0.0196(11)
C12	0.0468(17)	0.0570(18)	0.0380(15)	0.0275(14)	0.0250(13)	0.0352(15)
C13	0.0474(18)	0.0568(19)	0.0558(19)	0.0362(16)	0.0308(16)	0.0293(16)
C14	0.0541(19)	0.0460(18)	0.061(2)	0.0302(16)	0.0300(17)	0.0314(16)
C15	0.0561(19)	0.0449(17)	0.0556(19)	0.0250(15)	0.0328(16)	0.0346(16)
C16	0.0288(13)	0.0431(15)	0.0418(15)	0.0213(12)	0.0197(11)	0.0243(12)
N2	0.0218(10)	0.0332(11)	0.0340(11)	0.0154(9)	0.0151(9)	0.0146(9)
O2	0.0236(9)	0.0389(10)	0.0381(10)	0.0105(8)	0.0165(8)	0.0159(8)
C21	0.0243(12)	0.0360(13)	0.0311(12)	0.0158(11)	0.0149(10)	0.0150(10)
C22	0.0286(13)	0.0402(15)	0.0327(13)	0.0110(11)	0.0169(11)	0.0142(11)
C23	0.0380(15)	0.0371(15)	0.0406(15)	0.0166(12)	0.0211(13)	0.0160(12)
C24	0.0312(14)	0.0444(16)	0.0428(16)	0.0198(13)	0.0221(12)	0.0140(12)
C25	0.0305(13)	0.0456(16)	0.0454(16)	0.0208(13)	0.0247(12)	0.0185(12)
C26	0.0222(12)	0.0411(15)	0.0434(15)	0.0210(12)	0.0183(11)	0.0176(11)
O5	0.075(4)	0.134(6)	0.062(4)	0.033(4)	0.038(3)	0.063(4)
C51	0.035(3)	0.085(5)	0.031(3)	0.020(3)	0.020(3)	0.032(3)
C52A	0.0494(19)	0.110(3)	0.0410(17)	0.0321(19)	0.0290(15)	0.056(2)
C52	0.0494(19)	0.110(3)	0.0410(17)	0.0321(19)	0.0290(15)	0.056(2)
C53	0.0514(19)	0.077(2)	0.0418(17)	0.0151(16)	0.0211(15)	0.0475(19)
C54	0.0353(15)	0.0536(18)	0.0396(15)	0.0170(13)	0.0194(12)	0.0283(14)
C55	0.0235(12)	0.0533(16)	0.0303(13)	0.0165(12)	0.0141(10)	0.0244(12)
C56	0.0336(14)	0.063(2)	0.0398(15)	0.0251(14)	0.0220(12)	0.0276(14)
C57	0.0423(17)	0.099(3)	0.0492(19)	0.043(2)	0.0315(15)	0.045(2)
C80	0.0356(16)	0.0548(19)	0.0412(17)	0.0123(15)	0.0155(13)	0.0127(14)
Cl81	0.0465(5)	0.0725(6)	0.0618(5)	0.0277(5)	0.0267(4)	0.0267(4)
Cl82	0.0593(5)	0.0596(5)	0.0493(5)	0.0177(4)	0.0244(4)	0.0243(4)
Cl83	0.0613(6)	0.0749(7)	0.0876(7)	0.0355(6)	0.0487(6)	0.0153(5)

\* The anisotropic atomic displacement factor exponent takes the form:  $-2\pi^2 [h^2 a^{*2} U_{11} + \dots + 2hka^* b^* U_{12}]$ .



**Table 2-38.** Hydrogen atom coordinates and isotropic atomic displacement parameters ( $\text{\AA}^2$ ) for **22**.

Atom	$x/a$	$y/b$	$z/c$	$U_{\text{iso}}$
H12A	0.2536	0.5914	0.1558	0.046(9)
H12B	0.4118	0.6165	0.1558	0.049(10)
H13A	0.5281	0.8576	0.3202	0.049(10)
H13B	0.4356	0.8363	0.1780	0.056(11)
H14A	0.2216	0.8051	0.2155	0.049(10)
H14B	0.3672	0.9578	0.3095	0.059(11)
H15A	0.4024	0.8700	0.4756	0.051(10)
H15B	0.2373	0.8541	0.4219	0.061(11)
H16A	0.1838	0.6407	0.4411	0.041(9)
H16B	0.1455	0.6016	0.2950	0.040(9)
H22A	0.1703	0.0352	0.2323	0.041(9)
H22B	0.0556	0.0956	0.2004	0.046(9)
H23A	-0.0162	-0.1098	0.2733	0.046(9)
H23B	0.1056	0.0067	0.4112	0.042(9)
H24A	-0.1589	0.0112	0.2588	0.044(9)
H24B	-0.1453	-0.0420	0.3745	0.054(10)
H25A	0.0438	0.1923	0.5174	0.035(8)
H25B	-0.1070	0.1921	0.4368	0.053(10)
H26A	0.0183	0.2724	0.3019	0.034(8)
H26B	0.0760	0.3892	0.4356	0.030(7)
H51	0.1753	0.7726	0.9471	0.058
H52	0.1917	0.6805	0.8906	0.069
H53	0.3191	0.8536	0.8177	0.055(11)
H54	0.4087	0.7941	0.6705	0.031(8)
H56	0.2568	0.3916	0.6833	0.050(10)
H57	0.1617	0.4511	0.8250	0.060(11)
H80	0.3760	0.3015	0.1503	0.050(10)

**Table 2-39.** Bond lengths (Å), valence and torsion angles (°) for **22**.

Rh1-C55	1.995(3)	Rh1-N1	2.006(2)	Rh1-N2	2.028(2)
Rh1-O2#1	2.0745(19)	Rh1-O1#1	2.1040(19)	Rh1-Rh1#1	2.5190(4)
N1-C11	1.311(3)	N1-C16	1.467(3)	O1-C11	1.295(3)
O1-Rh1#1	2.1040(19)	C11-C12	1.510(4)	C12-C13	1.531(5)
C13-C14	1.522(5)	C14-C15	1.531(4)	C15-C16	1.520(4)
N2-C21	1.311(3)	N2-C26	1.478(3)	O2-C21	1.298(3)
O2-Rh1#1	2.0745(19)	C21-C22	1.515(4)	C22-C23	1.531(4)
C23-C24	1.522(4)	C24-C25	1.517(4)	C25-C26	1.531(4)
O5-C51	1.149(9)	C51-C52A	1.471(6)	C52A-C57	1.376(6)
C52A-C53	1.389(6)	C53-C54	1.400(4)	C54-C55	1.380(4)
C55-C56	1.406(4)	C56-C57	1.391(4)	C80-Cl83	1.753(3)
C80-Cl82	1.757(4)	C80-Cl81	1.762(4)		
C55-Rh1-N1	103.73(10)	C55-Rh1-N2	98.24(10)	N1-Rh1-N2	88.86(9)
C55-Rh1-O2#1	88.71(10)	N1-Rh1-O2#1	88.69(8)	N2-Rh1-O2#1	173.01(8)
C55-Rh1-O1#1	82.18(9)	N1-Rh1-O1#1	173.96(8)	N2-Rh1-O1#1	91.52(9)
O2#1-Rh1-O1#1	90.23(8)	C55-Rh1-Rh1#1	155.33(7)	N1-Rh1-Rh1#1	99.27(6)
N2-Rh1-Rh1#1	90.96(6)	O2#1-Rh1-Rh1#1	82.97(5)	O1#1-Rh1-Rh1#1	74.70(5)
C11-N1-C16	121.1(2)	C11-N1-Rh1	110.42(17)	C16-N1-Rh1	128.48(17)
C11-O1-Rh1#1	132.90(17)	O1-C11-N1	122.7(2)	O1-C11-C12	115.1(2)
N1-C11-C12	122.1(2)	C11-C12-C13	113.6(3)	C14-C13-C12	113.7(3)
C13-C14-C15	114.3(3)	C16-C15-C14	114.8(3)	N1-C16-C15	113.9(2)
C21-N2-C26	119.6(2)	C21-N2-Rh1	117.54(17)	C26-N2-Rh1	121.12(17)
C21-O2-Rh1#1	124.10(17)	O2-C21-N2	123.9(2)	O2-C21-C22	114.0(2)
N2-C21-C22	122.1(2)	C21-C22-C23	115.5(2)	C24-C23-C22	113.7(2)
C25-C24-C23	113.9(2)	C24-C25-C26	114.8(2)	N2-C26-C25	115.4(2)
O5-C51-C52A	132.0(8)	C57-C52A-C53	120.3(3)	C57-C52A-C51	114.6(5)
C53-C52A-C51	124.9(5)	C52A-C53-C54	120.4(3)	C55-C54-C53	119.2(3)
C54-C55-C56	120.3(3)	C54-C55-Rh1	120.3(2)	C56-C55-Rh1	119.3(2)
C57-C56-C55	119.6(3)	C52A-C57-C56	120.1(3)	Cl83-C80-Cl82	110.24(19)
Cl83-C80-Cl81	109.6(2)	Cl82-C80-Cl81	110.81(18)		
C55-Rh1-N1-C11	170.91(19)	N2-Rh1-N1-C11	-90.89(19)		
O2#1-Rh1-N1-C11	82.55(19)	Rh1#1-Rh1-N1-C11	-0.11(19)		
C55-Rh1-N1-C16	-9.3(2)	N2-Rh1-N1-C16	88.9(2)		
O2#1-Rh1-N1-C16	-97.7(2)	Rh1#1-Rh1-N1-C16	179.7(2)		
Rh1#1-O1-C11-N1	-1.5(4)	Rh1#1-O1-C11-C12	177.3(2)		
C16-N1-C11-O1	-179.0(2)	Rh1-N1-C11-O1	0.8(3)		
C16-N1-C11-C12	2.3(4)	Rh1-N1-C11-C12	-177.9(2)		
O1-C11-C12-C13	-114.0(3)	N1-C11-C12-C13	64.8(4)		
C11-C12-C13-C14	-79.5(3)	C12-C13-C14-C15	60.6(4)		
C13-C14-C15-C16	-60.2(4)	C11-N1-C16-C15	-67.9(3)		
Rh1-N1-C16-C15	112.3(2)	C14-C15-C16-N1	80.3(3)		
C55-Rh1-N2-C21	-155.8(2)	N1-Rh1-N2-C21	100.5(2)		
O1#1-Rh1-N2-C21	-73.44(19)	Rh1#1-Rh1-N2-C21	1.27(19)		
C55-Rh1-N2-C26	39.3(2)	N1-Rh1-N2-C26	-64.42(19)		
O1#1-Rh1-N2-C26	121.61(19)	Rh1#1-Rh1-N2-C26	-163.67(18)		
Rh1#1-O2-C21-N2	-8.8(4)	Rh1#1-O2-C21-C22	171.01(17)		

C26-N2-C21-O2	169.1(2)	Rh1-N2-C21-O2	3.9(3)
C26-N2-C21-C22	-10.6(4)	Rh1-N2-C21-C22	-175.83(19)
O2-C21-C22-C23	122.1(3)	N2-C21-C22-C23	-58.1(4)
C21-C22-C23-C24	80.4(3)	C22-C23-C24-C25	-62.3(3)
C23-C24-C25-C26	58.8(3)	C21-N2-C26-C25	72.1(3)
Rh1-N2-C26-C25	-123.3(2)	C24-C25-C26-N2	-79.2(3)
O5-C51-C52A-C57	-4.6(9)	O5-C51-C52A-C53	171.0(7)
C57-C52A-C53-C54	1.6(5)	C51-C52A-C53-C54	-173.7(4)
C52A-C53-C54-C55	-0.3(5)	C53-C54-C55-C56	-2.1(4)
C53-C54-C55-Rh1	-179.6(2)	N1-Rh1-C55-C54	-48.5(2)
N2-Rh1-C55-C54	-139.3(2)	O2#1-Rh1-C55-C54	39.9(2)
O1#1-Rh1-C55-C54	130.3(2)	Rh1#1-Rh1-C55-C54	109.9(3)
N1-Rh1-C55-C56	134.0(2)	N2-Rh1-C55-C56	43.1(2)
O2#1-Rh1-C55-C56	-137.7(2)	O1#1-Rh1-C55-C56	-47.3(2)
Rh1#1-Rh1-C55-C56	-67.7(3)	C54-C55-C56-C57	3.1(4)
Rh1-C55-C56-C57	-179.3(2)	C53-C52A-C57-C56	-0.5(5)
C51-C52A-C57-C56	175.3(4)	C55-C56-C57-C52A	-1.8(5)

---

Symmetry transformation codes: #1 -x+1,-y+1,-z+1

## MO Calculations.

**Computational details.** All geometry optimizations<sup>146</sup> were performed using the B3LYP three-parameter hybrid density functional method of Becke,<sup>147</sup> as implemented in the Gaussian03 suite of programs.<sup>148</sup> The basis functions consisted of the standard LANL2DZ for all atoms, which included the Hay and Wadt effective core potentials (ECP)<sup>149</sup> for Rh. Unless otherwise stated, the geometry optimizations were carried out without any symmetry constraint and the final geometries were characterized as local minima of the potential energy surface (PES) by verifying that all second derivatives of the energy were positive. MO calculations were performed on the optimized geometries using the Fenske-Hall LCAO-SCF method as implemented in JIMP 2.0 molecular modeling program.<sup>150</sup>

---

<sup>146</sup> Geometry optimizations were performed by Rinaldo Poli, Professor, Center for Coordination Chemistry, Toulouse, France.

<sup>147</sup> Becke, A. D., *J. Chem. Phys.* **1993**, 98, 5648-5652.

<sup>148</sup> Frisch, M. J., et al., *Gaussian 03, Revision B.04.* ed.; Gaussian, Inc.: Wallingford CT, 2003.

<sup>149</sup> Hay, P. J.; Wadt, W. R., *J. Chem. Phys.* **1985**, 82, 270-283.

<sup>150</sup> JIMP 2.0 is a free MO calculation software that uses Fenske-Hall LCAO functionals. The software was provided by researchers at Texas A & M. (a) Hall, M. B.; Fenske, R. F. *Inorg. Chem.* **1972**, 11, 768-779. (b) Manson, J.; Webster, C. E.; Pérez, L. M.; Hall, M. B. <http://www.chem.tamu.edu/jimp2/index.html>.

**Table 2-40.** Optimized geometry for **55** in Cartesian coordinates.

44  
scf done: -1359.096485

Rh	0.000000	0.000000	0.000000
N	0.000000	0.000000	2.021708
N	2.021844	0.000000	-0.023115
O	0.028346	0.302553	-2.116511
O	-2.116199	0.303932	0.051170
Rh	-0.033694	2.638696	-0.034113
O	-0.061844	2.335423	2.082611
O	2.082293	2.335520	-0.085510
N	-0.032686	2.638087	-2.056089
N	-2.055281	2.639283	-0.012025
C	-0.028512	1.165969	2.655088
C	2.654925	1.166003	-0.058826
C	-0.004378	1.471905	-2.689172
C	-2.688653	1.473513	0.023746
H	-0.024927	1.170604	3.752458
H	3.752274	1.170470	-0.067909
H	-0.007302	1.467120	-3.786554
H	-3.785998	1.469199	0.032155
H	0.042693	-0.844067	2.588253
H	2.589019	-0.843941	0.013245
H	-0.074910	3.481875	-2.623087
H	-2.622017	3.483502	-0.048777
C	0.122822	-1.994810	0.028302
C	-0.733943	-2.724241	0.871459
C	-0.687083	-4.134188	0.836919
C	0.214861	-4.798248	-0.017313
C	1.086247	-4.048846	-0.831711
C	1.046890	-2.684843	-0.776156
H	-1.396625	-2.210336	1.561009
H	-1.347095	-4.706453	1.486055
H	0.237298	-5.885141	-0.049226
H	1.820521	-4.536343	-1.470211
H	1.773026	-2.139837	-1.371508
C	-0.059202	4.637155	-0.059950
C	-0.924687	5.324948	0.809001
C	-0.985026	6.732981	0.738337
C	-0.179363	7.437444	-0.177523
C	0.703510	6.731670	-1.018124
C	0.775553	5.323565	-0.959424
H	-1.511497	4.782833	1.544198
H	-1.652401	7.273134	1.407171
H	-0.228308	8.522884	-0.225302
H	1.345894	7.270757	-1.711815
H	1.486808	4.780764	-1.574411

**Table 2-41.** Optimized geometry for **56** in Cartesian coordinates.

```
44
scf done: -1359.443398
Rh -0.132055 -0.167504 1.314328
O 1.975552 -0.118958 0.957122
N -0.119299 1.853750 1.366823
O -0.180402 -2.275306 0.956385
N -2.153031 -0.179236 1.367443
Rh -0.167504 -0.132055 -1.324328
O -0.118958 1.975552 -0.967122
O -2.275306 -0.180402 -0.966385
N 1.853750 -0.119299 -1.376823
N -0.179236 -2.153031 -1.377443
C -0.180953 -2.816847 -0.228180
C -2.816847 -0.180953 0.218180
C -0.117671 2.517263 0.217334
C 2.517263 -0.117671 -0.227334
H -2.697289 -0.161897 2.226936
H -0.136245 2.398463 2.226037
H 2.398463 -0.136245 -2.236037
H -0.161897 -2.697289 -2.236936
H -0.183612 -3.913961 -0.252479
H 3.614389 -0.114328 -0.251464
H -3.913961 -0.183612 0.242479
H -0.114328 3.614389 0.241464
C -0.524509 0.225595 -3.258181
C 0.225595 -0.524509 3.248181
C 0.227977 1.208006 -3.925762
C 0.016111 1.408428 -5.306445
C -0.944980 0.646860 -5.999633
C -1.710064 -0.311058 -5.305948
C -1.509979 -0.523369 -3.925339
H 0.936265 1.824204 -3.380461
H 0.594580 2.166572 -5.830916
H -1.105796 0.807911 -7.063146
H -2.470642 -0.886669 -5.830055
H -2.128537 -1.229076 -3.379343
C 1.208006 0.227977 3.915762
C 1.408428 0.016111 5.296445
C 0.646860 -0.944980 5.989633
C -0.311058 -1.710064 5.295948
C -0.523369 -1.509979 3.915339
H 1.824204 0.936265 3.370461
H 2.166572 0.594580 5.820916
H 0.807911 -1.105796 7.053146
H -0.886669 -2.470642 5.820055
H -1.229076 -2.128537 3.369343
```

**Table 2-42.** Optimized geometry for **57** in Cartesian coordinates.

44  
scf done: -1359.443735  
Rh -0.132245 0.066249 0.005599  
Rh 0.133020 -0.065588 2.632801  
N 1.913292 -0.086790 0.084883  
N -0.247093 -1.953263 -0.092036  
O -2.212920 0.169611 0.230005  
O 0.006045 2.155165 0.413743  
H 2.418373 -0.131484 -0.798974  
H -0.356931 -2.471011 -0.961213  
N -1.912516 0.087445 2.553511  
N 0.247858 1.953928 2.730441  
O 2.213696 -0.168933 2.408390  
O -0.005275 -2.154503 2.224662  
H -2.417599 0.132118 3.437369  
H 0.357687 2.471679 3.599617  
C 2.655209 -0.181978 1.180407  
C -0.157677 -2.654064 1.031116  
C -2.654433 0.182638 1.457988  
C 0.158437 2.654728 1.607288  
H 3.742331 -0.277142 1.069601  
H -0.214985 -3.748460 0.975724  
H -3.741555 0.277798 1.568796  
H 0.215735 3.749125 1.662680  
C 0.006229 0.468089 -1.948018  
C 0.917230 1.414384 -2.448890  
C 0.941881 1.673696 -3.835886  
C 0.061957 1.000988 -4.705176  
C -0.860527 0.073389 -4.183088  
C -0.896171 -0.196760 -2.799203  
H 1.561437 1.969688 -1.774417  
H 1.640131 2.410313 -4.228575  
H 0.084200 1.207238 -5.772668  
H -1.560757 -0.433298 -4.844259  
H -1.639812 -0.879696 -2.396312  
C -0.005478 -0.467459 4.586409  
C -0.916569 -1.413667 5.087275  
C -0.941237 -1.672993 6.474269  
C -0.061231 -1.000394 7.343562  
C 0.861346 -0.072888 6.821479  
C 0.896998 0.197286 5.437598  
H -1.560847 -1.968889 4.412802  
H -1.639562 -2.409541 6.866951  
H -0.083485 -1.206663 8.411050  
H 1.561643 0.433720 7.482640  
H 1.640705 0.880153 5.034713

**Table 2-43.** MO Calculations for **55** with energies (eV) and Atomic Orbital Contributions (%) [Values are only for the MOs used in Table 2-5].

MO #...		66( )	67( )	68( )	69( )	70( )	71( )	72( )	73( )	...
ENERGY =		-12.64	-11.19	-11.05	-11.03	-9.55	-9.51	-8.58	-6.94	
1C	2s	0.00	0.05	0.01	0.00	0.00	0.00	0.00	0.00	-0.03
1C	2px	0.00	0.00	0.00	0.00	0.18	0.07	0.00	0.00	0.01
1C	2py	0.00	0.00	0.16	1.16	0.00	0.01	0.06	0.06	-0.04
1C	2pz	0.00	0.03	0.21	1.08	0.00	0.02	0.06	0.06	-0.05
2C	2s	0.00	0.04	0.02	0.00	0.00	-0.01	0.00	0.00	-0.02
2C	2px	0.00	0.00	0.00	0.00	0.04	0.21	0.00	0.00	0.01
2C	2py	0.00	0.01	0.16	1.15	0.00	0.01	0.06	0.06	-0.04
2C	2pz	0.00	0.00	0.22	1.06	0.01	0.01	0.06	0.06	-0.05
3C	2s	0.00	0.05	0.01	0.00	0.00	0.00	0.00	0.00	-0.03
3C	2px	0.00	0.00	0.00	0.00	0.18	0.07	0.00	0.00	0.01
3C	2py	0.01	0.01	0.21	1.09	0.00	0.01	0.06	0.06	-0.04
3C	2pz	0.00	0.00	0.15	1.16	0.00	0.02	0.06	0.06	-0.06
4C	2s	0.00	0.04	0.02	0.00	0.00	-0.01	0.00	0.00	-0.03
4C	2px	0.00	0.00	0.00	0.00	0.04	0.22	0.00	0.00	0.01
4C	2py	0.00	0.00	0.22	1.10	0.00	0.01	0.06	0.06	-0.04
4C	2pz	0.00	0.03	0.13	1.13	0.01	0.01	0.06	0.06	-0.06
5C	2s	0.00	0.00	0.03	0.00	0.02	0.00	0.00	0.00	1.90
5C	2px	0.00	0.00	0.32	0.01	0.18	0.01	0.00	0.00	10.17
5C	2py	0.00	0.02	1.23	0.22	0.22	0.02	0.00	0.00	0.00
5C	2pz	0.01	0.26	0.00	0.00	0.02	0.15	0.00	0.00	0.00
6C	2s	0.00	0.04	0.00	0.00	0.00	0.04	0.00	0.00	0.00
6C	2px	0.01	0.14	0.02	0.00	0.00	0.12	0.00	0.00	-0.01
6C	2py	0.01	0.06	2.21	0.33	2.22	0.13	0.00	0.00	0.01
6C	2pz	0.00	0.39	0.02	0.00	0.01	0.33	0.00	0.00	0.08
7C	2s	0.00	0.01	0.00	0.00	0.00	0.01	0.00	0.00	0.04
7C	2px	0.01	0.05	0.02	0.00	0.00	0.05	0.00	0.00	0.40
7C	2py	0.01	0.00	0.22	0.04	0.06	0.00	0.00	0.00	0.00
7C	2pz	0.00	0.01	0.00	0.00	0.00	0.01	0.00	0.00	0.00
8C	2s	0.00	0.00	0.00	0.00	0.00	0.00	0.00	0.00	-0.01
8C	2px	0.00	0.00	0.00	0.00	0.00	0.00	0.00	0.00	0.00
8C	2py	0.00	0.07	3.32	0.49	2.72	0.16	0.00	0.00	0.03
8C	2pz	0.00	0.03	0.00	0.00	0.01	0.02	0.00	0.00	0.00
9C	2s	0.00	0.01	0.00	0.00	0.00	0.01	0.00	0.00	0.02
9C	2px	0.01	0.02	0.01	0.00	0.02	0.01	0.00	0.00	0.34
9C	2py	0.01	0.01	0.24	0.03	0.05	0.02	0.00	0.00	0.00
9C	2pz	0.00	0.02	0.00	0.00	0.00	0.01	0.00	0.00	0.00
10C	2s	0.00	0.04	0.00	0.00	0.00	0.05	0.00	0.00	0.00
10C	2px	0.01	0.09	0.00	0.00	0.01	0.08	0.00	0.00	-0.03
10C	2py	0.00	0.06	1.87	0.29	1.92	0.08	0.00	0.00	0.01
10C	2pz	0.00	0.39	0.02	0.00	0.00	0.39	0.00	0.00	0.04
11C	2s	0.00	0.00	0.02	0.02	0.01	0.00	0.00	0.00	1.80
11C	2px	0.00	0.01	0.31	0.11	0.05	0.01	0.00	0.00	10.33
11C	2py	0.00	0.01	1.14	0.21	0.16	0.02	0.00	0.00	0.05
11C	2pz	0.01	0.24	0.00	0.00	0.01	0.15	0.00	0.00	0.00
12C	2s	0.00	0.04	0.00	0.00	0.00	0.04	0.00	0.00	0.00
12C	2px	0.01	0.09	0.01	0.00	-0.01	0.14	0.00	0.00	-0.02
12C	2py	0.02	0.01	2.15	0.45	1.84	0.15	0.00	0.00	0.00
12C	2pz	0.00	0.39	0.01	0.01	0.06	0.33	0.00	0.00	0.06
13C	2s	0.00	0.01	0.00	0.00	0.00	0.01	0.00	0.00	0.03
13C	2px	0.00	0.03	0.00	0.00	0.01	0.05	0.00	0.00	0.39
13C	2py	0.04	0.00	0.22	0.04	0.03	0.02	0.00	0.00	0.00
13C	2pz	0.00	0.02	0.00	0.00	0.00	0.01	0.00	0.00	0.00
14C	2s	0.00	0.00	0.00	0.00	0.00	0.00	0.00	0.00	-0.01
14C	2px	0.00	0.00	0.02	0.00	0.01	0.00	0.00	0.00	0.00



14C	2py	0.00	0.01	3.18	0.67	2.21	0.21	0.00	0.00
14C	2pz	0.00	0.03	0.00	0.00	0.00	0.02	0.00	0.00
15C	2s	0.00	0.01	0.00	0.00	0.00	0.01	0.00	0.03
15C	2px	0.01	0.05	0.01	0.00	0.00	0.02	0.00	0.40
15C	2py	0.05	0.00	0.22	0.05	0.05	0.00	0.00	0.00
15C	2pz	0.00	0.02	0.00	0.00	0.00	0.01	0.00	0.00
16C	2s	0.00	0.04	0.00	0.00	0.01	0.04	0.00	0.00
16C	2px	0.02	0.14	0.00	0.00	0.05	0.07	0.00	-0.02
16C	2py	0.02	0.00	2.18	0.44	1.79	0.21	0.00	0.00
16C	2pz	0.01	0.40	0.02	0.00	0.03	0.31	0.00	0.07
17H	1s	0.00	0.18	0.06	0.01	0.11	0.01	0.00	0.26
18H	1s	0.00	0.13	0.11	0.01	0.05	0.08	0.00	0.27
19H	1s	0.00	0.15	0.08	0.02	0.12	0.00	0.00	0.26
20H	1s	0.00	0.16	0.12	0.02	0.06	0.10	0.00	0.23
21H	1s	0.00	0.08	0.04	0.02	0.25	0.09	0.00	0.01
22H	1s	0.00	0.05	0.05	0.01	0.07	0.27	0.00	0.00
23H	1s	0.00	0.08	0.05	0.01	0.25	0.08	0.00	0.01
24H	1s	0.00	0.05	0.08	0.00	0.07	0.28	0.00	0.01
25H	1s	0.00	0.04	0.00	0.00	0.01	0.02	0.00	0.09
26H	1s	0.00	0.07	0.01	0.00	0.00	0.05	0.00	0.06
27H	1s	0.00	0.00	0.00	0.00	0.00	0.00	0.00	0.04
28H	1s	0.00	0.07	0.00	0.00	0.01	0.05	0.00	0.04
29H	1s	0.00	0.06	0.01	0.00	0.00	0.04	0.00	0.12
30H	1s	0.00	0.05	0.01	0.00	0.00	0.02	0.00	0.11
31H	1s	0.00	0.06	0.00	0.00	0.01	0.05	0.00	0.05
32H	1s	0.00	0.00	0.00	0.00	0.00	0.00	0.00	0.04
33H	1s	0.00	0.07	0.01	0.00	0.00	0.04	0.00	0.06
34H	1s	0.00	0.04	0.00	0.00	0.01	0.03	0.00	0.10
35N	2s	0.00	0.03	0.00	0.00	0.04	0.05	0.00	0.12
35N	2px	0.04	0.06	0.03	0.02	0.14	0.04	0.01	-0.14
35N	2py	5.54	0.02	0.01	0.65	0.01	0.02	1.87	0.55
35N	2pz	5.21	1.04	0.26	0.29	0.01	0.05	1.74	0.37
36N	2s	0.00	0.01	0.00	0.00	0.00	0.06	0.00	0.15
36N	2px	0.03	0.05	0.06	0.01	0.04	0.13	0.00	-0.13
36N	2py	5.51	0.02	0.01	0.62	0.01	0.00	1.86	0.63
36N	2pz	5.07	0.65	0.46	0.30	0.02	0.00	1.70	0.46
37N	2s	0.00	0.02	0.01	0.00	0.05	0.04	0.00	0.12
37N	2px	0.04	0.06	0.04	0.00	0.13	0.05	0.01	-0.13
37N	2py	5.74	0.03	0.32	0.36	0.00	0.01	1.86	0.54
37N	2pz	5.57	0.79	0.00	0.70	0.00	0.03	1.73	0.36
38N	2s	0.00	0.02	0.01	0.00	0.01	0.07	0.00	0.12
38N	2px	0.04	0.06	0.06	0.00	0.04	0.13	0.00	-0.13
38N	2py	6.00	0.01	0.37	0.38	0.01	0.00	1.89	0.54
38N	2pz	5.52	0.86	0.03	0.66	0.02	0.01	1.74	0.35
39O	2s	0.01	0.03	0.00	0.00	0.02	0.03	0.00	0.05
39O	2px	0.08	2.00	0.74	0.20	1.24	0.47	0.00	-0.05
39O	2py	6.03	3.22	0.50	0.86	0.68	0.03	2.21	0.08
39O	2pz	7.37	0.75	1.86	0.01	0.68	0.10	2.36	0.19
40O	2s	0.01	0.02	0.00	0.00	0.00	0.04	0.00	0.05
40O	2px	0.14	1.64	1.22	0.18	0.34	1.43	0.00	-0.02
40O	2py	5.94	3.15	0.98	0.77	0.35	0.46	2.27	0.03
40O	2pz	7.80	0.52	2.27	0.01	0.24	0.71	2.33	0.12
41O	2s	0.01	0.02	0.00	0.00	0.03	0.03	0.00	0.06
41O	2px	0.08	1.98	0.97	0.17	1.18	0.51	0.00	-0.05
41O	2py	5.72	3.60	1.24	0.00	0.56	0.06	2.21	0.09
41O	2pz	7.02	0.74	0.99	0.83	0.59	0.18	2.36	0.22
42O	2s	0.01	0.02	0.01	0.00	0.00	0.04	0.00	0.06
42O	2px	0.12	1.59	1.56	0.14	0.28	1.31	0.00	-0.04
42O	2py	5.55	2.77	2.04	0.01	0.21	0.36	2.22	0.10
42O	2pz	6.96	0.51	1.27	0.74	0.17	0.56	2.31	0.22
43RH	4dz2	0.00	0.01	5.64	24.50	0.03	0.06	24.59	2.85
43RH	4dx2y2	0.01	0.23	0.76	10.78	0.00	0.14	8.83	6.43
43RH	4dxy	0.00	0.23	22.72	2.98	35.59	3.14	0.00	0.00
43RH	4dxz	1.13	32.62	0.20	0.00	3.18	39.16	0.00	0.25

43RH	4dyz	0.07	0.77	0.00	0.00	0.10	0.80	0.00	0.00
43RH	5s	0.00	0.01	0.66	0.05	0.42	0.14	0.00	1.37
43RH	5px	0.00	0.00	0.00	0.03	0.04	0.00	0.00	22.50
43RH	5py	0.00	0.00	0.38	0.00	0.45	0.03	0.00	0.28
43RH	5pz	0.01	0.58	0.00	0.00	0.04	0.50	0.00	0.00
44RH	4dz2	0.00	0.11	3.70	26.01	0.14	0.01	24.53	2.92
44RH	4dx2y2	0.00	0.01	1.33	10.32	0.08	0.00	8.85	6.48
44RH	4dxy	0.00	0.18	25.12	4.69	33.29	2.82	0.00	0.21
44RH	4dxz	1.16	32.73	0.36	0.03	3.48	39.39	0.00	0.03
44RH	4dyz	0.07	0.77	0.00	0.00	0.10	0.80	0.00	0.00
44RH	5s	0.00	0.00	0.24	0.08	0.22	0.03	0.00	1.39
44RH	5px	0.00	0.02	0.00	0.03	0.00	0.04	0.00	22.68
44RH	5py	0.00	0.00	0.35	0.14	0.43	0.03	0.00	0.30
44RH	5pz	0.01	0.57	0.01	0.00	0.05	0.50	0.00	0.00

---

**Table 2-44.** MO Calculations for **56** with energies (eV) and Atomic Orbital Contributions (%) [Values are only for the MOs used in Table 2-6].

MO	...66( )	67( )	68( )	69( )	70( )	71( )	72( )	73( )	...
ENERGY =	-12.68	-11.36	-11.18	-11.10	-10.31	-9.66	-8.70	-6.45	
1C 2s	0.00	0.04	0.00	0.02	0.00	0.00	0.00	0.00	-0.03
1C 2px	0.00	0.00	0.04	0.01	0.10	0.14	0.00	0.00	0.02
1C 2py	0.01	0.00	1.25	0.00	0.00	0.02	0.06	0.06	-0.02
1C 2pz	0.00	0.01	1.28	0.01	0.00	0.02	0.06	0.06	-0.05
2C 2s	0.00	0.04	0.00	0.02	0.00	0.00	0.00	0.00	-0.03
2C 2px	0.00	0.00	0.04	0.01	0.10	0.14	0.00	0.00	0.02
2C 2py	0.01	0.00	1.25	0.00	0.00	0.02	0.06	0.06	-0.02
2C 2pz	0.00	0.01	1.28	0.01	0.00	0.02	0.06	0.06	-0.05
3C 2s	0.00	0.04	0.00	0.02	0.00	0.00	0.00	0.00	-0.03
3C 2px	0.00	0.00	0.04	0.01	0.10	0.14	0.00	0.00	0.02
3C 2py	0.01	0.00	1.24	0.00	0.00	0.02	0.06	0.06	-0.02
3C 2pz	0.00	0.01	1.28	0.01	0.00	0.02	0.06	0.06	-0.05
4C 2s	0.00	0.04	0.00	0.02	0.00	0.00	0.00	0.00	-0.03
4C 2px	0.00	0.00	0.04	0.01	0.10	0.14	0.00	0.00	0.02
4C 2py	0.01	0.00	1.25	0.00	0.00	0.02	0.06	0.06	-0.02
4C 2pz	0.00	0.01	1.28	0.01	0.00	0.02	0.06	0.06	-0.05
5C 2s	0.00	0.00	0.01	0.11	0.21	0.00	0.00	0.00	1.61
5C 2px	0.00	0.00	0.01	1.17	1.50	0.00	0.00	0.00	8.90
5C 2py	0.00	0.00	0.18	1.76	0.69	0.00	0.00	0.00	0.08
5C 2pz	0.02	0.29	0.00	0.00	0.00	0.20	0.00	0.00	0.00
6C 2s	0.00	0.00	0.01	0.11	0.21	0.00	0.00	0.00	1.61
6C 2px	0.00	0.00	0.01	1.17	1.50	0.00	0.00	0.00	8.90
6C 2py	0.00	0.00	0.18	1.75	0.69	0.00	0.00	0.00	0.08
6C 2pz	0.02	0.29	0.00	0.00	0.00	0.20	0.00	0.00	0.00
7C 2s	0.00	0.04	0.00	0.00	0.00	0.05	0.00	0.00	0.00
7C 2px	0.01	0.11	0.00	0.00	0.04	0.12	0.00	0.00	-0.04
7C 2py	0.04	0.01	0.21	2.85	1.95	0.00	0.07	0.07	0.23
7C 2pz	0.03	0.41	0.00	0.00	0.04	0.39	0.00	0.00	0.04
8C 2s	0.00	0.01	0.00	0.01	0.00	0.01	0.00	0.00	0.03
8C 2px	0.00	0.04	0.00	0.07	0.09	0.04	0.00	0.00	0.34
8C 2py	0.06	0.03	0.03	0.33	0.10	0.00	0.00	0.00	0.00
8C 2pz	0.00	0.02	0.00	0.00	0.00	0.01	0.00	0.00	0.00
9C 2s	0.00	0.00	0.00	0.00	0.00	0.00	0.00	0.00	-0.01
9C 2px	0.00	0.00	0.00	0.03	0.00	0.00	0.00	0.00	0.00
9C 2py	0.00	0.00	0.33	4.28	2.59	0.00	0.08	0.08	0.27
9C 2pz	0.00	0.03	0.00	0.00	0.00	0.02	0.00	0.00	0.00
10C 2s	0.00	0.01	0.00	0.01	0.00	0.01	0.00	0.00	0.03
10C 2px	0.00	0.04	0.00	0.07	0.09	0.04	0.00	0.00	0.34
10C 2py	0.06	0.03	0.03	0.33	0.10	0.00	0.00	0.00	0.00
10C 2pz	0.00	0.02	0.00	0.00	0.00	0.01	0.00	0.00	0.00
11C 2s	0.00	0.04	0.00	0.00	0.00	0.05	0.00	0.00	0.00
11C 2px	0.01	0.11	0.00	0.00	0.04	0.12	0.00	0.00	-0.04
11C 2py	0.04	0.01	0.21	2.85	1.95	0.00	0.07	0.07	0.23
11C 2pz	0.03	0.41	0.00	0.00	0.04	0.39	0.00	0.00	0.04
12C 2s	0.00	0.04	0.00	0.00	0.00	0.05	0.00	0.00	0.00
12C 2px	0.01	0.11	0.00	0.00	0.04	0.12	0.00	0.00	-0.04
12C 2py	0.04	0.01	0.21	2.85	1.95	0.00	0.07	0.07	0.23
12C 2pz	0.03	0.41	0.00	0.00	0.03	0.39	0.00	0.00	0.04
13C 2s	0.00	0.01	0.00	0.01	0.00	0.01	0.00	0.00	0.03
13C 2px	0.00	0.04	0.00	0.07	0.09	0.04	0.00	0.00	0.34
13C 2py	0.06	0.03	0.03	0.33	0.10	0.00	0.00	0.00	0.00
13C 2pz	0.00	0.02	0.00	0.00	0.00	0.01	0.00	0.00	0.00
14C 2s	0.00	0.00	0.00	0.00	0.00	0.00	0.00	0.00	-0.01
14C 2px	0.00	0.00	0.00	0.03	0.00	0.00	0.00	0.00	0.00

14C	2py	0.00	0.00	0.33	4.28	2.58	0.00	0.08	0.27
14C	2pz	0.00	0.03	0.00	0.00	0.00	0.02	0.00	0.00
15C	2s	0.00	0.01	0.00	0.01	0.00	0.01	0.00	0.03
15C	2px	0.00	0.04	0.00	0.07	0.09	0.04	0.00	0.34
15C	2py	0.06	0.03	0.03	0.33	0.10	0.00	0.00	0.00
15C	2pz	0.00	0.02	0.00	0.00	0.00	0.01	0.00	0.00
16C	2s	0.00	0.04	0.00	0.00	0.00	0.05	0.00	0.00
16C	2px	0.01	0.11	0.00	0.00	0.04	0.12	0.00	-0.04
16C	2py	0.04	0.01	0.21	2.86	1.95	0.00	0.07	0.23
16C	2pz	0.03	0.41	0.00	0.00	0.04	0.39	0.00	0.04
17H	1s	0.00	0.07	0.00	0.11	0.13	0.19	0.00	0.06
18H	1s	0.00	0.07	0.00	0.11	0.13	0.19	0.00	0.06
19H	1s	0.00	0.07	0.00	0.11	0.13	0.19	0.00	0.06
20H	1s	0.00	0.07	0.00	0.11	0.13	0.19	0.00	0.06
21H	1s	0.00	0.17	0.01	0.03	0.00	0.05	0.00	0.27
22H	1s	0.00	0.17	0.01	0.03	0.00	0.05	0.00	0.27
23H	1s	0.00	0.17	0.01	0.03	0.00	0.05	0.00	0.27
24H	1s	0.00	0.17	0.01	0.03	0.00	0.05	0.00	0.27
25H	1s	0.00	0.05	0.00	0.01	0.02	0.03	0.00	0.09
26H	1s	0.01	0.07	0.00	0.01	0.02	0.05	0.00	0.04
27H	1s	0.00	0.00	0.00	0.02	0.01	0.00	0.00	0.03
28H	1s	0.01	0.07	0.00	0.01	0.02	0.05	0.00	0.04
29H	1s	0.00	0.05	0.00	0.01	0.02	0.03	0.00	0.09
30H	1s	0.00	0.05	0.00	0.01	0.02	0.03	0.00	0.09
31H	1s	0.01	0.07	0.00	0.01	0.02	0.05	0.00	0.04
32H	1s	0.00	0.00	0.00	0.02	0.01	0.00	0.00	0.03
33H	1s	0.01	0.07	0.00	0.01	0.02	0.05	0.00	0.04
34H	1s	0.00	0.05	0.00	0.01	0.02	0.03	0.00	0.09
35N	2s	0.00	0.02	0.00	0.04	0.09	0.05	0.00	0.05
35N	2px	0.24	0.06	0.00	0.03	0.08	0.10	0.06	-0.14
35N	2py	5.48	0.00	0.57	0.22	0.13	0.01	1.81	0.39
35N	2pz	5.26	0.88	0.64	0.10	0.02	0.02	1.81	0.20
36N	2s	0.00	0.02	0.00	0.04	0.09	0.05	0.00	0.05
36N	2px	0.24	0.06	0.00	0.03	0.08	0.10	0.06	-0.14
36N	2py	5.51	0.00	0.57	0.22	0.13	0.01	1.81	0.39
36N	2pz	5.29	0.88	0.64	0.10	0.02	0.02	1.81	0.20
37N	2s	0.00	0.02	0.00	0.04	0.09	0.05	0.00	0.05
37N	2px	0.24	0.06	0.00	0.03	0.08	0.10	0.06	-0.14
37N	2py	5.50	0.00	0.57	0.22	0.13	0.01	1.81	0.39
37N	2pz	5.28	0.88	0.64	0.10	0.02	0.02	1.81	0.20
38N	2s	0.00	0.02	0.00	0.04	0.09	0.05	0.00	0.05
38N	2px	0.24	0.06	0.00	0.03	0.08	0.10	0.06	-0.14
38N	2py	5.53	0.00	0.57	0.22	0.13	0.01	1.81	0.39
38N	2pz	5.30	0.88	0.64	0.10	0.02	0.02	1.81	0.20
39O	2s	0.01	0.02	0.00	0.00	0.06	0.03	0.00	0.05
39O	2px	0.00	2.50	0.07	0.61	1.09	1.06	0.05	-0.08
39O	2py	5.75	2.80	0.41	0.15	0.13	0.11	2.18	0.20
39O	2pz	7.39	0.66	0.10	0.95	0.10	0.41	2.44	0.45
40O	2s	0.01	0.02	0.00	0.00	0.06	0.03	0.00	0.05
40O	2px	0.00	2.50	0.07	0.61	1.09	1.06	0.05	-0.08
40O	2py	5.79	2.80	0.41	0.15	0.13	0.11	2.18	0.20
40O	2pz	7.42	0.66	0.10	0.95	0.10	0.41	2.44	0.45
41O	2s	0.01	0.02	0.00	0.00	0.06	0.03	0.00	0.05
41O	2px	0.00	2.49	0.07	0.61	1.09	1.06	0.05	-0.08
41O	2py	5.74	2.80	0.41	0.15	0.13	0.11	2.18	0.20
41O	2pz	7.36	0.66	0.10	0.95	0.10	0.41	2.44	0.45
42O	2s	0.01	0.02	0.00	0.00	0.06	0.03	0.00	0.05
42O	2px	0.00	2.50	0.07	0.61	1.09	1.06	0.05	-0.08
42O	2py	5.78	2.80	0.42	0.15	0.13	0.11	2.18	0.20
42O	2pz	7.39	0.66	0.10	0.95	0.10	0.41	2.44	0.45
43RH	4dz2	0.00	0.00	27.68	0.82	1.89	0.00	23.31	2.16
43RH	4dx2y2	0.00	0.00	11.98	0.03	0.18	0.00	8.92	6.18
43RH	4dxy	0.00	0.00	0.52	29.37	31.82	0.00	0.59	4.86
43RH	4dxz	1.21	33.01	0.00	0.00	0.00	43.42	0.00	0.00

43RH 4dyz	0.02	0.03	0.00	0.00	0.00	0.02	0.00	0.00
43RH 5s	0.00	0.00	0.01	0.12	0.21	0.00	0.00	0.88
43RH 5px	0.00	0.00	0.05	0.91	2.08	0.00	0.00	20.87
43RH 5py	0.00	0.00	0.00	0.30	0.44	0.00	0.00	0.00
43RH 5pz	0.01	0.60	0.00	0.00	0.00	0.53	0.00	0.00
44RH 4dz2	0.00	0.00	27.67	0.81	1.90	0.00	23.32	2.16
44RH 4dx2y2	0.00	0.00	11.97	0.03	0.18	0.00	8.93	6.18
44RH 4dxy	0.00	0.00	0.51	29.33	31.87	0.00	0.59	4.86
44RH 4dxz	1.22	32.99	0.00	0.00	0.00	43.45	0.00	0.00
44RH 4dyz	0.02	0.03	0.00	0.00	0.00	0.02	0.00	0.00
44RH 5s	0.00	0.00	0.01	0.12	0.21	0.00	0.00	0.88
44RH 5px	0.00	0.00	0.05	0.91	2.08	0.00	0.00	20.86
44RH 5py	0.00	0.00	0.00	0.30	0.44	0.00	0.00	0.00
44RH 5pz	0.01	0.60	0.00	0.00	0.00	0.53	0.00	0.00

**Table 2-45.** MO Calculations for **57** with energies (eV) and Atomic Orbital Contributions (%).

MO		...66( )	67( )	68( )	69( )	70( )	71( )	72( )	73( )...
ENERGY =		-12.73	-11.34	-11.33	-11.20	-10.32	-9.78	-8.77	-6.51
1C	2s	0.00	0.00	0.00	0.06	-0.01	0.00	0.00	0.00
1C	2px	0.00	0.05	0.00	0.03	0.12	0.12	0.00	-0.02
1C	2py	0.01	1.24	0.00	0.01	0.00	0.01	0.03	0.00
1C	2pz	0.00	1.44	0.00	0.01	-0.01	0.00	0.03	-0.05
2C	2s	0.00	0.00	0.06	0.00	0.00	0.00	0.00	-0.03
2C	2px	0.00	0.01	0.00	0.00	0.16	0.10	0.00	-0.03
2C	2py	0.01	1.41	0.01	0.00	-0.01	0.00	0.05	0.02
2C	2pz	0.00	1.38	0.01	0.00	0.00	0.01	0.06	-0.05
3C	2s	0.00	0.00	0.00	0.06	-0.01	0.00	0.00	-0.03
3C	2px	0.00	0.05	0.00	0.02	0.12	0.12	0.00	-0.02
3C	2py	0.01	1.24	0.00	0.01	0.00	0.01	0.03	0.00
3C	2pz	0.00	1.44	0.00	0.01	-0.01	0.00	0.03	-0.05
4C	2s	0.00	0.00	0.06	0.00	0.00	0.00	0.00	-0.03
4C	2px	0.00	0.01	0.00	0.00	0.16	0.10	0.00	-0.03
4C	2py	0.02	1.42	0.01	0.00	-0.01	0.00	0.05	0.02
4C	2pz	0.00	1.38	0.01	0.01	0.00	0.01	0.06	-0.05
5C	2s	0.01	0.00	0.02	0.11	0.21	0.00	0.00	-0.03
5C	2px	0.07	0.00	0.25	1.40	1.27	0.00	0.00	1.61
5C	2py	0.21	0.00	1.49	0.49	0.00	0.37	0.00	9.10
5C	2pz	0.00	0.01	0.06	0.11	0.30	0.00	0.00	0.03
6C	2s	0.00	0.00	0.01	0.03	0.05	0.00	0.00	0.01
6C	2px	0.00	0.01	0.00	0.02	0.17	0.01	0.00	0.00
6C	2py	0.17	0.00	1.76	0.87	0.02	2.17	0.00	-0.04
6C	2pz	0.00	0.01	0.18	0.14	0.57	0.00	0.01	0.00
7C	2s	0.00	0.00	0.00	0.00	0.02	0.00	0.00	0.00
7C	2px	0.00	0.01	0.01	0.02	0.17	0.00	0.00	0.02
7C	2py	0.00	0.00	0.35	0.15	0.00	0.12	0.00	0.28
7C	2pz	0.00	0.00	0.01	0.01	0.02	0.00	0.00	0.00
8C	2s	0.00	0.00	0.00	0.00	0.00	0.00	0.00	0.00
8C	2px	0.00	0.00	0.00	0.02	0.00	0.00	0.00	-0.01
8C	2py	0.21	0.00	3.01	1.38	0.02	2.76	0.00	0.00
8C	2pz	0.00	0.00	0.00	0.02	0.02	0.00	0.00	0.00
9C	2s	0.00	0.00	0.01	0.03	0.00	0.00	0.00	0.00
9C	2px	0.01	0.00	0.11	0.24	0.00	0.00	0.00	0.05
9C	2py	0.13	0.00	0.14	0.09	0.00	0.04	0.00	0.44
9C	2pz	0.00	0.00	0.00	0.00	0.01	0.00	0.00	0.00
10C	2s	0.00	0.00	0.02	0.03	0.03	0.00	0.00	0.00
10C	2px	0.01	0.00	0.17	0.21	0.04	0.00	0.00	0.00
10C	2py	0.02	0.00	2.00	1.00	0.01	2.27	0.00	0.00
10C	2pz	0.00	0.02	0.12	0.39	0.17	0.00	0.01	0.00
11C	2s	0.01	0.00	0.02	0.12	0.21	0.00	0.00	0.14
11C	2px	0.07	0.00	0.25	1.40	1.27	0.00	0.00	1.61
11C	2py	0.21	0.00	1.49	0.49	0.00	0.38	0.00	9.08
11C	2pz	0.00	0.01	0.05	0.11	0.31	0.00	0.00	0.03
12C	2s	0.00	0.00	0.01	0.03	0.05	0.00	0.00	0.01
12C	2px	0.00	0.01	0.00	0.02	0.17	0.01	0.00	0.00
12C	2py	0.18	0.00	1.76	0.86	0.02	2.18	0.00	-0.04
12C	2pz	0.00	0.02	0.18	0.14	0.57	0.00	0.01	0.00
13C	2s	0.00	0.00	0.00	0.00	0.02	0.00	0.00	0.00
13C	2px	0.00	0.01	0.01	0.02	0.17	0.00	0.00	0.02
13C	2py	0.00	0.00	0.35	0.15	0.00	0.12	0.00	0.28
13C	2pz	0.00	0.00	0.01	0.01	0.02	0.00	0.00	0.00
14C	2s	0.00	0.00	0.00	0.00	0.00	0.00	0.00	0.00
14C	2px	0.00	0.00	0.00	0.02	0.00	0.00	0.00	-0.01
14C	2py	0.21	0.00	3.00	1.37	0.02	2.77	0.00	0.00

14C	2pz	0.00	0.00	0.00	0.02	0.02	0.00	0.00	0.00
15C	2s	0.00	0.00	0.01	0.03	0.00	0.00	0.00	0.00
15C	2px	0.01	0.00	0.11	0.23	0.00	0.00	0.00	0.05
15C	2py	0.14	0.00	0.14	0.09	0.00	0.04	0.00	0.44
15C	2pz	0.00	0.00	0.00	0.00	0.01	0.00	0.00	0.00
16C	2s	0.00	0.00	0.02	0.03	0.03	0.00	0.00	0.00
16C	2px	0.01	0.00	0.17	0.21	0.04	0.00	0.00	0.00
16C	2py	0.02	0.00	2.00	0.99	0.01	2.28	0.00	0.00
16C	2pz	0.00	0.02	0.12	0.38	0.17	0.00	0.01	0.00
17H	1s	0.00	0.00	0.01	0.17	0.16	0.15	0.00	0.15
18H	1s	0.00	0.00	0.18	0.01	0.17	0.14	0.00	0.00
19H	1s	0.00	0.00	0.01	0.17	0.16	0.15	0.00	0.07
20H	1s	0.00	0.00	0.18	0.01	0.17	0.14	0.00	0.00
21H	1s	0.02	0.00	0.00	0.18	0.11	0.02	0.00	0.22
22H	1s	0.05	0.00	0.14	0.00	0.00	0.05	0.00	0.27
23H	1s	0.02	0.00	0.00	0.18	0.11	0.02	0.00	0.22
24H	1s	0.05	0.00	0.14	0.00	0.00	0.05	0.00	0.27
25H	1s	0.00	0.00	0.05	0.11	0.00	0.00	0.00	0.13
26H	1s	0.00	0.00	0.01	0.01	0.11	0.00	0.00	0.02
27H	1s	0.00	0.00	0.01	0.02	0.01	0.00	0.00	0.03
28H	1s	0.00	0.00	0.05	0.13	0.01	0.00	0.00	0.08
29H	1s	0.00	0.01	0.00	-0.01	0.08	0.00	0.00	0.06
30H	1s	0.00	0.00	0.05	0.11	0.00	0.00	0.00	0.13
31H	1s	0.00	0.00	0.01	0.01	0.11	0.00	0.00	0.02
32H	1s	0.00	0.00	0.01	0.02	0.01	0.00	0.00	0.03
33H	1s	0.00	0.00	0.05	0.13	0.01	0.00	0.00	0.08
34H	1s	0.00	0.01	0.00	-0.01	0.08	0.00	0.00	0.06
35N	2s	0.00	0.00	0.01	0.04	0.01	0.03	0.00	0.11
35N	2px	0.21	0.00	0.00	0.07	0.03	0.05	0.07	-0.11
35N	2py	4.32	0.26	0.02	0.30	0.04	0.00	1.63	0.49
35N	2pz	6.17	0.21	0.19	0.54	0.00	0.00	1.77	0.23
36N	2s	0.00	0.00	0.05	0.01	0.14	0.02	0.00	0.04
36N	2px	0.05	0.00	0.12	0.00	0.11	0.07	0.00	-0.14
36N	2py	4.72	0.70	0.58	0.00	0.10	0.00	2.01	0.21
36N	2pz	6.52	0.57	0.19	0.16	0.19	0.00	1.80	0.29
37N	2s	0.00	0.00	0.01	0.04	0.01	0.03	0.00	0.11
37N	2px	0.21	0.00	0.00	0.07	0.03	0.06	0.07	-0.11
37N	2py	4.31	0.25	0.03	0.30	0.04	0.00	1.63	0.48
37N	2pz	6.14	0.21	0.19	0.53	0.00	0.00	1.78	0.23
38N	2s	0.00	0.00	0.05	0.01	0.14	0.02	0.00	0.04
38N	2px	0.05	0.00	0.12	0.00	0.11	0.07	0.00	-0.14
38N	2py	4.69	0.71	0.57	0.00	0.09	0.00	2.02	0.21
38N	2pz	6.49	0.55	0.20	0.17	0.19	0.00	1.81	0.29
39O	2s	0.00	0.00	0.00	0.03	0.01	0.03	0.00	0.09
39O	2px	0.21	0.03	0.01	2.36	1.06	1.17	0.10	0.07
39O	2py	7.02	0.04	0.05	2.29	0.42	0.30	2.36	0.09
39O	2pz	6.32	0.00	0.01	2.25	0.94	0.51	2.37	0.14
40O	2s	0.00	0.00	0.02	0.01	0.10	0.01	0.00	0.05
40O	2px	0.05	0.01	2.70	0.04	1.58	0.74	0.00	-0.07
40O	2py	8.69	0.26	1.29	0.19	0.08	0.28	2.28	0.37
40O	2pz	4.42	0.23	2.08	0.08	0.14	0.15	2.50	0.29
41O	2s	0.00	0.00	0.00	0.03	0.01	0.03	0.00	0.09
41O	2px	0.21	0.02	0.01	2.36	1.07	1.18	0.10	0.06
41O	2py	7.05	0.04	0.05	2.29	0.42	0.30	2.36	0.09
41O	2pz	6.37	0.00	0.01	2.23	0.95	0.51	2.36	0.14
42O	2s	0.00	0.00	0.02	0.01	0.10	0.01	0.00	0.05
42O	2px	0.05	0.01	2.69	0.04	1.59	0.74	0.00	-0.07
42O	2py	8.81	0.28	1.27	0.19	0.08	0.28	2.28	0.38
42O	2pz	4.49	0.22	2.10	0.08	0.13	0.15	2.50	0.29
43RH	4dz2	0.00	31.74	0.01	0.02	0.17	0.00	24.88	2.11
43RH	4dx2y2	0.04	10.13	0.00	2.16	1.75	0.71	7.37	5.24
43RH	4dxy	0.04	0.21	20.30	7.82	0.43	36.70	0.21	0.09
43RH	4dxz	0.10	0.11	11.44	22.79	35.37	0.16	0.28	6.53
43RH	4dyz	0.00	0.00	0.00	0.05	0.01	0.00	0.00	0.01

43RH 5s	0.02	0.00	0.03	0.31	0.48	0.04	0.00	0.77
43RH 5px	0.01	0.00	0.30	0.63	2.17	0.00	0.00	20.76
43RH 5py	0.01	0.00	0.31	0.16	0.00	0.51	0.00	0.02
43RH 5pz	0.04	0.00	0.15	0.34	0.56	0.00	0.00	0.01
44RH 4dz2	0.00	31.57	0.00	0.01	0.16	0.00	25.06	2.10
44RH 4dx2y2	0.04	10.00	0.00	2.22	1.76	0.72	7.42	5.21
44RH 4dxy	0.04	0.18	20.22	7.76	0.43	36.89	0.21	0.09
44RH 4dxz	0.10	0.16	11.34	22.60	35.63	0.16	0.28	6.54
44RH 4dyz	0.00	0.00	0.00	0.05	0.01	0.00	0.00	0.01
44RH 5s	0.02	0.00	0.03	0.31	0.48	0.04	0.00	0.77
44RH 5px	0.01	0.00	0.30	0.64	2.16	0.00	0.00	20.73
44RH 5py	0.01	0.00	0.31	0.15	0.00	0.51	0.00	0.02
44RH 5pz	0.04	0.00	0.15	0.34	0.56	0.00	0.00	0.01

---



## Chapter 3

# The Oxidative Mannich Reaction: *tert*-Butylperoxyl Radical Oxidizes Dialkylanilines by Electron/Proton Transfer

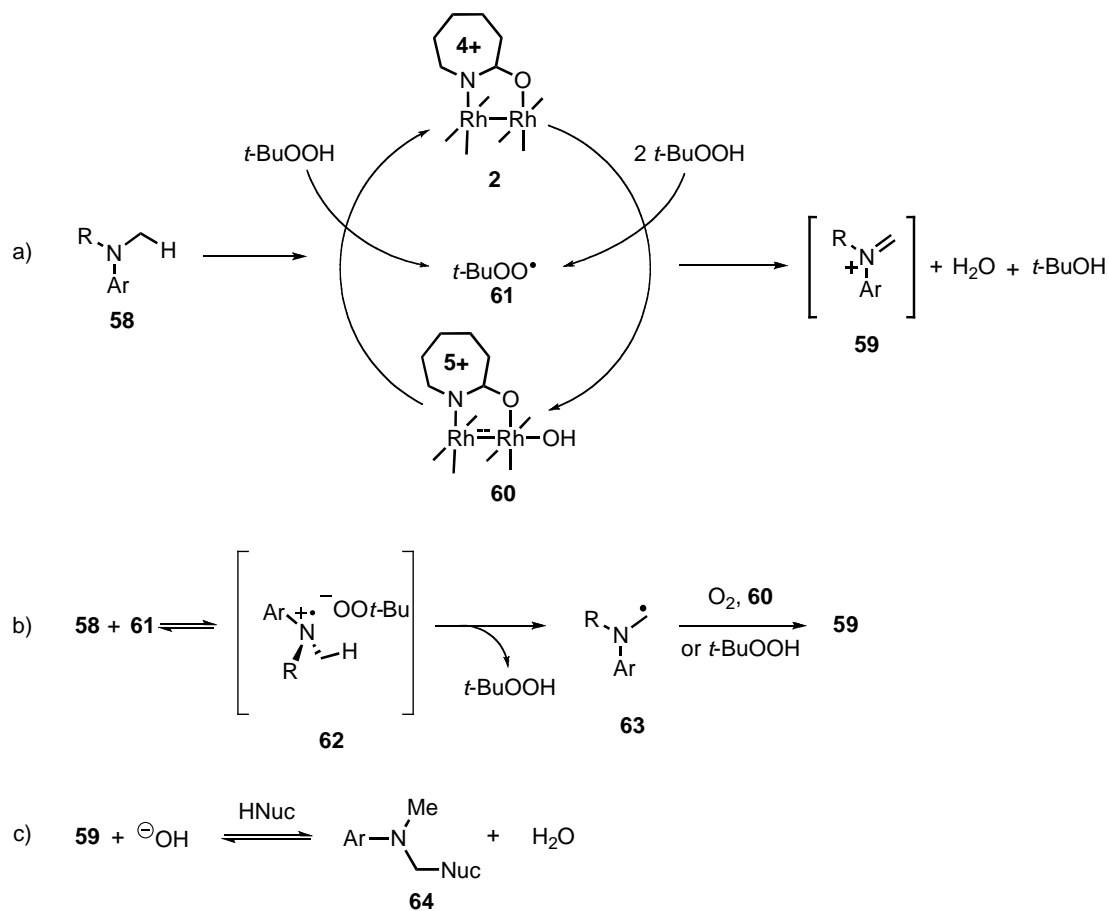
### I. Synopsis

The oxidation of amines is an important reaction in chemistry and biochemistry from both a transformative and a mechanistic standpoint. This chapter will focus on the mechanistic details of the oxidative Mannich reaction catalyzed by *tetrakis*( $\mu$ -caprolactamato)dirhodium(II) (**2**, Scheme 3-1a) with *tert*-butyl hydroperoxide (TBHP) that proceeds *via* oxidation of *N,N*-dialkylanilines (**58**) to iminium ions (**59**). The introduction of this chapter will present a brief description of the oxidative Mannich methodology and the theoretical development of a general model for the oxidative iminium ion formation based on the available literature.

An outline of the oxidation mechanism is proposed in Scheme 3-1. Dirhodium complexes **2** and **60** maintain a steady state of *tert*-butylperoxyl radical (**61**) in a one-electron redox cycle (Scheme 3-1a). Reaction of *N,N*-dialkylaniline (**58**) with the oxidation system yields the iminium ion (**59**). The oxidation proceeds with a two-step cleavage of the  $\alpha$ -amino CH-bond. The first step is an endergonic electron transfer (ET) between the *N,N*-dialkylaniline (**58**) and a *tert*-butylperoxyl radical (**61**) to yield a contact-ion pair (**62**, Scheme 3-1b). The ET reaction is coupled to a proton transfer (PT) that occurs as the second step to yield an  $\alpha$ -aminyl radical (**63**) as the initial product of oxidation. The ET and PT reactions occur as a thermodynamically coupled electron/proton transfer (ET-PT). The ET-PT step is followed by the oxidation of **63** by dissolved molecular oxygen, TBHP, or **60** to yield the iminium ion (**59**) as the final product of oxidation. The subsequent

C-C bond forming reaction between **60** and a nucleophile forms a functionalized dialkylaniline (**64**) and constitutes a formal Mannich addition (Scheme 3-1c). The addition occurs under thermodynamic control without the influence of **2** or **60**. Experimental identification of reaction intermediates, isotope effects profiles, linear free-energy relationships (LFER) with Hammett  $\sigma^+$  parameter and oxidation potentials ( $E_0$ ), and reactant molecularities are reported.

**Scheme 3-1.** Proposed mechanism of oxidative Mannich reaction. (Abbreviations: TBHP = *t*-BuOOH, *tert*-butyl hydroperoxide.)



## II. Introduction – Amine Oxidation and The Oxidative Mannich.

Oxidation technology is a venerable pillar of organic chemistry. From nature to the reaction flask, the synthesis of complex organic molecules requires the practitioner to not only make the skeleton of a molecule, but also control its oxidation state.<sup>151</sup> The impact of catalysis is particularly important in this area of chemistry. There is an enormous body of literature that provides examples of useful catalytic oxidants.<sup>152</sup> However, within that body of literature, there is much less discussion of their mechanisms of action. Mechanistic investigations remain relevant even for well-studied oxidation reactions. For example, the palladium catalyzed Wacker oxidation of ethylene to ethanal is a 70-year old reaction<sup>153</sup> that contributes to the production of more than 300 kilotons of ethanal each year in the United States alone.<sup>154</sup> The Wacker oxidation is an established industrial process; however, the organopalladium intermediates and their mechanisms of action continue to be a relevant topic of academic discussion.<sup>155</sup> The study of new oxidants and their mechanisms is not only of academic relevance, but cuts across scientific disciplines into the marketplace and remains an important area of investigation.

---

<sup>151</sup> Maimone, T. J.; Baran, P. S. *Nat. Chem. Bio.* **2007**, *3*, 396.

<sup>152</sup> For a variety of recent books and reviews on catalytic oxidations, see: a) Mijs, W. J.; De Jonge, C. R., *Organic Syntheses by Oxidation with Metal Compounds*. **1986**, b) Meunier, B., *Biomimetic Oxidations Catalyzed by Transition Metal Complexes*. Wiley: Weinheim, **2000**, c) Noyori, R.; Aoki, M.; Sato, K. *Chem. Commun.* **2003**, 1977, d) Bäckvall, J. E., *Modern Oxidation Methods*. Wiley: Weinheim, **2004**, e) Li, C.-J. *Chem. Rev.* **2005**, *105*, 3095, f) Punniyamurthy, T.; Velusamy, S.; Iqbal, J. *Chem. Rev.* **2005**, *105*, 2329, g) Herrerias, C. I.; Yao, X.; Li, Z.; Li, C.-J. *Chem. Rev.* **2007**, *107*, 2546.

<sup>153</sup> Smidt, J.; Hafner, W.; Jira, R.; Sedlmeier, J.; Sieber, R.; Ruttinger, R.; Kojer, H. *Angew. Chem., Int. Ed.* **1959**, *71*, 176.

<sup>154</sup> EPA. **1994**. Chemical Summary for Acetaldehyde. 749-F-94-003a. U.S. Environmental Protection Agency, Office of Pollution Prevention and Toxics.

<sup>155</sup> a) Keith, J. A.; Nielsen, R. J.; Oxgaard, J.; Goddard, W. A., III *J. Am. Chem. Soc.* **2007**, *129*, 12342, b) Keith, J. A.; Oxgaard, J.; Goddard, W. A., III *J. Am. Chem. Soc.* **2006**, *128*, 3132, c) Trend, R. M.; Ramtohul, Y. K.; Stoltz, B. M. *J. Am. Chem. Soc.* **2005**, *127*, 17778.

**The Oxidative Mannich Reaction.** Dirhodium(II) carboxamidates have emerged as excellent catalysts for oxidation using *tert*-butyl hydroperoxide (TBHP) as a terminal oxidant (Scheme 3-2). Methodologies for the oxidation of allylic (**65**),<sup>156</sup> benzylic (**67**),<sup>157</sup> and acetylenic (**69**) hydrocarbons<sup>158</sup> to their respective ketones (**66**, **68**, and **70**) are examples of chemoselective formation of C-O bonds from C-H bonds. Secondary amines (**71**) are oxidized to imines (**72**) to form C-N bonds<sup>159</sup> and phenols (**73**) are oxidized to *tert*-butyldioxy-semiquinones (**74**) to form C-O bonds.<sup>160</sup> In each case, the dirhodium(II) carboxamidates, and in particular Rh<sub>2</sub>(cap)<sub>4</sub> (**2**), are notable for both their catalytic efficiency as well as the mild reaction conditions that they require.

---

<sup>156</sup> a) Catino, A. J.; Forslund, R. E.; Doyle, M. P. *J. Am. Chem. Soc.* **2004**, *126*, 13622, b) Choi, H.; Doyle, M. P. *Organic Lett.* **2007**, *9*, 5349.

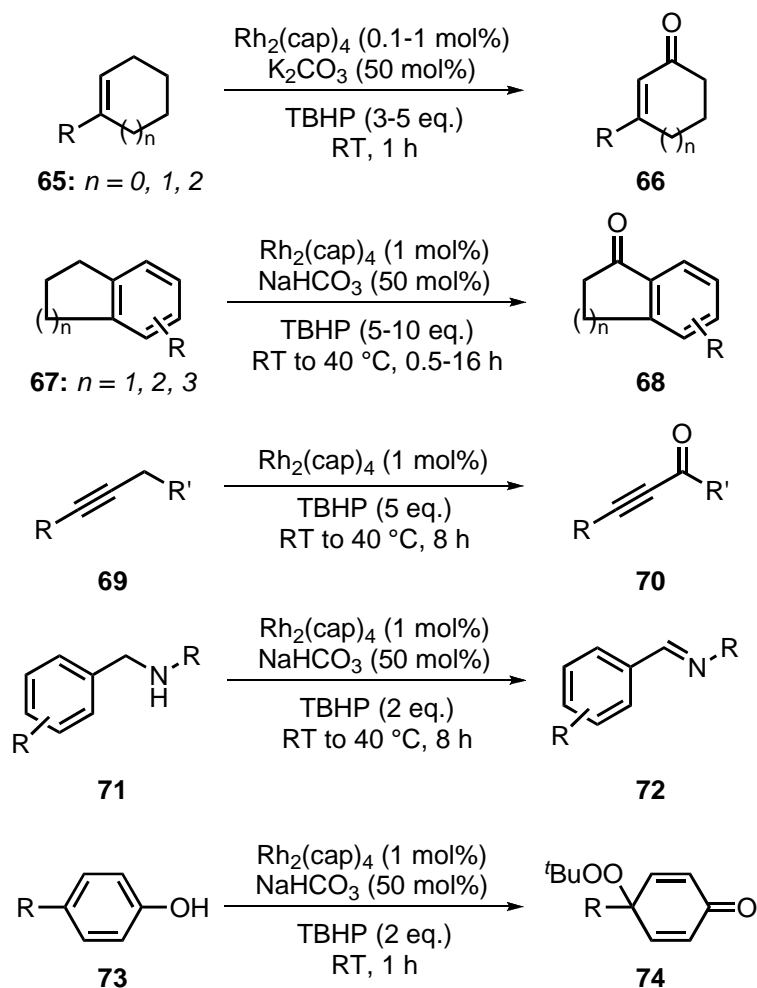
<sup>157</sup> Catino, A. J.; Nichols, J. M.; Choi, H.; Gottipamula, S.; Doyle, M. P. *Organic Lett.* **2005**, *7*, 5167.

<sup>158</sup> McLaughlin, E.; Doyle, M. P., Manuscript in preparation.

<sup>159</sup> Choi, H.; Doyle, M. P. *Chem. Commun.* **2007**, 745.

<sup>160</sup> a) Catino, A.; Khalafy, S., Doyle, M. P., Research Update, **2006**; b) A similar reaction has been reported that is catalyzed by ruthenium(II) chloride. b) Murahashi, S.-I.; Naota, T.; Miyaguchi, N.; Noda, S. *J. Am. Chem. Soc.* **1996**, *118*, 2509.

**Scheme 3-2.** Oxidations by the  $\text{Rh}_2(\text{cap})_4/\text{TBHP}$  system. (Abbreviations: TBHP = *tert*-butyl hydroperoxide)



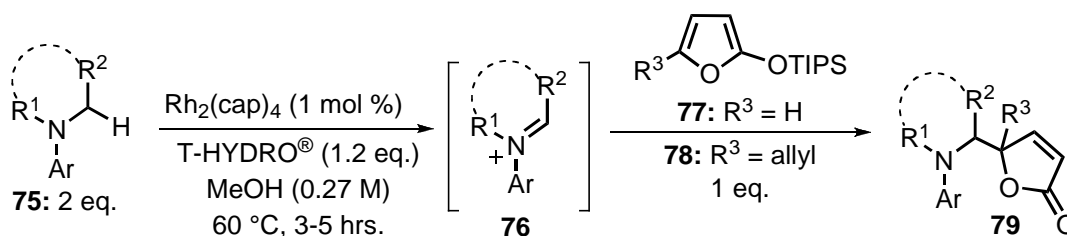
In addition to C-N and C-O bonds, the oxidation technology was leveraged to develop a C-C bond forming process based on the  $\text{Rh}_2(\text{cap})_4/\text{TBHP}$  catalyzed oxidation of tertiary amines (**75**) to iminium ions (**76**) (Scheme 3-3).<sup>161</sup> The oxidative Mannich<sup>162</sup> reaction is a catalytic C-C

<sup>161</sup> a) Catino, A. J.; Nichols, J. M.; Nettles, B. J.; Doyle, M. P. *J. Am. Chem. Soc.* **2006**, *128*, 5648, b) Catino, A. J., Oxidative C-H and C=C Bond Functionalization Catalyzed by Dirhodium Caprolactamate *Ph. D. Thesis*, University of Maryland, College Park, **2006**.

<sup>162</sup> Mannich reaction is defined as the addition of a resonance stabilized carbanion to an iminium ion: a) Royer, J.; Bonin, M.; Micouin, L. *Chem. Rev.* **2004**, *104*, 2311. b) Arend, M.; Westermann, B.; Risch, N. *Angew. Chem., Int. Ed.* **1998**, *37*, 1045.

bond forming methodology that can be used to prepare  $\gamma$ -aminobutenolides (**79**) from *N,N*-dialkylanilines and 2-(tri-isopropylsiloxy)furans<sup>163</sup> (**77** and **78**). The  $\gamma$ -aminobutenolides are synthetically useful cores of natural products and can be found in almost 10% of all naturally occurring molecules.<sup>164</sup> Recent examples in the literature have focused on the addition of pro-nucleophiles such as trimethylsilylcyanide,<sup>165</sup> nitro-olefins,  $\beta$ -ketoesters, indoles, and terminal acetylenes to catalytically form aryliminium ions.<sup>166</sup> The Rh<sub>2</sub>(cap)<sub>4</sub> oxidation system and the use of 2-siloxyfurans as a preformed nucleophile is a complementary protocol to these methodologies.

**Scheme 3-3.** General reaction scheme for the oxidative Mannich reaction with *N,N*-dialkylaniline (TIPS = tri-isopropylsilyl, T-HYDRO<sup>®</sup> = 70% w/w aqueous TBHP).



There were notable advantages of the dirhodium(II) catalyzed methodology. The reaction was tolerant of water as indicated by the use of

<sup>163</sup> For a review on the synthetic utility of 2-siloxyfurans, see: Rassu, G.; Zanardi, F.; Battistini, L.; Casiraghi, G. *Chem. Soc. Rev.* **2000**, 29, 109.

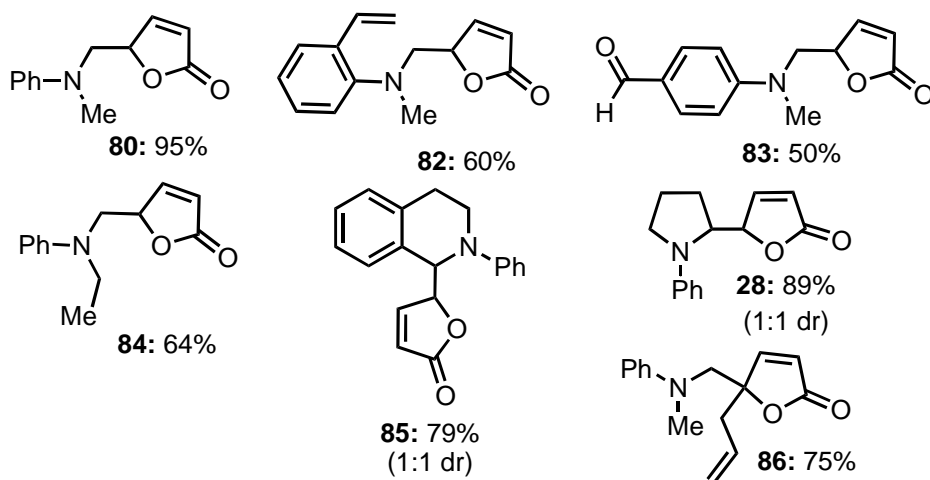
<sup>164</sup> For a review of natural products containing  $\gamma$ -butyrolactones, see: Seitz, M.; Reiser, O. *Curr. Opin. Chem. Biol.* **2005**, 9, 285.

<sup>165</sup> For Ru-catalyzed oxidations, see: a) Murahashi, S.-I.; Komiya, N., *Bioinspired oxidations catalyzed by ruthenium complexes*. In *Biomimetic Oxidations Catalyzed by Transition Metal Complexes*, Meunier, Ed. Imperial College Press: London, **2000**, 563-611, b) Murahashi, S.-I.; Komiya, N.; Terai, H.; Nakae, T. *J. Am. Chem. Soc.* **2003**, 125, 15312, c) Murahashi, S.-I.; Komiya, N.; Terai, H. *Angew. Chem., Int. Ed.* **2005**, 44, 6931.

<sup>166</sup> Cu/TBHP system. a) Li, Z.; Li, C.-J. *Eur. J. Org. Chem.* **2005**, 3173, b) Li, Z.; Li, C.-J. *J. Am. Chem. Soc.* **2005**, 127, 6968, c) Li, Z.; Li, C.-J. *J. Am. Chem. Soc.* **2005**, 127, 3672, d) Li, Z.; Bohle, D. S.; Li, C.-J. *Proc. Natl. Acad. Sci.* **2006**, 103, 8928, e) Li, Z.; Li, C.-J. *J. Am. Chem. Soc.* **2006**, 128, 56.

70% TBHP in water as the oxidant.<sup>167</sup> Catalyst loadings could be reduced to as low as 0.1 mol% with little impact on yield. The reaction was efficient with simple reaction partners, like *N,N*-dimethylaniline and **77**, to yield **80** in 95% isolated yield.<sup>168</sup> Although limited to arylamines, the methodology was tolerant of other oxidizable functionalities (Scheme 3-4). Noteworthy examples include a *N,N*-dimethylaniline with a proximal styrene (**81**) or 4-formyl-(*N,N*-dimethyl)-aniline (**82**). Unsymmetrical anilines (**83**) were selective for  $\alpha$ -CH<sub>3</sub> substitution as the regioisomeric  $\alpha$ -CH<sub>2</sub> addition-products were not observed. Cyclic amines were also good substrates, but occurred without diastereocontrol (**84** and **85**, 1:1 dr). Substituted 2-siloxyfurans, including 5-allyl-2-siloxyfuran (**78**) that generates a functionalized quaternary center (**86**) were also viable participants in the oxidative Mannich reaction. Overall, the methodology was tolerant of substitutional and functional variations on both the nucleophile and amine.

**Scheme 3-4.** Oxidative Mannich reaction scope. (Abbreviations: dr = diastereomeric ratio).



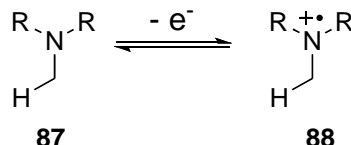
<sup>167</sup> Previous conditions for the Rh<sub>2</sub>(cap)<sub>4</sub> catalyzed oxidations (refs 156 and 157) as well as the other reported oxidative Mannich type reactions (refs 165 and 166) with TBHP were performed under anhydrous conditions.

<sup>168</sup> *N,N*-dimethylaniline was the substrate used to optimize reaction conditions.

**Basic Concepts in Amine Oxidation.** With the development of the oxidative Mannich methodology and, indeed, all of the dirhodium-catalyzed oxidation methodologies, there remained the question of reaction mechanism. The following discussion will compile a general model of amine oxidation as it appears in the literature for the conversion of tertiary amines to iminium ions.

In addition to their nucleophilic character, oxidation is a fundamental reactivity mode for amines. Tertiary amines have oxidation potentials ( $E_0$ ) of 0.5-1.3 eV vs. standard calomel electrode (SCE). These are some of the lowest  $E_0$  values of all organic compounds and are primarily due to stability enhancements of the radical cation intermediate.<sup>169</sup> Thus, the simplest oxidation process for a tertiary amine is single electron transfer (ET) from the non-bonding electron pair of the amine (**87**) to form a stable radical cation (**88**, Scheme 3-5).<sup>170</sup>

**Scheme 3-5.** ET formation of an aminium radical cation.



The oxidative formation of iminium ions from tertiary amines is a more complicated oxidation. The oxidation of a tertiary amine (**87**) to an iminium ion (**89**) is formally a hydride transfer (Scheme 3-6a). A hydride abstraction can be described by two fundamental reactions. The first is an ET reaction from an electron donor to an acceptor (Scheme 3-5). The other is a PT reaction from a proton donor to an acceptor. Thus, heterolytic  $\alpha$ -CH bond cleavage, or hydride transfer, can be thought of as the combination of two ETs and a PT. Similarly, homolytic  $\alpha$ -CH bond cleavage, or hydrogen-atom transfer (HAT),

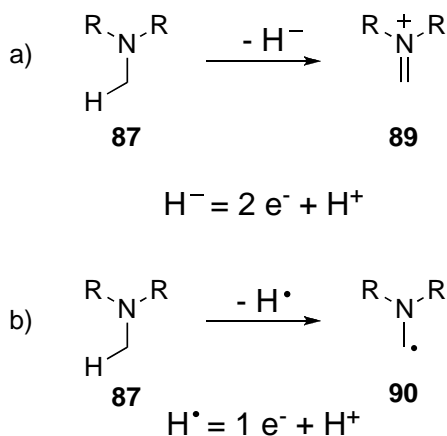
<sup>169</sup> Sumalekshmy, S.; Gopidas, K. R. *Chem. Phys. Lett.* **2005**, 413, 294.

<sup>170</sup> Das, S.; Suresh, V., *Electron-transfer reactions of amines*. In *Electron Transfer in Chemistry*, Balzani, Ed. Wiley: New York, **2001**, 2, 379-456.



can also be described as a combination of an ET and PT reaction that yields the  $\alpha$ -aminyl radical (**90**, Scheme 3-6b). The mechanistic complications for the heterolytic and homolytic process arise as the removal of electrons and protons need not happen at the same time or with the same agent. Thus, order of operations and the identity of bimolecular partners becomes a critical detail in the overall mechanistic picture.

**Scheme 3-6.** Basics of iminium ion formation.



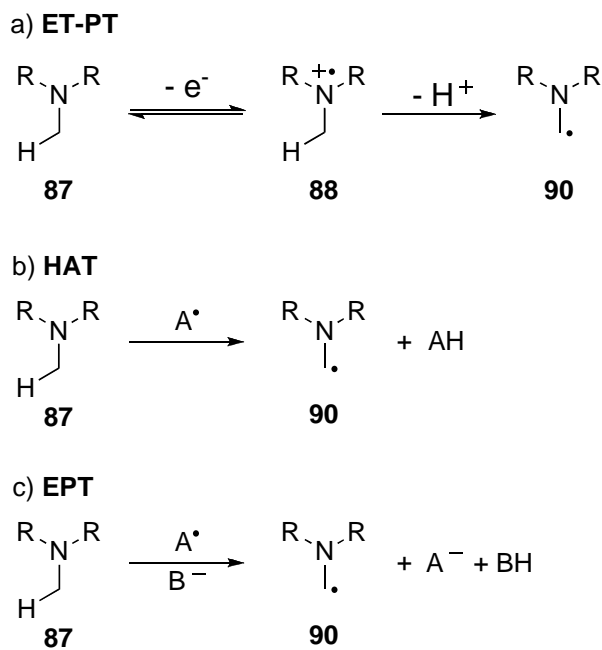
Researchers have made an effort to theoretically unify the permutations of concerted and stepwise ET/PT reactions under a single mechanism for oxidative CH-bond cleavage.<sup>171</sup> Consequently, a variety of terms have been created to refer to the kinetic and/or thermodynamic coupling of individual ET and PT reactions. Kinetically coupled ET/PT is defined as a set of ET and PT reactions in which the transfer of the proton and electron occurs through a common transition state, i.e. concerted transfer. This type of coupling has been called an electron/proton transfer (EPT), concerted proton/electron transfer (CPET), hydrogen-atom transfer

<sup>171</sup> For comprehensive reviews on the theoretical, experimental, and biological basis for PCET, see: a) Hammes-Schiffer, S. *Acc. Chem. Res.* **2001**, *34*, 273, b) Chang, C. J.; Chang, M. C. Y.; Damrauer, N. H.; Nocera, D. G. *Biochim. Biophys. Acta* **2004**, *1655*, 13, c) Mayer, J. M. *Annual Review of Physical Chemistry* **2004**, *55*, 363, d) Mayer, J. M.; Rhile, I. J. *Biochim. Biophys. Acta* **2004**, *1655*, 51, e) Meyer, T. J.; Huynh, M. H. V.; Thorp, H. H. *Angew. Chem., Int. Ed.* **2007**, *46*, 5284, f) Huynh, M. H. V.; Meyer, T. J. *Chem. Rev.* **2007**, *107*, 5004.

(HAT), and proton-coupled electron transfer (PCET). Thermodynamically coupled ET/PT reactions are defined as the coupling of the ground state intermediates of an ET and PT reaction on the same potential energy surface, i.e. a stepwise reaction. This type of coupling has been referred to as an electron transfer-proton transfer (ET-PT) and PCET.

The coupling of ET and PT reactions will be discussed specifically as they pertain to the oxidation of tertiary amines using the terminology of Hammes-Schiffer, Meyer, and Mayer where *all* such reactions are considered proton-coupled electron transfers (PCET). Using this terminology, a stepwise electron transfer-proton transfer process will be denoted as an ET-PT reaction (Scheme 3-7a). A concerted process will be denoted as a hydrogen-atom transfer (HAT) where the electron and proton acceptor are the same entity (Scheme 3-7b), and the term EPT will be used when the electron and proton acceptor are two different entities (Scheme 3-7c). The reader is encouraged to consult the cited reviews for a more complete description.

**Scheme 3-7.** Hammes-Schiffer, Meyer, and Mayer terminology for PCETs.



The complete mechanisms of amine oxidation remain sources of controversy across disciplines in part due to the kinetic and thermodynamic coupling of the component ET and PT reactions. For example, the oxidation of xenobiotics by cytochromes P450 is a vital biochemical process.<sup>172</sup> Cytochrome P450 is a monooxygenase super-family with over 1500 members isolated to date, and they are models for exquisite control of a catalytic, organometallic oxidation system.<sup>173</sup> The elucidation of the mechanism of P450 catalyzed oxidations of hydrocarbons and the role of the prosthetic iron-heme complex is one of the triumphs of modern bio-inorganic chemistry.<sup>174</sup> Despite this triumph, and the excellent work of many researchers, the relative contributions of ET-PT and EPT mechanisms in the oxidative dealkylation of tertiary amines by cytochrome P450 (Scheme 3-8),<sup>175,176</sup> and many other bio-inorganic oxidants,<sup>177</sup> remains a topic of considerable debate. In this reaction, the role of the biochemical oxidant ([O]) is to homolytically cleave the  $\alpha$ -CH bond of a tertiary amine (**89**) and make a C-O bond to generate a hemi-aminal (**91**). Hemi-aminal **91** spontaneously fragments to formaldehyde

---

<sup>172</sup> Lewis, D. F. V., *Cytochromes P450: Structure, Function and Mechanism*. Taylor & Francis: **1996**.

<sup>173</sup> a) Denisov, I. G.; Makris, T. M.; Sligar, S. G.; Schlichting, I. *Chem. Rev.* **2005**, *105*, 2253, b) Shaik, S.; Kumar, D.; de Visser, S. P.; Altun, A.; Thiel, W. *Chem. Rev.* **2005**, *105*, 2279.

<sup>174</sup> For excellent reviews on the mechanism of P450 oxidations, see: a) Meunier, B.; Bernadou, J. *Top. Catal.* **2002**, *21*, 47, b) Tani, F.; Matsu-Ura, M.; Nakayama, S.; Naruta, Y. *Coord. Chem. Rev.* **2002**, 226, 219, c) Meunier, B.; de Visser, S. P.; Shaik, S. *Chem. Rev.* **2004**, *104*, 3947.

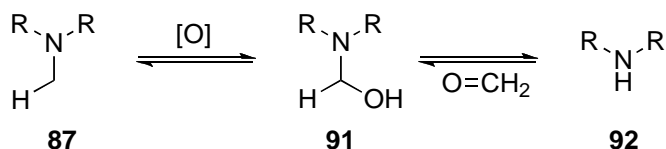
<sup>175</sup> For the ET-PT perspective of P450 mechanisms, see: a) Burka, L. T.; Guengerich, F. P.; Willard, R. J.; Macdonald, T. L. *J. Am. Chem. Soc.* **1985**, *107*, 2549, b) Guengerich, F. P.; Yun, C.-H.; Macdonald, T. L. *J. Biol. Chem.* **1996**, *271*, 27321, c) Guengerich, F. P. *Chem. Res. Toxicol.* **2001**, *14*, 611.

<sup>176</sup> For the HAT (concerted ET-PT) perspective, see: a) Shaffer, C. L.; Morton, M. D.; Hanzlik, R. P. *J. Am. Chem. Soc.* **2001**, *123*, 8502, b) Bhakta, M. N.; Wimalasena, K. *J. Am. Chem. Soc.* **2002**, *124*, 1844, c) Shaffer, C. L.; Harriman, S.; Koen, Y. M.; Hanzlik, R. P. *J. Am. Chem. Soc.* **2002**, *124*, 8268, d) Bhakta, M.; Hollenberg, P. F.; Wimalasena, K. *Chem. Comm.* **2005**, 265, e) Bhakta, M. N.; Wimalasena, K. *Eur. J. Org. Chem.* **2005**, 4801, f) Cerny, M. A.; Hanzlik, R. P. *J. Am. Chem. Soc.* **2006**, *128*, 3346.

<sup>177</sup> The reaction mechanisms of Cu containing mono-oxygenases are less clear than P450 oxidations. For some excellent reviews, see: a) Lewis, E. A.; Tolman, W. B. *Chem. Rev.* **2004**, *104*, 1047, b) Mirica, L. M.; Ottenwaelder, X.; Stack, T. D. P. *Chem. Rev.* **2004**, *104*, 1013, c) Decker, A.; Solomon, E. I. *Curr. Opin. Chem. Biol.* **2005**, *9*, 152.

(CH<sub>2</sub>=O) and the dealkylated secondary amine (**92**). The debate is centered on whether the  $\alpha$ -CH bond cleavage occurs as a stepwise ET-PT, or concertedly as a HAT or EPT reaction. Even in the case of cytochrome P450, where the active oxidant is well defined, the complexity of amine oxidation processes obfuscates mechanistic determinations for the biochemical systems.

**Scheme 3-8.** Oxidative dealkylation of amines (Abbreviations: [O] = oxidant).



In addition to the stepwise versus concerted ET/PT reactions, reaction complexity is compounded by the ancillary reactivity of the oxidation intermediates. Although useful bond constructions based on simple ET formation of a radical cation have been used to dramatic effect,<sup>178</sup> oxidation of a tertiary amine to its radical cation (**93**) can lead to a variety of fragmentations and further oxidations (Scheme 3-9). Loss of an electrofugal group from **93** (Scheme 3-9a) yields a reactive  $\alpha$ -aminyl radical (**90**).<sup>179</sup> The iminium ion (**89**) may be formed from the  $\beta$ -scission of a trimethylsilyl- or carboxylate radical leaving group (Scheme 3-9b)<sup>180</sup> or facile ET from **90** (Scheme 3-9c).<sup>181</sup> Finally, **93** can react with an appropriate acceptor like a

<sup>178</sup> a) Baran, P. S.; Richter, J. M. *J. Am. Chem. Soc.* **2005**, *127*, 15394, b) Beeson, T. D.; Mastracchio, A.; Hong, J.-B.; Ashton, K.; MacMillan, D. W. C. *Science* **2007**, *316*, 582.

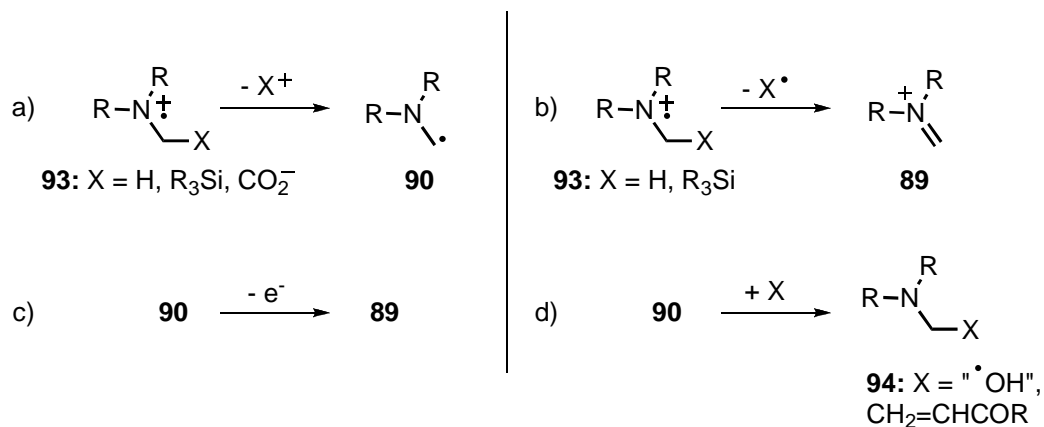
<sup>179</sup> a) Kim, H.-J.; Yoon, U.-C.; Jung, Y.-S.; Park, N. S.; Cederstrom, E. M.; Mariano, P. S. *J. Org. Chem.* **1998**, *63*, 860, b) Wu, X.-D.; Khim, S.-K.; Zhang, X.; Cederstrom, E. M.; Mariano, P. S. *J. Org. Chem.* **1998**, *63*, 841, c) Chen, C.; Mariano, P. S. *J. Org. Chem.* **2000**, *65*, 3252.

<sup>180</sup> And references therein Gaillard, E. R.; Whitten, D. G. *Acc. Chem. Res.* **1996**, *29*, 292.

<sup>181</sup> Jockusch, S.; Timpe, H. J.; Schnabel, W.; Turro, N. J. *J. Photochem. Photobiol., A* **1996**, *96*, 129.

hydroxyl radical donor,<sup>182</sup> or  $\alpha,\beta$ -unsaturated ketones to form new chemical bonds (Scheme 3-9d) in a radical termination product (**94**).<sup>183</sup>

**Scheme 3-9.** Fragmentations and oxidations of aminium radical cations.

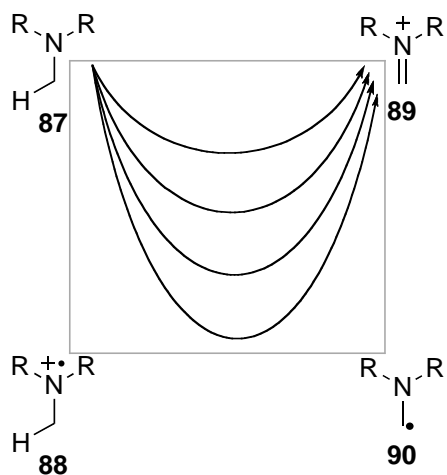


**Mechanistic Models of Amine Oxidation.** Considering the reactions described in Scheme 3-9 and the component ET and PT reactions, the mechanism of oxidative iminium ion formation can become quite complex. Before the mechanism of the oxidative Mannich reaction can be discussed, analysis of the simple bimolecular reactions and fragmentations that could compose the mechanism is a useful way of simplifying the issue and developing some mechanistic hypotheses. The products of the component ET and PT reactions are shown as intermediates in a square diagram (Scheme 3-10). These intermediates help define the "mechanistic space" for the oxidative formation of an iminium ion. Within this space, there are many paths connecting **87** to **89** that could intercept **88**, **90**, or both.

<sup>182</sup> See "oxygen rebound" mechanism for cytochrome P450 oxidations in ref. 172 for "OH" donor.

<sup>183</sup>  $\alpha,\beta$ -unsaturated ketones have been used as good acceptors that upon further oxidation yield the  $\gamma$ -amino ketone. Yoon, U. C.; Mariano, P. S. *Acc. Chem. Res.* **1992**, *25*, 233.

**Scheme 3-10.** Mechanistic space for iminium ion formation. Arrows graphically conceptualize the possibility of multiple paths from **87** to **89**.

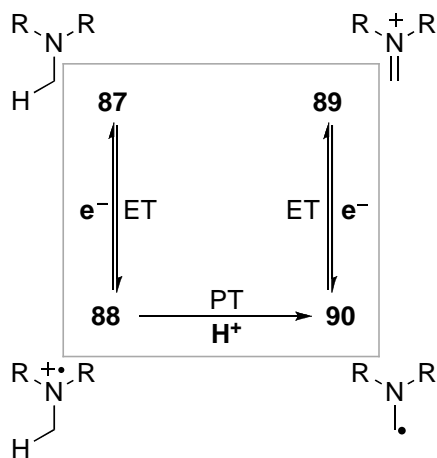


The diagram in Scheme 3-10 defines mechanistic boundaries for the formation of an iminium ion from a tertiary amine. Although an infinite number of pathways could exist, there are only three distinct mechanisms that formally intercept one or more of the oxidation intermediates **88** and/or **90**. The following discussion will describe three mechanisms and their distinguishing features. The first is an ET-PT/ET mechanism, followed by a description of the HAT/ET and ET/HAT pathways. Each of these pathways is a combination of concerted or stepwise ET and PT reactions to form an iminium ion from a tertiary amine.

The stepwise ET-PT/ET process is the first mechanistic family of tertiary amine oxidations (Scheme 3-11). The general reaction motif consists of three stepwise reactions beginning with a reversible ET between an amine (**87**) and an oxidant to form the radical cation (**88**). Irreversible PT from the radical cation generates the  $\alpha$ -aminyl radical (**90**) that rapidly undergoes a second ET with additional oxidant to generate an iminium ion (**89**). This mechanism is an example of a proton coupled electron transfer reaction in which the ET and PT steps are thermodynamically coupled.

A reaction model is given in Scheme 3-12 that will be used to derive a rate-law that will allow further classification of the thermodynamic extremes for this mechanism. The terms Am and Ox<sup>n+1</sup> refer to the amine and oxidant. The term [Am<sup>+</sup>(Ox<sup>n</sup>)] refers to the ion-pair produced upon electron transfer from **87** to **88**. The terms Am<sup>•</sup> and Ox<sup>n</sup>H refer to α-aminy radical and the reduced, protonated form of the oxidant. The model assumes that the PT step occurs directly between the ion-pair generated from the initial ET ([Am<sup>+</sup>(Ox<sup>n</sup>)]). This assumption holds only for oxidants that can act as both the ET and PT agent and is made to further simplify the derivation.<sup>184</sup> The α-aminy radical is a strongly reducing radical with a large, negative oxidation potential.<sup>185</sup> Therefore, the bimolecular ET reaction from the α-aminy radical will be excluded from the rate law for this model since it is not likely to contribute to rate-limitation and occurs after the CH-bond cleavage. This assumption makes the reaction model in Scheme 3-12 applicable only for the ET-PT portion of the ET-PT/ET reaction.

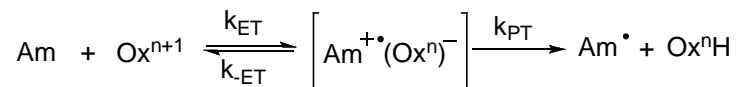
**Scheme 3-11.** Square diagram of the ET-PT/ET mechanism.



<sup>184</sup> The derivation for a base other than the oxidant would differ only in the definition of  $k_{PT}$ . In the presence of base (**B**) at constant concentration (buffered solution approximation),  $k'_{PT} = k_{PT}[\mathbf{B}]$ .

<sup>185</sup> Oxidation potential of α-aniliny radical = -0.85 vs. SCE in CH<sub>3</sub>CN. Wayner, D. D. M.; McPhee, D. J.; Griller, D. *J. Am. Chem. Soc.* **1988**, *110*, 132.

**Scheme 3-12.** Reaction definition for ET-PT/ET mechanism.



Eq. 3-1 is the general equation for the pseudo-1<sup>st</sup> order consumption of the oxidant ( $\text{Ox}^{n+1}$ ) in the presence of excess amine (Am) to form the  $\alpha$ -aminyl radical ( $\text{Am}^\bullet$ ) as described in Scheme 3-12. These conditions mimic those of a catalytic amine oxidation. Eq. 3-1 is an analytical expression for the observed rate constant ( $k_{\text{obs}}$ ) in terms of forward and backward electron transfer ( $k_{\text{ET}}$ ,  $k_{-ET}$ ) and proton transfer ( $k_{\text{PT}}$ ) rate constants. Applying limiting conditions to the ET and PT rate constants that make up  $k_{\text{obs}}$  yields a description of most mechanisms for tertiary amine oxidations that occur through initial electron transfer equilibria.<sup>186</sup> The limiting conditions provide a useful phenomenological grouping of ET-PT oxidations into four basic categories of unique rate-limiting steps that can be experimentally differentiated.<sup>187</sup>

$$\text{Eq. 3-1} \quad \frac{-d[\text{Ox}^{n+1}]}{dt} = k_{\text{obs}}[\text{Ox}^{n+1}] \quad k_{\text{obs}} = \frac{k_{\text{PT}}k_{\text{ET}}[\text{Am}]}{k_{\text{ET}}[\text{Am}] + k_{-ET} + k_{\text{PT}}}$$

The first two categories occur from an exergonic ET equilibrium between the reactants and ionic intermediate ( $\text{Am} + \text{Ox}^{n+1} \leftrightarrow [\text{Am}^{+\bullet}(\text{Ox}^n)^-]$ ). When the PT rate is much faster from the intermediate than either the forward or backward ET rate [ $k_{\text{PT}} \gg (k_{\text{ET}}[\text{Am}] + k_{-ET})$ ], then  $k_{\text{obs}}$  in Eq. 3-1 reduces to  $k_{\text{obs}} = k_{\text{ET}}[\text{Am}]$  (Eq. 3-2). Based on this equation, product formation only depends on the rate of forward electron transfer and the reaction proceeds by

<sup>186</sup> For the derivation of Eq. 3-1, see Section 3.V Experimental, pg 321. For derivation of eq. 3-1 for a specific system, and the resulting predictions for KIEs, see: Goto, Y.; Watanabe, Y.; Fukuzumi, S.; Jones, J. P.; Dinnocenzo, J. P. *J. Am. Chem. Soc.* **1998**, *120*, 10762.

<sup>187</sup> Due to the assumptions made in generating this model, the categorization applies only to oxidants that can be both ET and PT agents.



a simple, irreversible ET mechanism from starting amine. This will be referred to as a Type I ET-PT mechanism.

$$\text{Eq. 3-2} \quad \frac{-d[\text{Ox}^{n+1}]}{dt} = k_{\text{ET}}[\text{Am}][\text{Ox}^{n+1}] \text{ If } k_{\text{PT}} \gg k_{\text{ET}}[\text{Am}] + k_{-\text{ET}}$$

Conversely, if the forward ET rate is much faster than either the rate of PT or backwards ET [ $k_{\text{ET}}[\text{Am}] \gg (k_{\text{PT}} + k_{-\text{ET}})$ ], then  $k_{\text{obs}}$  in Eq. 3-1 reduces to  $k_{\text{obs}} = k_{\text{PT}}$  (Eq. 3-3). In this case, the reaction depends solely upon the rate of PT and the reaction proceeds by a simple PT mechanism from the rapid, quantitative formation of a radical cation. This will be referred to as a Type II ET-PT mechanism.

$$\text{Eq. 3-3} \quad \frac{-d[\text{Ox}^{n+1}]}{dt} = k_{\text{PT}}[\text{Ox}^{n+1}] \text{ If } k_{\text{ET}}[\text{Am}] \gg k_{\text{PT}} + k_{-\text{ET}}$$

The last two mechanistic categories occur in the case of an endergonic ET equilibrium between the reactants and ionic intermediate ( $\text{Am} + \text{Ox}^{n+1} \leftrightarrow [\text{Am}^+(\text{Ox}^n)]$ ). In the case of an endergonic ET equilibrium, it is unlikely that  $k_{\text{ET}}[\text{Am}]$  can be much larger than  $(k_{\text{PT}} + k_{-\text{ET}})$  since the bimolecular rate of forward ET would have to approach, or exceed, the diffusion controlled limit.<sup>188</sup> A more useful condition to consider is a situation where the rates of PT and backwards ET are competitive and faster than the forward ET reaction [ $k_{\text{ET}}[\text{Am}] \ll (k_{\text{PT}} + k_{-\text{ET}})$ ]. In this model, product formation depends on the relative rate of partitioning from a common intermediate. Assuming [ $k_{\text{ET}}[\text{Am}] \ll (k_{\text{PT}} + k_{-\text{ET}})$ ],  $k_{\text{obs}}$  in Eq. 3-1 reduces to a second general relationship (Eq. 3-4) for an endergonic ET equilibrium.

---

<sup>188</sup> Deprotonation rates as high as  $3.6 \times 10^9$  have been observed for electron deficient dialkylaniines Dombrowski, G. W.; Dinnocenzo, J. P.; Zielinski, P. A.; Farid, S.; Wosinska, Z. M.; Gould, I. R. *J. Org. Chem.* **2005**, 70, 3791.

$$\text{Eq. 3-4} \quad \frac{-d[\text{Ox}^{n+1}]}{dt} = k_{\text{obs}}[\text{Ox}^{n+1}] \quad k_{\text{obs}} = \frac{k_{\text{PT}}k_{\text{ET}}[\text{Am}]}{k_{\text{-ET}} + k_{\text{PT}}} \quad \text{If } k_{\text{-ET}} + k_{\text{PT}} \gg k_{\text{ET}}[\text{Am}]$$

Based on Eq. 3-4, two related but experimentally distinct types of ET-PT mechanisms that contain an endergonic ET process where  $k_{\text{-ET}}$  is not negligible. The first occurs when the PT rate is much faster than backwards electron transfer ( $k_{\text{PT}} \gg k_{\text{-ET}}$ ). Under this condition, Eq. 3-4 reduces to Eq. 3-5 and product formation is governed by the ET equilibrium. This will be referred to as a Type III ET-PT mechanism.

$$\text{Eq. 3-5} \quad \frac{-d[\text{Ox}^{n+1}]}{dt} = k_{\text{obs}}[\text{Ox}^{n+1}] \quad k_{\text{obs}} = \frac{k_{\text{ET}}}{k_{\text{-ET}}}[\text{Am}] \quad \text{If } k_{\text{PT}} \gg k_{\text{-ET}}$$

The final, experimentally distinct mechanism derived from Eq. 3-4 occurs when the backwards ET rate is much faster than PT ( $k_{\text{-ET}} \gg k_{\text{PT}}$ ). Under this condition, Eq. 3-4 reduces to Eq. 3-6, and product formation depends on both the ET equilibrium and PT. This will be referred to as a Type IV ET-PT mechanism.

$$\text{Eq. 3-6} \quad \frac{-d[\text{Ox}^{n+1}]}{dt} = k_{\text{obs}}[\text{Ox}^{n+1}] \quad k_{\text{obs}} = \frac{k_{\text{ET}}}{k_{\text{-ET}}} k_{\text{PT}} [\text{Am}] \quad \text{If } k_{\text{-ET}} \gg k_{\text{PT}}$$

Each of the four types of ET-PT mechanisms have a unique set of rate constants that govern rate limitation. These rate constants are physical descriptors of the transition state. There are a number of proposed relationships that relate the energy of a transition state to the free energy of a transformation. One such relationship is the Hammond postulate that states there is an intrinsic connection between the structure of the transition state and that of the nearest ground state of a molecule, or reactive complex, connected along a reaction coordinate. This connection between structures implies that reaction barriers for largely exothermic, or endothermic, reactions cannot be much larger than the energy differences between the reactants and

products.<sup>189</sup> Put simply, exergonic reactions are fast and endergonic reactions are slow.

While the Hammond postulate certainly does not apply in all cases,<sup>190</sup> its application to PT reactions yields the expected correlation of free-energy and reaction rate.<sup>191</sup> Marcus developed a related free energy/activation energy relationship for ET reactions that directly correlates reaction energy barriers for ET with the free-energy of the ET reaction.<sup>192</sup> Marcus theory predicts a similar relationship, i. e. exergonic ET is fast and endergonic ET is slow. Thus, the Hammond and Marcus relationships provide guidelines for describing the free energy relationship between reacting partners based on the rate constants in the kinetic models for ET-PT developed from Eq. 3-1. A fast ET, or PT, occurs from an exergonic relationship between reactants and products. Conversely, a slow ET, or PT, occurs from an endergonic relationship between reactants and products. With these guidelines, a reaction energy diagram can be made for the four types of ET-PT mechanisms.

---

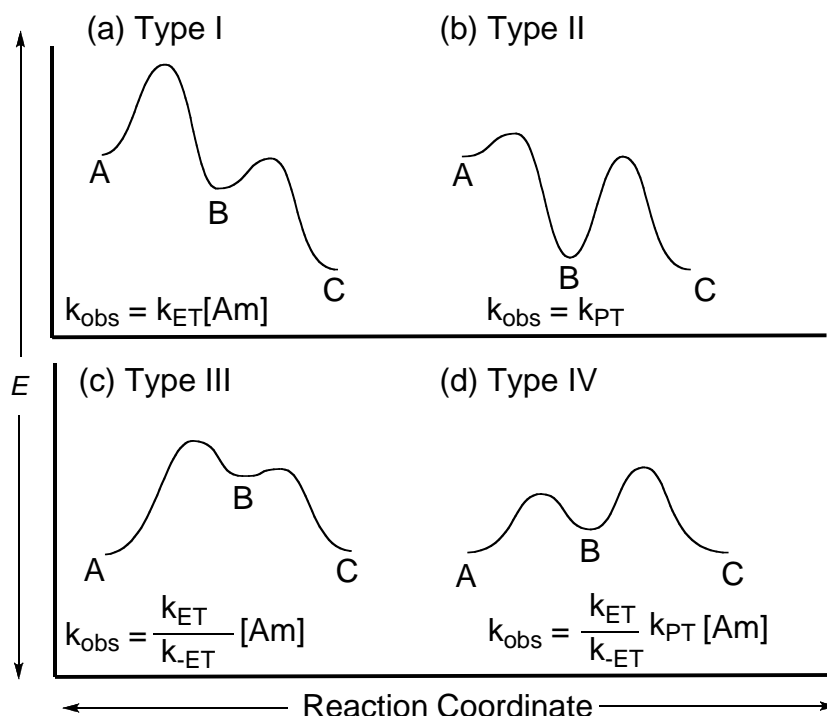
<sup>189</sup> a) Hammond, G. S. *J. Am. Chem. Soc.* **1955**, *77*, 334, b) Wales, D. J. *Science* **2001**, *293*, 2067.

<sup>190</sup> Johnson, C. D. *Chem. Rev.* **1975**, *75*, 755.

<sup>191</sup> a) Jencks, W. P. *Chem. Rev.* **1972**, *72*, 706, b) Agmon, N. *J. Chem. Soc., Faraday Trans. 2* **1978**, *74*, 388, c) Cioslowski, J. *J. Am. Chem. Soc.* **1991**, *113*, 6756, d) Pezacki, J. P. *Can. J. Chem.* **1999**, *77*, 1230.

<sup>192</sup> a) Marcus, R. A. *J. Chem. Phys.* **1957**, *26*, 872, b) Marcus, R. A. *J. Phys. Chem.* **1963**, *67*, 853, c) Marcus, R. A.; Eyring, H. *Ann. Rev. Phys. Chem.* **1964**, *15*, 155.

**Scheme 3-13.** Reaction energy diagrams of ET-PT/ET mechanisms (A = Am + Ox<sup>n+1</sup>, B = Am<sup>++</sup>(Ox<sup>n</sup>)<sup>-</sup>, C = Am<sup>•</sup> + Ox<sup>n</sup>H).



The rate-laws derived in Eq. 3-1 to Eq. 3-6 are summarized as reaction energy diagrams in Scheme 3-13. These energy diagrams are qualitative pictures of the thermodynamic relationship between the ET and PT reactions for each of the four ET-PT types and are not to be taken as an absolute definition of a reaction profile. The thermodynamic coupling of the ET equilibrium and the PT step can be seen graphically as the relationship between A, B, and C in Scheme 3-13 where A represents the reactants (Am + Ox<sup>n+1</sup>), B represents the electron transfer intermediate [Am<sup>++</sup>(Ox<sup>n</sup>)<sup>-</sup>], and C represents the products (Am<sup>•</sup> + Ox<sup>n</sup>H). Type I and II ET-PT mechanisms occur when  $k_{ET}[Am] \gg k_{-ET} + k_{PT}$ . Thus, they both proceed through an exergonic ET equilibrium and they simply differ by the kinetic barrier to PT from the electron transfer intermediate B. Type III and IV mechanisms occur when  $k_{-ET} + k_{PT} \gg k_{ET}[Am]$ . Thus, they both proceed through an endergonic ET equilibrium in which  $k_{-ET}$  is significant. The Type III and IV mechanisms also differ in the kinetic barrier to PT from the electron transfer intermediate B.

However, unlike the Type I and II ET-PT mechanisms, the ET equilibrium contributes to rate limitation in the Type III and IV mechanisms.

The free energy picture described in Scheme 3-13 has physical significance based on the properties of the reactants and products. The free energy of ET is the difference in oxidation potential between Am and Ox<sup>n+1</sup> and the free energy of PT can be thought as the difference in pKa between the base (Ox<sup>n</sup>)<sup>-</sup> and the acid (Am<sup>+</sup>) in the ET intermediate [Am<sup>+</sup>(Ox<sup>n</sup>)<sup>-</sup>]. A Type I ET-PT mechanism, described in Eq. 3-2, occurs in the case of an exergonic ET that generates a strong base to undergo a fast PT (Scheme 3-13a).<sup>193</sup> A Type II ET-PT mechanism, described in Eq. 3-3, occurs in the case of an exergonic ET that generates a weak base that undergoes slow PT (Scheme 3-13b). A Type III ET-PT mechanism, described in Eq. 3-5, occurs in the case of an endergonic ET equilibrium that generates a strong base that undergoes fast PT (Scheme 3-13c). Finally, a Type IV ET-PT mechanism, described in Eq. 3-6, occurs in the case of an endergonic ET equilibrium generating a weak base that undergoes slow PT (Scheme 3-13d). Although each type of ET-PT mechanism has a unique set of rate-limiting factors and can be thought of as different mechanisms experimentally, they represent the thermodynamic extremes of the same basic ET-PT pathway.

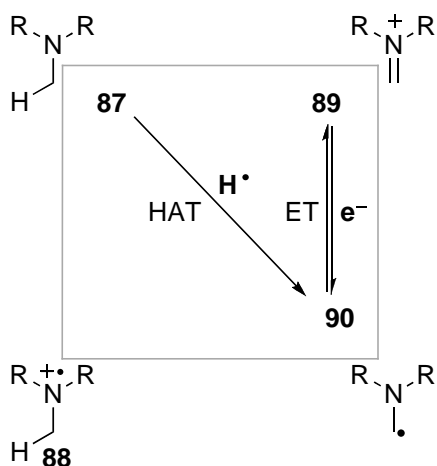
The HAT/ET mechanism is a second class of amine oxidations that is both experimentally *and* mechanistically different in nature. This mechanism is considerably simpler than the ET-PT/ET manifold. It begins with rate-limiting HAT from a tertiary amine (**87**) to generate the  $\alpha$ -aminyl radical (**90**) and ends with rapid ET from **90** to yield an iminium ion (**89**) (Scheme 3-14).

---

<sup>193</sup> Recent electrochemical methodologies for the preparation and use of iminium ions by anodic oxidation are examples of Type I ET/PT/ET processes. a) D'Oca, M. G. M.; Russowsky, D.; Canto, K.; Gressler, T.; Goncalves, R. S. *Organic Lett.* **2002**, *4*, 1763, b) Suga, S.; Watanabe, M.; Yoshida, J.-i. *J. Am. Chem. Soc.* **2002**, *124*, 14824, c) Sun, H.; Moeller, K. D. *Organic Lett.* **2002**, *4*, 1547, d) Suga, S.; Nishida, T.; Yamada, D.; Nagaki, A.; Yoshida, J. *J. Am. Chem. Soc.* **2004**, *126*, 14338, e) Maruyama, T.; Mizuno, Y.; Shimizu, I.; Suga, S.; Yoshida, J.-i. *J. Am. Chem. Soc.* **2007**, *129*, 1902.

The HAT/ET process is conceptually related to the ET-PT/ET process where the primary difference is the concerted nature of the initial ET-PT events. In the HAT/ET mechanism, the initial ET-PT process occurs during a concerted bimolecular reaction in which both the proton and the electron are transferred to the same intermediate. Ignoring the influence of the final ET step, a simple rate law can be derived (Eq. 3-7) with only the rate of HAT contributing to rate-limitation.

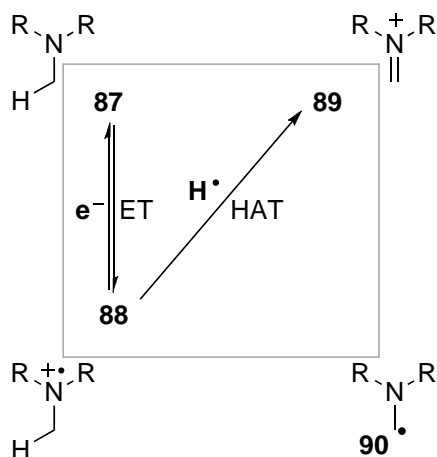
**Scheme 3-14.** HAT/ET mechanism.



Eq. 3-7 
$$\frac{-d[\text{Ox}^{n+1}]}{dt} = k_{\text{HAT}}[\text{Am}][\text{Ox}^{n+1}]$$

The third distinct mechanism for the oxidative formation of an iminium ion from a tertiary amine is the ET/HAT mechanism (Scheme 3-15). The ET/HAT process begins with a fast, reversible ET equilibrium to generate the aminium radical cation (**88**). Rate-limiting HAT from the radical cation then generates the iminium ion (**89**). The rate law is qualitatively similar to the ET-PT/ET process derived in Eq. 3-1 and is summarized in Eq. 3-8, except that  $k_{\text{PT}}$  is replaced by  $k_{\text{HAT}}$ . Therefore, despite the fact that the ET/HAT mechanism is fundamentally different in the way the CH-bond is broken, it would be mathematically indistinguishable from an ET-PT/ET process. Currently, there are no known examples of this type of reaction at this time and no further discussion will be presented here.

**Scheme 3-15.** ET/HAT mechanism.



$$\text{Eq. 3-8}^{194} \quad \frac{-d[\text{Ox}^{n+1}]}{dt} = k_{\text{obs}}[\text{Ox}^{n+1}] \quad k_{\text{obs}} = \frac{k_{\text{HAT}}k_{\text{ET}}[\text{Am}]}{k_{\text{ET}}[\text{Am}] + k_{-\text{ET}} + k_{\text{HAT}}}$$

The complete mechanistic picture of amine oxidations is by no means as clear as Eq. 3-1 to Eq. 3-8. Mechanistic departures are possible when organometallic complexes are formed during an oxidation. Moreover, the free energy of ET reactions can vary widely depending upon the relative  $E_0$  of the amine and oxidant. Consequently, the overall mechanism could be a composite of two or more contributing mechanisms in reactions where the free energy differences are not profound. In many cases, there are not sharp distinctions between the proposed reaction pathways. There are, however, many examples from the literature that demonstrate the concepts developed in Eq. 3-1 to Eq. 3-8.

In a beautiful set of laser spectroscopy experiments, Mariano, Falvey and co-workers measured the rate constants of PT from transient *p*-substituted anilinium radical cations using conditions that favored a Type II

<sup>194</sup> Eq. 3-8 is exactly the same as Eq. 3-1 except  $k_{\text{PT}} = k_{\text{HAT}}$ .

ET-PT mechanism (Scheme 3-16).<sup>195</sup> When irradiated at 308 nm (Scheme 3-16a), 4-R-*N,N*-dimethylaniline (**95**) and 1,4-dicyanobenzene (DCB) undergo a rapid ET to form their respective radical ions (**96**). Due to the stabilized nature of both ions, the backwards ET reaction is very slow ( $k_{\text{ET}} = 6.0 \times 10^{-10} \text{ M}^{-1}\text{s}^{-1}$  in MeCN) satisfying the conditions for a Type II ET-PT (Eq. 3-3). This technique allowed the researchers to measure the kinetic acidities as pseudo-first order PT rates ( $k'_{\text{PT}}$ ) of **96** with *tetra*-butylammonium acetate (TBAA) to form the  $\alpha$ -anilinyl radical (**97**). Second-order rate constants ( $k_{\text{PT}}$ ) were obtained by measuring  $k'_{\text{PT}}$  at varying concentrations of TBAA. The bimolecular rate constants followed a rational progression with varied aryl substitution (R) increasing from stabilizing (R = 4-MeO,  $k_{\text{obs}} = 8.0 \times 10^4 \text{ M}^{-1}\text{s}^{-1}$ ) to destabilizing (R = 4-CF<sub>3</sub>,  $k_{\text{obs}} = 8.9 \times 10^5 \text{ M}^{-1}\text{s}^{-1}$ ) substituents. Radical dimerization of the  $\alpha$ -anilinyl radical was the predominant product (**98**).<sup>196</sup>

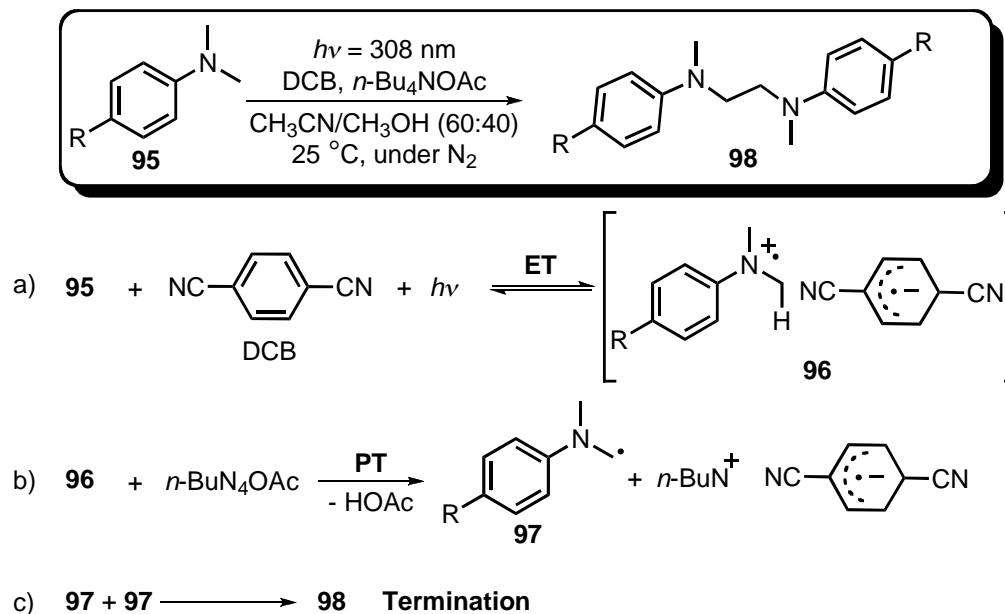
---

<sup>195</sup> a) Su, Z.; Falvey, D. E.; Yoon, U. C.; Mariano, P. S. *J. Am. Chem. Soc.* **1997**, *119*, 5261, b) Su, Z.; Mariano, P. S.; Falvey, D. E.; Yoon, U. C.; Oh, S. W. *J. Am. Chem. Soc.* **1998**, *120*, 10676.

<sup>196</sup> Others have measured the kinetic acidity of radical cations as well. a) Dinnocenzo, J. P.; Banach, T. E. *J. Am. Chem. Soc.* **1989**, *111*, 8646, b) Parker, V. D.; Tilset, M. *J. Am. Chem. Soc.* **1991**, *113*, 8778, c) Zhang, X.; Yeh, S.-R.; Hong, S.; Freccero, M.; Albin, A.; Falvey, D. E.; Mariano, P. S. *J. Am. Chem. Soc.* **1994**, *116*, 4211, d) Anne, A.; Fraoua, S.; Hapiot, P.; Moiroux, J.; Saveant, J.-M. *J. Am. Chem. Soc.* **1995**, *117*, 7412, e) Bockman, T. M.; Hubig, S. M.; Kochi, J. K. *J. Am. Chem. Soc.* **1996**, *118*, 4502.



**Scheme 3-16.** Determination of  $k_{PT}$  using Type II ET-PT/ET conditions.



The first experimental observations of a Type III ET-PT mechanism came from the oxidative dealkylation of tertiary alkylamines with aqueous  $\text{ClO}_2$  (Scheme 3-17).<sup>197</sup> In a series of elegant papers during the 1960's, Rosenblatt and co-workers probed the reaction of tertiary alkylamines with  $\text{ClO}_2$ .<sup>198</sup> Their work was the first to identify an ET-PT mechanism in amine oxidations.

Rosenblatt and co-workers observed that the first ET between the tertiary alkylamine (**99**) and  $\text{ClO}_2$  to form the radical cation (**100**) was rate-determining and reversible (Scheme 3-17a). The reversibility of the ET event was clearly established by observing a significant rate depression at high concentrations of chlorite ion ( $\text{ClO}_2^-$ ). The observation of a Hammett relationship with *p*-substituted arylamines ( $\rho = -0.92$  vs.  $\sigma$ ) denoted developing positive charge in the transition state consistent with rate-limiting

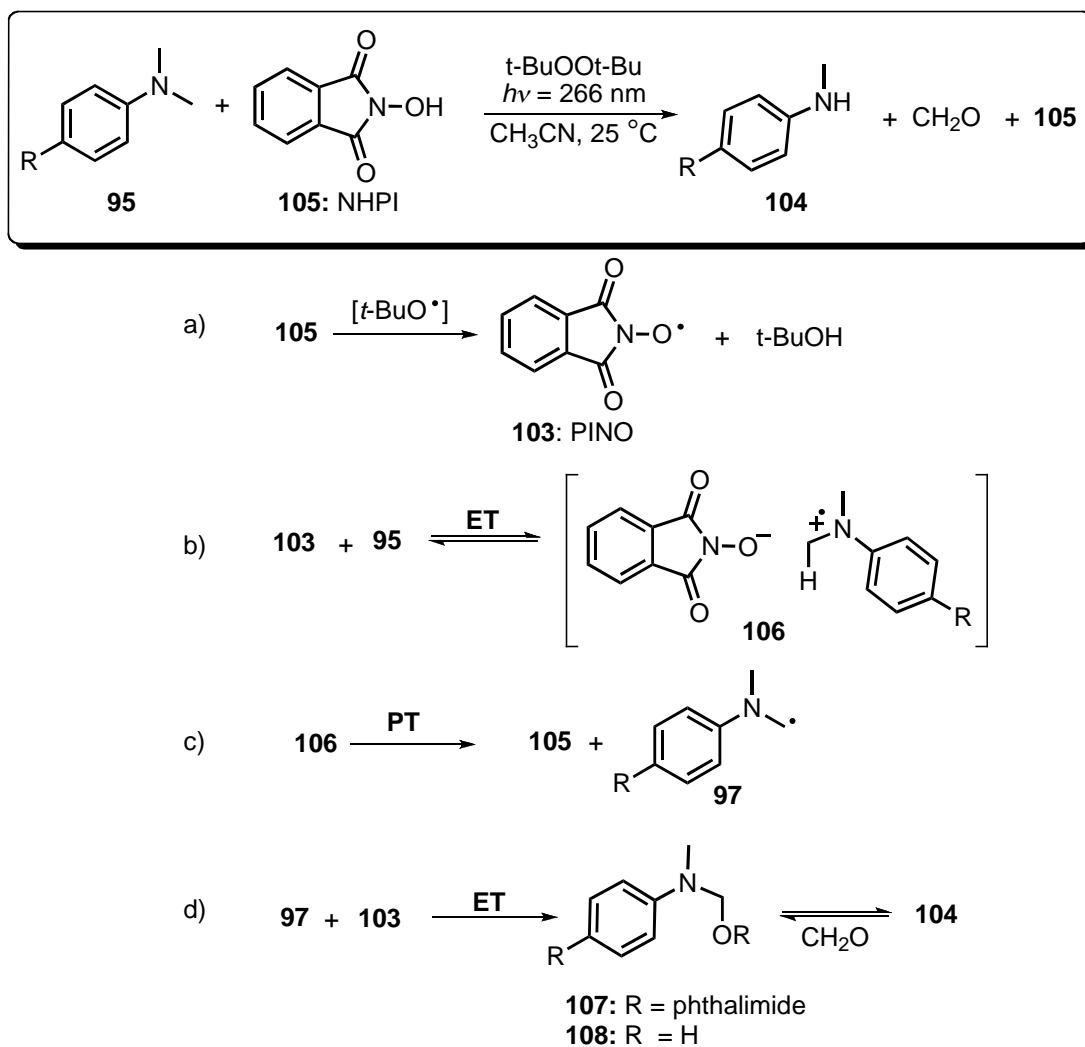
<sup>197</sup> Rosenblatt, D. H.; Hayes, A. J.; Harrison, B. L.; Streaty, R. A.; Moore, K. A. *J. Org. Chem.* **1963**, 28, 2790.

<sup>198</sup> The series and follow up studies is compiled in this review Chow, Y. L.; Danen, W. C.; Nelsen, S. F.; Rosenblatt, D. H. *Chem. Rev.* **1978**, 78, 243.



$\alpha$ -anilinyl radical (**97**) and regenerates **105**. Finally, rapid ET from the  $\alpha$ -anilinyl radical to **103** generates an aminal (**107**) that enters into a dealkylative equilibrium *via* the hemi-aminal (**108**) to yield **104**.

**Scheme 3-18.** PINO Oxidation: Type IV ET-PT/ET amine oxidation.



The contribution of the ET between the dimethylanilines (**95**) and the PINO radical (**103**) to rate-limitation was demonstrated by a linear correlation with both the Hammett parameter  $\sigma^+$  ( $\rho = -4.2$ ) and the oxidation potentials of the dialkylanilines (slope = -5.9). The contribution of PT to rate-limitation could be observed as significant deuterium KIEs for the comparative rates of  $h_6$  and  $d_6$  4-R-(*N,N*-dimethyl)-anilines (**95**). The KIEs for R = H and R = Br were  $k_H/k_D$

= 4.8 and 5.8, respectively. This data suggests a Type IV ET-PT reaction with both an ET and PT reaction contributing to overall rate-limitation.

The PINO example demonstrates the continuous relationship between the ET-PT mechanisms. A substrate dependent switch from a Type IV to a Type I ET-PT mechanism can be observed under the reaction conditions. As the oxidation potential of the dialkylaniline was decreased with increasing donating ability of the substituent, the value of the deuterium KIE decreased towards unity. For *p*-methoxy-*N,N*-dimethylaniline, the KIE value was equal to 1.0 indicating that proton transfer was no longer contributing to rate limitation and a Type I ET-PT mechanism was operative. This can be rationalized based on the oxidation potentials for PINO ( $E_0 = 0.92$  eV vs. NHE in  $\text{CH}_3\text{CN}$ ) and *p*-methoxy-*N,N*-dimethylaniline ( $E_0 = 0.69$  eV vs. NHE in  $\text{CH}_3\text{CN}$ ). The ET event is therefore significantly exergonic (0.23 eV or 5.3 kcal mol<sup>-1</sup>). This decreases the value of  $k_{\text{ET}}$  in Eq. 3-6 and the rate expression begins to approximate the Type I rate expression in Eq. 3-2. This free energy dependent change in behavior provides further support for the proposed general rate law in Eq. 3-1 and demonstrates the interrelationship between Type I and Type IV ET-PT; i.e. although the Type I and Type IV ET-PT mechanisms can be experimentally differentiated, they are opposite ends of the same mechanism.

In addition to the ET-PT/ET mechanisms for oxidative iminium ion formation, examples of the HAT/ET mechanism can be found in the literature. Rosenblatt and co-workers found that the oxidative dealkylation of benzylamine (**109**) to ammonia and benzaldehyde (**110**) with  $\text{ClO}_2$  occurs with significantly different reaction behavior as compared to that of triethyl- and trimethylamine. They attributed the deviation to a HAT/ET process (Scheme 3-19).<sup>200</sup> The HAT/ET mechanism begins with a hydrogen-atom

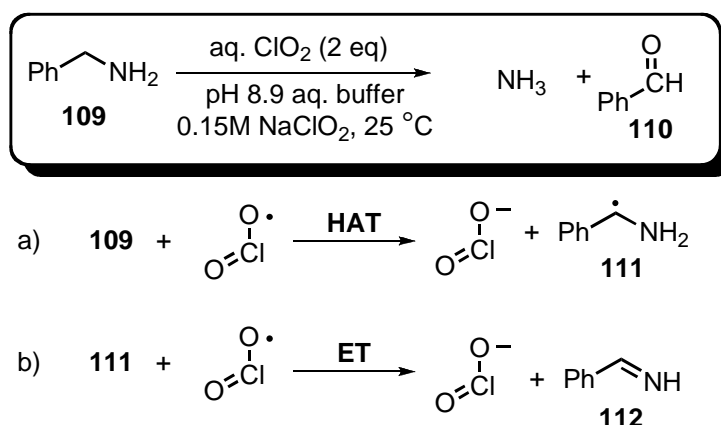
---

<sup>200</sup> a) Hull, L. A.; Davis, G. T.; Rosenblatt, D. H.; Williams, H. K. R.; Weglein, R. C. *J. Am. Chem. Soc.* **1967**, *89*, 1163, b) Rosenblatt, D. H.; Davis, G. T.; Hull, L. A.; Forberg, G. D. *J. Org. Chem.* **1968**, *33*, 1649.

transfer of the activated  $\alpha$ -benzyl-CH from benzylamine (**109**) to  $\text{ClO}_2$ . The resulting  $\alpha$ -aminyl radical (**111**) undergoes rapid ET to form the iminium ion (**112**) that then enters into a dealkylative equilibrium to generate benzaldehyde (**110**).

The mechanism was determined experimentally as follows. Inhibition of the triethylamine oxidation rate by added chlorite ion was observed with a linear dependence on chlorite ion over a broad range of concentrations. Similar experiments with benzylamine were not linearly dependent, but were asymptotic at high concentrations of chlorite ion. This behavior was an indication that a second mechanism existed for benzylamine that was independent of the Type III ET-PT mechanism determined for tertiary alkylamines (Scheme 3-17). Rosenblatt and co-workers suggested this mechanism was a HAT/ET process. The primary deuterium KIE of  $d_2$ -benzylamine ( $k_H/k_D = 3.0$ ) at high chlorite concentrations supported this assignment. Aside from being the first to experimentally observe such a mechanism, Rosenblatt and co-workers were the first to demonstrate the “duality” of amine oxidations and suggest that amine oxidations could have composite mechanisms.

**Scheme 3-19.** Classic  $\text{ClO}_2$ : HAT/ET amine oxidation.



Although the examples given here are by no means exhaustive,<sup>201, 202</sup> the models presented in Eq. 3-1 to Eq. 3-8 are a general rubric that can be applied to the oxidation of tertiary amines. In terms of the dirhodium(II) catalyzed oxidation of amines, the main goal was to determine the applicability of one of these established models to the formation of iminium ions in the oxidative Mannich reaction and to identify the reaction intermediates including potential organometallic oxidants.

### III. Results and Discussion

With an understanding of amine oxidation mechanisms, a three-part strategy was designed to approach the mechanism for the dirhodium(II) catalyzed oxidative Mannich reaction. First, key reaction intermediates, including the active oxidant, were experimentally identified and used to verify the applicability of the one of the tertiary amine oxidation models to the dirhodium-catalyzed process. Second, the nature of the rate-limiting step and the governing rate-law was determined by the method of isotope effects profiles. Finally, reactant molecularities and linear free energy relationships were measured to further characterize the transition state and establish the type of amine oxidation as well as the role of the dirhodium(II) complex.

---

<sup>201</sup> Recent electrochemical methodologies for the preparation and use of iminium ions by anodic oxidation are examples of Type I ET/PT/ET processes. a) D'Oca, M. G. M.; Russowsky, D.; Canto, K.; Gressler, T.; Goncalves, R. S. *Organic Lett.* **2002**, *4*, 1763, b) Suga, S.; Watanabe, M.; Yoshida, J.-i. *J. Am. Chem. Soc.* **2002**, *124*, 14824, d) Suga, S.; Nishida, T.; Yamada, D.; Nagaki, A.; Yoshida, J. *J. Am. Chem. Soc.* **2004**, *126*, 14338, c) Girard, N.; Hurvois, J.-P.; Moinet, C.; Toupet, L. *Eur. J. Org. Chem.* **2005**, 2269, d) Sperry, J. B.; Wright, D. L. *Chem. Soc. Rev.* **2006**, *35*, 605, e) Maruyama, T.; Mizuno, Y.; Shimizu, I.; Suga, S.; Yoshida, J.-i. *J. Am. Chem. Soc.* **2007**, *129*, 1902.

<sup>202</sup> For other examples of systems that follow a Type IV ET/PT/ET mechanism, see: a) Mahapatra, S.; Halfen, J. A.; Tolman, W. B. *J. Am. Chem. Soc.* **1996**, *118*, 11575, b) Baciocchi, E.; Lanzalunga, O.; Lapi, A.; Manduchi, L. *J. Am. Chem. Soc.* **1998**, *120*, 5783, c) Shearer, J.; Zhang, C. X.; Hatcher, L. Q.; Karlin, K. D. *J. Am. Chem. Soc.* **2003**, *125*, 12670, d) Nehru, K.; Seo, M. S.; Kim, J.; Nam, W. *Inorg. Chem.* **2007**, *46*, 293.

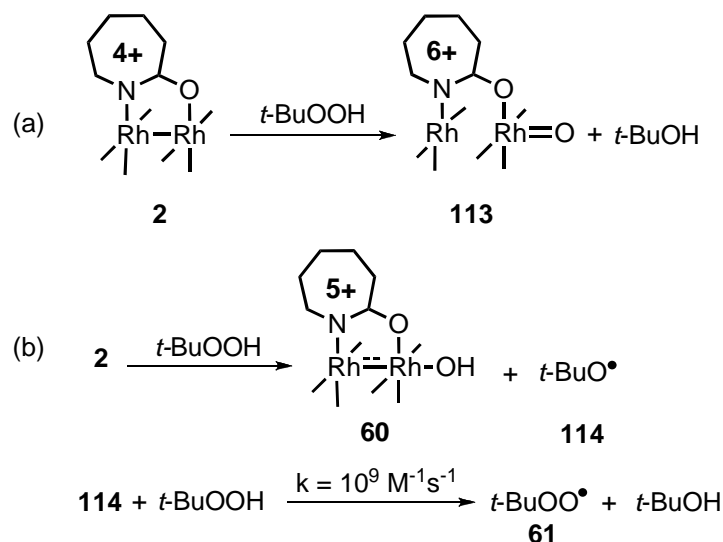
**Defining Reaction Intermediates.** The most logical first step in understanding a catalytic oxidation mechanism is to experimentally identify the oxidant. Thus, the reaction between  $\text{Rh}_2(\text{cap})_4$  (**2**) and TBHP was examined. In general, metal-catalyzed decomposition of TBHP follows either a one- or two-electron pathway shown schematically with **114** in Scheme 3-20.<sup>203</sup> The two-electron oxidation of **2** would yield a  $\text{Rh}_2^{6+}(\text{cap})_4\text{O}$  complex (**113**) with a metal-bound oxene ( $\text{O}^{2-}$ ) ligand and *tert*-butyl alcohol as the reduction products of TBHP. The one-electron oxidation of **2** would yield a  $\text{Rh}_2^{5+}(\text{cap})_4\text{OH}$  complex (**60**) with a metal-bound hydroxide ( $\text{OH}^-$ ) ligand and the *tert*-butoxyl radical (**114**) as the reduction products of TBHP. The reactive alkoxy radical **114** then propagates the radical chain decomposition of TBHP that ultimately generates the *tert*-butylperoxy radical (**61**).<sup>204</sup>

---

<sup>203</sup> Sheldon, R. A.; Kochi, J. K., *Metal-Catalyzed Oxidations of Organic Compounds*. Academic Press: New York, **1981**.

<sup>204</sup> a) Ref. 202, b) Hiatt, R. R.; Strachan, W. M. *J. Org. Chem.* **1963**, *28*, 1893, c) Hiatt, R. R.; Irwin, K. C.; Gould, C. W. *J. Org. Chem.* **1968**, *33*, 1430, d) Hiatt, R. R.; Mill, T.; Irwin, K. C.; Castleman, J. K. *J. Org. Chem.* **1968**, *33*, 1421, e) Minisci, F.; Fontana, F.; Araneo, S.; Recupero, F. *J. Chem. Soc., Chem. Commun.* **1994**, 1823, f) Araneo, S.; Fontana, F.; Minisci, F.; Recupero, F. *Tetrahedron Lett.* **1995**, *36*, 4307, g) Minisci, F.; Fontana, F.; Araneo, S.; Recupero, F.; Banfi, S.; Quici, S. *J. Am. Chem. Soc.* **1995**, *117*, 226, h) Walling, C. *Acc. Chem. Res.* **1998**, *31*, 155.

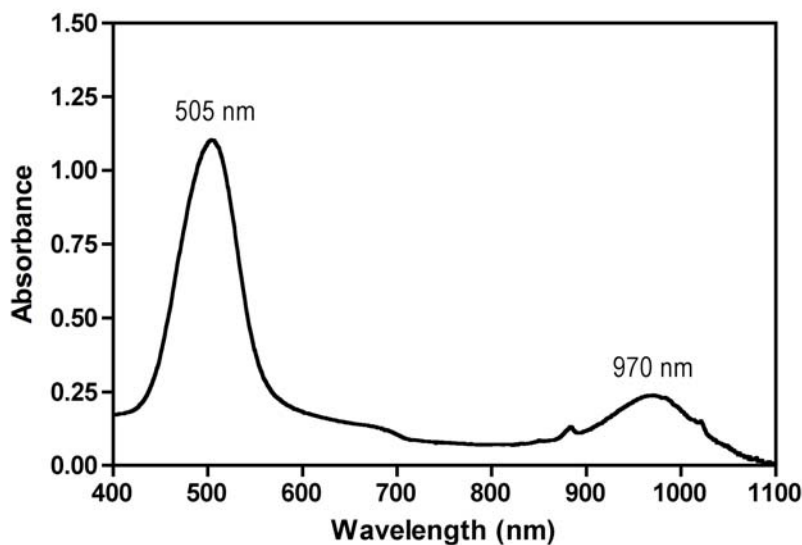
**Scheme 3-20.** Metal decomposition of *tert*-butylhydroperoxide, a) two-electron pathway; b) one-electron pathway.



The following experiments demonstrated that the  $\text{Rh}_2(\text{cap})_4/\text{TBHP}$  system operates in the one-electron oxidation manifold [ $\text{2} \rightarrow (\text{60} + \text{114}) \rightarrow \text{61}$ , Scheme 3-20b]. When  $\text{Rh}_2(\text{cap})_4$  was stoichiometrically oxidized with TBHP a hypsochromic shift in  $\lambda_{\text{max}}$  from 620 nm to 505 nm was observed as well as the appearance of another maximum at 970 nm characteristic of the oxidation from a  $\text{Rh}_2^{4+}$  to  $\text{Rh}_2^{5+}$  complex (Scheme 3-21). Attempts to make **113** with oxygen-transfer agents like *m*-chloroperoxybenzoic acid (*m*-CPBA) and iodosylbenzene ( $\text{PhI}=\text{O}$ ) yielded electronic spectra identical to **60** with no indication of  $\text{Rh}_2^{6+}$  complex formation at ~430 nm.



**Scheme 3-21.** Visible spectrum of **60** upon stoichiometric oxidation of  $\text{Rh}_2^{4+}$  to  $\text{Rh}_2^{5+}$  (**2**→**60**) by TBHP.



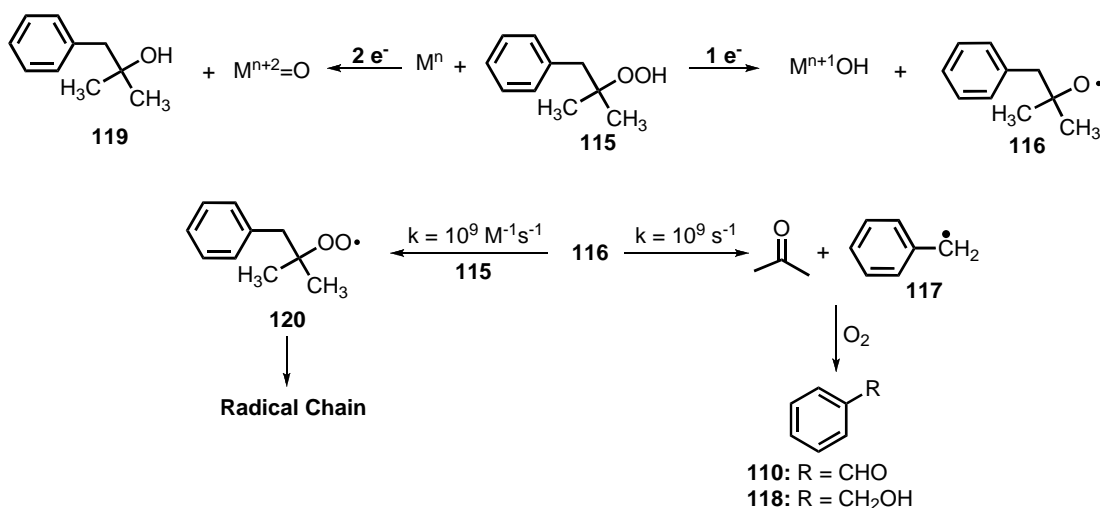
The observation of  $\text{Rh}_2^{5+}$  in the stoichiometric oxidation of  $\text{Rh}_2(\text{cap})_4$  indicated that a one-electron process was occurring that could initiate a radical chain process. 2-Methyl-1-phenylpropyl-2-hydroperoxide (**115**) was developed by Ingold and co-workers as a tool for detecting one and two electron oxidations of a metal by *tert*-alkyl hydroperoxides (Scheme 3-22).<sup>205</sup> Compound **115** acts as a reporter for alkoxy- or alkylperoxy radical intermediates in the amine oxidation. Single electron reduction of **115** by a metal (M) yields 1-phenyl-2-methyl-2-propoxy radical (**116**). The alkoxy radical **116** undergoes a rapid  $\beta$ -scission to yield acetone and benzyl radical (**118**) with a unimolecular rate constant of  $10^9 \text{ s}^{-1}$ . With **116** committing kinetic suicide, the formation of the alkylperoxy radical (**120**) is inhibited and the benzyl radical (**117**) is oxidized to benzaldehyde (**110**) and benzyl alcohol (**118**). These are observed as the major products of a one-electron reduction

---

<sup>205</sup> a) Arends, I. W. C. E.; Ingold, K. U.; Wayner, D. D. M. *J. Am. Chem. Soc.* **1995**, *117*, 4710, b) MacFaul, P. A.; Ingold, K. U.; Wayner, D. D. M.; Que, L., Jr. *J. Am. Chem. Soc.* **1997**, *119*, 10594.

of the alkyl hydroperoxide (**115**). In the event of a two-electron reduction of **115**, 1-phenyl-2-methyl-2-propanol (**119**) is observed as the major product.

**Scheme 3-22.** Hydroperoxide **115** as a suicide peroxide.<sup>206</sup>



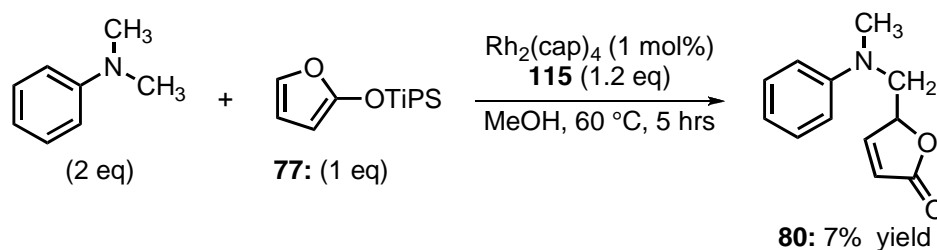
Stoichiometric decomposition of **115** by  $\text{Rh}_2(\text{cap})_4$  in a dilute solution of anhydrous benzene (3  $\mu\text{M}$ ) yielded  $\text{Rh}_2^{5+}$  in a one-electron oxidation. The organic decomposition products were mainly descended from the benzyl radical (**110**: 82%, **118**: <5%), acetone (85%), and **119** (10%) with full conversion of **115** to products. The ratio of single electron to two-electron products is 8:1 and suggests that the oxidation of  $\text{Rh}_2(\text{cap})_4$  by **115** occurs by a single-electron oxidation generating alkoxy radicals (Scheme 3-22b).

The rapid  $\beta$ -scission process from the alkoxy radical (**116**) effectively terminates the radical chain decomposition of the hydroperoxide (**115**) as it prevents the formation of additional alkoxy (**116**) and alkylperoxy (**120**) radical chain carrying species. Therefore, **115** was used to probe the role of alkoxy- and/or alkylperoxy radicals in the oxidation of amine substrates by  $\text{Rh}_2(\text{cap})_4$  (Scheme 3-23). When **115** was used as the terminal oxidant in the

<sup>206</sup> a) The rate constant for **116**→**120** is approximated based on the reaction of TBHP with *t*-BuO•, see ref. 203; b) The rate constant for **116**→**117** was measured by Arends and co-workers, see ref. 205a.

oxidative Mannich reaction with the 2-siloxyfuran (**77**) and *N,N*-dimethylaniline, the  $\gamma$ -butenolide product (**80**) is observed in less than 10% yield under the standard reaction conditions in comparison to 95% yield with TBHP. . Moreover, only 11% of the 2 equivalents of *N,N*-dimethylaniline was consumed.<sup>207</sup> This result, in conjunction with the stoichiometric decomposition of **115**, strongly implicate the  $\text{Rh}_2^{4+/5+}$  one-electron redox couple as a source of alkoxy and/or alkylperoxy radicals and suggests that these radicals are requisite intermediates along the amine oxidation pathway.

**Scheme 3-23.** Oxidative Mannich reaction fails with **115** as oxidant.



Considering the intermediacy of alkoxy and alkylperoxy radicals, the investigation turned to identifying the species primarily involved with the oxidation of substrates. It is not unreasonable to assume that the *tert*-butylperoxy radical is the radical intermediate of most significant concentration under the reaction conditions based on the reactivity of *tert*-butoxy radicals with TBHP.<sup>208</sup> This can be experimentally tested, however, through a selectivity assay based on the product distribution of an adamantane oxidation.

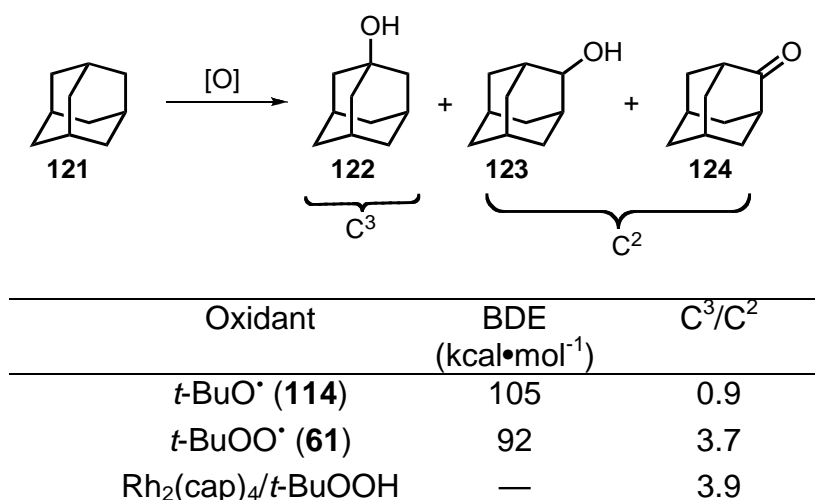
Using adamantane (**121**) as a substrate, the ratio of the oxidation products 1-adamantanol (**122**), 2-adamantanol (**123**), and 2-adamantanone (**124**) provide a diagnostic test that has been calibrated for both *tert*-butoxy

<sup>207</sup> Conversion was determined by  $^1\text{H}$  NMR against an internal standard of known concentration.

<sup>208</sup> Ref. 205.

and *tert*-butylperoxyl radicals.<sup>209</sup> Oxidation of one of the four tertiary (C<sup>3</sup>) and twelve secondary (C<sup>2</sup>) positions yields the products **122-124** and the ratio of C<sup>3</sup>/C<sup>2</sup> is a measure of selectivity (Scheme 3-24). The values for C<sup>3</sup>/C<sup>2</sup> reported in the literature follow a logical progression in terms of the homolytic bond dissociation energy (BDE) of the forming O-H bond upon hydrogen-atom transfer (HAT). For the *tert*-butoxyl radical, a strong O-H bond is formed (BDE = 105 kcal mol<sup>-1</sup>) and is reflected in a relatively unselective C<sup>3</sup>/C<sup>2</sup> ratio (0.9). *Tert*-butylperoxyl radical forms a much weaker O-H bond (BDE = 92 kcal mol<sup>-1</sup>) and consequently is much more selective for the oxidation of the weaker C<sup>3</sup> rather than the C<sup>2</sup> positions of adamantane (C<sup>3</sup>/C<sup>2</sup> = 3.7).

**Scheme 3-24.** Adamantane as an oxidation reporter.



The C<sup>3</sup>/C<sup>2</sup> ratio for the Rh<sub>2</sub>(cap)<sub>4</sub>/TBHP system was 3.9 indicating that the bond formed during the oxidation has a BDE very close to the *tert*-butyl hydroperoxide O-H bond. The BDEs measured for metal-hydroxide O-H bonds range from 75-80 kcal mol<sup>-1</sup>, well below that of TBHP.<sup>210</sup> Thus, the C<sup>3</sup>/C<sup>2</sup> selectivities of metal-centered oxidants can be much higher than the

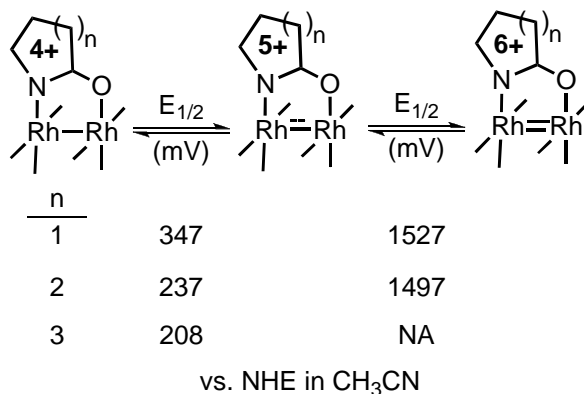
<sup>209</sup> f) Minisci, F.; Fontana, F.; Araneo, S.; Recupero, F.; Banfi, S.; Quici, S. *J. Am. Chem. Soc.* **1995**, *117*, 226.

<sup>210</sup> Mayer, J. M. *Acc. Chem. Res.* **1998**, *31*, 441.

*tert*-butylperoxyl radical (**61**).<sup>211</sup> This further eliminates the possibility of a metal-centered oxidant being responsible for CH-bond cleavage in the Rh<sub>2</sub>(cap)<sub>4</sub>/TBHP system. The C<sup>3</sup>/C<sup>2</sup> product ratio for the oxidation of adamantane by Rh<sub>2</sub>(cap)<sub>4</sub> and TBHP is consistent with an HAT by **61** that is generated from the Rh<sub>2</sub><sup>4+</sup>/Rh<sub>2</sub><sup>5+</sup> redox couple.

With the active oxidant identified as **61**, a brief discussion of the basic thermochemistry of the Rh<sub>2</sub>(cap)<sub>4</sub>/TBHP oxidation system follows. Dirhodium(II) carboxamidates feature some of the lowest redox potentials of all dirhodium(II) complexes (Scheme 3-25). They are readily oxidized from Rh<sub>2</sub><sup>4+</sup> to Rh<sub>2</sub><sup>5+</sup> at low potential with a small free energy penalty (1 mV = 0.023 kcal mol<sup>-1</sup>) and the reduction of Rh<sub>2</sub><sup>5+</sup> back to Rh<sub>2</sub><sup>4+</sup> also occurs at a low potential that yields very little free energy. Therefore, in a catalytic process that requires a metal-complex to cycle between oxidation states, dirhodium(II) carboxamidates can do so in the Rh<sub>2</sub><sup>4+/5+</sup> couple through a shallow free-energy well.

**Scheme 3-25.** Redox states for dirhodium(II) carboxamidates.<sup>212</sup>



<sup>211</sup> A C<sup>3</sup>/C<sup>2</sup> ratio of 9.2 was measured for a ruthenium oxidant. Murahashi, S.-I.; Komiya, N.; Oda, Y.; Kuwabara, T.; Naota, T. *J. Org. Chem.* **2000**, *65*, 9186.

<sup>212</sup> Ag/AgCl reference electrode converted to NHE by adding 197 mV to values found in: Doyle, M. P.; Ren, T., *The Influence of Ligands on Dirhodium(II) on Reactivity and Selectivity in Metal Carbene Reactions*. In *Progress in Inorganic Chemistry*, Karlin, Ed. Wiley: New York, **2001**, *49*, 113-168.

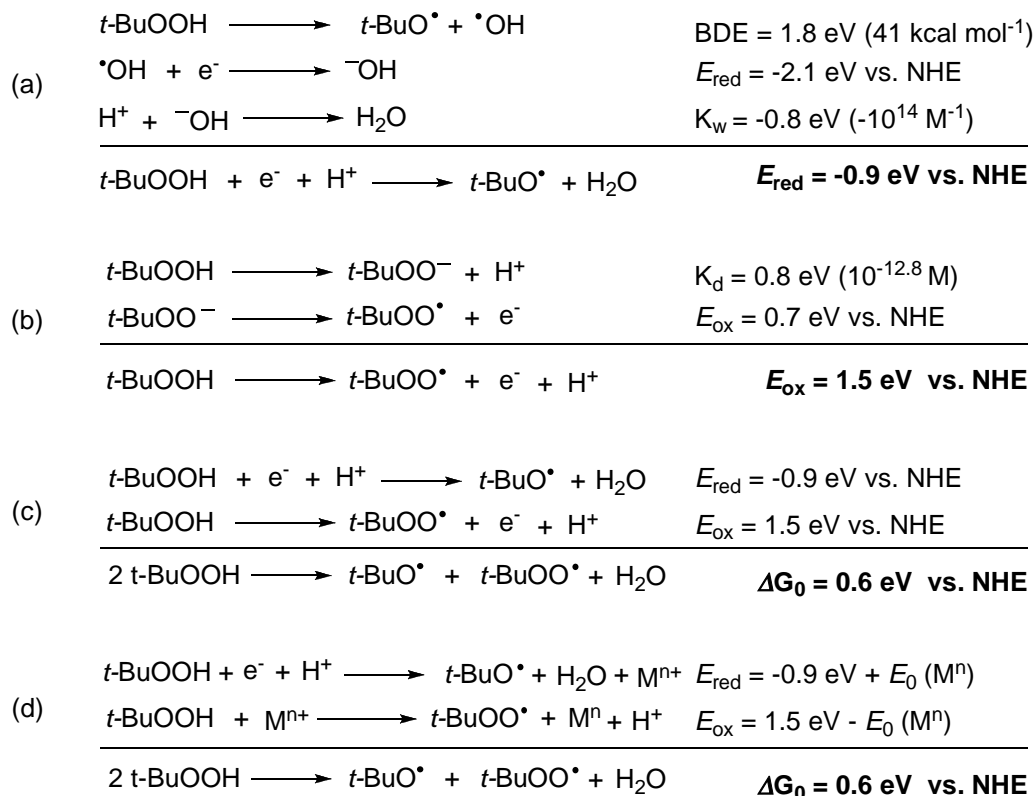
The oxidation/reduction potentials of TBHP are difficult to measure due to the induced radical chain decomposition that occurs concomitant with the electron transfer. Neglecting the formation molecular O<sub>2</sub> and *tert*-butyl alcohol, an estimate can be made for the individual oxidation and reduction half-reactions for TBHP based on the thermochemical data available for related reactions (Scheme 3-26). The reduction potential ( $E_{\text{red}}$ ) of TBHP is estimated to be -0.9 eV based on the thermochemical cycle in Scheme 3-26a.<sup>213</sup> The oxidation potential ( $E_{\text{ox}}$ ) of TBHP is estimated to be 1.5 eV by a similar thermochemical cycle in Scheme 3-26b.<sup>214</sup> Based on oxidation and reduction half-reactions, the decomposition of TBHP to the *tert*-butylperoxyl radical (**61**), *tert*-butoxyl radical (**114**) and water is an overall endergonic process of 0.6 eV (Scheme 3-26c).

---

<sup>213</sup> For the BDE of TBHP, see: Bach, R. D.; Ayala, P. Y.; Schlegel, H. B. *J. Am. Chem. Soc.* **1996**, *118*, 12758, For standard reduction potential of an aqueous hydroxy radical vs. NHE, see: Ritchie, C. D. *J. Am. Chem. Soc.* **1983**, *105*, 7313.

<sup>214</sup> For the reduction potential of the *tert*-butylperoxyl radical in water. a) Das, T. N.; Dhanasekaran, T.; Alfassi, Z. B.; Neta, P. *J. Phys. Chem. A* **1998**, *102*, 280, For the pK<sub>a</sub> of TBHP, see: Jonsson, M. *J. Phys. Chem.* **1996**, *100*, 6814.

**Scheme 3-26.** Thermochemical estimates of a) the reduction potential of TBHP ( $E_{\text{red}}$ ); b) the oxidation potential of TBHP ( $E_{\text{ox}}$ ),<sup>215</sup> and decomposition of TBHP ( $\Delta G_0 = E_{\text{red}} + E_{\text{ox}}$ ) in water. (Abbreviations: BDE = bond dissociation energy, NHE = normal hydrogen electrode, standard state = 1 atm, 298 K)

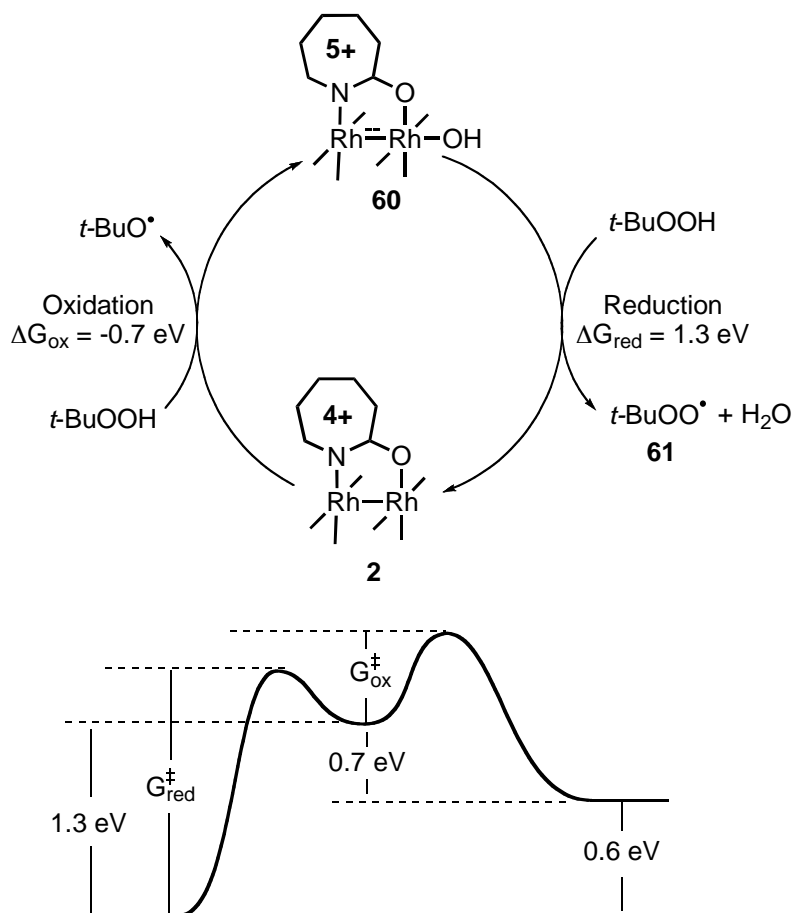


For metal catalyzed decompositions of TBHP, the metal donates and accepts the electron equivalents ( $e^-$ ) for each half-reaction (Scheme 3-26d). In each half-reaction,  $e^-$  is replaced with a metal using the relationship  $e^- + \text{M}^{n+1} = \text{M}^n$ . It becomes clear from such an analysis that the oxidation potential of the metal bears *no relevance to the overall free energy of the decomposition of TBHP*. Rather, the metal plays a role in determining the rate of the individual half-reactions.<sup>216</sup>

<sup>215</sup> This value matches the value reported for the oxidation of TBHP at pH = 0 reported in ref. 214a.

<sup>216</sup> The metal-catalyzed decomposition of TBHP is well-documented. a) Kharasch, M. S.; Fono, A.; Nudenberg, W. *J. Org. Chem.* **1951**, *16*, 105, b) Kharasch, M. S.; Pauson, P.;

**Scheme 3-27.** Decomposition of TBHP catalyzed by dirhodium(II) carboxamidates. (Abbreviations: TBHP = *t*-BuOOH, *tert*-butyl hydroperoxide.)



This concept is demonstrated using  $\text{Rh}_2(\text{cap})_4$  in the catalytic cycle shown in Scheme 3-27. The one-electron oxidation of  $\text{Rh}_2^{4+}(\text{cap})_4$  (**2**) by TBHP is thermodynamically favorable ( $\Delta G_{\text{ox}} = E_0(\text{Rh}_2) + E_{\text{red}}(\text{TBHP}) = -0.7 \text{ eV}$ ). Conversely, the one-electron reduction of  $\text{Rh}_2^{5+}(\text{cap})_4\text{OH}$  (**60**) by TBHP to form the *tert*-butylperoxyl radical (**61**) and water is thermodynamically unfavorable ( $\Delta G_{\text{red}} = E_{\text{ox}}(\text{TBHP}) - E_0(\text{Rh}_2) = 1.3 \text{ eV}$ ). In the catalytic decomposition of TBHP by  $\text{Rh}_2(\text{cap})_4$ , the turnover-limiting step will therefore be the endothermic reduction of **60** by TBHP. Thus, the oxidized form of  $\text{Rh}_2(\text{cap})_4$  (**60**) will be the resting state of the catalyst. The reaction energy

Nudenberg, W. *J. Org. Chem.* **1953**, *18*, 322, c) Hiatt, R. R.; Irwin, K. C.; Gould, C. W. *J. Org. Chem.* **1968**, *33*, 1430.



diagram in Scheme 3-27 summarizes the thermochemistry for the catalytic cycle starting from **60** and shows the rate-limiting nature of the metal reduction.

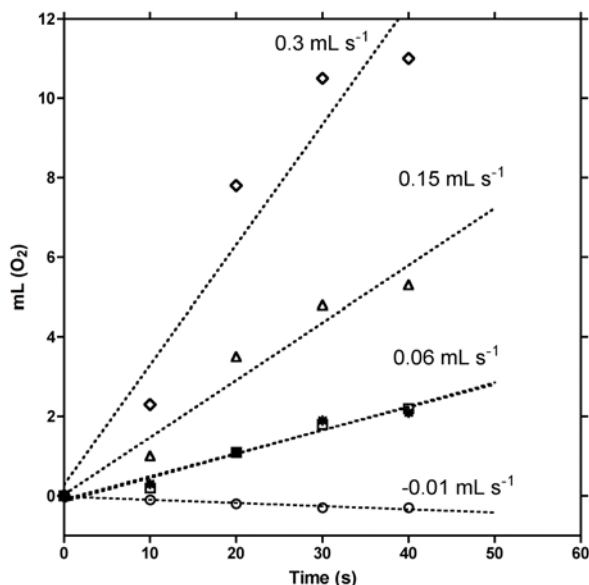
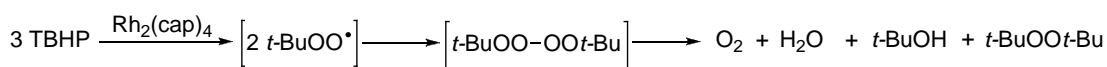
Although it would be difficult to separate the contributions of oxidation and reduction to the activation energy of TBHP decomposition, there is some experimental evidence to support the model posed in Scheme 3-27. The model predicts that, in the case of  $\text{Rh}_2(\text{cap})_4$ , the resting state of the catalytic cycle would be  $\text{Rh}_2^{5+}(\text{cap})_4$  (**60**) as a result of turnover-limiting reduction of **60** to  $\text{Rh}_2^{4+}(\text{cap})_4$  (**2**). This was observed spectrophotometrically as an immediate buildup of  $\text{Rh}_2^{5+}(\text{cap})_4$  complexes in solution at 505 nm during the decomposition of TBHP by **2** in the presence and absence of substrate under the oxidative Mannich reaction conditions.

The proposed model would also predict that the rate of TBHP decomposition would depend on pH or the base strength of an additive as  $\text{pK}_a$  is incorporated into the oxidation potential for TBHP. According to the thermodynamic cycle in Scheme 3-26b, as the extent of deprotonation increases the oxidation potential of TBHP ( $E_{\text{ox}}$ ) would decrease towards the limit of  $E_0$  for the *tert*-butylperoxy anion (0.71 eV). Considering the coupling of free energy and activation energy previously described for ET reactions, a commensurate lowering of the activation energy for the reduction of  $\text{Rh}_2^{5+}$ ,  $G_{\text{red}}^\ddagger$ , should occur as  $E_{\text{ox}}$  decreases. Thus, the decomposition would proceed at a faster rate.

To observe such a phenomenon, the initial rate ( $v_i$ ) of  $\text{O}_2$  liberation was measured from the catalytic decomposition of TBHP by **2** with additives of varying base strengths (Scheme 3-28) in anhydrous  $\text{CH}_2\text{Cl}_2$ . The evolution of  $\text{O}_2$  is a result of the dimerization of *tert*-butylperoxyl radicals (**61**) to form a highly unstable tetroxide that rapidly decomposes to yield  $\text{O}_2$  and di-*tert*-

butylperoxide.<sup>217</sup> The observed rate of O<sub>2</sub> evolution followed the predicted progression with increasing base strength;  $v_i$  (mL O<sub>2</sub>/s) = 0.1 with no additive and sodium bicarbonate (NaHCO<sub>3</sub>), 0.2 with potassium carbonate (K<sub>2</sub>CO<sub>3</sub>), and 0.3 with potassium *tert*-butoxide (KOt-Bu). Oxygen production was suppressed [ $v_i$  (mL O<sub>2</sub>/s) = 0.0] when acetic acid (AcOH) was used to inhibit the acid dissociation of TBHP. These observations are consistent with the model described in Scheme 3-27 and the half-reactions in Scheme 3-26.

**Scheme 3-28.** Base effect in catalytic decomposition of TBHP by **2**.

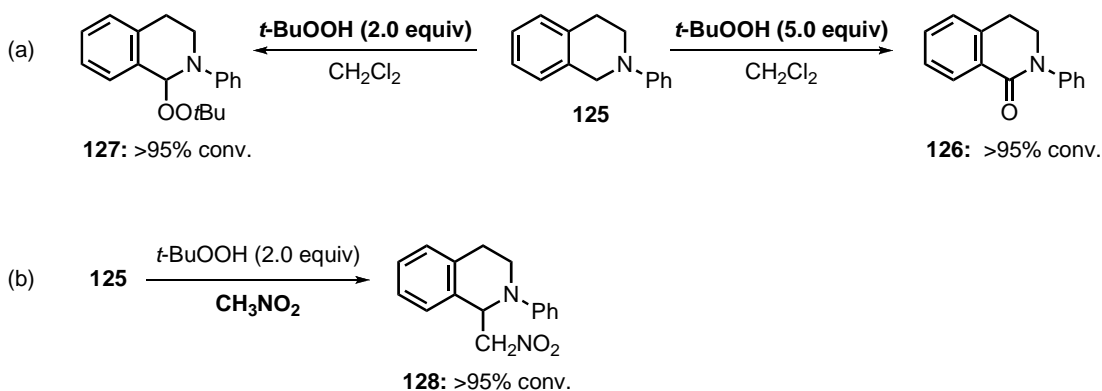


Reaction Conditions: Reaction was initiated by the addition of anhydrous TBHP in decane (0.010 mmol) to a stirring solution of **2** (0.001 mmol) and additive (0.010 mmol) in anhydrous CH<sub>2</sub>Cl<sub>2</sub>. The amount of O<sub>2</sub> was monitored using a gas burette charged with silicon oil. Additives:  $\diamond$ —KOt-Bu,  $\triangle$ —K<sub>2</sub>CO<sub>3</sub>,  $\ast$ —NaHCO<sub>3</sub>,  $\circ$ —AcOH,  $\square$ —none.

<sup>217</sup> The formation and decomposition of tetroxides from peroxy radicals is called the Russell termination. Russell, G. A. *J. Am. Chem. Soc.* **1957**, 79, 3871.

With the active oxidant, catalyst redox states, and basic thermodynamic model for the oxidation system defined, the next logical step was to determine the product of the reaction between the  $\text{Rh}_2(\text{cap})_4/\text{TBHP}$  oxidation system and amine substrates. The oxidative Mannich reaction was developed by assuming that an iminium ion was the product of the oxidation of *N,N*-dialkylanilines. This assumption was based on experiments performed by A. Catino and summarized in Scheme 3-29. When *N*-phenyl-tetrahydroisoquinoline (**125**) was oxidized under the general conditions for the benzylic oxidation (Scheme 3-29a), the known amide (**126**)<sup>218</sup> was generated in 95% conversion as determined by <sup>1</sup>H NMR. Simply reducing the amount of TBHP from 5 equiv. to 2 equiv. yielded the known dialkylperoxide (**127**).<sup>219</sup> When the reaction was run in a nucleophilic solvent like nitromethane, the solvent captured products **128** was observed in high conversion (Scheme 3-29b).<sup>220</sup> The observation of **127** and **128** suggested an iminium ion intermediate as the product of oxidation.

**Scheme 3-29.** Indirect observations of an iminium ion.<sup>221</sup>



As described in Scheme 3-8, the iminium ion from *N,N*-dimethylaniline in the presence of water will enter a dealkylative equilibrium to generate

<sup>218</sup> Cheng, C.-Y.; Tsai, H.-B.; Lin, M.-S. *J. Heterocycl. Chem.* **1995**, *32*, 73.

<sup>219</sup> Murahashi, S.; Naota, T.; Miyaguchi, N.; Nakato, T. *Tetrahedron Lett.* **1992**, *33*, 6991.

<sup>220</sup> Ref. 166a.

<sup>221</sup> Ref. 161b.



**Elements of Rate Limitation.** With the oxidation system and products defined, the focus shifted to the mechanism of action between *tert*-butylperoxyl radicals (**61**), and *N,N*-dialkylanilines to form iminium ions. A hydrogen-atom transfer between **61** and *N,N*-dialkylanilines that forms the  $\alpha$ -aniliny radical and TBHP was observed by Griller and co-workers (**63**, Scheme 3-1).<sup>222</sup> Based on this reactivity, the fate of **63** was chosen as a target for investigation. Intermediate **63** can either undergo a single-electron transfer to an oxidant to form the iminium ion (**59**, Scheme 3-1), or terminate in a radical coupling with **61** to form a peroxyaminal (**127**, Scheme 3-29) as an iminium ion precursor.

A simple model can be suggested based on the formation of the iminium ion precursor **127**. The Ingold-Fisher persistent radical effect (PRE) describes a set of conditions that can form mixed dialkylperoxides like **127** through selective radical termination events.<sup>223</sup> At its most fundamental, the PRE is a kinetic phenomenon that occurs when kinetically stable (persistent) and unstable (reactive) radicals are formed in a radical chain decomposition process at similar rates. Under this condition, the rate of persistent and reactive radical cross-termination is much faster than their individual dimerizations. The PRE mechanism has been proposed for metal-promoted TBHP oxidations of hydrocarbons where the relatively stable *tert*-butylperoxyl radical is formed alongside a reactive alkyl radical.<sup>224</sup>

A PRE model for the oxidation of *N,N*-dialkylanilines (**58**) by *tert*-butylperoxyl radicals (**61**) is presented in Scheme 3-31. The mechanism begins with a steady-state concentration of **61** provided by the  $\text{Rh}_2^{4+/5+}$  redox couple.

---

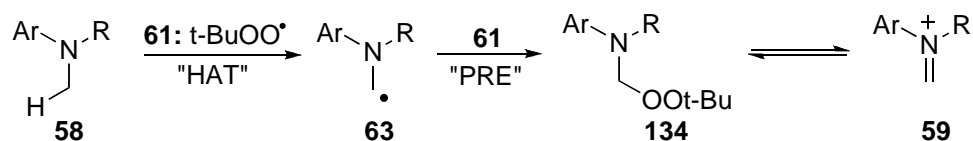
<sup>222</sup> Griller, D.; Howard, J. A.; Marriott, P. R.; Scaiano, J. C. *J. Am. Chem. Soc.* **1981**, *103*, 619.

<sup>223</sup> a) Fischer, H.; Souaille, M. *Macromol. Symp.* **2001**, *174*, 231, b) Studer, A. *Chem. Eur. J.* **2001**, *7*, 1159.

<sup>224</sup> a) Bravo, A.; Bjorsvik, H.-R.; Fontana, F.; Liguori, L.; Minisci, F. *J. Org. Chem.* **1997**, *62*, 3849, b) Minisci, F.; Recupero, F.; Cecchetto, A.; Gambarotti, C.; Punta, C.; Faletti, R.; Paganelli, R.; Pedulli, G. F. *Eur. J. Org. Chem.* **2004**, 109.

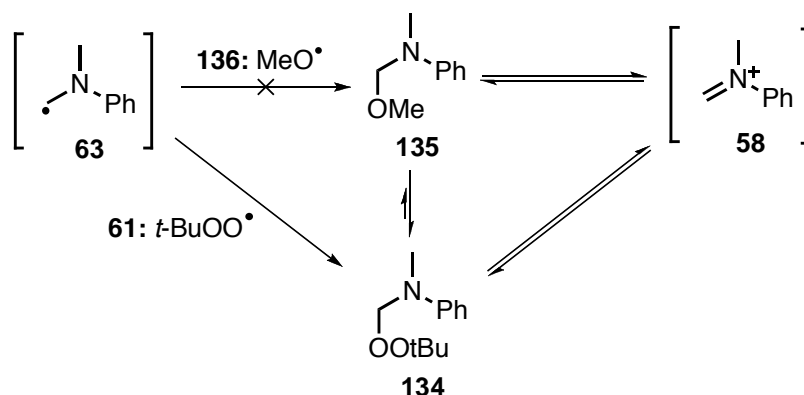
HAT between **58** and the *tert*-butylperoxyl radical (**61**) to generate the  $\alpha$ -aniliny radical (**63**). Selective termination of **63** with **61** generates the *tert*-butylperoxyaminal (**134**) that, upon elimination of TBHP, yields the iminium ion (**59**). If this model were operative in the case of dirhodium catalyzed amine oxidation, then **134** would be a common precursor to the iminium ion and all other observed products.

**Scheme 3-31.** PRE mechanism for iminium ion formation.



An experiment using *N,N*-dimethylaniline as the substrate was designed to test the common intermediacy of *N*-(*tert*-butyldioxyethyl)-*N*-methylaniline (**134**) in the production of *N*-(methoxymethyl)-*N*-methylaniline (**135**) (Scheme 3-32). Compound **134** was prepared separately by oxidation of *N,N*-dimethylaniline in  $\text{CH}_2\text{Cl}_2$  with  $\text{Rh}_2(\text{cap})_4$  and TBHP. Compound **135** was prepared by the same oxidation of *N,N*-dimethylaniline in  $\text{CH}_3\text{OH}$ . Compound **134** was placed in deuterated methanol (methanol-*d*) and allowed to stand at room temperature for 48 h. Periodic monitoring by  $^1\text{H}$  NMR showed incomplete conversion of **134** to **135** after the complex had come to equilibrium. The equilibrium was confirmed as no change in the relative amounts of **134** to **135** occurred after the first three hours. Moreover, the addition of excess TBHP caused the equilibrium to shift back towards **135**. The equilibrium constant between the two species (**134** $\leftrightarrow$ **135**) was measured as  $2 \times 10^{-3}$  based on  $^1\text{H}$  NMR analysis. This indicates that **134** is thermodynamically preferred over **135** by  $\sim 5 \text{ kcal mol}^{-1}$ .

**Scheme 3-32.** *tert*-Butylperoxyaminals are not common intermediates.

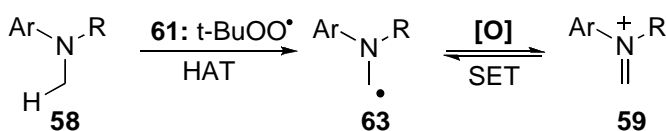


The oxidation of *N,N*-dimethylaniline to form (*N*-(trideuteriomethoxymethyl)-*N*-methylaniline ( $d^3$ -**135**) in methanol-*d* at room temperature was followed by  $^1\text{H}$  NMR over 1 h (Scheme 3-32). Based on homolytic BDEs of ROH (105 kcal mol $^{-1}$ ) and TBHP (92 kcal mol $^{-1}$ ), it is unlikely that there is any significant concentration of methoxyl radical (**136**) to support a separate PRE pathway to  $d^3$ -**135** in the presence of excess TBHP. Based on the solvolysis equilibrium constant, the intermediacy of **134** would lead to its build up under the reaction conditions to form  $d^3$ -**135**. This was not the case. The first product formed,  $d^3$ -**135**, was also the dominant product observed by  $^1\text{H}$  NMR (95% in 1 h). Therefore, the methoxy-aminal ( $d^3$ -**135**) must come from another process that does not involve the intermediacy of the alkylperoxy-aminal (**134**). A reasonable assumption is the solvolytic capture of an iminium ion generated directly from the oxidation of *N,N*-dimethylaniline by the  $\text{Rh}_2(\text{cap})_4/\text{TBHP}$  system.

Elimination of a PRE model leaves an ET process for oxidizing the  $\alpha$ -aminy radical (**63**) to the iminium ion (**59**). Therefore, other models must be considered. Scheme 3-33 shows the application of the HAT/ET model to the dirhodium/TBHP oxidation of *N,N*-dialkylanilines. A steady-state concentration of *tert*-butoxy radical (**61**) generated by the dirhodium-catalyzed decomposition of TBHP reacts with dialkylaniline (**58**) by HAT to form the  $\alpha$ -aminy radical (**63**). The intermediate **63** is oxidized to the iminium ion **59** by

ET to an oxidant (**[O]**). The oxidant could be molecular oxygen,  $\text{Rh}_2^{5+}(\text{cap})_4$ , or TBHP.

**Scheme 3-33.** HAT/ET mechanism for iminium ion formation.



A useful approach to test the HAT/ET model is to examine the influence of substrate oxidation potential ( $E_0$ ) on the deuterium isotope effect for CH-bond cleavage. The absence of an isotope effect for all substrates would indicate that an ET process is the rate-limiting step and the HAT/ET mechanism would not be valid. If an isotope effect exists and is insensitive to changes in substituents that affect  $E_0$ , then the HAT/ET mechanism is likely. However, if an isotope effect exists and its magnitude is influenced by the nature of the substituents, then the HAT/ET process is eliminated in favor of a Type IV ET-PT/ET mechanism. This approach is called an isotope effects free energy profile.

Dinnocenzo and coworkers developed a free energy profile for deuterium isotope effects as a powerful tool for discriminating between the ET-PT/ET and HAT/ET mechanisms.<sup>225</sup> For the HAT/ET mechanism the homolytic bond dissociation energies for substituted *N,N*-dialkylanilines are independent of the donor/acceptor ability of the substituent. Thus, there would be little difference for the magnitude of the isotope effect based on the substituent. For the ET-PT/ET mechanism, both a Type I and Type III ET-PT mechanism are limited by the electron transfer and no isotope effect would be observed. For the Type II ET-PT mechanism, only the proton transfer reaction contributes to rate-limitation and, much like the HAT/ET mechanism, only a small influence on the kinetic isotope effect would be expected.<sup>70</sup> The

<sup>225</sup> Ref. 186.



Type IV ET-PT mechanism provides a basis for which the free energy of the ET reaction can influence the observed KIE. The observed KIE will be denoted as  $k_{\text{Hobs}}/k_{\text{Dobs}}$  and substituted for  $k_{\text{obs}}$  in Eq. 3-4.<sup>226</sup> The absolute isotope effect for the PT reaction will be denoted as  $k_{\text{HPT}}/k_{\text{DPT}}$  and substituted for  $k_{\text{PT}}$  in Eq. 3-4. The results of this substitution are shown in Eq. 3-9.<sup>227</sup>

$$\text{Eq. 3-9} \quad \frac{k_{\text{Hobs}}}{k_{\text{Dobs}}} = \frac{k_{\text{HPT}}}{k_{\text{DPT}}} \left( \frac{k_{-\text{ET}} + k_{\text{DPT}}}{k_{-\text{ET}} + k_{\text{HPT}}} \right)$$

Inspection of Eq. 3-9 provides some useful diagnostic relationships for the observed isotope effects if a Type IV ET-PT/ET mechanism is operative. First, note that the isotope effects are independent of  $k_{\text{ET}}$ . This is consistent with the partitioning model in Eq. 3-4. Furthermore, this derivation does not violate the expected behavior of  $k_{\text{H}}/k_{\text{D}}$  based on the rate-limiting step. For the Type III ET-PT mechanism, where  $k_{\text{PT}} \gg k_{-\text{ET}}$ , then Eq. 3-9 simplifies to give  $k_{\text{Hobs}}/k_{\text{Dobs}} = 1$  consistent with a rate-limiting ET. For the Type II mechanism, where  $k_{-\text{ET}} \gg k_{\text{PT}}$ , then Eq. 3-9 simplifies to give  $k_{\text{Hobs}}/k_{\text{Dobs}} = k_{\text{HPT}}/k_{\text{DPT}}$  consistent with rate-limiting PT.

Perhaps the most important aspect of Eq. 3-9 is that it predicts a free energy dependence of  $k_{\text{Hobs}}/k_{\text{Dobs}}$  for a Type IV ET-PT/ET mechanism since the electron transfer rates  $k_{\text{ET}}$  and  $k_{-\text{ET}}$  are directly related to the free energy of the electron transfer.<sup>228</sup> Based on this analysis, systematic changes in  $E_0$  of the amine, and therefore  $k_{-\text{ET}}$ , provides a tool to identify the active mechanism so long as  $E_0$  does not substantially affect  $k_{\text{PT}}$  relative to  $k_{-\text{ET}}$ .<sup>229</sup> The free energy dependent isotope effect described in Eq. 3-9 predicts that as  $k_{-\text{ET}}$

---

<sup>226</sup> See pg. 274.

<sup>227</sup> For a full derivation of Eq. 3-9, see Section 3-V, Experimental, pg 323.

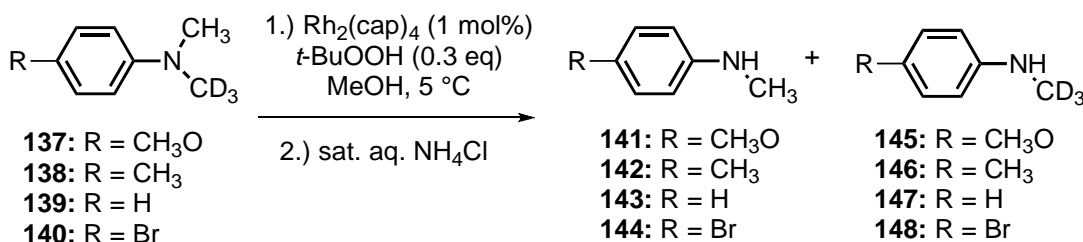
<sup>228</sup> a) Marcus, R. A. *J. Chem. Phys.* **1957**, 26, 872, b) Marcus, R. A. *J. Phys. Chem.* **1963**, 67, 853, c) Marcus, R. A.; Eyring, H. *Ann. Rev. Phys. Chem.* **1964**, 15, 155.

<sup>229</sup> Ref. 186.

increases (i.e. as  $E_0$  of the amine increases) the isotope effect will approach a maximum value of  $k_{\text{HPT}}/k_{\text{DPT}}$ .

Experimentally,<sup>230</sup> an isotope effects profile was generated for the dirhodium(II)/TBHP oxidation system with *p*-substituted *N,N*-dimethylanilines (DMAs). Two different profiles were measured. The first was based on *p*-substituted ( $h^3, d^3$ )-*N,N*-dimethylanilines (Scheme 3-34). The substrate incorporates *h* and *d* in the same molecule. Thus, the *h/d* ratio in the product of the ET equilibrium will remain constant and diminish the influence of an ET equilibrium isotope effect on the magnitude of the observed isotope effect. This provides an estimate of the theoretical maximum KIE ( $k_{\text{HPT}}/k_{\text{DPT}}$ ) for each substrate. The isotope effects derived from ( $h^3, d^3$ )-*N,N*-dimethylanilines will be referred to as a product isotope effect (PIE) depend primarily on the product forming PT reaction.

**Scheme 3-34.** Product isotope effects (PIE).

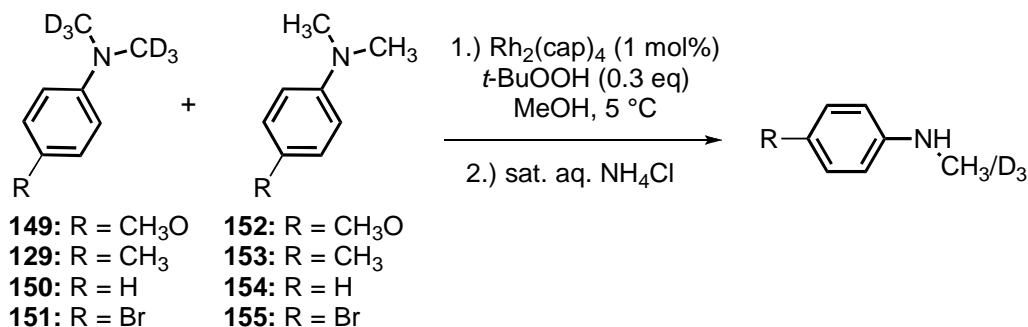


The second profile was measured with equivalent amounts of  $h^6$ - and  $d^6$ -*N,N*-dimethylanilines (Scheme 3-35). These substrates place *h* and *d* on separate molecules. In this measurement, the *h/d* ratio is not constant in the product of the ET equilibrium. Thus, the contribution of the ET equilibrium will influence the concentration of *h* and *d* in the intermediate through an equilibrium isotope effect. In this profile, the magnitude of the overall isotope effect will depend upon the magnitude of the equilibrium isotope effect. This will be called the kinetic isotope effect (KIE) as it is sensitive to all rate-limiting

<sup>230</sup> Work was done with J. M. Myslinski, undergraduate, University of Maryland.

factors including the ET equilibrium isotope effect and not just the product determining step. For both profiles, the *N*-(methoxymethyl)-*N*-methylaniline product was hydrolyzed in mild, aqueous acidic conditions to provide the *N*-methylanilines, and deuterium content was determined by GCMS. Each isotope ratio was measured at less than 10% conversion.

**Scheme 3-35.** Kinetic isotope effects (KIE).



The isotopic distributions for both the KIE and PIE profiles are listed in Table 3-1. For each substituent (R) the PIE is larger than the KIE. In both of the profiles, as  $E_0$  for the R-substituted *N,N*-dimethylanilines decreases, the value of the isotope effect decreases. If peroxy radical **61** were activating the dimethylaniline *via* the HAT/ET mechanism, there would be little difference between the KIE and PIE values and there would not be a LFER trend associated with the R-substituent. Surprisingly, the isotope effects profiles clearly indicate that an ET reaction is contributing to rate-limitation and eliminates the possibility of the HAT/ET mechanism.

**Table 3-1.** Free-energy profiles of PIE and KIE.

R	$E_0^{231}$ (eV vs. NHE)	BDE <sup>65</sup> (kcal mol <sup>-1</sup> )	PIE	KIE
CH <sub>3</sub> O	0.55	91	3.3 (1)	1.3 (1)
CH <sub>3</sub>	0.72	89.9 (2.5)	4.5 (5)	1.8 (1)
H	0.84	91.7 (1.3)	4.2 (2)	1.5 (1)
Br	0.89*	90*	5.1 (5)	2.9 (1)

\*Approximated from R = Cl

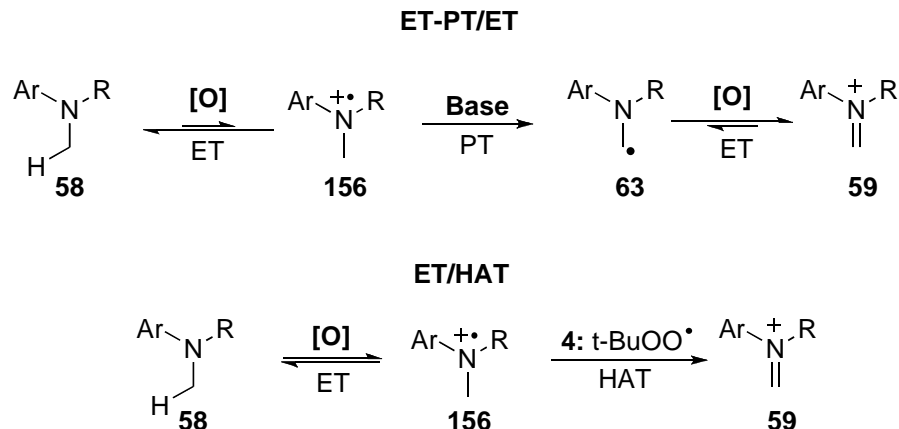
Based on the categorization of amine oxidation mechanisms,<sup>232</sup> the presence of an initial, endothermic ET equilibrium that contributes to rate-limitation is indicative of two possible mechanisms. These would be a Type IV ET-PT/ET or a similar ET/HAT mechanism (Scheme 3-36). The Type IV ET-PT/ET would start with an ET equilibrium between the dialkylaniline (**58**) and oxidant ([**O**]) that forms the anilinium radical cation (**156**). The intermediate **156** is deprotonated in a nearly irreversible proton-transfer (PT) to yield the  $\alpha$ -aminyl radical (**63**). Oxidation of **63** generates the iminium ion (**59**). The ET/HAT mechanism would also begin with an ET equilibrium between **58** and [**O**] to form **156**. In this mechanism, however, HAT from **156** generates the iminium ion directly. Unfortunately, the isotope effects profiles would be qualitatively similar in both cases as their rate expressions are mathematically identical (Eq. 3-1 and Eq. 3-8). Thus, the KIE profile cannot be used to distinguish the two mechanisms.

---

<sup>231</sup> Values for  $E_{ox}$  were measured vs. Fc/Fc+ in ref. 193 and converted to NHE (Fc/Fc+ = 400 mV vs. NHE). BDE's were also measured in ref. 193.

<sup>232</sup> See Section 3-I, Introduction.

**Scheme 3-36.** ET-PT/ET vs. ET/HAT.



**A Difference in Transition State.** A critical difference between the ET-PT/ET and ET/HAT mechanisms in the dirhodium/TBHP system is the identity of the initial electron transfer agent in the transition state. Although determining the oxidant post-CH activation (**63** to **59**, Scheme 3-36) would be difficult, determining the oxidant that contributes to rate-limiting CH activation (**58** to **156**, Scheme 3-36) is a more tenable challenge. There are three species that could behave as the initial electron transfer agent; molecular oxygen ( $O_2$ ), *tert*-butylperoxyl radical (**61**), and  $Rh_2^{5+}(cap)_4OH$  (**60**). The reduction of  $O_2$  by *N,N*-dialkylanilines is unlikely to be operative in the reaction as  $\Delta G_{ET}$  is too high and dialkylanilines are bench stable materials.<sup>233</sup> This leaves **61** or **60** as the likely oxidants available *in situ*. The oxidation has a clear dependence on the presence of **61**. If **61** were to behave as a HAT agent, then **60** would be left as the ET agent in the ET/HAT mechanism. If **61** were to behave as the ET agent in the Type IV ET-PT mechanism, then there would be no role for **60** as a partner in a bimolecular reaction with the amine. Thus, the ET/HAT mechanism would have **60** as the ET agent, and the ET-PT/ET mechanism would have **61**.

<sup>233</sup>  $E_0$  for  $O_2$  is -0.45 V vs. NHE in water.

Given that the ET reaction contributes to rate-limitation, there should be a linear free energy relationship (LFER) between the oxidation potentials of each reacting partner in ET reaction. Although varying the oxidation of the *tert*-butyl peroxy radical (**61**) is experimentally challenging, variations in the oxidation potentials of both the amine and Rh<sub>2</sub><sup>5+</sup> complex (**60**) are possible by varying substituents on each.<sup>234</sup> The LFER was measured first for the amine as the comparison of the initial rate ( $v_i$ , M<sup>-1</sup>s<sup>-1</sup>) of *N,N*-dimethylaniline consumption with various *p*-substituted *N,N*-dimethylanilines and greater than 10-fold excess of TBHP relative to aniline (Figure 3-1). The relative  $v_i$  were correlated with  $\sigma^+$  and  $E_0$  of the aniline. A linearly correlated LFER was established for substituted *N,N*-dimethylanilines with  $\sigma^+$  (-1.8,  $r^2 = 0.989$ , Figure 3-1a) and  $E_0$  (-5.2,  $r^2 = 0.990$ , Figure 3-1b). The large, negative slopes are consistent with the stabilization of positive charge in the transition state and support the proposal of an ET reaction contributing to rate-limitation.

With a clear LFER established for the amine, a similar relationship was measured for the dirhodium catalyst (Figure 3-2). *Tetrakis*-( $\mu$ -valerolactamato)-dirhodium(II) (**10**: Rh<sub>2</sub>(val)<sub>4</sub>) and *tetrakis*-[ $\mu$ -(methyl-2-oxopyrrolidine-5(S)-carboxylato)-dirhodium(II) (**157**: Rh<sub>2</sub>(5S-MEPY)<sub>4</sub>) have oxidation potentials of 217 mV and 555 mV vs. NHE in CH<sub>3</sub>CN respectively.<sup>235</sup> In the oxidation reaction, if a Rh<sub>2</sub><sup>5+</sup> complex (**60**) were the corresponding partner in the initial ET, then as the  $E_0$  of **60** is varied, a linear correlation should exist that is equal in magnitude and opposite in sign to the LFER established for the amine. Figure 3-2 shows the results of using Rh<sub>2</sub>(val)<sub>4</sub> and Rh<sub>2</sub>(5S-MEPY)<sub>4</sub> as the catalyst in the oxidation of *N,N*-dimethylaniline. No meaningful LFER was established for dirhodium complexes as all values were within experimental error of each other (slope = 0.5,  $r^2 = 0.74$ ).

---

<sup>234</sup> Work done with C. Edgely, undergraduate, University of Maryland.

<sup>235</sup> See ref. 212.

**Figure 3-1.** a) LFER calculated against  $\sigma^+$  for 4-R-*N,N*-dimethylanilines b) LFER calculated against  $E_0$  of 4-R-*N,N*-dimethylanilines.

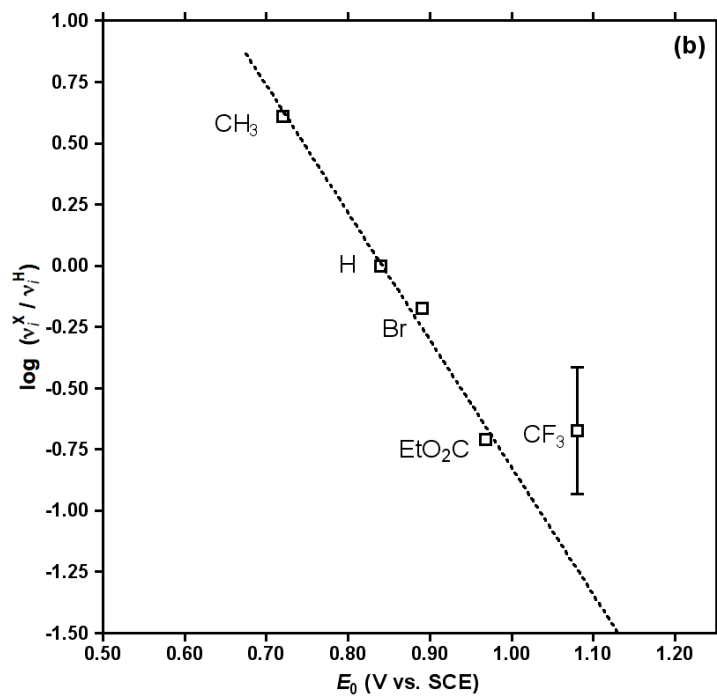
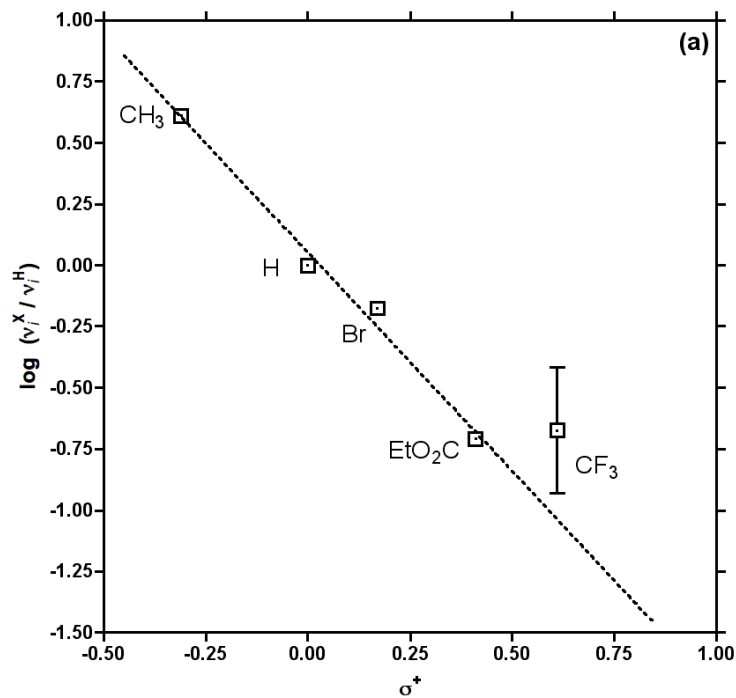
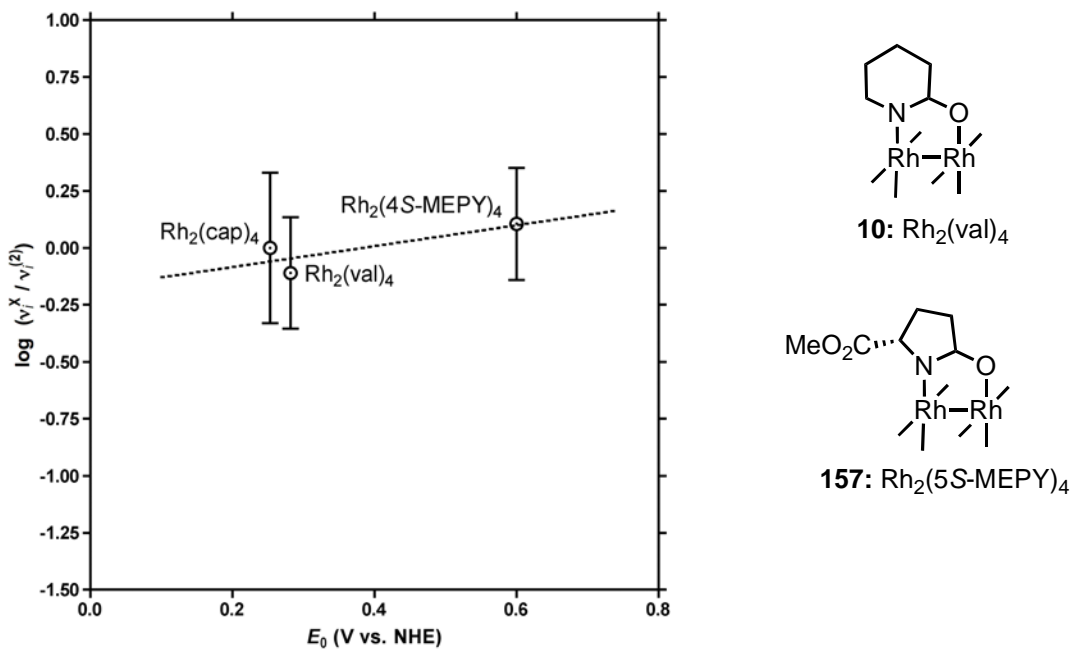


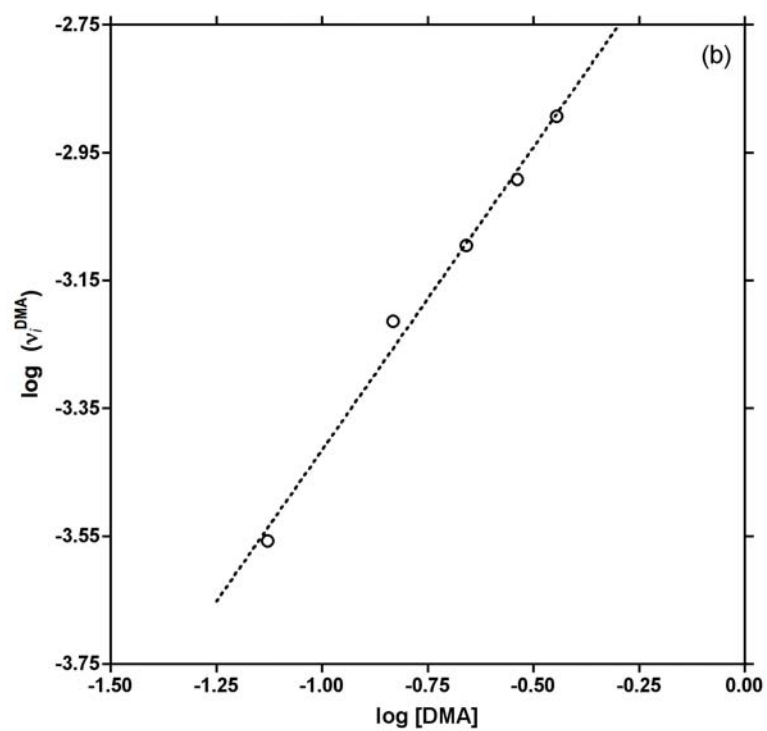
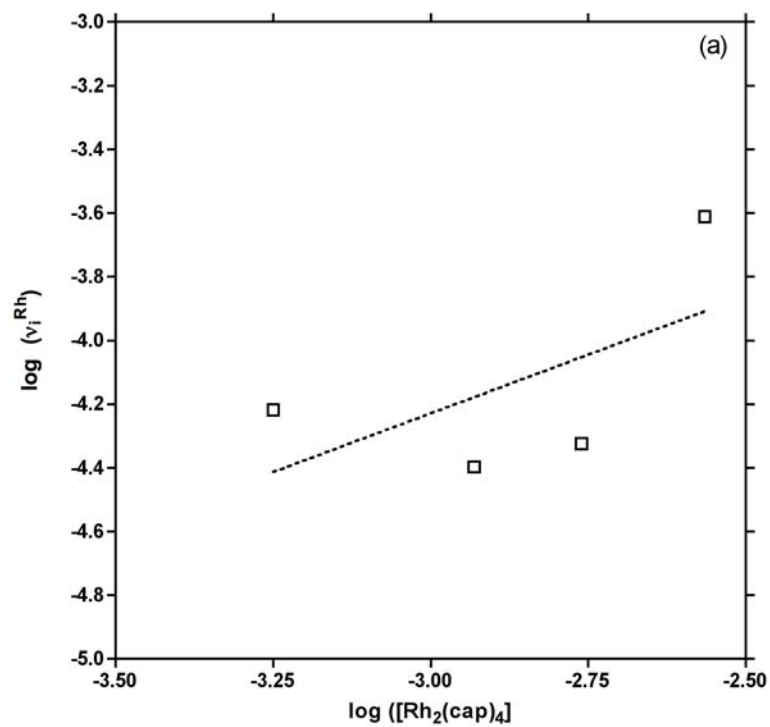
**Figure 3-2.** Graph showing lack of LFER for **60** and related complexes.



The influence of a  $\text{Rh}_2^{5+}$  complex in the electron transfer can be further probed by measuring reactant molecularities. Figure 3-3 shows the kinetic order determinations for the  $\text{Rh}_2(\text{cap})_4$  (**2**) catalyst and *N,N*-dimethylaniline (**154**). The kinetic orders were determined by measuring  $v_i$  (mmol/s) for the consumption of **154** with greater than 10-fold excess of TBHP relative to aniline at varying concentrations of **2** and **154**. The kinetic order of **2** was a fractional order of 0.74 with a poor linear correlation of  $\log(v_i)$  with  $\log([\text{Rh}_2])$ , ( $r^2 = 0.356$ , Figure 3-3a). The molecularity of **154** was 0.95 with good linear correlation of  $\log(v_i)$  with  $\log([\text{154}])$  ( $r^2 = 0.991$ ). Moreover, a pseudo-first order rate ( $k_{\text{obs}} = -1.3 \times 10^{-2} \text{ s}^{-1}$ ) was measured for greater than four half-lives with an excellent linear correlation of  $\ln([\text{154}])$  with time ( $r^2 = 0.9999$ , Figure 3-3b).



**Figure 3-3.** Kinetic order log/log plots for, a) **2** and b) *N,N*-dimethylaniline.



Based on the experimental evidence for the radical chain decomposition of TBHP by **2**, the complex kinetic order for **2** is most likely the result of **2** and **60** contributing to the steady-state concentration of **61** in the reaction. This is a typical observation for metal-promoted radical chain decompositions of TBHP where the kinetic order of the metal depends upon the radical chain length.<sup>236</sup> A mathematical description for this process written in terms of the starting materials (TBHP, amine, and **2**) is complicated by the nature of the radical chain decomposition of TBHP and makes it very challenging to write an analytical expression for the steady-state concentration of **61**. Experimentally, however, the reaction is first-order in *N,N*-dialkylaniline (**58**) over a large concentration range. Moreover, this first order behavior depends on the presence of a large excess of TBHP. This is consistent with a bimolecular reaction between **58** and **61**, with **61** maintained at constant concentration by the cycle between **2** and **60**. This cycle is kept constant at high concentrations of TBHP.

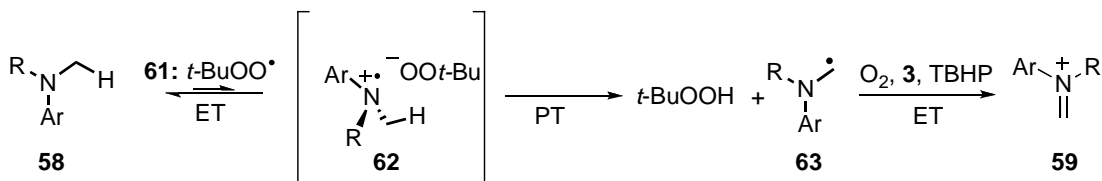
Without a strong LFER vs.  $E_0$ , or a kinetic order indicative of a bimolecular reaction between the  $\text{Rh}_2^{5+}$  complex (**60**) and **58**, **60** can be eliminated as the electron-transfer partner. This makes the corresponding ET/HAT reaction model that would require **60** as the ET agent much less likely and leaves **61** as the likely ET agent in a Type IV ET-PT/ET reaction. Scheme 3-37 shows the proposed mechanism for the bimolecular reaction between **58** and **61**. An initial, endergonic ET between **58** and **61** yields the anilinium radical cation salt (**62**). An intramolecular PT within **62** forms the  $\alpha$ -anilyl radical (**63**) and TBHP. Subsequent fast oxidation of **63** by  $\text{O}_2$ , **60**, or excess TBHP yields the iminium ion as the product of oxidation. This model is consistent with the isotope effects profile, LFER, and reactant

---

<sup>236</sup> The metal-catalyzed decomposition of TBHP is well-documented. a) Kharasch, M. S.; Fono, A.; Nudenberg, W. *J. Org. Chem.* **1951**, *16*, 105, b) Kharasch, M. S.; Pauson, P.; Nudenberg, W. *J. Org. Chem.* **1953**, *18*, 322, c) Hiatt, R. R.; Irwin, K. C.; Gould, C. W. *J. Org. Chem.* **1968**, *33*, 1430.

molarities. Moreover, the model suggests an interesting role for **61** as an electron transfer agent rather than a simple hydrogen-atom transfer agent in the oxidation of *N,N*-dialkylanilines.<sup>237</sup>

**Scheme 3-37.** Model for reaction between dialkylaniline and **4**.



An analysis of the available thermodynamic data illustrates the feasibility of the proposed pathway described in Scheme 3-37. The experimental reduction potential of *tert*-butylperoxyl radical (**61**) is 0.71 eV vs. NHE in water. The oxidation potential of *N,N*-dialkylaniline (**58**) is 0.86 eV vs. NHE in water for R = Me and Ar = phenyl. The electron transfer rate constant between the *tert*-butylperoxide anion and *N,N*-dimethylanilinium radical cation (**62**) to form **61** is  $2.1 \times 10^6 \text{ M}^{-1}\text{s}^{-1}$  in water.<sup>238</sup> This corresponds to the back-electron transfer rate in the Type IV ET-PT/ET model ( $k_{\text{ET}}$ ) for an endergonic electron transfer between **61** and *N,N*-dimethylaniline.

Based on this thermochemical data, the ET between **61** and *N,N*-dimethylaniline would be endergonic by  $\sim 0.2 \text{ eV}$  ( $5 \text{ kcal mol}^{-1}$ ) corresponding to a  $K_{\text{ET}} = 2 \times 10^{-3}$ . In the Type IV ET-PT/ET mechanism, the endergonic ET equilibrium must have a rate constant for back electron transfer ( $k_{\text{ET}}$ ) that is competitive with  $k_{\text{PT}}$  in order to satisfy the assumptions made in its derivation (Eq. 3-4). Bimolecular rate constants for proton-transfer from a *N,N*-dialkylanilinium radical cation to acetate range from  $10^7$  to  $10^9 \text{ M}^{-1}\text{s}^{-1}$  in  $\text{CH}_3\text{CN}$ .<sup>239</sup> Thus, the back-electron transfer rate constant ( $k_{\text{ET}} \sim 2 \times 10^6$

<sup>237</sup> Fukuzumi, S.; Shimoosako, K.; Suenobu, T.; Watanabe, Y. *J. Am. Chem. Soc.* **2003**, *125*, 9074.

<sup>238</sup> See ref. 214a.

<sup>239</sup> Ref. 188.

$M^{-1}s^{-1}$ ) is likely to be competitive with PT since the concentration of the base and electron-transfer agents are approximately equal in the proposed charge transfer complex **62**. Thus, the thermodynamic condition is satisfied for the proposed reaction model in Scheme 3-37 and Eq. 3-4.

In line with the ET-PT/ET mechanism, a potential change in mechanism was observed in the LFER relationship determined for dialkylanilines. There is a significant deviation from the LFER with 4-trifluoromethyl-(*N,N*-dimethyl)-aniline (**158**) that is beyond the error limits of the assay. The deviation is most likely due to the influence of an alternate mechanism for the reaction with electron deficient substrates. The Type IV ET-PT/ET reaction model predicts that at the limits of exergonic and endergonic initial ET reactions, the mechanism will switch to a Type I ET-PT/ET or a HAT/ET mechanism, respectively (see Introduction).

In the case of **158**, the initial electron transfer would be the most endergonic of the substrates measured ( $\Delta G_0 \sim 0.6$  V,  $K_{ET} = 7 \times 10^{-11} M^{-1}$ ). If the ET-PT/ET mechanism were to remain active, the reaction would occur at an extremely slow rate based on  $K_{ET}$ . The extremely small  $K_{ET}$  for the reaction between the *tert*-butylperoxyl radical and **158** make a Type IV ET-PT/ET highly unlikely. Given the thermodynamic parameters, the deviation for **158** is consistent with a mechanistic break occurring at the limit of an endergonic initial ET in favor of the neutral HAT/ET reaction pathway. Based on this observation, an upper limit for  $\Delta G_{ET}$  of  $\sim 0.5$  V ( $12 \text{ kcal mol}^{-1}$ ) can be estimated for the ET-PT/ET mechanism to be operative with the *tert*-butylperoxyl radical.

## IV. Conclusion

Dirhodium(II) complexes catalyze the oxidation of *N,N*-dialkylanilines (**58**) to aryliminium ions (**59**) with TBHP as a terminal oxidant (Scheme 3-1). The role of dirhodium(II) complexes in the oxidation is to provide a steady-state concentration of *tert*-butylperoxyl radicals (**61**) through a one-electron redox cycle with TBHP. The active oxidant under the reaction conditions is **61**. The peroxy radical oxidizes the *N,N*-dialkylaniline to an  $\alpha$ -aniliny radical (**63**) by a thermodynamically coupled electron transfer-proton transfer (ET-PT) rather than the expected hydrogen-atom transfer (HAT). Rapid oxidation of the  $\alpha$ -aniliny radical to an iminium ion provides the electrophile in the oxidative Mannich reaction. The ET reactivity attributed to **61** suggests that oxidations of substrates with low oxidation potentials by **61** may not proceed *via* exclusive HAT mechanisms. Moreover, the proposed model suggests that **61** is the general oxidant for dirhodium(II) catalyzed oxidations with TBHP.

## V. Experimental

**General.** All reactions were performed under ambient atmosphere unless otherwise noted. All reagents were commercially obtained unless otherwise noted. T-HYDRO<sup>®</sup> (aqueous TBHP 70 % w/w) and anhydrous *tert*-butyl hydroperoxide in decane were obtained from Aldrich and used as received. All deuterated reagents (> 98% incorporation of deuterium) were obtained from Cambridge Isotopes.

<sup>1</sup>H (400 MHz) and <sup>13</sup>C NMR (100 MHz) spectra were obtained on a Bruker DRX-400 NMR spectrometer as solutions in CDCl<sub>3</sub> unless otherwise noted. Chemical shifts are reported in parts per million (ppm, δ) downfield from Me<sub>4</sub>Si (TMS). GCMS analyses were performed on a Varian Saturn 2100T mass spectrometer with a Varian 3900 gas chromatograph equipped with a Varian Factor Four capillary column. Gas chromatographic analysis was performed by flame ionization detection on an HP-5890 gas chromatograph equipped with a Supelco SPB-5 capillary column. Preparative chromatographic purification was performed using SiliCycle (60 Å, 40 – 63 mesh) silica gel according to the method of Still.<sup>240</sup> Thin layer chromatography (TLC) was performed on Merck 0.25 mm silica gel 60 F<sub>254</sub> plates with visualization by fluorescence quenching or chemical stain. UV/Visible spectra were obtained on a Varian Cary 50 spectrophotometer using a xenon flash lamp. IR spectra were recorded on a JASCO FT/IR 4100 spectrometer. Anhydrous CH<sub>2</sub>Cl<sub>2</sub> and tetrahydrofuran were purified prior to use by nitrogen forced-flow over activated alumina as described by Grubbs.<sup>241</sup> Melting points were recorded using an Electrothermal Mel-Temp apparatus and were reported without correction.

---

<sup>240</sup> Still, W. C.; Kahn, M.; Mitra, A. *J. Org. Chem.* **1978**, *43*, 2923.

<sup>241</sup> Pangborn, A. B.; Giardello, M. A.; Grubbs, R. H.; Rosen, R. K.; Timmers, F. J. *Organometallics* **1996**, *15*, 1518.

*Tetrakis*-( $\mu$ -caprolactamato)-dirhodium(II) (**2**),<sup>242</sup> *tetrakis*-( $\mu$ -valerolactamato)-dirhodium(II) (**10**),<sup>243</sup> and *tetrakis*-[ $\mu$ -(*S*-methyl-2-oxopyrrolidine-5-carboxylato)]-dirhodium(II)<sup>244</sup> (**157**) were prepared according to published procedures. 2-triisopropylsiloxyfuran (**77**) and *N*-phenyl-1,2,3,4-tetrahydroisoquinoline (**125**) were prepared according to the methods of Denmark and colleagues.<sup>245</sup> *N*-methyl-*N*-(trideuteriomethyl)-*p*-anisidine (**137**), *N*-methyl-*N*-(trideuteriomethyl)-*p*-toluidine<sup>247b</sup> (**138**), *N*-methyl-*N*-(trideuteriomethyl)-aniline (**139**)<sup>247a</sup> were prepared by the methods of Baciocchi<sup>246</sup> and Karki.<sup>247</sup> A representative procedure is presented for *N*-methyl-*N*-(trideuteriomethyl)-*p*-bromoaniline (**140**) on page 328. *Bis*-(*N*-trideuteriomethyl)-*p*-anisidine (**149**), *bis*-(*N*-trideuteriomethyl)-*p*-toluidine (**129**), *bis*-(*N*-trideuteriomethyl)-aniline (**150**)<sup>247a</sup> were prepared by the methods of Shearer<sup>248</sup> and Karki.<sup>247</sup> A representative procedure is presented for *bis*-(*N*-trideuteriomethyl)-*p*-bromoaniline (**151**) on page 329. *N*-(trideuteriomethyl)-*p*-anisidine (**145**), *N*-(trideuteriomethyl)-*p*-toluidine (**146**), *N*-(trideuteriomethyl)-aniline (**147**)<sup>247a</sup> were prepared by the methods of Baciocchi<sup>246</sup> and Karki.<sup>247</sup> A representative procedure for *N*-(trideuteriomethyl)-*p*-bromoaniline (**148**) is presented on page 329. The percent deuterium content of the synthesized deuterated compounds was determined by gas

---

<sup>242</sup> Doyle, M. P.; Westrum, L. J.; Wolthuis, W. N. E.; See, M. M.; Boone, W. P.; Bagheri, V.; Pearson, M. M. *J. Am. Chem. Soc.* **1993**, *115*, 958.

<sup>243</sup> Bear, J. L.; Lifsey, R. S.; Chau, L. K.; Ahsan, M. Q.; Korp, J. D.; Chavan, M.; Kadish, K. M. *J. Chem. Soc., Dalton Trans.* **1989**, 93.

<sup>244</sup> Doyle, M. P.; Winchester, W. R.; Hoorn, J. A. A.; Lynch, V. *J. Am. Chem. Soc.* **1993**, *115*, 9968.

<sup>245</sup> Beutner, G. L.; Denmark, S. E. *J. Amer. Chem. Soc.* **2003**, *125*, 7800.

<sup>246</sup> See ref. 199.

<sup>247</sup> a) Dinnocenzo, J. P.; Karki, S. B.; Jones, J. P. *J. Am. Chem. Soc.* **1993**, *115*, 7111. b) Karki, S. B.; Dinnocenzo, J. P.; Jones, J. P.; Korzekwa, K. R. *J. Am. Chem. Soc.* **1995**, *117*, 3657.

<sup>248</sup> See ref. 202c.

chromatography-mass spectrometry (GC-MS) to be  $\geq 95\%$  in all cases (Table 3-3).<sup>249</sup>

### Synthesis and Characterizations.

**Dirhodium catalyzed decomposition of TBHP (Scheme 3-28).** A 10 dr vial equipped with a stirbar was charged with  $\text{Rh}_2(\text{cap})_4$  (7  $\mu\text{mol}$ ), additive (0.14 mmol), and  $\text{CH}_2\text{Cl}_2$  (5 mL). The reaction vessel was sealed to allow the inclusion of air and fixed with a gas burette charged with silicon oil. TBHP (1.36 mmol) was added *via* syringe and volume of gas evolution (mL) was monitored for 60 s. Four additives were tested: potassium *tert*-butoxide, potassium carbonate, sodium bicarbonate, and acetic acid.

**Deuterium scrambling in the formation of 5-[[tri-deuteriomethyl(4-methylphenyl)amino]methyl]furan-2(5H)-one (130).** T-HYDRO<sup>®</sup> (0.652 mmol) was added in one portion to a stirring solution of *N,N*-bis(*d*<sup>3</sup>-methyl)-*p*-toluidine (**129**: 0.542 mmol), 2-triisopropoxysilylfuran (**77**: 0.542 mmol), formaldehyde (aqueous 37% by wt., 2.72 mmol), and  $\text{Rh}_2(\text{cap})_4$  (**2**: 5.4  $\mu\text{mol}$ ) in MeOH (2 mL). The reaction mixture was heated at 60 °C for 5 hrs. The solvent was removed under reduced pressure and the crude oil was purified by chromatography on silica gel (5:1  $\rightarrow$  1:1 hexanes/EtOAc) to yield an orange oil (0.30 mmol, 59%) consistent with reported characterization.<sup>250</sup> **<sup>1</sup>H NMR** (400 MHz,  $\text{CDCl}_3$ )  $\delta$  7.47 (dd, 1H,  $J = 5.8, 1.5$  Hz), 7.07 (d, 2H,  $J = 8.4$  Hz), 6.64 (d, 2H,  $J = 8.8$  Hz), 6.11 (d, 1H,  $J = 6.0$  Hz), 5.24-5.27 (comp, 1H), 3.65 (d, 1.98H,  $J = 6.0$  Hz), 2.26 (s, 3H) ppm; **<sup>13</sup>C NMR** (100 MHz)  $\delta$  172.7, 154.5, 146.2, 129.9, 126.7, 122.1, 112.6, 82.0, 55.3, 39.1, 20.2 ppm.

---

<sup>249</sup> Each of the prepared anilines is a deuterated version of a commercially available compound. The compounds that have been characterized in the literature are noted and their spectral data are identical to the protonated compounds except in the number of protons. Thus, GC-MS analysis was used to characterize materials and provide a measure of deuterium incorporation. See page 329.

<sup>250</sup> Characterization for **130** was consistent with literature values for the protonated compound, ref. 161.



Deuterium incorporation was calculated as the integration of the CH<sub>2</sub> signal at 3.65 ppm against the ideal value of 2.00.

**2-Methyl-1-phenylpropyl-2-hydroperoxide (115).** The product was prepared according to published procedures.<sup>251</sup> Pure **115** was obtained by recrystallization from boiling pentane to yield white needles (35 % yield). **<sup>1</sup>H NMR** (400 MHz, CD<sub>3</sub>OD)<sup>252</sup>  $\delta$  7.21-7.31 (comp, 5H), 2.89 (s, 3H), 1.22 (s, 6H) ppm; Melting Point (°C) 43-44, lit. = not reported.

**Oxidation with 2-methyl-1-phenylpropyl-2-hydroperoxide (115) to form 5-[[methyl(phenyl)amino]methyl]furan-2(5H)-one (130).**<sup>253</sup> Hydroperoxide **115** (0.652 mmol) was added in one portion to a NMR tube charged with dimethylaniline (1.09 mmol), 2-triisopropoxysilylfuran (**77**: 0.542 mmol), Rh<sub>2</sub>(cap)<sub>4</sub> (**2**: 5.4  $\mu$ mol) and biphenyl (1.0 mmol) in CD<sub>3</sub>OD (1 mL). The reaction mixture was heated at 60 °C for 5 hrs. The conversion of dimethylaniline was determined by <sup>1</sup>H NMR relative to biphenyl. The solvent was removed under reduced pressure, and the crude oil was purified by chromatography on silica gel (5:1  $\rightarrow$  1:1 hexanes/EtOAc) to yield an orange oil (0.04 mmol, 7%) consistent with the reported characterization. **<sup>1</sup>H NMR** (400 MHz, CDCl<sub>3</sub>)  $\delta$  7.47 (dd, 1H, *J* = 5.8, 1.5 Hz), 7.25 (t, 2H, *J* = 8.0 Hz), 6.77 (t, 1H, *J* = 7.3 Hz), 6.72 (d, 2H, *J* = 8.0 Hz), 6.13 (dd, 1H, *J* = 5.8, 2.0 Hz), 5.27 (tt, 1H, *J* = 5.8, 2.0 Hz), 3.69 (d, 2H, *J* = 5.8 Hz), 3.02 (s, 3H) ppm.

---

<sup>251</sup> b) Hiatt, R. R.; Strachan, W. M. *J. Org. Chem.* **1963**, *28*, 1893.

<sup>252</sup> The <sup>1</sup>H NMR spectrum of **115** in CDCl<sub>3</sub> was commensurate with the reported spectrum. The spectrum reported in this manuscript is recorded in CD<sub>3</sub>OD. Signals at 2.77 and 1.24 ppm are trace amounts of 1-phenyl-2-methylpropan-2-ol that are always present as an impurity due to decomposition of the peroxide.

<sup>253</sup> See ref. 161.

***N*-[(*tert*-Butylperoxy)methyl]-*N*-methylaniline (134).** T-HYDRO<sup>®</sup> (0.652 mmol) was added in one portion to a stirring solution of *N,N*-dimethylaniline (1.1 mmol) and Rh<sub>2</sub>(cap)<sub>4</sub> (**2**: 5.4 μmol) in CH<sub>2</sub>Cl<sub>2</sub> (2 mL). The reaction mixture was heated at 60 °C for 5 hrs. The solvent was removed under reduced pressure, and the crude oil was purified by chromatography on silica gel (20:1 hexanes/EtOAc) to yield a light yellow oil (0.45 mmol, 41%) consistent with the reported characterization;<sup>254</sup> **<sup>1</sup>H NMR** (400 MHz, CDCl<sub>3</sub>) δ 7.26 – 7.22 (comp, 2H), 6.87 (d, 2H, *J* = 8.0 Hz), 6.78 (t, 1H, *J* = 7.2 Hz), 5.15 (s, 2H), 3.14 (s, 3H), 1.20 (s, 9H).

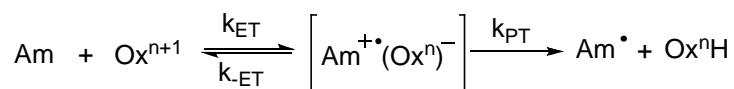
***N*-(Methoxymethyl)-*N*-methylaniline (135).** T-HYDRO<sup>®</sup> (0.652 mmol) was added in one portion to a stirring solution of aniline (1.1 mmol) and Rh<sub>2</sub>(cap)<sub>4</sub> (**2**: 5.4 μmol) in MeOH (2 mL). The reaction mixture was heated at 60 °C for 5 hrs. The solvent was removed under reduced pressure, and the crude oil was purified by chromatography on silica gel (25:1 hexanes/EtOAc) to yield a light yellow oil (0.37 mmol, 34%) consistent with the reported characterization;<sup>255</sup> **<sup>1</sup>H NMR** (400 MHz, CDCl<sub>3</sub>) δ 7.28 – 7.17 (comp, 3H), 6.89 – 6.71 (comp, 2H), 4.75 (s, 2H), 3.31 (s, 3H), 3.10 (s, 3H).

---

<sup>254</sup> Murahashi, S.; Naota, T.; Yonemura, K. *J. Am. Chem. Soc.* **1988**, *110*, 8256.

<sup>255</sup> Murahashi, S.; Naota, T.; Miyaguchi, N.; Nakato, T. *Tetrahedron Lett.* **1992**, *33*, 6991.

**General rate equation for ET-PT/ET mechanism (Eq. 3-1).** The following is the derivation of the general rate law for ET-PT/ET mechanism from the model shown below from Scheme 3-12. This derivation can be found in ref. 186 for an iron catalyzed oxidation of dimethylanilines. The term AmOx refers to the ion-pair produced upon electron transfer ( $[Am^{+•}(Ox^n)^-]$ ) and the terms Am and  $Ox^{n+1}$  refer to the starting amine and oxidant. The terms Am $\cdot$  and  $Ox^nH$  refer to  $\alpha$ -aminy radical and the reduced, protonated form of the oxidant. The derivation seeks to write an expression for the consumption of the oxidant ( $Ox^{n+1}$ ) in terms of the amine (Am) and  $Ox^{n+1}$ .



Eq. 3-10 describes the consumption rate of the ET intermediate [AmOx] in terms bimolecular reactions that form and consume AmOx.

$$\text{Eq. 3-10} \quad \frac{-d[AmOx]}{dt} = k_{ET}[Am][Ox^{n+1}] - k_{-ET}[AmOx] - k_{PT}[AmOx]$$

Eq. 3-11 describes the consumption rate of the oxidant [ $Ox^{n+1}$ ] in terms bimolecular reactions that form and consume  $Ox^{n+1}$ .

$$\text{Eq. 3-11} \quad \frac{-d[Ox^{n+1}]}{dt} = k_{-ET}[AmOx] - k_{ET}[Am][Ox^{n+1}]$$

Summing eqs. 3-10 and 3-11 yields the basic expression for the formation of the product (Am $\cdot$ ).

Eq. 3-12

$$\frac{-d[Ox^{n+1}]}{dt} + \frac{-d[AmOx]}{dt} = (k_{-ET}[AmOx] - k_{ET}[Am][Ox^{n+1}]) + (k_{ET}[Am][Ox^{n+1}] - k_{-ET}[AmOx] - k_{PT}[AmOx])$$

Simplification of the expression in Eq. 3-12 yields Eq. 3-13 as the rate equation in terms of the oxidant ( $\text{Ox}^{n+1}$ ) and the intermediate ( $\text{AmOx}$ ).

$$\text{Eq. 3-13} \quad \frac{-d[\text{Ox}^{n+1}]}{dt} + \frac{-d[\text{AmOx}]}{dt} = -k_{\text{PT}}[\text{AmOx}]$$

Applying the steady-state approximation ( $-d[\text{AmOx}]/dt = 0$ ) to Eq. 3-10 provides an expression for the steady-state concentration of  $[\text{AmOx}]$ .

$$\text{Eq. 3-14} \quad [\text{AmOx}] = \frac{k_{\text{ET}}[\text{Am}][\text{Ox}^{n+1}]}{k_{-\text{ET}} + k_{\text{PT}}}$$

Substitution of the value for  $[\text{AmOx}]$  into Eq. 3-13 gives Eq. 3-15 and allows the equation to be written entirely in terms of the oxidant ( $\text{Ox}^{n+1}$ ).

$$\text{Eq. 3-15} \quad \frac{-d[\text{Ox}^{n+1}]}{dt} + \frac{-d \left[ \frac{k_{\text{ET}}[\text{Am}][\text{Ox}^{n+1}]}{k_{-\text{ET}} + k_{\text{PT}}} \right]}{dt} = k_{\text{PT}} \frac{k_{\text{ET}}[\text{Am}][\text{Ox}^{n+1}]}{k_{-\text{ET}} + k_{\text{PT}}}$$

Applying a pseudo-first order approximation ( $[\text{Am}] = \text{constant}$ ) allows for the separation of variables (Eq. 3-16). As constants, the rate constants can be separated from the differential expression.<sup>256</sup>

$$\text{Eq. 3-16} \quad \frac{-d[\text{Ox}^{n+1}]}{dt} + \left( \frac{k_{\text{ET}}[\text{Am}]}{k_{-\text{ET}} + k_{\text{PT}}} \right) \frac{-d[\text{Ox}^{n+1}]}{dt} = k_{\text{PT}} \frac{k_{\text{ET}}[\text{Am}][\text{Ox}^{n+1}]}{k_{-\text{ET}} + k_{\text{PT}}}$$

Consolidation of terms gives the relationship shown in Eq. 3-17.

$$\text{Eq. 3-17} \quad \left( \frac{k_{\text{ET}}[\text{Am}]}{k_{-\text{ET}} + k_{\text{PT}}} + 1 \right) \frac{-d[\text{Ox}^{n+1}]}{dt} = k_{\text{PT}} \frac{k_{\text{ET}}[\text{Am}][\text{Ox}^{n+1}]}{k_{-\text{ET}} + k_{\text{PT}}}$$

---

<sup>256</sup> This is a simple example of the “chain rule”, e. g.  $d(3x^2)/dx = 3*(dx^2/dx) = 6x$ .

Defining “1” as  $(k_{-ET} + k_{PT})/(k_{-ET} + k_{PT})$  gives a common denominator facilitating the consolidation of terms that gives Eq. 3-18.

$$\text{Eq. 3-18} \quad \left( \frac{k_{ET}[Am] + k_{-ET} + k_{PT}}{k_{-ET} + k_{PT}} \right) \frac{-d[Ox^{n+1}]}{dt} = k_{PT} \frac{k_{ET}[Am][Ox^{n+1}]}{k_{-ET} + k_{PT}}$$

Consolidating rate constants yields the expression in the form of “ $dx/dt = f(x)$ ” reported in Eq. 3-1.

$$\text{Eq. 3-1} \quad \frac{-d[Ox^{n+1}]}{dt} = k_{obs}[Ox^{n+1}] \quad k_{obs} = \frac{k_{PT}k_{ET}[Am]}{k_{ET}[Am] + k_{-ET} + k_{PT}}$$

**Dependence of  $k_H/k_D$  on the free energy of ET (Eq. 3-9).** The following equation derives the expression for the observed isotope effect ( $k_{Hobs}/k_{Dobs}$ ). Writing  $k_H/k_D$  using  $k_{HPT}$  and  $k_{DPT}$  in the expression for  $k_{obs}$  into the expression used to derive the Type IV ET-PT/ET mechanism (Eq. 3-4) gives Eq. 3-19. Consolidation of terms yields the expression in Eq. 3-9.

$$\text{Eq. 3-4} \quad \frac{-d[Ox^{n+1}]}{dt} = k_{obs}[Ox^{n+1}] \quad k_{obs} = \frac{k_{PT}k_{ET}[Am]}{k_{-ET} + k_{PT}} \quad \text{If } k_{-ET} + k_{PT} \gg k_{ET}[Am]$$

$$\text{Eq. 3-19} \quad \frac{k_{Hobs}}{k_{Dobs}} = \frac{k_{HPT}k_{ET}[Am]}{k_{-ET} + k_{HPT}} \left( \frac{k_{DPT}k_{ET}[Am]}{k_{-ET} + k_{DPT}} \right)^{-1}$$

$$\text{Eq. 3-9} \quad \frac{k_{Hobs}}{k_{Dobs}} = \frac{k_{HPT}}{k_{DPT}} \left( \frac{k_{-ET} + k_{DPT}}{k_{-ET} + k_{HPT}} \right)$$

**Adamantane oxidation assay.** Anhydrous TBHP in decane (100  $\mu$ L, 0.63 mmol)<sup>257</sup> was added in a single portion to a stirring solution of adamantane (1.144 mmol), Rh<sub>2</sub>(cap)<sub>4</sub> (0.013 mmol), and NaHCO<sub>3</sub> (0.550 mmol) in anhydrous CH<sub>2</sub>Cl<sub>2</sub> (5 mL) was added. Samples were taken as 50  $\mu$ L aliquots and diluted to 1 mL in a volumetric flask over time (1, 5, 10, 30, and 60 min.). At each timepoint, the C<sup>3</sup>/C<sup>2</sup> ratio and conversion was determined by GC analysis. Response factors (RF) were measured by injection of a standard solution of known concentration containing adamantane (RF = 1.00), 1-adamantanol (RF = 1.07), and 2-adamantanol/one (RF = 1.09). The C<sup>3</sup>/C<sup>2</sup> ratio was calculated as the response area of 1-adamantanol to the sum of 2-adamantanol and 2-adamantanone. Conversion was measured as a corrected area percent based on the total sum of 1-adamantanol, 2-adamantanol, 2-adamantanone, and adamantane. Reported C<sup>3</sup>/C<sup>2</sup> ratio is the average of each time point measured.

**Table 3-2.** Compiled raw data for adamantane product distribution.

Time (min).	C <sup>3</sup> /C <sup>2</sup>	% conv.
1	3.9	3
5	3.6	7
10	3.7	11
30	4.0	12
60	4.3	11
Mean	3.9	

**Solvolysis equilibrium (K<sub>solv</sub>).** A <sup>1</sup>H NMR tube was charged with *N*-(*tert*-butyldioxy)-*N*-methylaniline (**134**) (0.24 mmol), biphenyl as an internal standard (0.60 mmol), and CD<sub>3</sub>OD (0.75 mL). The mixture was left to sit at ambient temperature over 48 h. After three hours there was no change in the relative amount of **134** and *N*-(methoxymethyl)-*N*-methylaniline (**135**) was determined by the relative integrations of the aminal CH<sub>2</sub> signal at 5.15 and

<sup>257</sup> Conversions were kept low by using a substoichiometric amount of oxidant.

4.75 ppm, respectively. These signals were converted to a molar quantity relative to the internal standard. The equilibrium constant  $K_{\text{solv}}$  was calculated to be  $2 \times 10^{-3}$  using the following equation:

$$K_{\text{solv}} = ([\mathbf{135}][\text{TBHP}])/([\mathbf{134}][\text{CD}_3\text{OD}]), [\text{TBHP}] = [\mathbf{134}]_0 - [\mathbf{135}]$$

The concentration of the solvent,  $[\text{CD}_3\text{OD}]$ , was taken as the density of the solvent expressed as a molar quantity:  $\rho(\text{CH}_3\text{OH}) @ 298 \text{ K} = 32.03 \text{ mol/L}$ .<sup>258</sup>

#### **Decomposition of 2-methyl-1-phenylpropyl-2-hydroperoxide (115) assay.**

A solution of **115** (0.037 mmol, 0.037 M) was prepared in a 1 mL volumetric flask in  $\text{C}_6\text{D}_6$  (1.000 mL). An NMR tube was charged with  $\text{Rh}_2(\text{cap})_4$  (2.2 mg, 3.0  $\mu\text{mol}$ ) and biphenyl as the internal standard (44  $\mu\text{mol}$ ) and diluted with  $\text{C}_6\text{D}_6$  (1.00 mL). The reaction was initiated by injection of solution containing **115** (81  $\mu\text{L}$ , 0.030  $\mu\text{mol}$ ). The reaction solution was sonicated for 1 minute and allowed to stand at room temperature. At 1 h, a  $^1\text{H}$  NMR was taken and products quantified against the internal standard.

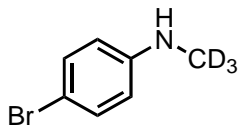
**General procedure for measuring isotope effects.** A stirring solution of *N,N*-dialkylaniline (0.272 mmol),  $\text{Rh}_2(\text{cap})_4$  (3.0 mmol), and biphenyl as the internal standard (0.042 mmol) in MeOH (1 mL) was allowed to equilibrate for 15 min. in a controlled temperature bath ( $5.0 \pm 0.2 \text{ }^\circ\text{C}$ ). T-HYDRO<sup>®</sup> (0.330 mmol) was added in a single portion to initiate the reaction ( $t = 0 \text{ min}$ ). After 180 s, the entire reaction solution was quenched in a biphasic mixture of saturated  $\text{NH}_4\text{Cl}$  (25 mL) and  $\text{CH}_2\text{Cl}_2$  (10 mL). The solution was made basic using NaOH (5.0 M) to  $\text{pH} > 8$  and the organic layer was extracted for GCMS analysis. The  $k_{\text{H}}/k_{\text{D}}$  value was determined as the ratio of *N*-methylaniline/*N*-(trideuteriomethyl)aniline for three independent measurements. Quantitative

---

<sup>258</sup>E.W. Lemmon, M.O. McLinden and D.G. Friend, "Thermophysical Properties of Fluid Systems" in *NIST Chemistry WebBook, NIST Standard Reference Database Number 69*, Eds. P.J. Linstrom and W.G. Mallard, June 2005, National Institute of Standards and Technology, Gaithersburg MD, 20899 (<http://webbook.nist.gov>).

measurements were made based on single-point calibration curves generated with standards of known concentration for each analyte. Error is reported as ( $\pm$ ) one standard deviation.

***N*-(trideuteriomethyl)-*p*-bromoaniline (148. d3-BrNMA).**<sup>259</sup> A 125 mL



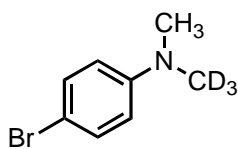
separatory funnel was charged with a saturated solution of sodium carbonate (10 mL), ethyl acetate (25 mL), and 4-bromo-aniline (1.00 g, 5.81 mmol). Isobutylchloroformate (0.824 g, 6.17 mmol) was added portion-wise and the reaction was periodically shaken until starting material was completely consumed by TLC analysis. The organic phase was washed with water (25 mL) and brine (25 mL) and concentrated under reduced pressure to yield a crude solid. The crude *N*-aryl-isobutylchloroformate was taken up in anhydrous THF (50 mL), transferred to a 250 mL round-bottomed flask, and cooled to 0 °C. LiAlD<sub>4</sub> (0.478 g, 11.4 mmol) was added portion-wise to the cold, stirring solution to minimize gas evolution. After addition, the reaction vessel was fitted with a condenser, sealed with a septum, and purged with N<sub>2</sub>. After 10 minutes, the reaction vessel was heated to reflux overnight. The solution was allowed to cool to rt. The reaction mixture was taken up in ether (50 mL) and cooled to 0 °C. A saturated solution of Na<sub>2</sub>SO<sub>4</sub> was added drop-wise until gas evolution ceased and a white fluffy solid formed. The mixture was filtered over Celite, dried over Mg<sub>2</sub>SO<sub>4</sub>, and concentrated to yield crude material. Bulb-to-bulb distillation afforded the analytically pure compound as a yellow oil (1.1g, 5.8 mmol). <sup>1</sup>H NMR (CDCl<sub>3</sub>) 7.70 (1H, s), 6.61 (2H, d, *J* = 8.4 Hz), 5.67 (2H, d, *J* = 8.4 Hz) ppm.

---

<sup>259</sup> This procedure was adapted from ref. 199 and used to prepare compounds **145**, **146**, and **147**.



***N*-methyl-*N*-(trideuteriomethyl)-*p*-bromoaniline (140).**<sup>260</sup> A solution of ZnCl<sub>2</sub>



(0.397 g, 2.91 mmol), sodium cyanoborohydride (0.219 g, 3.49 mmol), and methanol (25 mL) was added portion-wise to a stirring solution of 4-bromo-*N*-(trideuteriomethyl)-aniline (1.1 g, 5.8 mmol), aqueous formaldehyde (37% by wt., 0.710 mL, 10.7 mmol) and methanol (25 mL). After the addition, the reaction was allowed to stir until TLC analysis showed consumption of starting material. The reaction mixture was poured directly into a separatory funnel containing 2M NaOH (150 mL) and the aqueous layer was extracted with diethyl ether (2 x 50 mL). The combined ethereal layers were then washed with brine (2 x 100 mL), dried over MgSO<sub>4</sub>, and concentrated under reduced pressure to yield a crude oil. Purification by preparative silica gel chromatography provided the pure material as a white solid (4.9 mmol, 85%). <sup>1</sup>H NMR (CDCl<sub>3</sub>) 7.28 (2H, d, *J* = 8.0 Hz), 6.58 (2H, d, *J* = 8.0 Hz), 2.91 (3H, s) ppm.

***Bis*-(*N*-trideuteriomethyl)-*p*-bromoaniline (151. d<sub>6</sub>-bromo-DMA).**

Following the procedure of Karki et al.,<sup>261</sup> *d*<sup>3</sup>-methyl iodide (17.9 mmol, 99.5% deuterium) was added in a single portion to a vigorously stirring mixture of 4-bromoaniline (1.00 g, 5.81 mmol) and K<sub>2</sub>CO<sub>3</sub> (1.61 g, 11.6 mmol) in acetone (20 mL).<sup>262</sup> The reaction vessel was fitted with a condenser and the mixture was allowed to stir. After 20 minutes, the reaction was heated to reflux overnight. After cooling to room temperature, the organic layer was taken up in ether (50 mL) and washed with water, NaHCO<sub>3</sub>, and brine (50 mL each), dried over MgSO<sub>4</sub>, and concentrated to afford a crude solid. Purification by preparative silica gel chromatography provided the pure material as a white

---

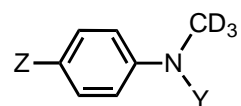
<sup>260</sup> This procedure was adapted from ref. 202c and used to prepare compounds **137**, **138**, and **139**.

<sup>261</sup> This procedure was adapted from ref. 247 and used to prepare compounds **150** and **129**.

<sup>262</sup> Alternative conditions reported in ref. 247b were used to prepare **149**. These conditions use tetrabutylammonium iodide and sodium hydroxide in a benzene and water mixture (10:1) rather than acetone to avoid overalkylation with electron rich anilines such as anisidine.

solid (4.0 mmol, 68%).  $^1\text{H NMR}$  ( $\text{CDCl}_3$ ) 7.28 (2H, d,  $J = 8.0$  Hz), 6.58 (2H, d,  $J = 8.0$  Hz), 2.91 (6H, s) ppm.

**Table 3 - 3. Deuterium incorporations for deuterated substrates.**



Compound	Y	Z	% $^2\text{H}$
<b>148</b>	H	Br	99.7
<b>140</b>	$\text{CH}_3$	Br	98.7
<b>151</b>	$\text{CD}_3$	Br	98.8
<b>147</b>	H	H	96.2
<b>139</b>	$\text{CH}_3$	H	98.3
<b>150</b>	$\text{CD}_3$	H	96.4
<b>146</b>	H	$\text{CH}_3$	97.4
<b>138</b>	$\text{CH}_3$	$\text{CH}_3$	98.0
<b>129</b>	$\text{CD}_3$	$\text{CH}_3$	95.4
<b>145</b>	H	$\text{CH}_3\text{O}$	98.1
<b>137</b>	$\text{CH}_3$	$\text{CH}_3\text{O}$	98.6
<b>149</b>	$\text{CD}_3$	$\text{CH}_3\text{O}$	98.7

**Kinetic isotope effects [KIE] assay.** For  $R = \text{H}, \text{MeO}, \text{Br},$  and  $\text{CH}_3$ , *N,N*-dimethyl-4-*R*-aniline (0.272 mmol) and *bis*-(*N*-trideuteriomethyl)-4-*R*-aniline (0.272 mmol) were assayed using the general procedure for measuring isotope effects.

**Table 3-4.** Data for KIE values.

R	$k_{\text{H}}/k_{\text{D}}$ <sup>RUN 1</sup>	$k_{\text{H}}/k_{\text{D}}$ <sup>RUN 2</sup>	$k_{\text{H}}/k_{\text{D}}$ <sup>RUN 3</sup>	Mean (SD)
MeO	3.18	3.23	3.44	3.28 (0.13)
Me	4.42	3.92	4.87	4.40 (0.48)
H	4.01	4.13	4.39	4.17 (0.20)
Br	5.58	4.51	5.05	5.05 (0.53)

**Product isotope effects [PIE] assay.** For R = H, MeO, Br, and CH<sub>3</sub>, *N*-(trideuteriomethyl)-*N*-methyl-4-*R*-aniline (0.272 mmol) was assayed using the general procedure for measuring isotope effects.

**Table 3-5.** Data for PIE values.

R	$k_H/k_D$ <sup>RUN 1</sup>	$k_H/k_D$ <sup>RUN 2</sup>	$k_H/k_D$ <sup>RUN 3</sup>	Mean $k_H/k_D$ (SD)
MeO	1.40	1.36	1.31	1.32 (0.07)
Me	1.70	1.76	1.90	1.79 (0.10)
H	1.61	1.39	1.53	1.51 (0.11)
Br	2.82	2.91	3.05	2.93 (0.12)

**General procedure for determining initial rates ( $v_i$ ).** All liquid *N,N*-dialkylanilines were freshly distilled prior to use. *N,N*-dimethylanisidine and 4-(trifluoromethyl)-(*N,N*-dimethyl)-aniline were solids and were purified by silica gel chromatography prior to use. All dirhodium compounds were recrystallized prior to use. A reactants solution of *N,N*-dialkylaniline (0.27 M) and *d*-TBHP (2.7 M) was prepared with CD<sub>3</sub>OD in a 10 mL volumetric flask. A catalyst solution of Rh<sub>2</sub>L<sub>4</sub> was prepared in a 1 mL volumetric flask with CD<sub>2</sub>Cl<sub>2</sub>/CD<sub>3</sub>OD (1:1, 1.000 mL).<sup>263</sup> A NMR tube equipped with a capillary standard of neat nitrobenzene was charged with 1.000 mL of the reactants solution, purged with N<sub>2</sub>, and sealed. After equilibration to constant temperature,<sup>264</sup> the reaction was initiated with an aliquot of the catalyst solution (20 μL) to give a final volume of 1.020 mL. Concentrations were corrected for *N,N*-dialkylaniline (0.265 M), *d*-TBHP (2.65 M), and Rh<sub>2</sub>L<sub>4</sub> according to the final volume. The reaction was monitored by single-pulse <sup>1</sup>H NMR scans to minimize delay between measurements. For each determination of  $v_i$  by <sup>1</sup>H NMR, the singlet corresponding to the *N*-methyl groups of the *N,N*-dimethylaniline was calibrated to 2.95 ppm and monitored.

<sup>263</sup> Rh<sub>2</sub>L<sub>4</sub> concentrations were varied in some cases and calculated as mol/L based on the mass of the complex.

<sup>264</sup> For all determinations of  $v_i$ , the temperature of the <sup>1</sup>H NMR probe was 18 °C as determined by the chemical shift of the OH proton in a 1% CH<sub>3</sub>OH in CD<sub>3</sub>OD solution.

**General procedure for the preparation of *tert*-butyl hydroperoxide in D<sub>2</sub>O (*d*-TBHP).** Deuterated TBHP was prepared by extracting 70% w/w aqueous TBHP (100 mL) with CH<sub>2</sub>Cl<sub>2</sub> (3 x 50 mL) in an extraction funnel. The combined organic layers were washed with D<sub>2</sub>O (3 x 15 mL) allowing the mixture to stand for 0.5 h between each wash. After the last wash, the organic layer was left to partition in the extraction funnel with D<sub>2</sub>O (15 mL) overnight. The mixture was transferred to a flask and the CH<sub>2</sub>Cl<sub>2</sub> was removed under reduced pressure to yield a biphasic solution of TBHP and D<sub>2</sub>O. The solution was transferred to an extraction funnel and washed with D<sub>2</sub>O (5 mL). The organic layer was separated to yield a clear solution of D<sub>2</sub>O saturated TBHP. TBHP concentration was determined by iodometric titration.<sup>265</sup> <sup>1</sup>H NMR (400 MHz, CD<sub>3</sub>OD) δ 1.21 (s, 9H) ppm.

**Linear free energy relationship [LFER] of substituted dimethylanilines.**

Values of  $v_i$  were measured using the general method for initial rate determination with a 0.020 M (15 mg/mL) solution of Rh<sub>2</sub>(cap)<sub>4</sub>. The reaction was initiated by adding a solution of Rh<sub>2</sub>(cap)<sub>4</sub> (20 μL, 0.00040 mmol) in CD<sub>2</sub>Cl<sub>2</sub>/CD<sub>3</sub>OD (1:1) to an NMR tube containing 4-R-(*N,N*-dimethyl)-anilines (0.27 mmol) and *d*-TBHP (2.7 mmol) in CD<sub>3</sub>OD (1.00 mL). The reaction was performed in triplicate for R = CH<sub>3</sub>, H, Br, CO<sub>2</sub>Et, and CF<sub>3</sub> with  $v_i$  reported as the mean and error as (±) one standard deviation.

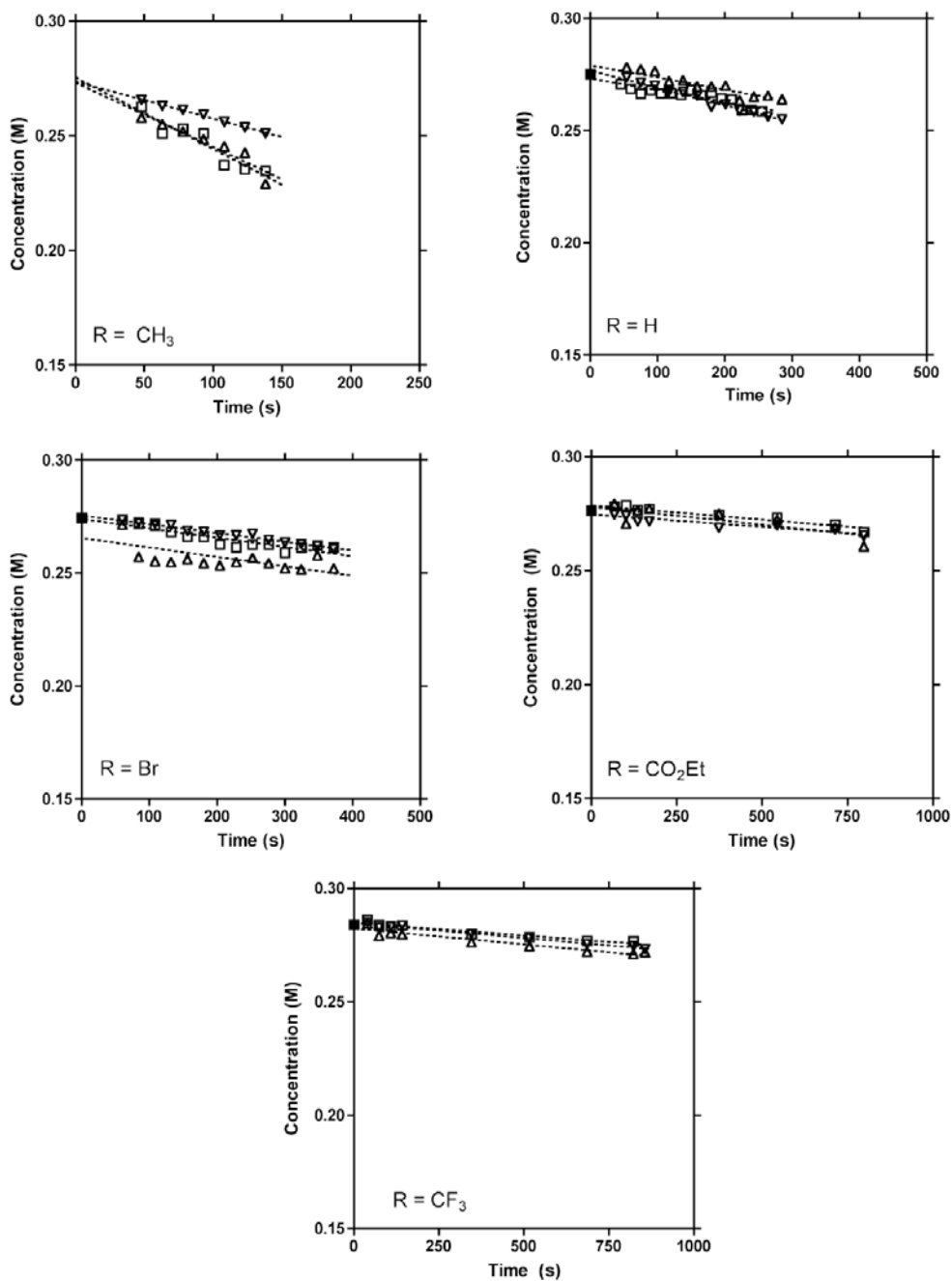
**Table 3-6.** Compiled raw data for LFER of amine,  $v_i$  and  $\log(v_i^{\text{rel}})$ .

R	$v_i^a$ RUN1	$v_i^a$ RUN2	$v_i^a$ RUN3	Mean $v_i^{a,b}$	$\log(v_i^R/v_i^H)^b$
CH <sub>3</sub>	-3.11	-2.81	-1.61	-2.53 (6)	0.6 (3)
H	-0.52	-0.54	-0.77	-0.6 (1)	0.0 (3)
Br	-0.41	-0.42	-0.39	-0.41 (2)	-0.2 (2)
CO <sub>2</sub> Et	-0.12	-0.16	-0.11	-0.13 (3)	-0.7 (3)
CF <sub>3</sub>	-0.11	-0.14	-0.13	-0.13 (1)	-0.7 (3)

<sup>a</sup>(x10<sup>-4</sup> M s<sup>-1</sup>). <sup>b</sup>Numbers in parentheses are the uncertainty in the last reported digit.

<sup>265</sup> Sharpless, K. B.; Verhoeven, T. R. *Aldrichimica Acta* **1979**, 12, 63.

**Figure 3-4.** Plots of  $v_i$  for each substituted 4-R-N,N-dimethylaniline;  $\diamond$ —Run 1,  $\triangle$ —Run 2,  $\square$ —Run 3.



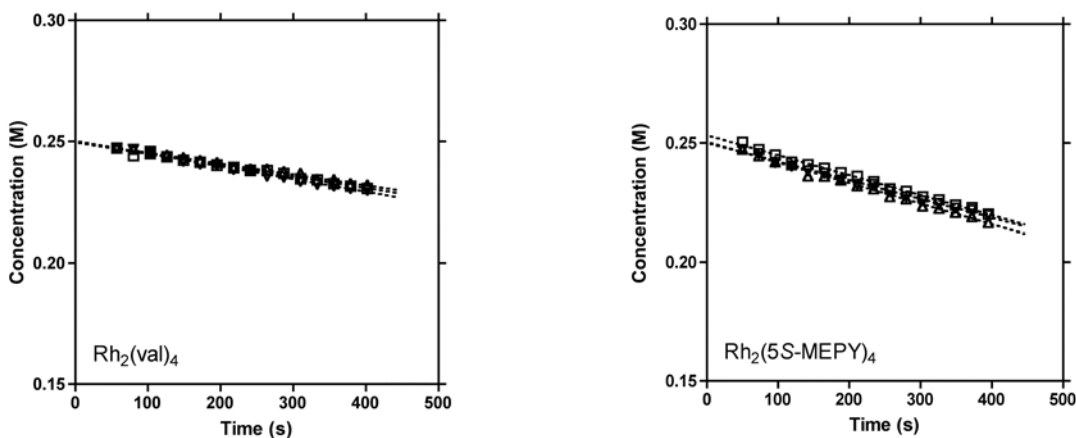
**LFER of dirhodium(II) catalyst.** Values of  $v_i$  were measured using the general method for initial rate determination with a 0.020 M solution of  $Rh_2L_4$ . The reaction was initiated with the addition of a solution of dirhodium(II) complex (20  $\mu$ L, 0.00040 mmol) to an NMR tube containing *N,N*-dimethylaniline (0.27 mmol) and *d*-TBHP (2.7 mmols) in  $CD_3OD$  (1.00 mL). The experiment was performed in triplicate for  $Rh_2(cap)_4$  (**2**),  $Rh_2(val)_4$  (**10**), and  $Rh_2(5S-MEPY)_4$  (**157**). The reported  $v_i$  is the mean of three independent measurements with error reported as ( $\pm$ ) one standard deviation.

**Table 3-7.** Compiled raw data for LFER of catalyst,  $v_i$  and  $\log(v_i^{rel})$ .

$Rh_2L_4$	$v_i^a$ RUN1	$v_i^a$ RUN2	$v_i^a$ RUN3	Mean <sup>b</sup>	$\log(v_i^R/v_i^{CAP})^b$
$Rh_2(cap)_4$ ( <b>2</b> ) <sup>c</sup>	-0.52	-0.54	-0.77	-0.61 (14)	0.0 (3)
$Rh_2(val)_4$ ( <b>10</b> )	-0.47	-0.45	-0.53	-0.48 (4)	-0.1 (4)
$Rh_2(5S-MEPY)_4$ ( <b>157</b> )	-0.86	-0.79	-0.84	-0.83 (4)	0.1 (2)

<sup>a</sup>( $\times 10^{-4}$  M s<sup>-1</sup>). <sup>b</sup>Numbers in parentheses are the uncertainty in the last reported digit. <sup>c</sup>Values taken from previous experiment (Table 3-6).

**Figure 3-5.** Plots of  $v_i$  for each dirhodium(II) complex;  $\diamond$ —Run 1,  $\triangle$ —Run 2,  $\square$ —Run 3.



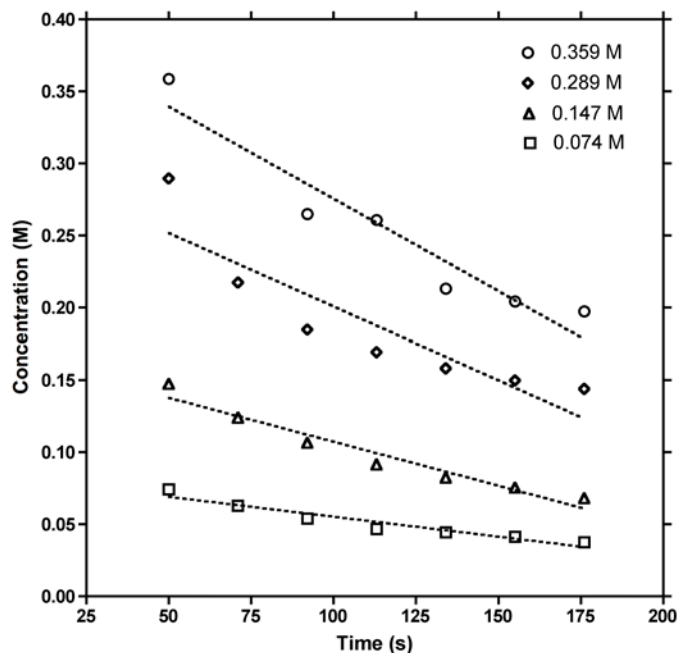
**Kinetic order of dialkylaniline.** Values of  $v_i$  were measured using the general method for initial rate determination with a 0.020 M solution of  $Rh_2(cap)_4$ . The reaction was initiated with the addition of a solution of  $Rh_2(cap)_4$  (20  $\mu$ L, 0.00040 mmol) in  $CD_2Cl_2/CD_3OD$  (1:1) to an NMR tube containing *N,N*-dimethylaniline at various concentrations and *d*-TBHP (2.72 M) in  $CD_3OD$  (1.00 mL). The reported  $v_i$  is from a single measurement at each concentration.

**Table 3-8.** Compiled raw data for kinetic order of *N,N*-dimethylaniline.

[DMA] mM	$v_i^a$	log [DMA]	log ( $v_i$ )
74.3	-0.28	-1.13	-3.56
147.4	-0.61	-0.83	-3.21
289.5	-1.02	-0.54	-2.99
358.8	-1.28	-0.45	-2.89

<sup>a</sup>( $\times 10^{-4}$  M s<sup>-1</sup>)

**Figure 3-6.** Plots of  $v_i$  for each concentration of *N,N*-dimethylaniline.



**Kinetic order of dirhodium catalyst.** The kinetic order of  $\text{Rh}_2(\text{cap})_4$  was calculated from values of  $v_i$  measured using the general method for initial rate determination. The reaction was initiated with 100  $\mu\text{L}$  of  $\text{Rh}_2(\text{cap})_4$  at various concentrations in  $\text{CD}_2\text{Cl}_2:\text{CD}_3\text{OD}$  (1:1) to an NMR tube containing *N,N*-dimethylaniline (0.272 mmol) and *d*-TBHP (2.72 mmol) in  $\text{CD}_3\text{OD}$  (1.000 mL). The concentrations measured were  $[\text{Rh}_2(\text{cap})_4] = 2.72, 1.73, 1.17,$  and 0.56 mM.

**Figure 3-7.** Plots of  $v_i$  for each concentration of  $\text{Rh}_2(\text{cap})_4$ ;  $\diamond$ —Run 1,  $\triangle$ —Run 2,  $\square$ —Run 3.

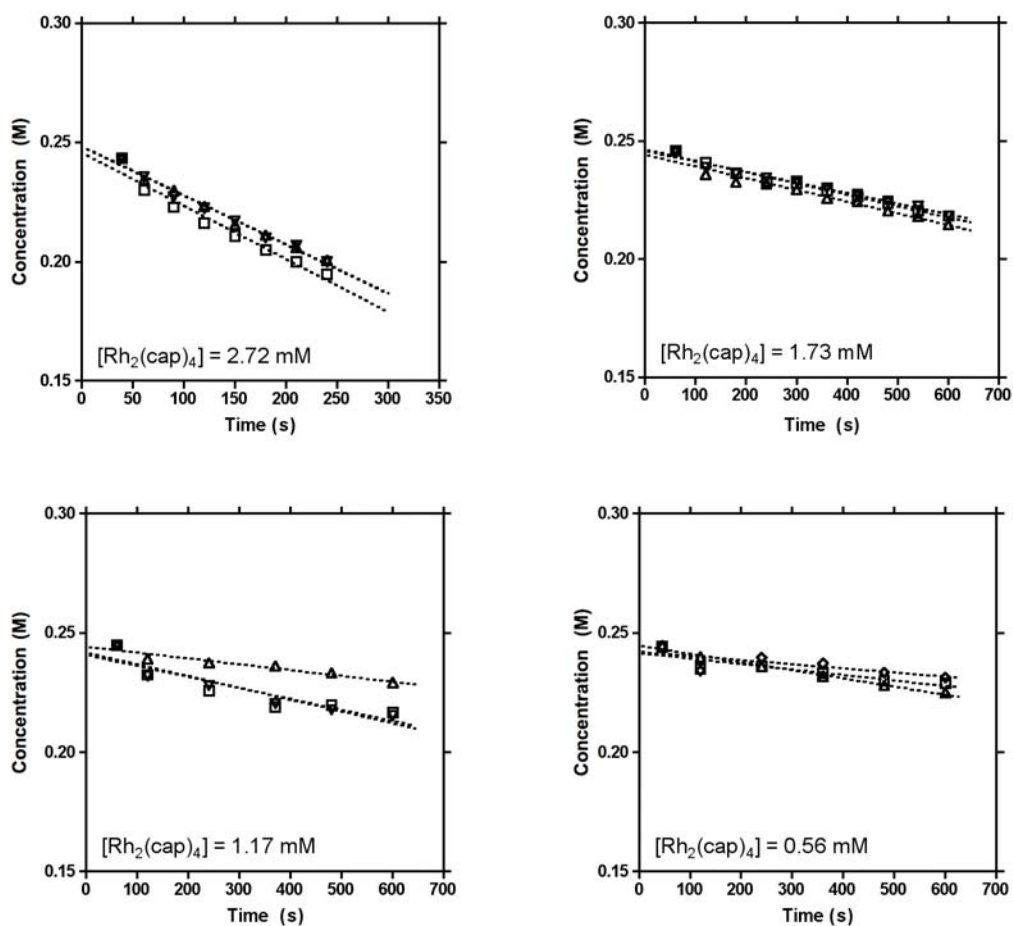




**Table 3-9.** Compiled raw data for kinetic order of dirhodium catalyst.

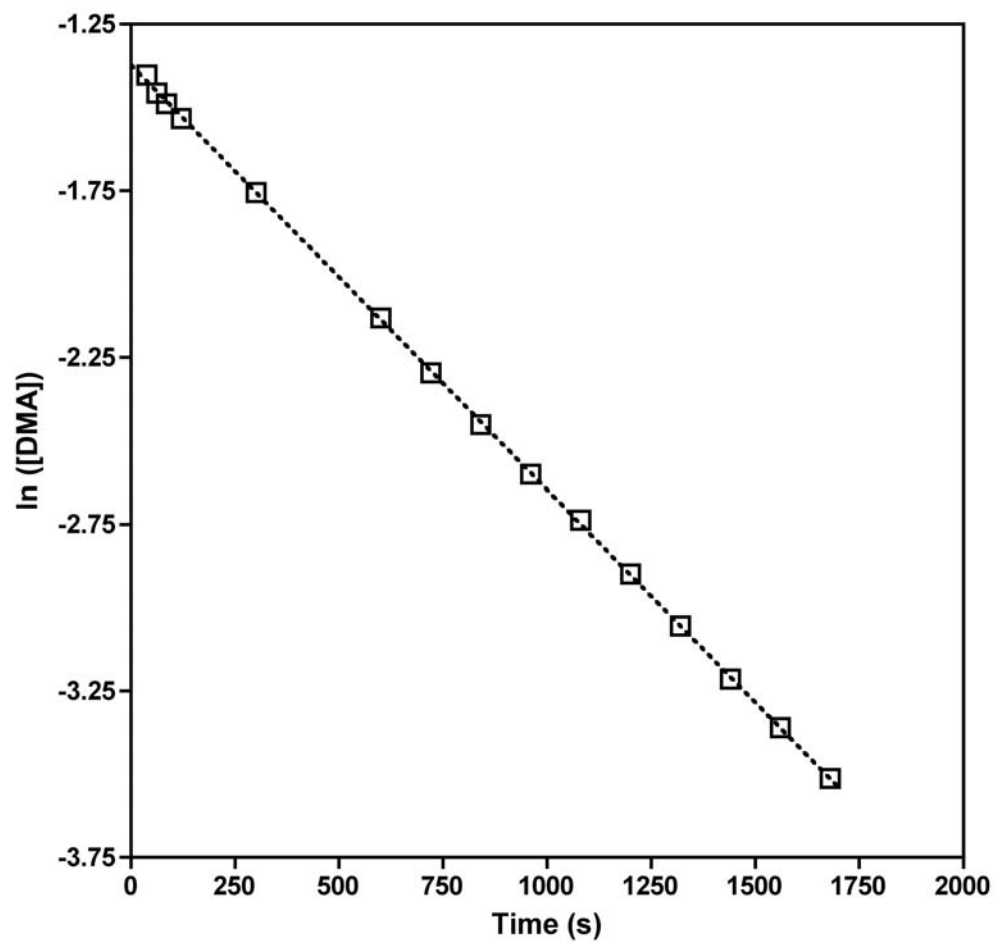
[Rh <sub>2</sub> (cap) <sub>4</sub> ] mM	$v_i^a$ RUN1	$v_i^a$ RUN2	$v_i^a$ RUN3	Mean $v_i^a$	log ( $v_i$ ) <sup>a</sup>
2.72	-2.56	-2.56	-2.31	-2.5 (2)	-3.6 (1)
1.73	-0.48	-0.50	-0.45	-0.5 (3)	-4.3 (6)
1.17	-0.46	-0.25	-0.50	-0.8 (1)	-3.4 (1)
0.56	-0.39	-0.40	-0.38	-0.4 (1)	-4.4 (3)

<sup>a</sup>Numbers in parentheses are the uncertainty in the last reported digit.

**Pseudo-first order kinetic validation for the oxidation of *N,N*-dimethylaniline with excess TBHP.** A 1 mL volumetric was charged with *N,N*-dimethylaniline (0.272 mmol) and *d*-TBHP (2.72 mmol) and diluted to volume with CD<sub>3</sub>OD (1.000 mL). A 0.027 M solution of Rh<sub>2</sub>(cap)<sub>4</sub> (20 mg/mL) was prepared in a 1 mL volumetric flask. This solution was transferred to an NMR tube equipped with a capillary standard of neat nitrobenzene. After equilibration to constant temperature,<sup>266</sup> the reaction was initiated by addition of a solution of Rh<sub>2</sub>(cap)<sub>4</sub> (100 μL, 0.0027 mmol) in CD<sub>2</sub>Cl<sub>2</sub>:CD<sub>3</sub>OD (1:1). Reaction progress was followed by single-pulse <sup>1</sup>H NMR over time monitoring the singlet corresponding to the *N*-methyl groups of the *N,N*-dimethylaniline was calibrated to 2.95 ppm. The doublet corresponding to the *o*-nitro CH of nitrobenzene was used as the integration reference.

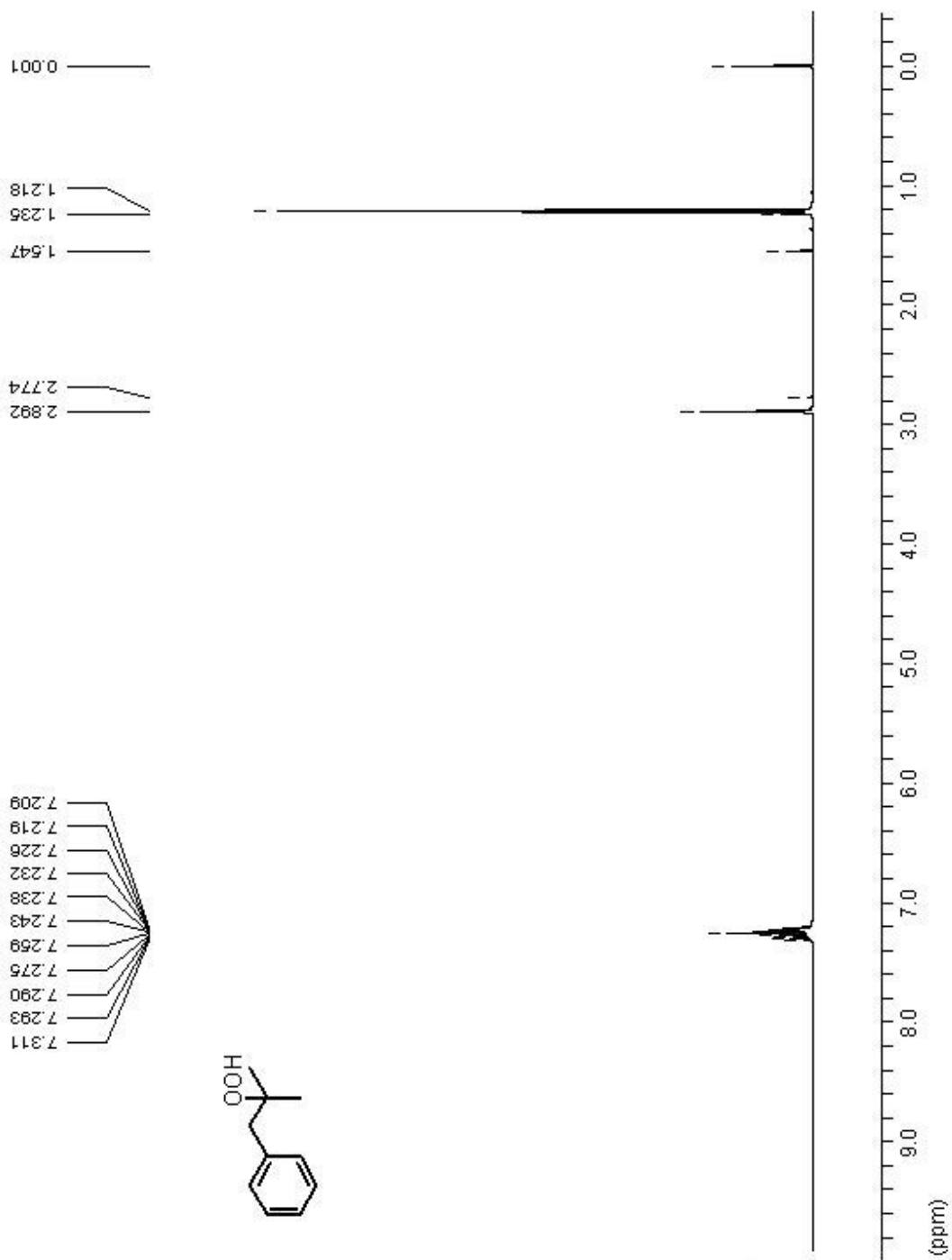
<sup>266</sup> The temperature of the <sup>1</sup>H NMR probe was 18 °C as determined by the chemical shift of the OH proton in a 1% CH<sub>3</sub>OH/CD<sub>3</sub>OD solution.

**Figure 3-8.** 1<sup>st</sup> order plot of ln[DMA] vs. time ( $k_{\text{obs}} = -1.3 \times 10^{-3} \text{ s}^{-1}$ ;  $r^2 = 0.9999$ ).

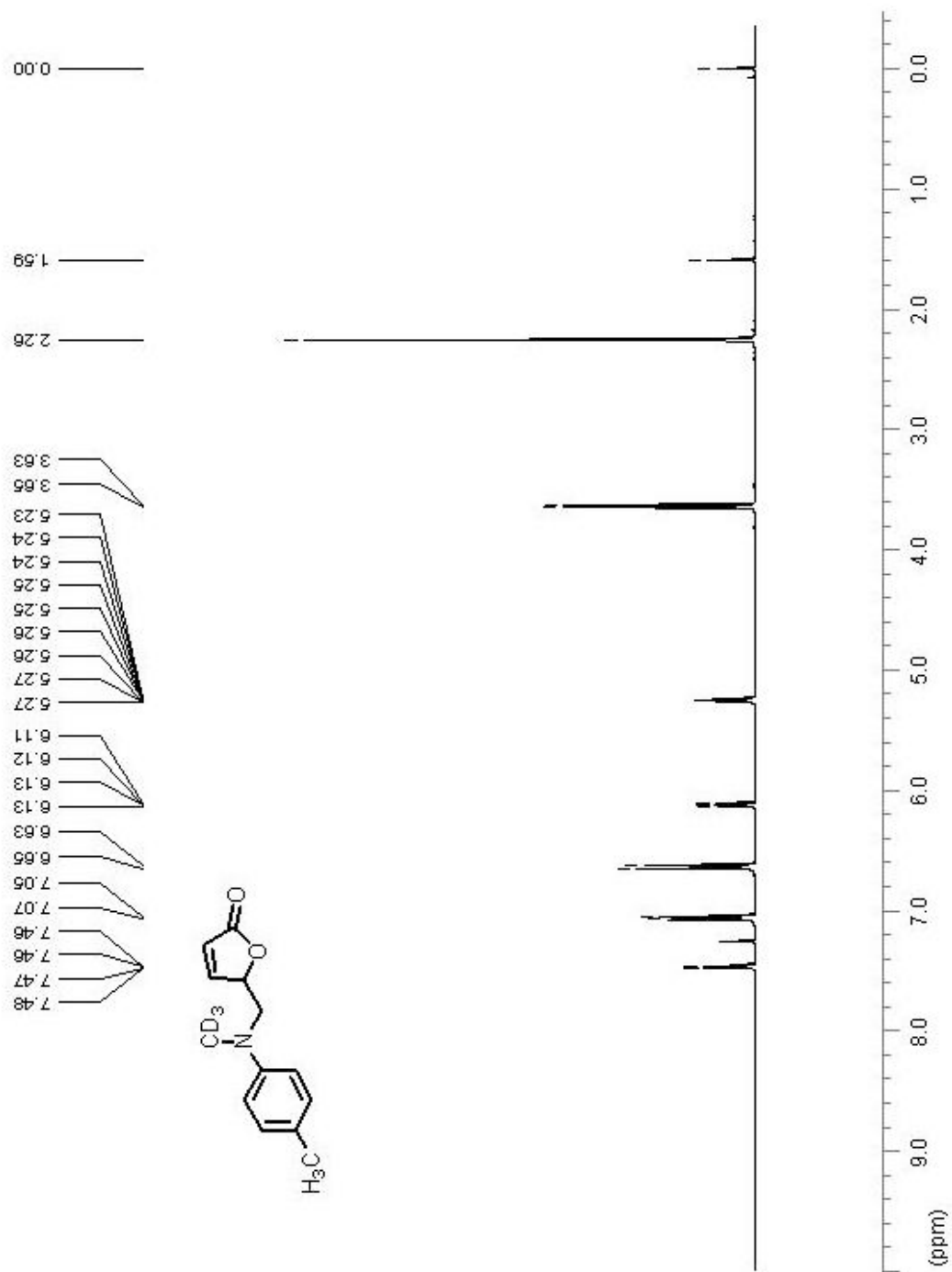


## Spectral Traces

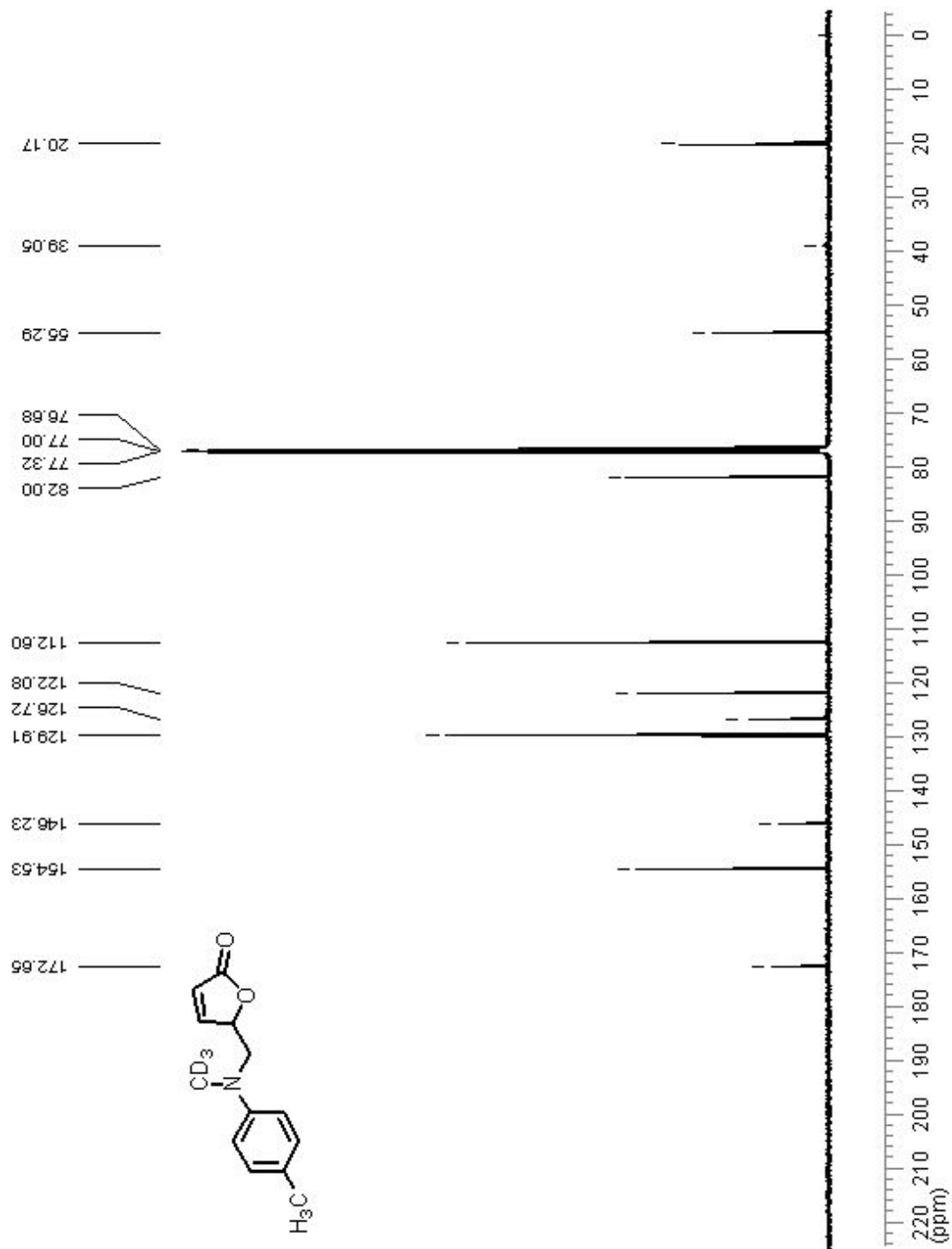
### $^1\text{H}$ NMR Spectrum – (115)



<sup>1</sup>H NMR Spectrum – (130)



<sup>13</sup>C NMR Spectrum – (130)



## Bibliography

- Adams, R. D.; Captain, B.; Herber, R. H.; Johansson, M.; Nowik, I.; Smith, J. L., Jr.; Smith, M. D. "Addition of Palladium and Platinum Tri-*tert*-Butylphosphine Groups to Re-Sn and Re-Ge Bonds" *Inorg. Chem.* **2005**, *44*, 6346.
- Adams, R. D.; Captain, B.; Zhu, L. "Platinum Promoted Insertion of an Alkyne into a Metal-Hydrogen Bond" *J. Am. Chem. Soc.* **2006**, *128*, 13672.
- Adams, R. D.; Captain, B.; Trufan, E.; Zhu, L. "Activation of Metal Hydride Complexes by Tri-*tert*-Butylphosphine-platinum and -Palladium Groups" *J. Am. Chem. Soc.* **2007**, *129*, 7545.
- Adams, R. D.; Captain, B.; Zhu, L. "Facile Activation of Hydrogen by an Unsaturated Platinum-Osmium Cluster Complex" *J. Am. Chem. Soc.* **2007**, *129*, 2454.
- Agmon, N. "Quantitative Hammond postulate" *J. Chem. Soc., Faraday Trans.* **1978**, *74*, 388.
- Aguirre, J. D.; Lutterman, D. A.; Angeles-Boza, A. M.; al., e. "Effect of Axial Coordination on the Electronic Structure and Biological Activity of Dirhodium(II,II) Complexes" *Inorg. Chem.* **2007**, *46*, 7494.
- Ahsan, M. Q.; Bernal, I.; Bear, J. L. "Reaction of *tetrakis*(Acetato)dirhodium with Acetamide: Crystal and Molecular Structure of *tetrakis*(Acetamido)diaquadirhodium Trihydrate" *Inorg. Chem.* **1986**, *25*, 260.
- Albrecht, M.; Crabtree, R. H.; Mata, J.; Peris, E. "Chelating Bis-carbene Rhodium(III) Complexes in Transfer Hydrogenation of Ketones and Imines" *Chem. Commun.* **2002**, 32.
- Angaridis, P.; Cotton, F. A.; Murillo, C. A.; Villagran, D.; Wang, X. "Paramagnetic Precursors for Supramolecular Assemblies: Selective Syntheses, Crystal Structures, and Electrochemical and Magnetic Properties of  $Ru_2(O_2CMe)_{4-n}(formamidinate)_nCl$  Complexes,  $n = 1-4$ " *Inorg. Chem.* **2004**, *43*, 8290.
- Anne, A.; Fraoua, S.; Hapiot, P.; Moiroux, J.; Saveant, J. M. "Steric and Kinetic Isotope Effects in the Deprotonation of Cation Radicals of NADH Synthetic Analogs" *J. Am. Chem. Soc.* **1995**, *117*, 7412.

- Araneo, S.; Fontana, F.; Minisci, F.; Recupero, F. "Redox Catalysis in Free-Radical Reactions: New, Simple, Convenient Intramolecular Homolytic Aromatic Substitutions" *Tetrahedron Lett.* **1995**, 36, 4307.
- Arend, M.; Westermann, B.; Risch, N. "Modern Variants of the Mannich Reaction" *Angew. Chem., Int. Ed.* **1998**, 37, 1045.
- Arends, I. W. C. E.; Ingold, K. U.; Wayner, D. M. "A Mechanistic Probe for Oxygen Activation by Metal Complexes and Hydroperoxides and Its Application to Alkane Functionalization by  $[\text{Fe}^{\text{III}}\text{Cl}_2\text{tris}(2\text{-pyridinylmethyl)amine}]^+\text{BF}_4^-$ " *J. Am. Chem. Soc.* **1995**, 117, 4710.
- Aresta, M.; Quaranta, E.; Tommasi, I.; Derien, S.; Dunach, E. "Tetraphenylborate Anion as a Phenylating Agent: Chemical and Electrochemical Reactivity of  $\text{BPh}_4^-$ -Rh Complexes toward Mono- and Dienes and Carbon Dioxide" *Organometallics* **1995**, 14, 3349.
- Astruc, D., "Electron-Transfer and Radical Processes in Transition Metal Chemistry" Wiley: New York, **1995**.
- Bach, R. D.; Ayala, P. Y.; Schlegel, H. B. "A Reassessment of the Bond Dissociation Energies of Peroxides. An *ab Initio* Study" *J. Am. Chem. Soc.* **1996**, 118, 12758.
- Baciacchi, E.; Lanzalunga, O.; Lapi, A.; Manduchi, L. "Kinetic Deuterium Isotope Effect Profiles and Substituent Effects in the Oxidative *N*-Demethylation of *N,N*-Dimethylanilines Catalyzed by *Tetrakis*(pentafluorophenyl)porphyriniron(III) Chloride" *J. Am. Chem. Soc.* **1998**, 120, 5783.
- Baciacchi, E.; Bietti, M.; Gerini, M. F.; Lanzalunga, O. "Electron-Transfer Mechanism in the *N*-Demethylation of *N,N*-Dimethylanilines by the Phthalimide-*N*-oxyl Radical" *J. Org. Chem.* **2005**, 70, 5144.
- Bäckvall, J. E., *Modern Oxidation Methods*. 1st ed.; Wiley: Weinheim, **2004**.
- Baran, P. S.; Richter, J. M. "Enantioselective Total Syntheses of Welwitindolinone A and Fischerindoles I and G" *J. Am. Chem. Soc.* **2005**, 127, 15394.
- Bard, A. J.; Faulkner, L. R., "Electrochemical Methods: Fundamentals and Applications" Wiley: New York, **1980**.
- Barral, M. C.; Gallo, T.; Herrero, S.; Jimenez-Aparicio, R.; Torres, M. R.; Urbanos, F. A. "Equatorially Connected Diruthenium(II,III) Units toward

- Paramagnetic Supramolecular Structures with Singular Magnetic Properties" *Inorg. Chem.* **2006**, *45*, 3639.
- Barybin, M. V.; Chisholm, M. H.; Dalal, N. S.; Holovics, T. H.; Patmore, N. J.; Robinson, R. E.; Zipse, D. J. "Long-Range Electronic Coupling of MM Quadruple Bonds (M = Mo or W) via a 2,6-Azulenedicarboxylate Bridge" *J. Am. Chem. Soc.* **2005**, *127*, 15182.
- Bear, J. L.; Chen, W. Z.; Han, B.; Huang, S.; Wang, L. L.; Thuriere, A.; Van Caemelbecke, E.; Kadish Karl, M.; Ren, T. "Cyanide Adducts on the Diruthenium Core of [Ru<sub>2</sub>(L)<sub>4</sub>](+) (L = ap, CH<sub>3</sub>ap, Fap, or F3ap). Electronic Properties and Binding Modes of the Bridging Ligand" *Inorg. Chem.* **2003**, *42*, 6230.
- Bear, J. L.; Lifsey, R. S.; Chau, L. K.; Ahsan, M. Q.; Korp, J. D.; Chavan, M.; Kadish, K. M. "Structural, Spectroscopic, and Electrochemical Characterization of *tetrakis*- $\mu$ -(2-Pyrrolidinonato)dirhodium(II) and *tetrakis*- $\mu$ -( $\delta$ -Valerolactamato)dirhodium(II)" *J. Chem. Soc., Dalton Trans.* **1989**, 93.
- Bear, J. L.; Han, B.; Huang, S. "Molecular Structure and Electrochemistry of Ru<sub>2</sub>(dpf)<sub>4</sub>(C<sub>2</sub>C<sub>6</sub>H<sub>5</sub>)<sub>2</sub> (dpf = N,N'-Diphenylformamidinate Ion): A Novel Ruthenium(III)-Ruthenium(III) Dimer" *J. Am. Chem. Soc.* **1993**, *115*, 1175.
- Bear, J. L.; Han, B.; Huang, S.; Kadish, K. M. "Effect of Axial Ligands on the Oxidation State, Structure, and Electronic Configuration of Diruthenium Complexes. Synthesis and Characterization of Ru<sub>2</sub>(dpf)<sub>4</sub>Cl, Ru<sub>2</sub>(dpf)<sub>4</sub>(C<sub>2</sub>C<sub>6</sub>H<sub>5</sub>), Ru<sub>2</sub>(dpf)<sub>4</sub>(C<sub>2</sub>C<sub>6</sub>H<sub>5</sub>)<sub>2</sub>, and Ru<sub>2</sub>(dpf)<sub>4</sub>(CN)<sub>2</sub> (dpf = N,N'-Diphenylformamidinate)" *Inorg. Chem.* **1996**, *35*, 3012.
- Beeson, T. D.; Mastracchio, A.; Hong, J.-B.; Ashton, K.; MacMillan, D. W. C. "Enantioselective Organocatalysis Using SOMO Activation" *Science* **2007**, *316*, 582.
- Bennett, M. J.; Cotton, F. A.; Foxman, B. M.; Stokely, P. F. "Structures of Two Compounds Containing Strong Metal-to-Metal Bonds" *J. Am. Chem. Soc.* **1967**, *89*, 2759.
- Berry, J. F.; Cotton, F. A.; Huang, P.; Murillo, C. A.; Wang, X. "A Hardwon Dirhodium Paddlewheel with Guanidinate-type (hpp) Bridging Ligands" *J. Chem. Soc., Dalton Trans.* **2005**, 3713.
- Berry, J. F.; Cotton, F. A.; Ibragimov, S. A.; Murillo, C. A.; Wang, X. "Searching for Precursors to Metal-Metal Bonded Dipalladium Species: A Study of Pd<sub>2</sub><sup>4+</sup> Complexes" *Inorg. Chem.* **2005**, *44*, 6129.



- Berry, J. F.; Bothe, E.; Cotton, F. A.; Ibragimov, S. A.; Murillo, C. A.; Villagran, D.; Wang, X. "Metal-Metal Bonding in Mixed Valence Ni<sub>2</sub><sup>5+</sup> Complexes and Spectroscopic Evidence for a Ni<sub>2</sub><sup>6+</sup> Species" *Inorg. Chem.* **2006**, *45*, 4396.
- Bersuker, I. B. "Modern Aspects of the Jahn-Teller Effect Theory and Applications to Molecular Problems" *Chem. Rev.* **2001**, *101*, 1067.
- Bhakta, M.; Hollenberg, P. F.; Wimalasena, K. "Evidence for a Hydrogen Abstraction Mechanism in P450-Catalyzed *N*-dealkylations" *Chem. Commun.* **2005**, 265.
- Bhakta, M. N.; Wimalasena, K. "Microsomal P450-Catalyzed *N*-Dealkylation of *N,N*-Dialkylanilines: Evidence for a C $\alpha$ -H Abstraction Mechanism" *J. Am. Chem. Soc.* **2002**, *124*, 1844.
- Bhakta, M. N.; Wimalasena, K. "A Mechanistic Comparison Between Cytochrome P450- and Chloroperoxidase-catalyzed *N*-Dealkylation of *N,N*-Dialkylanilines" *Eur. J. Org. Chem.* **2005**, 4801.
- Blum, A. S.; Ren, T.; Parish, D. A.; Trammell, S. A.; Moore, M. H.; Kushmerick, J. G.; Xu, G. L.; Deschamps, J. R.; Pollack, S. K.; Shashidhar, R. "Ru<sub>2</sub>(ap)<sub>4</sub>-oligo(phenyleneethynyl) Molecular Wires: Synthesis and Electronic Characterization" *J. Am. Chem. Soc.* **2005**, *127*, 10010.
- Bockman, T. M.; Hubig, S. M.; Kochi, J. K. "Direct Observation of Carbon-Carbon Bond Cleavage in Ultrafast Decarboxylations" *J. Am. Chem. Soc.* **1996**, *118*, 4502.
- Bravo, A.; Bjorsvik, H.-R.; Fontana, F.; Liguori, L.; Minisci, F. "Ingold-Fischer 'Persistent Radical Effect', Solvent Effect, and Metal Salt Oxidation of Carbon-Centered Radicals in the Synthesis of Mixed Peroxides from *tert*-Butyl Hydroperoxide" *J. Org. Chem.* **1997**, *62*, 3849.
- Brown, H. C.; Bhat, N. G.; Somayaji, V. "Organoboranes. 30. Convenient Procedures for the Synthesis of Alkyl- and Alkenylboronic Acids and Esters" *Organometallics* **1983**, *2*, 1311.
- Bruker. SMART and SAINT. Bruker AXS Inc., Madison, Wisconsin, USA. **1999**.
- Burka, L. T.; Guengerich, F. P.; Willard, R. J.; Macdonald, T. L. "Mechanism of Cytochrome P-450 Catalysis. Mechanism of *N*-Dealkylation and Amine Oxide Deoxygenation" *J. Am. Chem. Soc.* **1985**, *107*, 2549.

- Bursten, B. E. "Some Comments on Approximate LCAO Molecular Orbital Theory in Organometallic Chemistry: Getting More by Doing Less?" *Pure Appl. Chem.* **1991**, 63, 839.
- Cadenas, E.; Davies, K. J. A. "Mitochondrial Free Radical Generation, Oxidative Stress, and Aging" *Free Rad. Biol. Med.* **2000**, 29, 222.
- Catino, A. J.; Forslund, R. E.; Doyle, M. P. "Dirhodium(II) Caprolactamate: An Exceptional Catalyst for Allylic Oxidation" *J. Am. Chem. Soc.* **2004**, 126, 13622.
- Catino, A. J.; Nichols, J. M.; Choi, H.; Gottipamula, S.; Doyle, M. P. "Benzylic Oxidation Catalyzed by Dirhodium(II,III) Caprolactamate" *Organic Lett.* **2005**, 7, 5167.
- Catino, A. J.; Nichols, J. M.; Forslund, R. E.; Doyle, M. P. "Efficient Aziridination of Olefins Catalyzed by Mixed-valent Dirhodium(II,III) Caprolactamate" *Organic Lett.* **2005**, 7, 2787.
- Catino, A. J. Oxidative C-H and C=C Bond Functionalization Catalyzed by Dirhodium Caprolactamate. Ph. D. Thesis, University of Maryland, College Park, **2006**.
- Catino, A. J.; Nichols, J. M.; Nettles, B. J.; Doyle, M. P. "The Oxidative Mannich Reaction Catalyzed by Dirhodium Caprolactamate" *J. Am. Chem. Soc.* **2006**, 128, 5648.
- Cerny, M. A.; Hanzlik, R. P. "Cytochrome P450-Catalyzed Oxidation of *N*-Benzyl-*N*-cyclopropylamine Generates Both Cyclopropanone Hydrate and 3-Hydroxypropionaldehyde via Hydrogen Abstraction, Not Single Electron Transfer" *J. Am. Chem. Soc.* **2006**, 128, 3346.
- Chang, C. J.; Chang, M. C. Y.; Damrauer, N. H.; Nocera, D. G. "Proton-coupled Electron Transfer: A Unifying Mechanism for Biological Charge Transport, Amino Acid Radical Initiation and Propagation, and Bond Making/Breaking Reactions of Water and Oxygen" *Biochim. Biophys. Acta* **2004**, 1655, 13.
- Chavan, M. Y.; Zhu, T. P.; Lin, X. Q.; Ahsan, M. Q.; Bear, J. L.; Kadish, K. M. "Axial-ligand Dependent Electrochemical and Spectral Properties of a Series of Acetate- and Acetamidate Bridged Dirhodium Complexes" *Inorg. Chem.* **1984**, 23, 4538.
- Chavan, M. Y.; Zhu, T. P.; Lin, X. Q.; Ahsan, M. Q.; Bear, J. L.; Kadish, K. M. "Axial-ligand-dependent electrochemical and spectral properties of a

- series of acetate- and acetamidate-bridged dirhodium complexes" *Inorg. Chem.* **1984**, *23*, 4538.
- Chen, C.; Mariano, P. S. "An Oxidative Prins Cyclization Methodology" *J. Org. Chem.* **2000**, *65*, 3252.
- Chen, W.-Z.; Ren, T. "Synthesis and Characterization of  $Ru_2(DMBA)_4X_2$  ( $X = CN, N_3, N(CN)_2, I$ ): Controlling Structural, Redox, and Magnetic Properties with Axial Ligands" *Inorg. Chem.* **2003**, *42*, 8847.
- Chen, W.-Z.; Fanwick, P. E.; Ren, T. "Dendronized Diruthenium Compounds via the Copper(I)-Catalyzed Click Reaction" *Inorg. Chem.* **2007**, *46*, 3429.
- Chifotides, H. T.; Dunbar, K. R., "Rhodium Compounds" In *Multiple Bonds between Metal Atoms*, 3rd ed.; Cotton, F. A.; Murillo, C. A.; Walton, R. A., Eds. Springer Science and Business Media, Inc.: New York, **2005**, 465-589.
- Chifotides, H. T.; Dunbar, K. R. "Interactions of Metal-Metal-Bonded Antitumor Active Complexes with DNA Fragments and DNA" *Acc. Chem. Res.* **2005**, *38*, 146.
- Chisholm, M. H.; Gallucci, J.; Hadad, C. M.; Huffman, J. C.; al., e. " $M_2(hpp)_4Cl_2$  and  $M_2(hpp)_4$ , Where  $M = Mo$  and  $W$ : Preparations, Structure and Bonding, and Comparisons with  $C_2$ ,  $C_2H_2$ , and  $C_2Cl_2$  and the Hypothetical Molecules  $M_2(hpp)_4(H)_2$ " *J. Am. Chem. Soc.* **2003**, *125*, 16041.
- Choi, H.; Doyle, M. P. "Oxidation of Secondary Amines Catalyzed by Dirhodium Caprolactamate" *Chem. Commun.* **2007**, 745.
- Choi, H.; Doyle, M. P. "Optimal TBHP Allylic Oxidation of 5-Steroids Catalyzed by Dirhodium Caprolactamate" *Organic Lett.* **2007**, *9*, 5349.
- Chow, Y. L.; Danen, W. C.; Nelsen, S. F.; Rosenblatt, D. H. "Nonaromatic Aminium Radicals" *Chem. Rev.* **1978**, *78*, 243.
- Cioslowski, J. "Quantifying the Hammond Postulate: Intramolecular Proton Transfer in Substituted Hydrogen Catecholate Anions" *J. Am. Chem. Soc.* **1991**, *113*, 6756.
- Cornell, C. N.; Sigman, M. S. "Recent Progress in Wacker Oxidations: Moving toward Molecular Oxygen as the Sole Oxidant" *Inorg. Chem.* **2007**, *46*, 1903.

- Cotton, F. A.; Harris, C. B. "Molecular Orbital Calculations for Complexes of Heavier Transition Elements. III. The Metal-Metal Bonding and Electronic Structure of  $\text{Re}_2\text{Cl}_8^{2-}$ " *Inorg. Chem.* **1967**, 6, 924.
- Cotton, F. A.; Robinson, W. R.; Walton, R. A. "Stability and Reactivity of a New Form of Rhenium (IV) Chloride: Studies on its Disproportionation in Solution" *Inorg. Chem.* **1967**, 6, 223.
- Cotton, F. A.; Dunbar, K. R. "Isolation and Structure of the Novel Dirhodium(II) Compound  $\text{Rh}_2(\text{dmpm})_2[(\text{C}_6\text{H}_5)_2\text{P}(\text{C}_6\text{H}_4)]_2\text{Cl}_2$  with Bridging Bis(dimethylphosphino)methane and Orthometalated Triphenylphosphine Ligands" *J. Am. Chem. Soc.* **1987**, 109, 3142.
- Cotton, F. A.; Matusz, M.; Poli, R.; Feng, X. "Dinuclear Formamidinato Complexes of Nickel and Palladium" *J. Am. Chem. Soc.* **1988**, 110, 1144.
- Cotton, F. A.; Feng, X. "Density Functional Theory Study of Transition-Metal Compounds Containing Metal-Metal Bonds. 1. Molecular Structures of Dinuclear Compounds by Complete Geometry Optimization" *J. Am. Chem. Soc.* **1997**, 119, 7514.
- Cotton, F. A.; Yokochi, A. "The Apparent Flexibility of Bonds in Paddlewheel-Type Compounds." *Inorg. Chem.* **1997**, 36, 2461.
- Cotton, F. A.; Feng, X. "Density Functional Theory Study of Transition-Metal Compounds Containing Metal-Metal Bonds. 2. Molecular Structures and Vibrational Spectra of Dinuclear Tetracarboxylate Compounds of Molybdenum and Rhodium" *J. Am. Chem. Soc.* **1998**, 120, 3387.
- Cotton, F. A.; Gu, J.; Murillo, C. A.; Timmons, D. J. "The First Dinuclear Complex of Palladium(III)" *J. Am. Chem. Soc.* **1998**, 120, 13280.
- Cotton, F. A.; Nocera, D. G. "The Whole Story of the Two-Electron Bond, with the  $\delta$  Bond as a Paradigm" *Acc. Chem. Res.* **2000**, 33, 483.
- Cotton, F. A.; Lin, C.; Murillo, C. A. "Supramolecular Arrays Based on Dimetal Building Units" *Acc. Chem. Res.* **2001**, 34, 759.
- Cotton, F. A.; Gruhn, N. E.; Gu, J.; Huang, P.; Lichtenberger, D. L.; Murillo, C. A.; Van Dorn, L. O.; Wilkinson, C. C. "Closed-Shell Molecules That Ionize More Readily Than Cesium" *Science* **2002**, 298, 1971.
- Cotton, F. A.; Hillard, E. A.; Murillo, C. A. "The First Dirhodium Tetracarboxylate Molecule without Axial Ligation: New Insight into the Electronic Structures of Molecules with Importance in Catalysis and Other Reactions" *J. Am. Chem. Soc.* **2002**, 124, 5658.

- Cotton, F. A.; Lin, C.; Murillo, C. A. "The Use of Dimetal Building Blocks in Convergent Syntheses of Large Arrays" *Proc. Natl. Acad. Sci.* **2002**, *99*, 4810.
- Cotton, F. A.; Liu, C. Y.; Murillo, C. A. "Systematic Preparation of Mo<sub>2</sub><sup>4+</sup> Building Blocks for Supramolecular Assemblies" *Inorg. Chem.* **2004**, *43*, 2267.
- Cotton, F. A., "Physical, Spectroscopic and Theoretical Results on Multiple Bonds Between Metal Atoms" In *Multiple Bonds between Metal Atoms*, 3rd ed.; Cotton, F. A.; Murillo, C. A.; Walton, R. A., Eds. Springer Science and Business Media, Inc.: New York, **2005**, 707-796.
- Cotton, F. A.; Murillo, C. A.; Walton, R. A.; Editors, *Multiple Bonds Between Metal Atoms*. 3rd ed.; Springer Science and Business Media, Inc.: New York, **2005**; p 818 pp.
- Cotton, F. A.; Murillo, C. A.; Yu, R. "Chiral Supramolecules: Organometallic Molecular Loops Made from Enantiopure R-[*cis*-Rh<sub>2</sub>(C<sub>6</sub>H<sub>4</sub>PPh<sub>2</sub>)<sub>2</sub>(CH<sub>3</sub>CN)<sub>6</sub>](BF<sub>4</sub>)<sub>2</sub>" *Inorg. Chem.* **2005**, *44*, 8211.
- Cotton, F. A.; Donahue, J. P.; Gruhn, N. E.; Lichtenberger, D. L.; Murillo, C. A.; Timmons, D. J.; Van Dorn, L. O.; Villagran, D.; Wang, X. "Facilitating Access to the Most Easily Ionized Molecule: An Improved Synthesis of the Key Intermediate, W<sub>2</sub>(hpp)<sub>4</sub>Cl<sub>2</sub>, and Related Compounds" *Inorg. Chem.* **2006**, *45*, 201.
- Cotton, F. A.; Koshevoy, I. O.; Lahuerta, P.; Murillo, C. A.; Sanau, M.; Ubeda, M. A.; Zhao, Q. "High Yield Syntheses of Stable, Singly Bonded Pd<sub>2</sub><sup>6+</sup> Compounds" *J. Am. Chem. Soc.* **2006**, *128*, 13674.
- Cotton, F. A.; Liu, C. Y.; Murillo, C. A.; Wang, X. "Dimolybdenum-Containing Molecular Triangles and Squares with Diamidate Linkers: Structural Diversity and Complexity" *Inorg. Chem.* **2006**, *45*, 2619.
- Cotton, F. A.; Murillo, C. A.; Villagran, D.; Yu, R. "Uniquely Strong Electronic Communication between [Mo<sub>2</sub>] Units Linked by Dioxolene Dianions" *J. Am. Chem. Soc.* **2006**, *128*, 3281.
- Cotton, F. A.; Murillo, C. A.; Wang, X.; Wilkinson, C. C. "Homologues of the Easily Ionized Compound Mo<sub>2</sub>(hpp)<sub>4</sub> Containing Smaller Bicyclic Guanidines" *Inorg. Chem.* **2006**, *45*, 5493.
- Cotton, F. A.; Li, Z.; Liu, C. Y.; Murillo, C. A. "Modulating Electronic Coupling Using O- and S-donor Linkers" *Inorg. Chem.* **2007**, *46*, 7840.

- Cotton, F. A.; Li, Z.; Murillo, C. A. "Precursors for Assembly of Supramolecules Containing Quadruply Bonded  $\text{Cr}_2^{4+}$  Units: Systematic Preparation of  $\text{Cr}_2(\text{formamidinate})_n(\text{acetate})_{4-n}$  ( $n = 2-4$ )" *Eur. J. Inorg. Chem.* **2007**, 3509.
- Cotton, F. A.; Liu, C. Y.; Murillo, C. A.; Zhao, Q. "Electronic Localization versus Delocalization Determined by the Binding of the Linker in an Isomer Pair" *Inorg. Chem.* **2007**, 46, 2604.
- Crawford, C. L.; Barnes, M. J.; Peterson, R. A.; Wilmarth, W. R. "Copper-catalyzed Sodium Tetraphenylborate, Triphenylborane, Diphenylborinic acid and Phenylboronic Acid Decomposition Kinetic Studies in Aqueous Alkaline Solutions" *J. Organomet. Chem.* **1999**, 581, 194.
- D'Oca, M. G. M.; Russowsky, D.; Canto, K.; Gressler, T.; Goncalves, R. S. "Electrochemical Oxidation of *N-p*-Toluenesulfonamides" *Organic Lett.* **2002**, 4, 1763.
- Daminelli, G.; Widany, J.; Di Carlo, A.; Lugli, P. "Tuning the Optical Properties of Thiophene Oligomers Toward Infrared Emission: A Theoretical Study" *J. Chem. Phys.* **2001**, 115, 4919.
- Danhauser, W.; Cole, R. H. "Dielectric Properties of Liquid Butyl Alcohols" *J. Chem. Phys.* **1955**, 23, 1762.
- Das, S.; Suresh, V., "Electron-transfer reactions of amines" In *Electron Transfer in Chemistry*, Balzani, V., Ed. Wiley: New York, **2001**, 2, 379-456.
- Das, T. N.; Dhanasekaran, T.; Alfassi, Z. B.; Neta, P. "Reduction Potential of the *tert*-Butylperoxyl Radical in Aqueous Solutions" *J. Phys. Chem. A* **1998**, 102, 280.
- Davies, H. M. L.; Bruzinski, P. R.; Fall, M. J. "Effect of diazoalkane structure on the stereoselectivity of rhodium(II) (S)-N-(arylsulfonyl)prolinate catalyzed cyclopropanations" *Tetrahedron Lett.* **1996**, 37, 4133.
- Davies, H. M. L.; Rusiniak, L. "Effect of catalyst on the diastereoselectivity of methyl phenyldiazoacetate cyclopropanations" *Tetrahedron Lett.* **1998**, 39, 8811.
- Davis, G. T.; Demek, M. M.; Rosenblatt, D. H. "Oxidations of Amines. X. Detailed Kinetics in the Reaction of Chlorine Dioxide with Triethylenediamine" *J. Am. Chem. Soc.* **1972**, 94, 3321.
- Dean, J. A., *Lange's Handbook of Chemistry*. McGraw-Hill: New York, **1992**.

- Decker, A.; Solomon, E. I. "Dioxygen Activation by Copper, Heme and Non-heme Iron Enzymes: Comparison of Electronic Structures and Reactivities" *Curr. Opin. Chem. Biol.* **2005**, *9*, 152.
- Denisov, I. G.; Makris, T. M.; Sligar, S. G.; Schlichting, I. "Structure and Chemistry of Cytochrome P 450" *Chem. Rev.* **2005**, *105*, 2253.
- Dennis, A. M.; Howard, R. A.; Kadish, K. M.; Bear, J. L.; Brace, J.; Winograd, N. "X-ray Photoelectron Spectra of Some Dirhodium Carboxylate Complexes" *Inorg. Chim. Acta* **1980**, *44*, L139.
- Dequeant, M. Q.; McGuire, R.; McMillin, D. R.; Ren, T. "One-Dimensional Supramolecular Assemblies Based on a  $\text{Re}_2(\text{III},\text{III})$  Synthons and Their Solid-State Phosphorescence" *Inorg. Chem.* **2005**, *44*, 6521.
- Dequeant, M. Q.; Fanwick, P. E.; Ren, T. "Synthesis and Structural Characterization of Several Dirhenium(III) Compounds" *Inorg. Chim. Acta* **2006**, *359*, 4191.
- DiLabio, G. A.; Johnson, E. R. "Lone Pair- $\pi$ ; and  $\pi$ - $\pi$  Interactions Play an Important Role in Proton-Coupled Electron Transfer Reactions" *J. Am. Chem. Soc.* **2007**, *129*, 6199.
- Dinnocenzo, J. P.; Banach, T. E. "Deprotonation of Tertiary Amine Cation Radicals. A Direct Experimental Approach" *J. Am. Chem. Soc.* **1989**, *111*, 8646.
- Dinnocenzo, J. P.; Karki, S. B.; Jones, J. P. "On Isotope Effects for the Cytochrome P-450 Oxidation of Substituted *N,N*-Dimethylanilines" *J. Am. Chem. Soc.* **1993**, *115*, 7111.
- Dombrowski, G. W.; Dinnocenzo, J. P.; Farid, S.; Goodman, J. L.; Gould, I. R. " $\alpha$ C-H Bond Dissociation Energies of Some Tertiary Amines" *J. Org. Chem.* **1999**, *64*, 427.
- Dombrowski, G. W.; Dinnocenzo, J. P.; Zielinski, P. A.; Farid, S.; Wosinska, Z. M.; Gould, I. R. "Efficient Unimolecular Deprotonation of Aniline Radical Cations" *J. Org. Chem.* **2005**, *70*, 3791.
- Doyle, M. P.; Brandes, B. D.; Kazala, A. P.; Pieters, R. J.; Jarstfer, M. B.; Watkins, L. M.; Eagle, C. T. "Chiral Rhodium(II) Carboxamides. A New Class of Catalysts for Enantioselective Cyclopropanation Reactions" *Tetrahedron Lett.* **1990**, *31*, 6613.

- Doyle, M. P.; Westrum, L. J.; Wolthuis, W. N. E.; See, M. M.; Boone, W. P.; Bagheri, V.; Pearson, M. M. "Electronic and Steric Control in Carbon-Hydrogen Insertion Reactions of Diazoacetoacetates Catalyzed by Dirhodium(II) Carboxylates and Carboxamides" *J. Am. Chem. Soc.* **1993**, *115*, 958.
- Doyle, M. P.; Winchester, W. R.; Hoorn, J. A. A.; Lynch, V.; al., e. "Dirhodium(II) *tetrakis*-(carboxamidates) with chiral ligands. Structure and selectivity in catalytic metal-carbene transformations " *J. Am. Chem. Soc.* **1993**, *115*, 9968.
- Doyle, M. P.; Winchester, W. R.; Hoorn, J. A. A.; Lynch, V.; Simonsen, S. H.; Ghosh, R. "Dirhodium(II) Tetrakis(carboxamidates) with Chiral Ligands. Structure and Selectivity in Catalytic Metal-carbene Transformations" *J. Am. Chem. Soc.* **1993**, *115*, 9968.
- Doyle, M. P.; Zhou, Q.-L.; Charnsangavej, C.; Longoria, M. A.; McKervey, M. A.; Garcia, C. F. "Chiral Catalysts for Enantioselective Intermolecular Cyclopropanation Reactions with Methyl Phenyl diazoacetate. Origin of the Solvent Effect in Reactions Catalyzed by Homochiral Dirhodium(II) Prolinates" *Tetrahedron Lett.* **1996**, *37*, 4129.
- Doyle, M. P.; Zhou, Q.-L.; Raab, C. E.; Roos, G. H. P.; Simonsen, S. H.; Lynch, V. "Synthesis and Structures of (2,2-cis)-Dirhodium(II) Tetrakis[methyl 1-acyl-2-oxoimidazolidine-4(S)-carboxylates]. Chiral Catalysts for Highly Stereoselective Metal Carbene Transformations" *Inorg. Chem.* **1996**, *35*, 6064.
- Doyle, M. P.; Raab, C. E.; Roos, G. H. P.; Lynch, V.; Simonsen, S. H. "(4,0)-Dirhodium(II) Tetrakis[methyl 1-acetyl-2-oxoimidazolidine-4(S)-carboxylate]. Implications for the Mechanism of Ligand Exchange Reactions" *Inorg. Chim. Acta* **1997**, *266*, 13.
- Doyle, M. P.; McKervey, M. A.; Ye, T., "Modern Catalytic Methods for Organic Synthesis with Diazo Compounds: From Cyclopropanes to Ylides" Wiley: New York, **1998**.
- Doyle, M. P.; Ren, T., "The Influence of Ligands on Dirhodium(II) on Reactivity and Selectivity in Metal Carbene Reactions" In *Progress in Inorganic Chemistry*, Karlin, K., Ed. Wiley: New York, **2001**, *49*, 113-168.
- Doyle, M. P.; Morgan, J. P.; Fetting, J. C.; Zavalij, P. Y.; Colyer, J. T.; Timmons, D. J.; Carducci, M. D. "'Matched/Mismatched" Diastereomeric Dirhodium(II) Carboxamidate Catalyst Pairs. Structure-Selectivity Correlations in Diazo Decomposition and Hetero-Diels-Alder Reactions" *J. Org. Chem.* **2005**, *70*, 5291.



- Eberson, L.; Shaik, S. S. "Electron-transfer Reactions of Radical Anions: Do They Follow Outer- or Inner-sphere Mechanisms?" *J. Am. Chem. Soc.* **1990**, *112*, 4484.
- Espino, C. G.; Fiori, K. W.; Kim, M.; DuBois, J. "Expanding the Scope of C-H Amination through Catalyst Design" *J. Am. Chem. Soc.* **2004**, *126*, 15378.
- Evans, P. A.; Editor, "Modern Rhodium-Catalyzed Organic Reactions" Wiley: Weinheim, **2005**.
- Fagnou, K.; Lautens, M. "Rhodium-Catalyzed Carbon-Carbon Bond Forming Reactions of Organometallic Compounds" *Chem. Rev.* **2003**, *103*, 169.
- Fiori, K. W.; Fleming, J. J.; Du Bois, J. "N,O-Acetals: Rh-catalyzed Amination of Etheral C $\alpha$ -H bonds: A Versatile Strategy for the Synthesis of Complex Amines" *Angew. Chem., Int. Ed.* **2004**, *43*, 4349.
- Fischer, H.; Souaille, M. "The Persistent Radical Effect in Living Radical Polymerization - Borderline Cases and Side-Reactions" *Macromol. Symp.* **2001**, *174*, 231.
- Forward, J. M.; Fackler, J. P., Jr.; Staples, R. J. "Synthesis and Structural Characterization of the Luminescent Gold(I) Complex [(MeTPA)<sub>3</sub>Au]I<sub>3</sub>. Use of NaBPh<sub>4</sub> as a Phenyl-Transfer Reagent To Form [(MeTPA)AuPh](BPh<sub>4</sub>) and (TPA)AuPh" *Organometallics* **1995**, *14*, 4194.
- Fukuzumi, S.; Shimoosako, K.; Suenobu, T.; Watanabe, Y. "Mechanisms of Hydrogen-, Oxygen-, and Electron-transfer Reactions of Cumylperoxyl Radical" *J. Am. Chem. Soc.* **2003**, *125*, 9074.
- Gaillard, E. R.; Whitten, D. G. "Photoinduced Electron Transfer Bond Fragmentations" *Acc. Chem. Res.* **1996**, *29*, 292.
- Gassman, P. G.; Macomber, D. W.; Willging, S. M. "Isolation and Characterization of Reactive Intermediates and Active Catalysts in Homogeneous Catalysis" *J. Am. Chem. Soc.* **1985**, *107*, 2380.
- Girard, N.; Hurvois, J.-P.; Moinet, C.; Toupet, L. "Total Synthesis of (+)-Pumiliotoxin C: An Electrochemical Approach" *Eur. J. Org. Chem.* **2005**, 2269.
- Gois, P. M.; Trindade, A. F.; Veiros, L. F.; Andre, V.; Duarte, M. T.; Afonso, C. A.; Caddick, S.; Cloke, F. G. "Tuning the Reactivity of Dirhodium(II) Complexes with Axial N-Heterocyclic Carbene Ligands: The Arylation of Aldehydes" *Angew. Chem., Int. Ed.* **2007**, *46*, 5750.

- Goto, Y.; Watanabe, Y.; Fukuzumi, S.; Jones, J. P.; Dinnocenzo, J. P. "Mechanisms of *N*-Demethylations Catalyzed by High-Valent Species of Heme Enzymes: Novel Use of Isotope Effects and Direct Observation of Intermediates" *J. Am. Chem. Soc.* **1998**, *120*, 10762.
- Griller, D.; Howard, J. A.; Marriott, P. R.; Scaiano, J. C. "Absolute Rate Constants For the Reactions of *tert*-Butoxyl, *tert*-Butylperoxyl, and Benzophenone Triplet with Amines: the Importance of a Stereoelectronic Effect" *J. Am. Chem. Soc.* **1981**, *103*, 619.
- Guengerich, F. P.; Yun, C.-H.; Macdonald, T. L. "Evidence for a 1-Electron Oxidation Mechanism in *N*-Dealkylation of *N,N*-Dialkylanilines by Cytochrome P450 2B1. Kinetic Hydrogen Isotope Effects, Linear Free Energy Relationships, Comparisons with Horseradish Peroxidase, and Studies with Oxygen Surrogates" *J. Biol. Chem.* **1996**, *271*, 27321.
- Guengerich, F. P. "Common and Uncommon Cytochrome P450 Reactions Related to Metabolism and Chemical Toxicity" *Chem. Res. Toxicol.* **2001**, *14*, 611.
- Guirado, G.; Fleming, C. N.; Lingenfelter, T. G.; Williams, M. L.; Zuilhof, H.; Dinnocenzo, J. P. "Nanosecond Redox Equilibrium Method for Determining Oxidation Potentials in Organic Media" *J. Am. Chem. Soc.* **2004**, *126*, 14086.
- Hammes-Schiffer, S. "Theoretical Perspectives on Proton-Coupled Electron Transfer Reactions" *Acc. Chem. Res.* **2001**, *34*, 273.
- Hammond, G. S. "A Correlation of Reaction Rates" *J. Am. Chem. Soc.* **1955**, *77*, 334.
- Hansch, C.; Leo, A.; Taft, R. W. "A Survey of Hammett Substituent Constants and Resonance and Field Parameters" *Chem. Rev.* **1991**, *91*, 165.
- Harvey, J. N.; Poli, R.; Smith, K. M. "Understanding the Reactivity of Transition Metal Complexes Involving Multiple Spin States" *Coord. Chem. Rev.* **2003**, *239*, 347.
- Hiatt, R. R.; Strachan, W. M. "Effect Of Structure On Thermal Stability Of Hydroperoxides" *J. Org. Chem.* **1963**, *28*, 1893.
- Hiatt, R. R.; Irwin, K. C.; Gould, C. W. "Homolytic Decompositions of Hydroperoxides. IV. Metal-catalyzed Decompositions" *J. Org. Chem.* **1968**, *33*, 1430.

- Hiatt, R. R.; Mill, T.; Irwin, K. C.; Castleman, J. K. "Homolytic Decompositions of Hydroperoxides. II. Radical-induced Decompositions of *tert*-Butyl Hydroperoxide" *J. Org. Chem.* **1968**, 33, 1421.
- Hicks, R. G.; Nodwell, M. B. "Synthesis and Electronic Structure Investigations of  $\alpha$ ,  $\omega$ -Bis(arylthio)oligothiophenes: Toward Understanding Wire-Linker Interactions in Molecular-Scale Electronic Materials" *J. Am. Chem. Soc.* **2000**, 122, 6746.
- Hilderbrand, S. A.; Lim, M. H.; Lippard, S. J. "Dirhodium Tetracarboxylate Scaffolds as Reversible Fluorescence-Based Nitric Oxide Sensors" *J. Am. Chem. Soc.* **2004**, 126, 4972.
- Hirao, T. "Oxovanadium(V)-induced Oxidative Transformations of Main-group Organometallics" *Coord. Chem. Rev.* **2003**, 237, 271.
- Horner, J. H.; Martinez, F. N.; Musa, O. M.; Newcomb, M.; Shahin, H. E. "Kinetics of Dialkylaminium Cation Radical Reactions: Radical Clocks, Solvent Effects, Acidity Constants, and Rate Constants for Reactions with Hydrogen Atom Donors" *J. Am. Chem. Soc.* **1995**, 117, 11124.
- Hull, L. A.; Davis, G. T.; Rosenblatt, D. H.; Williams, H. K. R.; Weglein, R. C. "Oxidations of Amines. III. Duality of Mechanism in the Reaction of Amines with Chlorine Dioxide" *J. Am. Chem. Soc.* **1967**, 89, 1163.
- Hull, L. A.; Davis, G. T.; Rosenblatt, D. H. "Oxidations of Amines. IX. Correlation of Rate Constants for Reversible One-electron Transfer in Amine Oxidation with Reactant Potentials" *J. Am. Chem. Soc.* **1969**, 91, 6247.
- Hurst, S. K.; Ren, T. "Synthesis, Characterization and Electrochemistry of Diruthenium Complexes Linked by Aryl Acetylide Bridges" *J. Organomet. Chem.* **2002**, 660, 1.
- Huynh, M. H. V.; Meyer, T. J. "Proton-Coupled Electron Transfer" *Chem. Rev.* **2007**, 107, 5004.
- Isborn, C.; Hrovat, D. A.; Borden, W. T.; Mayer, J. M.; Carpenter, B. K. "Factors Controlling the Barriers to Degenerate Hydrogen Atom Transfers" *J. Am. Chem. Soc.* **2005**, 127, 5794.
- Jencks, W. P. "General acid-base catalysis of complex reactions in water" *Chem. Rev.* **1972**, 72, 706.
- Jensen, K. P.; Roos, B. O.; Ryde, U. "Performance of Density Functionals for First Row Transition Metal Systems" *J. Chem. Phys.* **2007**, 126, 14103.

- Jerzykiewicz, L.; Mierzwicki, K.; Latajka, Z.; Sobota, P. "The First Structurally Characterized Nonorganometallic Titanium(III) Alkoxo-Bridged Dinuclear Complexes" *Inorg. Chem.* **2003**, *42*, 267.
- Johnson, C. D. "Linear Free Energy Relations and the Reactivity-selectivity Principle" *Chem. Rev.* **1975**, *75*, 755.
- Jonsson, M. "Thermochemical Properties of Peroxides and Peroxyl Radicals" *J. Phys. Chem.* **1996**, *100*, 6814.
- Kadish, K. M.; Phan, T. D.; Giribabu, L.; Van Caemelbecke, E.; Bear, J. L. "Substituent and Isomer Effects on Structural, Spectroscopic, and Electrochemical Properties of Dirhodium(III,II) Complexes Containing Four Identical Unsymmetrical Bridging Ligands" *Inorg. Chem.* **2003**, *42*, 8663.
- Karki, S. B.; Dinnocenzo, J. P. "On the Mechanism of Amine Oxidations by P450" *Xenobiotica* **1995**, *25*, 711.
- Karki, S. B.; Dinnocenzo, J. P.; Jones, J. P.; Korzekwa, K. R. "Mechanism of Oxidative Amine Dealkylation of Substituted *N,N*-Dimethylanilines by Cytochrome P-450: Application of Isotope Effect Profiles" *J. Am. Chem. Soc.* **1995**, *117*, 3657.
- Kawamura, T.; Maeda, M.; Miyamoto, M.; Usami, H.; Imaeda, K.; Ebihara, M. "Geometrical Difference and Electron Configuration of Lantern-Type  $Rh_2^{4+}$  and  $Rh_2^{5+}$  Complexes: X-ray Structural and DFT Study" *J. Am. Chem. Soc.* **1998**, *120*, 8136.
- Kertesz, M.; Choi, C. H.; Yang, S. J. "Conjugated Polymers and Aromaticity" *Chem. Rev.* **2005**, *105*, 3448.
- Kharasch, M. S.; Fono, A.; Nudenberg, W. "The Chemistry of Hydroperoxides .5. The Thermal Decomposition of *Tert*-Alkyl Peroxides" *J. Org. Chem.* **1951**, *16*, 105.
- Kharasch, M. S.; Pauson, P.; Nudenberg, W. "The Chemistry of Hydroperoxides. XII. The Generation and Properties of Free *tert*-Butylperoxyl Radicals" *J. Org. Chem.* **1953**, *18*, 322.
- Khaskin, E.; Zavalij, P. Y.; Vedernikov, A. N. "Oxidatively Induced Methyl Transfer from Boron to Platinum in Dimethyldi(2-pyridyl)boratoplatinum Complexes" *Angew. Chem., Int. Ed.* **2007**, *46*, 6309.

- Kim, H.-J.; Yoon, U.-C.; Jung, Y.-S.; Park, N. S.; Cederstrom, E. M.; Mariano, P. S. "Oxidative Pictet-Spengler Cyclizations" *J. Org. Chem.* **1998**, *63*, 860.
- Launay, J. P. "Long-distance Intervalence Electron Transfer" *Chem. Soc. Rev.* **2001**, *30*, 386.
- Lebel, H.; Janes, M. K.; Charette, A. B.; Nolan, S. P. "Structure and Reactivity of Unusual *N*-Heterocyclic Carbene (NHC) Palladium Complexes Synthesized from Imidazolium Salts" *J. Am. Chem. Soc.* **2004**, *126*, 5046.
- Levanda, C.; Bechgaard, K.; Cowan, D. O. "Mixed Valence Cations. Chemistry of  $\pi$ -bridged Analogues of Biferrocene and Biferrocenylene" *J. Org. Chem.* **1976**, *41*, 2700.
- Lewis, D. F. V., "Cytochromes P450: Structure, Function and Mechanism" Taylor & Francis: **1996**.
- Lewis, E. A.; Tolman, W. B. "Reactivity of Dioxygen-Copper Systems" *Chem. Rev.* **2004**, *104*, 1047.
- Li, W.; Nelson, D. P.; Jensen, M. S.; Hoerrner, R. S.; Cai, D. "An Improved Protocol for the Preparation of 3-Pyridyl-and Some Arylboronic Acids" *J. Org. Chem.* **2002**, *67*, 5394.
- Li, Y.; Han, B.; Kadish, K. M.; Bear, J. L. "A Novel Diamagnetic Diruthenium(III) Complex Bridged by Four Unsymmetrical Carboxylate-type Ligands. Synthesis, Molecular Structure, Electrochemistry, and Spectroelectrochemistry of  $\text{Ru}_2(\text{pfap})_4(\text{C}_2\text{C}_6\text{H}_5)_2$ , Where pfap is 2,3,4,5,6-Pentafluoro-2-anilinopyridinate" *Inorg. Chem.* **1993**, *32*, 4175.
- Li, Z.; Li, C.-J. "Highly Efficient CuBr-catalyzed Cross-dehydrogenative Coupling (CDC) Between Tetrahydroisoquinolines and Activated Methylene Compounds" *Eur. J. Org. Chem.* **2005**, 3173.
- Li, Z.; Li, C.-J. "CuBr-catalyzed Direct Indolation of Tetrahydroisoquinolines via Cross-dehydrogenative Coupling Between  $\text{sp}_3$  C-H and  $\text{sp}_2$  C-H Bonds" *J. Am. Chem. Soc.* **2005**, *127*, 6968.
- Li, Z.; Li, C.-J. "Highly Efficient Copper-catalyzed nitro-Mannich Type Reaction: Cross-dehydrogenative-Coupling Between  $\text{sp}_3$  C-H Bond and  $\text{sp}_3$  C-H Bond" *J. Am. Chem. Soc.* **2005**, *127*, 3672.
- Li, Z.; Bohle, D. S.; Li, C.-J. "Cu-catalyzed Cross-dehydrogenative Coupling: A Versatile Strategy for C-C Bond Formations via the Oxidative Activation of  $\text{sp}_3$  C-H Bonds" *Proc. Natl. Acad. Sci.* **2006**, *103*, 8928.

- Li, Z.; Li, C.-J. "Catalytic Allylic Alkylation via the Cross-Dehydrogenative-Coupling Reaction between Allylic  $sp^3$  C-H and Methylenic  $sp^3$  C-H Bonds" *J. Am. Chem. Soc.* **2006**, *128*, 56.
- Lichtenberger, D. L.; Lynn, M. A.; Chisholm, M. H. "Quadruple Metal-Metal Bonds with Strong Donor Ligands. Ultraviolet Photoelectron Spectroscopy of  $M_2(\text{form})_4$  ( $M = \text{Cr, Mo, W}$ ;  $\text{form} = \text{N,N}'\text{-diphenylformamidinate}$ )" *J. Am. Chem. Soc.* **1999**, *121*, 12167.
- Lifsey, R. S.; Lin, X. Q.; Chavan, M. Y.; Ahsan, M. Q.; Kadish, K. M.; Bear, J. L. "Reaction of Rhodium(II) Acetate with *N*-Phenylacetamide: Substitution Products and Geometric Isomers" *Inorg. Chem.* **1987**, *26*, 830.
- Lin, C.; Ren, T.; Valente, E. J.; Zubkowski, J. D. "Synthesis, Spectroscopy and Electrochemistry of *Tetrakis*-[ $\mu$ -(*N, N'*-diarylformamidinato)-*bis*-( $\sigma$ -phenylethynyl)]diruthenium(III)" *J. Chem. Soc., Dalton Trans.* **1998**, 571.
- Lin, C.; Ren, T.; Valente, E. J.; Zubkowski, J. D. "Probing Diruthenium  $\sigma$ -Alkynyl Bonding Interactions *via* Substituent Effects. Linear Free Energy Relationships in Dinuclear Compounds VI" *J. Organomet. Chem.* **1999**, *570*, 114.
- Lin, S. Y.; Chen, I. W. P.; Chen, C. h.; Hsieh, M. H.; Yeh, C. Y.; Lin, T. W.; Chen, Y. H.; Peng, S. M. "Effect of Metal-Metal Interactions on Electron Transfer: an STM Study of One-Dimensional Metal String Complexes" *J. Phys. Chem. B* **2004**, *108*, 959.
- Lo Schiavo, S.; Bruno, G.; Zanello, P.; Laschi, F.; Piraino, P. "New Adducts of Dirhodium(II) Formamidinate Complexes with Polycyano Acceptor Molecules. X-ray Crystal Structure of the Tricyanomethanide Complex  $\text{Rh}_2(\text{form})_4[\text{C}(\text{CN})_3]$  ( $\text{form} = \text{N,N}'\text{-Di-p-tolylformamidinate}$ )" *Inorg. Chem.* **1997**, *36*, 1004.
- Lo Schiavo, S.; Serroni, S.; Puntoriero, F.; Tresoldi, G.; Piraino, P. "Synthesis and Characterization of Dirhodium(II,II)-porphyrin Based Multiredox Systems" *Eur. J. Inorg. Chem.* **2002**, 79.
- Lo Schiavo, S.; Serroni, S.; Puntoriero, F.; Tresoldi, G.; Piraino, P. "Synthesis and characterization of dirhodium(II,II)-porphyrin-based multiredox systems" *Eur. J. Inorg. Chem.* **2002**, 79.
- MacFaul, P. A.; Ingold, K. U.; Wayner, D. D. M.; Que, L., Jr. "A Putative Monooxygenase Mimic Which Functions *via* Well-Disguised Free Radical Chemistry" *J. Am. Chem. Soc.* **1997**, *119*, 10594.

- Macintosh, A. M.; Chisholm, M. H. "Linking Multiple Bonds between Metal Atoms: Clusters, Dimers of "Dimers", and Higher Ordered Assemblies" *Chem. Rev.* **2005**, *105*, 2949.
- Mahapatra, S.; Halfen, J. A.; Tolman, W. B. "Mechanistic Study of the Oxidative *N*-Dealkylation Reactions of Bis( $\mu$ -oxo)dicopper Complexes" *J. Am. Chem. Soc.* **1996**, *118*, 11575.
- Maimone, T. J.; Baran, P. S. "Modern Synthetic Efforts Toward Biologically Active Terpenes" *Nat. Chem. Bio.* **2007**, *3*, 396.
- Manchester, J. I.; Dinnocenzo, J. P.; Higgins, L. A.; Jones, J. P. "A New Mechanistic Probe for Cytochrome P450" *J. Am. Chem. Soc.* **1997**, *119*, 5069.
- Marcus, R. A. "The Theory of Oxidation-reduction Reactions Involving Electron Transfer. III. Applications to Data on the Rates of Organic Redox Reactions" *J. Chem. Phys.* **1957**, *26*, 872.
- Marcus, R. A. "The Theory of Oxidation-reduction Reactions Involving Electron Transfer. V. Comparison and Properties of Electrochemical and Chemical Rate Constants" *J. Phys. Chem.* **1963**, *67*, 853.
- Marcus, R. A.; Eyring, H. "Chemical and Electrochemical Electron-transfer Theory" *Ann. Rev. Phys. Chem.* **1964**, *15*, 155.
- Mariano, P. S. "Electron-transfer Mechanisms in Photochemical Transformations of Iminium Salts" *Acc. Chem. Res.* **1983**, *16*, 130.
- Maruyama, T.; Mizuno, Y.; Shimizu, I.; Suga, S.; Yoshida, J.-i. "Reactions of a *N*-Acyliminium Ion Pool with Benzylsilanes. Implication of a Radical/Cation/Radical Cation Chain Mechanism Involving Oxidative C-Si Bond Cleavage" *J. Am. Chem. Soc.* **2007**, *129*, 1902.
- Mayer, J. M. "Hydrogen Atom Abstraction by Metal-Oxo Complexes: Understanding the Analogy with Organic Radical Reactions" *Acc. Chem. Res.* **1998**, *31*, 441.
- Mayer, J. M., "Thermodynamic influences on C-H bond oxidation" In *Biomimetic Oxidations Catalyzed by Transition Metal Complexes*, Meunier, B., Ed. Imperial College Press: London, **2000**, 1-43.
- Mayer, J. M. "Proton-coupled Electron Transfer: A Reaction Chemist's View" *Ann. Rev. Phys. Chem.* **2004**, *55*, 363.

- Mayer, J. M.; Rhile, I. J. "Thermodynamics and Kinetics of Proton-coupled Electron Transfer: Stepwise vs. Concerted Pathways" *Biochim. Biophys. Acta* **2004**, *1655*, 51.
- Mendiratta, A.; Cummins, C. C.; Cotton, F. A.; Ibragimov, S. A.; Murillo, C. A.; Villagran, D. "A Diamagnetic Ditungsten(III) Paddlewheel Complex with No Direct Metal-Metal Bond" *Inorg. Chem.* **2006**, *45*, 4328.
- Mendiratta, A.; Cummins, C. C.; Cotton, F. A.; Ibragimov, S. A.; Murillo, C. A.; Villagran, D. *Inorg. Chem.* **2006**, *45*, 4328.
- Meunier, B.; Bernadou, J. "Metal-Oxo Species in P450 Enzymes and Biomimetic Models. Oxo-Hydroxo Tautomerism with Water-Soluble Metalloporphyrins" *Top. Catal.* **2002**, *21*, 47.
- Meunier, B.; de Visser, S. P.; Shaik, S. "Mechanism of Oxidation Reactions Catalyzed by Cytochrome P450 Enzymes" *Chem. Rev.* **2004**, *104*, 3947.
- Meyer, T. J.; Huynh, M. H. V.; Thorp, H. H. "The Possible Role of Proton-coupled Electron Transfer (PCET) in Water Oxidation by Photosystem II" *Angew. Chem., Int. Ed.* **2007**, *46*, 5284.
- Minisci, F.; Fontana, F.; Araneo, S.; Recupero, F. "New Syntheses of Mixed Peroxides under Gif-Barton Oxidation of Alkylbenzenes, Conjugated Alkenes and Alkanes; a Free-radical Mechanism" *J. Chem. Soc., Chem. Commun.* **1994**, 1823.
- Minisci, F.; Fontana, F.; Araneo, S.; Recupero, F.; Banfi, S.; Quici, S. "Kharasch and Metalloporphyrin Catalysis in the Functionalization of Alkanes, Alkenes, and Alkylbenzenes by t-BuOOH. Free Radical Mechanisms, Solvent Effect, and Relationship with the Gif Reaction" *J. Am. Chem. Soc.* **1995**, *117*, 226.
- Minisci, F.; Recupero, F.; Cecchetto, A.; Gambarotti, C.; Punta, C.; Faletti, R.; Paganelli, R.; Pedulli, G. F. "Mechanisms of the Aerobic Oxidation of Alcohols to Aldehydes and Ketones, Catalysed Under Mild Conditions by Persistent and Non-persistent Nitroxyl Radicals and Transition Metal Salts - Polar, Enthalpic, and Captodative Effects" *Eur. J. Org. Chem.* **2004**, 109.
- Mirica, L. M.; Ottenwaelder, X.; Stack, T. D. P. "Structure and Spectroscopy of Copper-Dioxygen Complexes" *Chem. Rev.* **2004**, *104*, 1013.
- Mitsumi, M.; Goto, H.; Umebayashi, S.; Ozawa, Y.; Kobayashi, M.; Yokoyama, T.; Tanaka, H.; Kuroda, S.-i.; Toriumi, K. "A Neutral Mixed-Valent Conducting Polymer Formed by Electron Transfer between Metal d and Ligand Orbitals" *Angew. Chem., Int. Ed.* **2005**, *44*, 4164.



- Miyaura, N.; Suzuki, A. "Palladium-Catalyzed Cross-Coupling Reactions of Organoboron Compounds" *Chem. Rev.* **1995**, *95*, 2457.
- Moinet, C.; Hurvois, J.-P.; Jutand, A. "Organic and metal-catalyzed electrosynthesis" *Adv. Org. Synth.* **2005**, *1*, 403.
- Murahashi, S.; Naota, T.; Yonemura, K. "Ruthenium-catalyzed Cytochrome P-450 Type Oxidation of Tertiary Amines with Alkyl Hydroperoxides" *J. Am. Chem. Soc.* **1988**, *110*, 8256.
- Murahashi, S.; Naota, T.; Miyaguchi, N.; Nakato, T. "Ruthenium-catalyzed Oxidation of Tertiary Amines with Hydrogen Peroxide in the Presence of Methanol" *Tetrahedron Lett.* **1992**, *33*, 6991.
- Murahashi, S.-I.; Naota, T.; Miyaguchi, N.; Noda, S. "Ruthenium-Catalyzed Oxidation of Phenols with Alkyl Hydroperoxides. A Novel, Facile Route to 2-Substituted Quinones" *J. Am. Chem. Soc.* **1996**, *118*, 2509.
- Murahashi, S.-I.; Komiya, N., "Bioinspired oxidations catalyzed by ruthenium complexes" In *Biomimetic Oxidations Catalyzed by Transition Metal Complexes*, Meunier, B., Ed. Imperial College Press: London, **2000**, 563-611.
- Murahashi, S.-I.; Komiya, N.; Oda, Y.; Kuwabara, T.; Naota, T. "Ruthenium-Catalyzed Oxidation of Alkanes with tert-Butyl Hydroperoxide and Peracetic Acid" *J. Org. Chem.* **2000**, *65*, 9186.
- Murahashi, S.-I.; Komiya, N.; Terai, H.; Nakae, T. "Aerobic Ruthenium-catalyzed Oxidative Cyanation of Tertiary Amines with Sodium Cyanide" *J. Am. Chem. Soc.* **2003**, *125*, 15312.
- Murahashi, S.-I.; Komiya, N.; Terai, H. "Ruthenium-catalyzed Oxidative Cyanation of Tertiary Amines with Hydrogen Peroxide and Sodium Cyanide" *Angew. Chem., Int. Ed.* **2005**, *44*, 6931.
- Murphy, S.; Schuster, G. B. "A Kinetic Method for Determination of Redox Potentials: Oxidation of Tetraarylborates" *J. Phys. Chem.* **1995**, *99*, 511.
- Musa, O. M.; Horner, J. H.; Shahin, H.; Newcomb, M. "A Kinetic Scale for Dialkylaminy Radical Reactions" *J. Am. Chem. Soc.* **1996**, *118*, 3862.
- Nehru, K.; Seo, M. S.; Kim, J.; Nam, W. "Oxidative N-Dealkylation Reactions by Oxoiron(IV) Complexes of Nonheme and Heme Ligands" *Inorg. Chem.* **2007**, *46*, 293.

- Ni, Z.; Yassar, A.; Antoun, T.; Yaghi, O. M. "Porous Metal-Organic Truncated Octahedron Constructed from Paddle-Wheel Squares and Terthiophene Links" *J. Am. Chem. Soc.* **2005**, *127*, 12752.
- Nichols, J. M.; Wolf, J.; Zavalij, P.; Varughese, B.; Doyle, M. P. "Bis(phenyl)dirhodium(III) Caprolactamate: A Dinuclear Paddlewheel Complex with No Metal-Metal Bond" *J. Am. Chem. Soc.* **2007**, *129*, 3504.
- Pangborn, A. B.; Giardello, M. A.; Grubbs, R. H.; Rosen, R. K.; Timmers, F. J. "Safe and Convenient Procedure for Solvent Purification" *Organometallics* **1996**, *15*, 1518.
- Parker, V. D.; Tilset, M. "Facile Proton-transfer Reactions of *N,N*-Dimethylaniline Cation Radicals" *J. Am. Chem. Soc.* **1991**, *113*, 8778.
- Pauling, L. "The Nature of the Bonds Formed by the Transition Metals with Hydrogen, Carbon and Phosphorus" *Acta Crystallogr., Sect. B: Struct. Sci* **1978**, *B34*, 746.
- Pearson, R. G. "Jahn-Teller Effects" *Proc. Natl. Acad. Sci.* **1975**, *72*, 2104.
- Petrie, S.; Stranger, R. "DFT and Metal-metal Bonding: A Dys-functional Treatment for Multiply Charged Complexes?" *Inorg. Chem.* **2004**, *43*, 2597.
- Pezacki, J. P. "Normal Acid/base Behaviour in Proton Transfer Reactions to Alkoxy Substituted Carbenes: Estimates for Intrinsic Barriers to Reaction and pK Values" *Can. J. Chem.* **1999**, *77*, 1230.
- Powers, M. J.; Meyer, T. J. "Intervalence Transfer in Mixed-Valence Biferrocene Ions" *J. Am. Chem. Soc.* **1978**, *100*, 4393.
- Prater, M. E.; Pence, L. E.; Clerac, R.; Finniss, G. M.; Campana, C.; Auban-Senzier, P.; Jerome, D.; Canadell, E.; Dunbar, K. R. "A Remarkable Family of Rhodium Acetonitrile Compounds Spanning Three Oxidation States and with Nuclearities Ranging from Mononuclear and Dinuclear to One-Dimensional Chains" *J. Am. Chem. Soc.* **1999**, *121*, 8005.
- Pretsch, E.; Clerc, T.; Seibl, J.; Simon, W., "Tables of Spectral Data for Structure Determination of Organic Compounds" Springer-Verlag: Berlin, **1983**.
- Pruchnik, F. P.; Jakimowicz, P.; Ciunik, Z.; Stanislawek, K.; Oro, L. A.; Tejel, C.; Ciriano, M. A. "Rhodium Wires Based on Binuclear Acetate-bridged Complexes" *Inorg. Chem. Commun.* **2001**, *4*, 19.

- Punniyamurthy, T.; Velusamy, S.; Iqbal, J. "Recent Advances in Transition Metal Catalyzed Oxidation of Organic Substrates with Molecular Oxygen" *Chem. Rev.* **2005**, *105*, 2329.
- Radhakrishnan, S.; Parthasarathi, R.; Subramanian, V.; Somanathan, N. "Molecular Orbital Calculations on Polythiophenes Containing Heterocyclic Substituents: Effect of Structure on Electronic Transitions" *J. Phys. Chem. B* **2006**, *110*, 14078.
- Rassu, G.; Zanardi, F.; Battistini, L.; Casiraghi, G. "The Synthetic Utility of Furan-, Pyrrole- and Thiophene-based 2-Silyloxydienes" *Chem. Soc. Rev.* **2000**, *29*, 109.
- Reece, S. Y.; Hodgkiss, J. M.; Stubbe, J.; Nocera, D. G. "Proton-coupled Electron Transfer: The Mechanistic Underpinning for Radical Transport and Catalysis in Biology" *Philos. Trans. R. Soc. London, Ser. B* **2006**, *361*, 1351.
- Ren, T. "Substituent Effects in Dinuclear Paddlewheel Compounds: Electrochemical and Spectroscopic Investigations" *Coord. Chem. Rev.* **1998**, *175*, 43.
- Ren, T.; Xu, G. L. "Diruthenium Metallaynes: Versatile Chromophores and Electrophores" *Comments Inorg. Chem.* **2002**, *23*, 355.
- Ren, T. "Diruthenium  $\sigma$ -Alkynyl Compounds: A New Class of Conjugated Organometallics" *Organometallics* **2005**, *24*, 4854.
- Ren, T.; Parish, D. A.; Xu, G.-L.; Moore, M. H.; Deschamps, J. R.; Ying, J.-W.; Pollack, S. K.; Schull, T. L.; Shashidhar, R. "Synthesis and Characterization of Wire-like  $\text{Ru}_2(\text{ap})_4^-$ -[ $\sigma$ -oligo(phenylene-ethynyl)] Compounds." *J. Organomet. Chem.* **2005**, *690*, 4734.
- Ren, T.; Chen, W. "The Synthesis and Characterization of  $\text{Ru}_2(\text{DMBA})_4\text{XCl}$  with X as Br and I" *J. Cluster Sci.* **2007**, ASAP, DOI: 10.1007/s10876.
- Rhile, I. J.; Mayer, J. M. "One-Electron Oxidation of a Hydrogen-Bonded Phenol Occurs by Concerted Proton-Coupled Electron Transfer" *J. Am. Chem. Soc.* **2004**, *126*, 12718.
- Ritchie, C. D. "Cation-anion Combination Reactions. 24. Ionization Potentials, Solvation Energies, and Reactivities of Nucleophiles in Water" *J. Am. Chem. Soc.* **1983**, *105*, 7313.

- Rosenblatt, D. H.; Hayes, A. J.; Harrison, B. L.; Streaty, R. A.; Moore, K. A. "The Reaction of Chlorine Dioxide with Triethylamine in Aqueous Solution" *J. Org. Chem.* **1963**, *28*, 2790.
- Rosenblatt, D. H.; Hull, L. A.; De Luca, D. C.; Davis, G. T.; Weglein, R. C.; Williams, H. K. R. "Oxidations of Amines. II. Substituent Effects in Chlorine Dioxide Oxidations" *J. Am. Chem. Soc.* **1967**, *89*, 1158.
- Rosenblatt, D. H.; Davis, G. T.; Hull, L. A.; Forberg, G. D. "Oxidations of Amines. V. Duality of Mechanism in the Reactions of Aliphatic Amines with Permanganate" *J. Org. Chem.* **1968**, *33*, 1649.
- Roy, C. D.; Brown, H. C. "Stability of Boronic Esters – Structural Effects on the Relative Rates of Transesterification of 2-(phenyl)-1,3,2-dioxaborolane" *J. Organomet. Chem.* **2007**, *692*, 784.
- Royer, J.; Bonin, M.; Micouin, L. "Chiral Heterocycles by Iminium Ion Cyclization" *Chem. Rev.* **2004**, *104*, 2311.
- Russell, G. A. "Deuterium-isotope Effects in the Autoxidation of Alkyl hydrocarbons. Mechanism of the Interaction of Peroxy Radicals" *J. Am. Chem. Soc.* **1957**, *79*, 3871.
- Sargent, A. L.; Rollog, M. E.; Eagle, C. T. "Electronic Structure of Axially Ligated Rhodium Carboxylates.  $\pi$ -Back-bonding Revisited" *Theor. Chem. Acc.* **1997**, *97*, 283.
- Seitz, M.; Reiser, O. "Synthetic Approaches Towards Structurally Diverse  $\gamma$ -Butyrolactone Natural-product-like Compounds" *Curr. Opin. Chem. Biol.* **2005**, *9*, 285.
- Seo, H.; Hotta, C.; Fukuyama, H. "Toward Systematic Understanding of Diversity of Electronic Properties in Low-Dimensional Molecular Solids" *Chem. Rev.* **2004**, *104*, 5005.
- Shaffer, C. L.; Morton, M. D.; Hanzlik, R. P. "*N*-Dealkylation of an *N*-Cyclopropylamine by Horseradish Peroxidase. Fate of the Cyclopropyl Group" *J. Am. Chem. Soc.* **2001**, *123*, 8502.
- Shaffer, C. L.; Harriman, S.; Koen, Y. M.; Hanzlik, R. P. "Formation of Cyclopropanone during Cytochrome P450-Catalyzed *N*-Dealkylation of a Cyclopropylamine" *J. Am. Chem. Soc.* **2002**, *124*, 8268.
- Shaik, S.; de Visser, S. P.; Ogliaro, F.; Schwarz, H.; Schroeder, D. "Two-state reactivity Mechanisms of Hydroxylation and Epoxidation by Cytochrome P-450 Revealed by Theory" *Curr. Opin. Chem. Biol.* **2002**, *6*, 556.

- Shaik, S.; Kumar, D.; de Visser, S. P.; Altun, A.; Thiel, W. "Theoretical Perspective on the Structure and Mechanism of Cytochrome P450 Enzymes" *Chem. Rev.* **2005**, *105*, 2279.
- Sharma, P. K.; De Visser, S. P.; Shaik, S. "Can a Single Oxidant with Two Spin States Masquerade as Two Different Oxidants? A Study of the Sulfoxidation Mechanism by Cytochrome P450" *J. Am. Chem. Soc.* **2003**, *125*, 8698.
- Sharpless, K. B.; Verhoeven, T. R. "Metal-catalyzed, Highly Selective Oxygenations of Olefins and Acetylenes with *tert*-Butyl Hydroperoxide. Practical Considerations and Mechanisms" *Aldrichim. Act.* **1979**, *12*, 63.
- Shearer, J.; Zhang, C. X.; Hatcher, L. Q.; Karlin, K. D. "Distinguishing Rate-Limiting Electron versus H-Atom Transfers in Cu<sub>2</sub>(O<sub>2</sub>)-Mediated Oxidative N-Dealkylations: Application of Inter- versus Intramolecular Kinetic Isotope Effects" *J. Am. Chem. Soc.* **2003**, *125*, 12670.
- Shearer, J.; Zhang, C. X.; Zakharov, L. N.; Rheingold, A. L.; Karlin, K. D. "Substrate Oxidation by Copper-dioxygen Adducts: Mechanistic Considerations" *J. Am. Chem. Soc.* **2005**, *127*, 5469.
- Sheldon, R. A.; Kochi, J. K., "Metal-Catalyzed Oxidations of Organic Compounds" Academic Press: New York, **1981**.
- Sheldrick, G. M. "Phase Annealing in SHELX-90: Direct Methods for Larger Structures" *Acta Crystallogr., Sect. A: Found. Crystallogr.* **1990**, *A46*, 467.
- Sheldrick, G. M. SADABS. University of Göttingen, Germany, **1996**.
- Sheldrick, G. M. SHELXL-97. University of Göttingen, Germany, **1999**.
- Shi, Y.-H.; Chen, W.-Z.; John, K. D.; Da Re, R. E.; Cohn, J. L.; Xu, G.-L.; Eglin, J. L.; Sattelberger, A. P.; Hare, C. R.; Ren, T. "Diosmium(III) Compounds Supported by 2-Anilinopyridinate and Novel Alkynyl Derivatives" *Inorg. Chem.* **2005**, *44*, 5719.
- Shi, Y. H.; Yee, G. T.; Wang, G. B.; Ren, T. "A New Direction in Carbon-Rich Organometallic Wires: Diruthenium Compounds Bridged by *E*-Hex-3-ene-1,5-diyne-diyl" *J. Am. Chem. Soc.* **2004**, *126*, 10552.
- Smidt, J.; Hafner, W.; Jira, R.; Sedlmeier, J.; Sieber, R.; Ruttinger, R.; Kojer, H. "Catalytic Reactions of Olefins on Compounds of the Platinum Group" *Angew. Chem., Int. Ed.* **1959**, *71*, 176.

- Solomon, E. I.; Chen, P.; Metz, M.; Lee, S.-K.; Palmer, A. E. "Oxygen Binding, Activation, and Reduction to Water by Copper Proteins" *Angew. Chem., Int. Ed.* **2001**, *40*, 4570.
- Speckamp, W. N.; Moolenaar, M. J. "New Developments in the Chemistry of *N*-acyliminium Ions and Related Intermediates" *Tetrahedron* **2000**, *56*, 3817.
- Sperry, J. B.; Wright, D. L. "The Application of Cathodic Reductions and Anodic Oxidations in the Synthesis of Complex Molecules" *Chem. Soc. Rev.* **2006**, *35*, 605.
- Starmans, W. A. J.; Thijs, L.; Zwanenburg, B. "Novel chiral dirhodium catalysts derived from aziridine- and azetidinedicarboxylic acid for intermolecular cyclopropanation reactions with methyl phenyldiazoacetate" *Tetrahedron* **1998**, *54*, 629.
- Still, W. C.; Kahn, M.; Mitra, A. "Rapid Chromatographic Technique for Preparative Separations with Moderate Resolution" *J. Org. Chem.* **1978**, *43*, 2923.
- Strauss, S. H. "The Search for Larger and More Weakly Coordinating Anions" *Chem. Rev.* **1993**, *93*, 927.
- Studer, A. "The Persistent Radical Effect in Organic Synthesis" *Chem. Eur. J.* **2001**, *7*, 1159.
- Su, Z.; Falvey, D. E.; Yoon, U. C.; Mariano, P. S. "The Dynamics of  $\alpha$ -Anilinocarboxylate and Related Cation Radical  $\alpha$ -Heterolytic Fragmentation Processes" *J. Am. Chem. Soc.* **1997**, *119*, 5261.
- Su, Z.; Mariano, P. S.; Falvey, D. E.; Yoon, U. C.; Oh, S. W. "Dynamics of Anilinium Radical  $\alpha$ -Heterolytic Fragmentation Processes. Electrofugal Group, Substituent, and Medium Effects on Desilylation, Decarboxylation, and Retro-Aldol Cleavage Pathways" *J. Am. Chem. Soc.* **1998**, *120*, 10676.
- Suga, S.; Watanabe, M.; Yoshida, J.-i. "Electroauxiliary-Assisted Sequential Introduction of Two Carbon Nucleophiles on the Same  $\alpha$ -Carbon of Nitrogen: Application to the Synthesis of Spiro Compounds" *J. Am. Chem. Soc.* **2002**, *124*, 14824.
- Suga, S.; Nishida, T.; Yamada, D.; Nagaki, A.; Yoshida, J. "Three-component Coupling Based on the "Cation Pool" Method" *J. Am. Chem. Soc.* **2004**, *126*, 14338.

- Sumalekshmy, S.; Gopidas, K. R. "Reaction of Aromatic Amines with  $\text{Cu}(\text{ClO}_4)_2$  in Acetonitrile as a Facile Route to Amine Radical Cation Generation" *Chem. Phys. Lett.* **2005**, 413, 294.
- Sun, H.; Moeller, K. D. "Silyl-Substituted Amino Acids: New Routes to the Construction of Selectively Functionalized Peptidomimetics" *Organic Lett.* **2002**, 4, 1547.
- Sun, H.; Martin, C.; Kesselring, D.; Keller, R.; Moeller, K. D. "Building Functionalized Peptidomimetics: Use of Electroauxiliaries for Introducing N-Acyliminium Ions into Peptides" *J. Am. Chem. Soc.* **2006**, 128, 13761.
- Szuchmacher Blum, A.; Ren, T.; Parish, D. A.; Trammell, S. A.; Moore, M. H.; Kushmerick, J. G.; Xu, G. L.; Deschamps, J. R.; Pollack, S. K.; Shashidhar, R. " $\text{Ru}_2(\text{ap})_4(\sigma\text{-oligo(phenyleneethynyl)})$  Molecular Wires: Synthesis and Electronic Characterization" *J. Am. Chem. Soc.* **2005**, 127, 10010.
- Timmons, D. J.; Doyle, M. P., "Chiral dirhodium(II) catalysts and their applications" In *Multiple Bonds between Metal Atoms*, 3rd ed.; Cotton, F. A.; Murillo, C. A.; Walton, R. A., Eds. Springer Science and Business Media, Inc.: New York, **2005**, 591-632.
- Wales, D. J. "A Microscopic Basis for the Global Appearance of Energy Landscapes" *Science* **2001**, 293, 2067.
- Walling, C. "Intermediates in the Reactions of Fenton Type Reagents" *Acc. Chem. Res.* **1998**, 31, 155.
- Wayner, D. D. M.; McPhee, D. J.; Griller, D. "Oxidation and Reduction Potentials of Transient Free Radicals" *J. Am. Chem. Soc.* **1988**, 110, 132.
- Welch, C. J.; Tu, Q.; Wang, T.; Raab, C.; Wang, P.; Jia, X.; Bu, X.; Bykowski, D.; Hohenstaufen, B.; Doyle, M. P. "Observations of Rhodium-containing Reaction Intermediates Using HPLC with ICP-MS and ESI-MS Detection" *Adv. Synth. Catal.* **2006**, 348, 821.
- Wu, X.-D.; Khim, S.-K.; Zhang, X.; Cederstrom, E. M.; Mariano, P. S. "An Oxidative Mannich Cyclization Methodology for the Stereocontrolled Synthesis of Highly Functionalized Piperidines" *J. Org. Chem.* **1998**, 63, 841.
- Xu, G.; DeRosa, M. C.; Crutchley, R. J.; Ren, T. "*trans*-Bis(alkynyl) Diruthenium(III) Tetra(amidinate): An Effective Facilitator of Electronic Delocalization" *J. Am. Chem. Soc.* **2004**, 126, 3728.

- Xu, G.; Wang, C.; Ni, Y.; Goodson, T. G.; Ren, T. "Iterative Synthesis of Oligoynes Capped by a Ru<sub>2</sub>(ap)<sub>4</sub>-terminus and Their Electrochemical and Optoelectronic Properties" *Organometallics* **2005**, *24*, 3247.
- Yakelis, N. A.; Bergman, R. G. "Safe Preparation and Purification of Sodium Tetrakis[(3,5-trifluoromethyl)phenyl]borate (NaBARF<sub>24</sub>): Reliable and Sensitive Analysis of Water in Solutions of Fluorinated Tetraarylborates" *Organometallics* **2005**, *24*, 3579.
- Ying, J.; Cordova, A.; Ren, T. Y.; Xu, G.; Ren, T. "Bis-alkynyl Diruthenium Compounds with Built-in Electronic Asymmetry: Toward an Organometallic Aviram-Ratner Diode" *Chem. Eur. J.* **2007**, *13*, 6874.
- Ying, J. W.; Sobransingh, D. R.; Xu, G. L.; Kaifer, A. E.; Ren, T. "Sulfide-capped Wire-like Metallaynes as Connectors for Au Nanoparticle Assemblies" *Chem. Commun.* **2005**, 357.
- Ying, J. W.; Cordova, A.; Ren, T. Y.; Xu, G. L.; Ren, T. "Bis-alkynyl diruthenium compounds with built-in electronic asymmetry: toward an organometallic Aviram-Ratner diode" *Chem. Eur. J.* **2007**, *13*, 6874.
- Yoon, U. C.; Mariano, P. S. "Mechanistic and Synthetic Aspects of Amine-one Single Electron Transfer Photochemistry" *Acc. Chem. Res.* **1992**, *25*, 233.
- Yoon, U. C.; Mariano, P. S. "The Synthetic Potential of Phthalimide SET Photochemistry" *Acc. Chem. Res.* **2001**, *34*, 523.
- Zhang, T.-G.; Zhao, Y.; Asselberghs, I.; Persoons, A.; Clays, K.; Therien, M. J. "Design, Synthesis, Linear, and Nonlinear Optical Properties of Conjugated (Porphinato)zinc(II)-Based Donor-Acceptor Chromophores Featuring Nitrothiophenyl and Nitrooligothiophenyl Electron-Accepting Moieties" *J. Am. Chem. Soc.* **2005**, *127*, 9710.
- Zhang, X.; Yeh, S.-R.; Hong, S.; Freccero, M.; Albin, A.; Falvey, D. E.; Mariano, P. S. "Dynamics of  $\alpha$ -CH Deprotonation and  $\alpha$ -Desilylation Reactions of Tertiary Amine Cation Radicals" *J. Am. Chem. Soc.* **1994**, *116*, 4211.
- Zhao, P.; Incarvito, C. D.; Hartwig, J. F. "Directly Observed Transmetalation from Boron to Rhodium.  $\beta$ -Aryl Elimination from Rh(I) Arylboronates and Diarylborinates" *J. Am. Chem. Soc.* **2007**, *129*, 1876.
- Zou, G.; Alvarez, J. C.; Ren, T. "Ru- $\sigma$ -alkynyl Compounds of Tetraanilinopyridinato-diruthenium(II,III) Core: Synthesis and Structural Characterization" *J. Organomet. Chem.* **2000**, *152*, 152.